

## **Copyright Warning & Restrictions**

The copyright law of the United States (Title 17, United States Code) governs the making of photocopies or other reproductions of copyrighted material.

Under certain conditions specified in the law, libraries and archives are authorized to furnish a photocopy or other reproduction. One of these specified conditions is that the photocopy or reproduction is not to be “used for any purpose other than private study, scholarship, or research.” If a user makes a request for, or later uses, a photocopy or reproduction for purposes in excess of “fair use” that user may be liable for copyright infringement,

This institution reserves the right to refuse to accept a copying order if, in its judgment, fulfillment of the order would involve violation of copyright law.

**Please Note: The author retains the copyright while the New Jersey Institute of Technology reserves the right to distribute this thesis or dissertation**

Printing note: If you do not wish to print this page, then select “Pages from: first page # to: last page #” on the print dialog screen

The Van Houten library has removed some of the personal information and all signatures from the approval page and biographical sketches of theses and dissertations in order to protect the identity of NJIT graduates and faculty.



SCANNING ELECTRON MICROSCOPY AND  
X-RAY ENERGY DISPERSIVE SPECTROSCOPIC  
ANALYSIS OF SELECTED SORBENT MATERIALS

by

Elhamy Amin Sedhom

Thesis submitted to the Faculty of the Graduate School  
of the New Jersey Institute of Technology in partial fulfillment  
of the requirements for the degree of  
Master of Engineering Science  
1981

Blank Page

APPROVAL OF THESIS  
SCANNING ELECTRON MICROSCOPY AND  
X-RAY ENERGY DISPERSIVE SPECTROSCOPIC  
ANALYSIS OF SELECTED SORBENT MATERIALS

BY

ELHAMY AMIN SEDHOM

FOR

DEPARTMENT OF CHEMICAL ENGINEERING AND CHEMISTRY  
NEW JERSEY INSTITUTE OF TECHNOLOGY

BY

FACULTY COMMITTEE

APPROVED:

NEWARK, NEW JERSEY

MAY 1981

VITA

Name: Elhamy Amin Sedhom

Permanent address:

Degree and date to be conferred: Master of Analytical Chemistry, 1981

Date of birth:

Place of birth:

Secondary education: Abnoub Elementary & High School

Collegiate institutions attended	Dates	Degree	Date of Degree
Ein Shams University Faculty of Science	1959-63	B.Sc.	1963
New Jersey Institute of Technology, N.J.	1975-81	M.Sc.	1981

Major: Analytical Chemistry

## ABSTRACT

A previous study<sup>(1)</sup> showed that a combination of acidic and basic sorbents in a layered system is required to reduce to safe levels the contaminants present in the leachates emanating from industrial landfills. The sorbents used were fly ash, vermiculite, kaolinite, illite, zeolite, apautagite, bentonite, activated carbon and bauxite.

The purpose of this investigation is to study the physical properties, elemental composition and the distribution of the aforementioned solid sorbents. Properties of interest are particle size, shape and distribution and also the chemical composition and the distribution of the elements within the sample particles.

Scanning Electron Microscopy (SEM) and X-ray Energy Dispersive Spectroscopy (EDS) were used in this study of two fly ash and eight clay samples. This study revealed the particle size distribution and the minimum average and maximum particle size of each sample. Also, the morphological details of particles such as surface roughness, micro and macro pores and cracks were illustrated by the SEM micrographs.

Elemental X-ray images and X-ray energy spectra were obtained and show the elemental distribution in each sample and the variations in their concentration between the sample

particles. The X-ray images and X-ray energy spectra also illustrated the relationship between the particle shape and its chemical composition.

Area scans were obtained to illustrate the general chemical composition of the sample, while point scans were obtained to show the elemental composition of some individual particles. These two methods served to point out the difference between the particle elemental composition and other particles in the same sample. Finally, by using the X-ray images and X-ray energy spectra, simple phase analysis could be obtained.

## TABLE OF CONTENTS

	<u>PAGE</u>
ABSTRACT	ii
TABLE OF CONTENTS	iv
ACKNOWLEDGEMENT	v
LIST OF DIAGRAMS	vi
LIST OF FIGURES	vii
1 - INTRODUCTION	1
2 - MATERIALS DESCRIPTION	3
3 - SAMPLE PREPARATION	12
4 - INSTRUMENTATION	23
5 - EXPERIMENTAL RESULTS AND DISCUSSION	45
6 - CONCLUSIONS	284
7 - REFERENCES	287

## ACKNOWLEDGEMENT

I would like to express my appreciation to Professors H. Kimmel, L. Dauerman and R. Trattner for their support. I would like to thank Mrs. L. Zydorski for her skillful typing and Mrs. Eve Jonas for her help in drawing the diagrams. I am deeply grateful to Dr. M.A. DeSesa and Dr. R.K. Darlington for the encouragement they gave me during this work. Finally, I wish to express my sincere gratitude to Dr. C.A. Cody for the direction, advice and support given to me through this study.



## LIST OF DIAGRAMS

	<u>PAGE</u>
I. Vacuum Evaporator	19
II. Sputter Coater	22
III. Schematic Drawing of the Electron and X-ray Optics of the SEM	24
IV. The Electron Gun	26
V. Illustration Showing the Depth of Signal Generation when the Primary Electron Beam Interacts with the Sample Surface	27
VI. Schematic Drawing Showing Origin of Spherical Aberration	30
VII. Schematic Drawing Showing Origin of Chromatic Aberration	30
VIII. Schematic Drawing Showing Diffraction at a Lens Aperture	34
IX. Optimum Positions of the Secondary and Backscattered Detectors	36
Xa. Possible Paths (1 to 5) of Backscattered Electrons in a Solid Sample	37
Xb. Secondary Electrons Produced by Electron-Electron Collisions are Shown by 6 and 7	37
XI. Si(Li) Detector of an X-ray Energy Dispersive Spectrometer	44

## LIST OF FIGURES

SEM Images, X-ray Image and X-ray Energy Spectra

	<u>PAGE</u>
SAMPLE IDENTIFICATION	
Apautagite	48
Fly Ash (Acidic)	73
Bentonite	106
Vermiculite	134
Fly Ash (Basic)	151
Activated Carbon	186
Illite	195
Kaolinite	223
Zeolite	238
Bauxite	267

SECTION 1  
INTRODUCTION.

The ultimate and safe disposal of liquid and solid wastes is currently one of the most important concerns of environmental protection and public health authorities. There are only a few, acceptable waste disposal practices. However, none of them is easy, foolproof, or inexpensive.

Incineration of combustible waste greatly reduces the volume of the original waste; however, it creates smoke and odor nuisance, and some volatile compounds or elements may escape into the atmosphere.

Some coastal cities, such as New York City, have dumped digested sewage sludge into designated dumping grounds within coastal waters. As a result of the alleged hazard to marine life and public health, the City of New York is under court order to terminate the dumping by 1981.

Waste disposal on land is by far the most common method. Michaels<sup>(2)</sup> has estimated that landfills are used to dispose of in excess of 90% of all solid waste. A major concern in the landfill method is the protection of ground water from leachates which form from the wastes. Disposal of solid waste by sanitary landfill is very well documented<sup>(3-5)</sup>

The EPA definition of sanitary landfill is "an engineered method of disposing of solid wastes on land in a manner that minimizes environmental hazards by spreading the solid wastes in thin layers, compacting the solid wastes

to the smallest practical volume and applying and compacting cover material at the end of each operating day"<sup>(6)</sup>.

A properly operated sanitary landfill is free of odor, flies and rodents. In some cases, it may be necessary to protect ground water from leachate-rainwater that passes through the landfill and picks up dissolved, colloidal, and suspended solids in concentration that vary widely with local conditions. Leachate can become highly concentrated and therefore must be collected and treated before it is discharged to the environment.

The study reported herein enables the users of selected sorbents to relate efficiency versus physical and chemical properties for the treatment of leachate contaminants from a landfill.

The efficiency is related to properties such as particle size, shape and distribution, micro and macro structures of the particles surface, elemental composition and distribution. These properties of the ten samples have been studied by the Scanning Electron Microscope (SEM) and the X-ray Energy Dispersive Spectrometer (EDS).

SECTION 2  
MATERIALS DESCRIPTION

Introduction

Ten sorbent materials were used in this study; eight are clays while the other two are waste products. These materials are: apautagite, fly ash (acidic and basic), bentonite, vermiculite, activated carbon, illite, kaolinite, zeolite and bauxite. The clay minerals are used because they have the property of sorbing certain anions and cations and retaining these in an exchangeable state. These ions can be exchanged for other anions or cations by treatment of such ions in a water solution. Also, the exchange reaction can take place in a non-aqueous environment. The exchange reaction is stoichiometric.

The exchangeable ions are held around the outside of the silica-alumina clay mineral structural unit, and the exchange reaction generally does not affect the structure of the silica-alumina pocket. For example, the ion-exchange reaction is used for the softening of water. Here the sorbents are zeolites or carbon exchangers.

The property of exchange capacity is measured in terms of milliequivalents per gram or more frequently milliequivalents per 100 g. Exchange capacity is determined at neutrality, i.e, pH 7. In clay minerals, the most common exchangeable cations are  $\text{Ca}^{++}$ ,  $\text{Mg}^{++}$ ,  $\text{H}^+$ ,  $\text{K}^+$  and  $\text{Na}^+$ , while

the common exchangeable anions in clay minerals are  $\text{SO}_4^-$ ,  $\text{Cl}^-$ ,  $\text{PO}_4^{3-}$  and  $\text{NO}_3^-$  (7).

#### Sample Description

##### Apautagite:

Apautagite is commonly known as greensand or glauconite and is mined in the state of New Jersey. It is a complex hydrated silicate or ferrous-ferric iron and potassium which usually contains some magnesium and aluminum. The chemical formula is approximately  $\text{K}\cdot\text{Mg}\cdot(\text{Fe}, \text{Al})\text{SiO}_2\cdot 3\text{H}_2\text{O}$ . Apautagite is usually found as rounded or subangular granules which appear blackish-green in reflected light<sup>(8)</sup>.

World Production: The U.S.A. is the largest producer of apautagite (greensand). Practically the entire American output comes from Burlington and Gloucester Counties, New Jersey and Calvert County, Maryland<sup>(8)</sup>. Next in production to the U.S.A. is Australia which has the bulk of its production coming from GinGin, in the Western part of Australia. The Australian greensand, after treatment, is largely exported to Europe under the name "Mallinite". Small quantities of greensand are also mined in other countries<sup>(8)</sup>.

Uses: Apautagite can be used as: a base exchange water softener, in the preparation of some pigments, for fertilizers, and as a source of potash salts and sorbent<sup>(8)</sup>.

##### Fly Ash:

Fly ash is a powder of fine particulates collected from stacks. It is a waste product of electric power generation where coal is used as a fuel. It is collected by

electrostatic precipitation from the flue gases before they escape through the stack.

The elemental composition and the surface structures of the particles forming the fly ash vary according to the type of coal used and also on the degree of combustion. It is estimated that a total of 30 million tons of fly ash is generated every year in the U.S.A. The pH of the fly ash particles in water varies from acidic to basic (alkaline). Fly ash has been used for treatment of COD (chemical oxygen demand) and to remove some other contaminants from chemical waste. Acidic and basic fly ash examined in this study was supplied by the Public Service Electric and Gas Company, Hudson Generating Station, Jersey City, New Jersey<sup>(1&9)</sup>.

#### Bentonite:

The name bentonite is applied to a variety of naturally occurring clay-like products. Each adsorbs water to a greater extent than ordinary clays, and also has a much greater capacity for cation exchange than that shown by kaolinic clays. In some types of bentonite, the adsorption of water is accompanied by a considerable increase in volume and the formation of a gelatinous mass. Bentonites are also distinguished from other clays in that they are almost entirely crystalline. Minerals comprising the montmorillonite family may be represented, in general, by the formula  $(\text{Mg}\cdot\text{Ca})\text{O}\cdot\text{Al}_2\text{O}_3\cdot 5\text{SiO}_2\cdot n\text{H}_2\text{O}$  where  $n$  is = 8. Bentonite was formed by alteration of volcanic ash<sup>(1,7,8&10)</sup>.

Bentonite is known and marketed under many names such as soap clay, mineral soap, wilkinite, staylite, val-clay,

aquagel, ardmorite and refinite. Several clays, prepared or treated as organo-bentonites, are sold under names such as Baragel or Tixogel.

World Supply: The U.S.A. is the world's chief supplier of bentonite. The mineral is found in nearly every state west of the Mississippi River, and also in a belt extending from Kentucky to the Gulf of Mexico. Over one-half of the output comes from the Wyoming-South Dakota area, which yields the sodium, or high-swelling type. There is a non-swelling bentonite which contains high levels of calcium. This type is mined at Panther Creek, Mississippi. Bentonite is also found in Canada, West Germany, Italy, Algeria and Morocco<sup>(7,8&10)</sup>.

Uses: Bentonite can be used for a variety of purposes, including rotary drilling mud, filtration aids for decolorization of oils, foundry sand bonding material and as sorbents and emulsifying agents for asphaltic and resinous substances in soaps, paints and pharmaceutical products. Bentonite is used as an adhesive agent in sprays and insecticides or as a plasticizer in ceramic bodies.

Specifications and analytical methods were developed in the U.S.A. for bentonite<sup>(10)</sup>. Some minor uses for bentonite include alkali-bentonite mixed with glycerine for facial beauty creams, the de-inking of old newsprint and as a thixotropic agent to prevent settling of mixed paints<sup>(10)</sup>.

Vermiculite:

Vermiculite is a name given to a group of minerals which have a platy, laminated structure similar to the platy



structure of the mica group minerals, Vermiculite, when heated exfoliates to a remarkable extent in a direction at a right angle to the laminae. Because of the exfoliation property of vermiculite, it is a commercially valuable material.

Chemical analyses of commercial vermiculite show wide ranges of concentrations of the major elements. The amount of water has a major effect in its degree of exfoliation during heating and its volume increases up to 100 times. The average molecular composition of vermiculite is  $22\text{MgO} \cdot 5\text{Al}_2\text{O}_3 \cdot \text{Fe}_2\text{O}_3 \cdot 22\text{SiO}_2 \cdot 40\text{H}_2\text{O}$ . The vermiculites have a high cation-exchange capacity (150 milliequivalents per 100 g).

The structure of vermiculite consists of trioctahedral mica sheets separated by double layers of water and is unbalanced by substitution of aluminum far in the tetrahedral layer. Vermiculite will also absorb some organic molecules between the mica layers<sup>(1,7,8&10)</sup>. The vermiculite used in this study was received from W.R. Grace & Company, Trenton, New Jersey. The sample was examined without grinding.

Uses: Vermiculite is used in home insulation, acoustical plastics, agricultural chemicals, ceramics, insulating refractories and fertilizers. Other uses for vermiculite include: poultry litter, as a lubricant, filler, absorbent, packaging and shipping material for acids and chemicals (because it is inert) and as a decorative material<sup>(7,8&10)</sup>.

### Activated Carbon:

Activated carbon consists of black large particles, highly porous and having a very great absorption capacity for vapors, gases and colloidal solids. Activated carbon is produced by the destructive distillation of some carbonaceous materials and is activated by heating to 800-900°C in a steam or carbon dioxide to prevent oxidation. This treatment greatly increases the porosity. The surface area of one gram can range from 600 to 2000 square meters<sup>(1&9)</sup>. The sample used for this study was obtained from Witco Chemical, Activated Carbon Division, New York, New York and was examined as received.

### Illite:

Illite deposits are sedimentary in origin although illite has been found in hydrothermal and residual deposits. Illite is not a specific mineral name, but instead a general term for the clay minerals of argillaceous sediments of the mica-like clay minerals. The basic structural unit is a layer composed of two silica tetrahedral sheets and a central octahedral sheet. This unit is similar to that of montmorillonite except that more aluminum ions replace silicon in the tetrahedral sheet. This causes a greater charge deficiency. This charge deficiency is balanced by potassium ions. The potassium ions act as a bridge between the unit layers, tying them together. The strength of the bridging is such that the illite minerals are nonexpandable.

Illite is a name given to the aluminum, magnesium, and iron-rich mica-like clays found in the state of Illinois.

The illites have a moderate cation-exchange capacity. In most cases the illite clays have no special use other than relatively common structural clay products such as brick and tile<sup>(1,7,8&10)</sup>.

The sample used for this study was supplied by A.P. Green Refractory Company, Morris, Illinois. It was received in rock form, was ground to powder and passed through an 80 - mesh screen before examination.

Kaolinite:

Kaolinite is the most common member of the kaolin minerals (China clay). The structure of kaolinite consists of a single silica tetrahedral sheet and a single alumina octahedral sheet combined into the kaoline unit layer. These unit layers are stacked one on top of the other; variations in orientation of the unit layers and in stacking differences within the kaolinite mineral group lead to differences in various minerals of the kaolin group.

Kaolinite contains a relatively high ratio of aluminum to silicon, high hydrogen, but low sodium, potassium, calcium and no magnesium and very low concentrations of iron. Broken bonds around the edges of the silica-alumina units are the major cause of its exchange capacity. Because of this, it may have sorptive characteristics. The general chemical formula for kaolinite is  $\text{Al}_2\text{O}_3 \cdot 2\text{SiO}_2 \cdot 2\text{H}_2\text{O}$ <sup>(7,8&10)</sup>.

World Production: The largest producer of kaolinite is Great Britain. Kaolinite minerals are also found in the United States, West Germany, Austria, India, Algeria, France, Spain, Italy and Australia<sup>(7,8&10)</sup>.

Uses: The prepared kaolinite has many applications, e.g., in the paper industries, in ceramics, rubber, plastics, paints, pharmaceuticals, polishes, ultramarine, oilcloth, insecticides, fertilizers; textiles, sorbents, etc. (7,8&10). The kaolinite used for this study was obtained from Georgia Kaolin Company, Elizabeth, New Jersey.

Zeolite:

The zeolites are hydrous sodium calcium aluminum silicates which commonly occur as secondary minerals of volcanic rocks, especially basalts. Zeolite minerals have four silica tetrahedral arranged in the form of a ring. Aluminum ions are arranged as tetrahedral units. This atomic structure causes the particles of zeolite minerals to have a fibrous or columnar shape.

Uses: The zeolites are mainly used for water treatment because of their large ion-exchange capacity. Zeolites have great sorption characteristics. The sample used for this study was supplied by the Double Eagle Petroleum and Mining Company, Casper, Wyoming (1,7,8&10).

Bauxite:

Bauxite is a name given to rocks or earthly deposits in which the main constituent is aluminum oxide,  $\text{Al}_2\text{O}_3 \cdot 2\text{H}_2\text{O}$ , and the composition as  $\text{Al}_2\text{O}_3$ , 73.9%;  $\text{H}_2\text{O}$ , 26.1%. A specific mineral of this composition has never been identified by microscopic, chemical or X-ray examination. Therefore, it is concluded that bauxite is a rock consisting of one or more aluminum minerals together with some impurities, such

as silica in the form of clay minerals (kaolinite, halloysite and others) or quartz, iron oxide (as hematite or goethite), titania (as leucaxene or rutile), iron sulfide (as pyrite or marcasite), iron carbonate (siderite), and calcium carbonate (as calcite). The last three are minor impurities.

Traces of less common elements such as vanadium and beryllium can also be found as impurities in bauxite minerals. Bauxite, which is an aluminum ore, can be constituted as (alpha trihydrate)  $\text{Al}_2\text{O}_3 \cdot 3\text{H}_2\text{O}$  ( $\text{Al}_2\text{O}_3$ , 65.4%;  $\text{H}_2\text{O}$ , 34.6%) or (alpha monohydrate),  $\text{Al}_2\text{O}_3 \cdot \text{H}_2\text{O}$  ( $\text{Al}_2\text{O}_3$ , 85%;  $\text{H}_2\text{O}$ , 15%), and as a mixture of both the mono- and trihydrates<sup>(8,10)</sup>.

World Distribution: Bauxite minerals are widely distributed throughout many countries. Some examples are: Haiti, Jamaica, U.S.A. (North America), Brazil, British Guiana, Surinan (South America), Austria, France, West Germany, Greece, Hungary, Italy, Rumania, Spain, U.S.S.R., Yugoslavia (Europe), India, Indonesia, Malaya, Pakistan, Sawawak (Asia), Republic of Guinea, Ghana, Mozambique (Africa) and Australia.

Uses: The main industrial uses of bauxite as a raw material are as follows: (a) for the production of metallic aluminium, (b) for the manufacture of salts of aluminum, (c) as a major constituent of refractory bricks, (d) for producing fused alumina, which can be used as abrasive, (e) as a constituent of aluminous rapid hardening cement, (f) in oil refining and (g) as a sorbent<sup>(8)</sup>.

SECTION 3  
SAMPLE PREPARATION

One of the greatest strengths of Scanning Electron Microscopy is the ease of sample preparation. It should be pointed out, however, that poor sample preparation technique will result in micrographs of poor quality. This results because of poor electrical conduction from the sample to the sample holder. To obtain high resolution images one must employ proper sample preparation<sup>(11)</sup>.

The methods which were used in preparing samples are as follows:

1. For Samples of Small Particle Size:

Ultra pure carbon stubs (1" dia. x 1" height) were used. This type of spectroscopically pure carbon was used because it is ideal for virtually any type of X-ray analysis, particularly EDS since the X-ray signal generated from the carbon substrate is not detected.

The surface of the carbon mounts (stubs) were cleaned by using a very smooth polishing paper (600 grit), and a double-sided adhesive tape was placed on the clean surface of the carbon stub. A representative portion of the sample was sprinkled on the double-sided tape. The carbon stub was tapped gently to make sure that the particles of the sample had adhered to the surface of the double-sided tape. A microscopically clean compressed gas (Refrigerant 12-dichlorodifluoromethane) was used to remove all the loose particles.

## 2. For Samples of Large Particle Size:

A very thin film of epoxy glue was spread on the clean surface of the carbon stub and a representative portion of the sample was dusted onto the wet epoxy film. About five minutes were necessary for the epoxy to harden. The extra particles were removed by the compressed gas (Refrigerant 12-dichlorodifluoromethane).

Nearly all non-conductive specimens examined in an Electron Microscope or analyzed in any micro analyzer need to be coated with a very thin film of conducting material. The importance of this coating layer is to eliminate or reduce the electric charge which builds up rapidly in a non-conducting specimen when scanned by an electron beam of high energy electrons.

In the absence of a coating layer, a non-conductive specimen will exhibit a charging phenomenon which results in image distortion and thermal damage. Alternatives to coating can be used but none of these techniques will produce a better final image or allow elemental analysis to be carried on with the same accuracy as that which can be obtained from properly coated materials (11,12,14,15&17).

The following section explains in some detail why samples have to be coated before analysis can be carried out by the Scanning Electron Microscope and/or the Energy Dispersive Spectrometer.

### Conductivity:

The single most important reason for coating samples is to increase the electrical conductivity of the sample.

Materials of high resistance will rapidly build up charge under the incident beam and thus may develop a potential sufficient to cause dielectric breakdown in certain regions of the sample. This leads to variations in the surface potential giving rise to complex image artifacts commonly known as "charging". These artifacts are manifested as deflections of the low energy secondary electrons, increased emission of secondaries within the structures of a rough sample, periodic bursts of secondary electron emission and deflection of the electron beam, all of which will decrease the resolving power and analytical capabilities of the system. The resulting astigmatism will lead to undue brightness and misleading X-ray signals<sup>(11)</sup>.

Thermal Damage:

Specimen heating is not usually a problem for most samples examined in the SEM because the probe current is usually too low to cause any thermal damage. Undue heating in the SEM can lead to sample movement and instability and, in extreme situations, to breakdown and destructions of the sample. The phenomenon described as "beam damage" can be noticed in the form of blisters, cracks, dark areas and holes in SEM micrographs of the sample surface. This problem is more serious in biological samples. These types of problems were not encountered during the present analysis.

Thermal damage can be reduced by using a low beam current. The sample should be in contact with a good thermal conductor and may be coated with a thin film of a good heat



conductive material such as Cu, Al, Cr, Ag, Au or Pd, to reduce thermal damage<sup>(11,12,14&17)</sup>.

#### Secondary Electron Emissions:

The secondary electrons which form the bulk of the emitted electrons leaving the surface of the sample have relatively low energies and form a broad energy distribution which is more or less independent of the primary energy. For most solid materials the maximum for this broad curve is only a few ev (electron volt) and it is the secondary electrons originating from within 1 to 2 microns ( $\mu$ ) of the surface which are used in the secondary mode of operation in the SEM. The largest number of secondaries occur at the point of impact of the primary beam where the highest density of exiting electrons occurs (Diagram V).

As the angle between the primary beam and the surface of the sample is decreased, there is a greater proportion of secondary electrons generated. Surface irregularities can enhance or diminish the emission of secondary electrons, and also give rise to the topographical contrast seen in all SEM micrographs.

Secondary electrons can also be produced by back scattered primaries as the beam penetrates deeper into the sample. As the primary beam energy increases and penetrates further into the sample, the yield of secondary electrons decreases.

The thin film of metal which is usually applied to a non-conductive material to make it electrically and thermally

conductive is also a source of the secondary electrons. This source can be responsible for the bulk of the secondary electrons (11,12&14).

Beam Penetration:

The greater the penetration of the primary beam into the sample, the more the high resolution of the SEM is diminished. Also, the beam damage in the case of organic samples is increased. Primary beam penetration can be reduced by coating the sample with a thin layer of heavy metal. Also, beam penetration can be reduced by lowering the primary beam energy (11&12).

Mechanical Stability:

In the case of powdered sample or fragile materials, they can be held in position by coating the sample with a thin layer of carbon or any other suitable material. It is even possible to place such powder directly onto the carbon stub and stabilize it with a very thin layer of carbon or other coating material without using adhesive or double-sided tape (11&12).

For the present investigation each one of the samples examined was coated twice. First each sample was coated with carbon to study the elemental composition and distribution. A vacuum evaporation technique was used. Next in order to study the particle size, shape and distribution, a thin layer of Au-Pd was deposited on the sample by using a sputter coater.

### Vacuum Evaporation:

A vacuum evaporator made by Denton Vacuum Inc. (Model No. DV515) was used to coat samples with a very thin layer of carbon. The following is a description of this unit and the principles of operation.

Many metals when heated in vacuum will evaporate once their temperature has been raised sufficiently for their vapor pressure to exceed  $10^{-2}$  torr. The high temperatures which are necessary to permit the evaporation of the material can be achieved by three different methods. The electric arc method used in the Model No. DV515. An arc is struck between two conductors (carbon rods), and rapid evaporation of the conductor surface occurs. This is the usual way by which carbon and some other high melting point metals are evaporated, and it is usual to strike the arc several times in quick succession to avoid undue heating of the sample.

The carbon may be evaporated by the arc or resistive method using spectroscopically pure carbon rods. For the resistive method carbon rods are prepared as follows: two carbon rods 6 mm in diameter are treated so that the end of one is ground down to a tip of 1.5 mm diameter by 5.0 mm long and the other rod left with a squared-off 6.0 mm tip or ground to a 45° angle with the angled face turned towards the sample. The rods are held coaxially and kept in contact by springs. In this method the carbon rods should be gently heated to a dull redness at high vacuum and before back

filling with argon gas in order to remove any volatile substances. The evaporation is carried out using a power source of 30 V and up to 20 A. A few bursts of power are given at 10 second intervals while the sample is rotated in all directions until the desired thickness of coating is achieved. The carbon layer is typically 50-100 Å thick<sup>(11,12,14&17)</sup>.

#### The Vacuum Evaporator:

The vacuum evaporator consists of a system to obtain and measure the necessary high vacuum, a container in which the evaporation can take place, and electrical connections to enable the evaporant (carbon) to be heated and the sample rotated about three mutually perpendicular axes, Diagram I.

#### Sputtering:

The unit which was used is made by Technic Inc. (Model Hummer II). The sputter coating method is a cathodic disintegration. It is one of the most widely used thin film deposition techniques. Here a surface is bombarded by a heavy ionized gas such as argon, so that it is progressively eroded away, with the eroded particles going off in all directions. The material to be sputtered is made the cathode and the sample to be coated is placed on the anode.

Sputtering is carried out at 2-3 Kev in an atmosphere of argon ( $10^{-2}$  to  $10^{-1}$  torr). The ionized argon forms a plasma and the positive ions sputter away the target atoms and are deposited on the sample in the form of very thin layers. In this method the particles of the sample will be coated from all directions with an even layer of Pd-Au (the cathode which was used in coating the samples). The

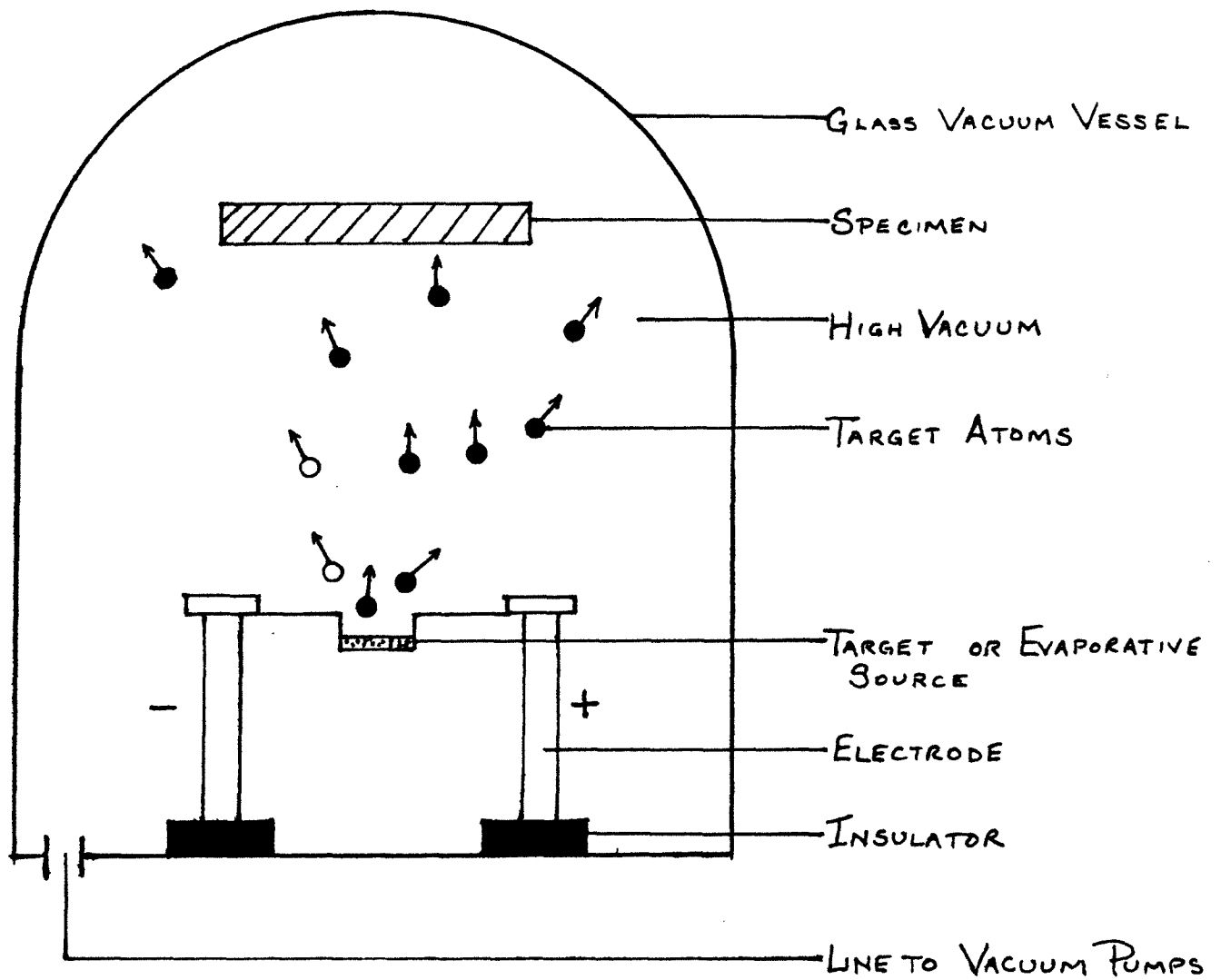


DIAGRAM I: VACUUM EVAPORATOR

uniform sputter coating will prevent any kind of charging and help in getting quality micrographs especially at very high magnifications<sup>(11,12,13,14&17)</sup>.

The Sputter Coater:

The Model Hummer II is a diode or direct current sputter coater. It consists of a small bell-jar containing the cathode target (Pd-Au) and specimen holder (anode). The bell-jar sits on the top of a control module containing a vacuum gauge, high voltage power supplies, leak valve and a timer. To obtain vacuum, a rotary pump can be used which is located inside the control module, Diagram II.

This technique provides a continuous even coating layer on those parts of the sample which are not in the line of sight of the target. This is because the target atoms suffer many collisions and are travelling in all directions as they arrive at the surface of the sample. The complete coating is achieved without rotating or tilting the sample.

One can readily obtain a thin non-porous film that forms a strong, closely adhering surface layer which will faithfully follow the surface features of the sample particles, and all the surface structures will be seen clearly in the SEM micrographs.

Thermal damages can be reduced or eliminated because the thin uniform layer coating the sample will give it enough protection from any electron beam effect.

There is no need for a diffusion pump. A vacuum or rotary pump is sufficient to reach the proper vacuum for

sputtering. In one minute a vacuum needed for coating or deposition can be achieved while in the evaporator 15 to 20 minutes are required<sup>(11,12,13&15)</sup>.

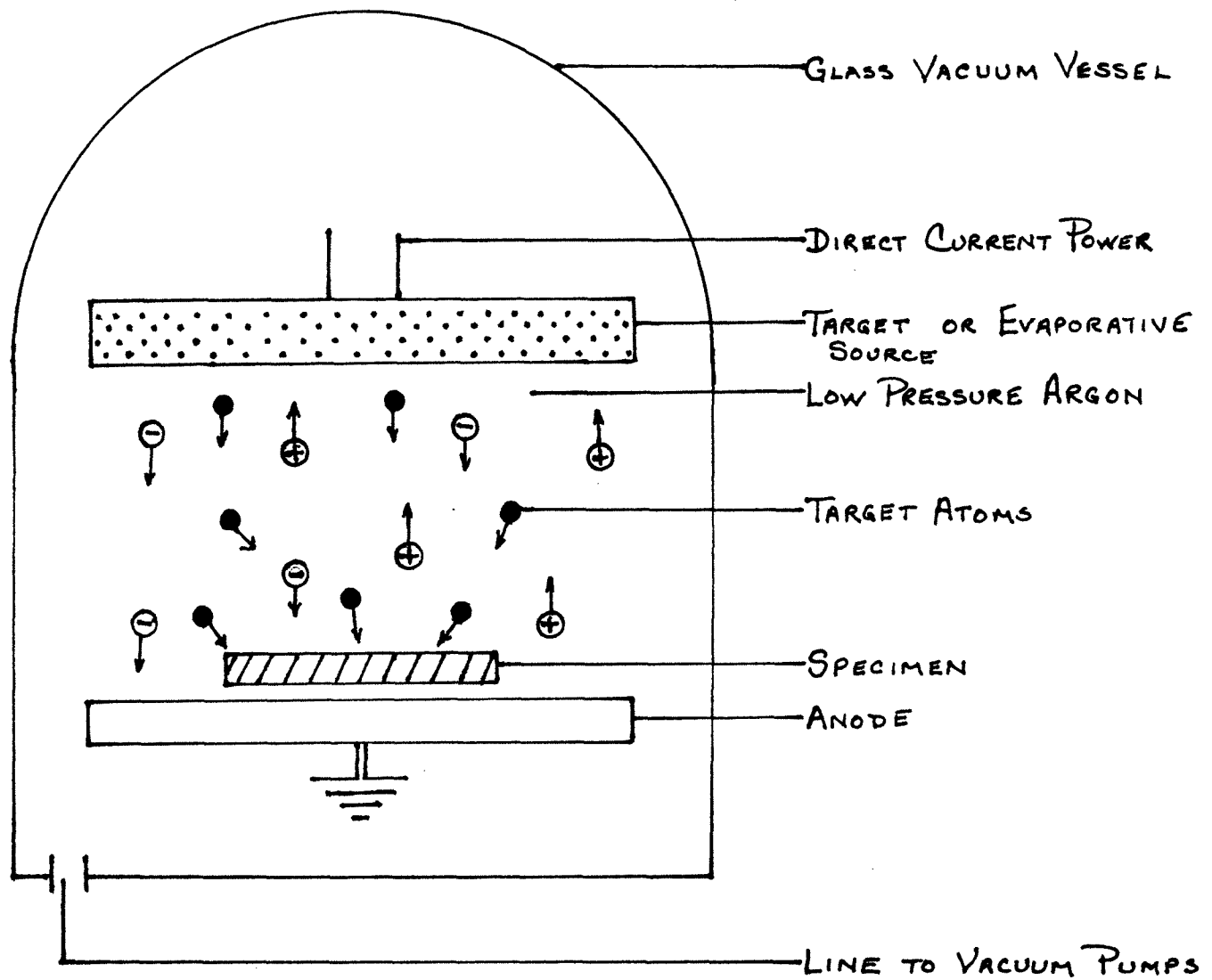


DIAGRAM II: SPUTTER COATER



## SECTION 4

### INSTRUMENTATION

#### Introduction

The Scanning Electron Microscope (SEM) when used in conjunction with an X-ray Energy Dispersive Spectrometer (EDS) is a very powerful tool in the characterization and examination of clay and fly ash samples. These two instruments were employed to study the structures (particle size, shape and distribution), and also to determine the elemental composition and distribution of elements within the ten samples.

#### The Scanning Electron Microscope

The SEM has no equal in its ability to reveal surface morphology of particles. The SEM is also an ideal instrument to examine the micro and macro structures of all solid samples with very simple sample preparation while simultaneously producing micrographs which are in most cases easy to interpret.

#### Principles of Operation

A JEOL-JSM 35C Model Scanning Electron Microscope was employed. The SEM image is produced without the interposition of any lens between the sample and the viewing screen (CRT) or the camera. The schematic in Diagram III illustrates the SEM uses an optical system to focus an electron beam upon the sample.

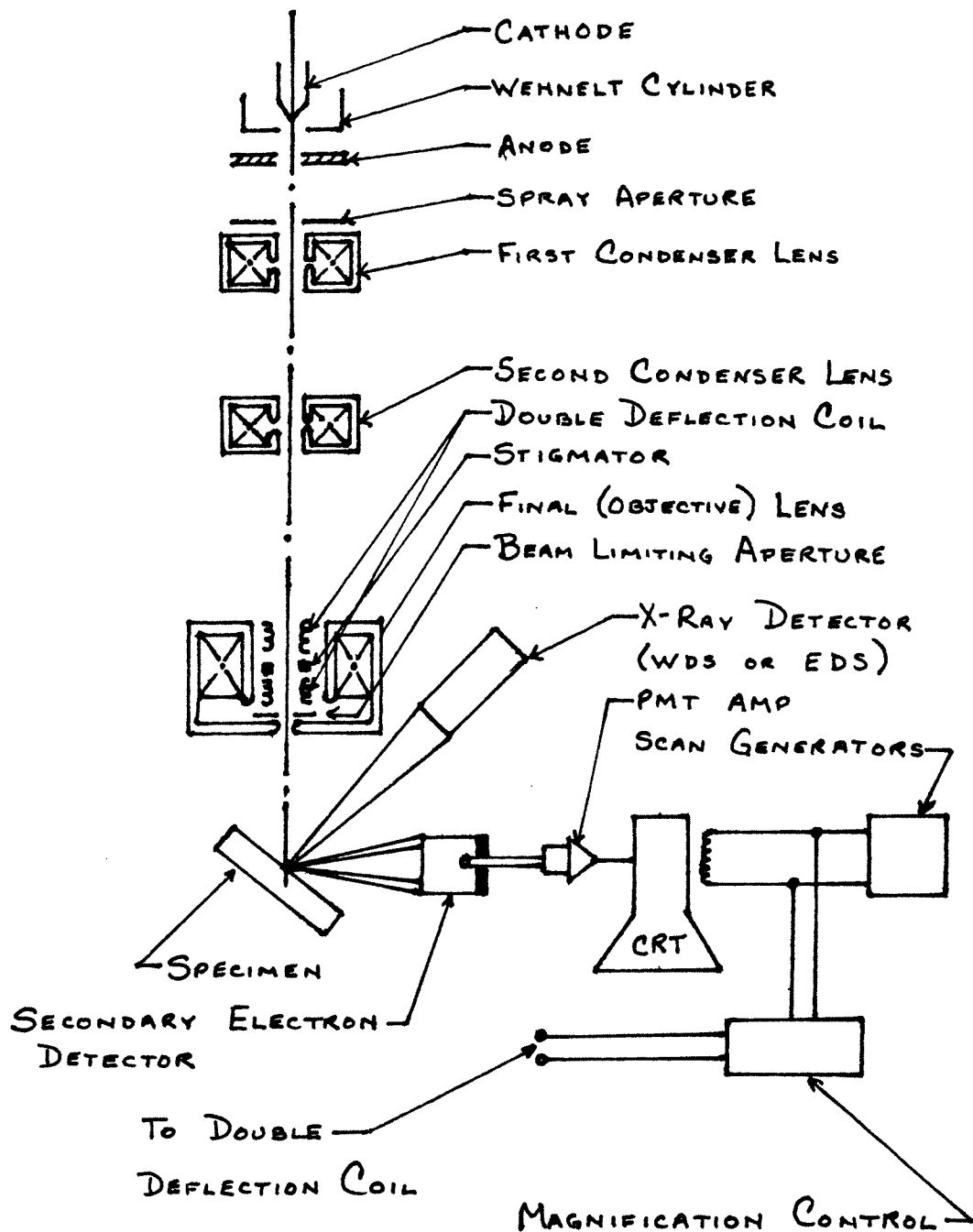


DIAGRAM III: SCHEMATIC DRAWING OF THE ELECTRON AND X-RAY OPTICS OF THE SEM

The electron gun (an electrically heated tungsten W filament cathode) is held at a negative potential of 1 to 30,000 volts with respect to the anode, generating an intense primary electron beam of a large diameter (20 to 40  $\mu\text{m}$ ) - see Diagram IV.

The beam then travels towards and passed through a small hole in the anode. The beam is demagnified on passing through condenser and objective lenses to produce a microfocused image of the tungsten filament tip at the plane of the sample. The diameter of the electron beam is approximately 50 to 200  $\text{A}^\circ$  as it reaches the surface of the sample. The diameter of the electron beam can be changed depending upon the purpose of the analysis. The beam current ( $I_B$ ) at the sample surface is now reduced to  $\approx 10^{-11}$  amperes. This great reduction in current is primarily the result of electrons being trapped and scattered by apertures on their way down the electron optical column.

As the focused primary electron beam hits the sample surface several different kinds of signals are generated, Diagram V, such as low energy secondary electrons (0-50 eV), primary backscattered electron with higher energy (50 or more eV), auger electrons and characteristic X-ray signals from the very small area being irradiated by the electron beam.

The secondary electrons (low energy <50 eV) travel to the secondary electron detector. The signal produced is then amplified by a suitable video amplifier and is displayed

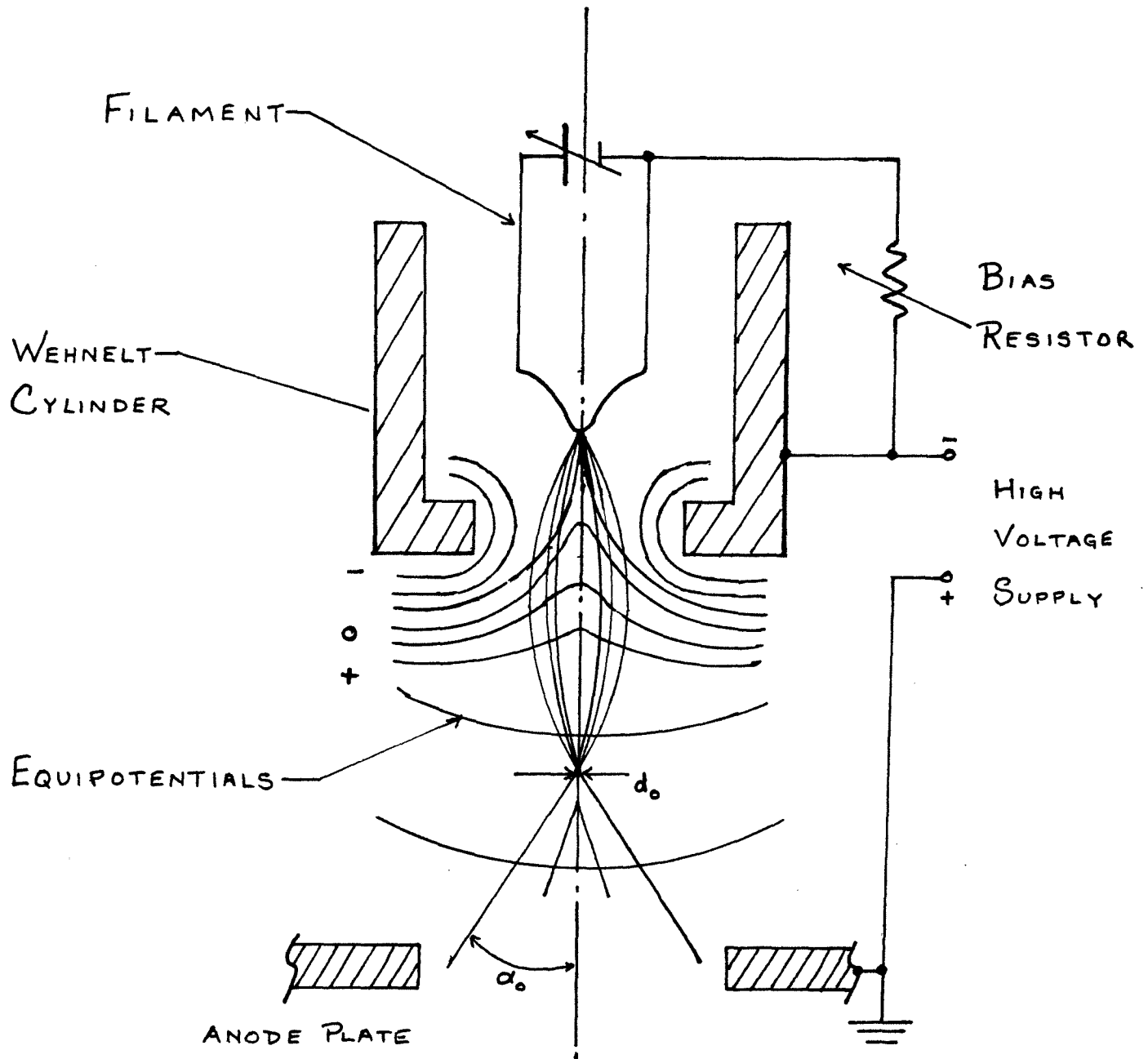


DIAGRAM IV: THE ELECTRON GUN

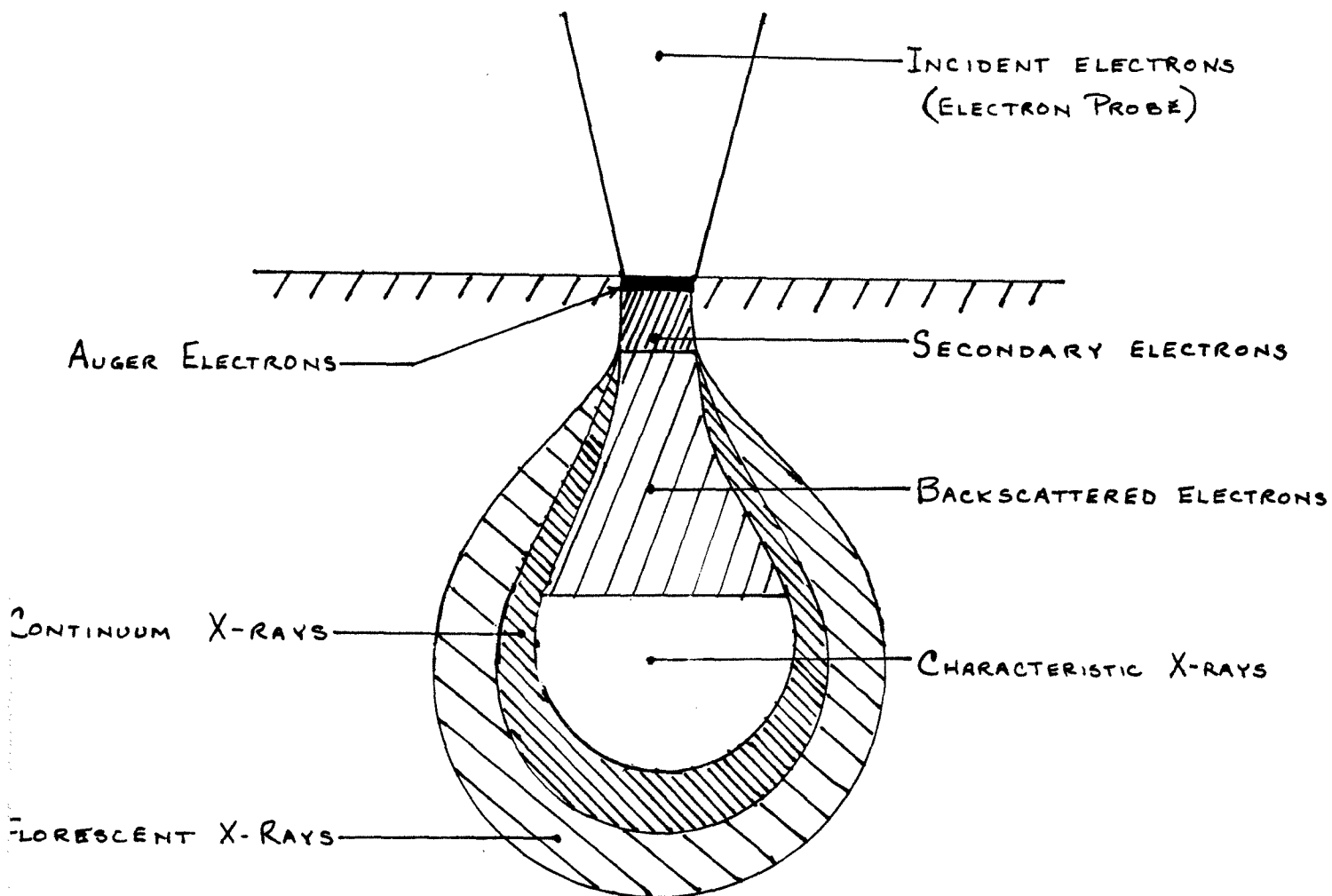


DIAGRAM V: ILLUSTRATION SHOWING THE DEPTH OF  
 SIGNAL GENERATION WHEN THE PRIMARY ELECTRON  
 BEAM INTERACTS WITH THE SAMPLE SURFACE

as an intensity modulated spot on the cathode ray tube (CRT). The brightness of the image spot depends primarily on the number of the collected secondary electrons emitted from the electron irradiated spot on the sample surface.

The scan generator produces a signal which, when applied to the scanning coils, move the electron beam across the irradiated area of the sample to form what is known as the raster (image). The number of lines and points in each line controls the resolution. The ratios of this current,  $I_{CD}$ , to the current,  $I_D$ , in the scanning coils circuit of the cathode ray tube (CRT) determine the magnification of the SEM. By changing the current, one can vary the magnification. The magnification in the JEOL-JSM 35C Scanning Microscope (which was used for the analysis) ranges from 10X to 180,000X<sup>(18-19)</sup>.

There are many important factors affecting the resolution of the scanning electron microscope. Some of these include current density of the primary beam, fluctuations in the electron probe current, the acceleration voltage, number of scan lines in the raster and lens aberrations. Lens aberration include spherical aberration, chromatic aberration, diffraction and astigmatism. All these factors can be expressed in a mathematical equation which relates most of these factors to a theoretical minimum beam diameter.

There are three types of electron guns (sources). Each has a great influence on the ultimate resolution of the SEM. The tungsten electron gun has a limited beam

brightness ( $\beta = 10^5 \text{ ACM}^{-2} \text{ steradian}^{-1}$ ) which leads to a sample current of about  $10^{-11}$  amperes.

The Langmuir equation relates the beam current of the electron probe at the sample to its maximum theoretical aberrationless beam diameter.

$$d_0^2 = \frac{4i}{\pi^2 \beta} \alpha^{-2}$$

where  $\alpha$  = semi-angular aperture of the final lens  
in radians

$i$  = final beam current in amperes

Since  $\beta$  is a function of the type of electron emission and emitter, the only way to improve  $d_0$  is to find a method to make  $\beta$  a large value.

The lanthanum hexaboride ( $\text{LaB}_6$ ) electron gun can produce a  $\sim 50$ - $100$  times brighter electron beam than the tungsten one. The use of  $\text{LaB}_6$  electron source requires a higher vacuum than that used in the case of the tungsten electron gun. There is a third type which is even better than the W or  $\text{LaB}_6$ ; the field emission cathode. The field emission cathode produces an electron beam 1,000 times brighter than that one produced by the W electron gun where  $\beta$  has the value of  $10^8 \text{ amp/cm}^2 \text{ steradians}$  (18-19).

### Lens Aberrations

#### Spherical Aberration:

Spherical aberration arises because electrons moving in trajectories which are further away from the optical axis are focused more strongly than those near the axis (see Diagram VI).

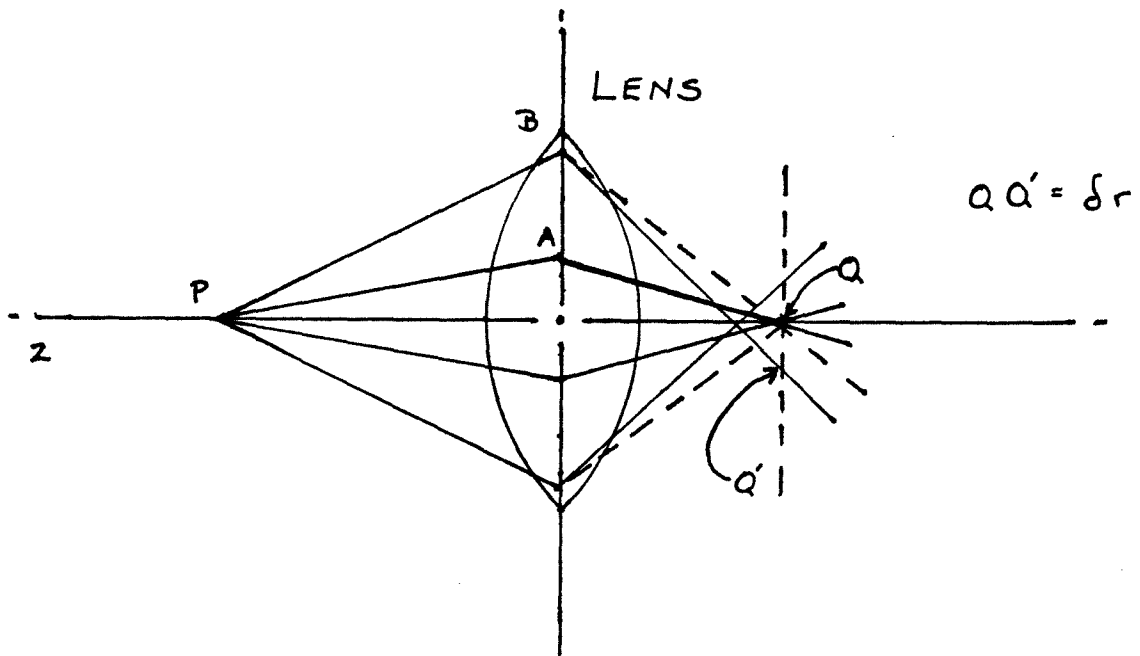


DIAGRAM VI: SCHEMATIC DRAWING SHOWING ORIGIN OF SPHERICAL ABERRATION

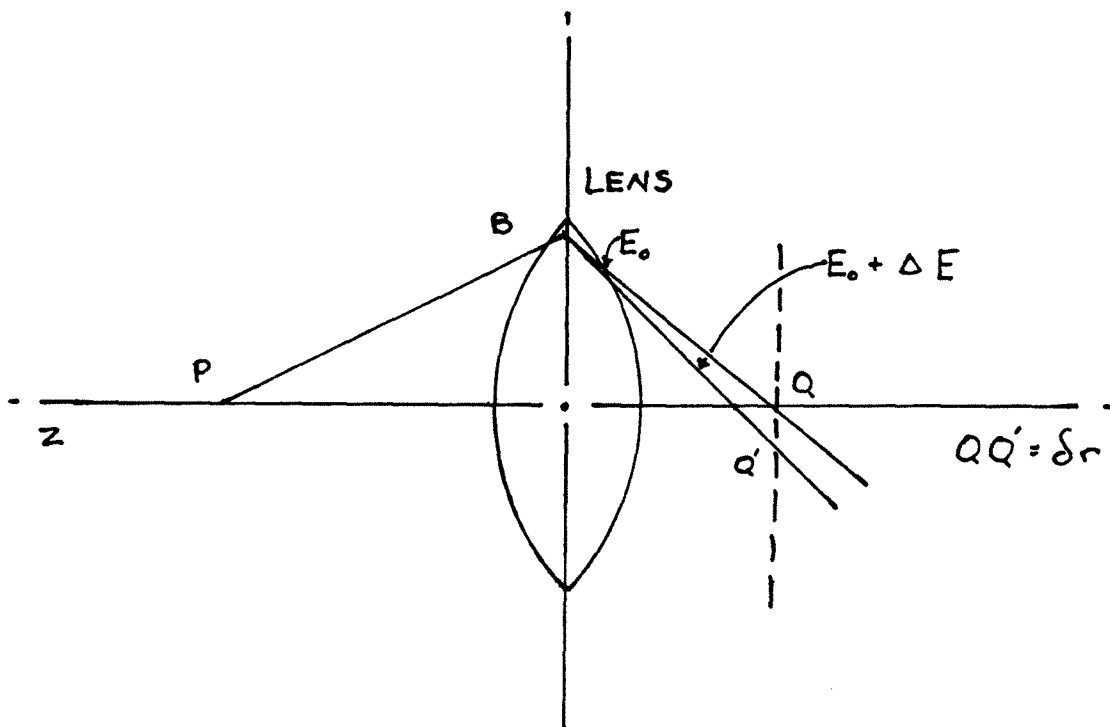


DIAGRAM VII: SCHEMATIC DRAWING SHOWING ORIGIN OF CHROMATIC ABERRATION



Electrons that diverge from point p and follow a path PA close to the optical axis will be focused to a point Q. Electrons that follow the path PB, which is the maximum divergence by the aperture of the lens, will be focused more strongly. These rays are focused on the axis closer to the lens than point Q. The rays traveling along the path PB are focused to a point Q' at the image plane. This process causes a disk of confusion in the image plane  $Sr = QQ'$  of point P. The diameter of the disk of the minimum confusion can be expressed as:

$$d_s = 1/2 C_s \alpha^3$$

where  $\alpha$  is the divergence angle at the image plane formed between BQ and the optical axis,  $C_s$  is the spherical aberration coefficient and is related to the beam energy  $E_0$  and the focal length  $f$  of the lens. The spherical aberration  $d_s$  can be made smaller by decreasing  $\alpha$ . To do this, however, the objective aperture size must be decreased which will decrease the current of the final spot. To avoid decreasing the current of the final spot, the working distance can be decreased by using a higher sample position (i.e., the sample will be closer to the final lens pole piece) (18-19).

#### Chromatic Aberration:

A variation in the energy  $E_0$  and the corresponding velocity  $v$  of the electrons passing through the lens or a variation in the magnetic field  $H$  of the lens will change the point at which the electrons are focused.

Diagram VII shows what may happen if the voltage of the electrons in the diverging ray PB are different rays of energies  $E_0$  and  $E_0 + \Delta E$ . Some of the electrons will be focused to point Q while others will be focused to point Q' at the image plane.

As in the case for spherical aberration, there is again a disk of confusion in the image plane,  $\delta_r = QQ'$ , of point P. The diameter  $d_c$  of the disk of least confusion is written as:

$$d_c = (\Delta E/E_0) C_c \alpha$$

where  $\alpha$  is the divergence angle of the image plane between BQ and the electron optical axis;  $\Delta E/E_0$  is the fractional variation in the electron beam energy, and  $C_c$  is the chromatic aberration coefficient. The chromatic aberration is directly related to the focal length of the lens.

Variations in  $E_0$  and H are due to unstable power supplies. By stabilizing the lens current or the high voltage to one part in  $10^6$  per minute, the effect due to the variation in H and  $E_0$  will be minimized. There still exists variation in the energy of the electrons equal to  $\Delta E$ . This is due to the Maxwellian distribution of initial velocities, that is, the spread of the initial velocities (energy) leaving the cathode. The value of  $d_c$  can be decreased by decreasing the divergence angle  $\alpha$  at the specimen as is the cause for spherical aberration<sup>(18-19)</sup>.

### Diffraction

If the spherical and chromatic aberrations were insignificant, the image of a point P would still be of

finite dimensions, due to the wave nature of the electrons and the aperture size of the final lens. The intensity distribution of the point source at the image plane caused by diffraction is illustrated in Diagram VIII. The radius of the first minimum  $\delta_r$  subtends an angle  $\theta$  at the lens. The effect of diffraction yields a disk of confusion of diameter  $d_d$  which is given by:

$$d_d = 1.22 \lambda / \alpha$$

where  $\lambda$  is the wavelength of the electrons given by  $\lambda = 12.26/E_0^{1/2}$  with  $\lambda$  in  $\text{A}^\circ$ ,  $E_0$  in electron volts (ev) and  $\alpha$  the angle between the converging ray and the electron optical axis in radians. In the diffraction aberration the larger the value of  $\alpha$  the smaller the contribution of  $d_d$  (18-19).

#### Astigmatism

Even with today's high technology it has not been possible to produce a magnetic lens with perfect axial symmetry. The result is that the image plane for objects laying in one direction will be different than the image plane for objects lying in another direction. If a lens system has elliptical and not circular symmetry, electrons diverging from a line focus will converge to two separate line foci at right angles to each other rather than to a line focus. This astigmatism effect will enlarge the effective size of the final electron probe diameter. A stigmator can be used in the final lens to supply a weak correcting

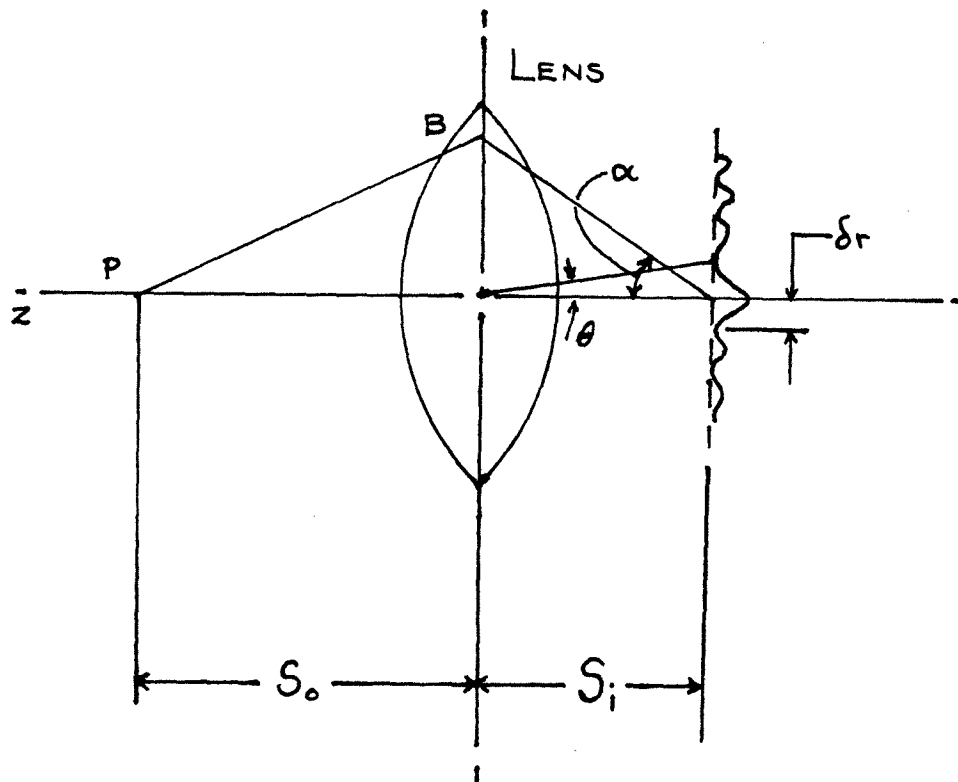


DIAGRAM VIII: SCHEMATIC DRAWING SHOWING  
DIFFRACTION AT A LENS APERTURE

field to produce the desired symmetric field in the lens. Any stigmator usually has two major controls, one to correct for the magnitude of the symmetry and another to correct for the direction of the symmetry of the main field<sup>(18-19)</sup>.

#### Signal Generation, Collection and Contrast

The diameter of the electron beam and its current density or brightness is usually considered the most important factor in producing an acceptable SEM micrograph. However, equally important, is a strong, clean video signal, i.e., high signal to noise ratio. The amplitude (picture contrast) of the video signal is a function of many variables some of which are the secondary yield of the sample, the collection efficiency of the secondary detector and the frequency response and noise of the video amplifier.

When the electron beam scans the sample, secondary and primary backscattered electrons are generated. Diagram VI illustrates why 1/10 or less of the total signal collected by the secondary electron detector is backscattered electrons. Since backscattered electrons are emitted in line of sight, a small fraction will reach the small aperture of the secondary electron detector. In Diagram IX the location of the backscattered detector is placed in a position for maximum collection efficiency<sup>(20)</sup>.

Diagram Xa illustrates what happens when moderate energy electrons (10 to 20 Kev) hit the sample. The primary electron beam penetrates the sample in a statistical manner generating an infinite variety of electron trajectories. The trajectories shown represent a summary of scattering

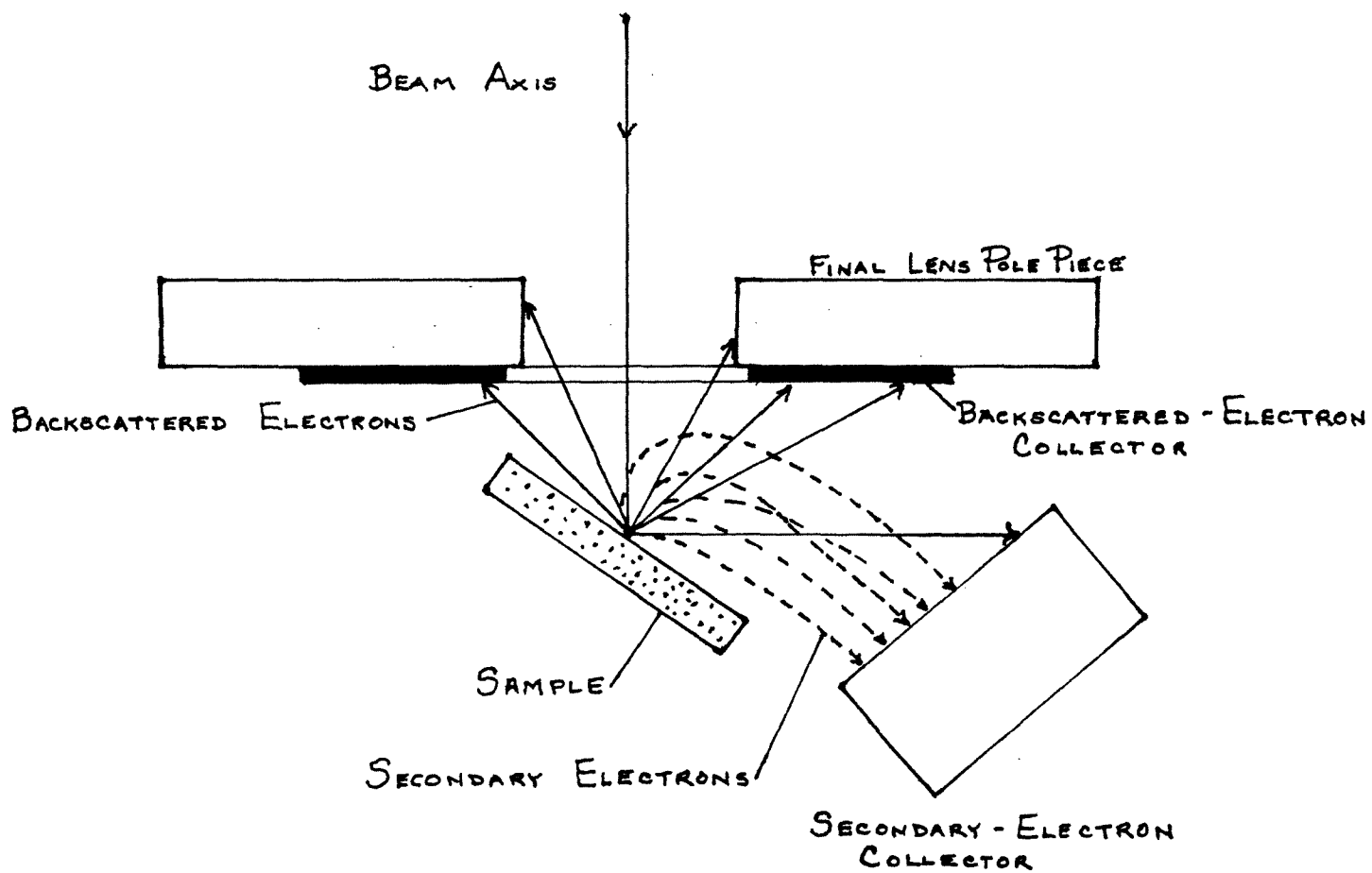


DIAGRAM IX: OPTIMUM POSITIONS OF THE  
SECONDARY AND BACKSCATTERED DETECTORS

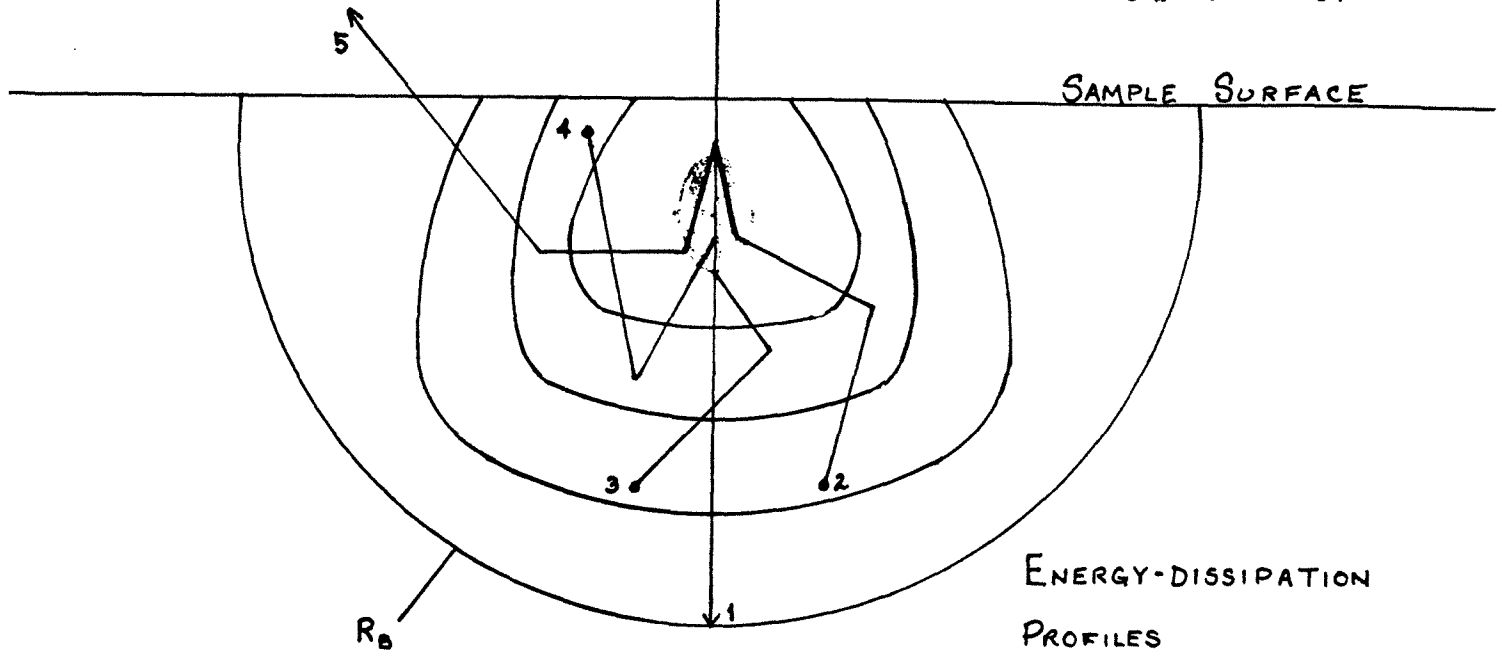


DIAGRAM Xa: POSSIBLE PATHS (1 TO 5) OF BACKSCATTERED ELECTRONS IN A SOLID SAMPLE

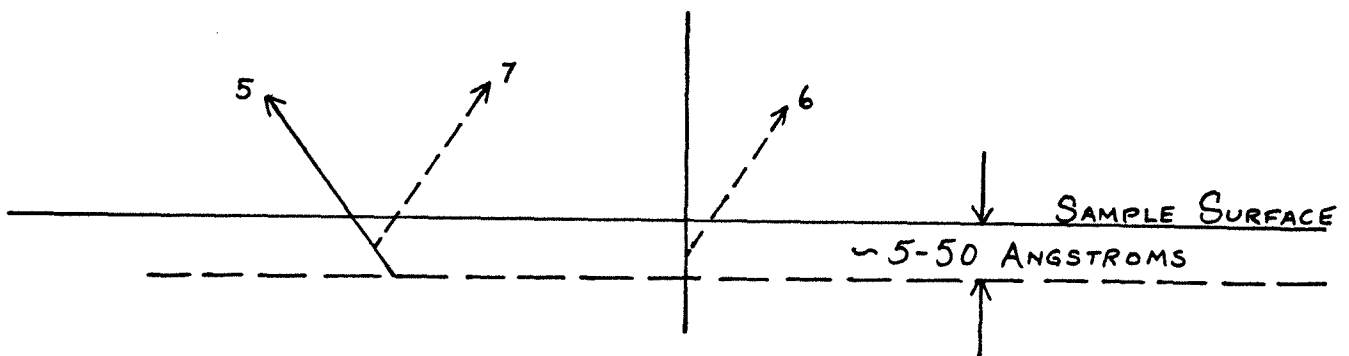


DIAGRAM Xb: SECONDARY ELECTRONS PRODUCED BY ELECTRON-ELECTRON COLLISIONS ARE SHOWN BY 6 AND 7

events that can happen. Trajectories 1 to 4 occur as a result of multiple scattering and collisions resulting in loss of the probe electrons in the sample. The contour lines are successive regions in which scattered electrons to the Bohr-Bethe range ( $\sim 1\mu$ ) representing the greatest depth of generation of the beam at a particular energy and a given sample density<sup>(21)</sup>. Trajectory 5 is an example of an emitted backscattered electron that has undergone plural scattering then emerging from the sample in a straight line. Most backscattered electrons emerge from the sample with an energy slightly less than the main beam energy<sup>(20)</sup>. The main result of these scattering mechanisms is that an electron beam of  $\sim 25$  KeV focused to a probe diameter of  $100\text{\AA}$  generates an emitting area of backscattered electrons =  $1.0\mu$  in diameter and results in an apparent probe size of this diameter. A larger probe size will result by tilting the sample.

Diagram 10b demonstrates the mechanism of generation of secondary electrons in trajectory 6 by unscattered electrons from the primary beam and a secondary produced by a scattered electron in trajectory 7. The secondary electrons emitted from trajectory 6 contributed to the useful signal while the secondary electrons emitted from trajectory 7 only contribute to the noise of the system.

The image information obtained in the SEM is mainly composed of emitted secondary electrons generated within the sample by the probe. The probability that the secondary



electrons will escape from the sample decreases as the point of generation becomes deeper in the sample. Therefore, those electrons that do emerge come from a surface layer which is only  $\approx$  5 to 100  $\text{\AA}$  in depth for metals and slightly deeper for lighter materials. The secondary electrons emerge with energies ranging from  $<1$  eV to 50 eV; the maximum energy is around 5 eV. The secondary electrons are generated from an area of the surface roughly  $20\text{\AA}^2$  greater in diameter than the original probe diameter. This diameter results because of the electrons very short mean free-path in matter. The extended diameter of the emitting area, which cannot be prevented, is one of the principal limitations affecting the resolution in this type of scanning electron microscope. Close to the sample two electron detectors are placed which collect, detect and amplify the secondary and backscattered electrons ejected from the sample.

The contrast (amplitude) of the video signal produced is directly proportional to the amount of signal collected. This not only depends on the operating conditions of the detector but also on the current density of the probe, the chemical composition of the sample, the angle made by the probe to the sample surface, the charge on and the conductivity of the sample, the surface roughness of the sample and finally the secondary yield of the sample. A good contrast can be produced by using heavy metal or metal oxides, tilting the sample, placing the sample in the direction of the detector, using a sample which has a rough

or irregular surface or coarse powders and by coating the sample surface with a heavy metal such as Pb-Au. The Pd-Au layer will give the highest secondary electron yield of any metal.

After successfully capturing and amplifying the secondary electrons emitted from the sample, the resultant video signal modulates the scanning beam of a high resolution cathode ray tube (CRT) from which SEM micrographs can be produced.

### X-Ray Energy Dispersive Spectrometer (EDS)

#### Introduction:

When the primary electron beam interacts with the surface of the sample, characteristic X-ray will be generated from the sample. By using a Wave Length Spectrometer (WDS) and/or an X-ray Energy Dispersive Spectrometer (EDS) very important information about the chemical composition of a sample can be revealed. Also qualitative or quantitative analysis can be performed.

The EDS technique was used to study the elemental composition and distribution of the clay and fly ash samples. Nondestructive and micro analysis can be conducted with the aid of the EDS and/or the WDS when they are attached to the SEM. By the use of the SEM and EDS together, one can perform elemental analysis for a certain field in the sample, for a very small area (reduced field), or even for a very small particle  $\approx 0.5\mu$ . These methods are usually known as area scan or point scan, respectively.

### Principles of Operation:

A Kevex Ray Model 5000A EDS was used in this study. Diagram XI illustrates the solid state detector. The characteristic X-ray signal generated from the sample passes through a thin beryllium window into an evacuated chamber containing a cooled, reverse-bias p-i-n (p-type, intrinsic, n-type) lithium-drifted silicon crystal. Absorption of the X-rays in the intrinsic region results in the formation of electron-hole pairs which are collected by the applied bias to form a charge pulse, which is then converted to a voltage pulse by a charge sensitive preamplifier. The signal is then amplified and shaped by a main amplifier and passed to a multichannel analyzer (MCA) where the pulses are sorted by voltage. The energy distribution is then displayed on a cathode ray tube and/or an X-Y recorder.

The operating characteristics of the main amplifier in a Si(Li) detector system are more critical than in the case of WDS because all of the spectral dispersion is done electronically. Special circuitry must be used to ensure maximum linearity, low noise, rapid overload recovery and stable high-count-rate performance. Most amplifiers use pole zero cancellation network to compensate for pulse overshoot when internal AC coupling is used, and a DC restoration circuit to clamp the pulse baseline to stable reference voltage.

In the case of Si(Li) detector system high-counting-rate effects cause serious problems, where loss of resolution

and peak shifts due to pulse pileup can occur, causing peak overlap and inaccurate count rate and energy determinations. To avoid these problems a pulse pileup rejector and live-time corrector can be used. Pulse pileup occurs when the time duration between pulses approaches the processing time of the main amplifier. It shows up as energy distortion, either of the second of two closely spaced pulses or of both pulses, if the peak amplitude of the first is not reached before the arrival of the second. The resulting effect is to subtract pulses from their proper channels and to add them to channels of higher energy. Pulse pileup rejection is accomplished by placing a circuit in parallel with the main amplifier, which can gate the multichannel analyzer input off if a second pulse arrives within a predetermined time after the main amplifier begins to process a previous pulse.

Live time refers to that portion of time during an analysis in which the system can accept and process X-ray pulses. Most multichannel analyzers provide the option of reselection either live time or clock time as the period for data collection. If live time is chosen, then the counting periods will be extended over clock time to compensate for any process that temporarily gates the multichannel analyzer off. These processes include pulsed optical feedback, pulse pileup rejection, and pulse measurements and storage in the multichannel analyzer. If accurate quantitative analysis is necessary it must be performed in the live time mode.

The use of the multichannel analyzer (MCA) is to collect, sort, store and display the pulses received from the main amplifier, by using an analog-to-digital converter interfaced to a hard-wired computer memory. Pulses are first given an acceptance test using an upper and lower level discriminator to check if they are within a preset level of acceptability and also to determine if any internal events cause the system to be busy. If they are accepted, the standard method of conversion is from pulse amplitude to time. This is done by charging a special capacitor to a voltage proportional to the peak value of the input signal and counting the number of clock pulses that occur while the capacitor discharges to its original level.

The MCA's display data is presented as a data histogram of X-ray intensity vs. atomic number or X-ray energy in Kev. The Kevex-Ray unit which was used in the analysis combines graphical and alphanumeric display to read out energy and element identification directly<sup>(18-19)</sup>.

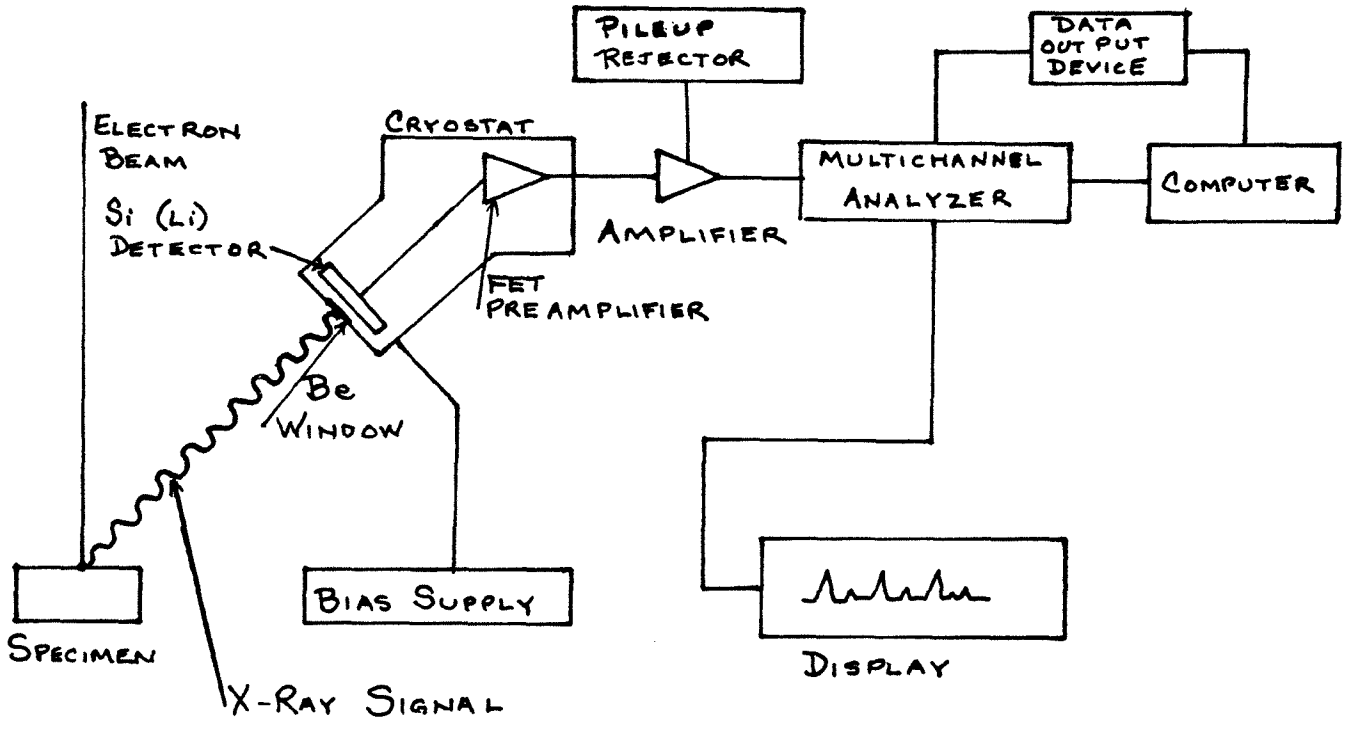


DIAGRAM XI: Si(Li) DETECTOR OF AN X-RAY ENERGY DISPERSIVE SPECTROMETER

SECTION 5  
EXPERIMENTAL, RESULTS AND DISCUSSION

Introduction

A number of SEM micrographs were obtained at various magnifications in order to study the properties of the particles; properties of interest included size, shape, distribution and surface structures. X-ray images were also obtained to study the elemental distribution within particles.

SEM micrographs were obtained at low magnification (10 to 300X) to cover the large field of the sample. This also gives a general idea about the particle size range. The maximum particle size was measured from these SEM images.

The average particle size was measured from the SEM micrographs obtained at 1000X to 3000X or less in some cases. SEM micrographs which were taken at very high magnifications (3000X to 20000X) were used to measure the minimum particle size, and also to illustrate the detailed structures on the surface of the particles.

The elemental X-ray images were obtained to illustrate the concentration of the elements in a specific field. X-ray energy spectra were recorded at a fixed time of 1.0 minutes to show the relative intensities of the elements present in each sample. Area and point scan analysis were also carried out.

## Results

### Apautagite or Greensand of New Jersey:

#### Structural Analysis:

Most of the apautagite particles were irregular in shape, some were elongated and very few of them were fibrous. Compare Figures 4, 6, 7 and 9. The edges of nearly all the particles were rounded. The surface of the particles was quite smooth, and many very fine particles ( $\approx 0.2\mu$ ) were found to be attached to the surfaces of the large particles. No pores or cracks were observed on the surface of the small or large particles. The maximum, average and minimum particle size were measured in microns ( $\mu$ ) as follows:

Maximum	Average	Minimum
100.0	11.0	0.1

#### Elemental Composition and Distribution:

Mg, Al, Si, S, K, Ca, Ti and Fe were detected from the sample. Figure 15, for example, illustrates the general elemental distribution and shows that the major element in most of the particles is Si while the other elements are minor. This also is illustrated in the X-ray energy spectrum, Figure 51.

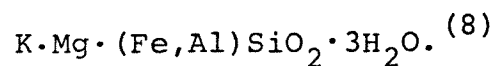
Figure 23 indicates that a large particle in the middle of the field contained a very high concentration of Fe-S and a very low concentration of Mn. This is also shown in the X-ray images (Figures 27 and 28) and in the X-ray energy spectrum, Figure 54.



The elemental distribution of particles seen in Figure 29 was similar to those in Figure 15, i.e., Si was the major element. A particle in the left side of the field in Figure 36 was found to contain very high concentrations of K as indicated by the X-ray image in Figure 41 and the X-ray energy spectrum, Figure 52.

Figure 43 shows the presence of a particle in the lower left side of the field which contained very high levels of Ca (possible as Ca oxide or carbonate), see supporting data in Figure 48 and X-ray energy spectrum, Figure 56. A particle in the lower right of the field contained high concentrations of Ti (possible Ti oxide), see also X-ray image Figure 49 and X-ray energy spectrum, Figure 57. Three small particles of high Fe (possible Fe oxide) and traces of Mn were present in this field and they can be seen in X-ray image Figure 50 and X-ray energy spectra, Figure 51.

Elements as S, Ca, Ti and Mn were present as contaminants in the sample if it is assumed that the approximate chemical formula of greensand is:



SEM IMAGES OF SAMPLE #

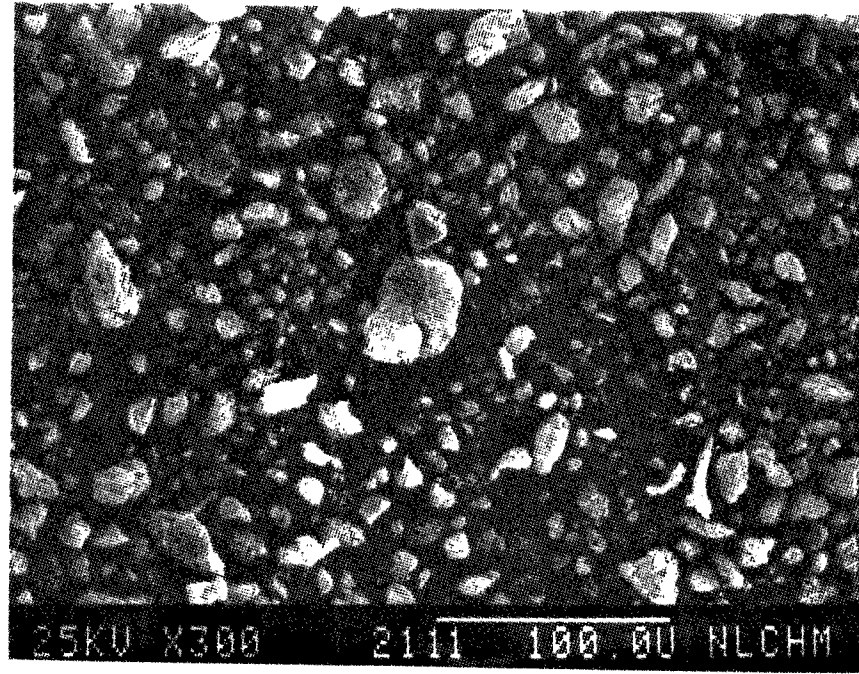


Figure 1

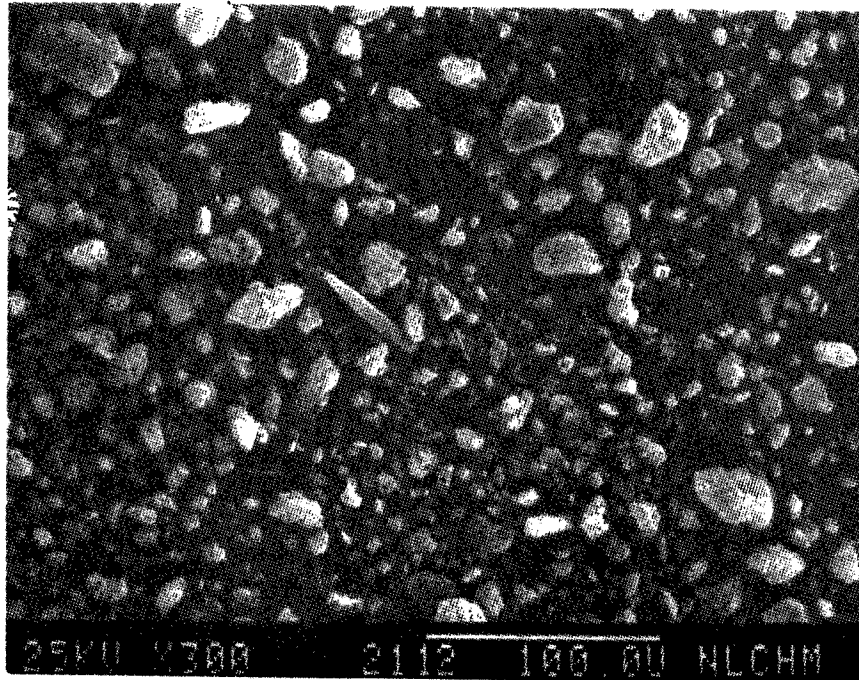


Figure 2

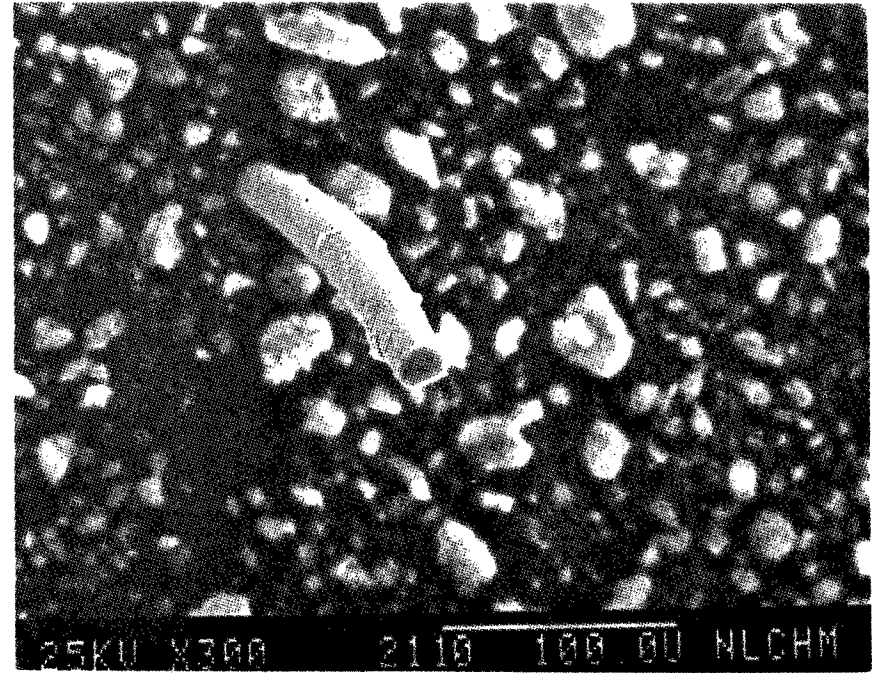


Figure 3

SEM IMAGES OF SAMPLE #

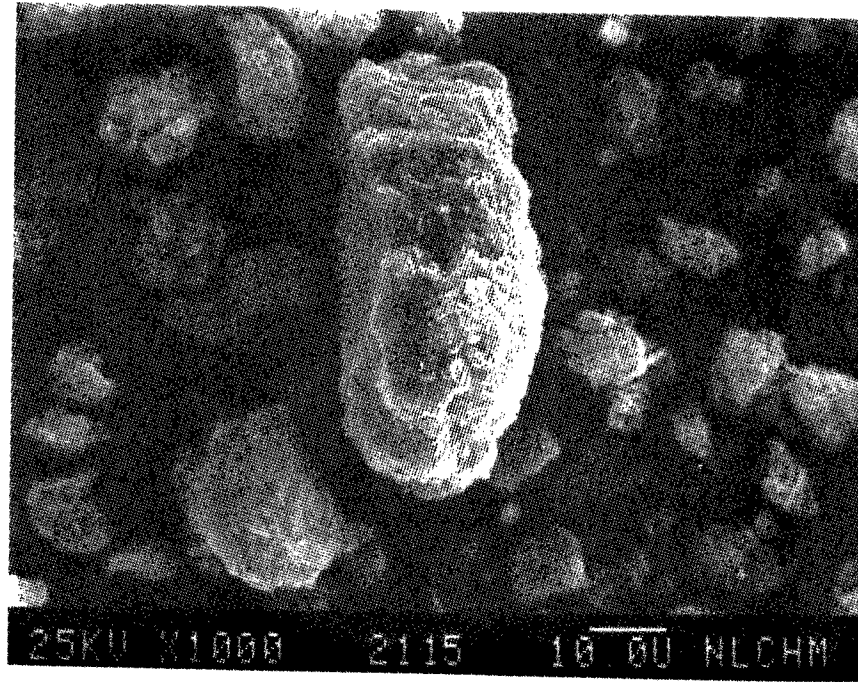


Figure 4

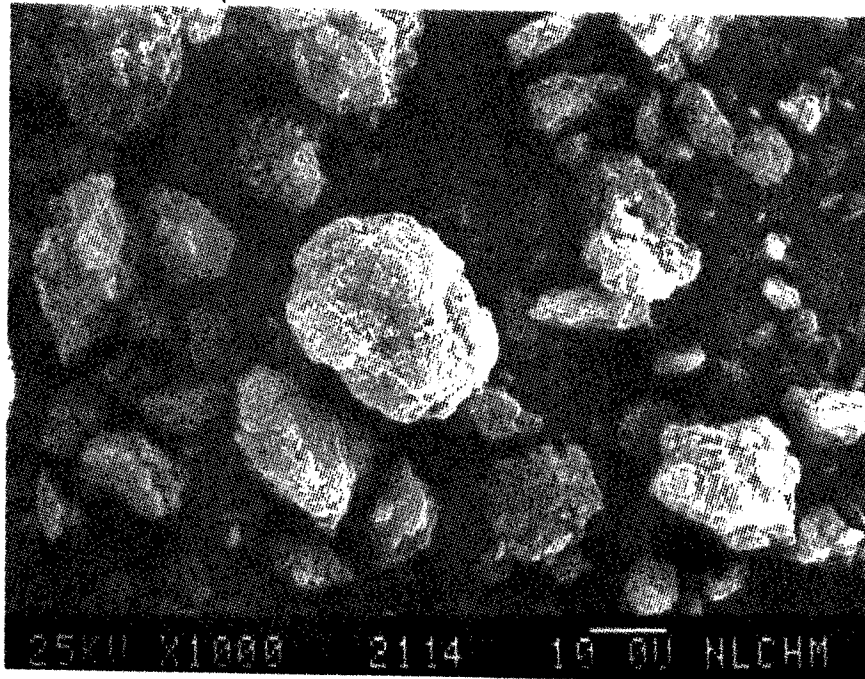


Figure 5

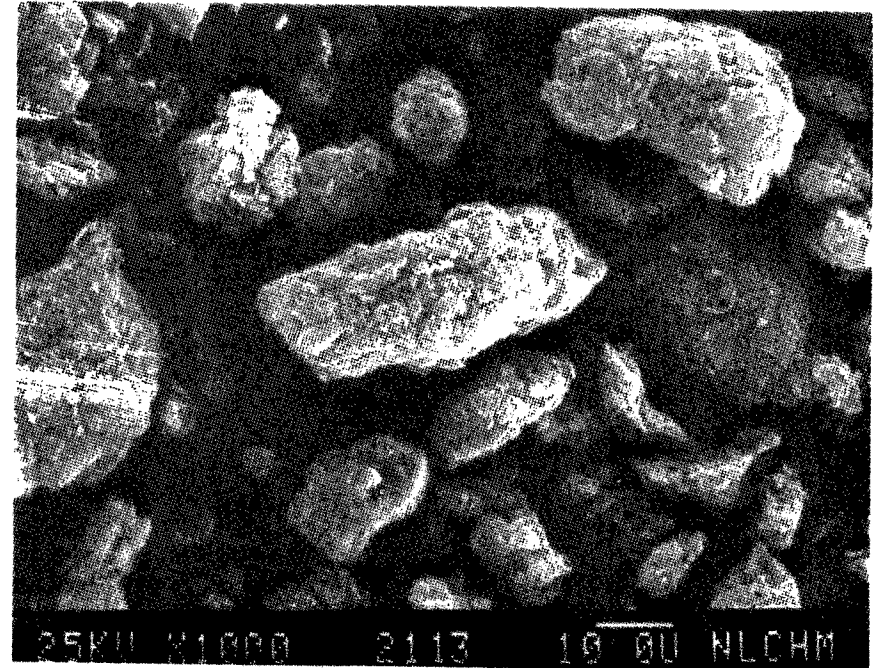


Figure 6

SEM IMAGES OF SAMPLE #

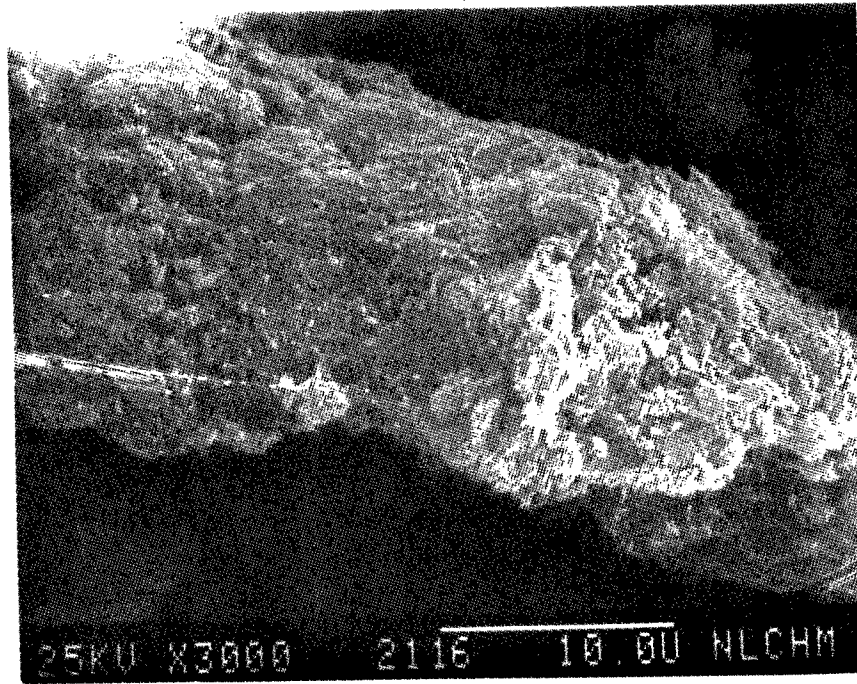


Figure 7

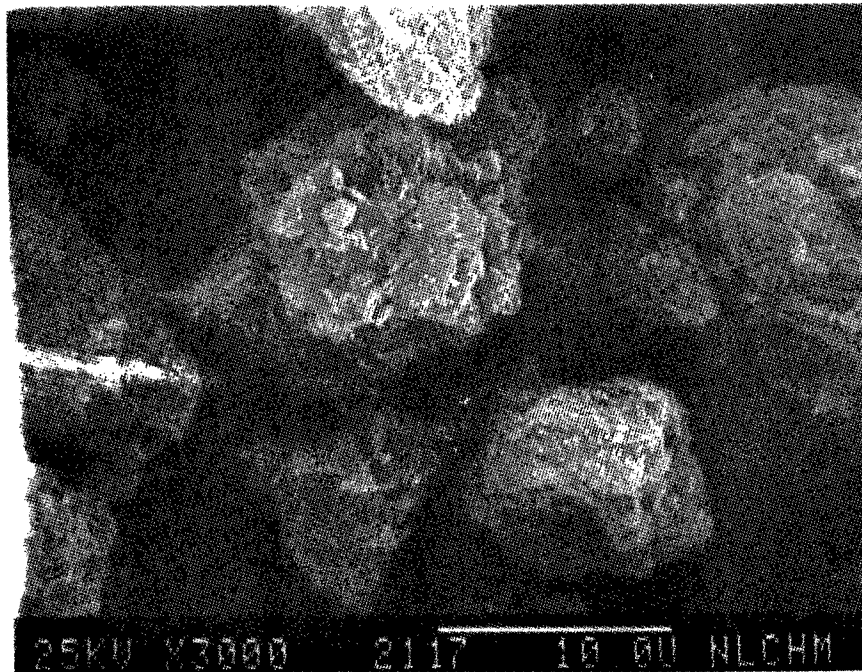


Figure 8

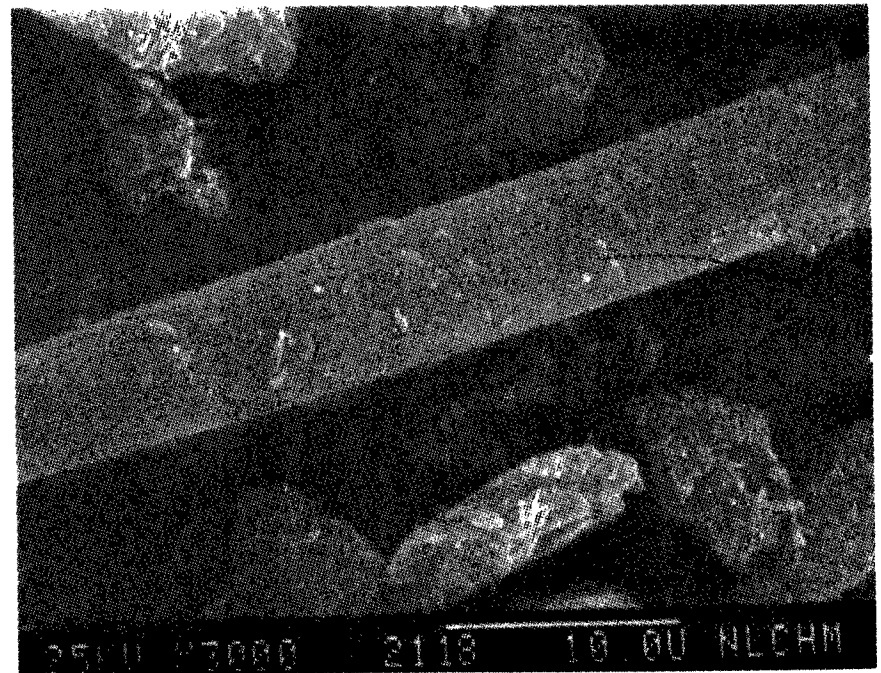


Figure 9



SEM IMAGES OF SAMPLE #

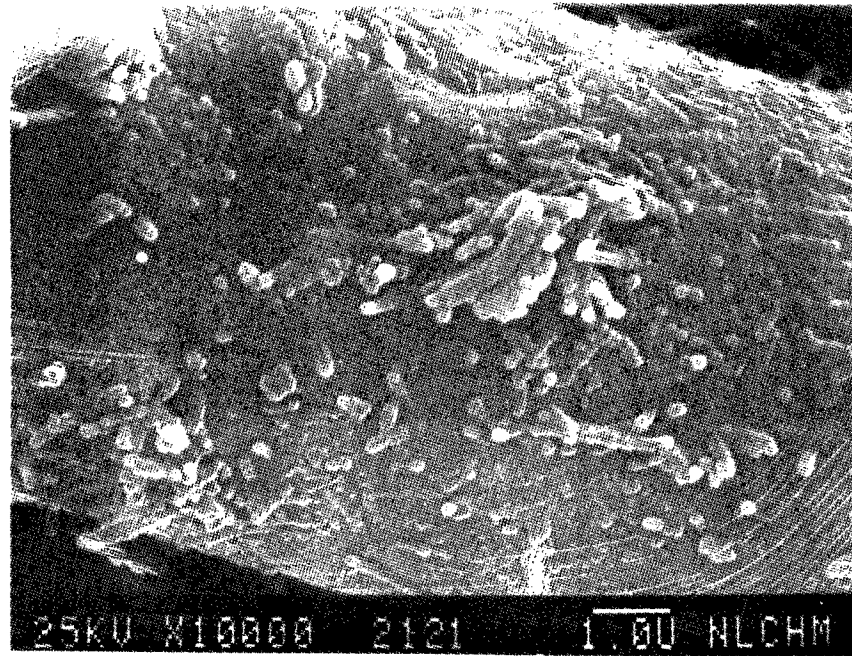


Figure 10

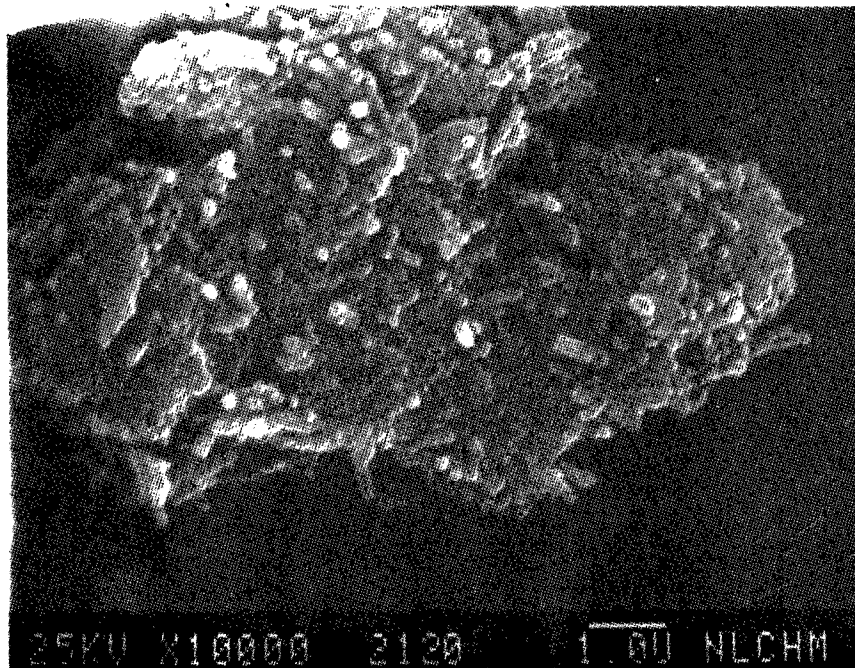


Figure 11

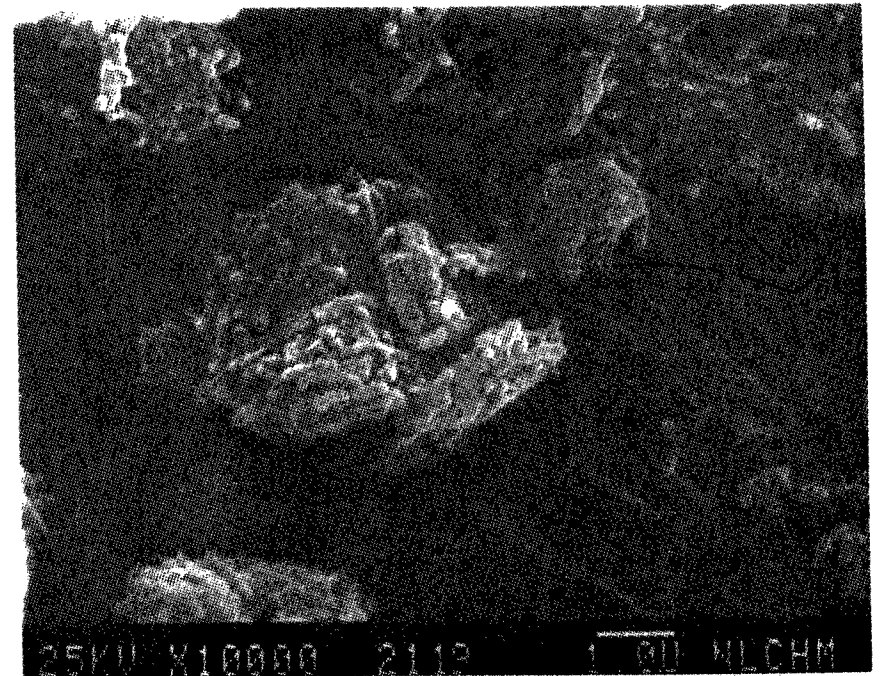


Figure 12

SEM IMAGES OF SAMPLE #

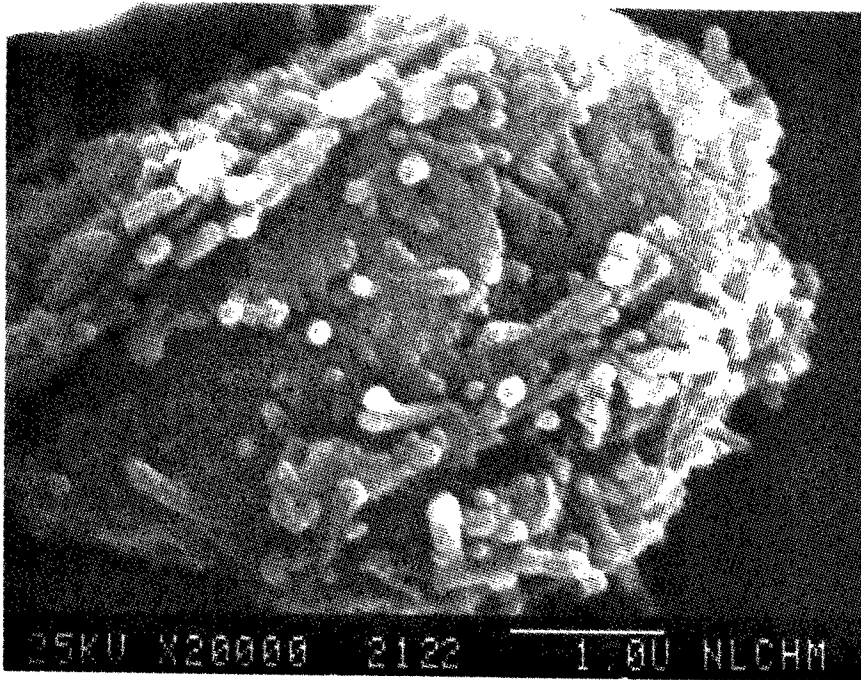


Figure 13

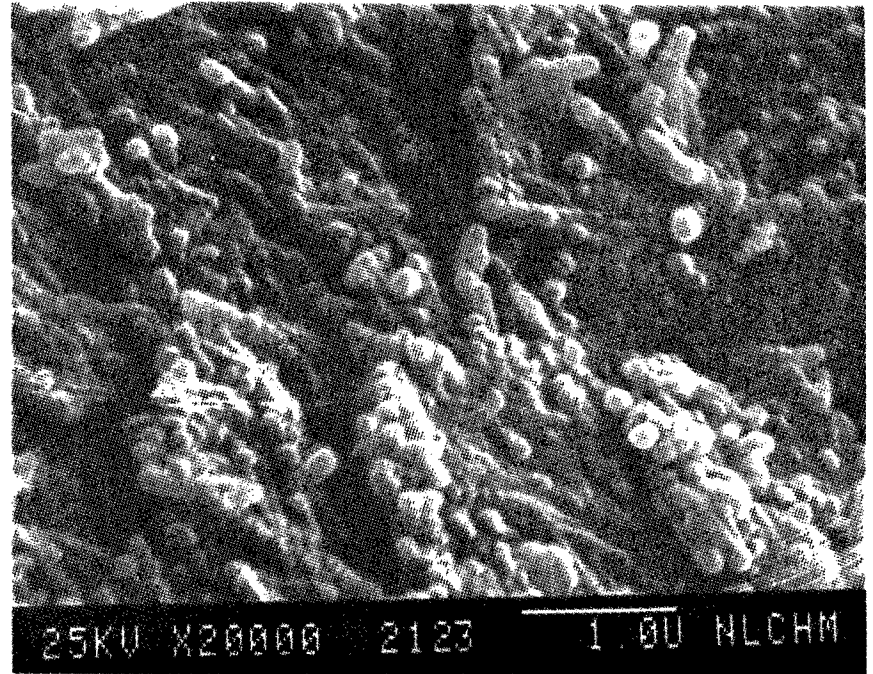


Figure 14

SEM IMAGES OF SAMPLE #

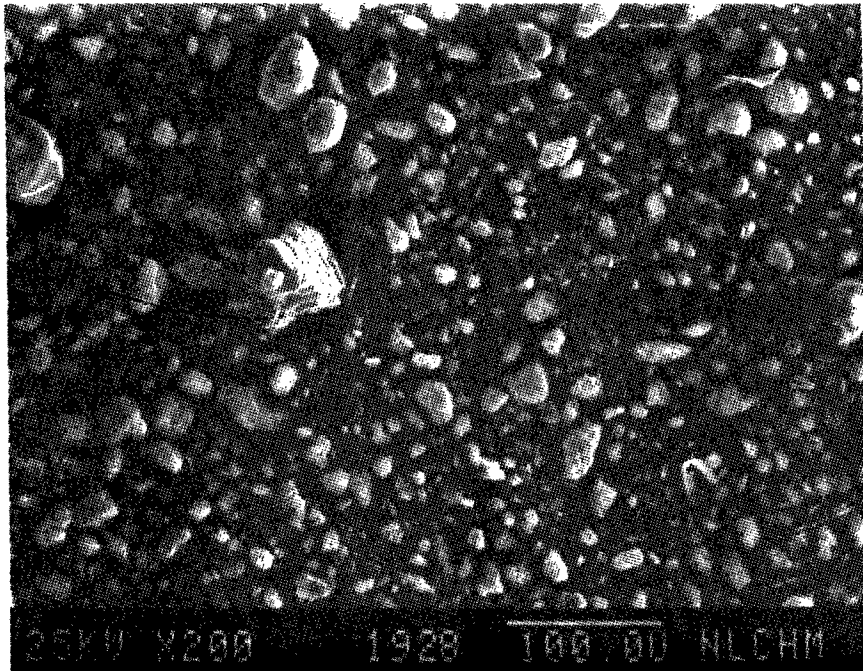


Figure 15

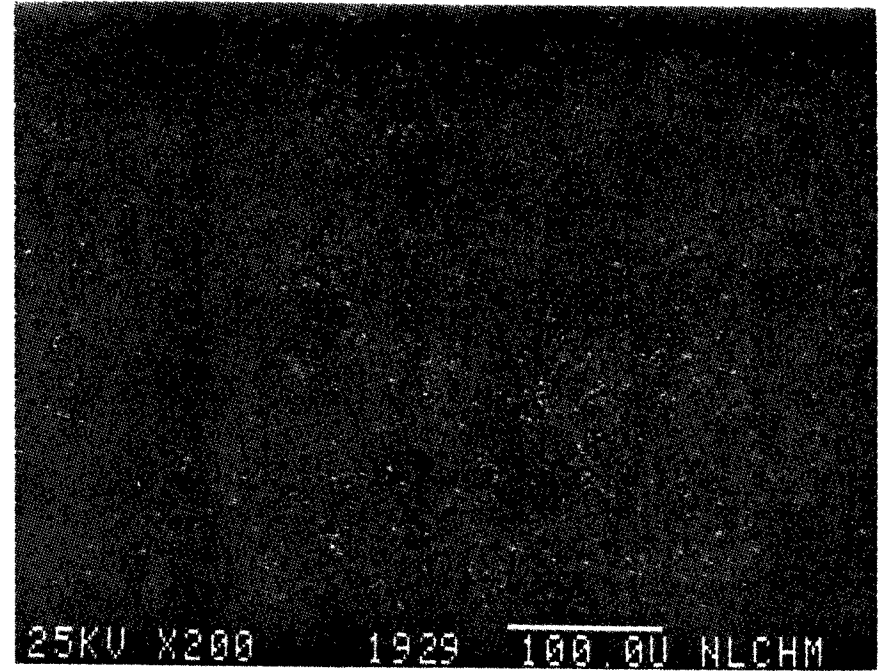


Figure 16

Mg X-Ray Image of Figure 15

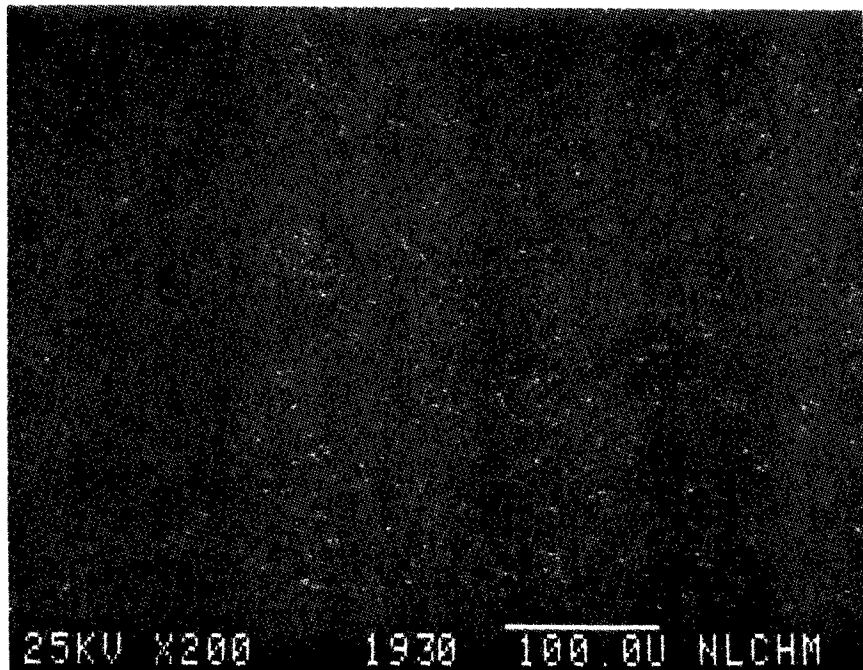


Figure 17

Al X-Ray Image of Figure 15

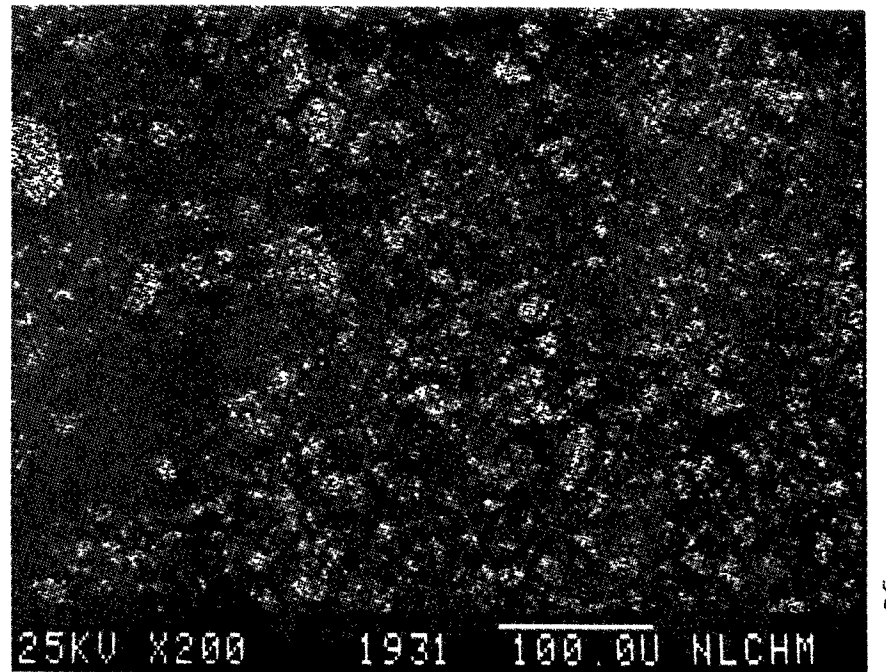


Figure 18

Si X-Ray Image of Figure 15

SEM IMAGES OF SAMPLE #

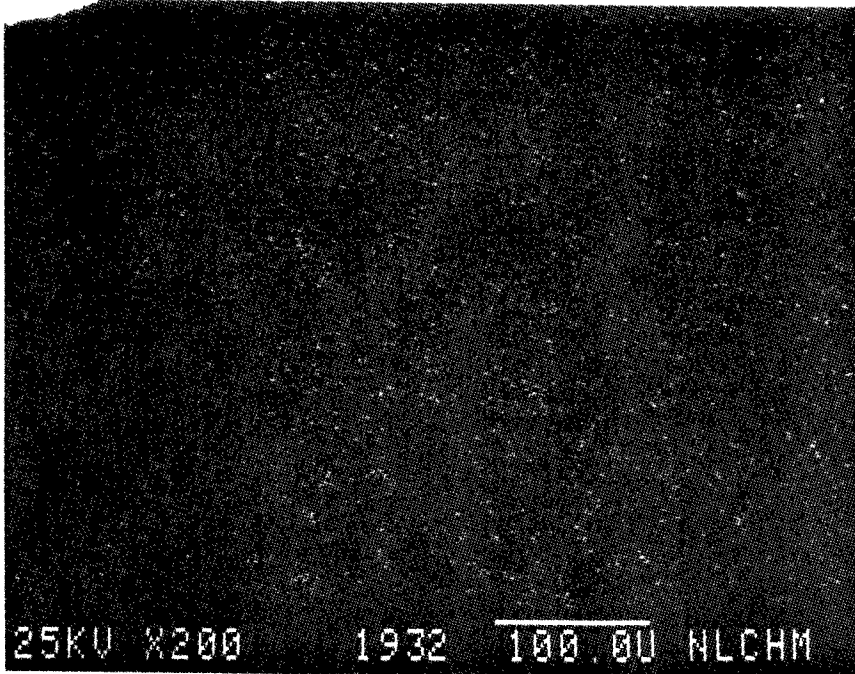


Figure 19 S X-Ray Image of Figure 15

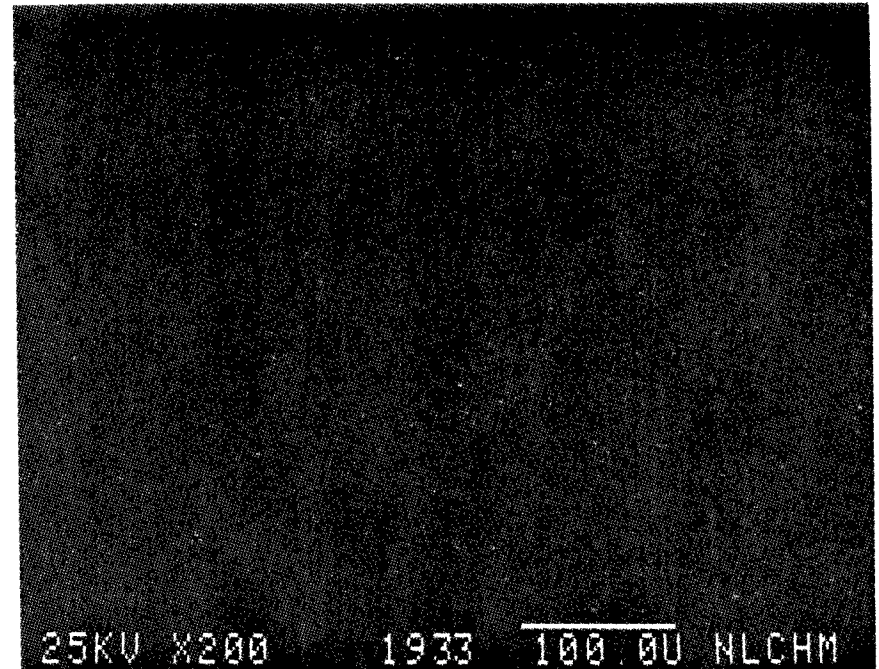


Figure 20 K X-Ray Image of Figure 15

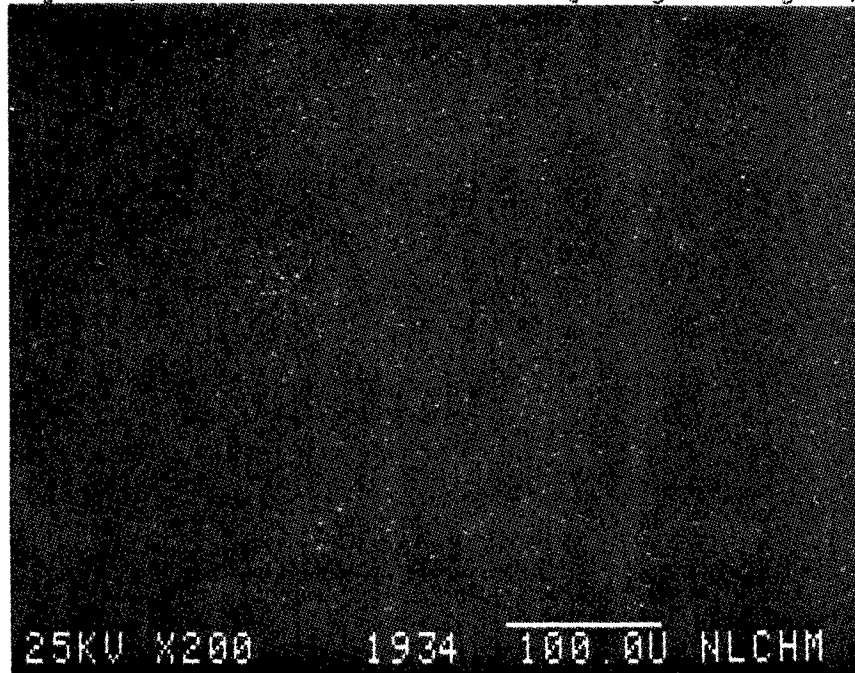


Figure 21 Ca X-Ray Image of Figure 15

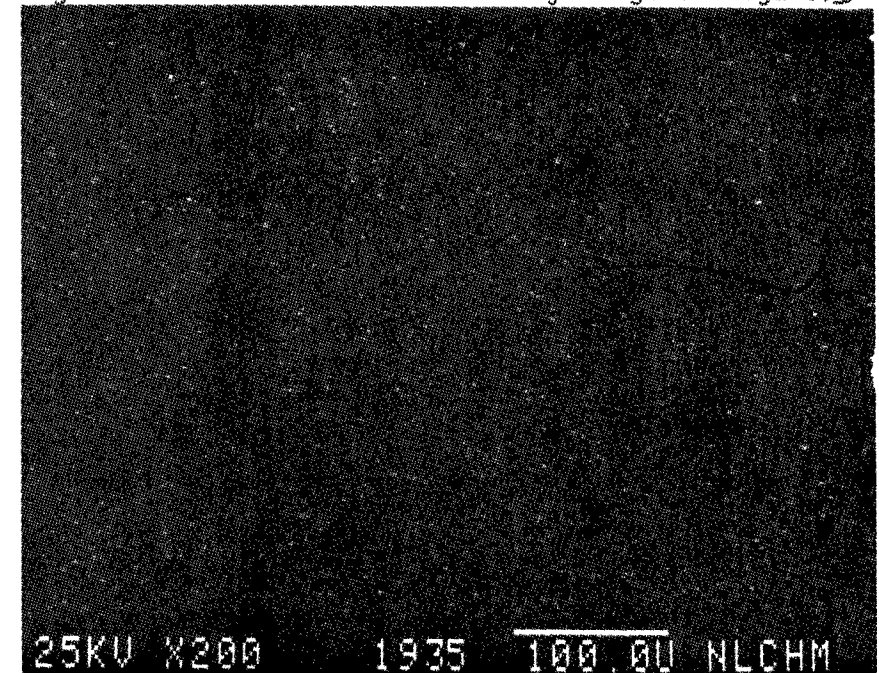


Figure 22 Fe X-Ray Image of Figure 15



SEM IMAGES OF SAMPLE #



Figure 23

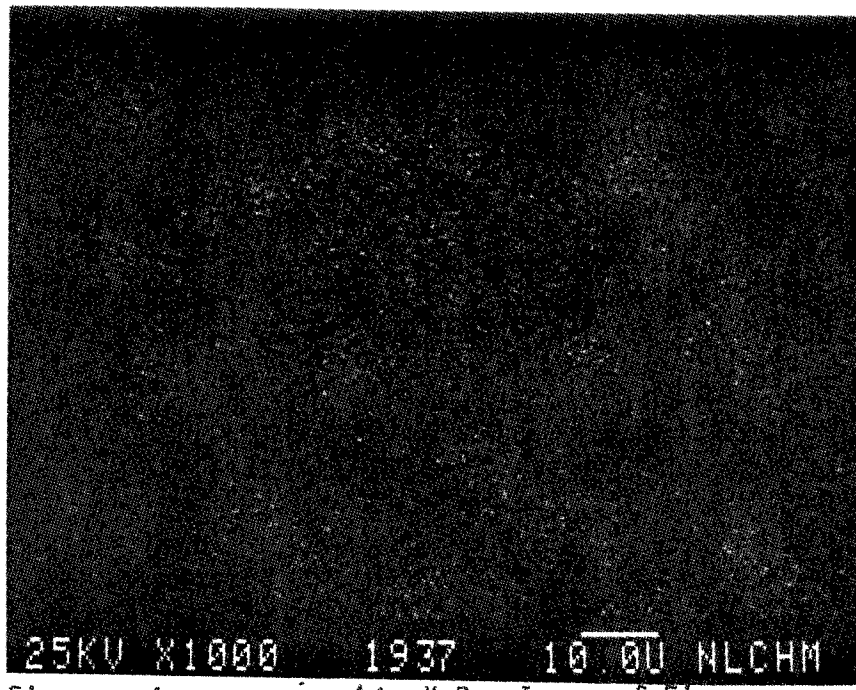


Figure 24

Mg X-Ray Image of Figure 23

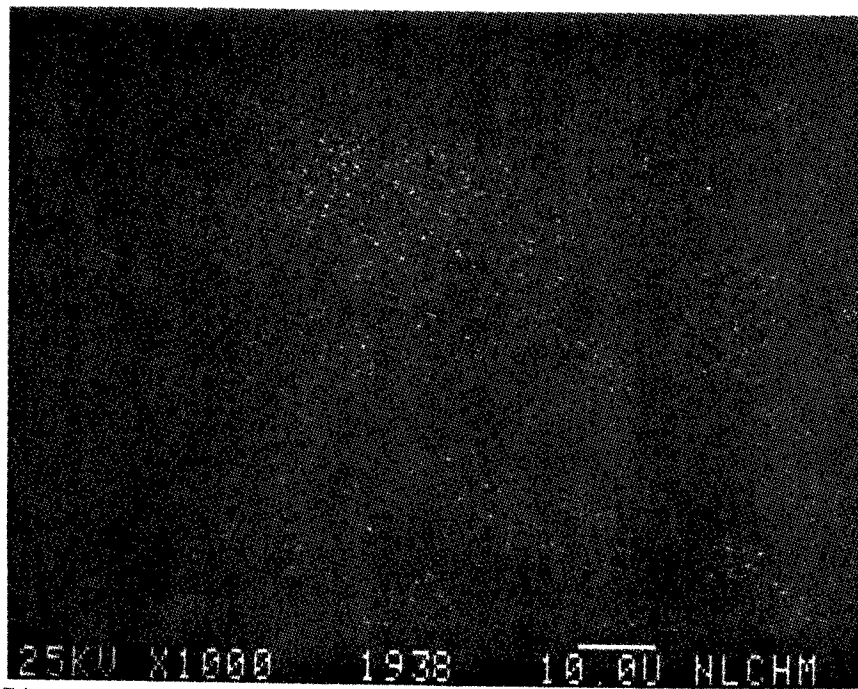


Figure 25

AL X-Ray Image of Figure 23

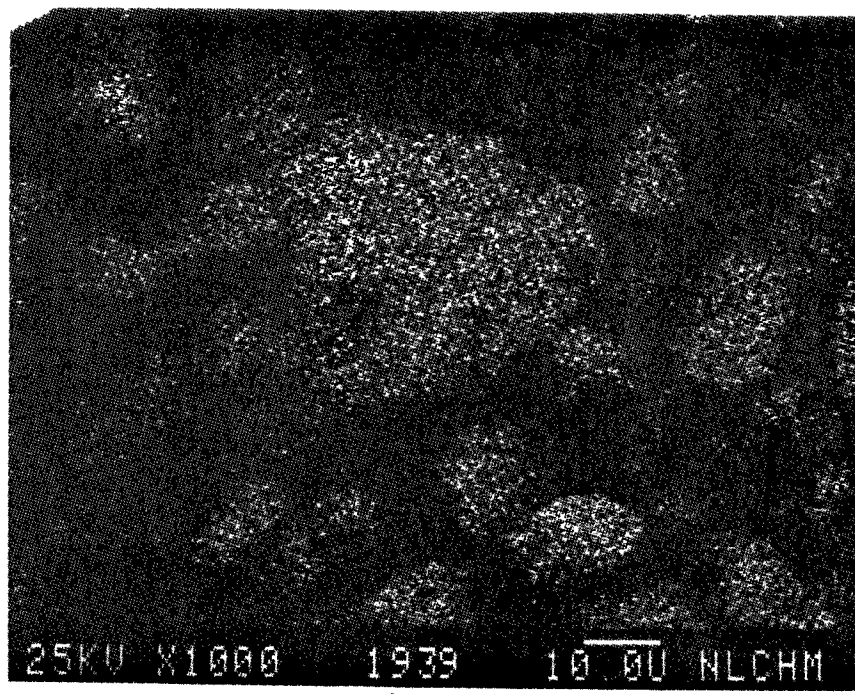


Figure 26

Si X-Ray Image of Figure 23

SEM IMAGES OF SAMPLE #

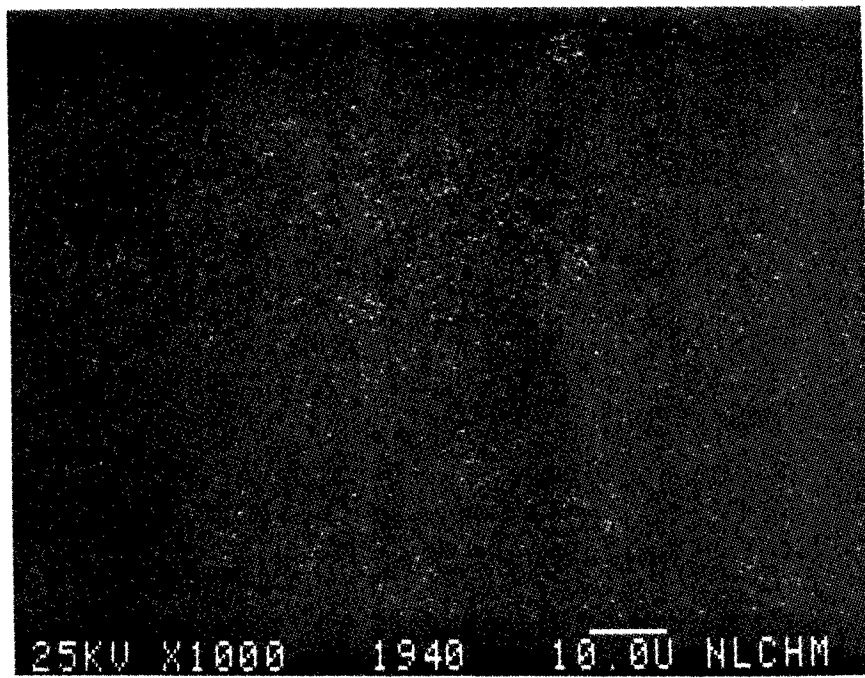


Figure 27

S X-Ray Image of Figure 23

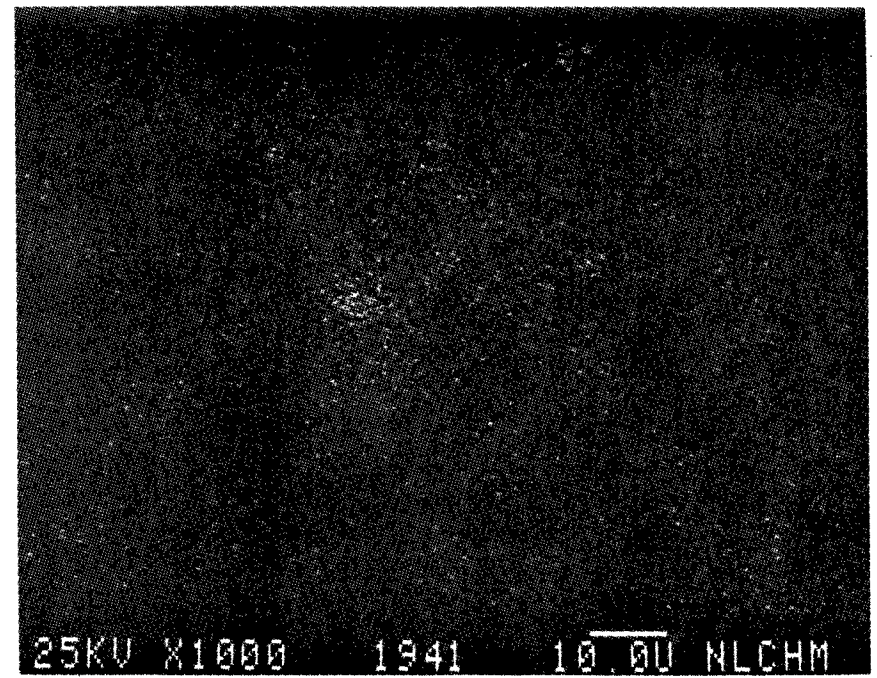


Figure 28

Fe X-Ray Image of Figure 23

SEM IMAGES OF SAMPLE #

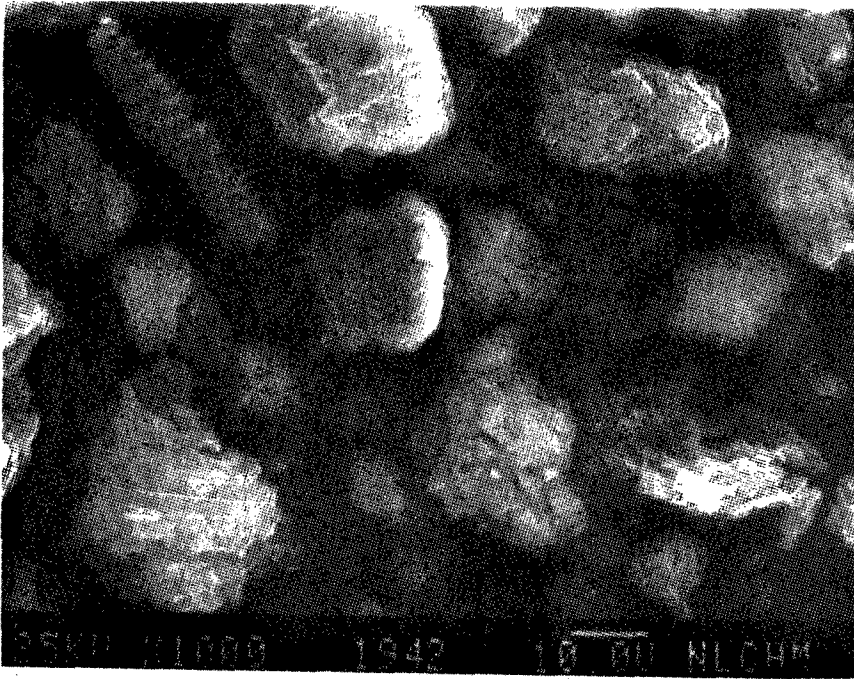


Figure 29

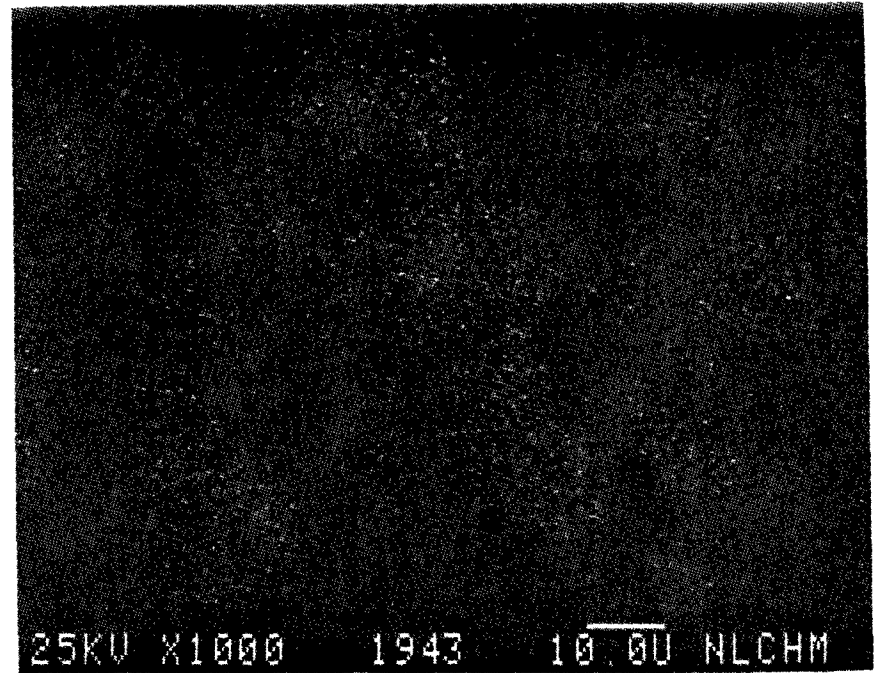


Figure 30

Mg X-Ray Image of Figure 29

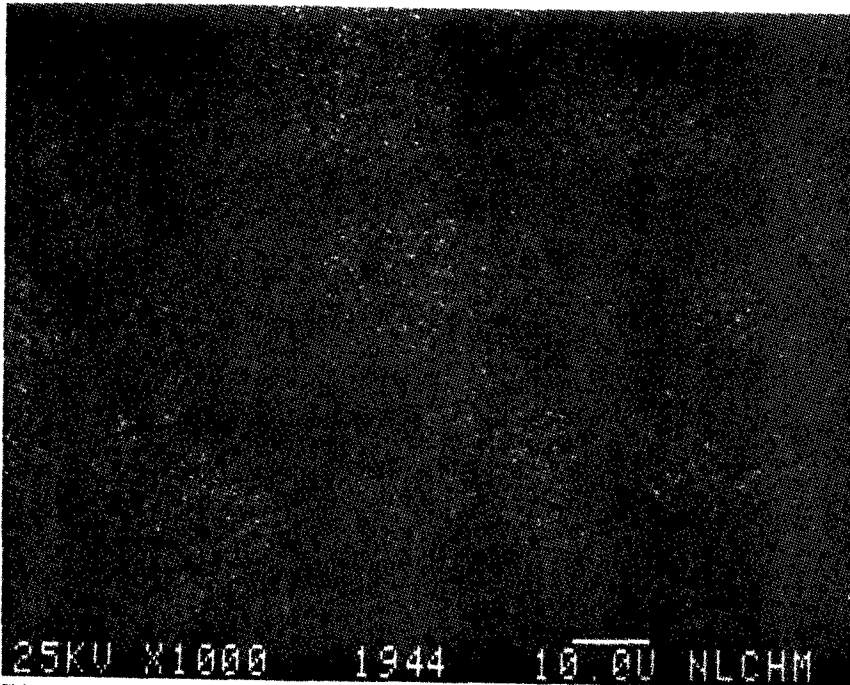


Figure 31

Al X-Ray Image of Figure 29

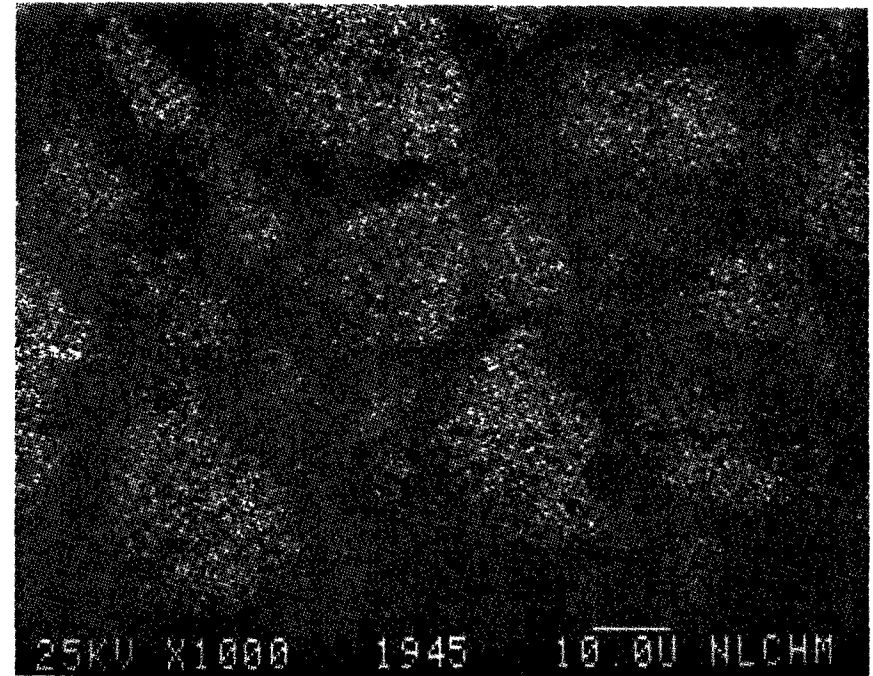


Figure 32

Si X-Ray Image of Figure 29

SEM IMAGES OF SAMPLE #

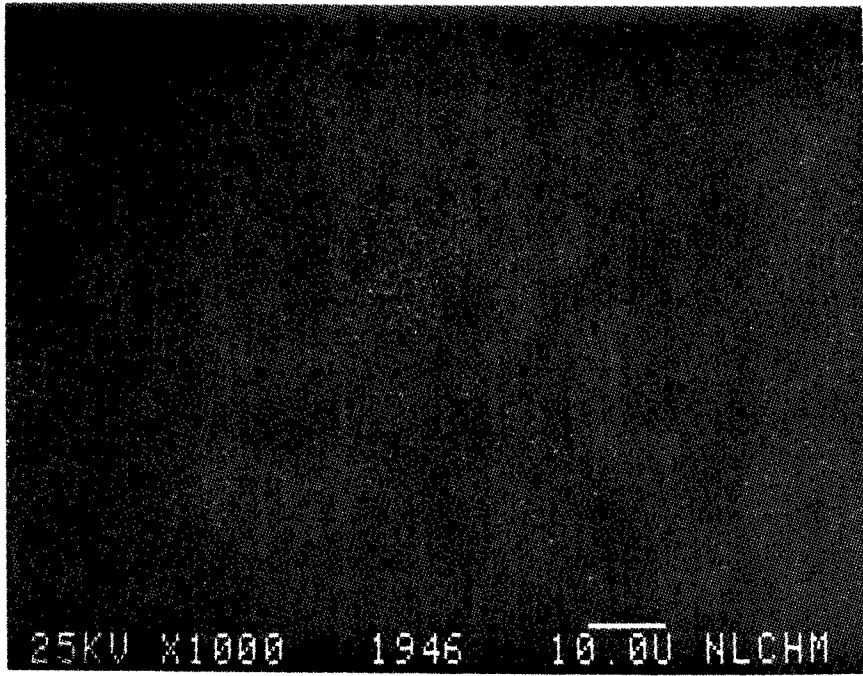


Figure 33

K X-Ray Image of Figure 29

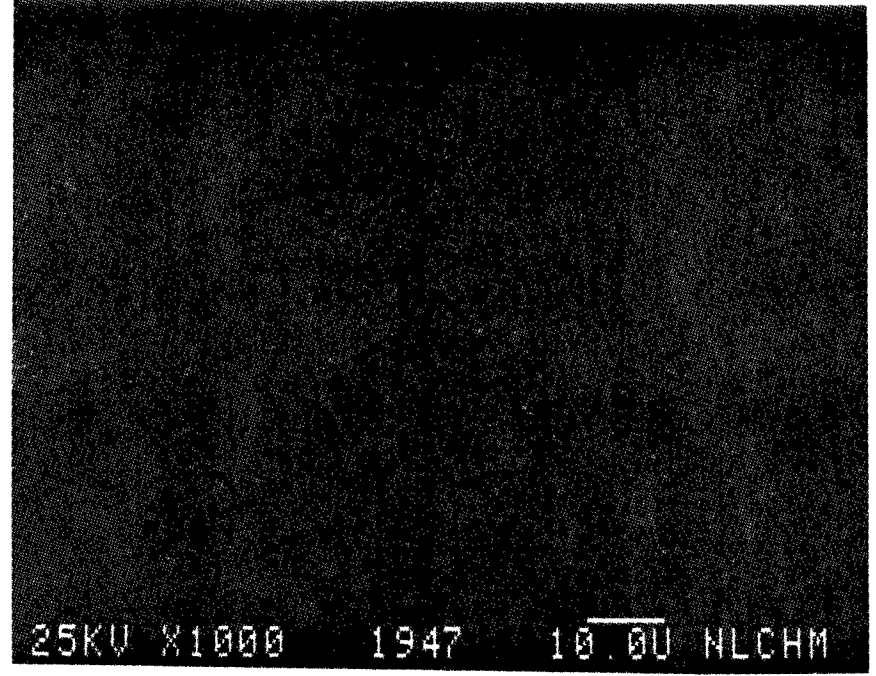


Figure 34

Ca X-Ray Image of Figure 29

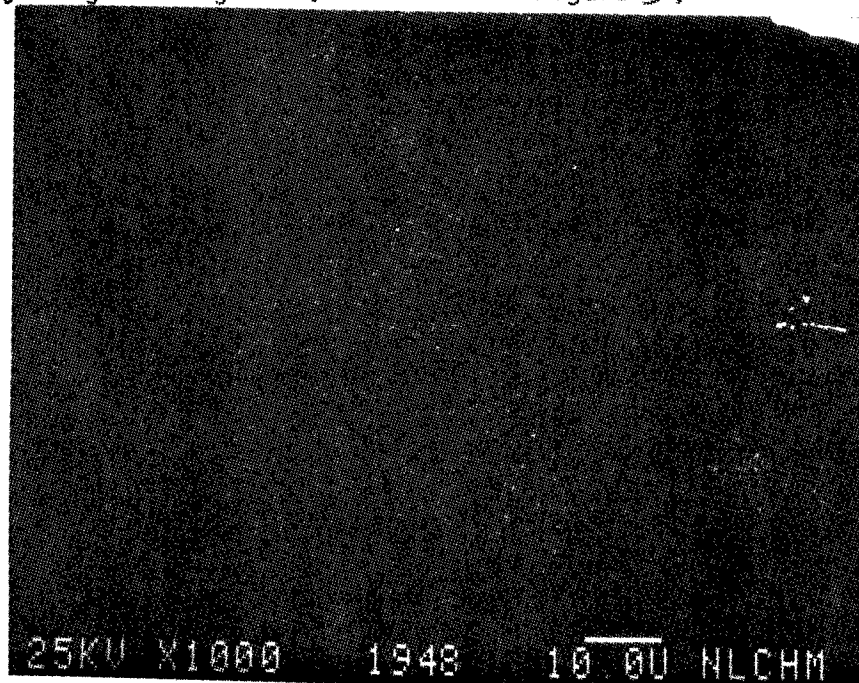


Figure 35

Fe X-Ray Image of Figure 29



Figure 36

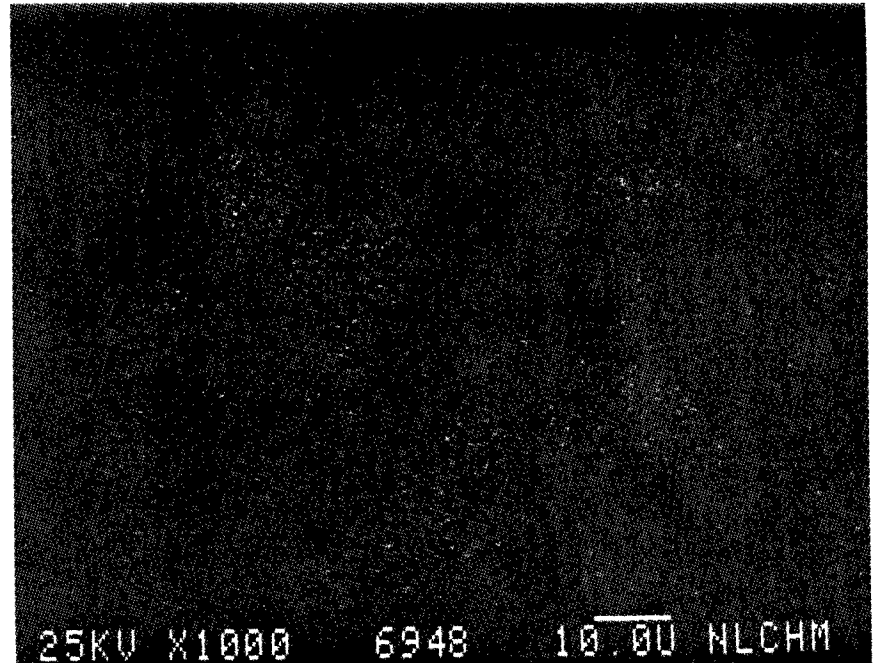


Figure 37

Mg X-Ray Image of Figure 36

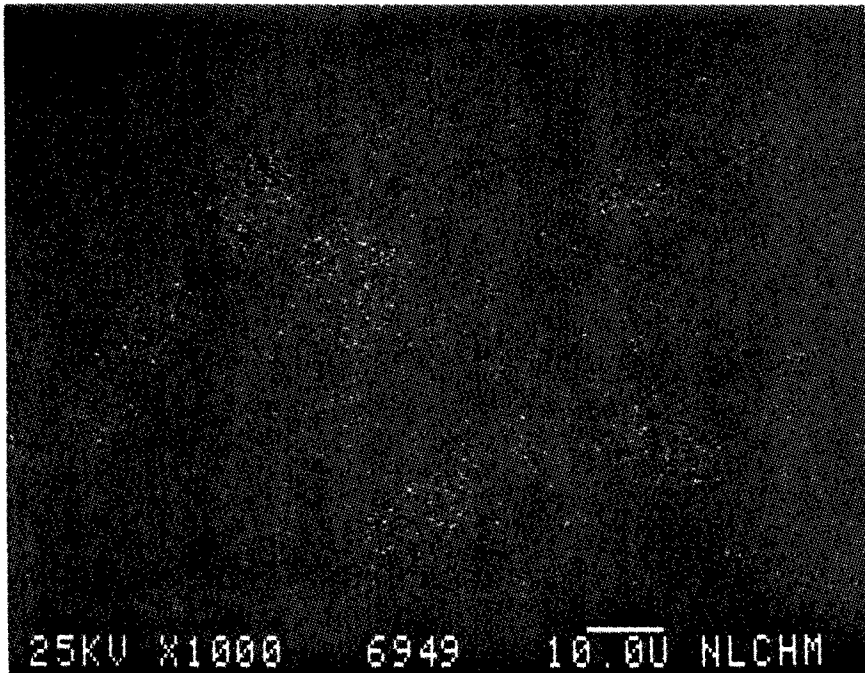


Figure 38

AL X-Ray Image of Figure 36

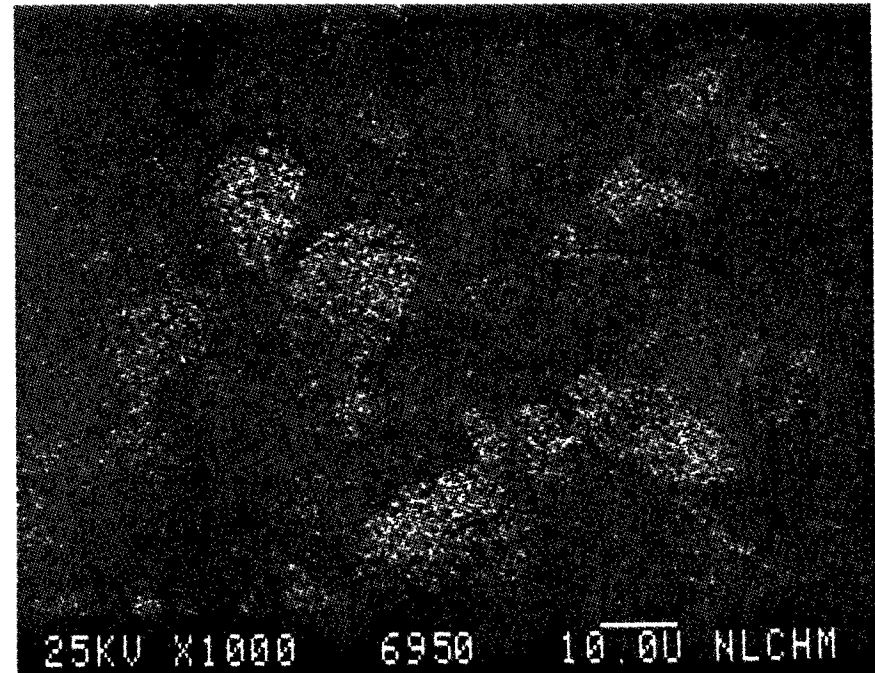


Figure 39

Si X-Ray Image of Figure 36



SEM IMAGES OF SAMPLE #

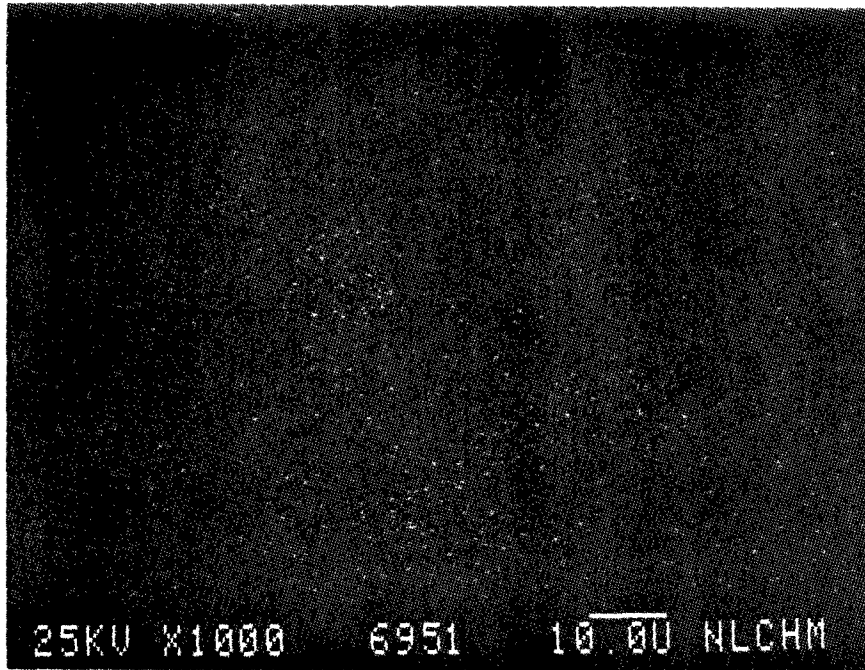


Figure 40

S X-Ray Image of Figure 36

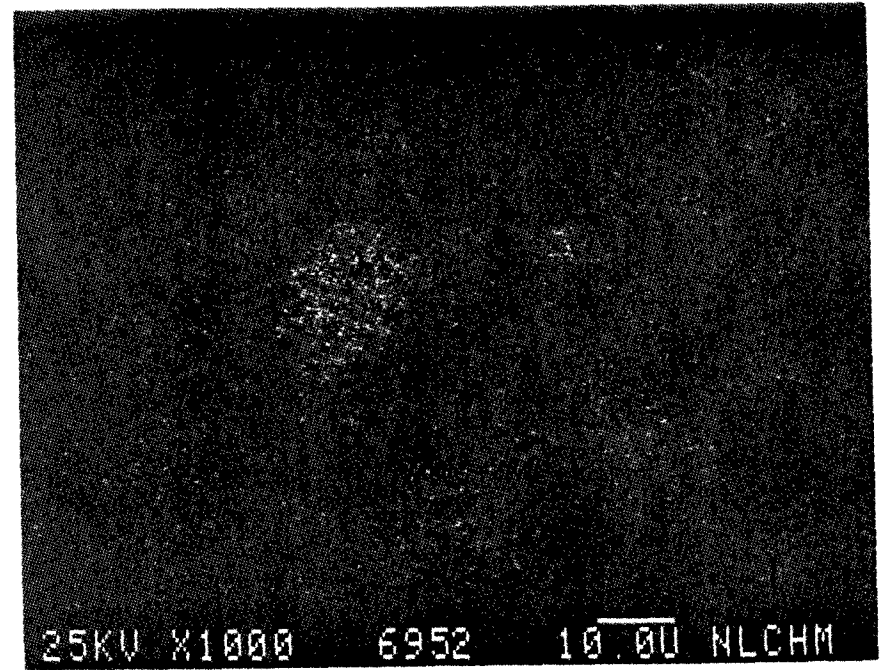


Figure 41

K X-Ray Image of Figure 36

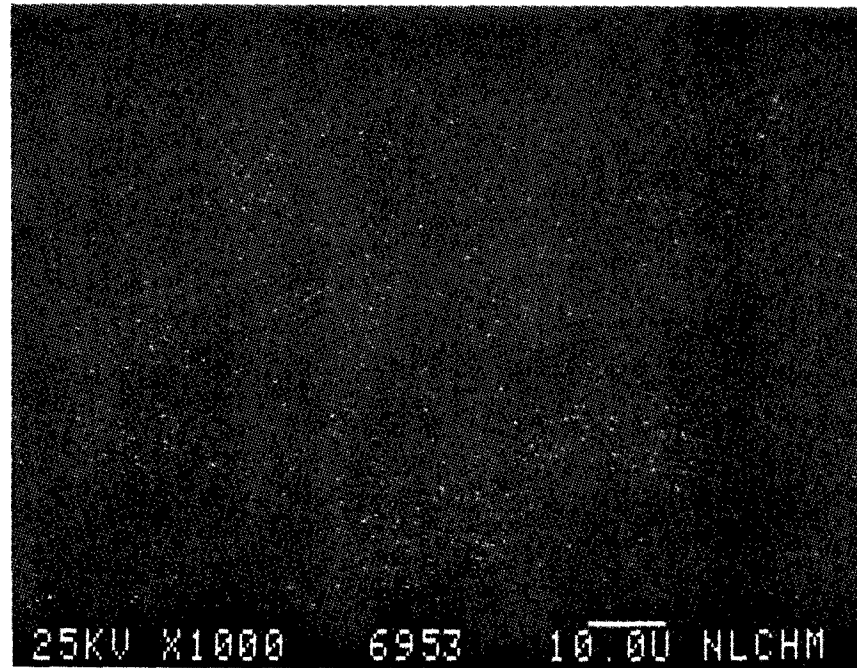


Figure 42

Fe X-Ray Image of Figure 36

SEM IMAGES OF SAMPLE #



Figure 43

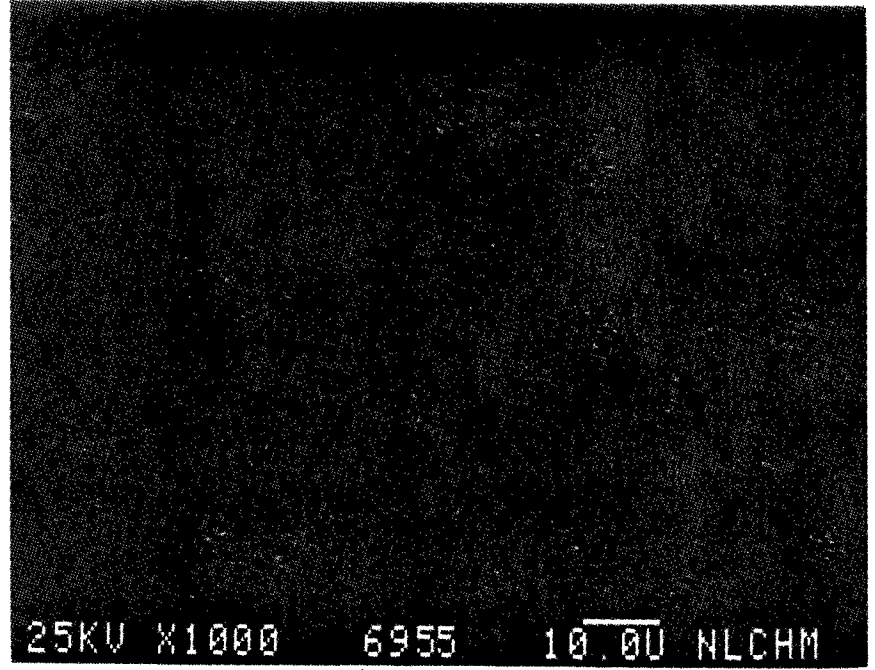


Figure 44

Mg X-Ray Image of Figure 43

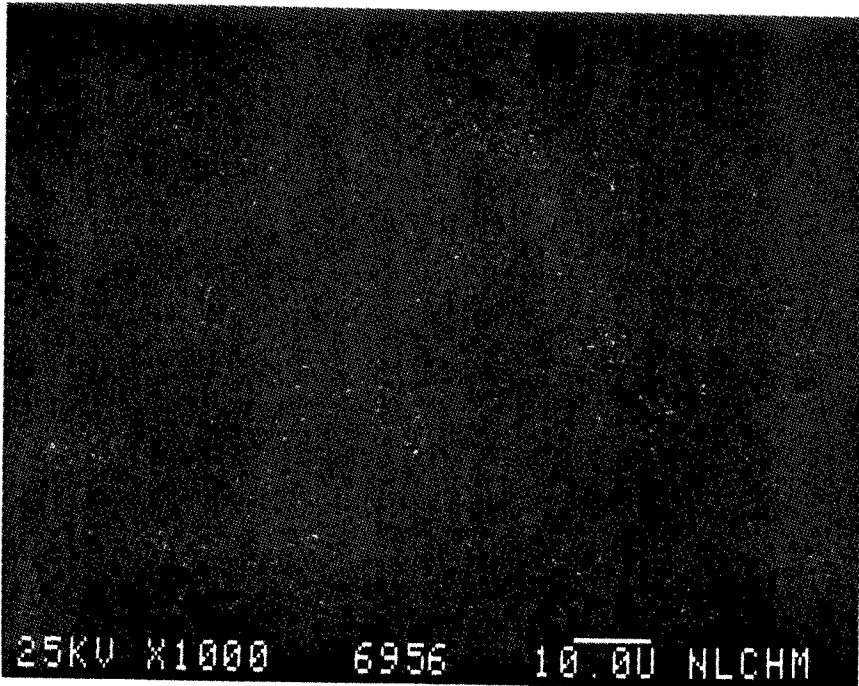


Figure 45

Al X-Ray Image of Figure 43

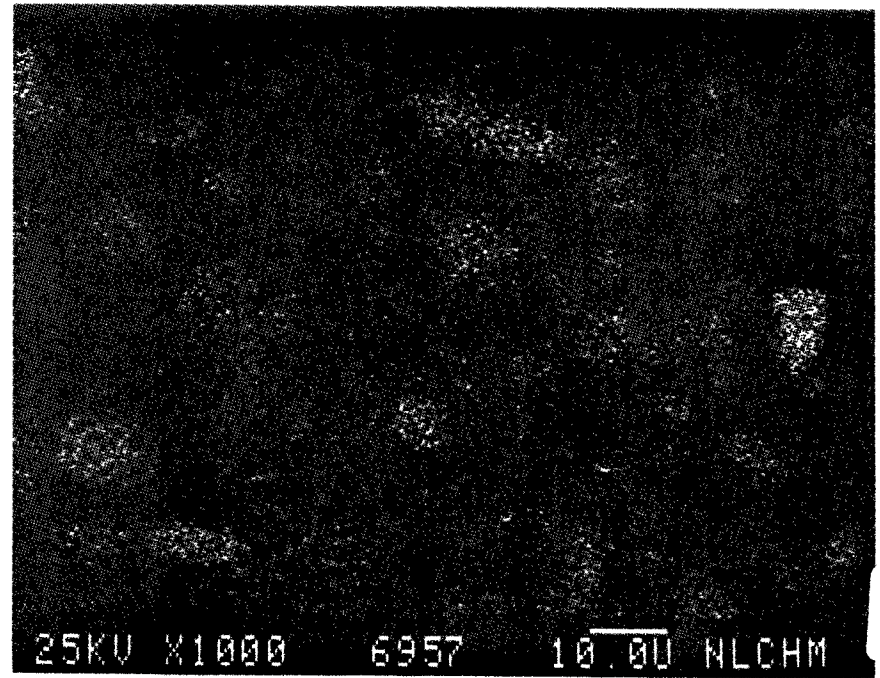


Figure 46

Si X-Ray Image of Figure 43

SEM IMAGES OF SAMPLE #

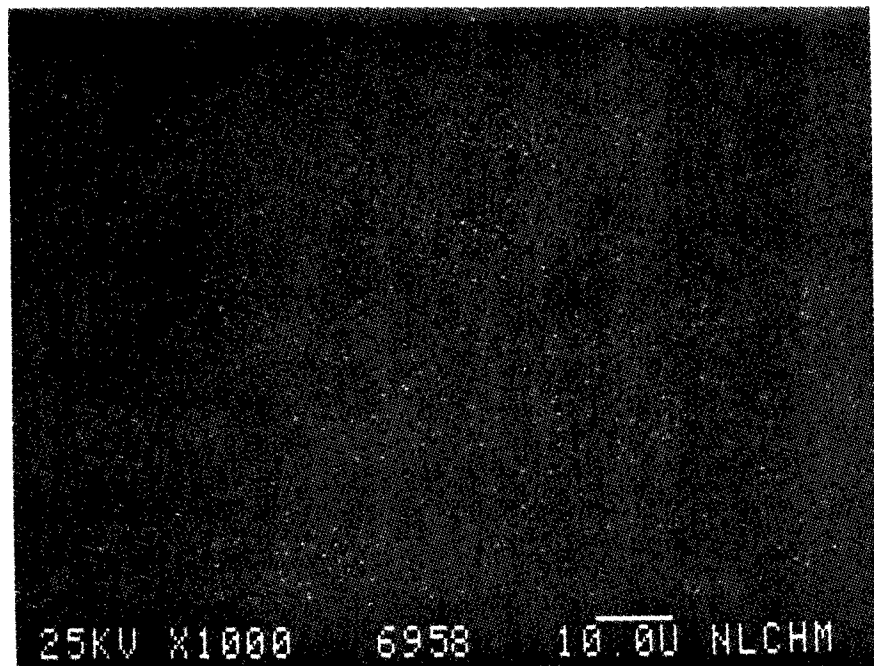


Figure 47

K X-Ray Image of Figure 43

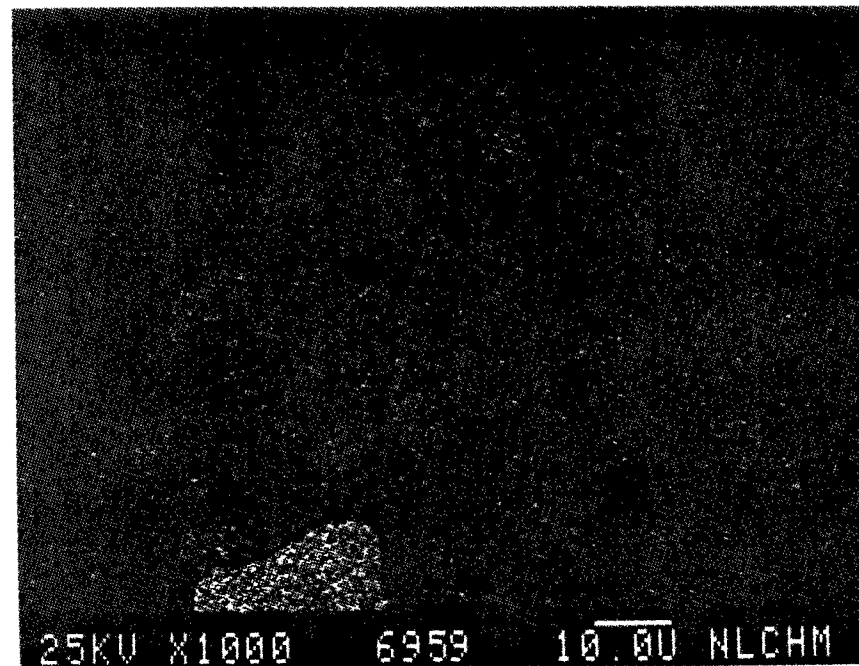


Figure 48

Ca X-Ray Image of Figure 43

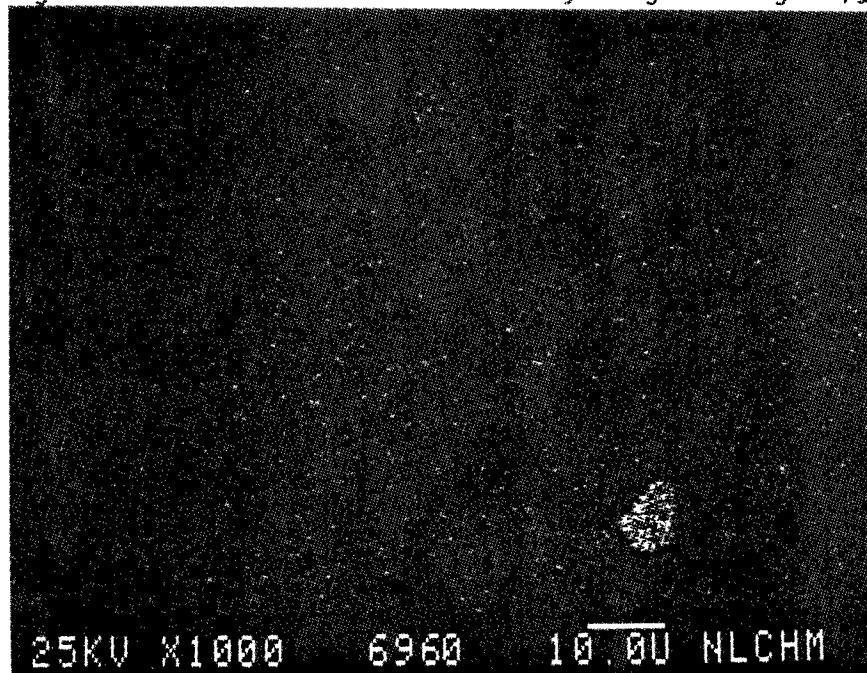


Figure 49

Ti X-Ray Image of Figure 43

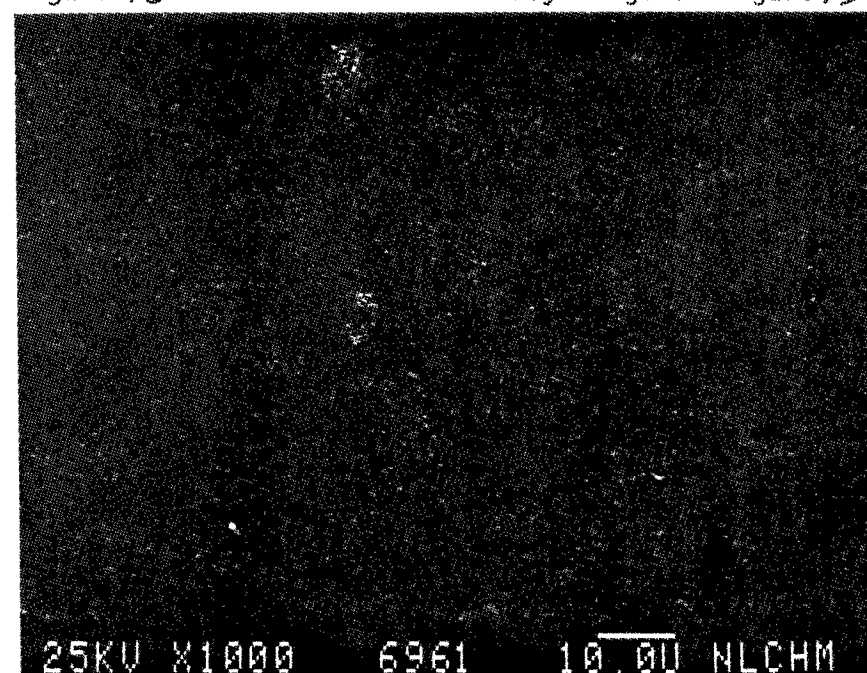


Figure 50

Fe X-Ray Image of Figure 43



ENERGY DISPERSIVE X-RAY ANALYSIS

Analytical Number Apautagite

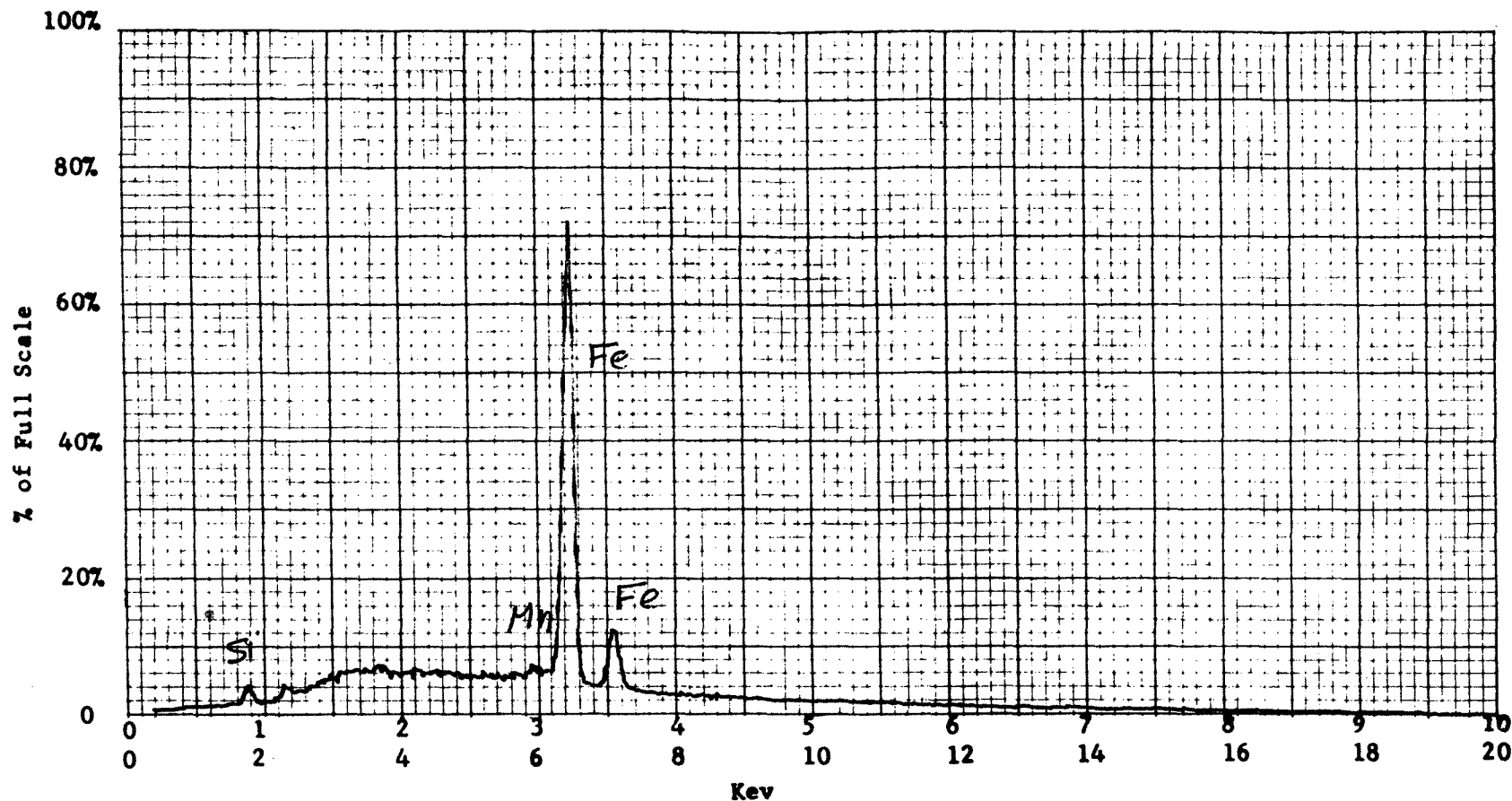
Operator \_\_\_\_\_ Date \_\_\_\_\_

Accelerating Potential 25 KeV

Total Counts Acquired 1.0 min.

Number Counts Full Scale 5K

Number of eV per channel 20



Sample peculiarities and remarks: FIGURE 51: POINT SCAN ON A HIGH Fe PARTICLE  
IN FIGURE 43

ENERGY DISPERSIVE X-RAY ANALYSIS

Analytical Number Apautagite

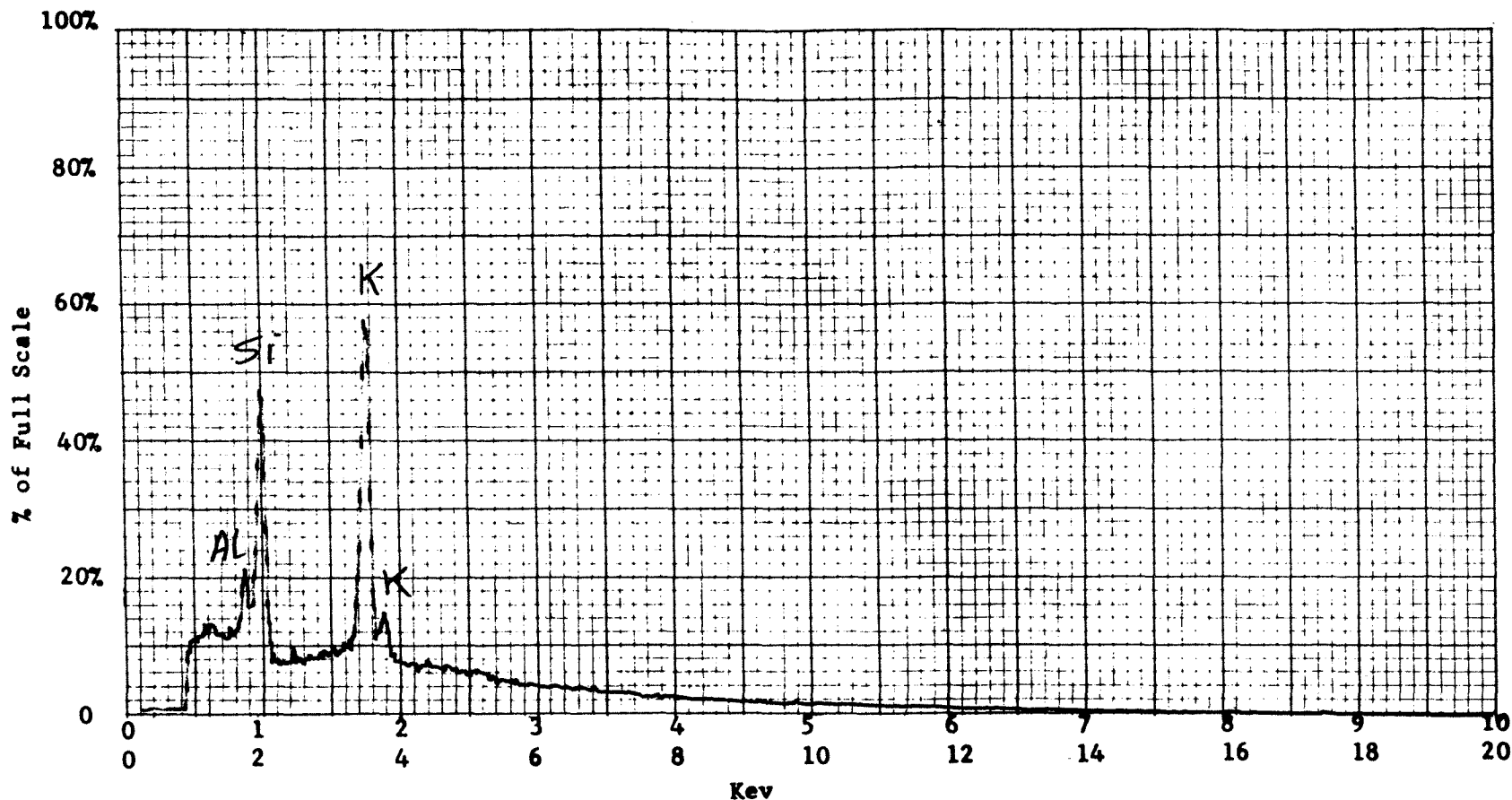
Operator \_\_\_\_\_ Date \_\_\_\_\_

Accelerating Potential 25 KeV

Total Counts Acquired 1.0 min.

Number Counts Full Scale 5K

Number of eV per channel 20



Sample peculiarities and remarks: FIGURE 52: POINT SCAN ON A HIGH K PARTICLE  
IN FIGURE 36

ENERGY DISPERSIVE X-RAY ANALYSIS

Analytical Number Apautagite

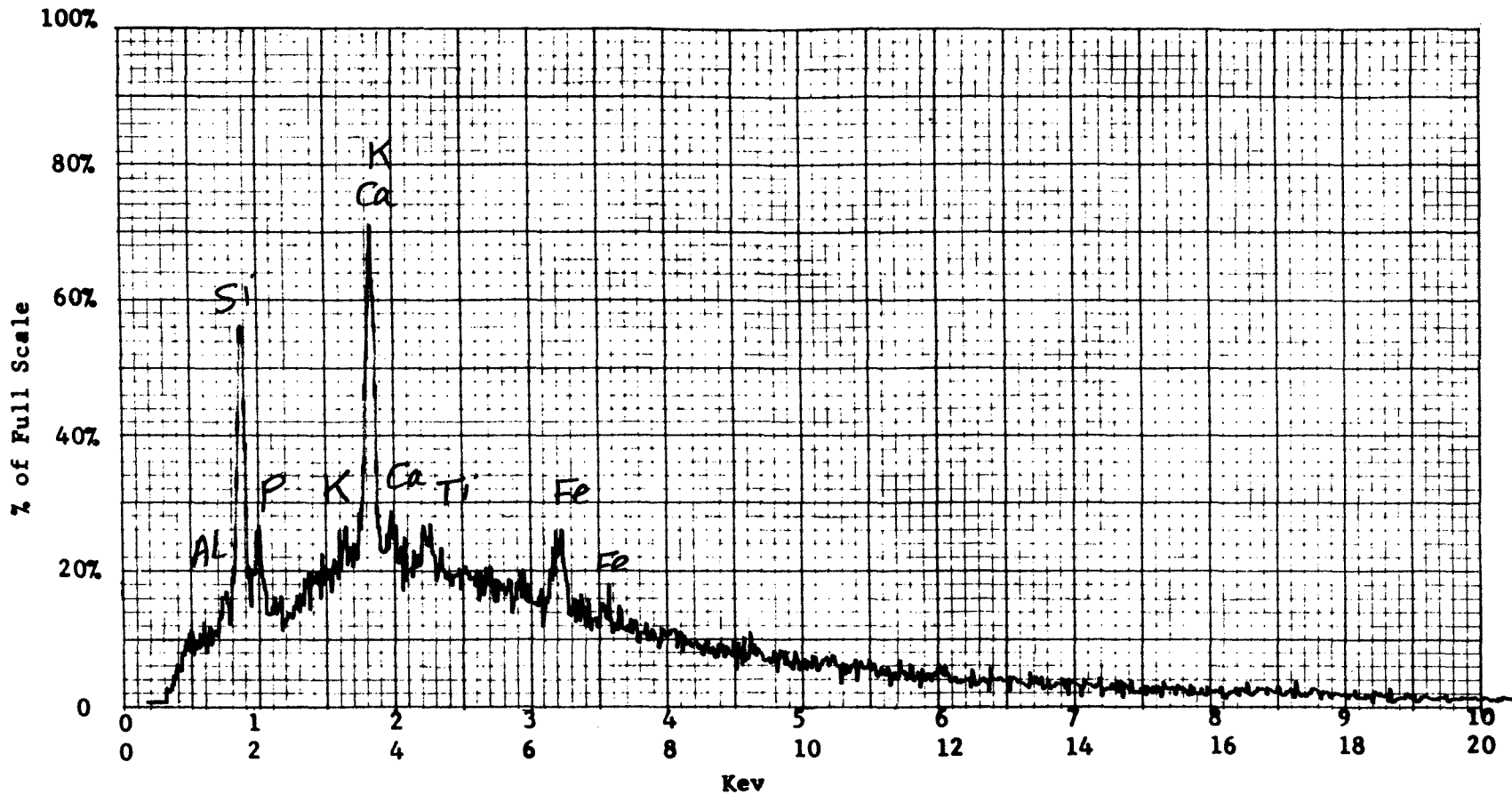
Operator \_\_\_\_\_ Date \_\_\_\_\_

Accelerating Potential 25 KeV

Total Counts Acquired 1.0 min.

Number Counts Full Scale 1 K

Number of eV per channel 20



Sample peculiarities and remarks: FIGURE 53: AREA SCAN ON FIGURE 43

ENERGY DISPERSIVE X-RAY ANALYSIS

Analytical Number Apautagite

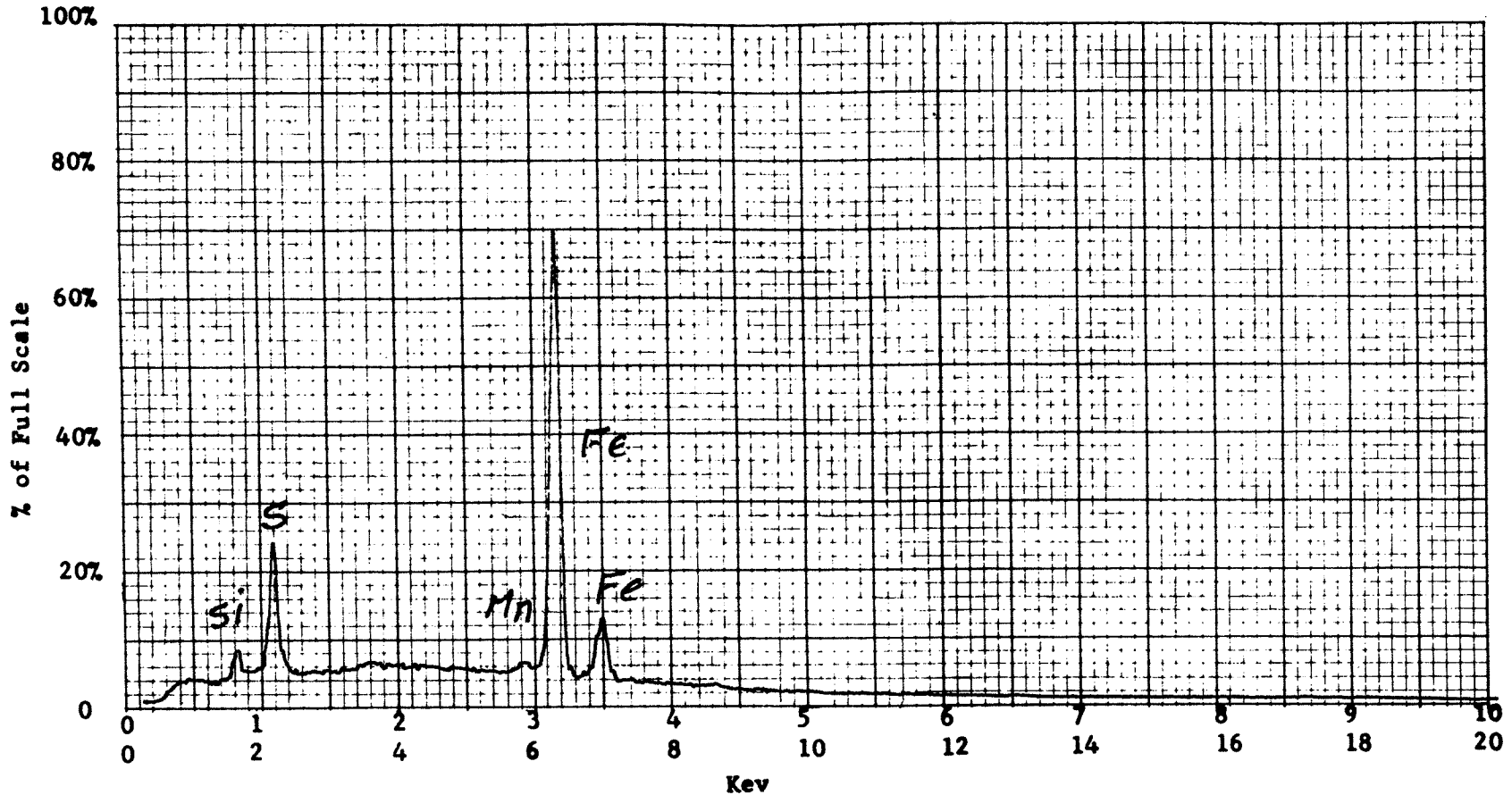
Operator \_\_\_\_\_ Date \_\_\_\_\_

Accelerating Potential 25 KeV

Total Counts Acquired 1.0 min.

Number Counts Full Scale 5K

Number of eV per channel 20



Sample peculiarities and remarks: FIGURE 54: POINT SCAN ON A HIGH Fe-S PARTICLE IN FIGURE 23

ENERGY DISPERSIVE X-RAY ANALYSIS

Analytical Number Apautagite

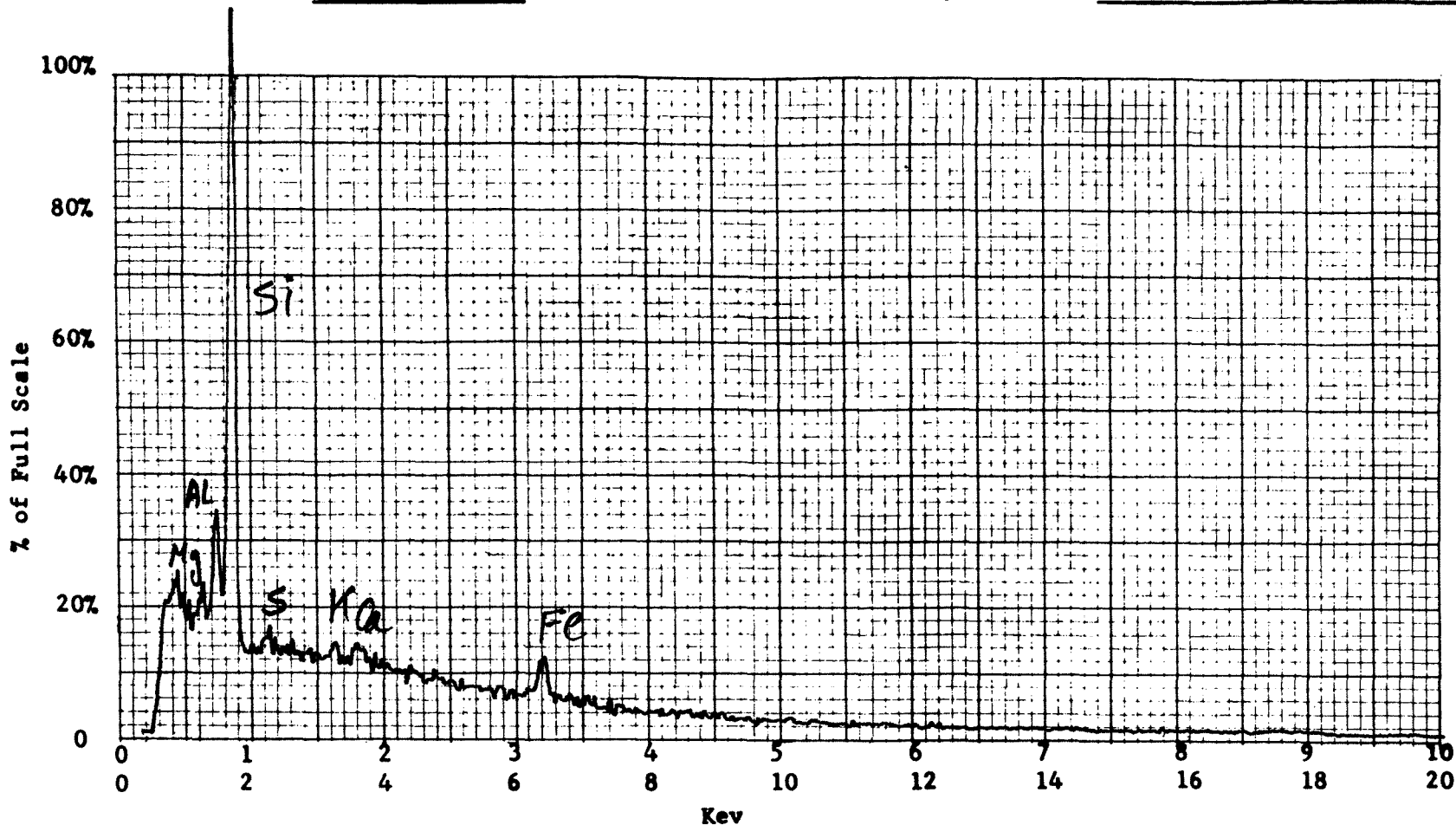
Operator \_\_\_\_\_ Date \_\_\_\_\_

Accelerating Potential 25 KeV

Total Counts Acquired 1.0 min.

Number Counts Full Scale 2K

Number of eV per channel 20



Sample peculiarities and remarks: FIGURE 55: AREA SCAN

**ENERGY DISPERSIVE X-RAY ANALYSIS**

Analytical Number Apautagite

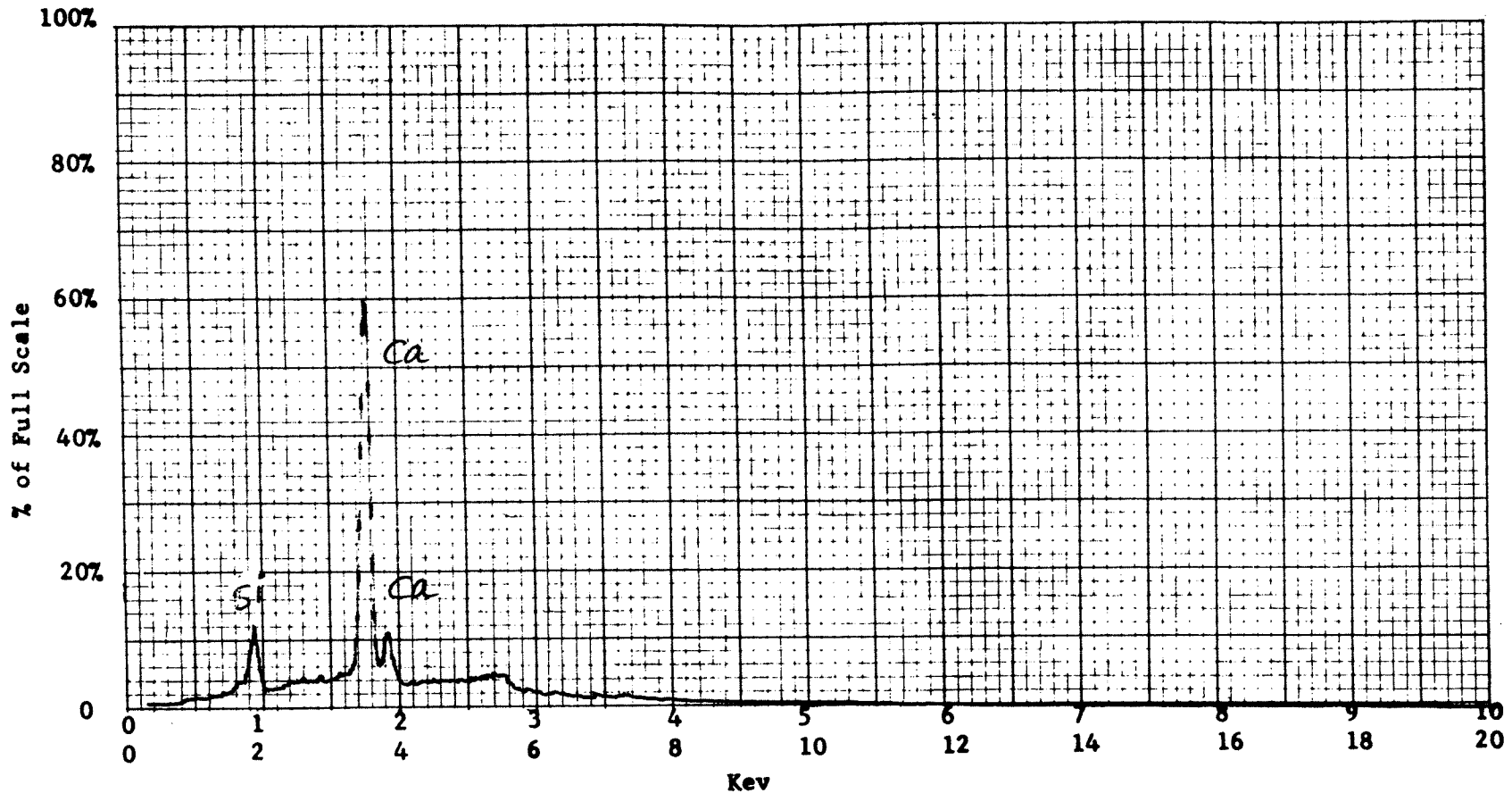
Operator \_\_\_\_\_ Date \_\_\_\_\_

Accelerating Potential 25 KeV

Total Counts Acquired 1.0 min.

Number Counts Full Scale 5K

Number of eV per channel 20



Sample peculiarities and remarks: FIGURE 56: POINT SCAN ON A HIGH Ca PARTICLE  
IN FIGURE 43

ENERGY DISPERSIVE X-RAY ANALYSIS

Analytical Number Apautagite

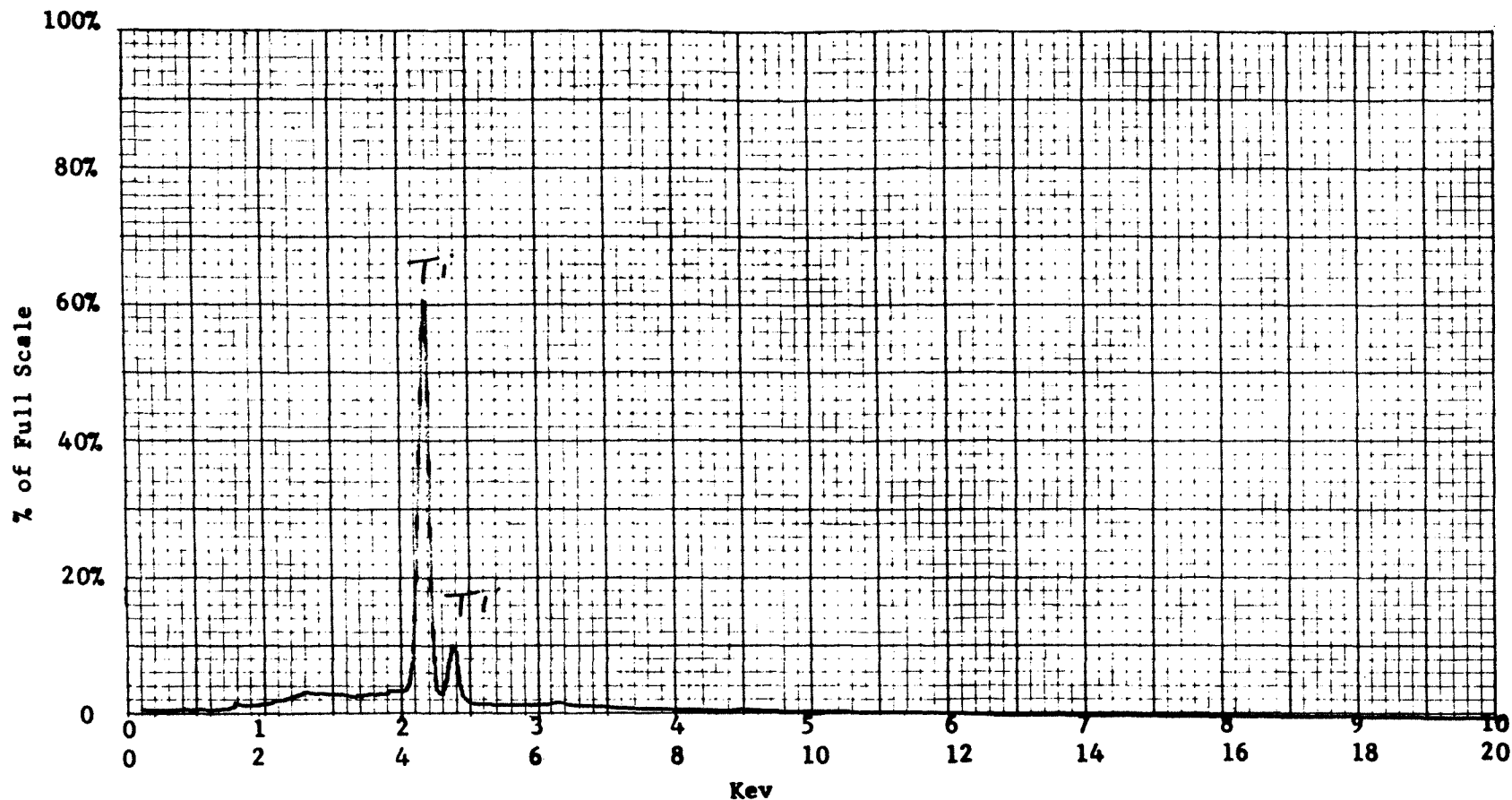
Operator \_\_\_\_\_ Date \_\_\_\_\_

Accelerating Potential 25 KeV

Total Counts Acquired 1.0 min.

Number Counts Full Scale 10K

Number of eV per channel 20



Sample peculiarities and remarks: FIGURE 57: POINT SCAN ON A HIGH Ti PARTICLE  
IN FIGURE 43

Fly Ash (Acidic):Structural Analysis:

A large percentage of the acidic fly ash particles were spherical in shape, either as individual particles or agglomerates. Small spheres ( $\approx 0.15\mu$ ) were found attached to the surfaces of larger particles. One angular particle was detected; its general shape is illustrated in Figure 77. A very small elongated particle is shown in Figures 82 and 88.

Coal fly ash is produced by burning coal; the temperature at which the coal burns will affect the shape, size and the surface structure of the particles. Also, the location of the fly ash collector in the chimney stocks will have a great effect on the size and shape. This is true because the distance the particles have to travel from the burning area to where the collector is located has a great effect on the cooling rate which in turn affects the size, shape and the surface structures of the particles.

SEM micrographs at 10,000X or 20,000X indicate that the surface of some elongated or spherical particles was rough. The maximum, average and minimum particle size were measured in microns ( $\mu$ ) as following:

Maximum	Average	Minimum
105.0	11.0	0.14

Elemental Composition and Distribution:

Al, Si, S, K, Ca, Ti and Fe make up the bulk of the sample. For example, Figures 90 and 97 illustrate the



general elemental distribution. In these figures, Al and Si are present as major elements, while K, Ca, S and Ti are minor and Fe is concentrated in a few particles. This aspect of distribution is also illustrated by the area scan in the X-ray energy spectrum, Figure 148.

Figure 104 indicated that a large particle in the middle of the field (large spherical particle with several other smaller irregular and spherical particles attached) contained very high Ca levels (from the small agglomerated particles) and very high concentrations of Fe (from the large spherical particle).

The elemental distribution of particles in Figure 111 shows the presence of a few small spheres of high Ca and many others of very high Fe concentrations.

Most of the particles in Figure 118 contained high Al and Si, while the other elements were present in very low levels.

A large spherical particle with a rough surface, see Figure 125, was found to contain very high concentrations of Ca and S; the distribution of these elements is shown in the X-ray images, Figure 128 for S and 130 for Ca. See also X-ray energy spectrum, Figure 149.

In the middle of Figure 133 a particle of very high Ca (possible Ca oxide or carbonate) was detected. The X-ray image, Figure 138, shows that the Ca level in this particle is very high while in the other particles the Ca concentration is very low.

Two particles of very high Fe (possible Fe oxide) and one particle of Ti (possible Ti oxide) were observed in Figure 141. X-ray images, Figures 146 and 147, illustrate the distribution of Ti and Fe throughout this field. X-ray energy spectrum, Figure 150, illustrates the relative intensity of Ti by using the point scan technique on a high Ti concentration particle.

SEM IMAGES OF SAMPLE #

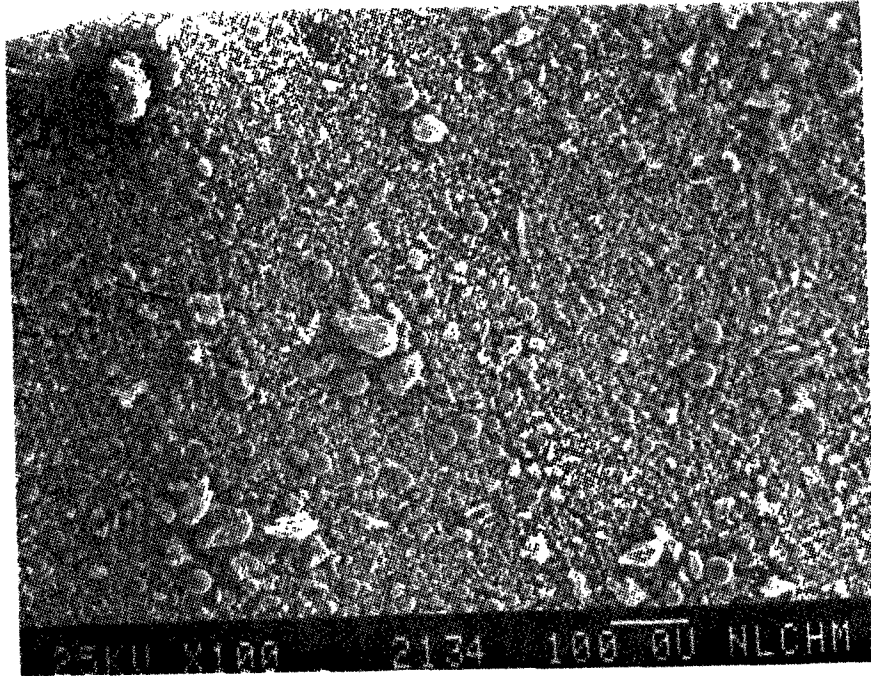


Figure 58

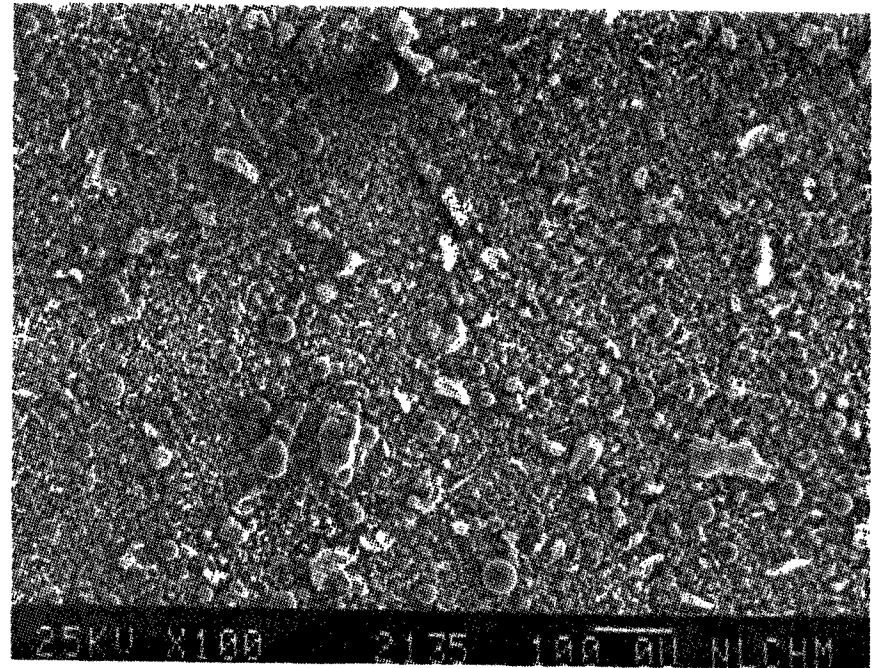


Figure 59

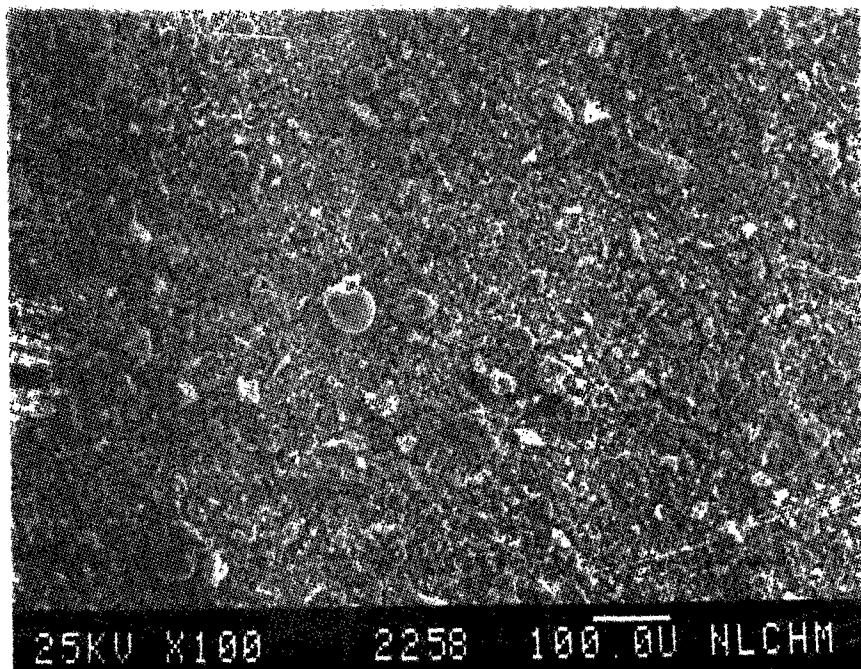


Figure 60

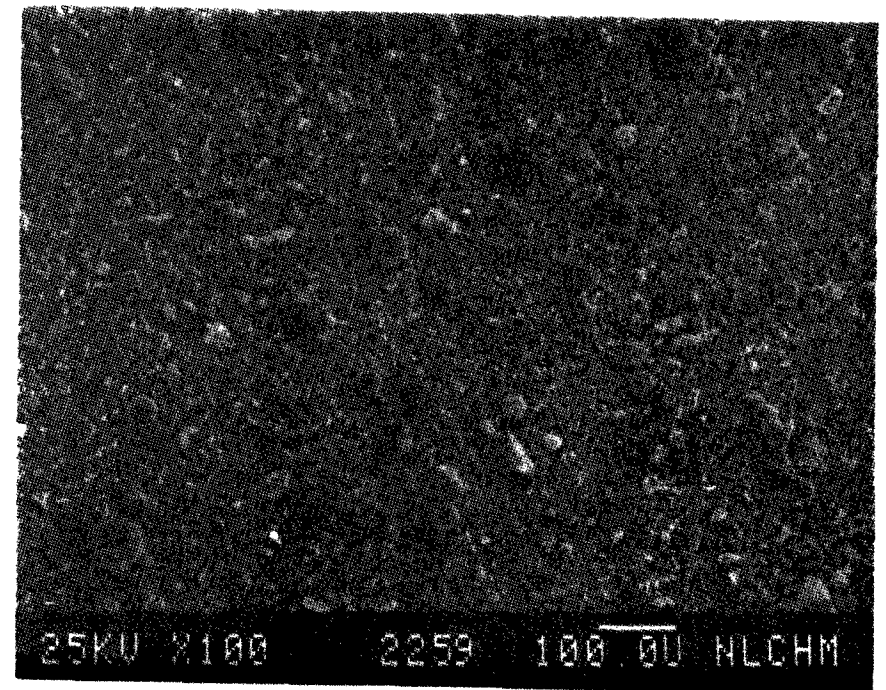


Figure 61

SEM IMAGES OF SAMPLE #

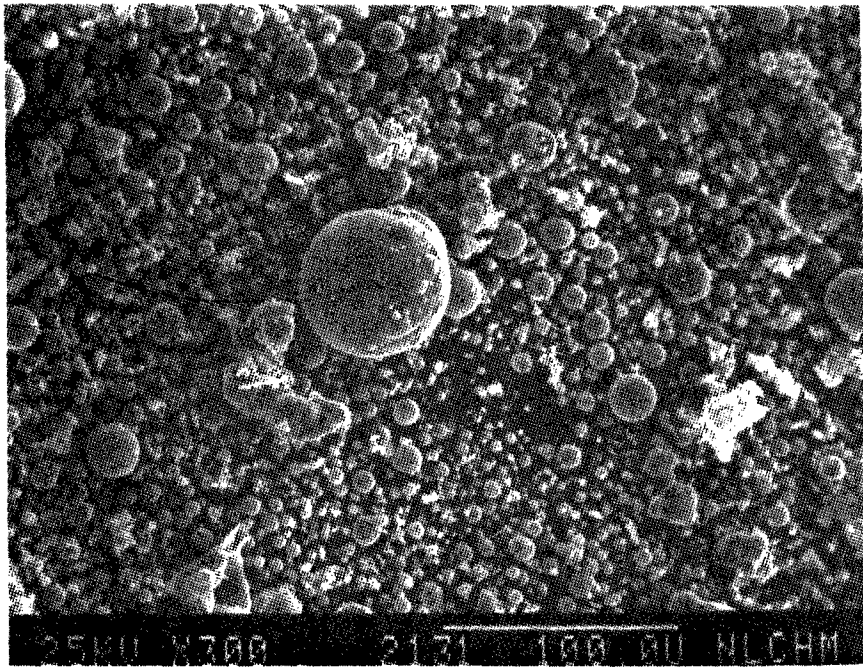


Figure 62

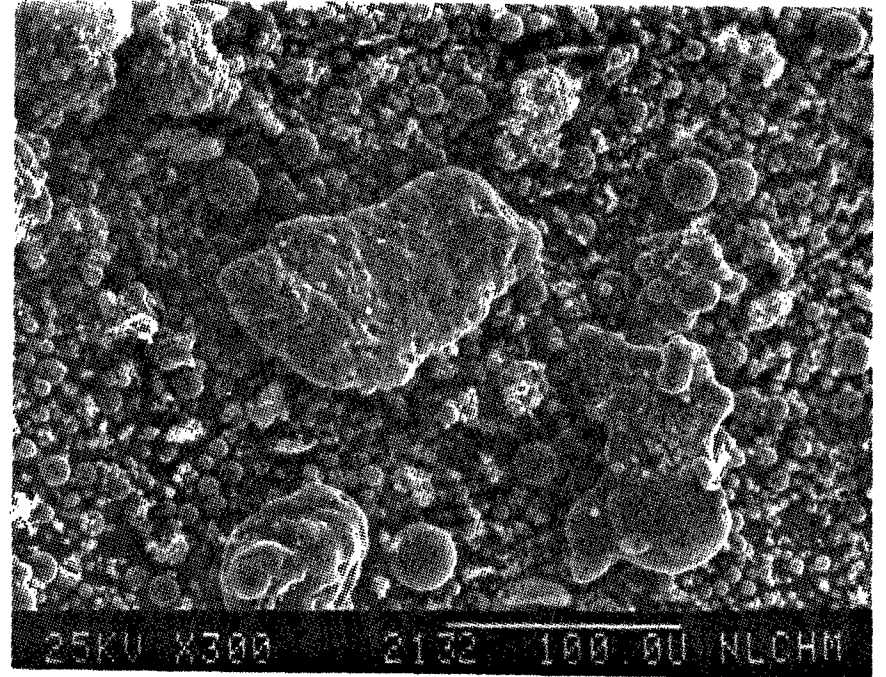


Figure 63

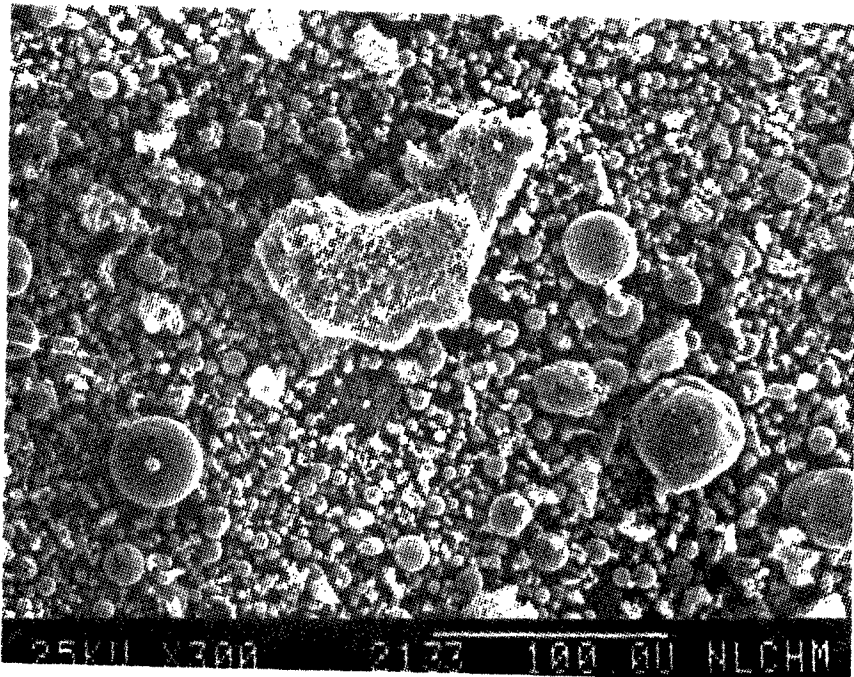


Figure 64

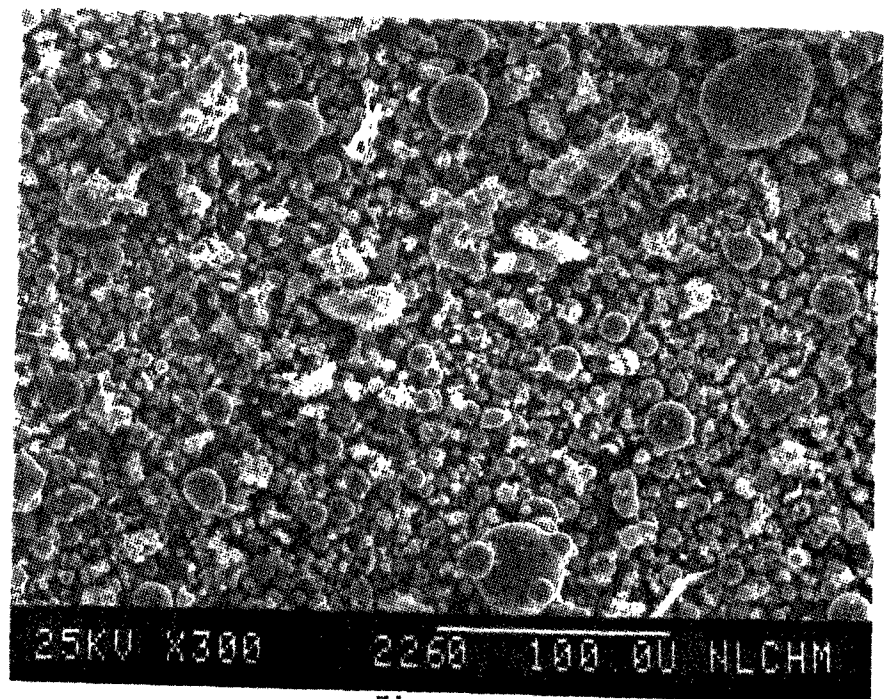


Figure 65



SEM IMAGES OF SAMPLE #

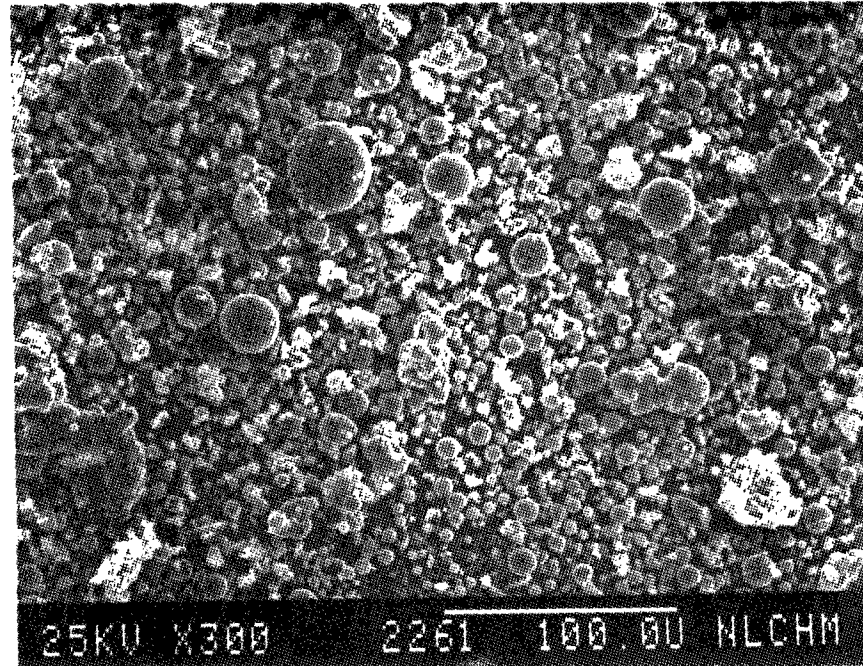


Figure 66

SEM IMAGES OF SAMPLE #

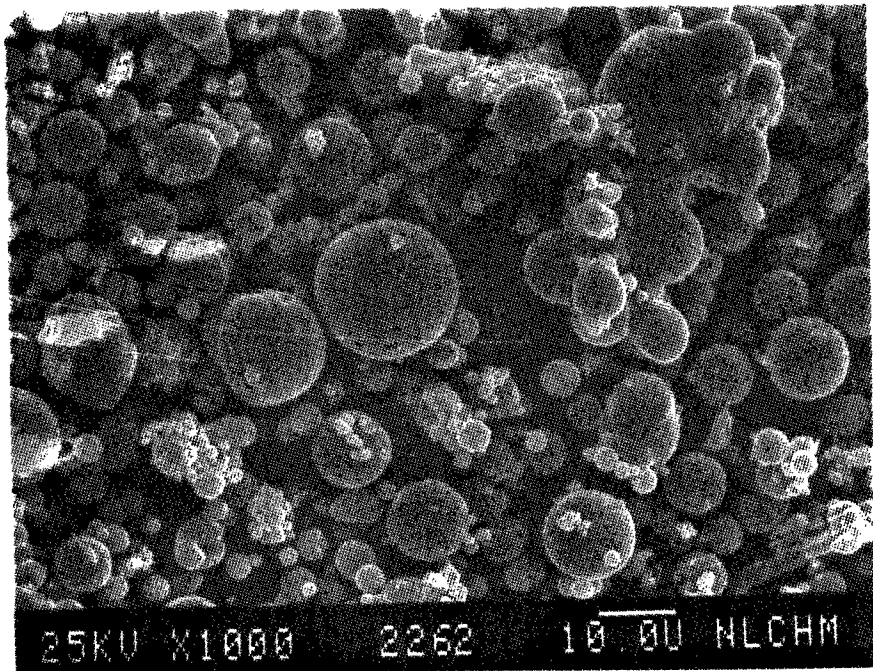


Figure 67

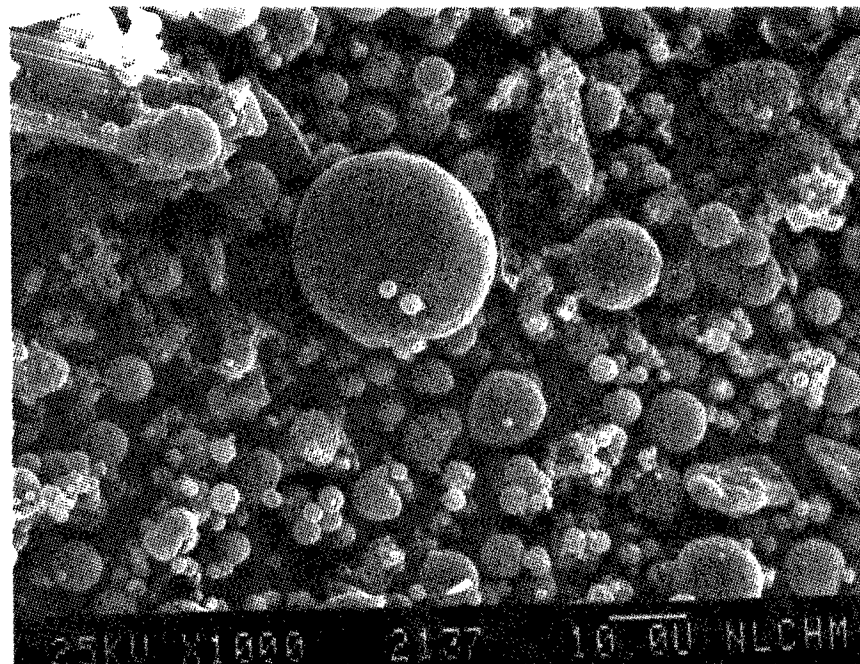


Figure 68

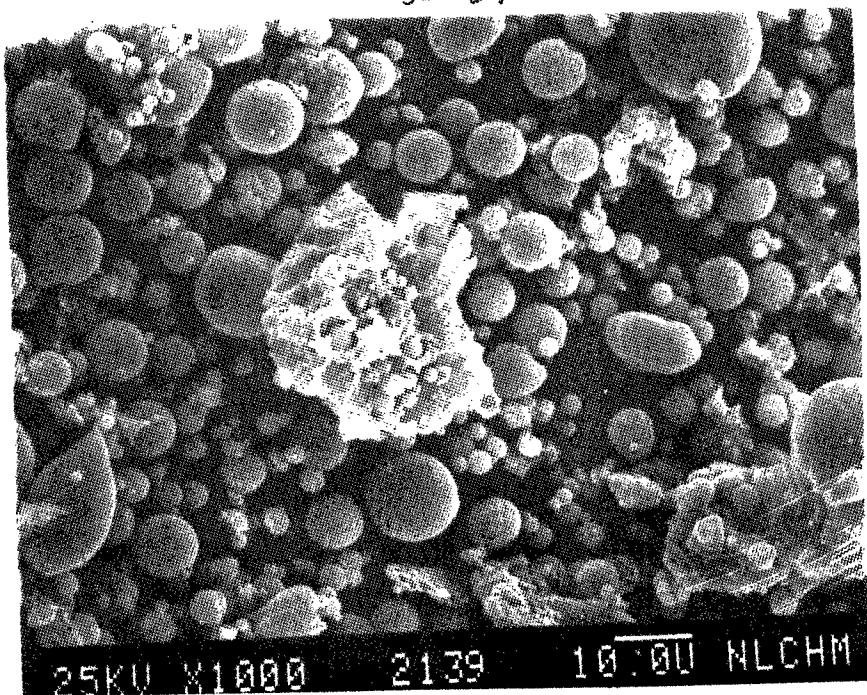


Figure 69

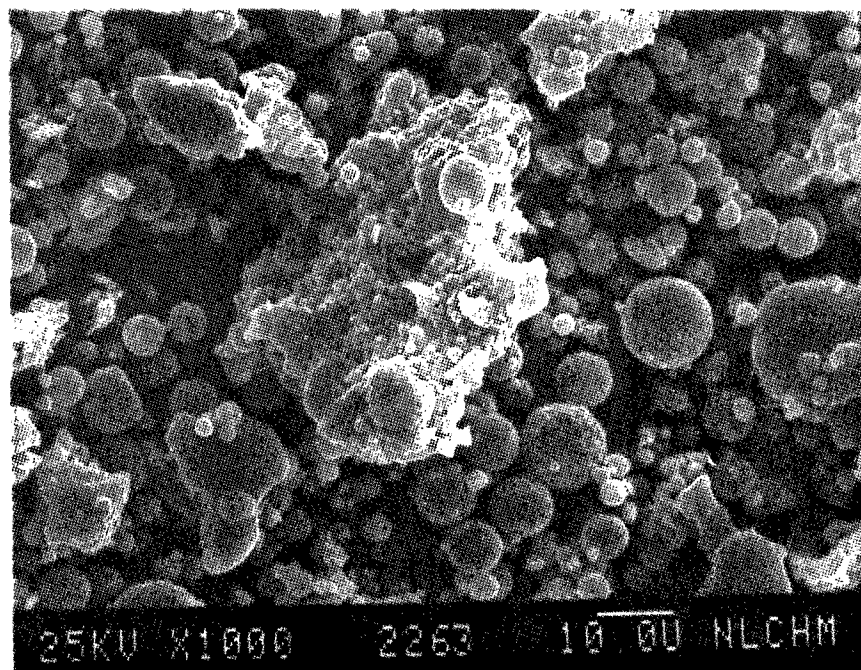


Figure 70

SEM IMAGES OF SAMPLE #

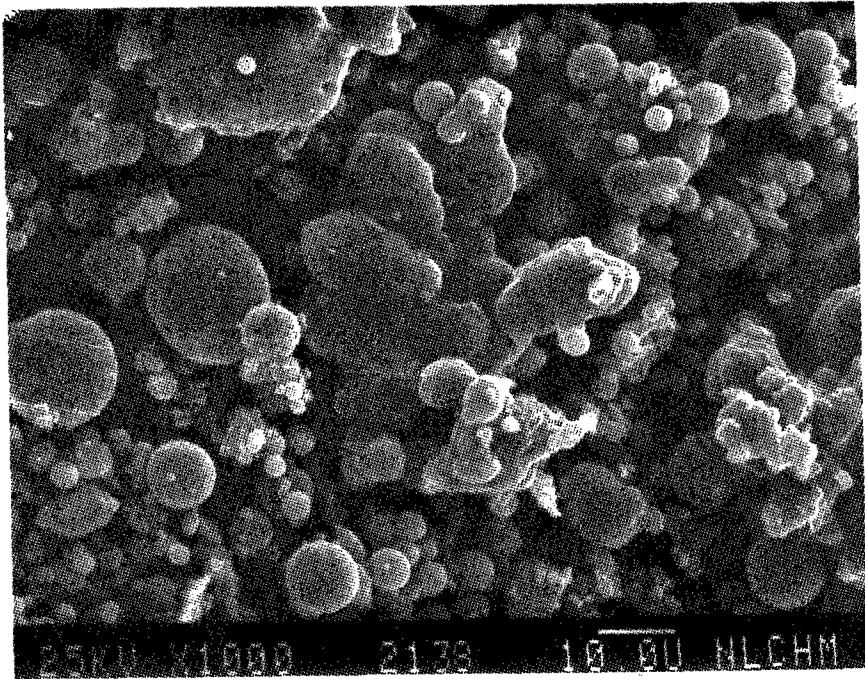


Figure 71

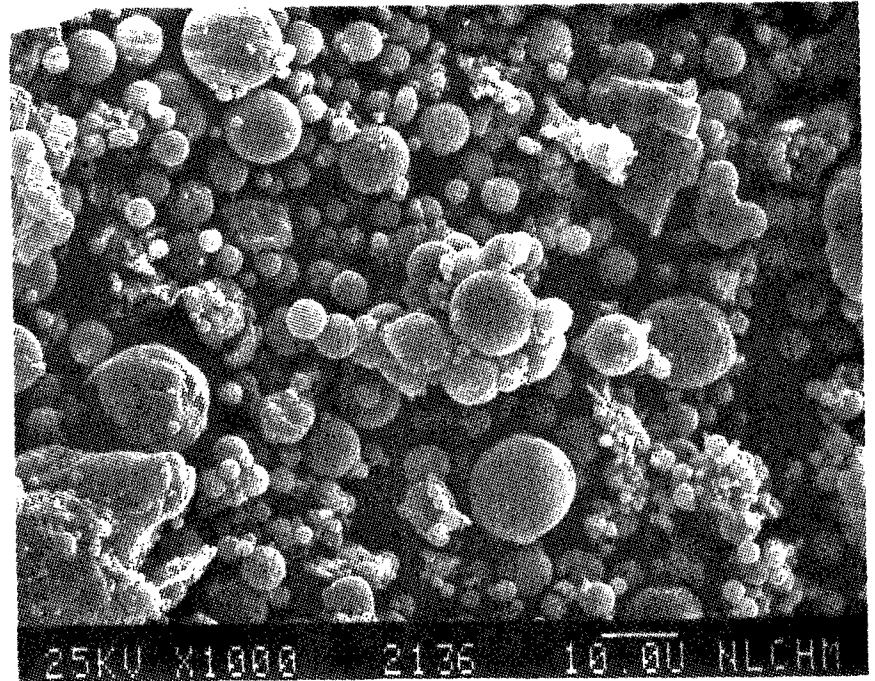


Figure 72



SEM IMAGES OF SAMPLE #

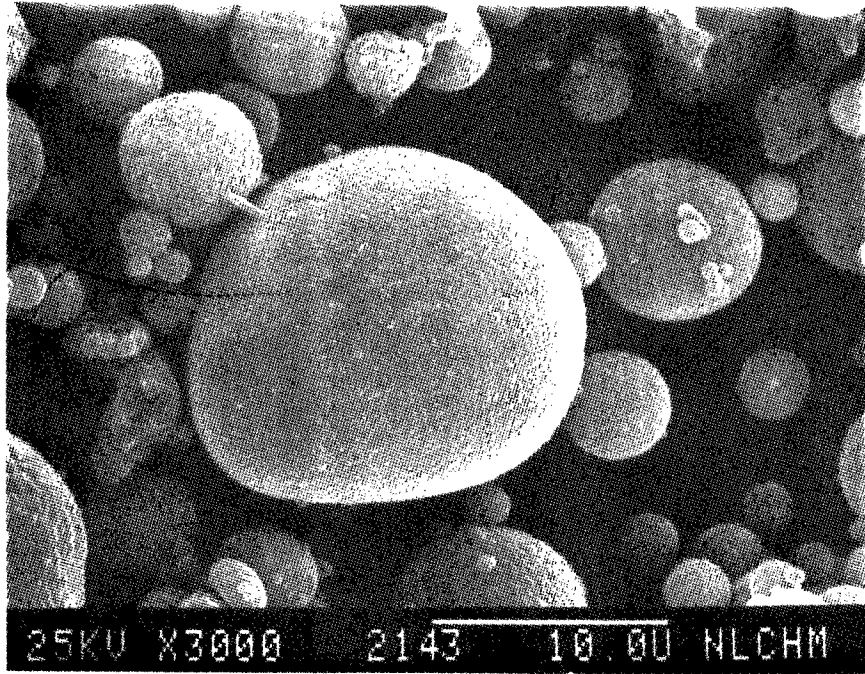


Figure 73

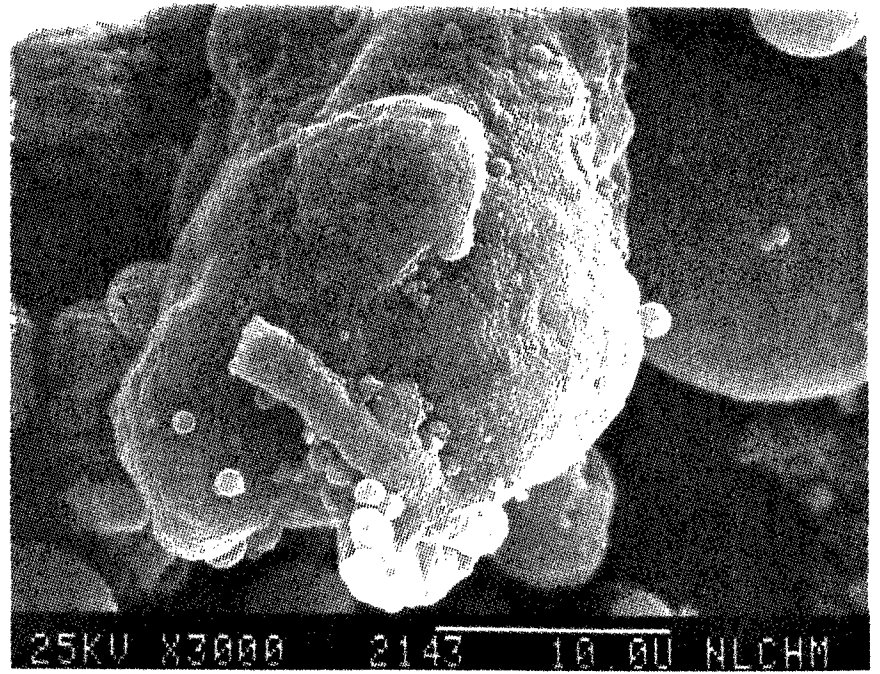


Figure 74

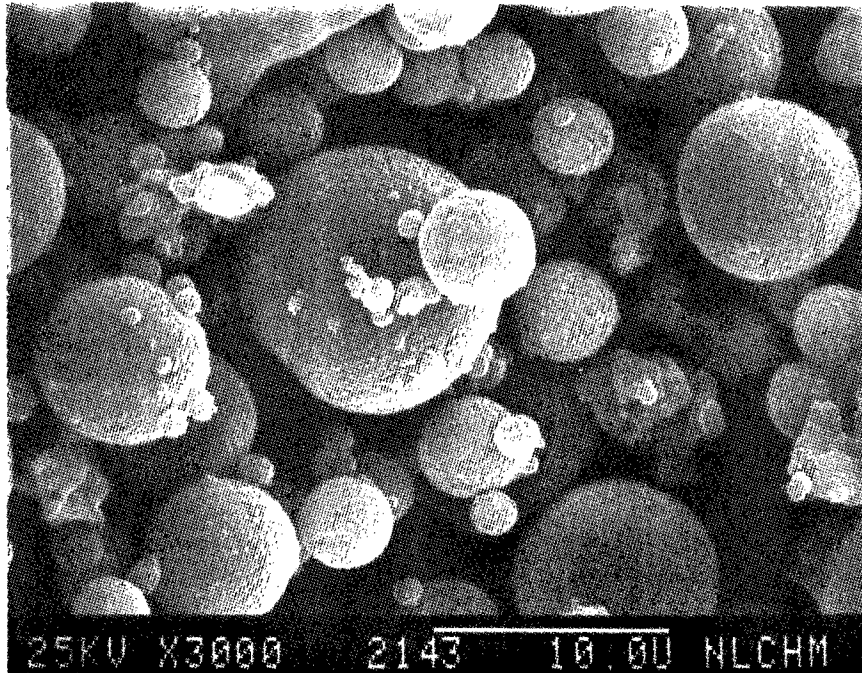


Figure 75

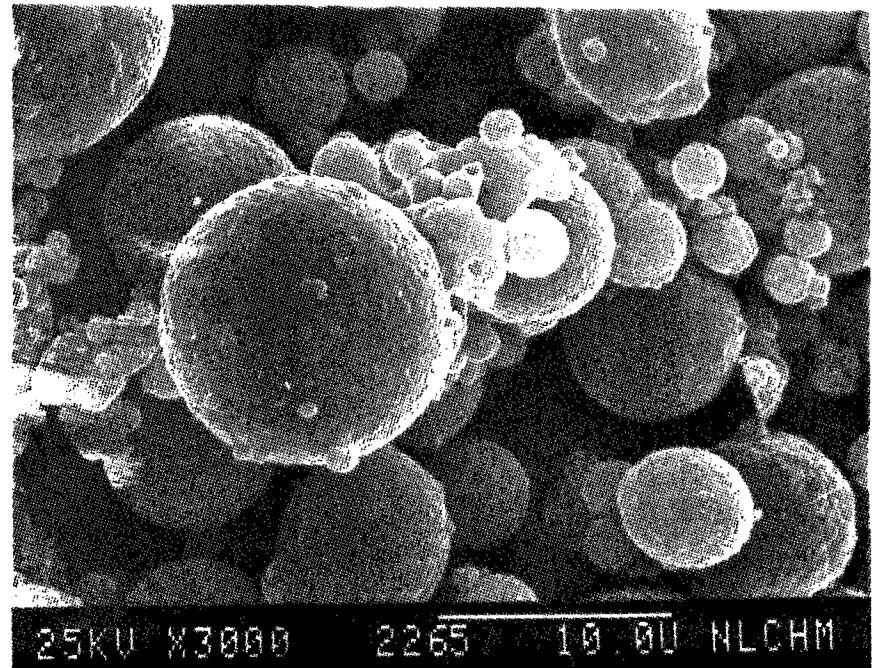


Figure 76



SEM IMAGES OF SAMPLE #

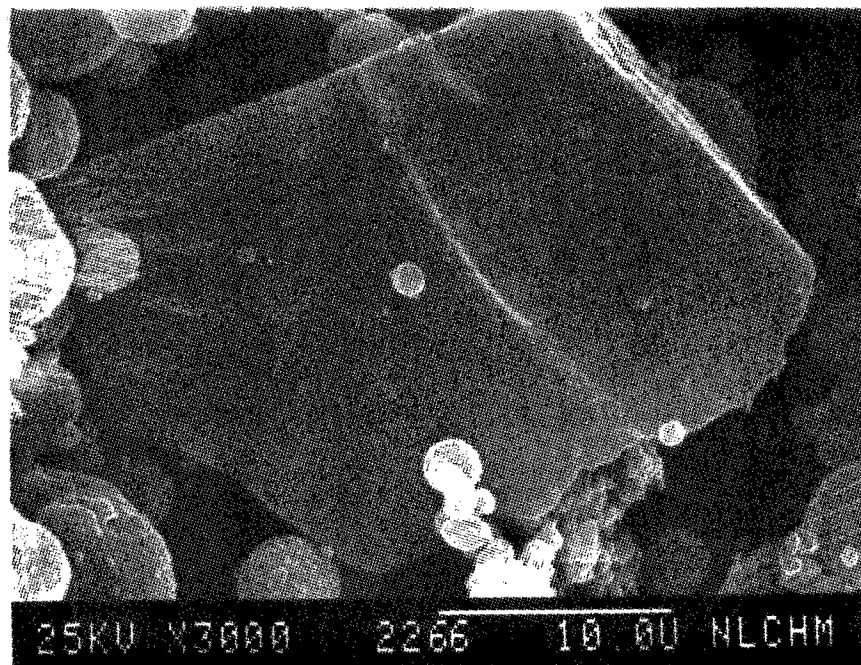


Figure 77

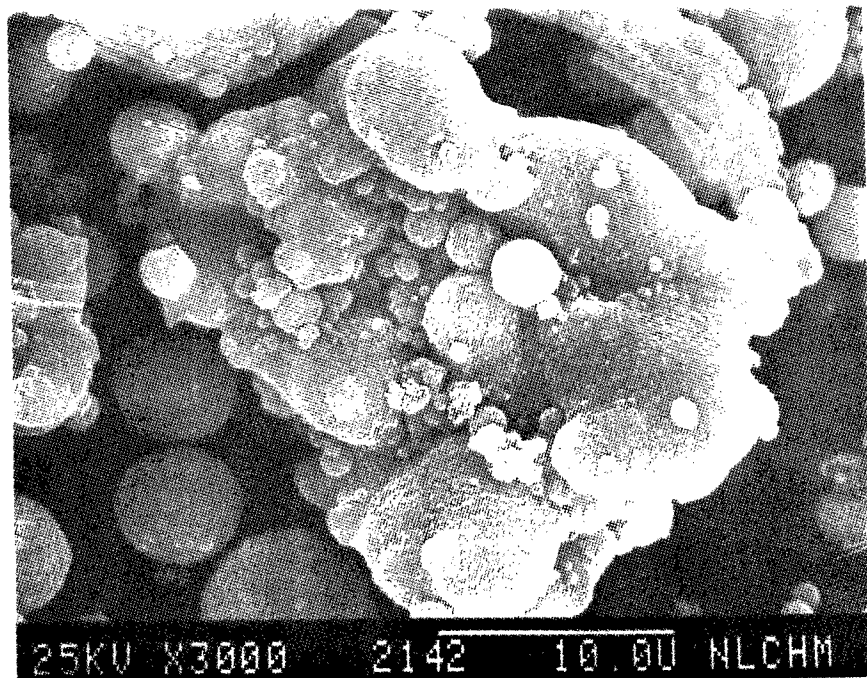


Figure 78

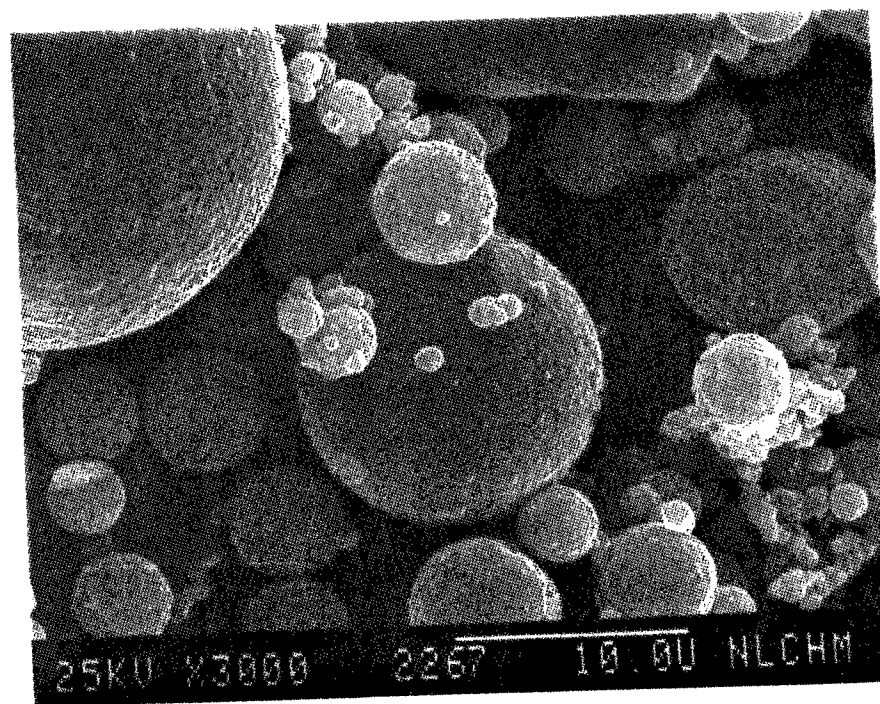


Figure 79

SEM IMAGES OF SAMPLE #

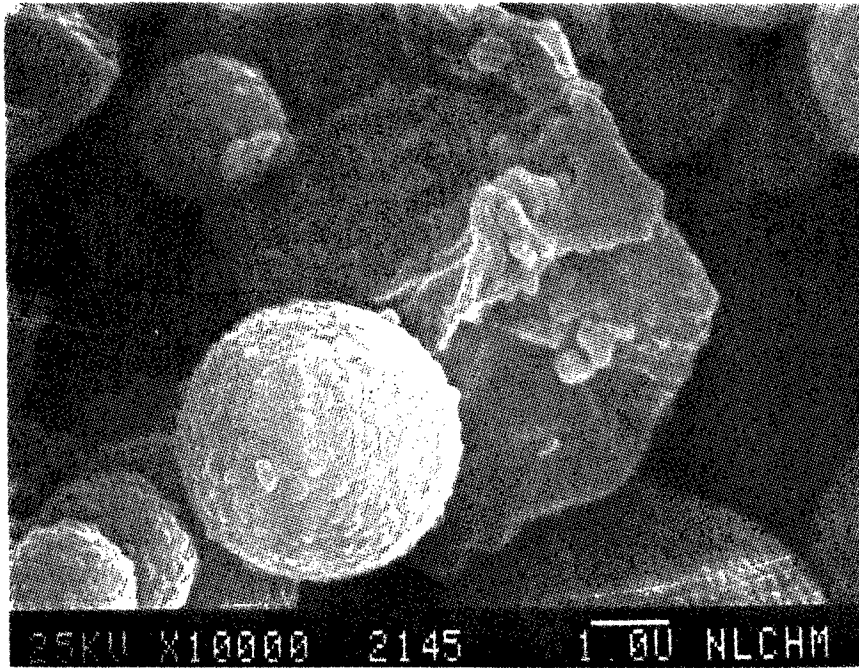


Figure 80

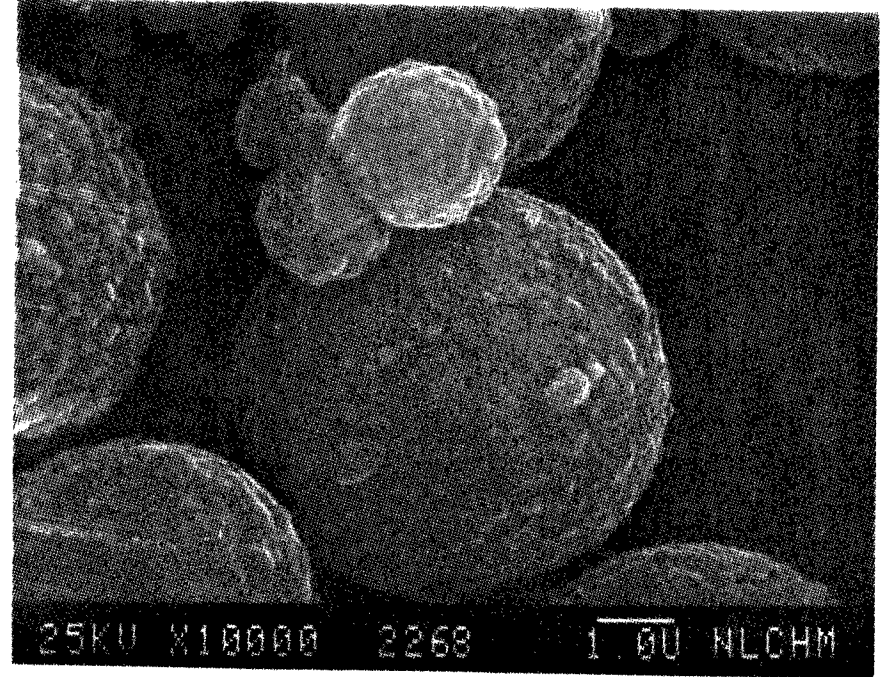


Figure 81

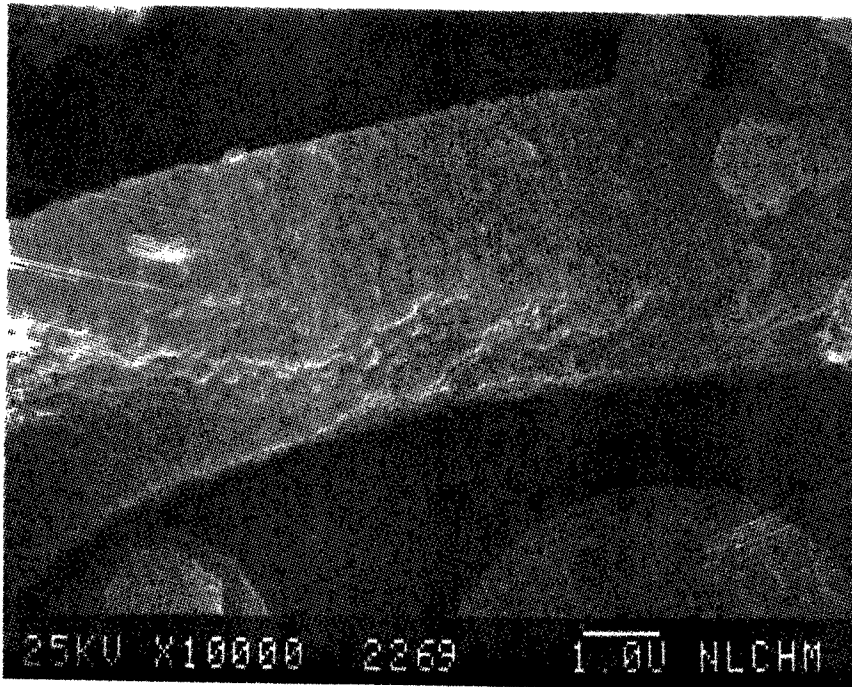


Figure 82

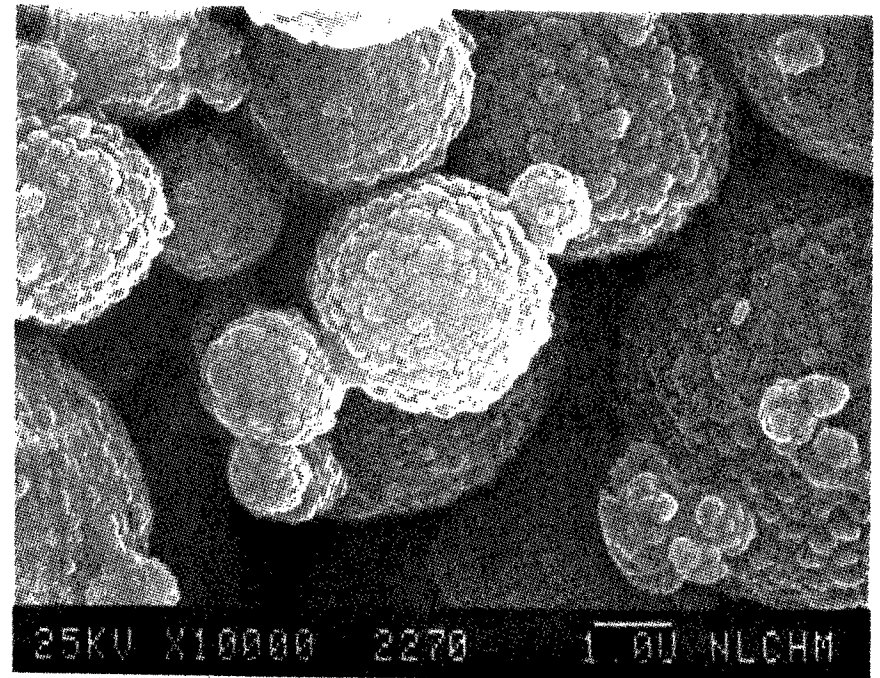


Figure 83



SEM IMAGES OF SAMPLE #

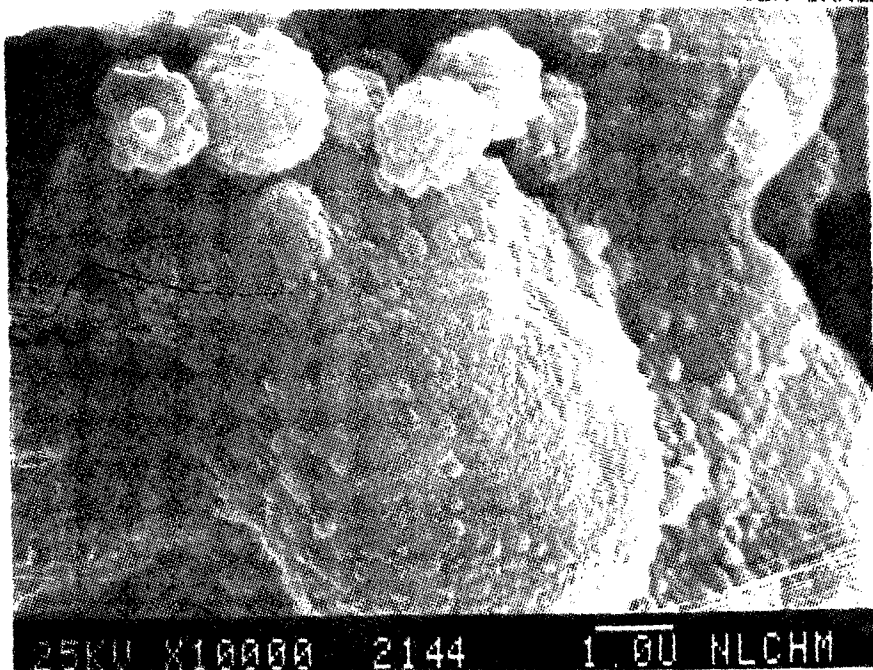


Figure 84

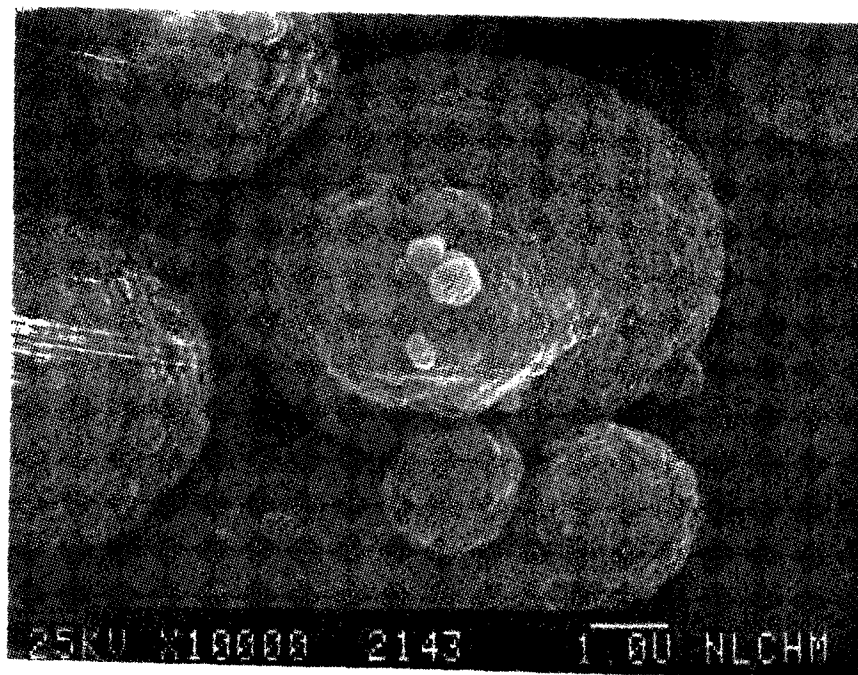


Figure 85

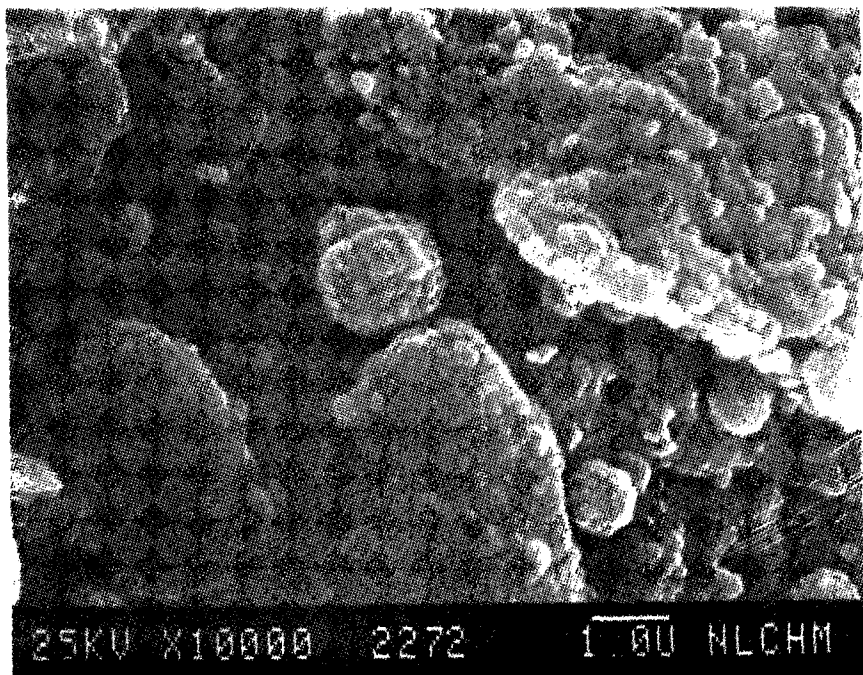


Figure 86

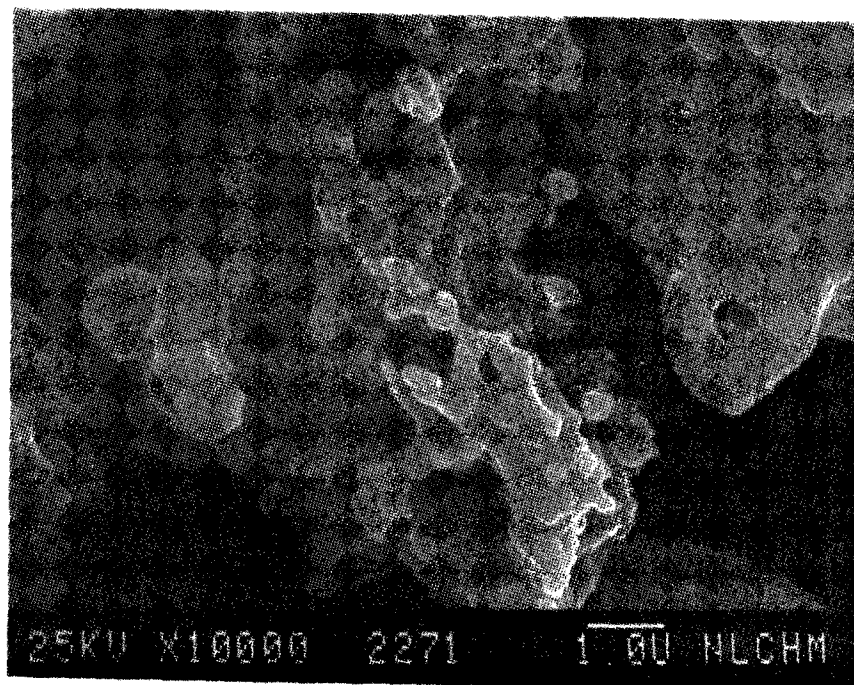


Figure 87

SEM IMAGES OF SAMPLE #

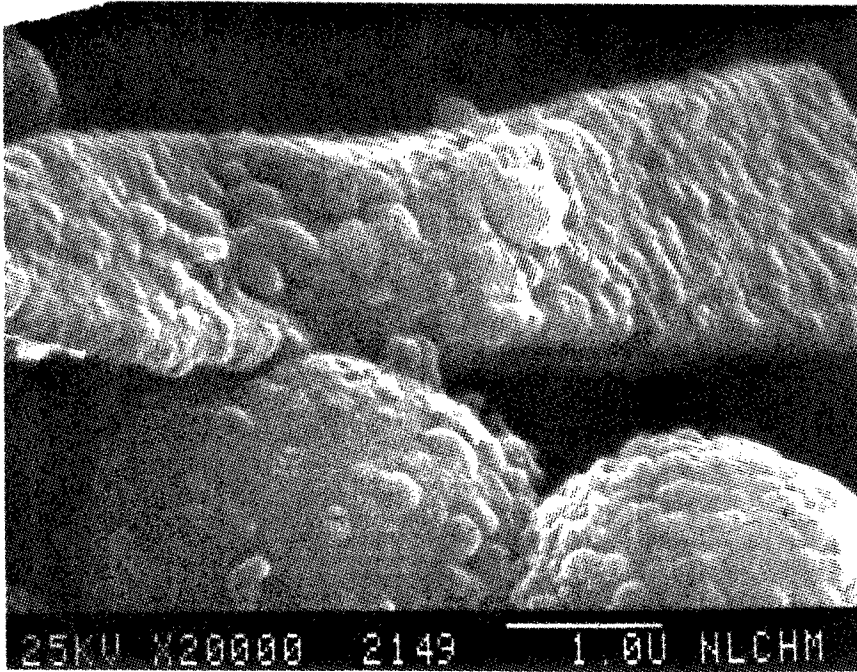


Figure 88

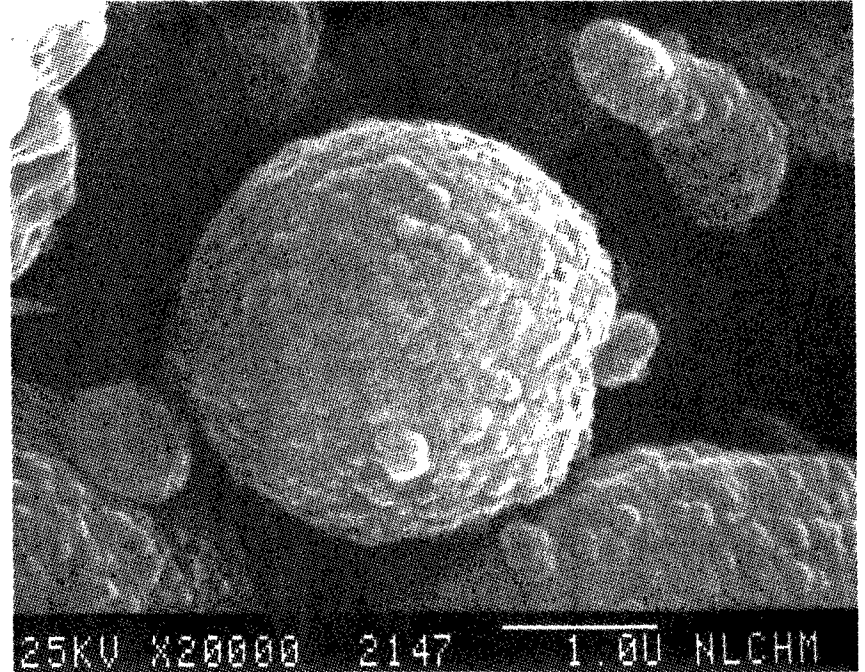


Figure 89

SEM IMAGES OF SAMPLE #

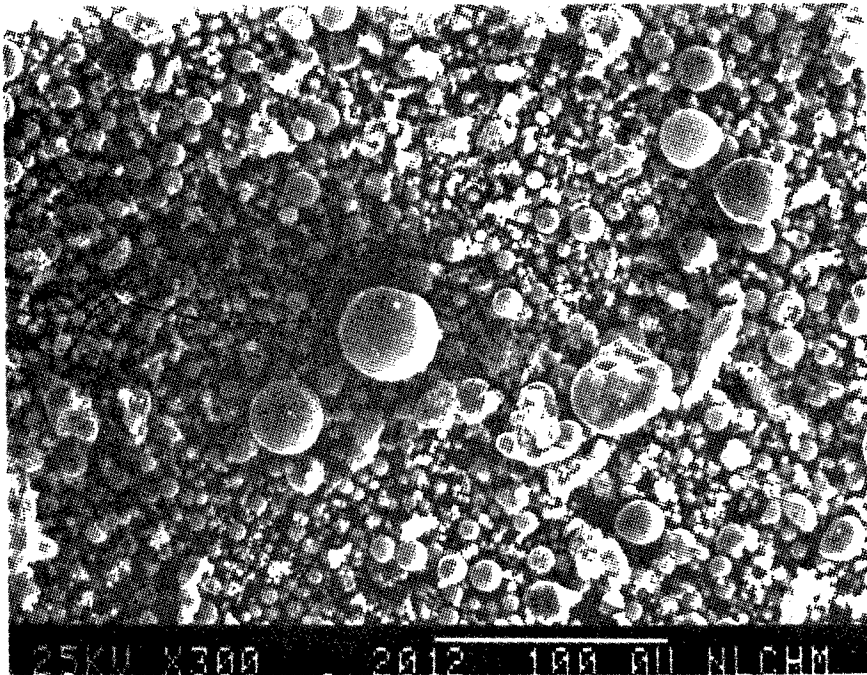


Figure 90

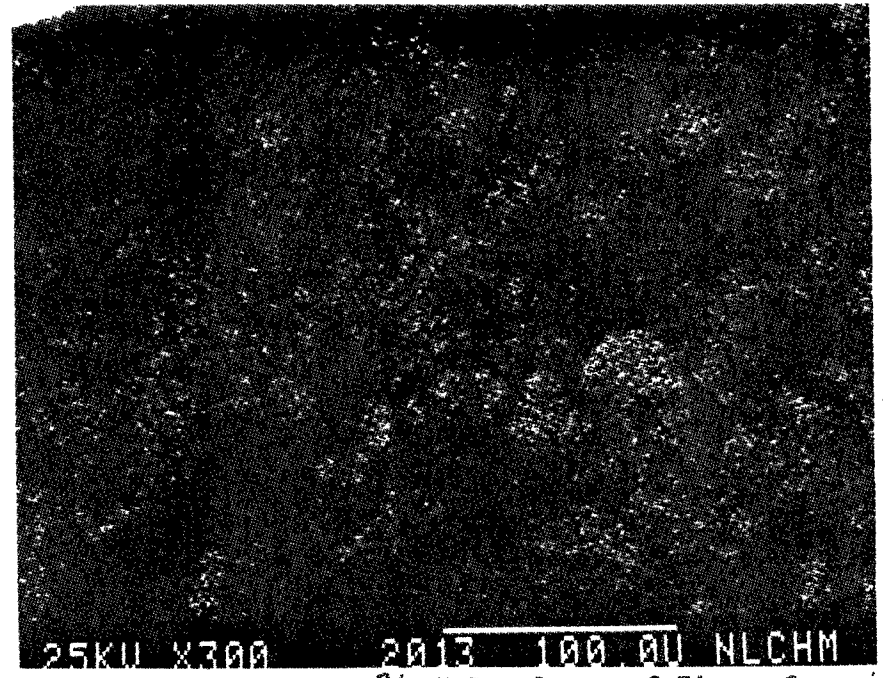


Figure 91

AL X-Ray Image of Figure 90

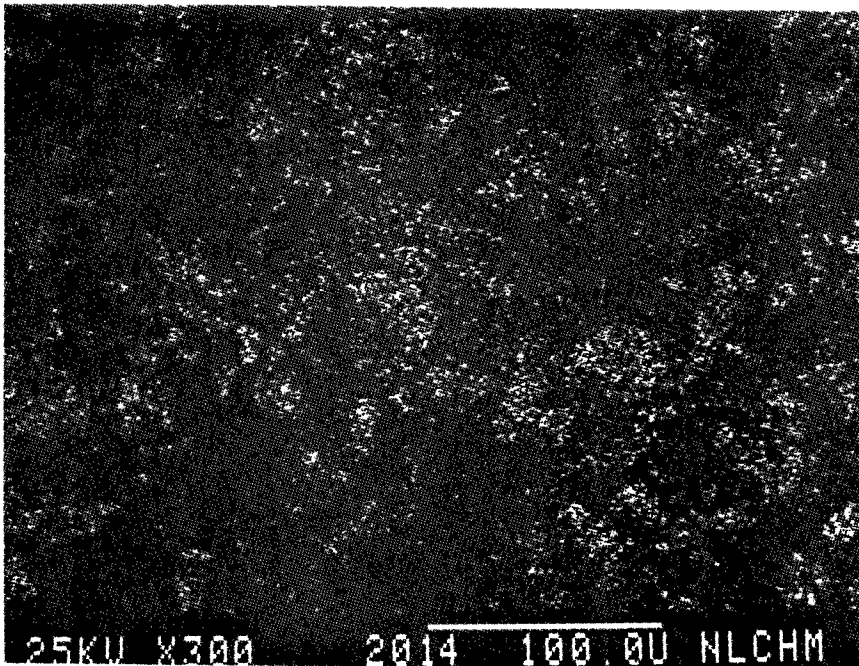


Figure 92

Si X-Ray Image of Figure 90

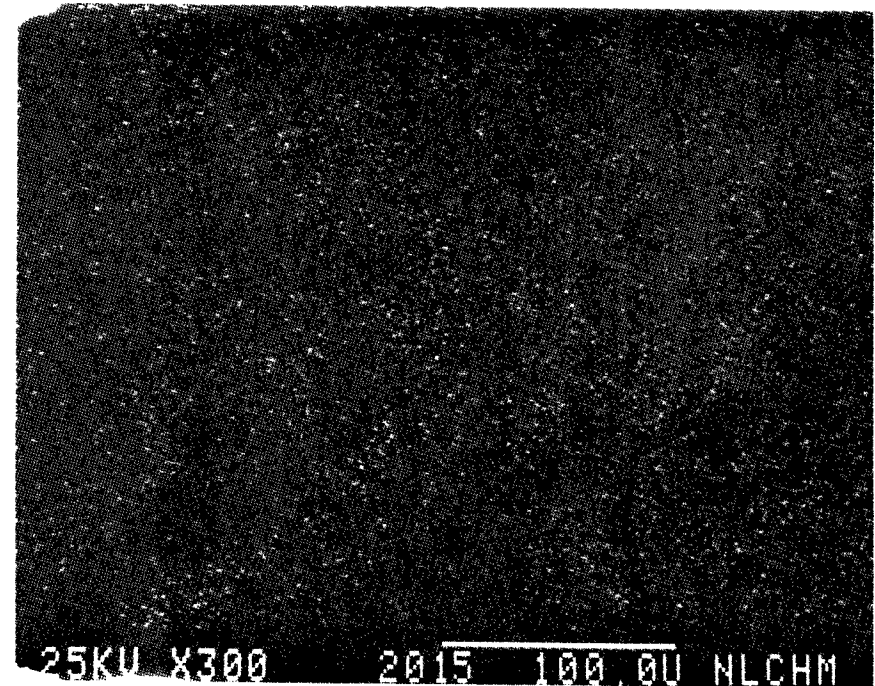


Figure 93

K X-Ray Image of Figure 90



SEM IMAGES OF SAMPLE #

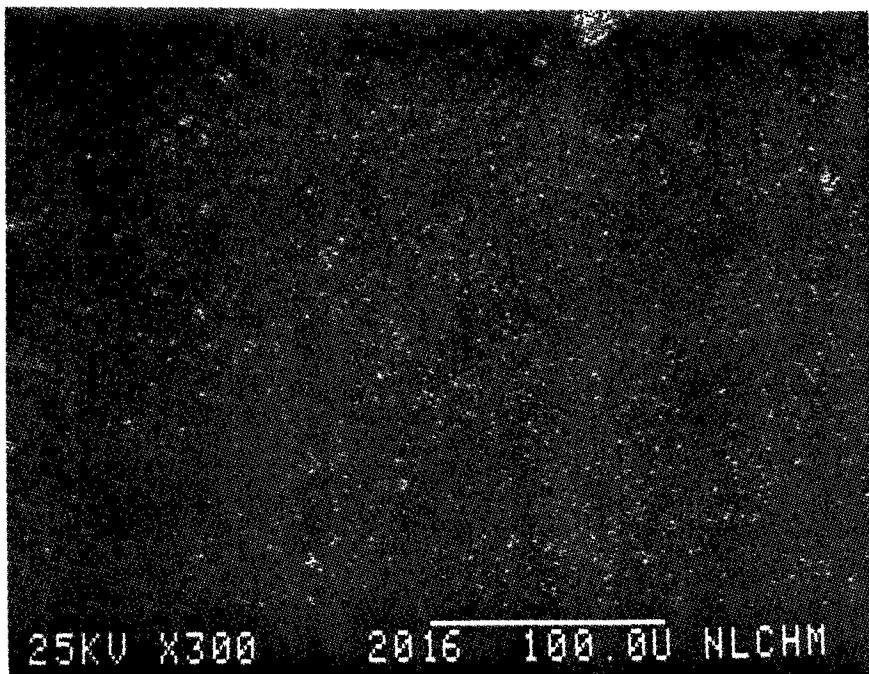


Figure 94. Ca X-Ray Image of Figure 90

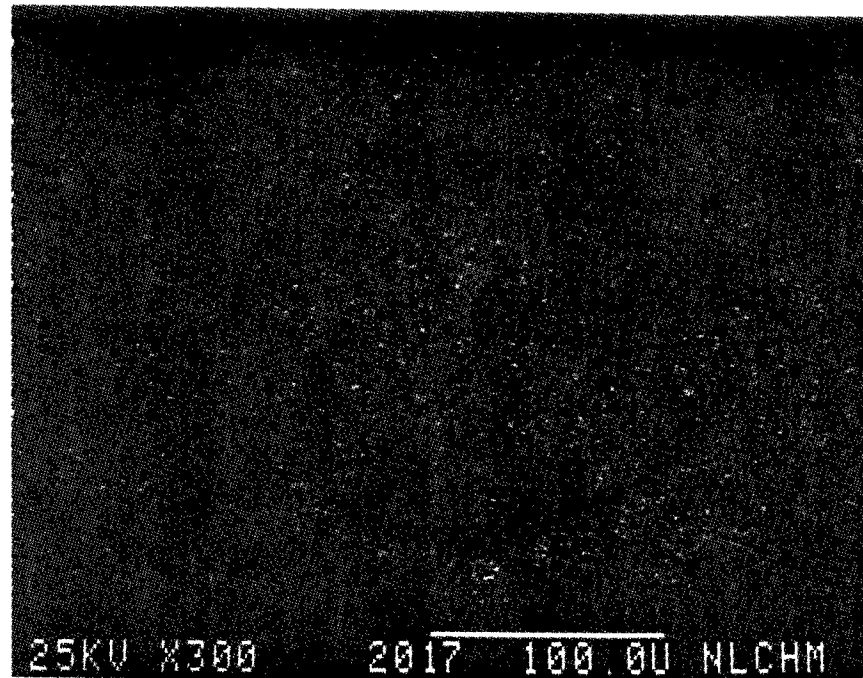


Figure 95 Ti X-Ray Image of Figure 90

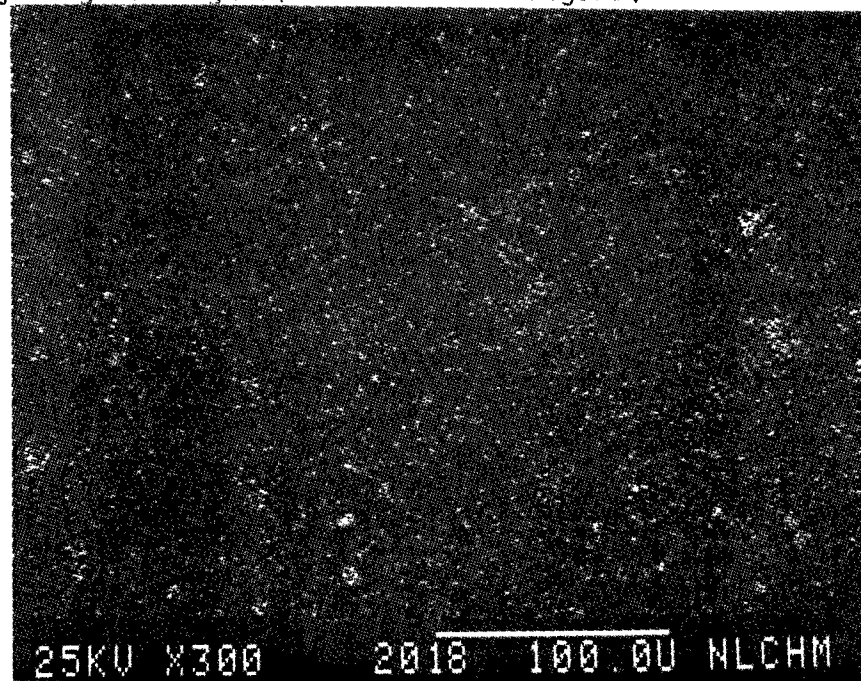


Figure 96 Fe X-Ray Image of Figure 90

SEM IMAGES OF SAMPLE #

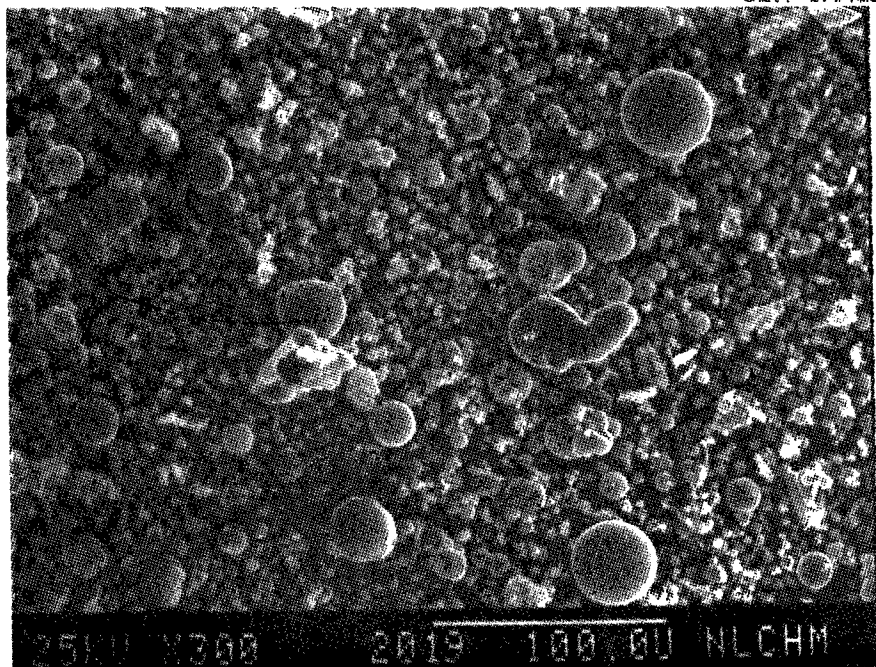


Figure 97

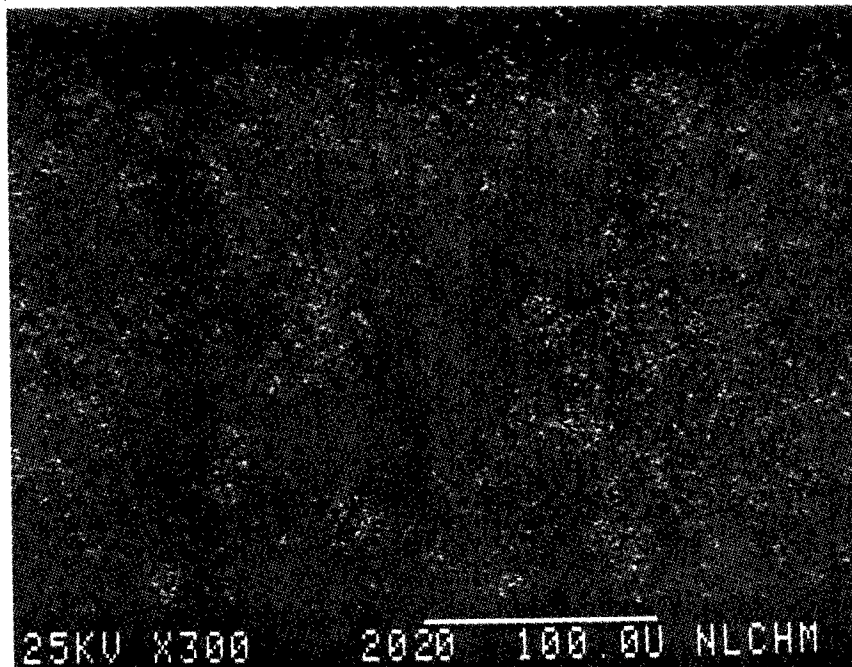


Figure 98

AL X-Ray Image of Figure 97

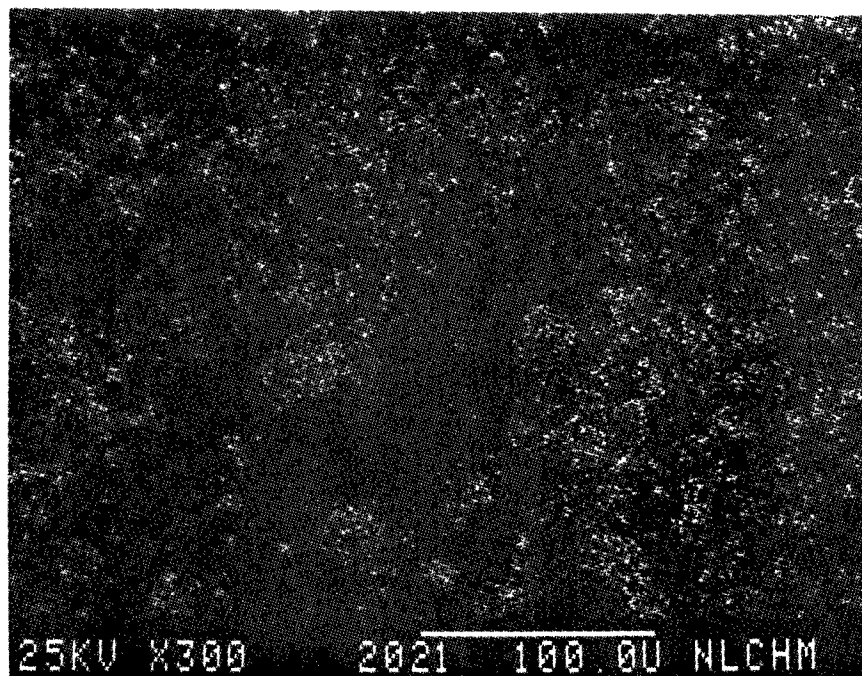


Figure 99

Si X-Ray Image of Figure 97

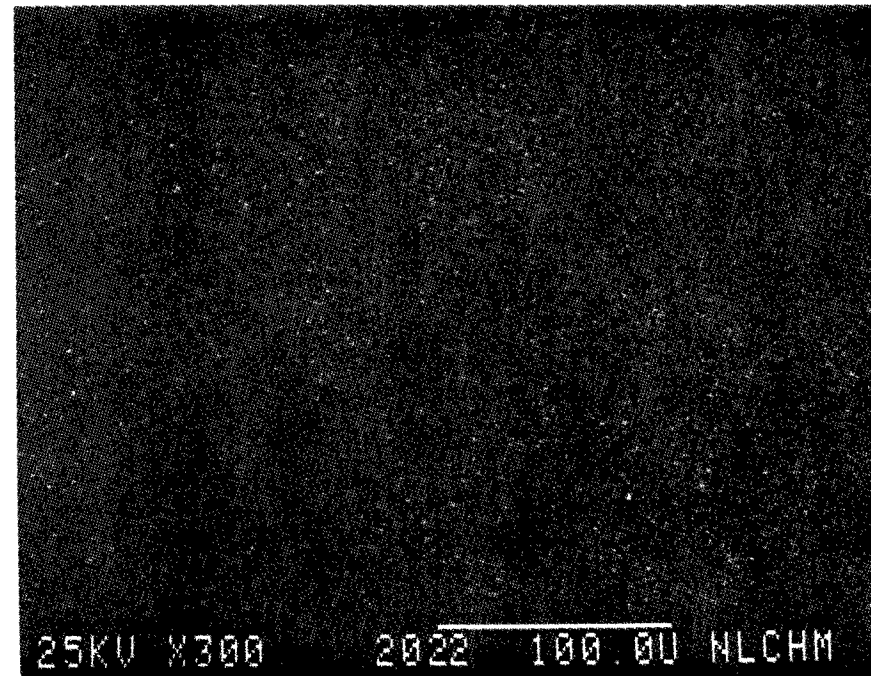


Figure 100

K X-Ray Image of Figure 97

SEM IMAGES OF SAMPLE #

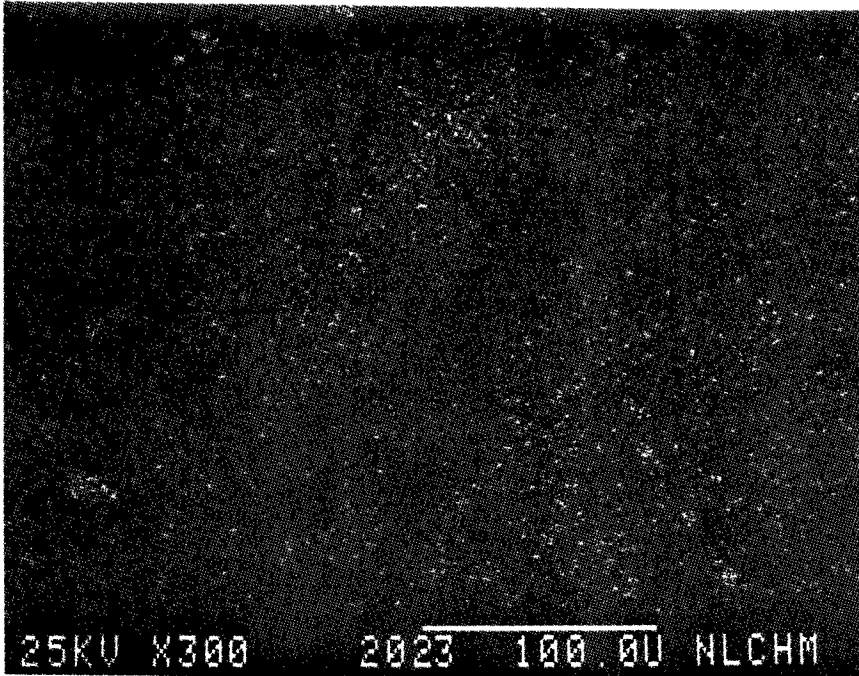


Figure 101

Ca X-Ray Image of Figure 97

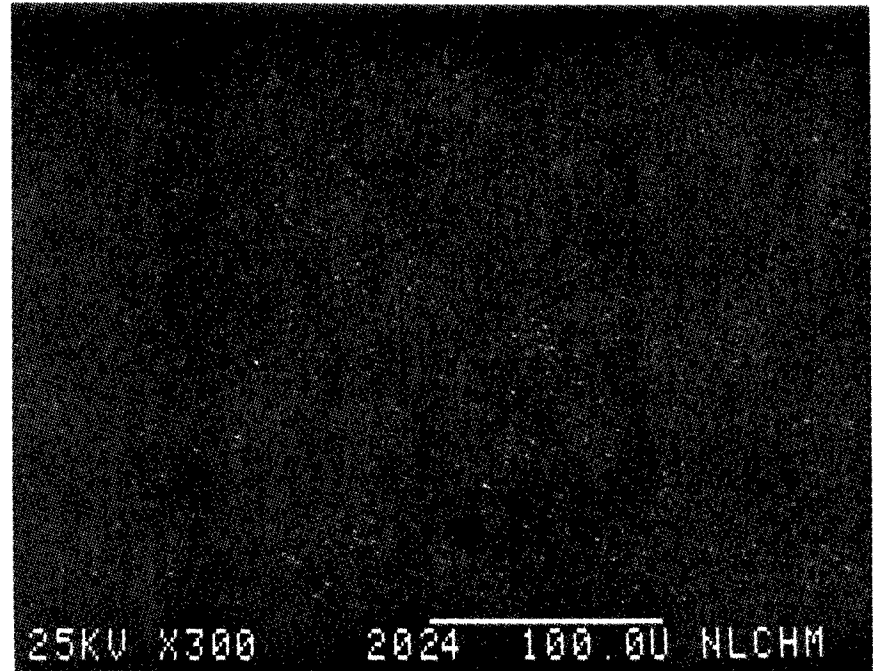


Figure 102

Ti X-Ray Image of Figure 97

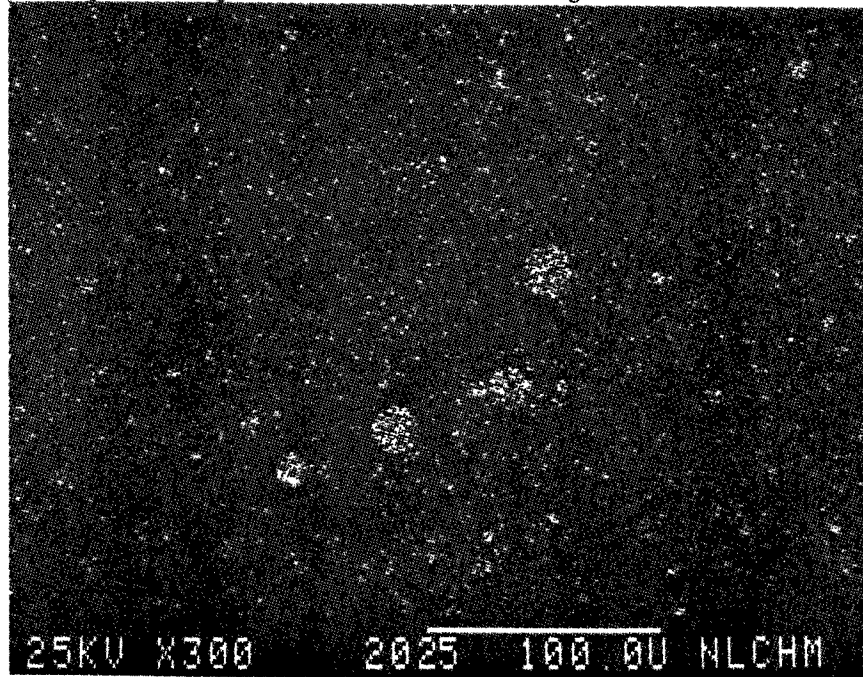


Figure 103

Fe X-Ray Image of Figure 97



SEM IMAGES OF SAMPLE #

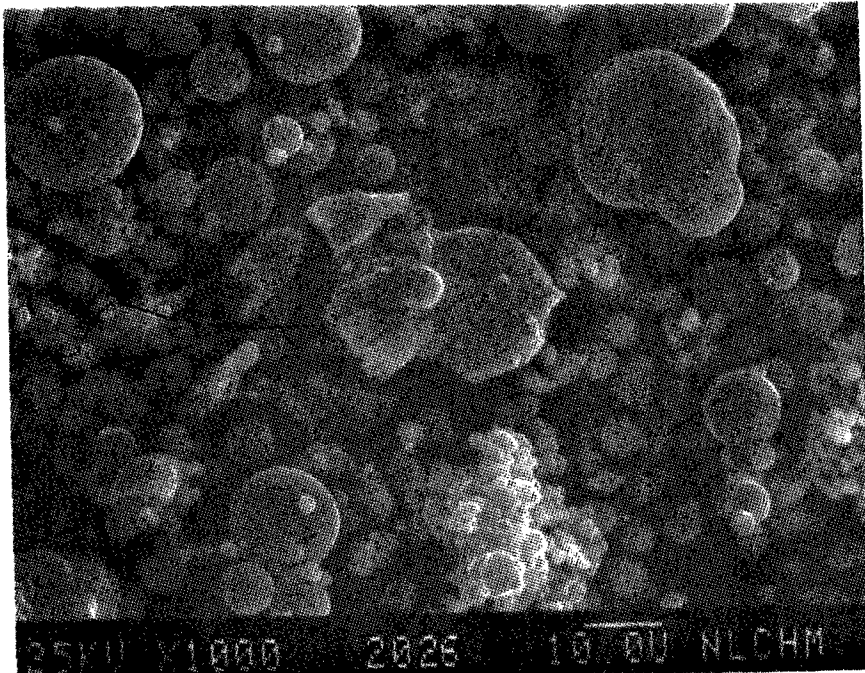


Figure 104

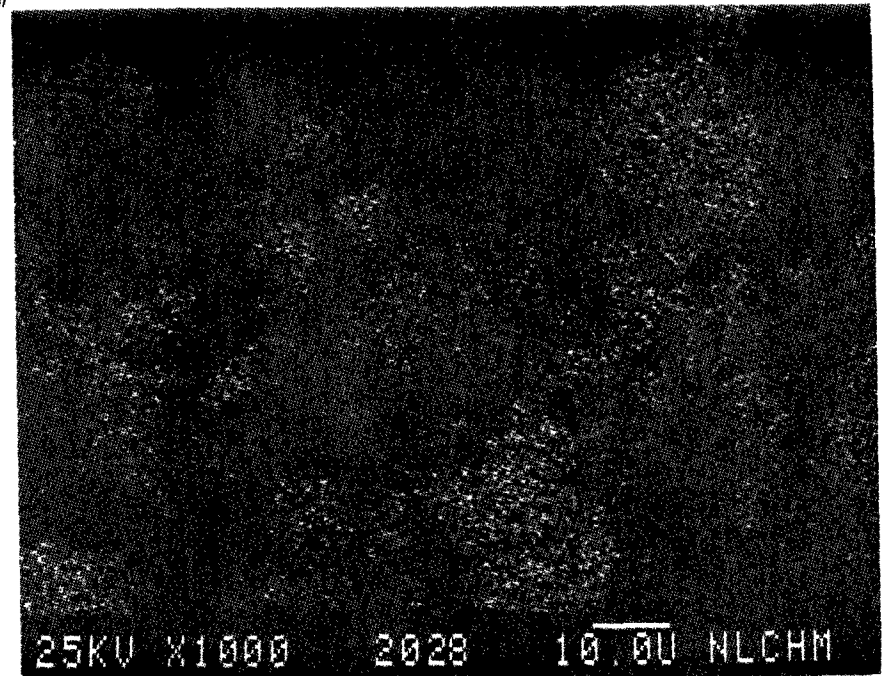


Figure 105

AL X-Ray Image of Figure 104

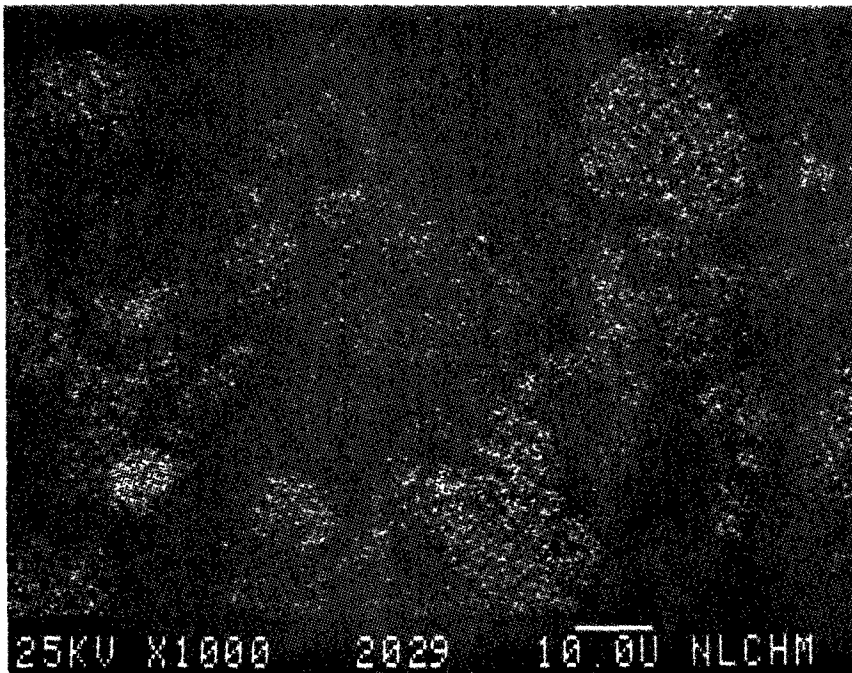


Figure 106

Si X-Ray Image of Figure 104

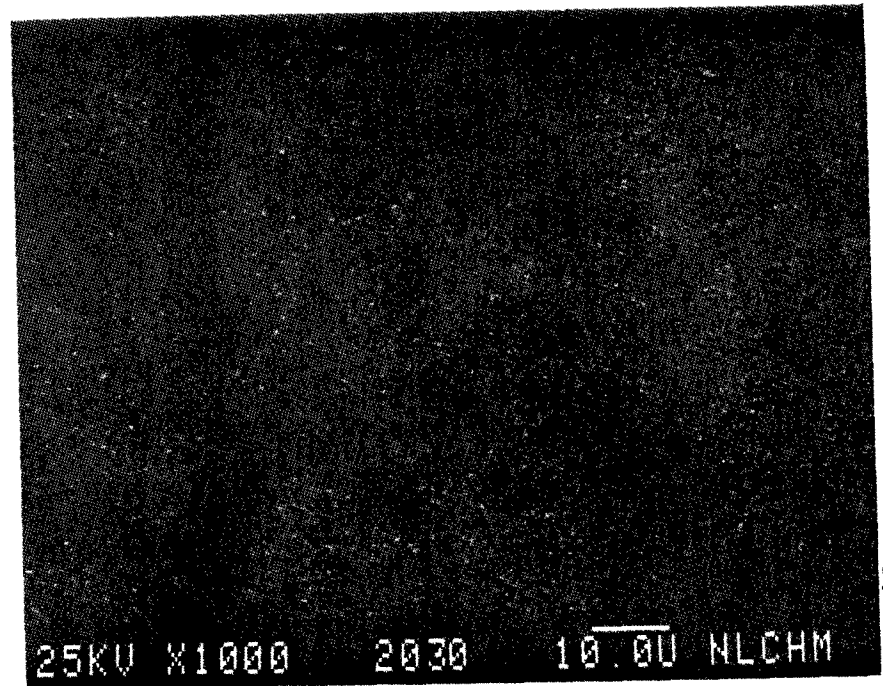


Figure 107

K X-Ray Image of Figure 104

SEM IMAGES OF SA1 #

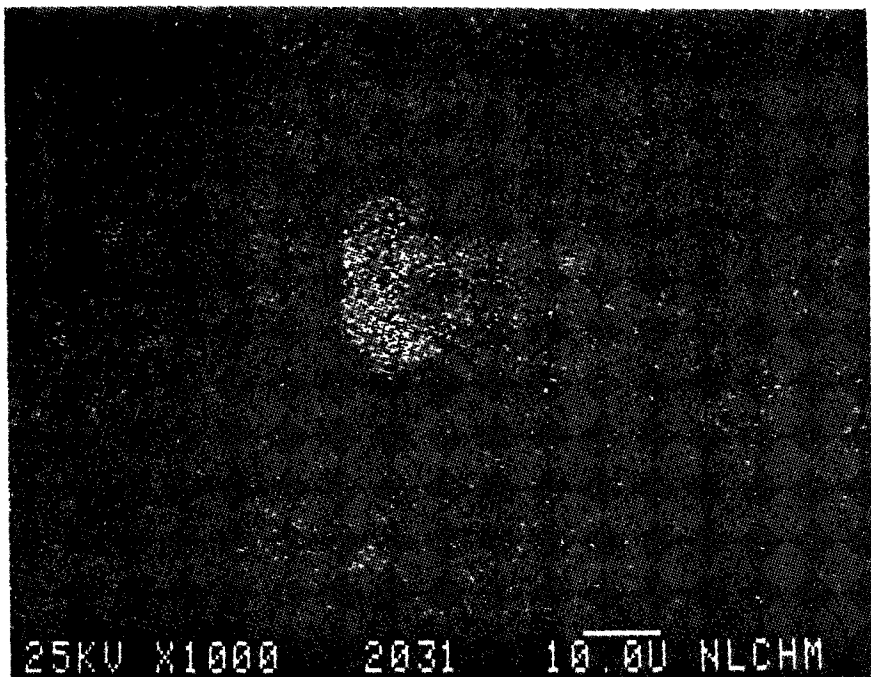


Figure 108

Ca X-Ray Image of Figure 104

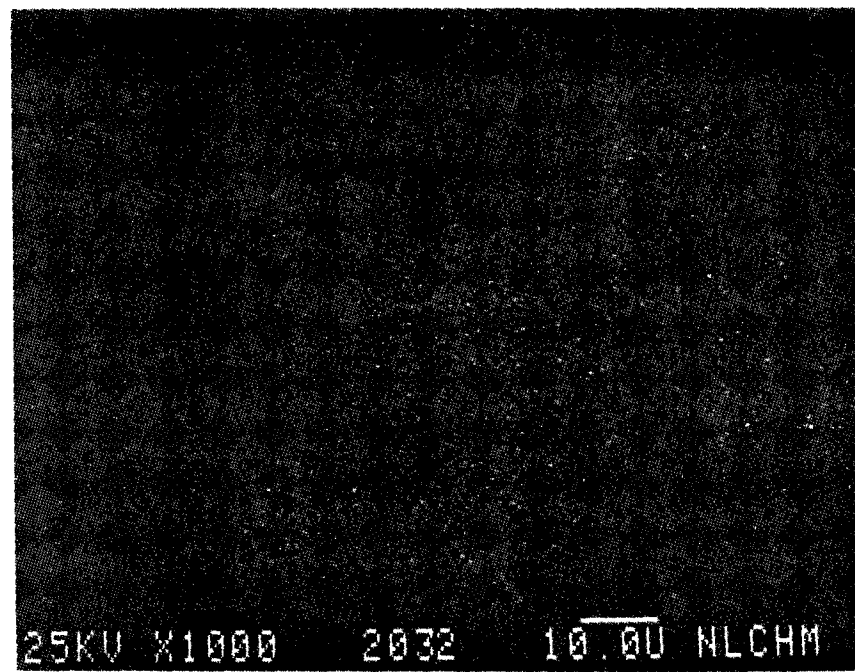


Figure 109

Ti X-Ray Image of Figure 104

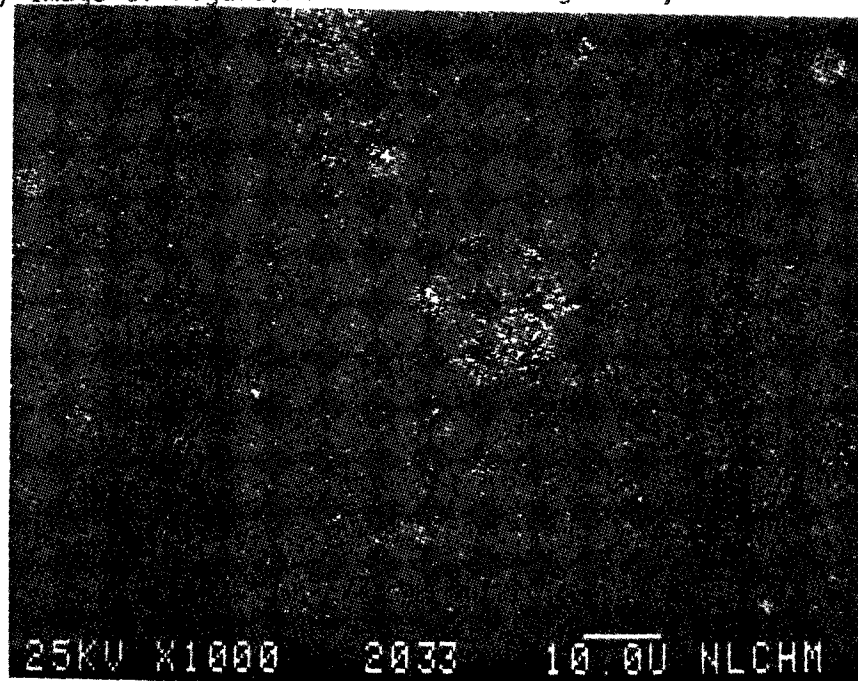


Figure 110

Fe X-Ray Image of Figure 104

SEM IMAGES OF SAMPLE #

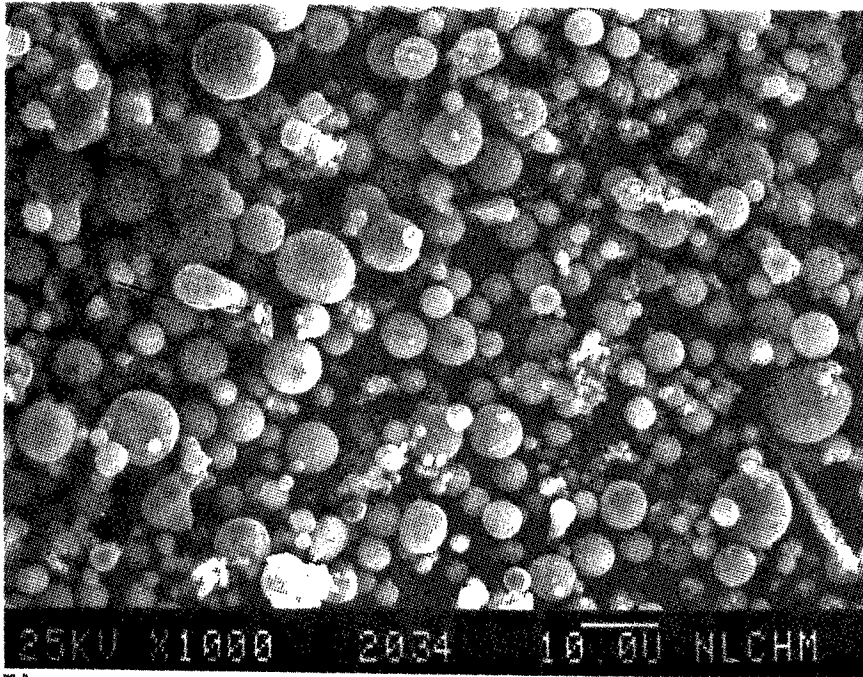
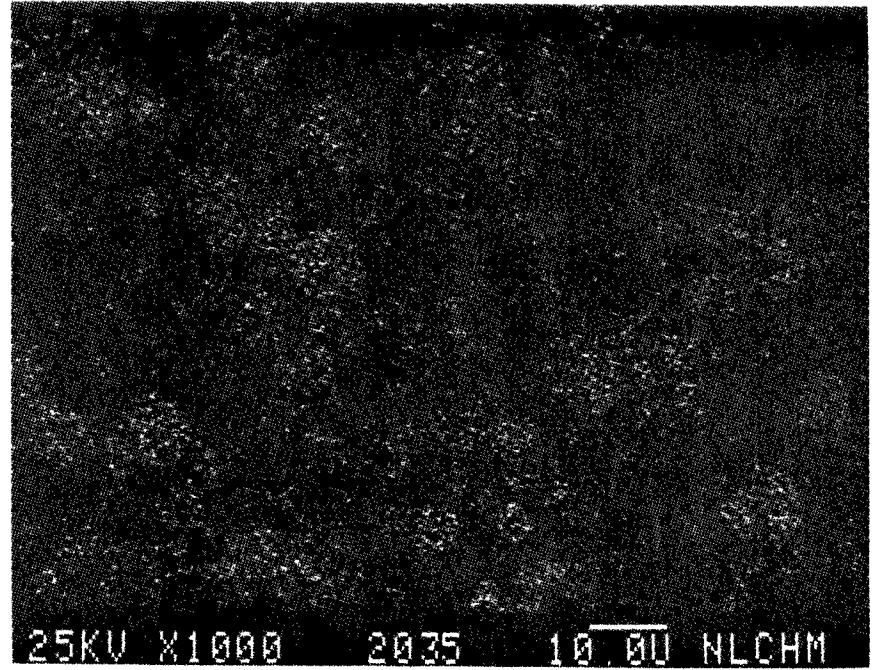


Figure ///



Figure//2

AL X-Ray Image of Figure ///

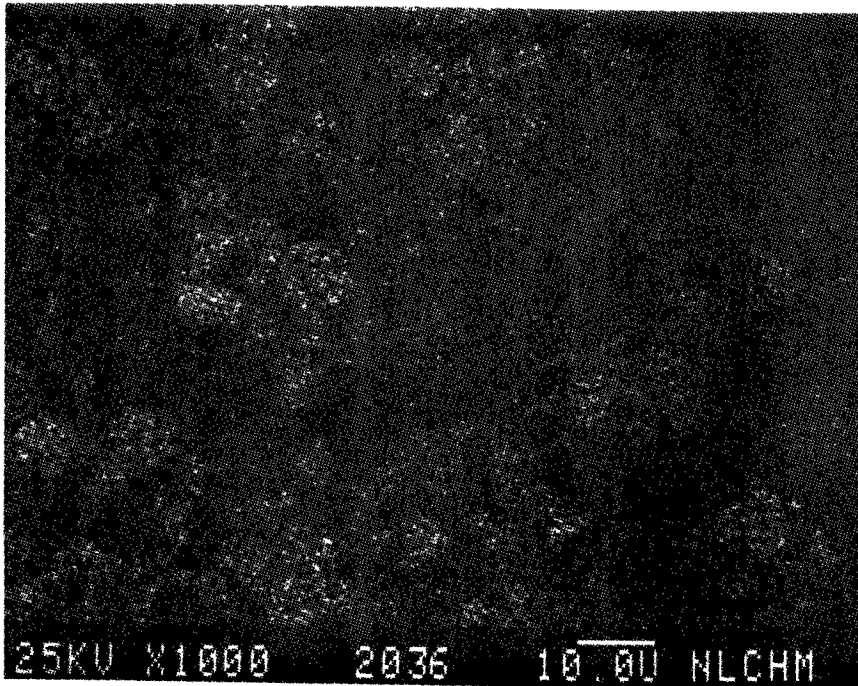
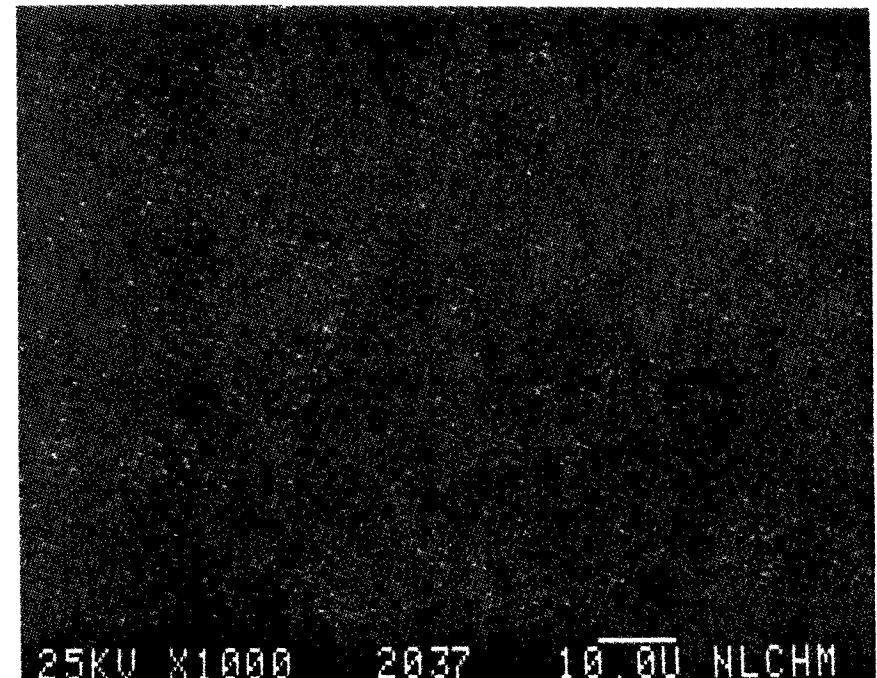


Figure //3

Si X-Ray Image of Figure///



Figure//4

K X-Ray Image of Figure ///

SEM IMAGES OF SAMPLE #

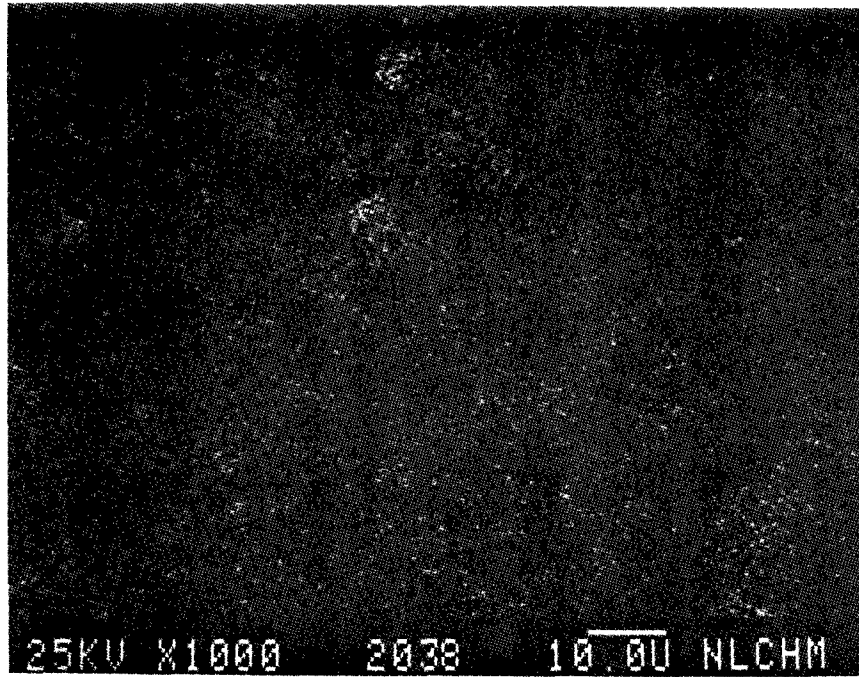


Figure //5

Ca X-Ray Image of Figure //

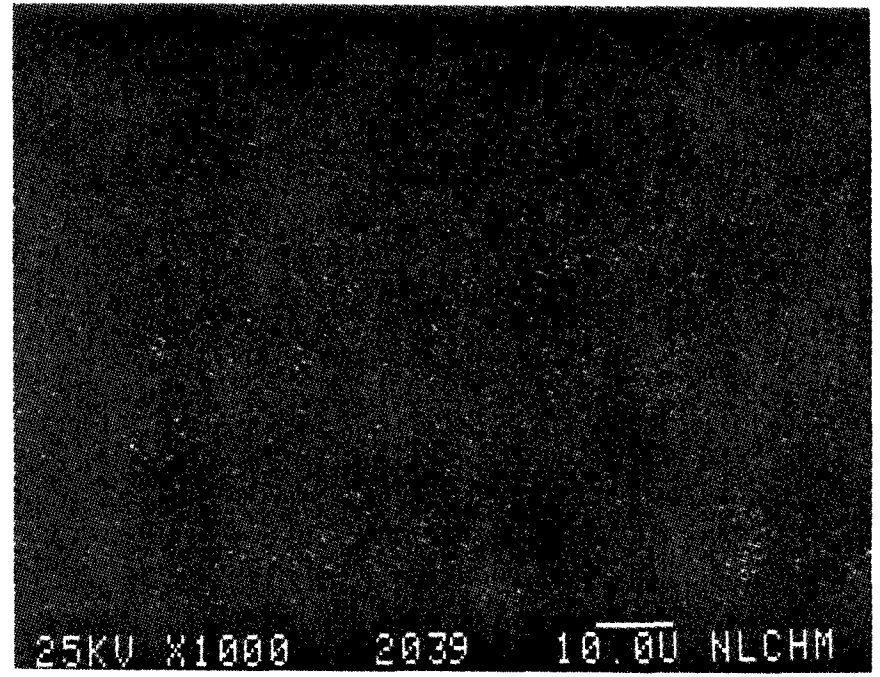


Figure //6

Ti X-Ray Image of Figure //

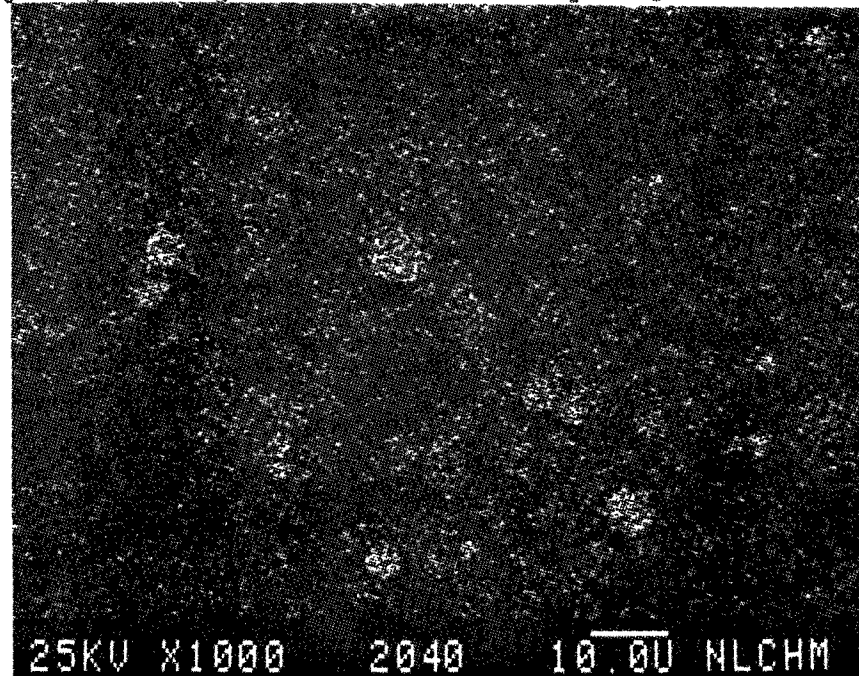


Figure //7

Fe X-Ray Image of Figure //



SEM IMAGES OF SAMPLE #

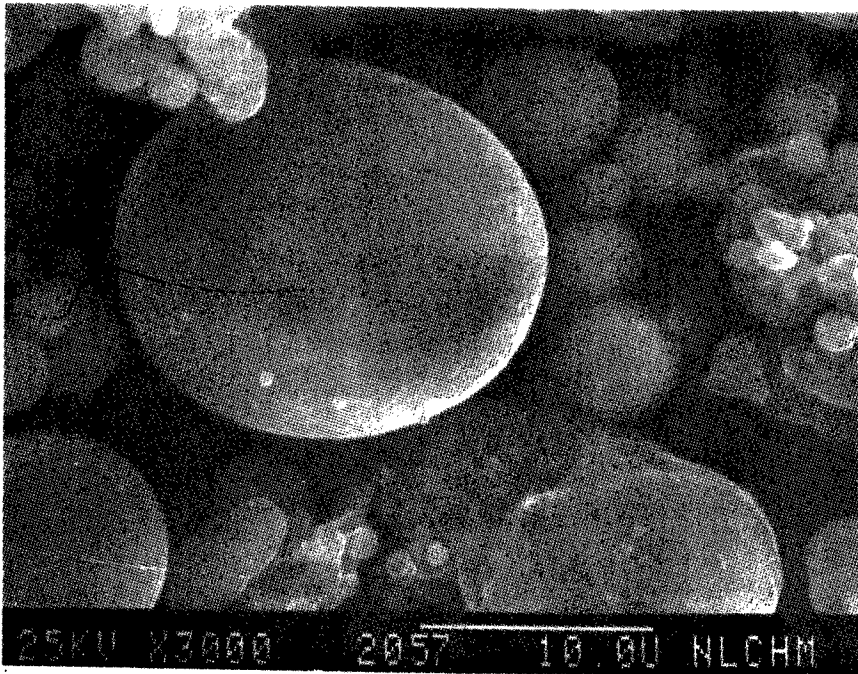


Figure 118

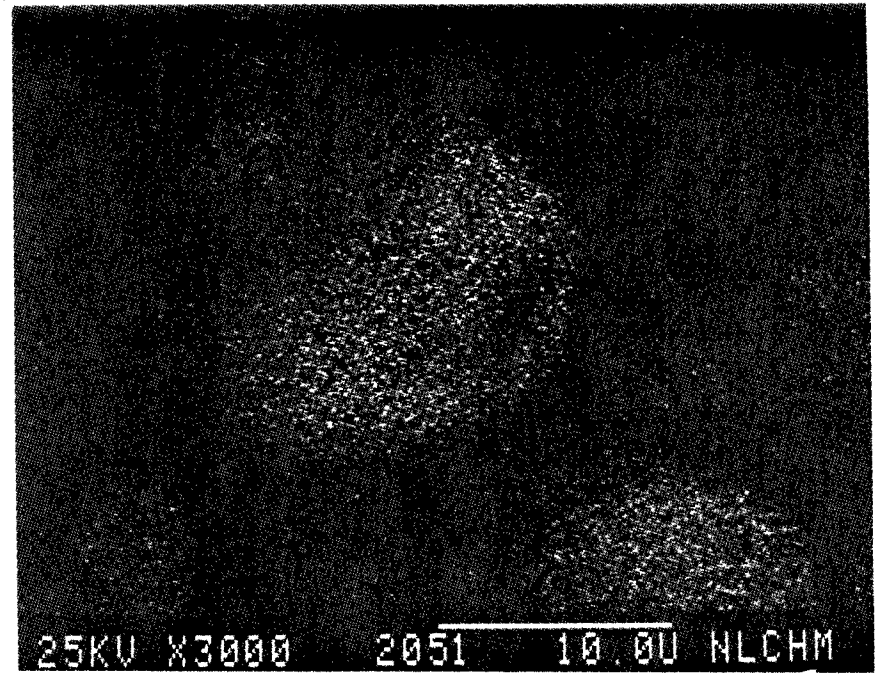


Figure 119

AL X-Ray Image of Figure 118

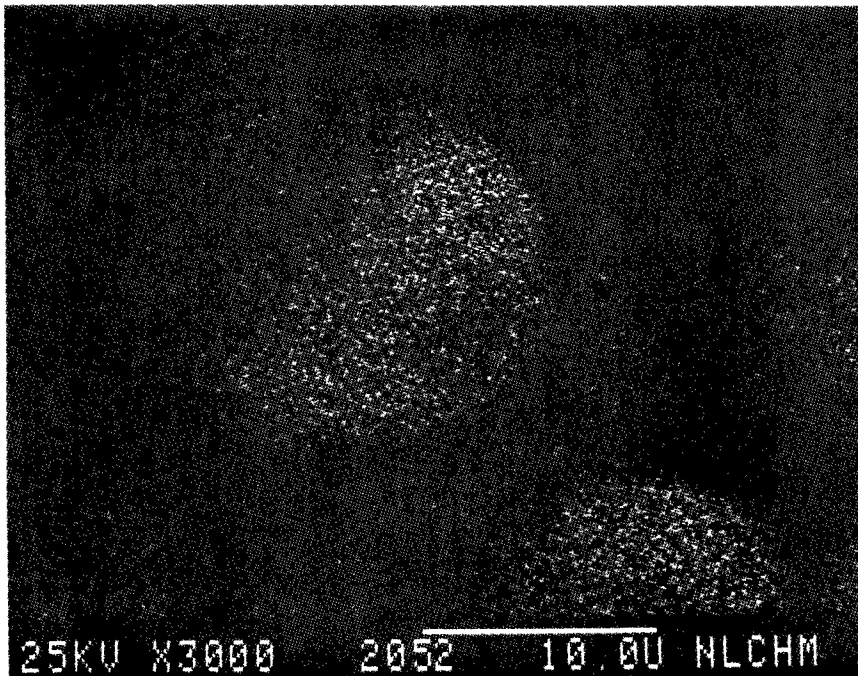


Figure 120

Si X-Ray Image of Figure 118

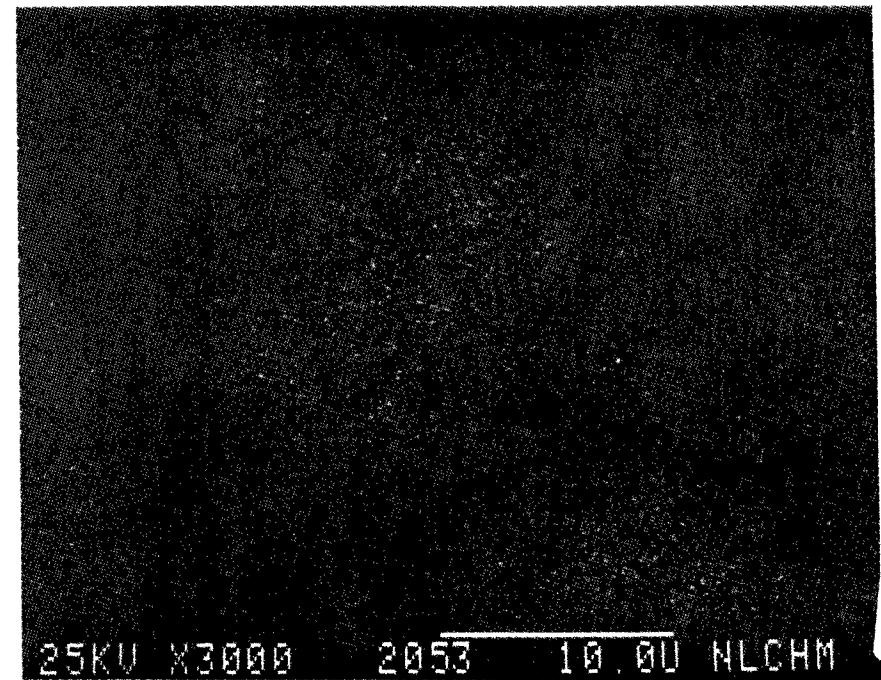


Figure 121

K X-Ray Image of Figure 118

SEM IMAGES OF SAMPLE #

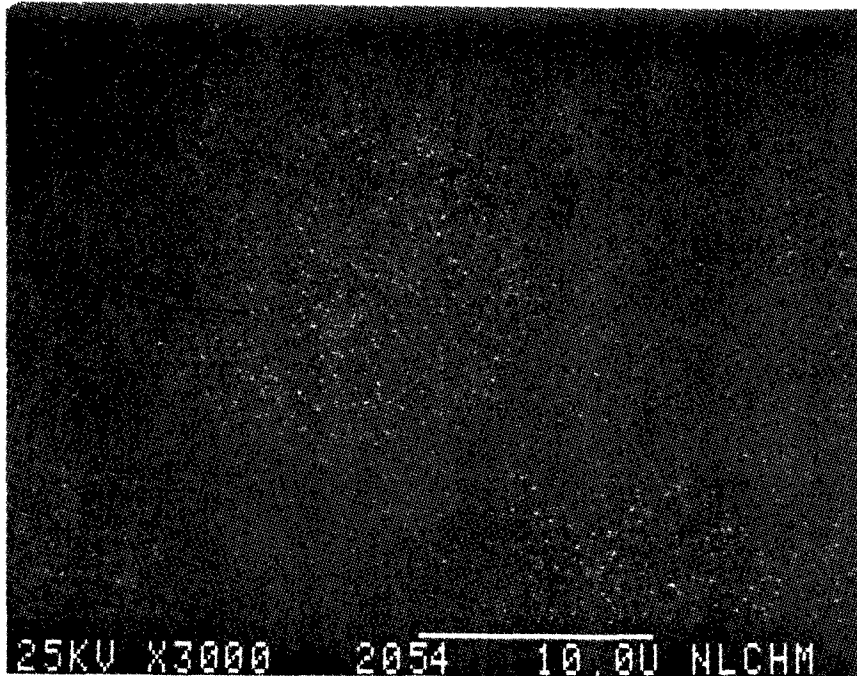


Figure 122

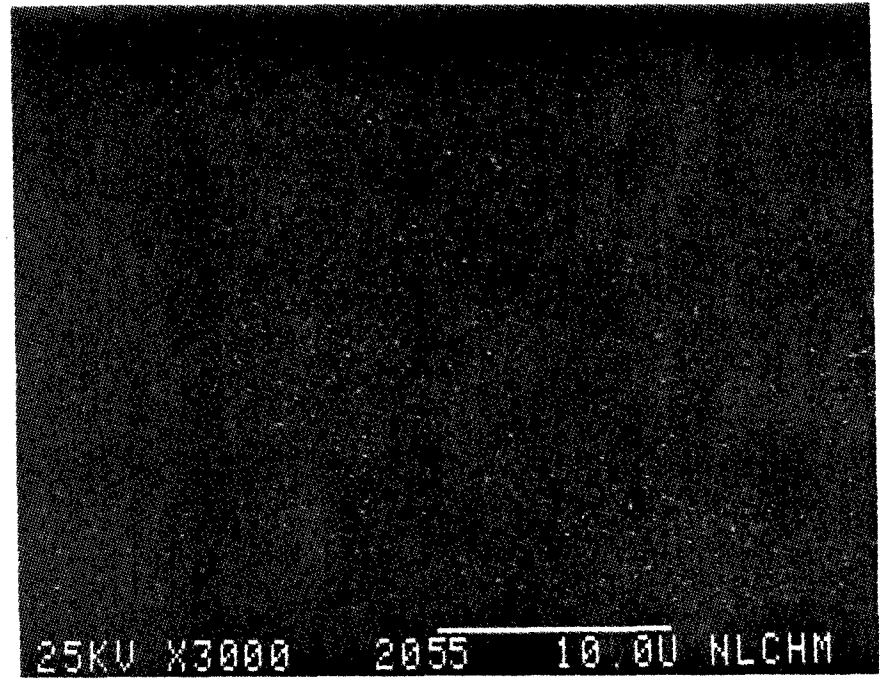


Figure 123

Ca X-Ray Image of Figure 118

Ti X-Ray Image of Figure 118

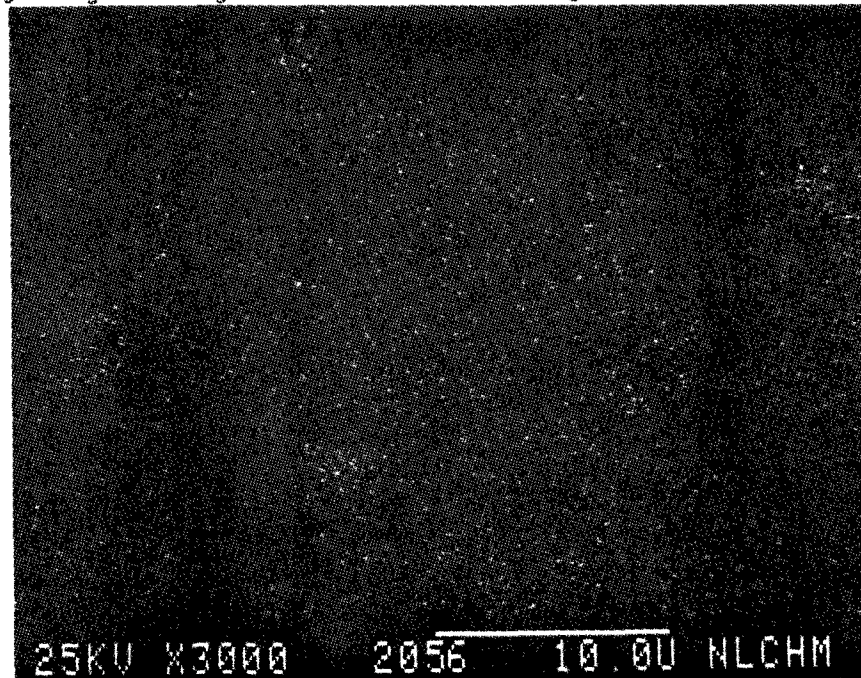
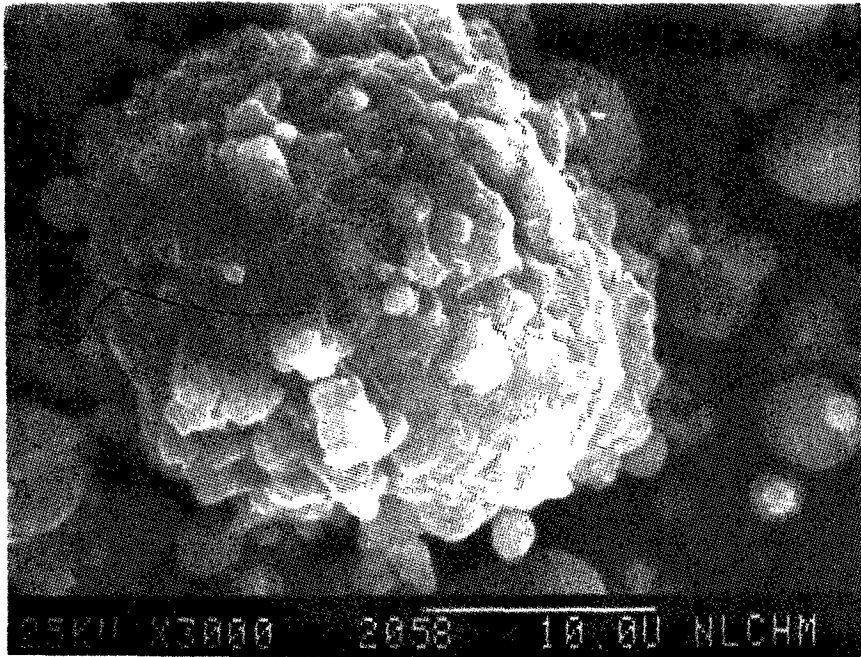


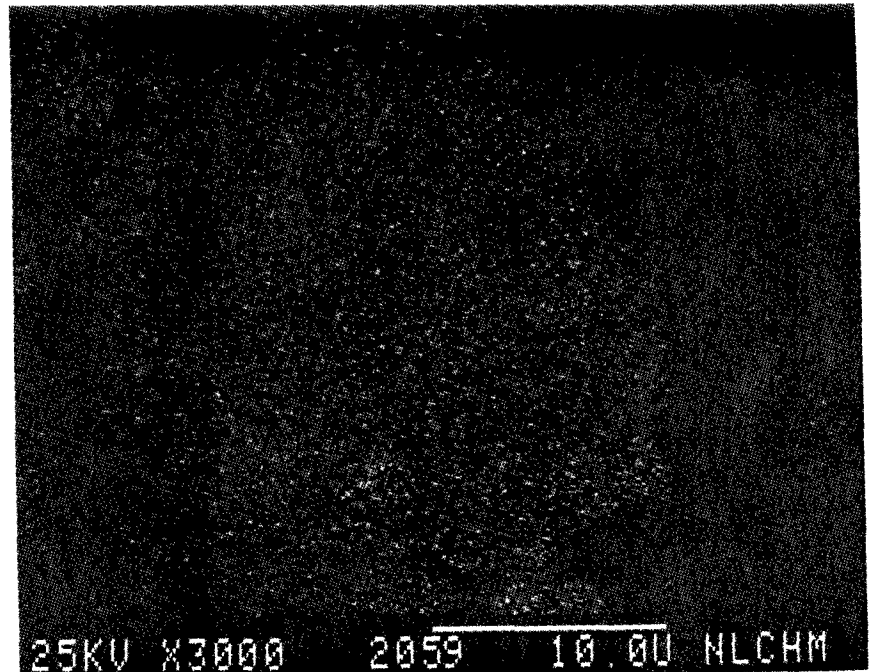
Figure 124

Fe X-Ray Image of Figure 118

SEM IMAGES OF SAMPLE #



Figure/25 .



Figure/26

AL X-Ray Image of Figure/25

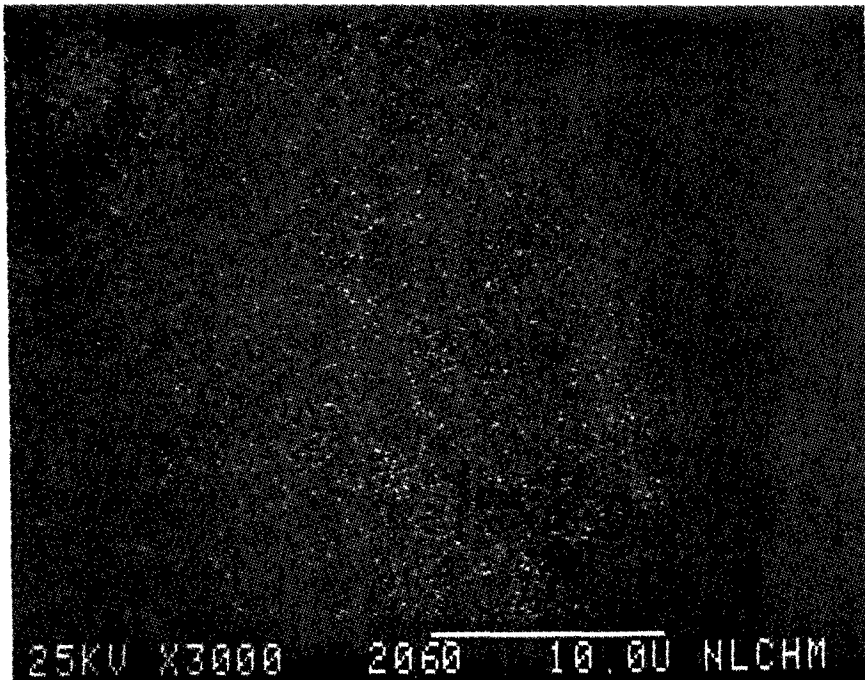
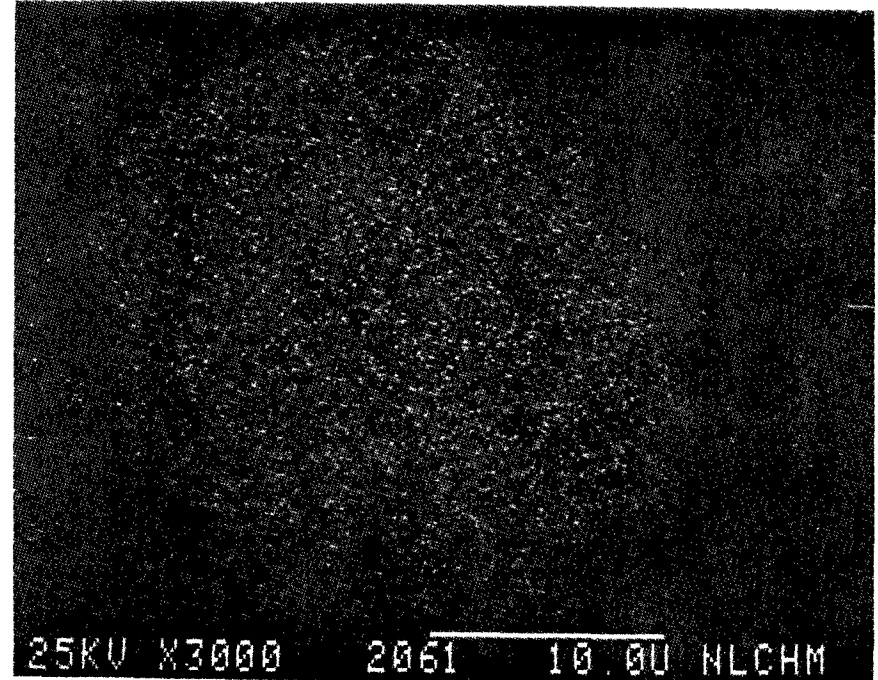


Figure /27

Si X-Ray Image of Figure/25



Figure/28

S X-Ray Image of Figure/25

SEM IMAGES OF SAMPLE #

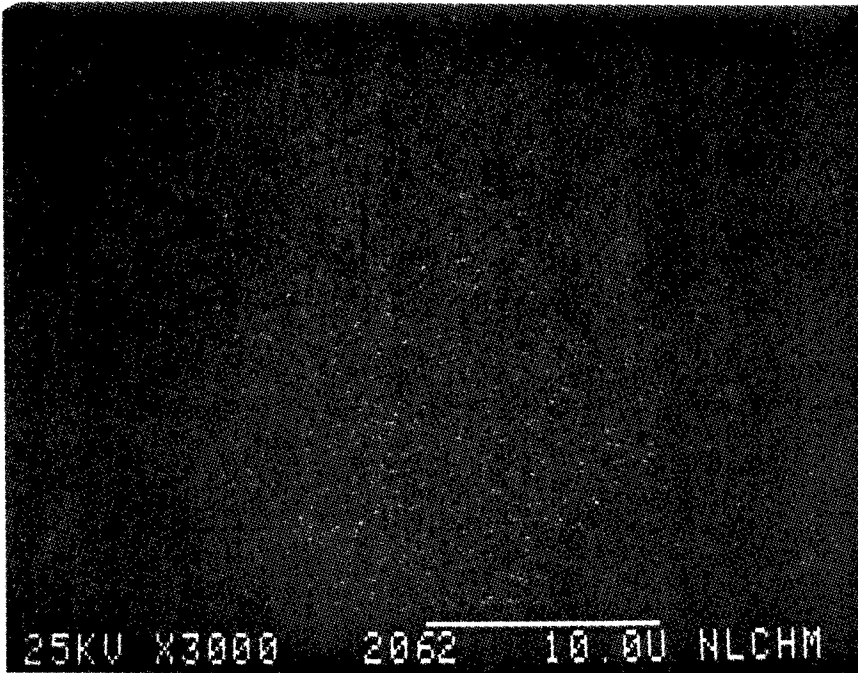


Figure 129

K X-Ray Image of Figure 125

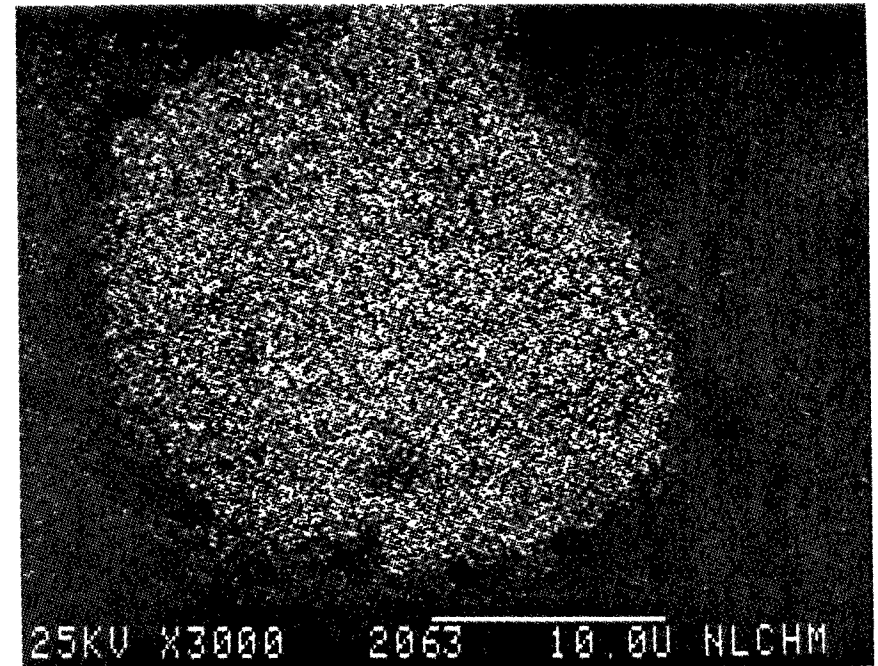


Figure 130

Ca X-Ray Image of Figure 125

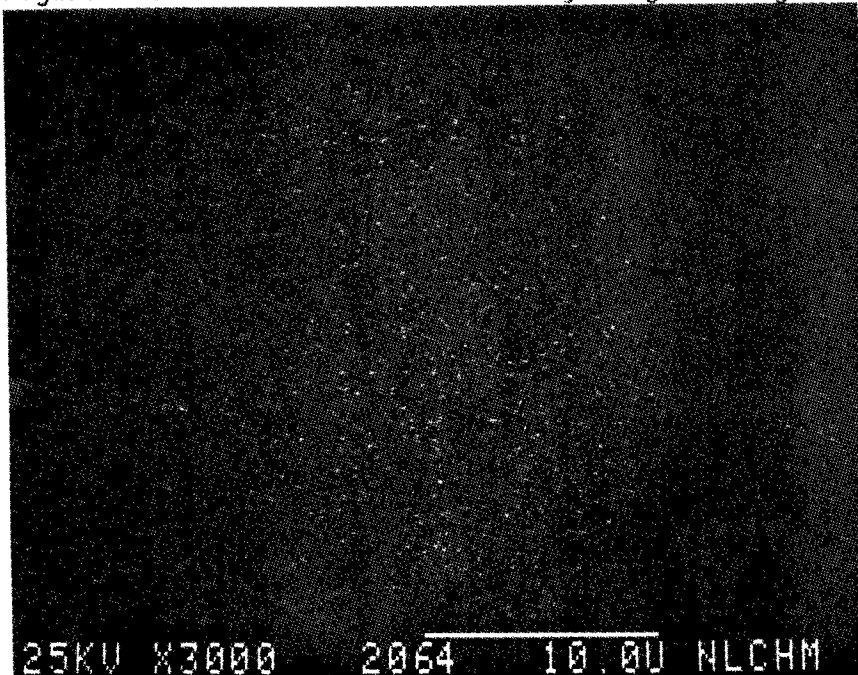


Figure 131

Ti X-Ray Image of Figure 125



Figure 132

Fe X-Ray Image of Figure 125



SEM IMAGES OF SAMPLE #

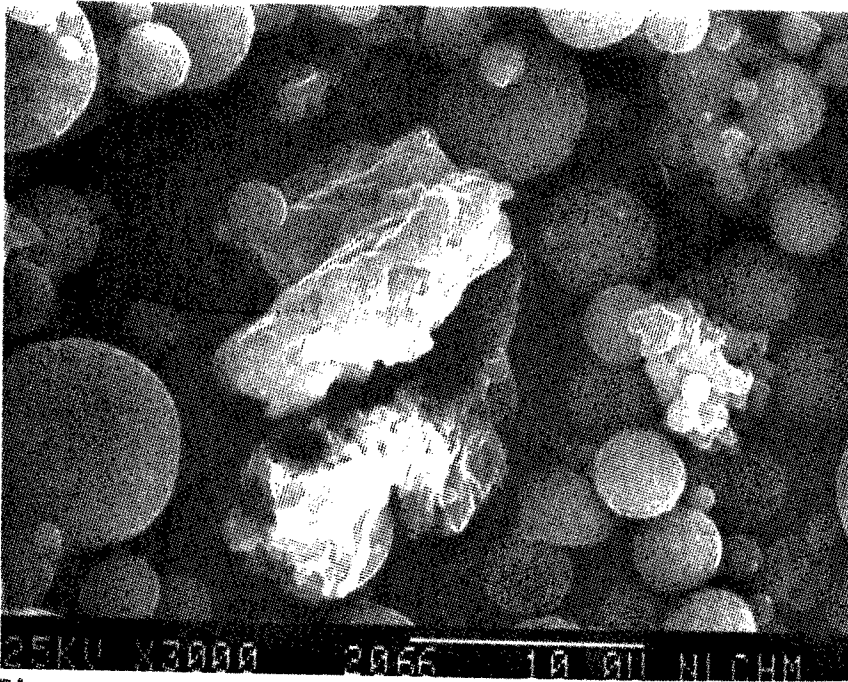


Figure 133.

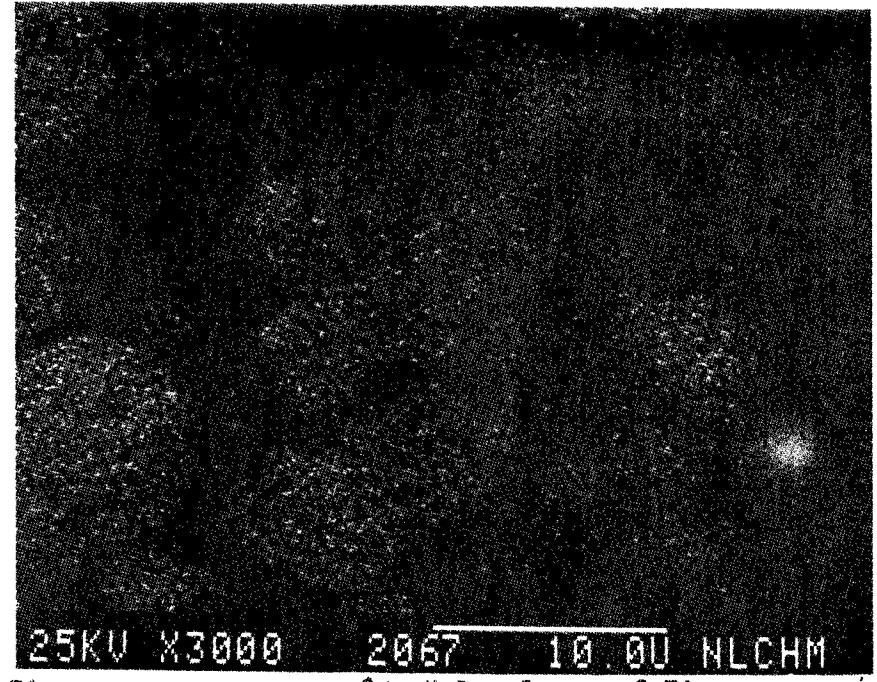


Figure 134

AL X-Ray Image of Figure 133

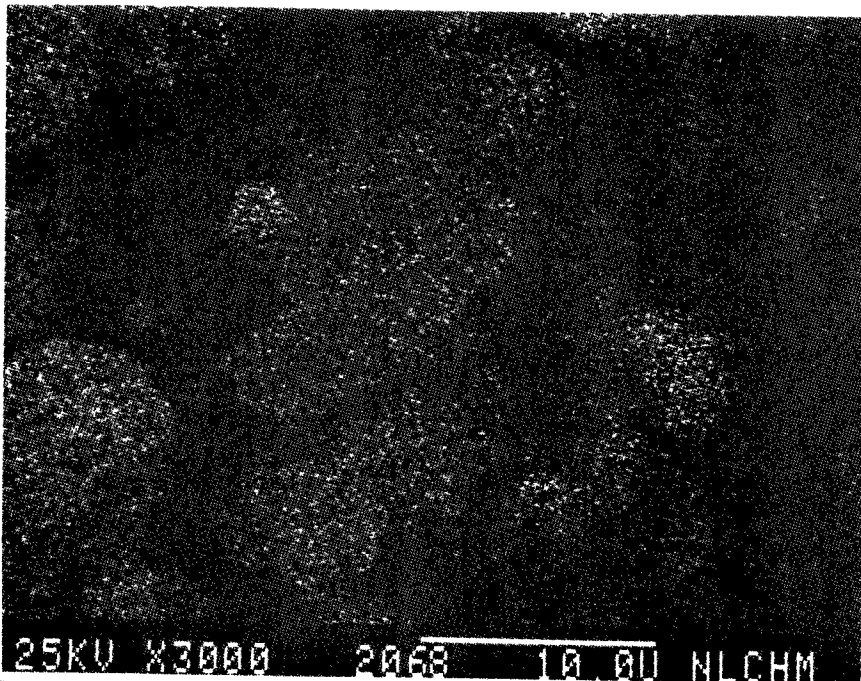


Figure 135

Si X-Ray Image of Figure 133

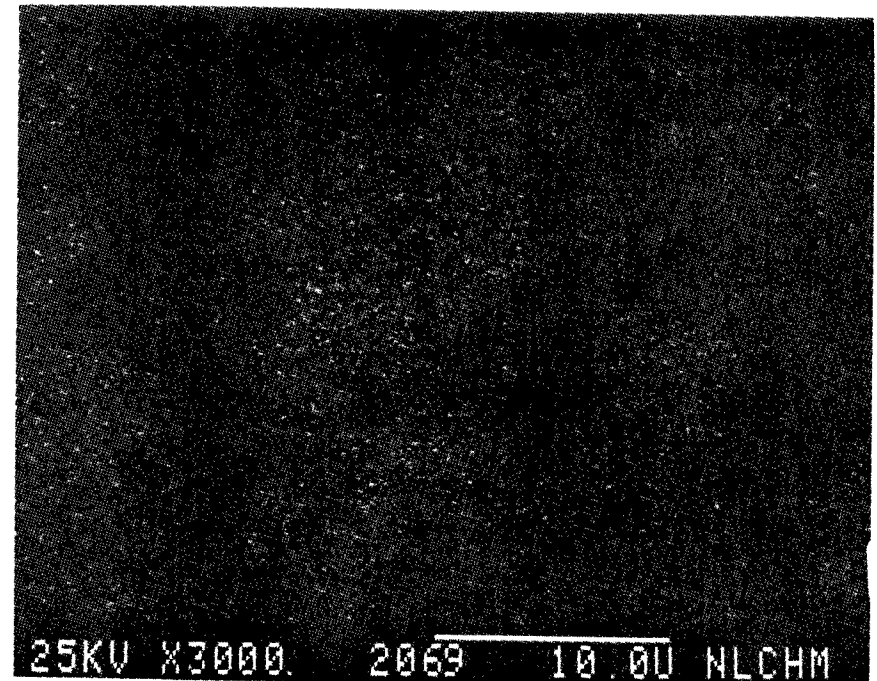


Figure 136

S X-Ray Image of Figure 133

SEM IMAGES OF SAMPLE #

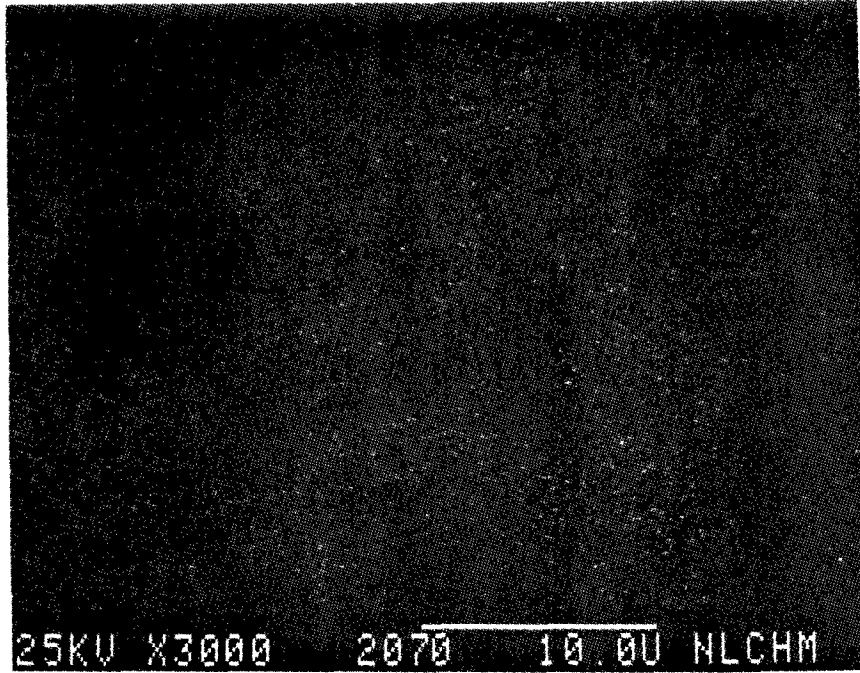


Figure 137

K X-Ray Image of Figure 133

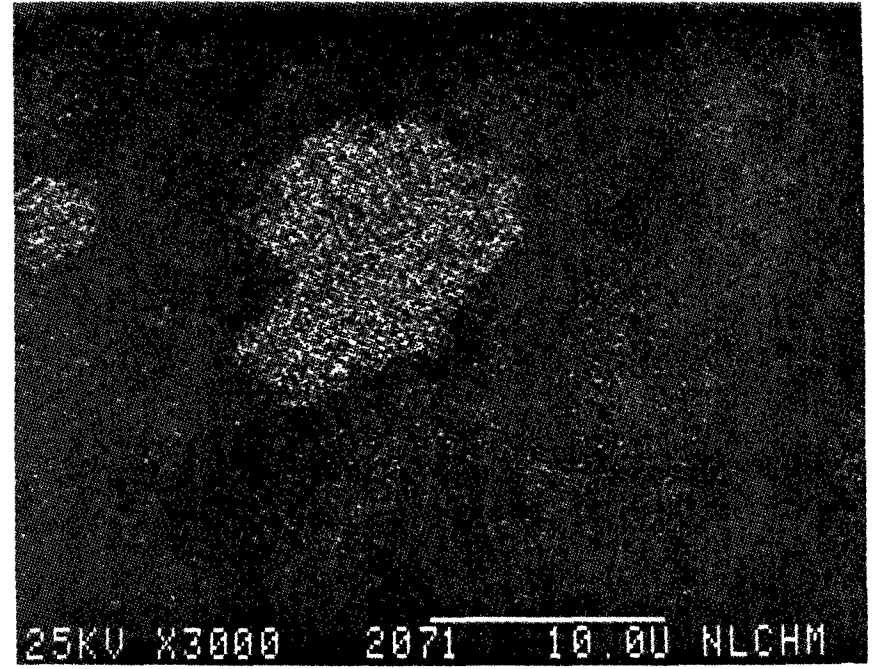


Figure 138

Ca X-Ray Image of Figure 133

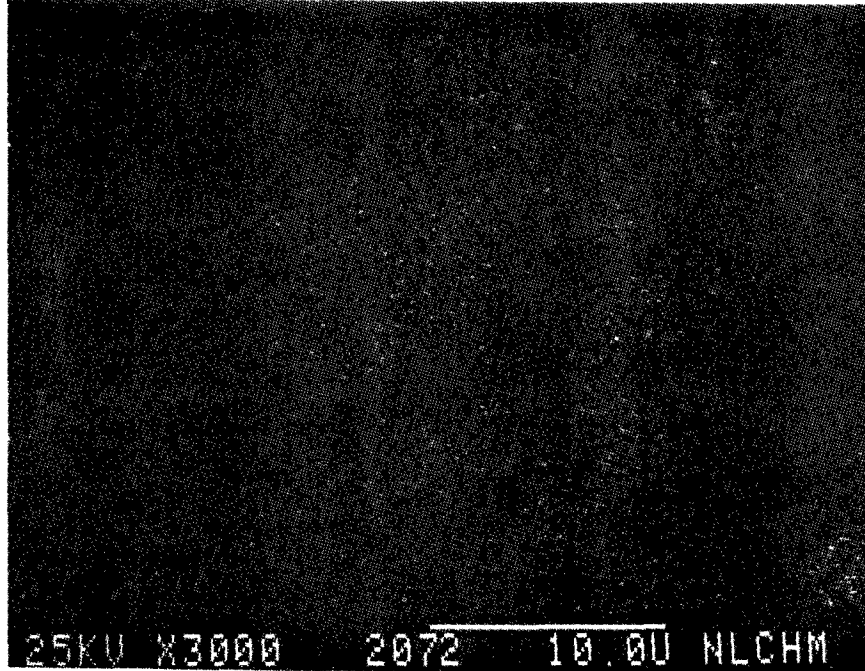


Figure 139

Ti X-Ray Image of Figure 133

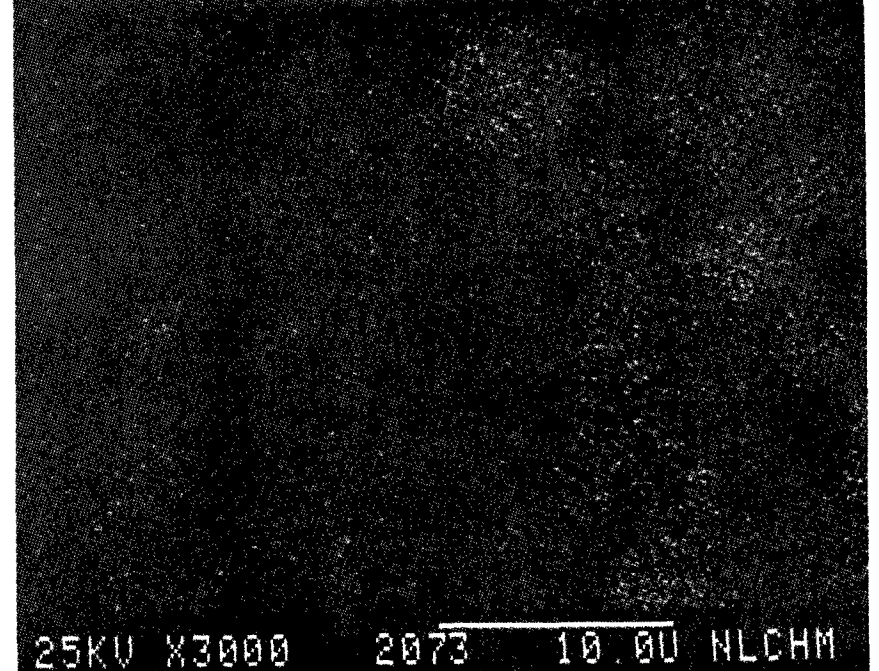


Figure 140

Fe X-Ray Image of Figure 133

SEM IMAGES OF SAMPLE #

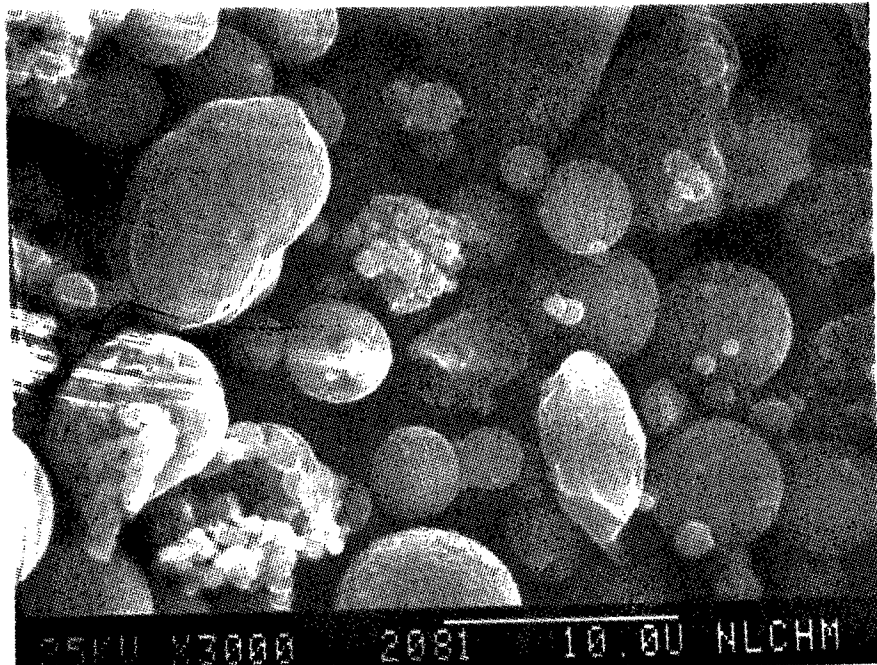


Figure 141

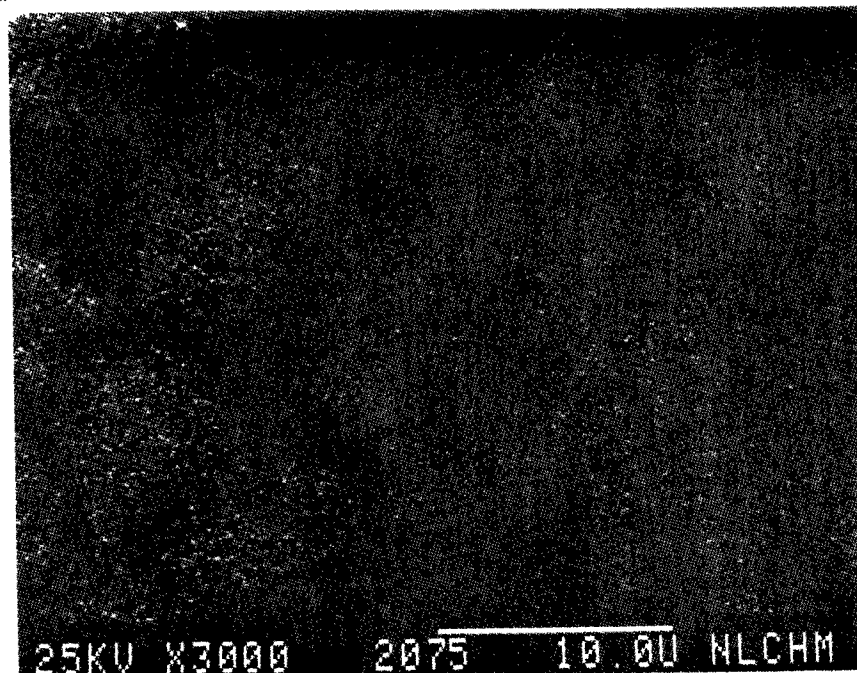


Figure 142

AL X-Ray Image of Figure 141

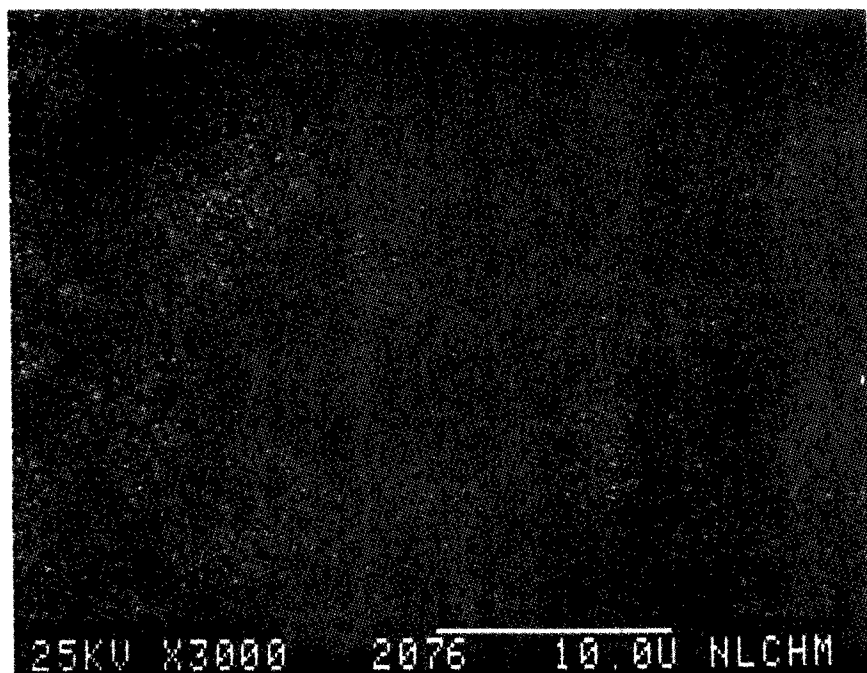


Figure 143

Si X-Ray Image of Figure 141

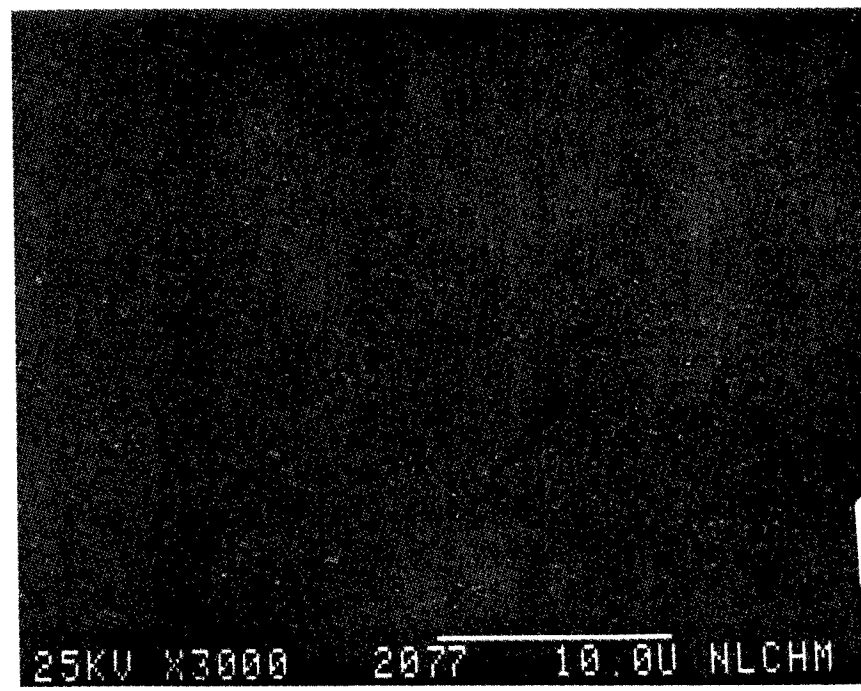


Figure 144

K X-Ray Image of Figure 141

SEM IMAGES OF SAMPLE #

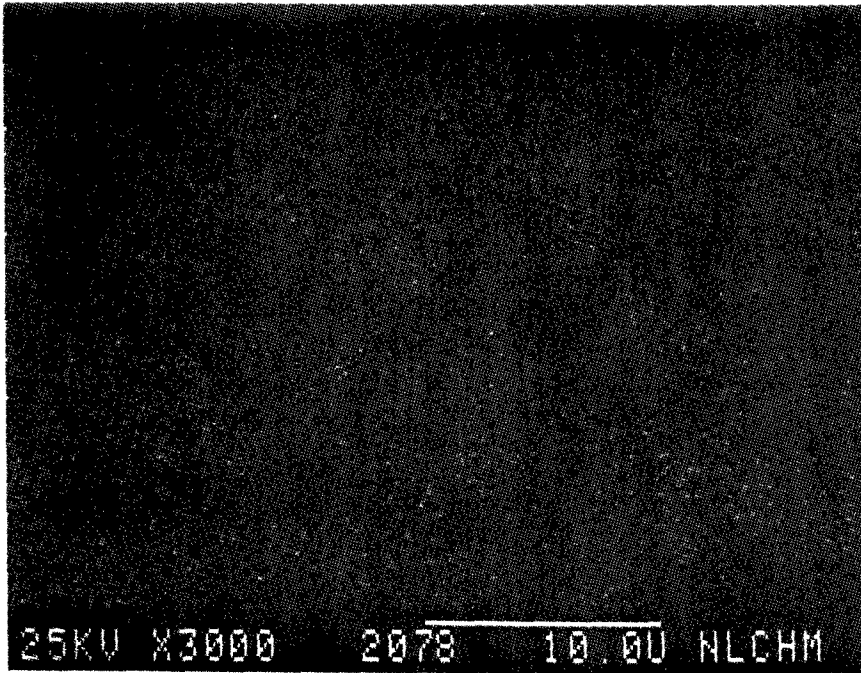


Figure 145

CR X-Ray Image of Figure 141

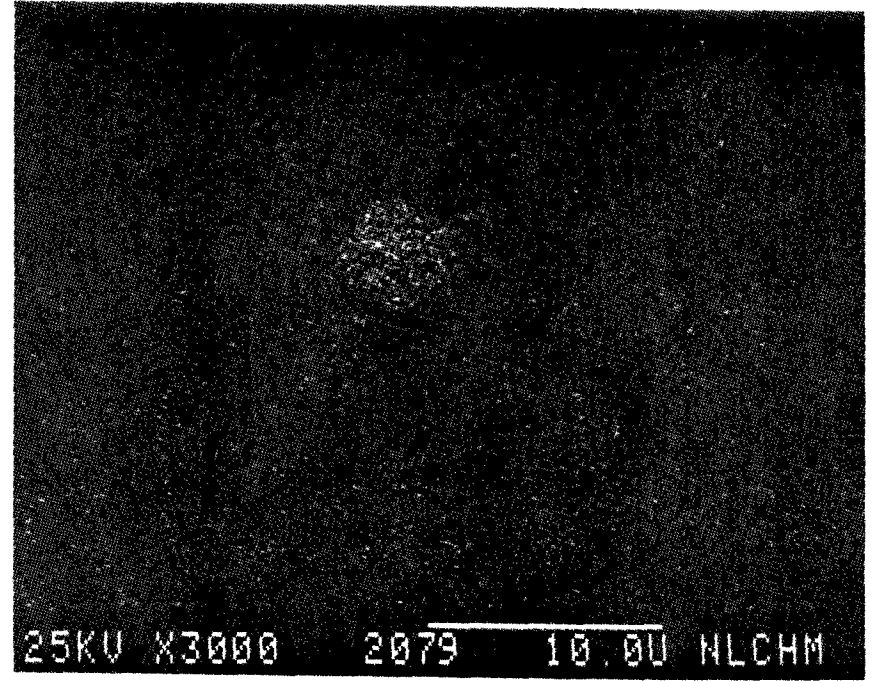


Figure 146

Ti X-Ray Image of Figure 141

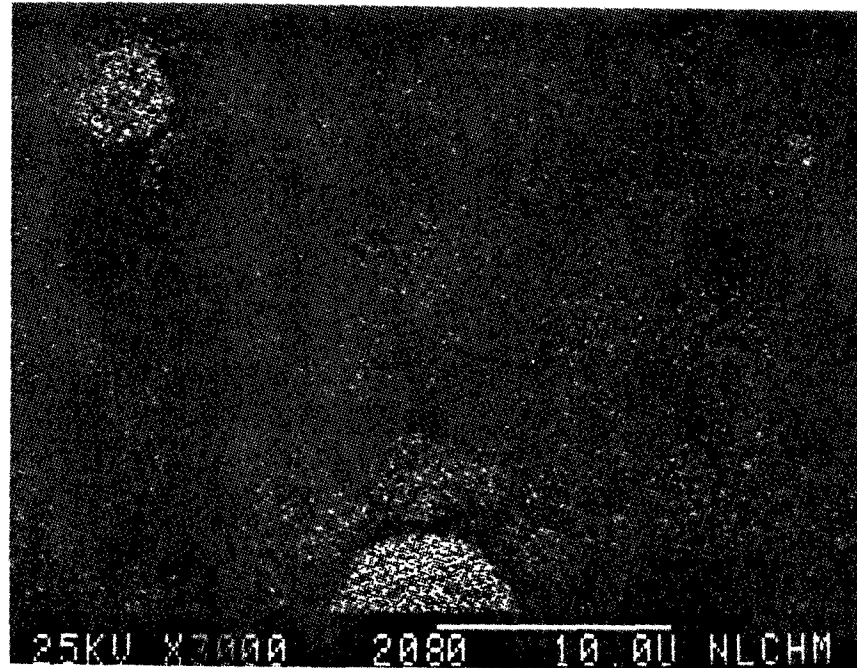


Figure 147

Fe X-Ray Image of Figure 141

ENERGY DISPERSIVE X-RAY ANALYSIS

Analytical Number Fly Ash (Acidic)

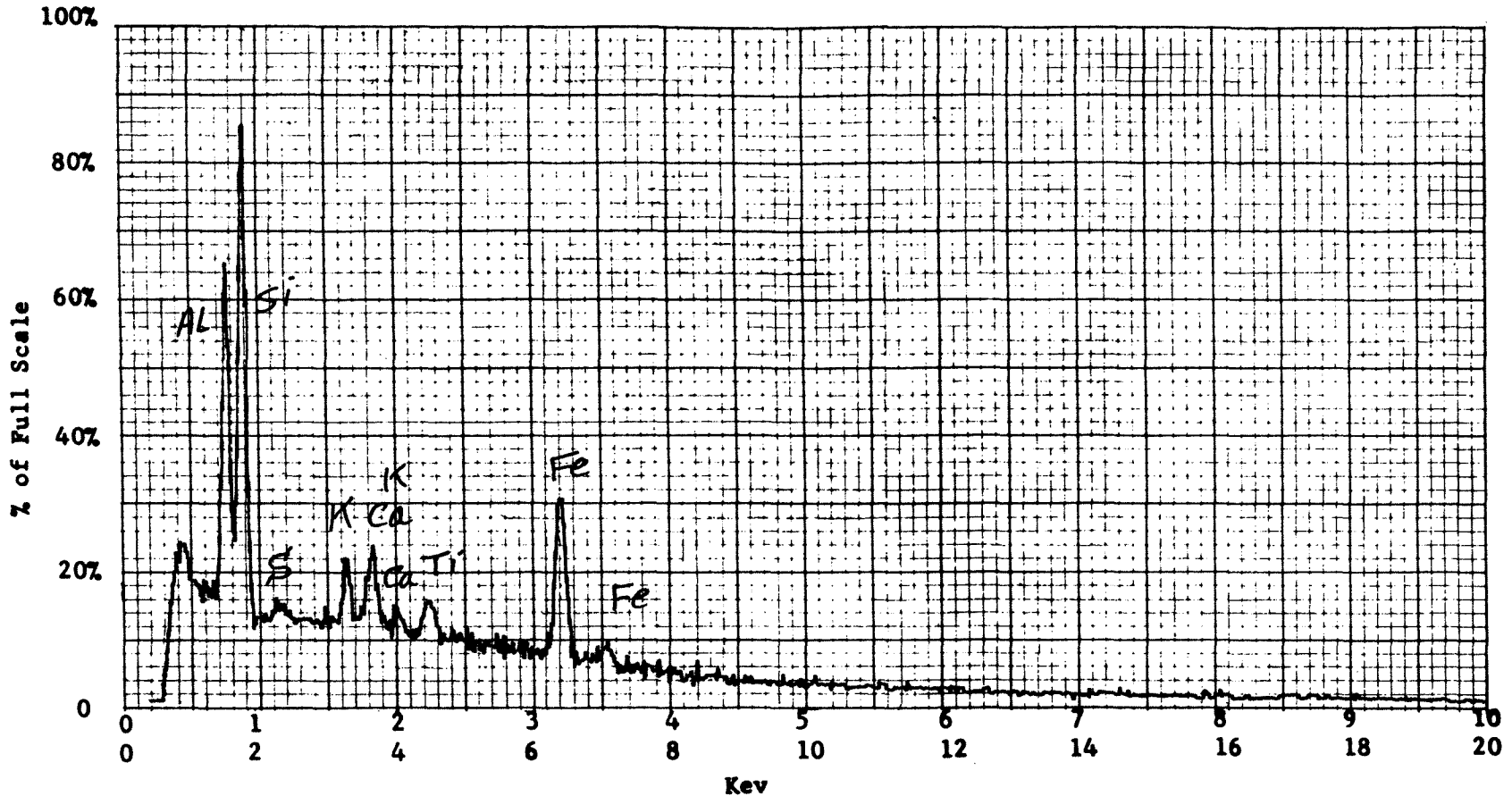
Operator \_\_\_\_\_ Date \_\_\_\_\_

Accelerating Potential 25 KeV

Total Counts Acquired 1.0 min.

Number Counts Full Scale 2K

Number of eV per channel 20



Sample peculiarities and remarks:

FIGURE 148: AREA SCAN



ENERGY DISPERSIVE X-RAY ANALYSIS

Analytical Number Fly Ash (Acidic)

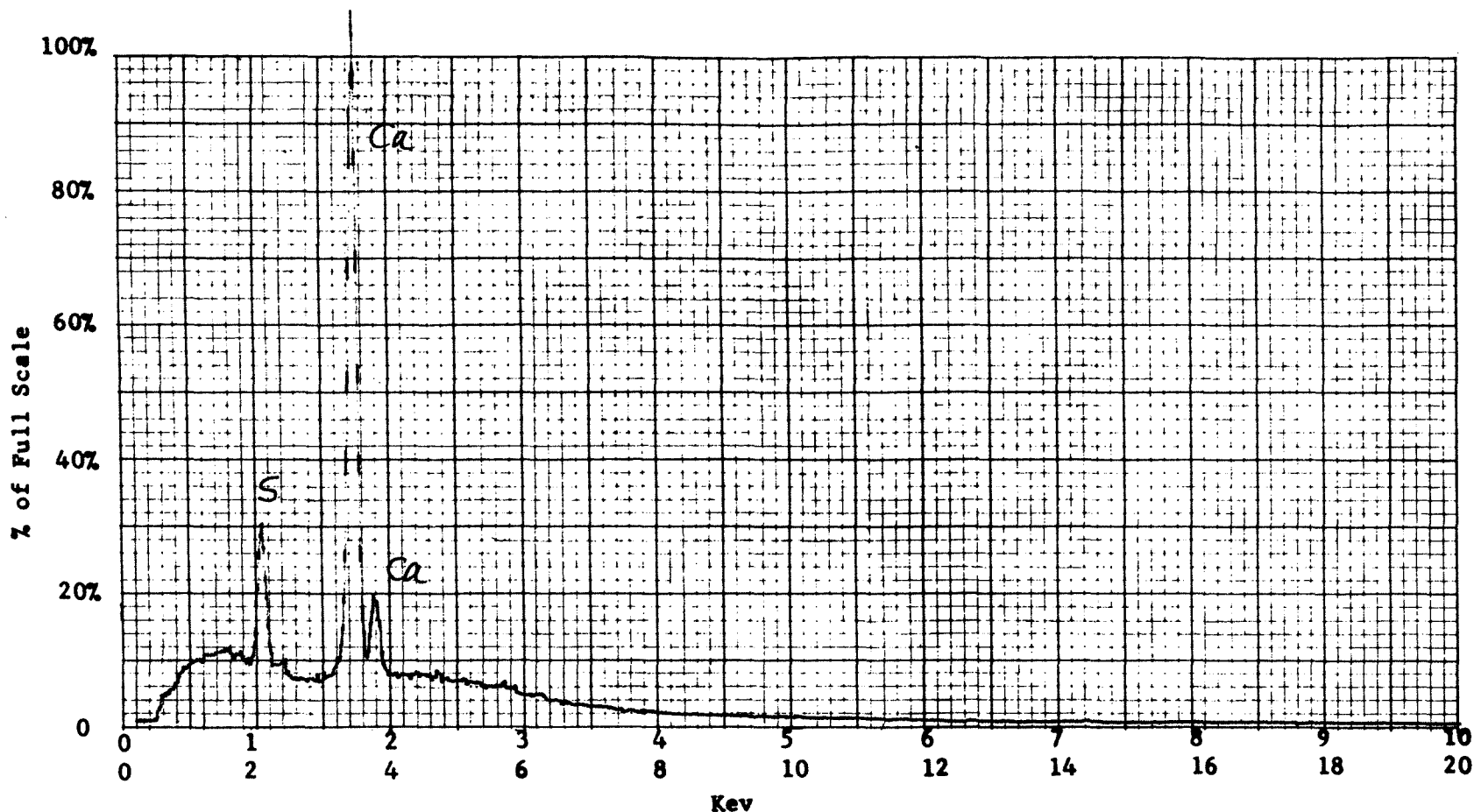
Operator \_\_\_\_\_ Date \_\_\_\_\_

Accelerating Potential 25 KeV

Total Counts Acquired 1.0 min.

Number Counts Full Scale 2K

Number of eV per channel 20



Sample peculiarities and remarks: FIGURE 149: POINT SCAN ON A HIGH Ca-S PARTICLE  
IN FIGURE 125

ENERGY DISPERSIVE X-RAY ANALYSIS

Analytical Number Fly Ash (Acidic)

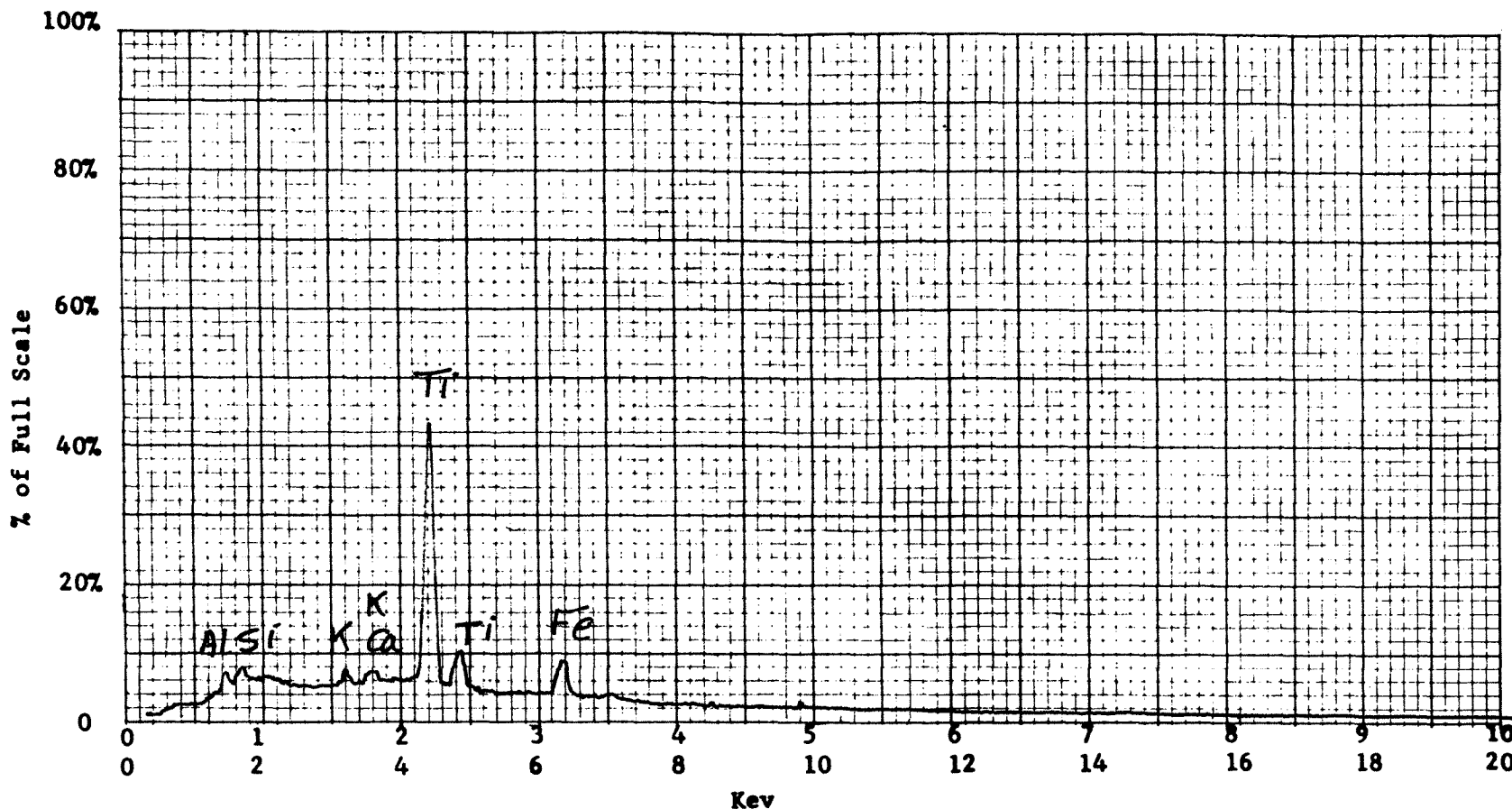
Operator \_\_\_\_\_ Date \_\_\_\_\_

Accelerating Potential 25 KeV

Total Counts Acquired 1.0 min.

Number Counts Full Scale 5K

Number of eV per channel 20



Sample peculiarities and remarks: FIGURE 150: POINT SCAN ON A HIGH Ti PARTICLE  
IN FIGURE 141

ENERGY DISPERSIVE X-RAY ANALYSIS

Analytical Number Fly Ash (Acidic)

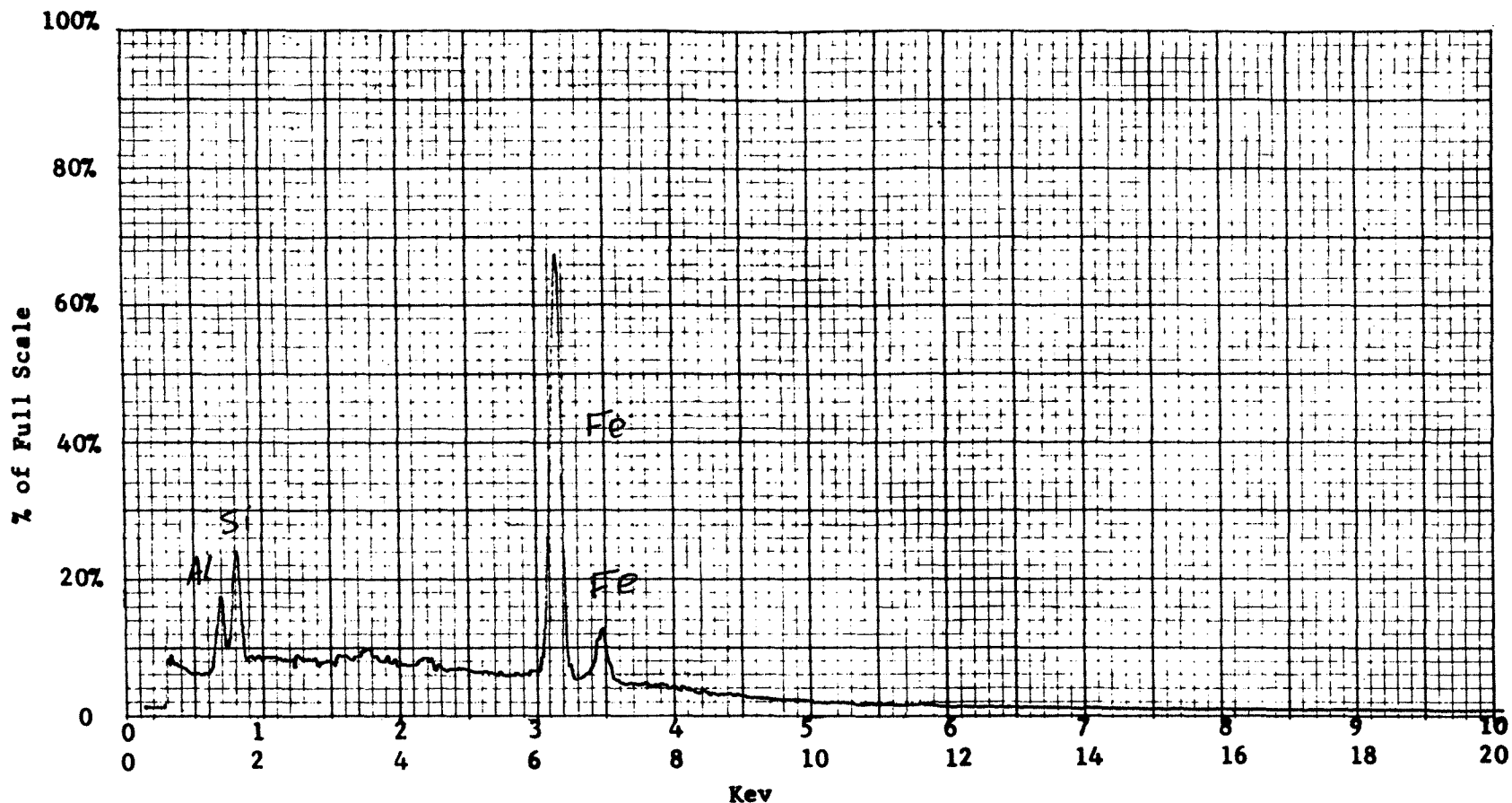
Operator \_\_\_\_\_ Date \_\_\_\_\_

Accelerating Potential 25 KeV

Total Counts Acquired 1.0 min.

Number Counts Full Scale 5K

Number of eV per channel 20



Sample peculiarities and remarks: FIGURE 151: POINT SCAN ON A HIGH Fe (LARGE SPHERE) PARTICLE



ENERGY DISPERSIVE X-RAY ANALYSIS

Analytical Number Fly Ash (Acidic)

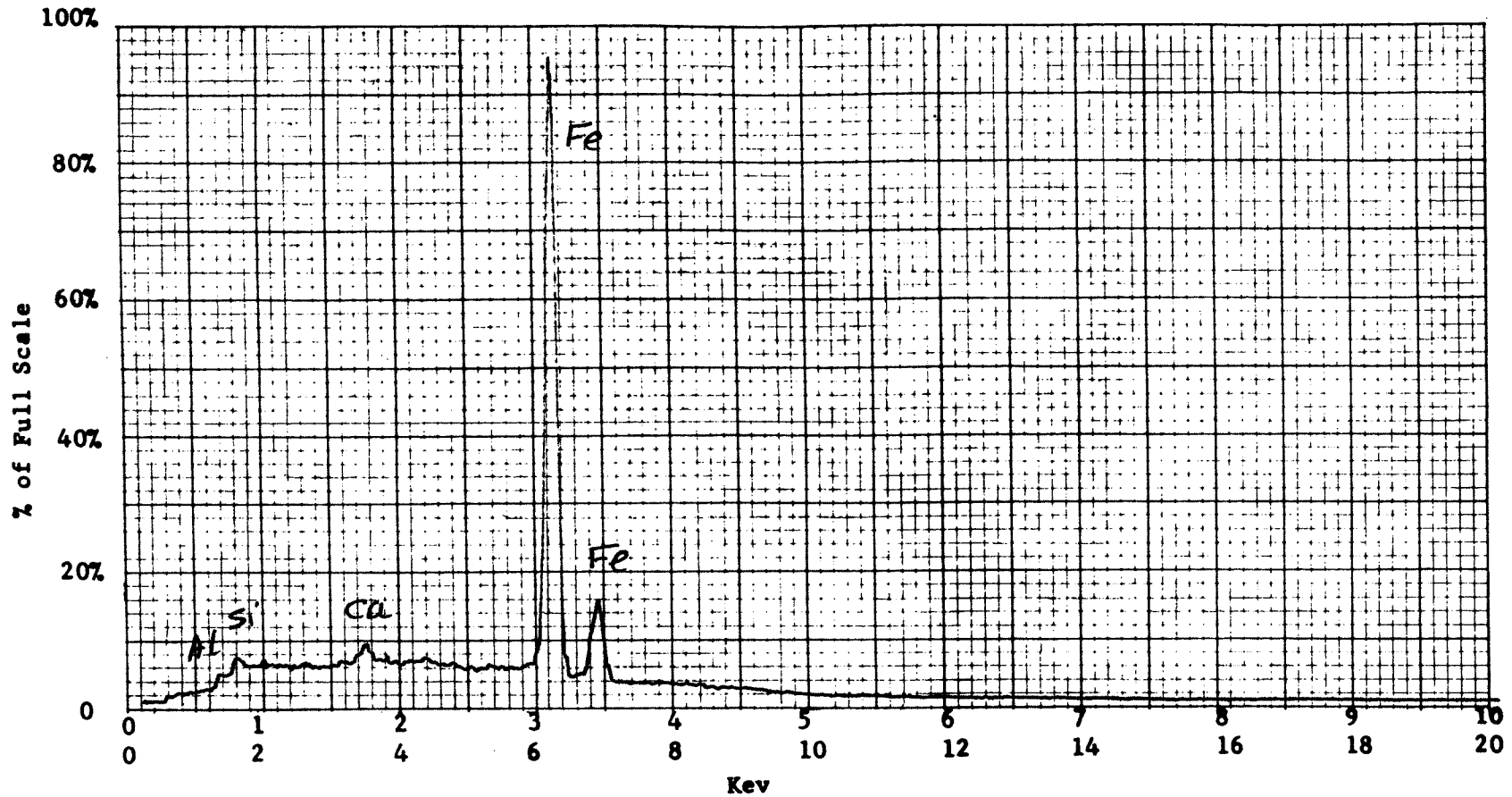
Operator \_\_\_\_\_ Date \_\_\_\_\_

Accelerating Potential 25 KeV

Total Counts Acquired 1.0 min.

Number Counts Full Scale 5K

Number of eV per channel 20



Sample peculiarities and remarks: FIGURE 152: POINT SCAN ON AN AVERAGE SIZE SPHERICAL PARTICLE CONTAINING HIGH Fe

Bentonite:Structural Analysis:

All the bentonite particles were observed to be irregular in shape, and their surfaces were relatively rough. SEM micrographs obtained at high magnifications, such as 3000X, 10,000X and 20,000X, showed the presence of cracks and pores in some particles while other particles had very fine fibrous shape structures on their surfaces.

The maximum, average and minimum particle size were measured in microns ( $\mu$ ) as follows:

Maximum	Average	Minimum
135.0	26.0	1.2

Elemental Composition and Distribution:

Area scan analysis indicated the presence of Al, Si, S, Ca and Ti in the particles. Figures 177 and 182 were obtained at low magnification (200X) to illustrate the general elemental distribution. These figures indicated that the major element in most of the bentonite particles is Si, while other elements are present in minor amounts.

Figure 187 indicates that a large particle in the middle of the field contained very high concentrations of Ca and S (possible Ca sulphate); this is shown in the sulfur X-ray image (Figure 190), calcium X-ray image (Figure 191) and in the X-ray energy spectrum, Figure 211.

A large rectangular particle in the middle of the field of Figure 193 was found to contain very high levels of Ca while no S was detected (possible Ca oxide or carbonate).

This is illustrated by the calcium X-ray image (Figure 197) and X-ray energy spectrum, Figure 212.

Another Ca and S containing particle was observed in Figure 204. The presence of high Ca and S is illustrated in the sulfur X-ray image (Figure 207), calcium X-ray image (Figure 208) and in the X-ray energy spectrum, Figure 215.

A very small particle in Figure 199 indicated the presence of very high Fe content (possible Fe oxide). This is illustrated by the iron X-ray image, see Figure 203, and in the X-ray energy spectrum, Figure 214. In the same figure (i.e., Figure 199) a large particle in the right lower corner of the field was found to contain Al, Si, S, Ca and Fe, but the Fe level was much higher than for any other bentonite particle. This can be seen in the elemental X-ray images (Figures 200, 201, 202 and 203) and also in the X-ray energy spectrum, Figure 213.

SEM IMAGES OF SAMPLE #

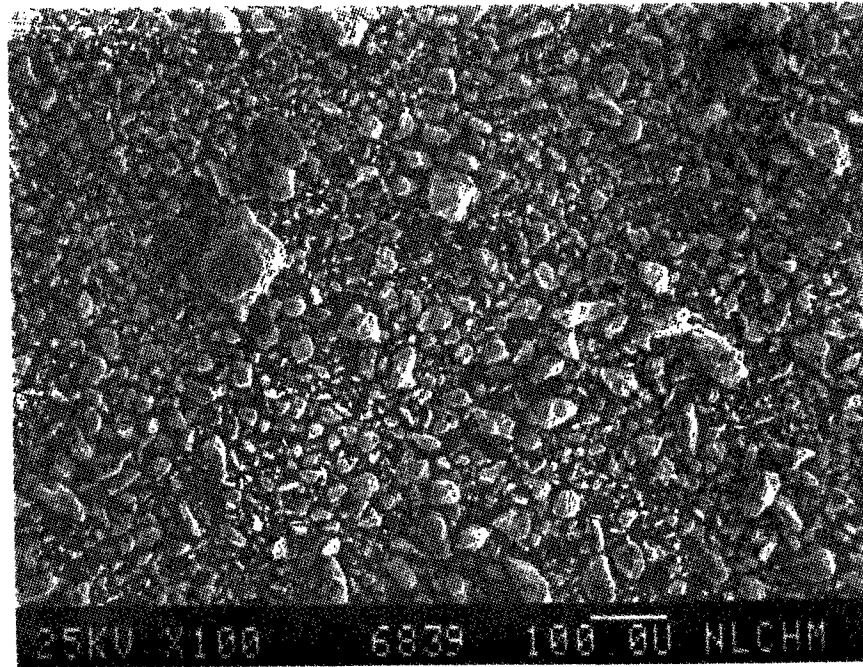


Figure 153

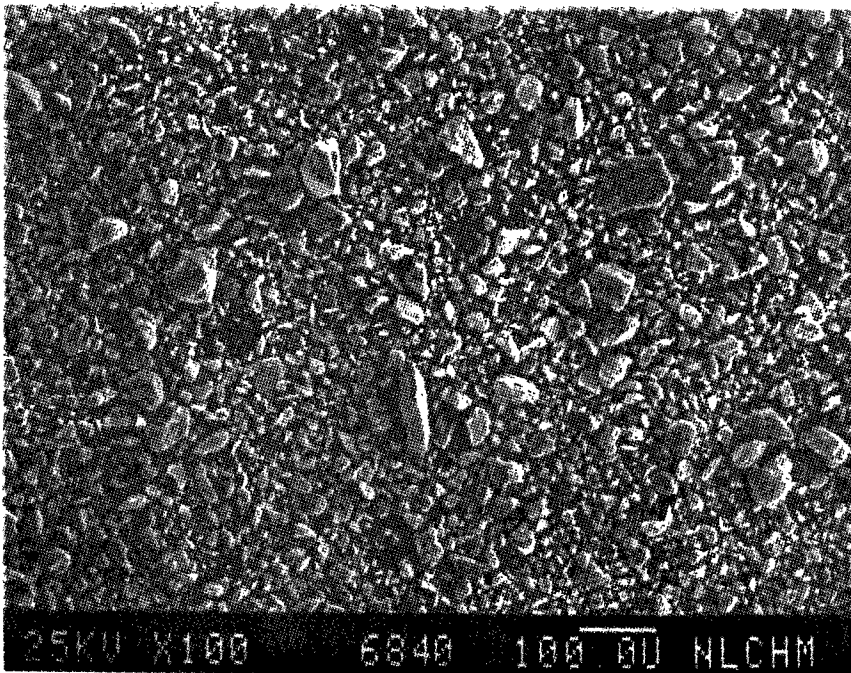


Figure 154

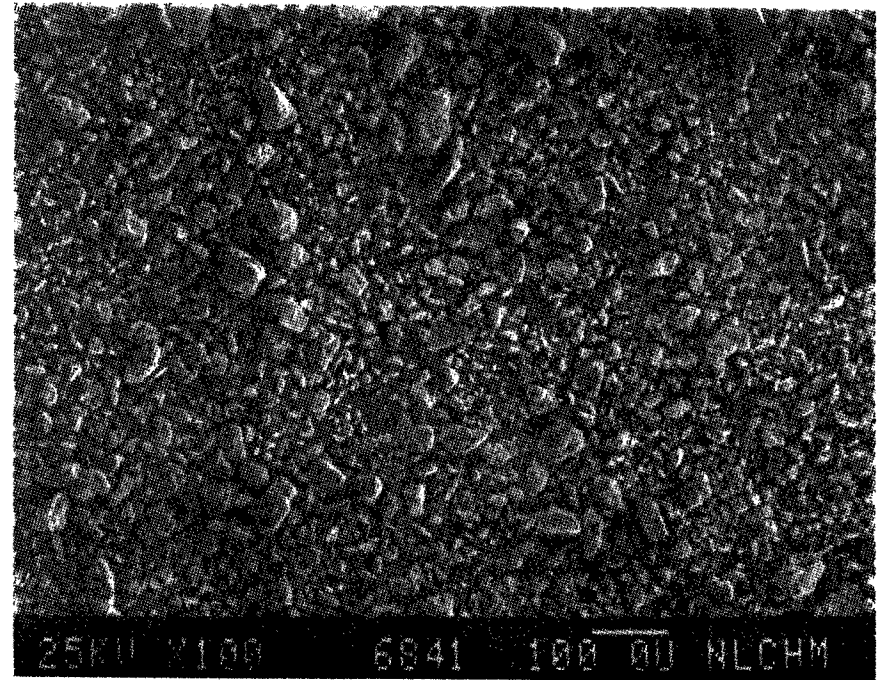


Figure 155

SEM IMAGES OF SAMPLE #

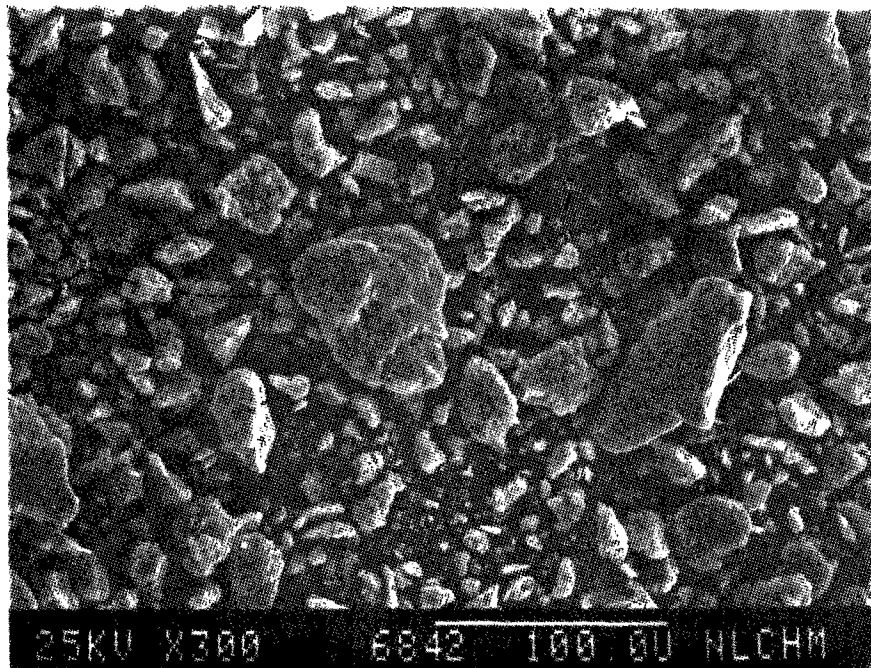


Figure 156

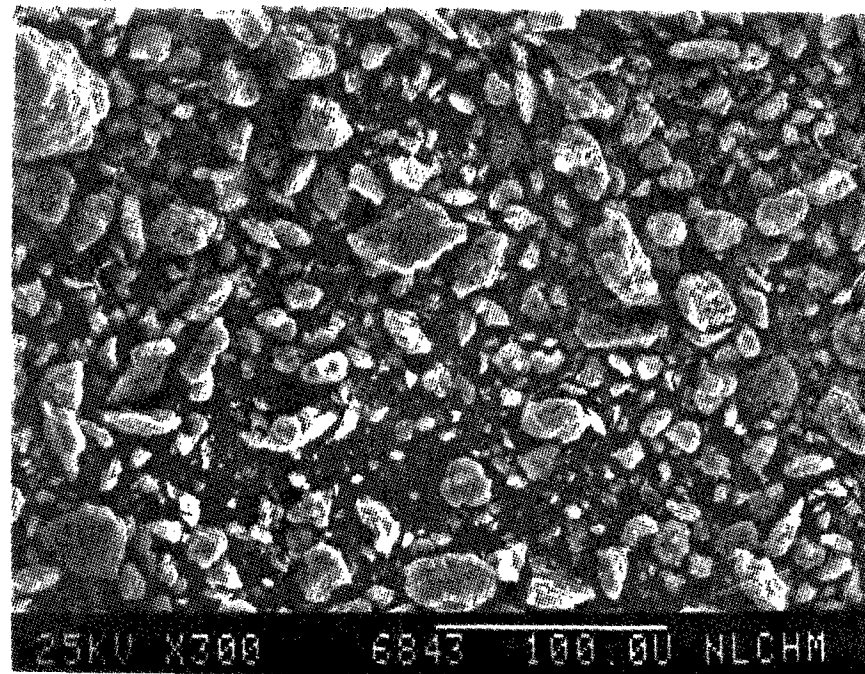


Figure 157

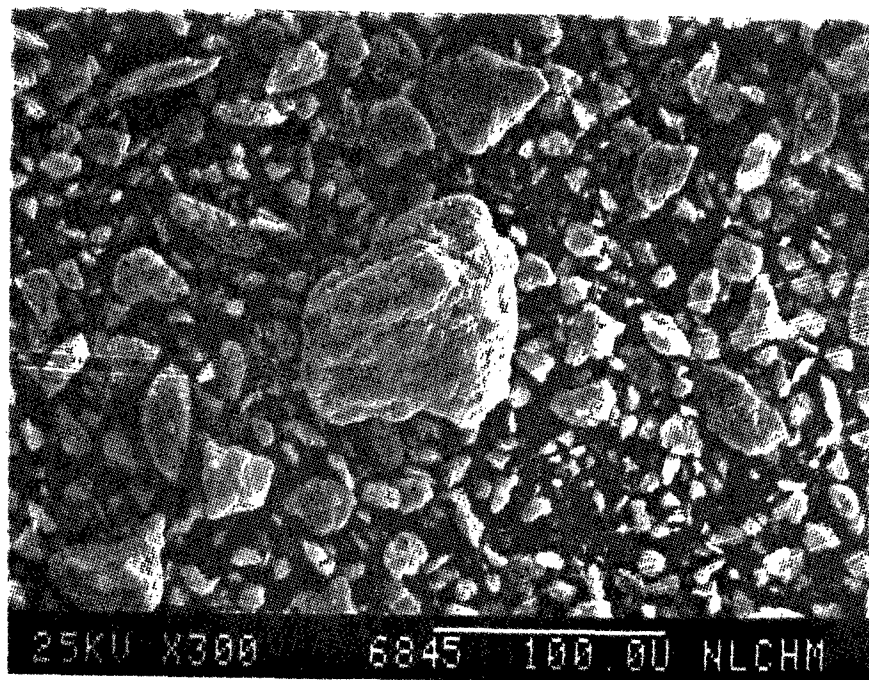


Figure 158

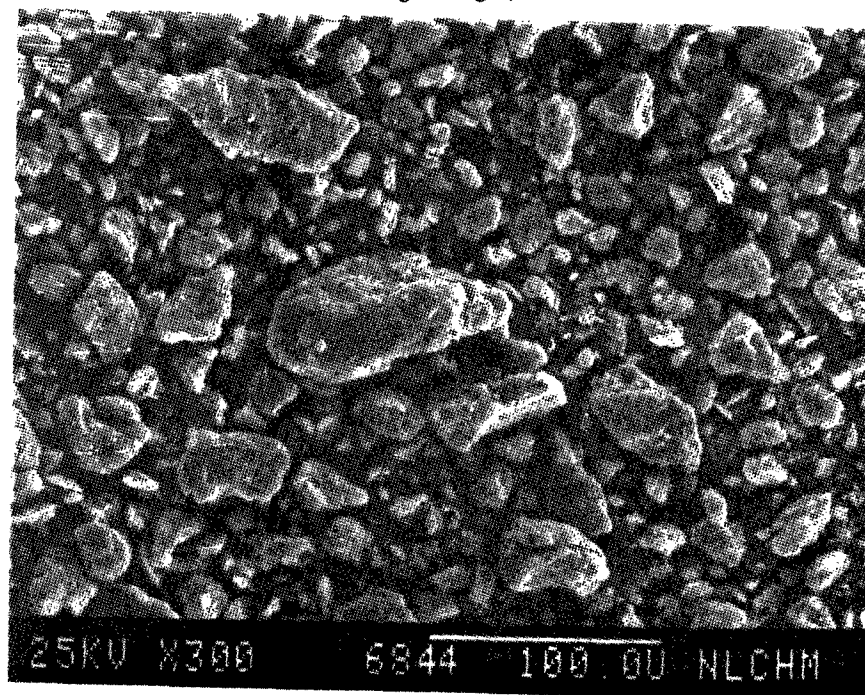


Figure 159



SEM IMAGES OF SAMPLE #

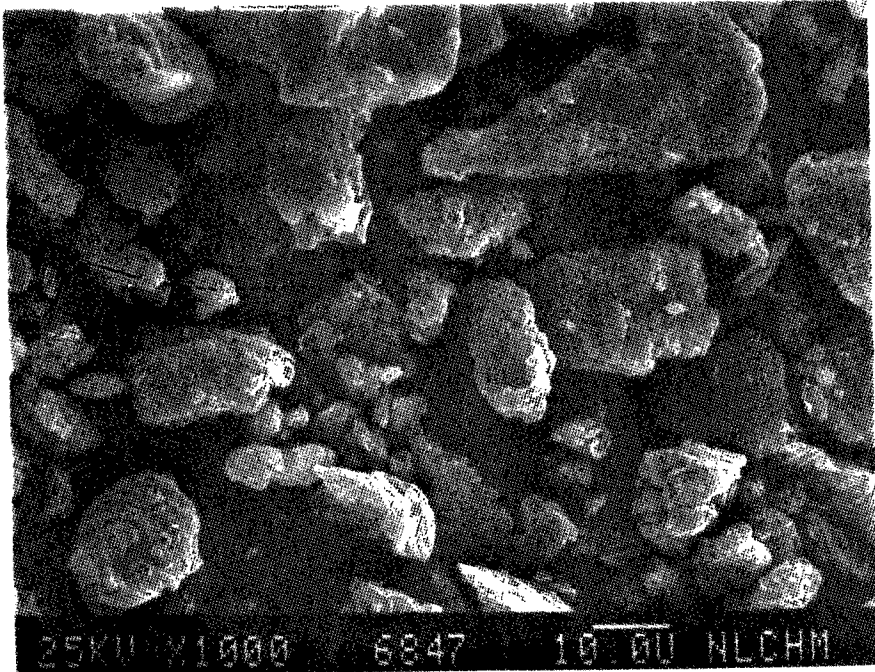


Figure 160

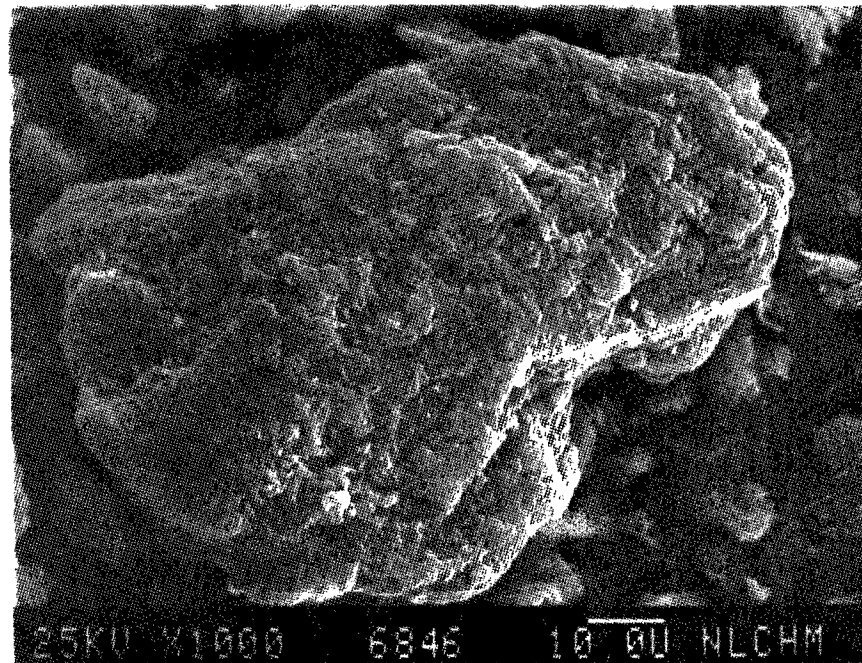


Figure 161

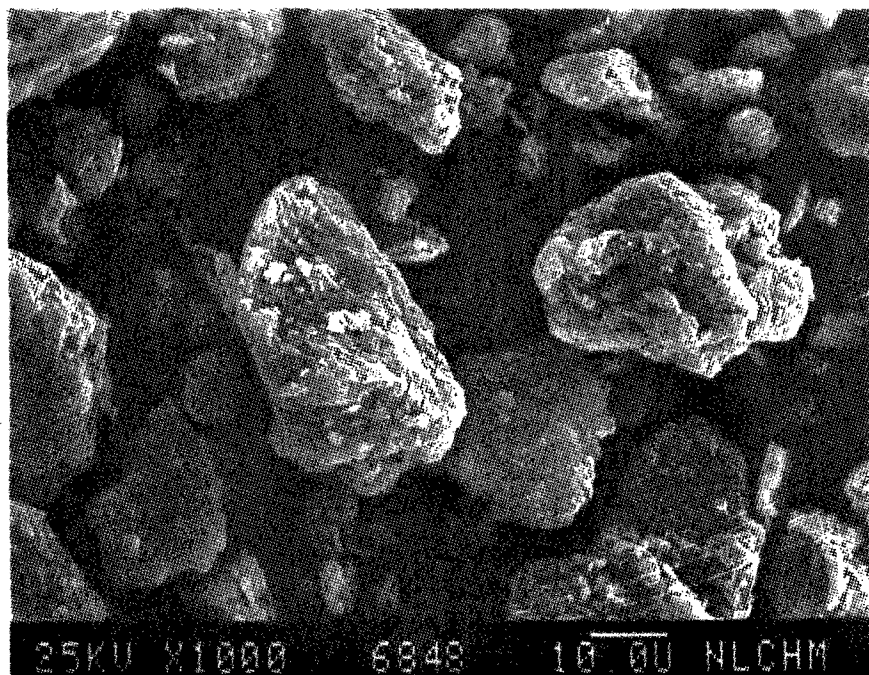


Figure 162



Figure 163

SEM IMAGES OF SAMPLE #

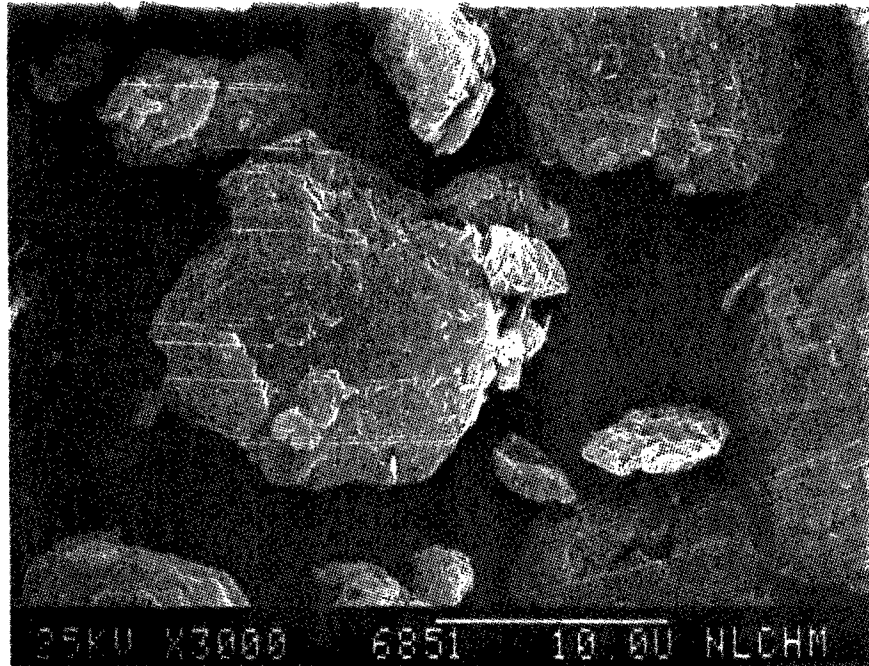


Figure 164

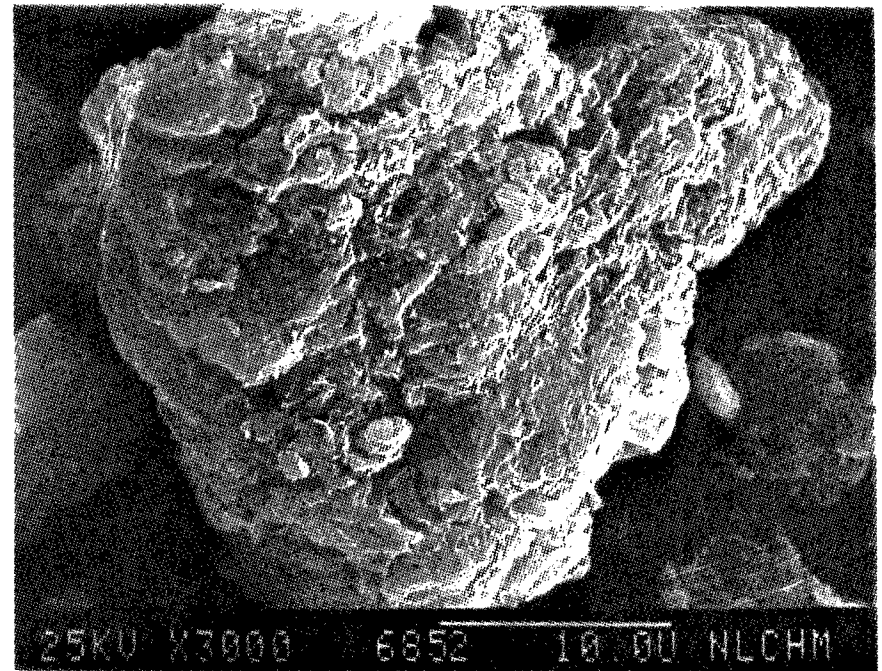


Figure 165

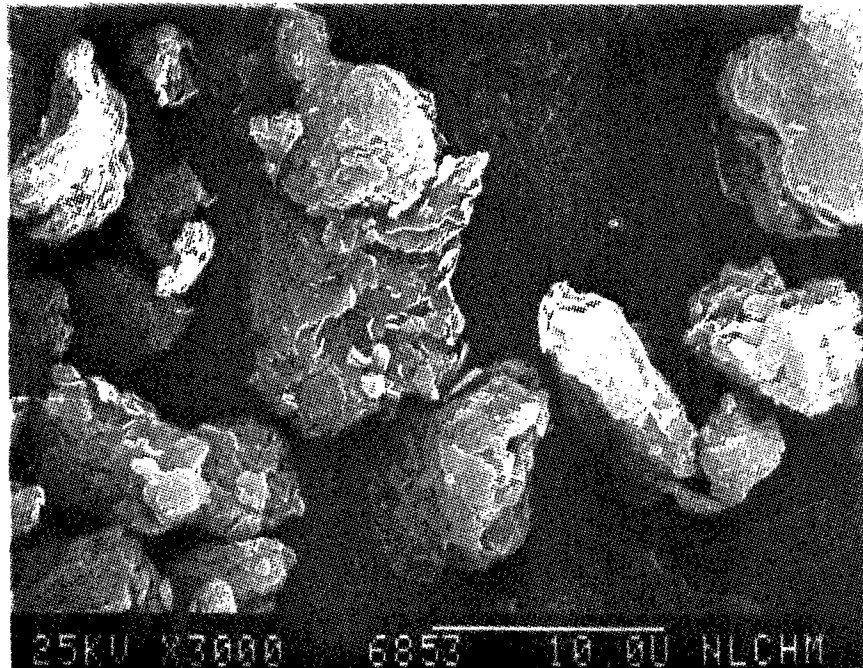


Figure 166

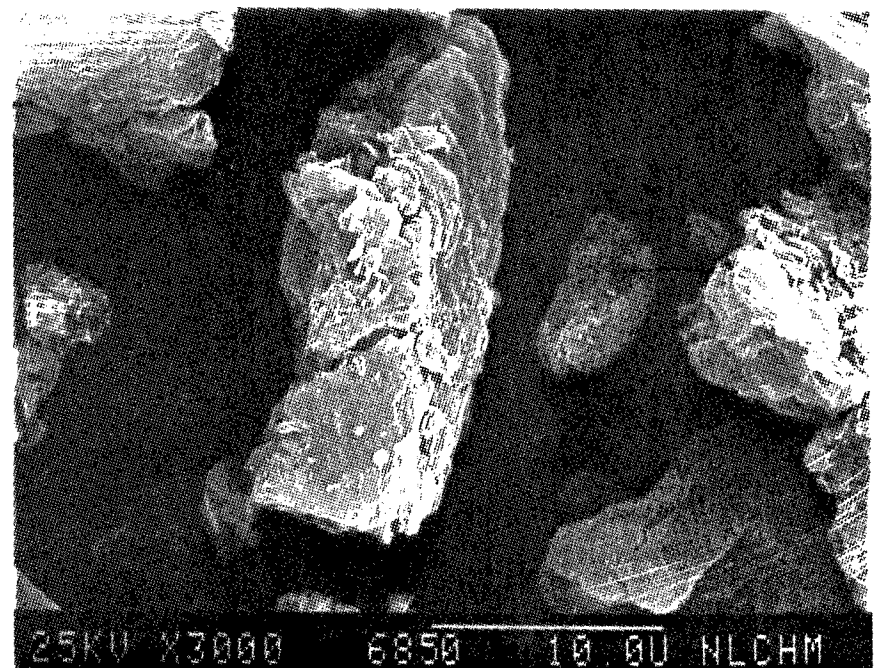


Figure 167

SEM IMAGES OF SAMPLE #

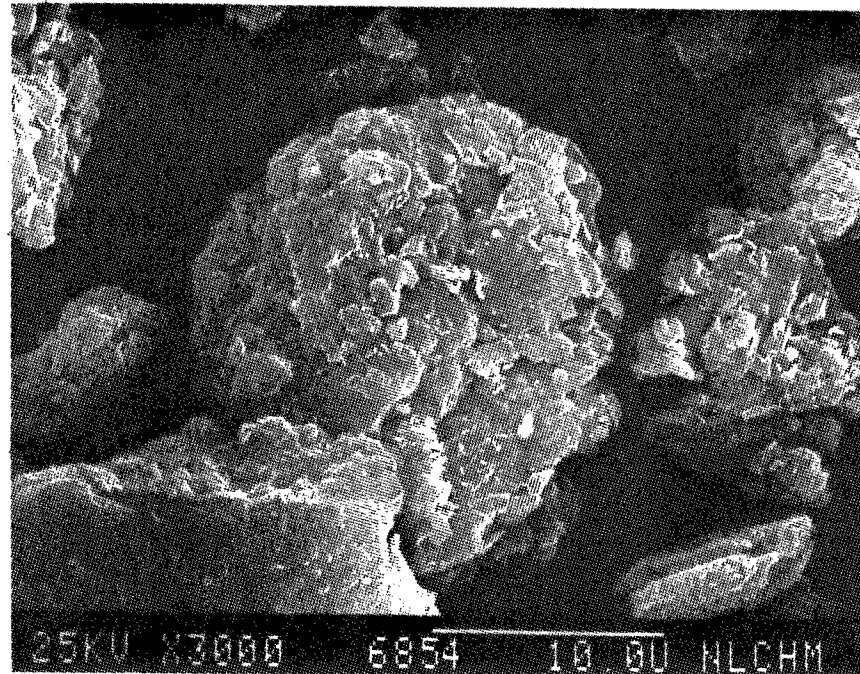


Figure 168



SEM IMAGES OF SAMPLE #

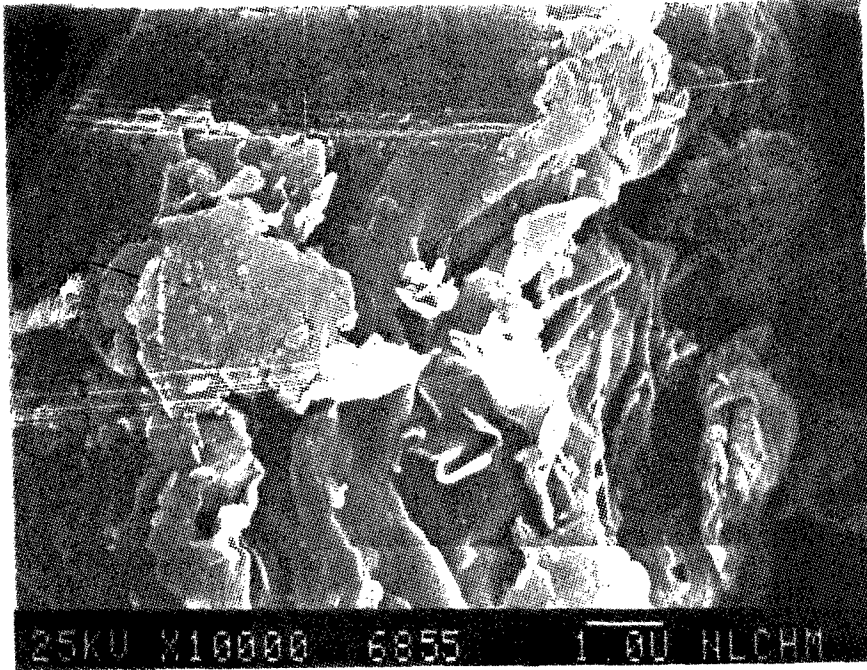


Figure 169

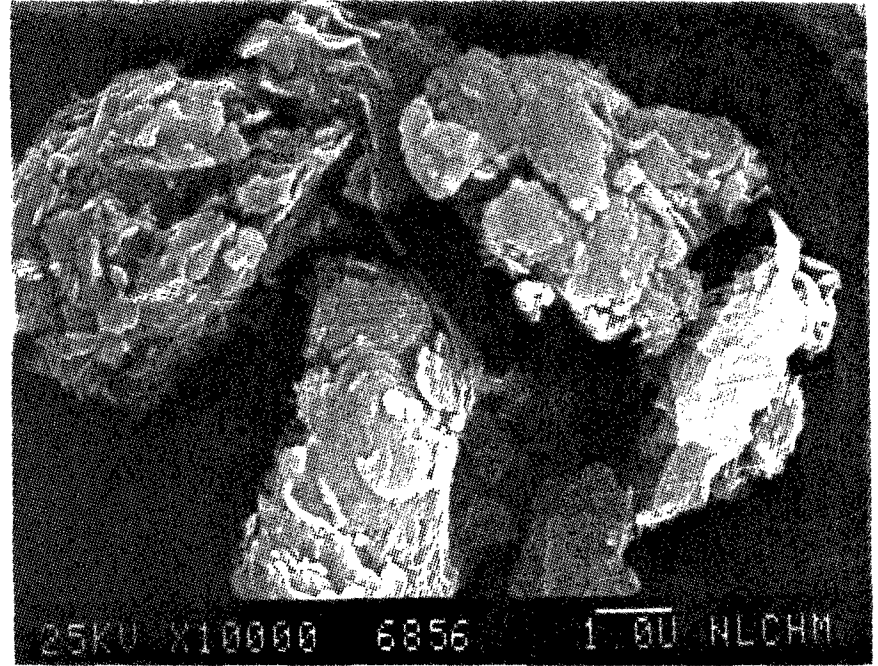


Figure 170

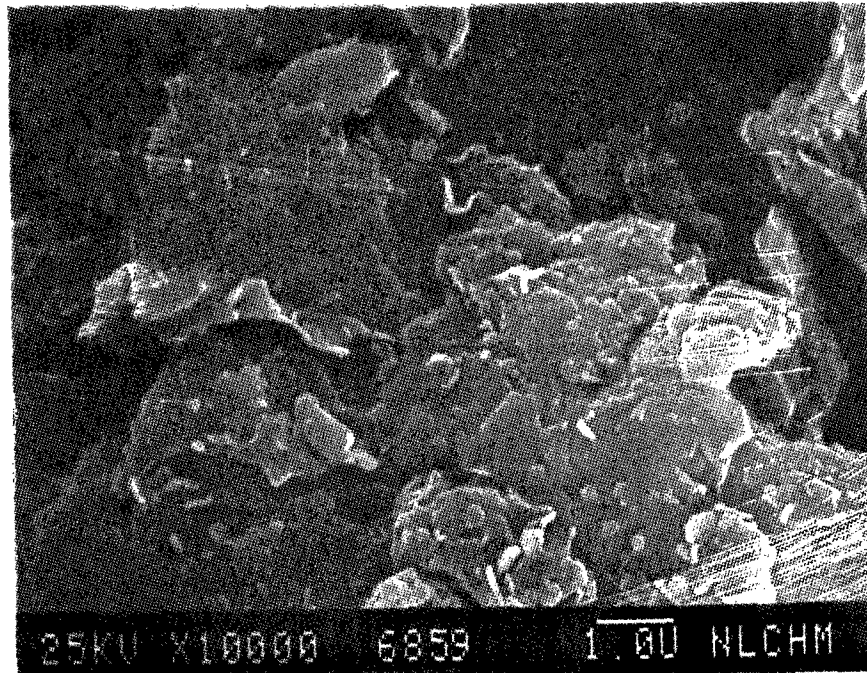


Figure 171



Figure 172

SEM IMAGES OF SAMPLE #

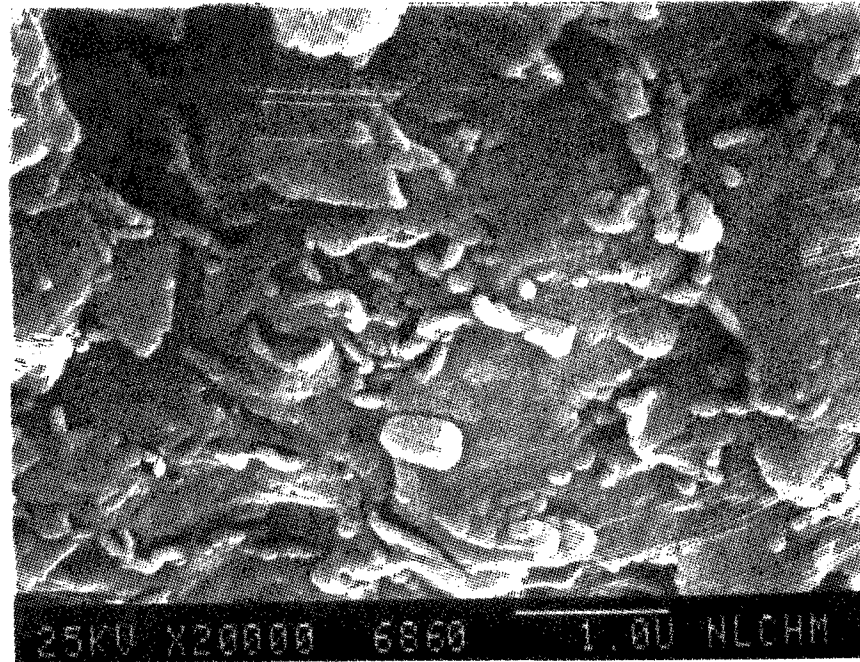


Figure 173

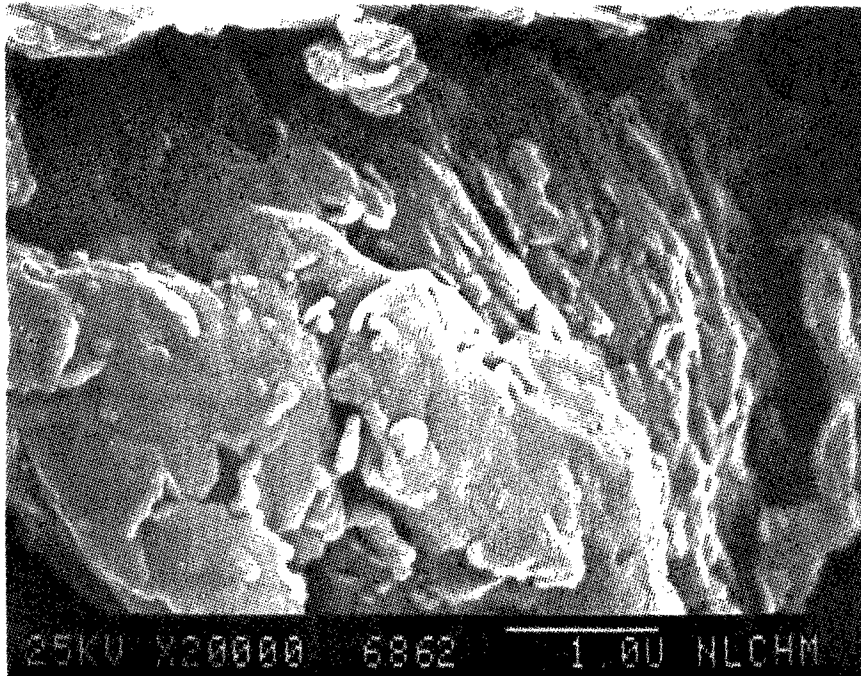


Figure 174

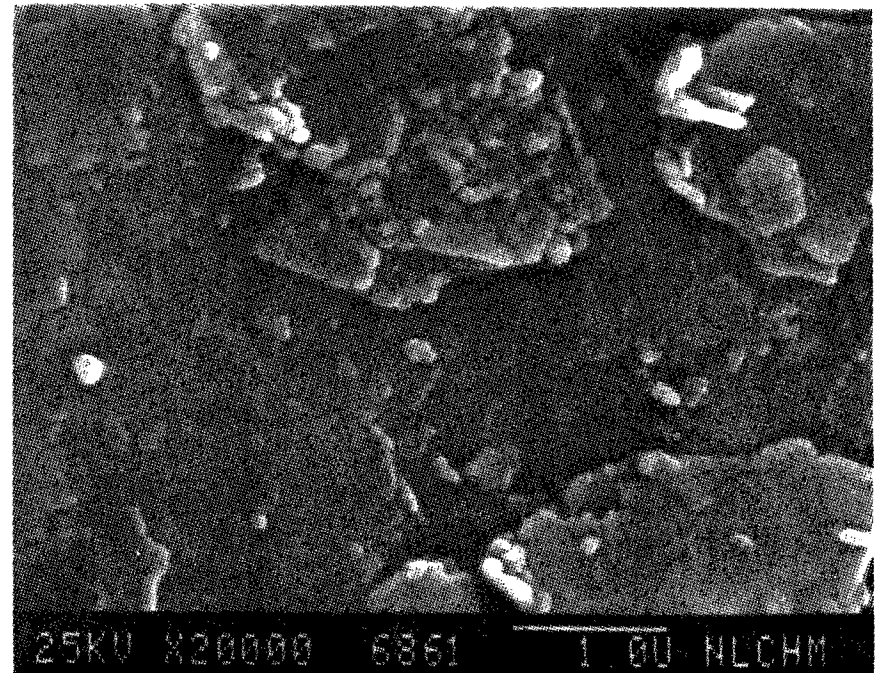


Figure 175

SEM IMAGES OF SAMPLE #

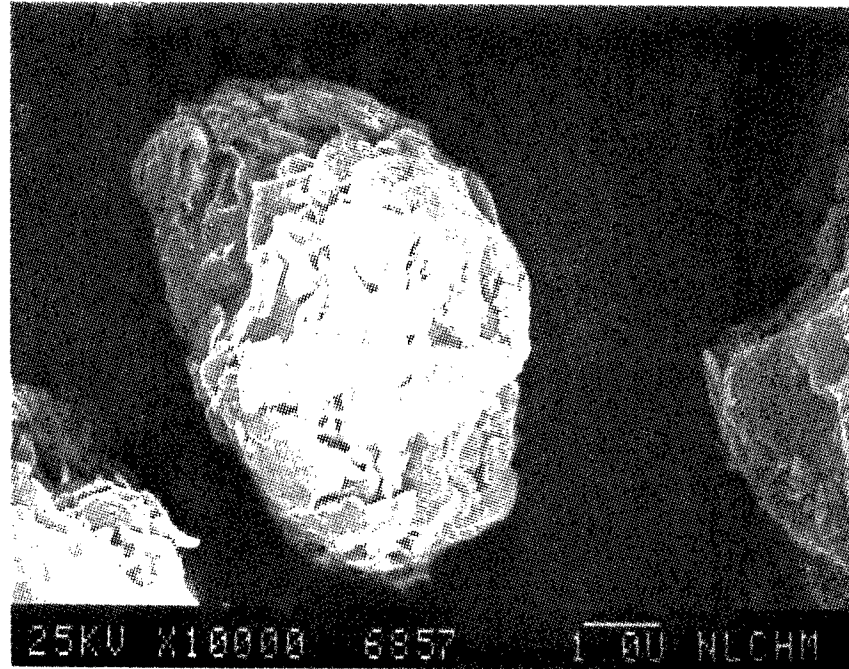


Figure 176



SEM IMAGES OF SAMPLE #

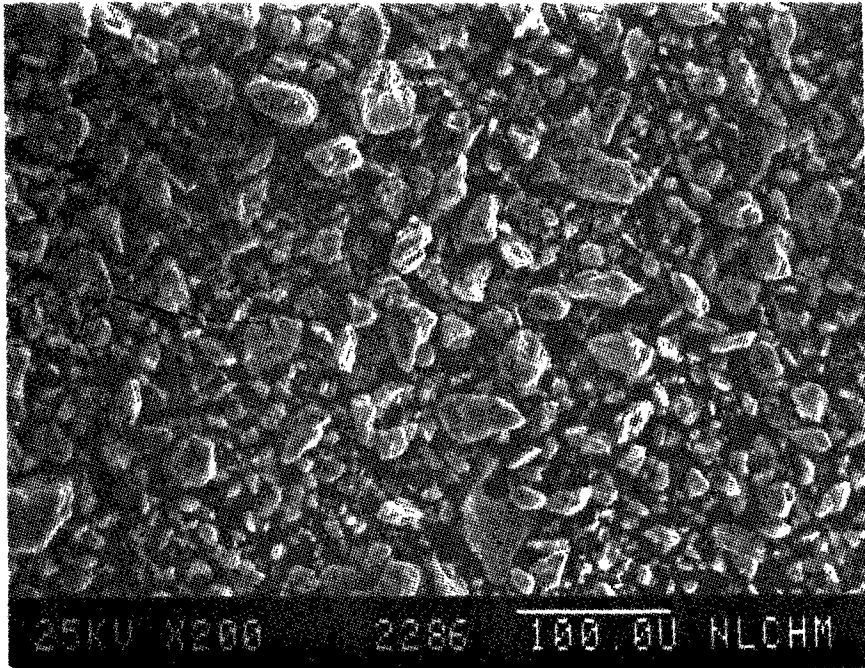


Figure 177

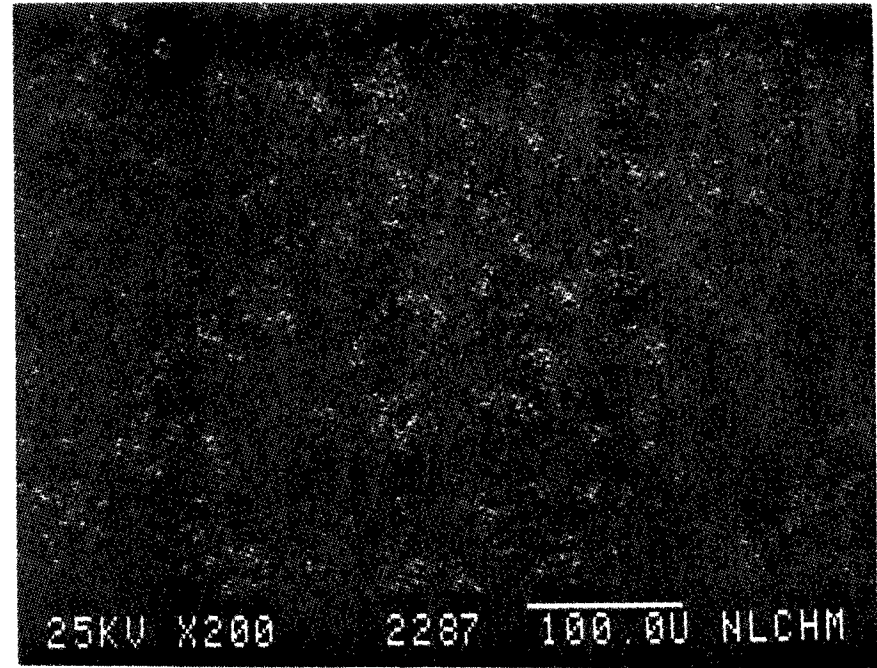


Figure 178

AL X-Ray Image of Figure 177

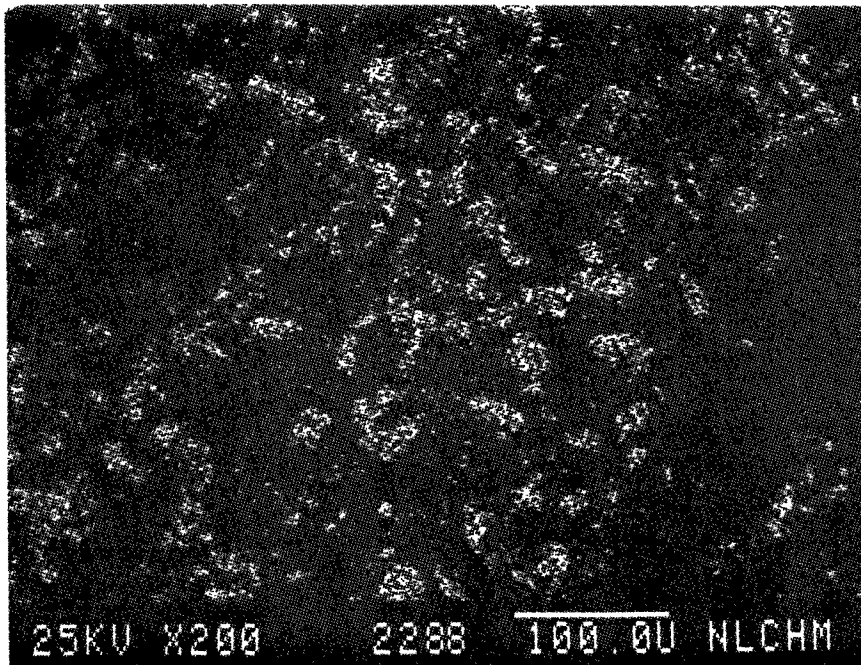


Figure 179

Si X-Ray Image of Figure 177

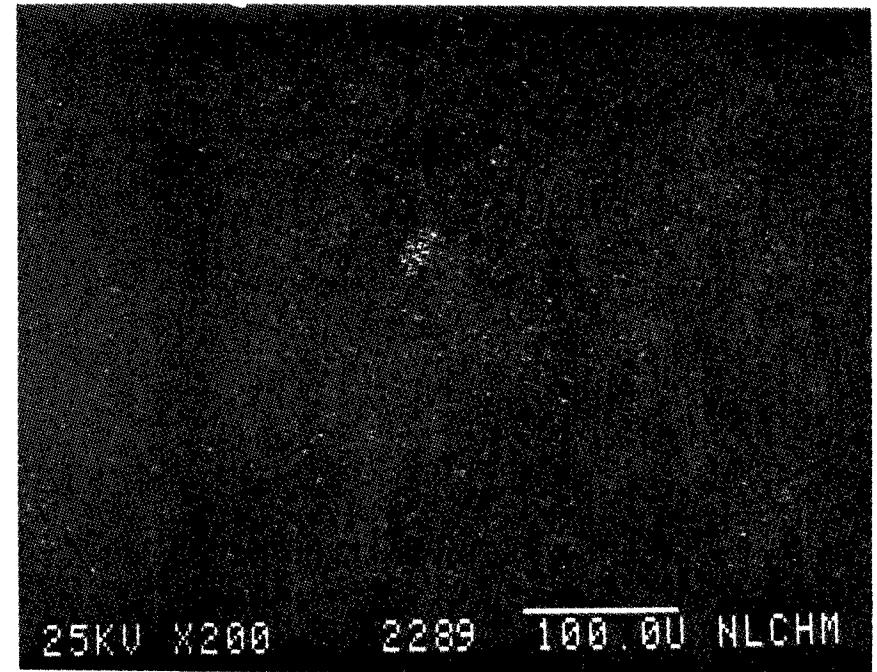


Figure 180

Ca X-Ray Image of Figure 177

SEM IMAGES OF SAMPLE #

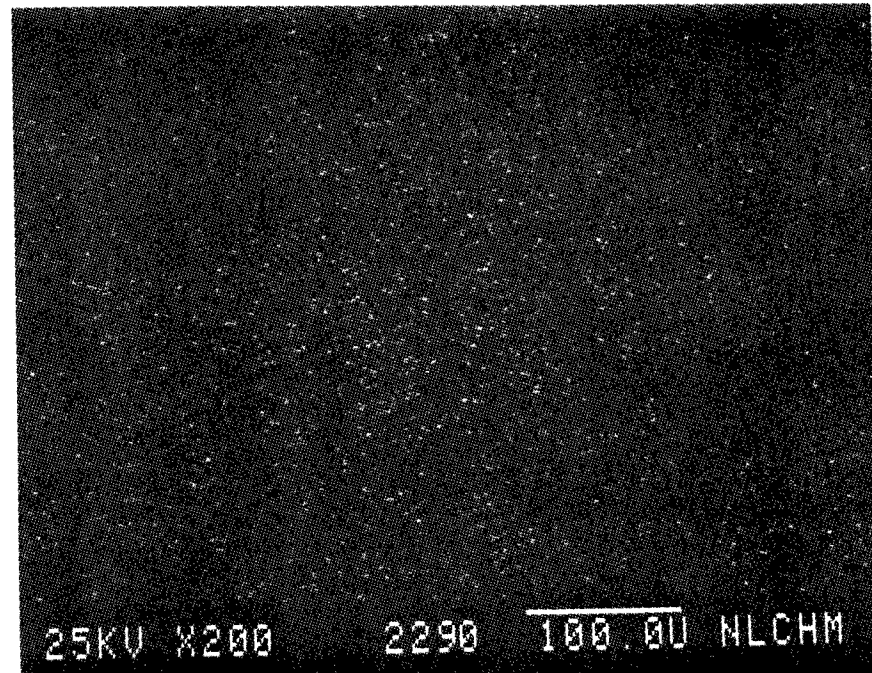


Figure 181

Fe X-Ray Image of Figure 177

SEM IMAGES OF SAMPLE #

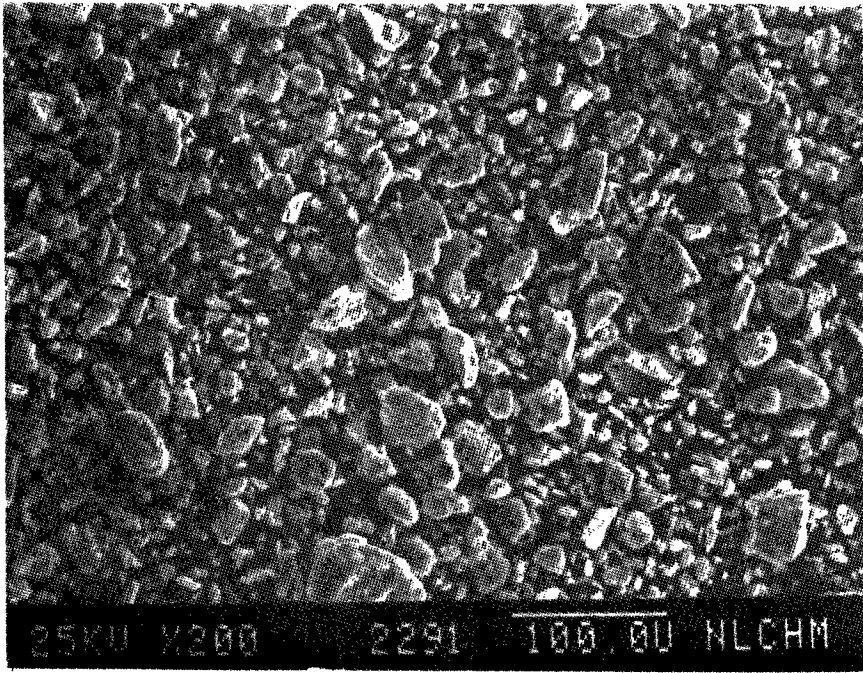


Figure 182

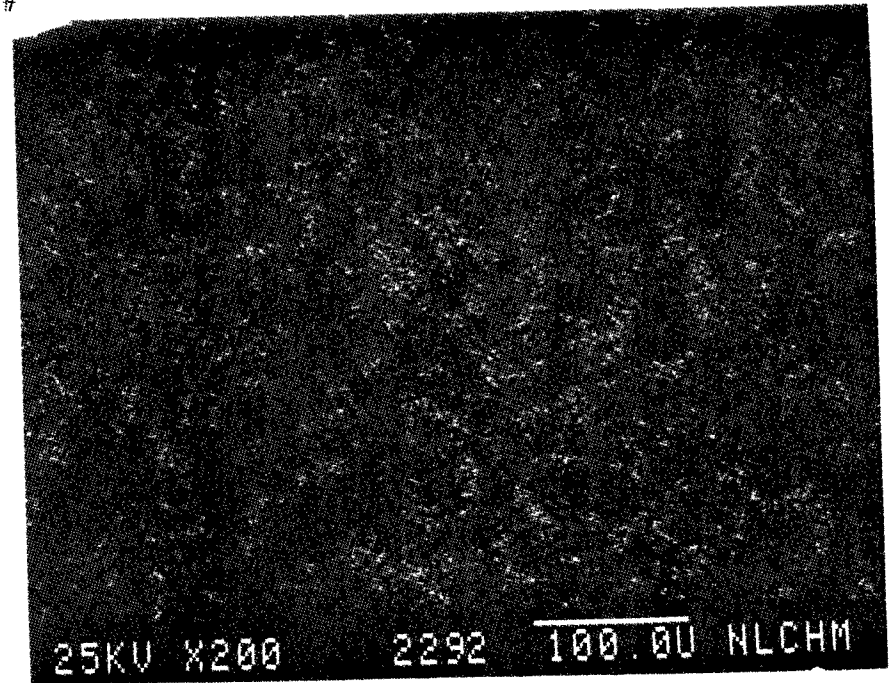


Figure 183

AL X-Ray Image of Figure 182

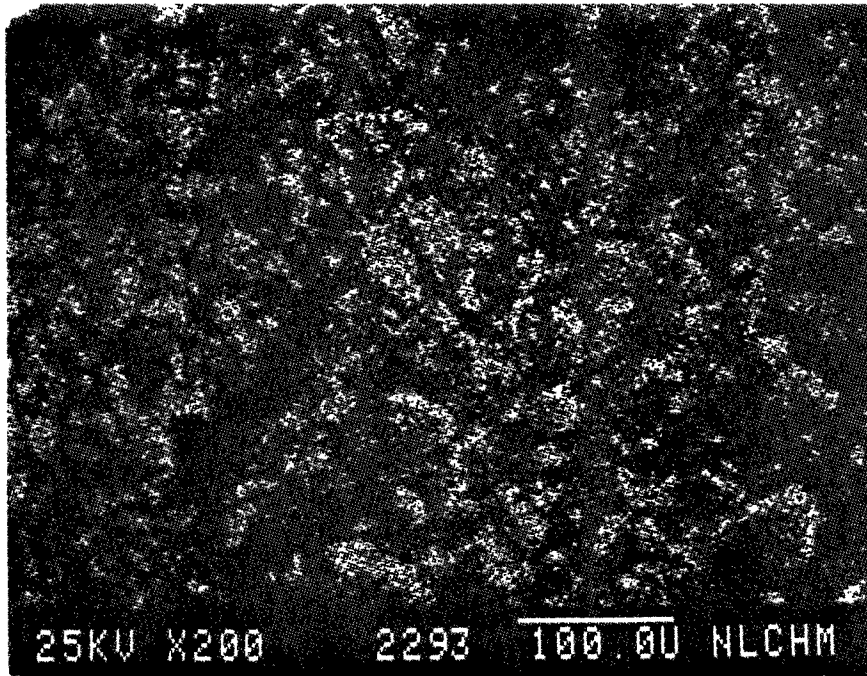


Figure 184

Si X-Ray Image of Figure 182

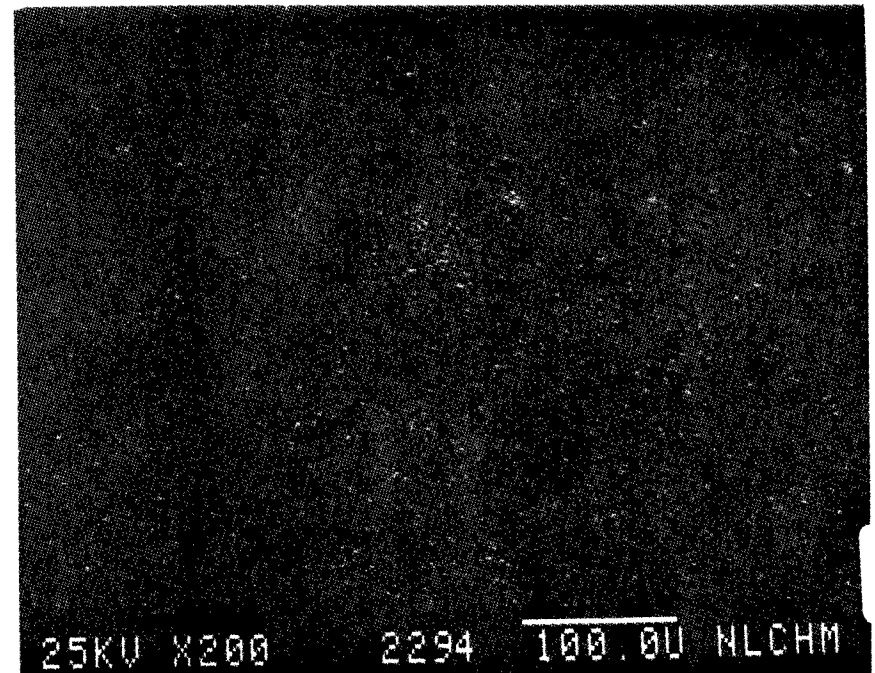


Figure 185

Ca X-Ray Image of Figure 182

SEM IMAGES OF SAMPLE #

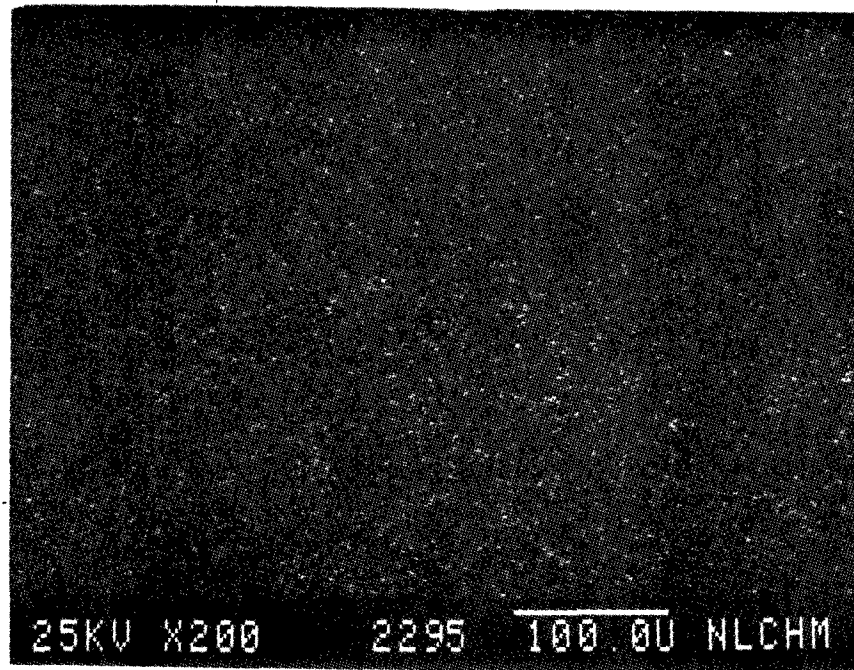


Figure 186

Fe X-Ray Image of Figure 182



SEM IMAGES OF SAMPLE #

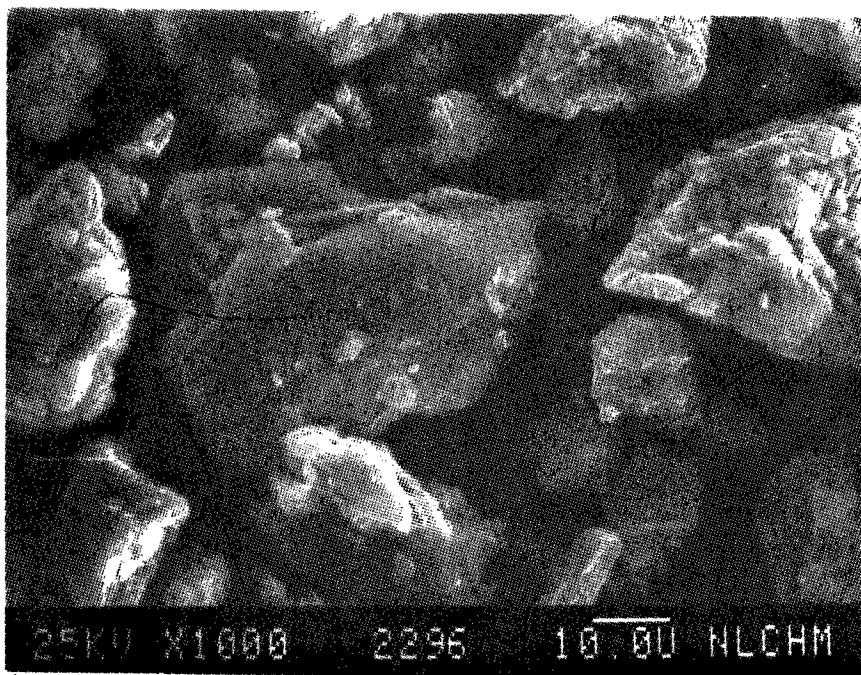


Figure 187

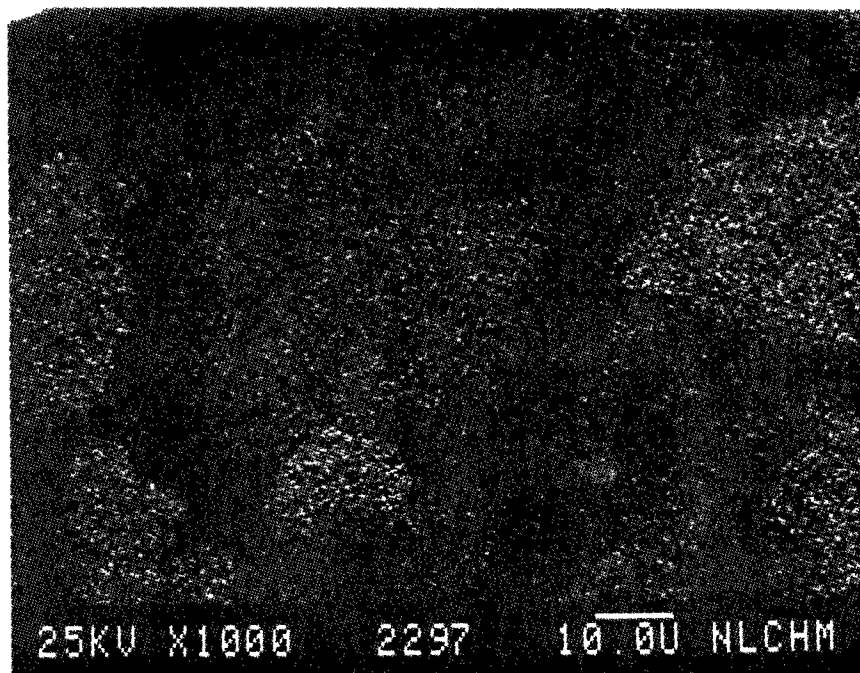


Figure 188

AL X-Ray Image of Figure 187

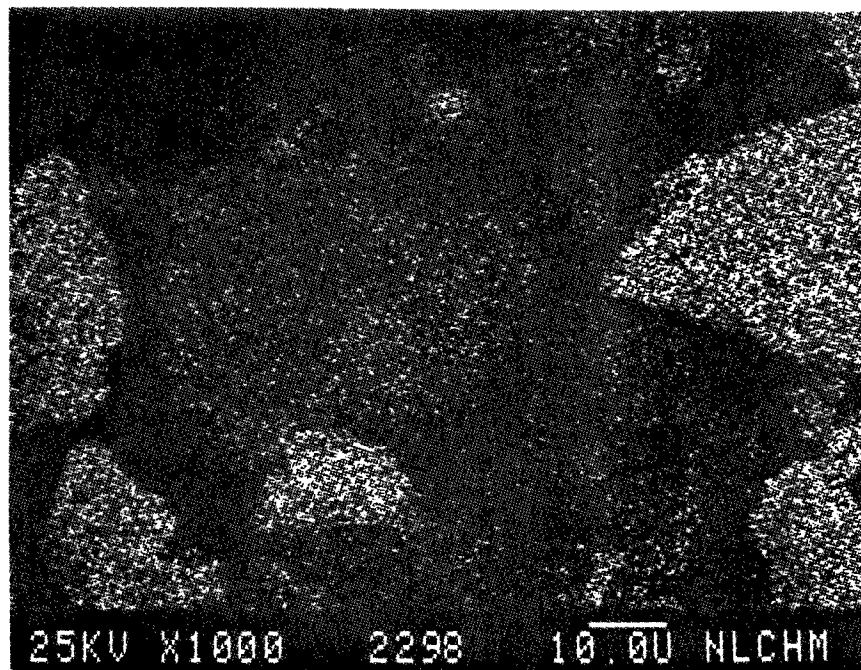


Figure 189

Si X-Ray Image of Figure 187

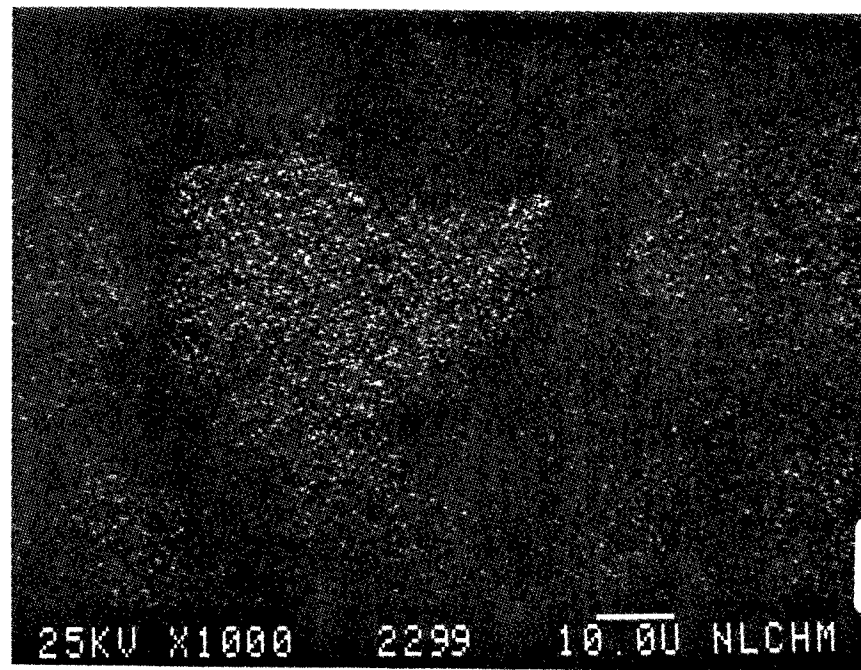


Figure 190

S X-Ray Image of Figure 187

SEM IMAGES OF SAMPLE #

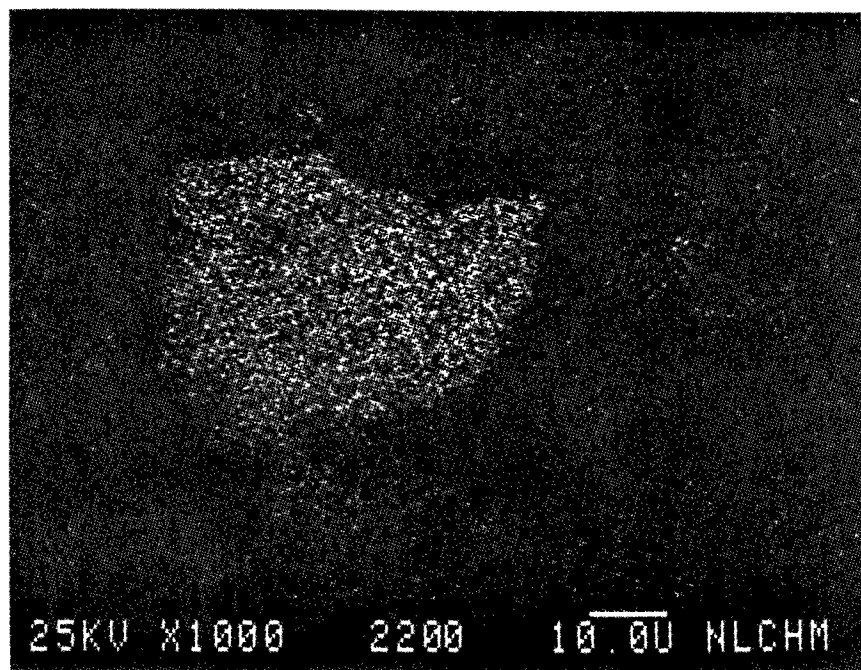


Figure 191

Ca X-Ray Image of Figure 187

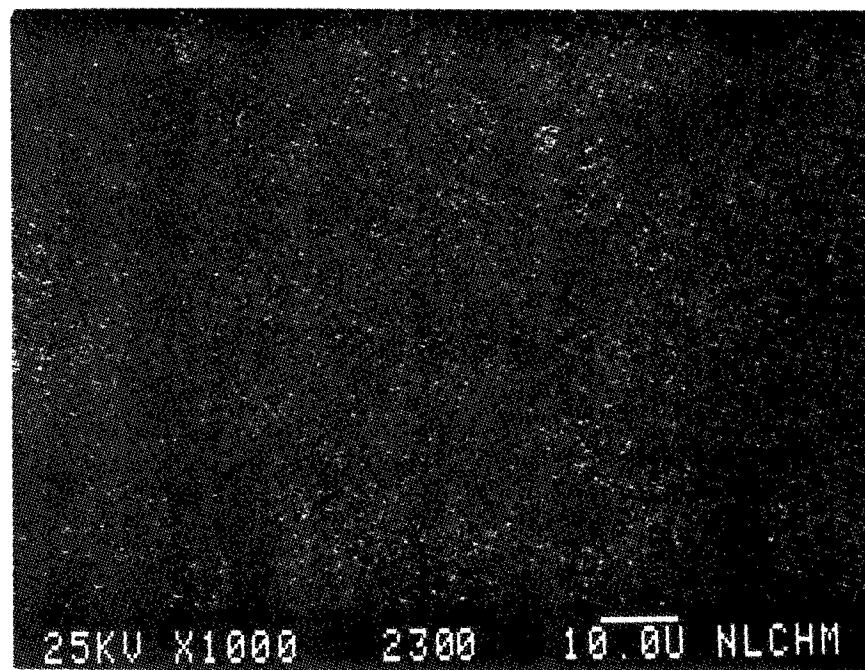


Figure 192

Fe X-Ray Image of Figure 187

SEM IMAGES OF SAMPLE #

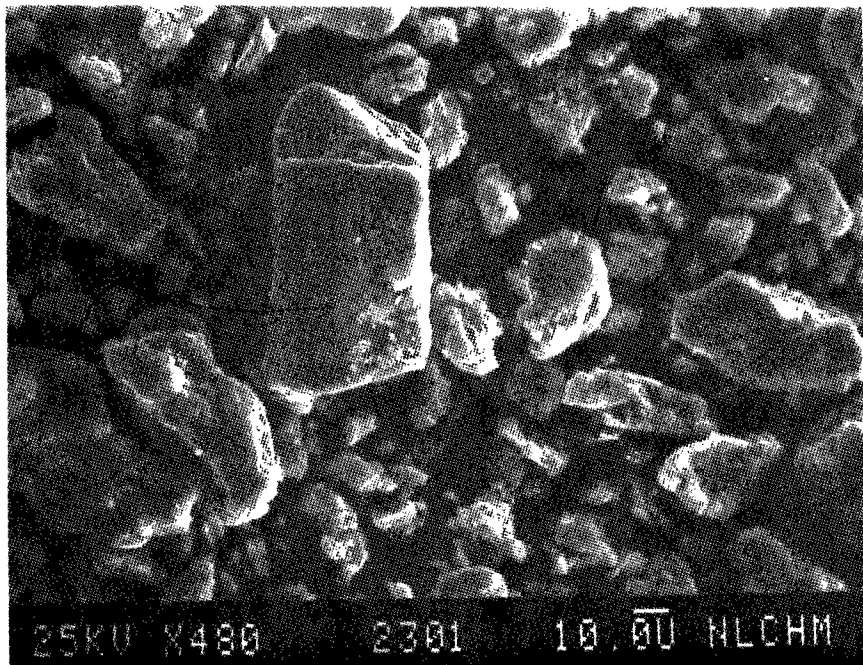


Figure 193

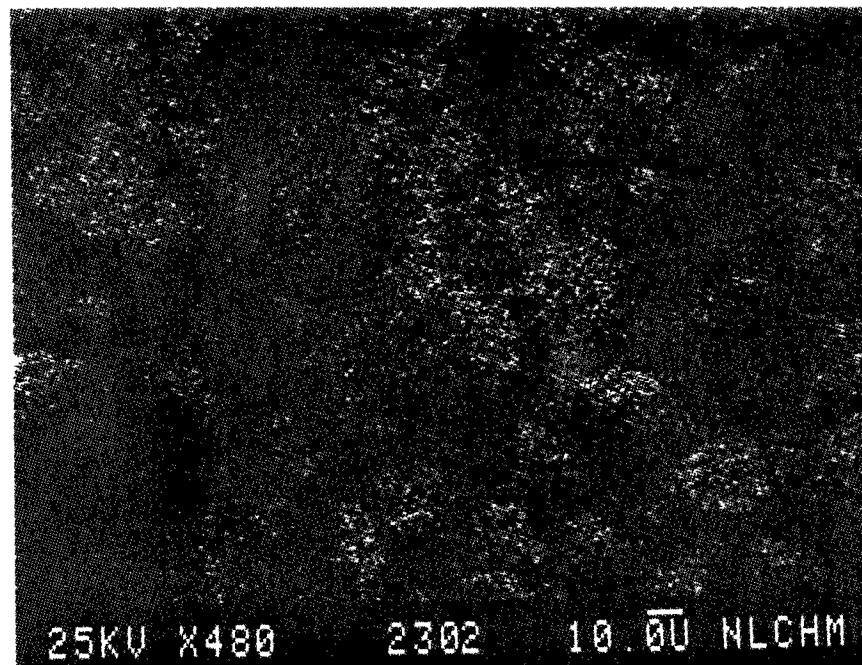


Figure 194

AL X-Ray Image of Figure 193

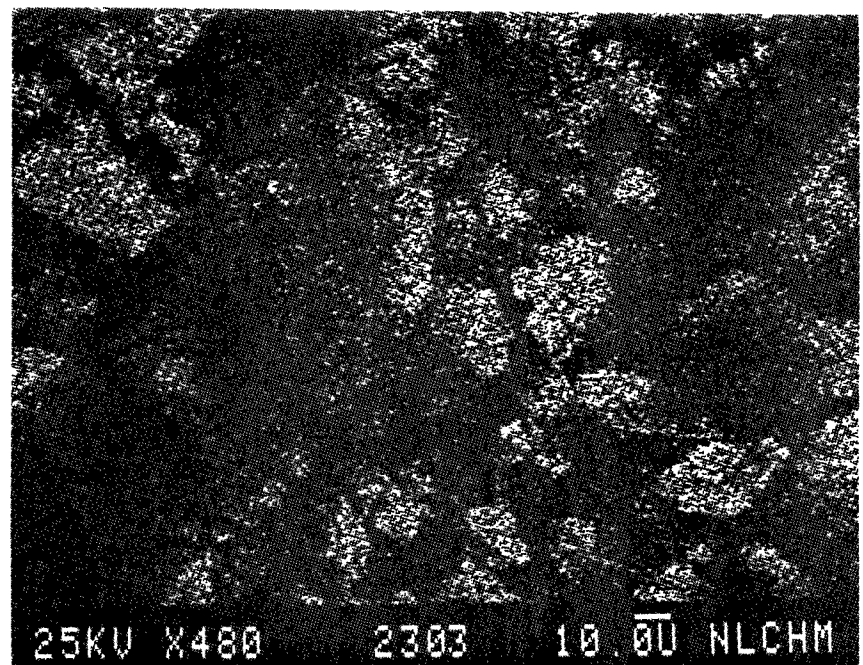


Figure 195

Si X-Ray Image of Figure 193

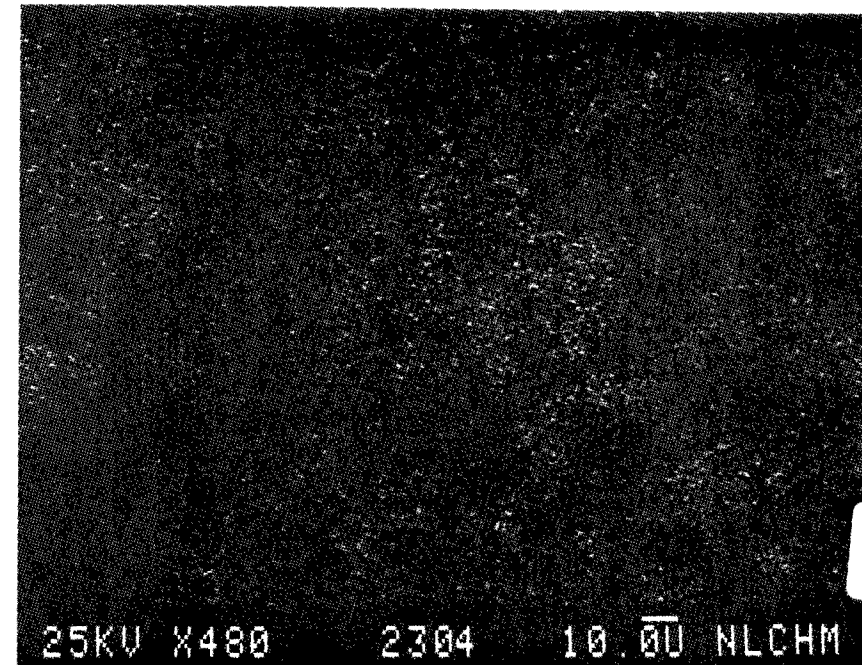


Figure 196

S X-Ray Image of Figure 193

SEM IMAGES OF SAMPLE #

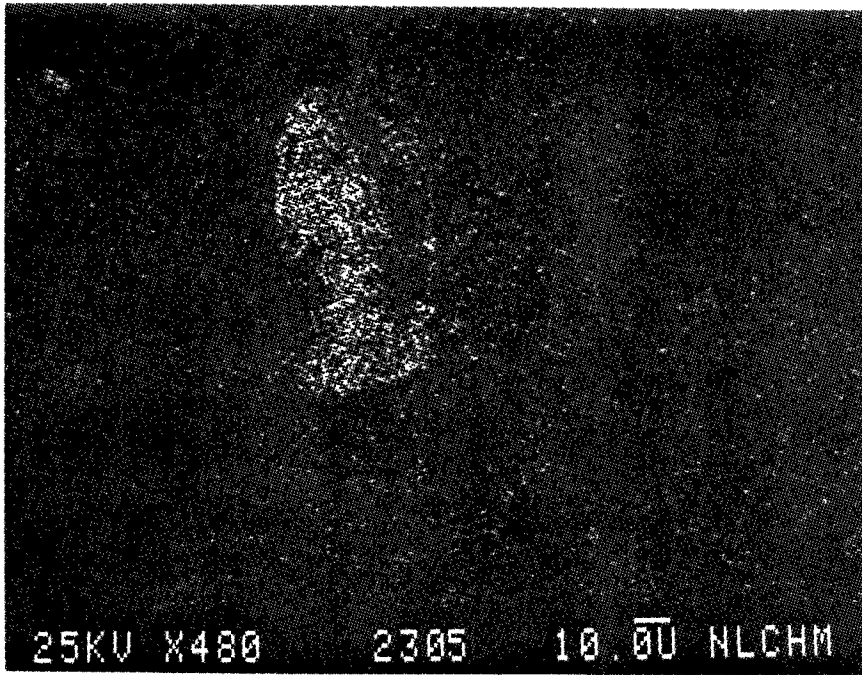


Figure 197

Ca X-Ray Image of Figure 193

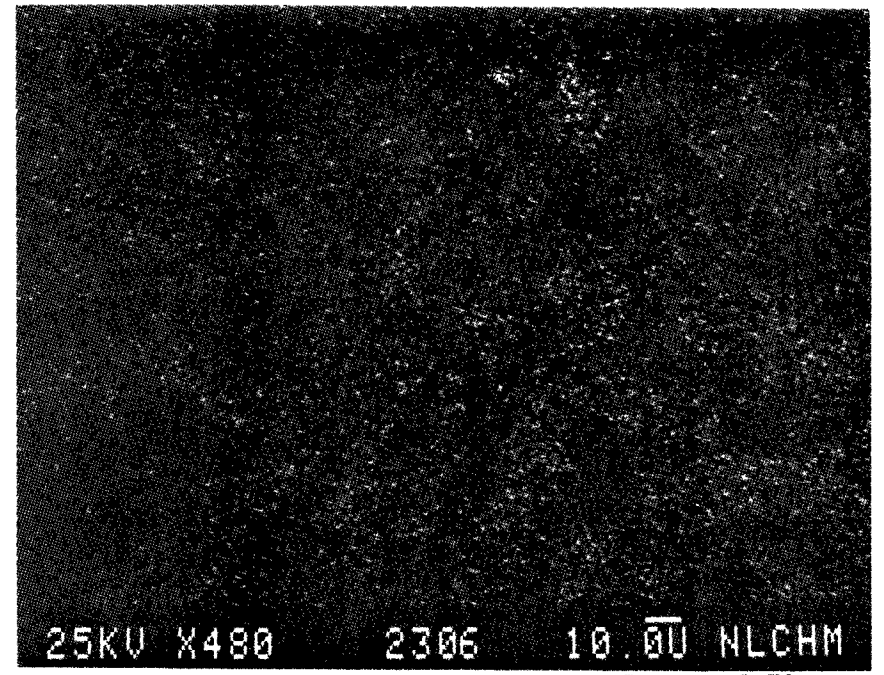


Figure 198

Fe X-Ray Image of Figure 193



SEM IMAGES OF SAMPLE #

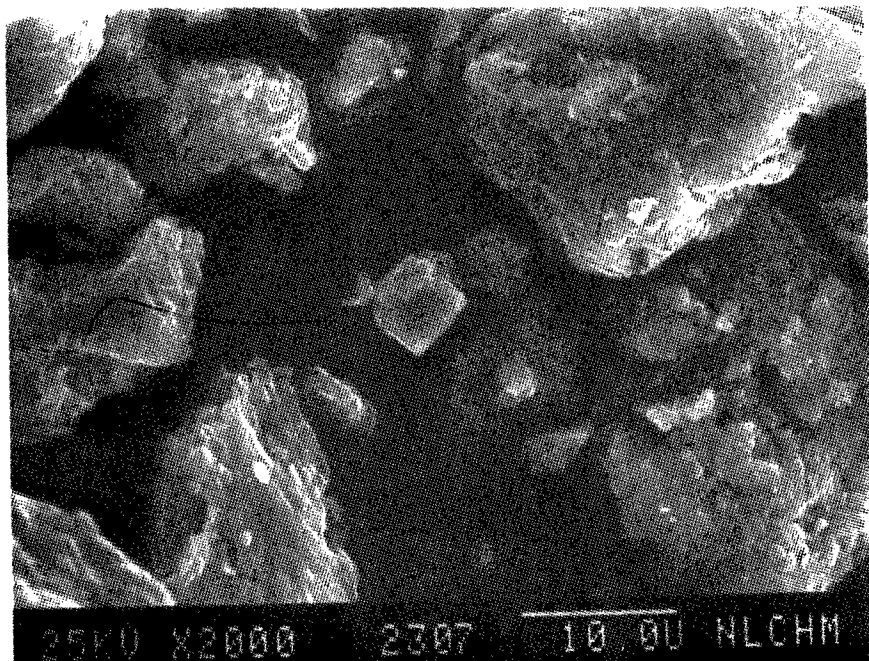


Figure 199

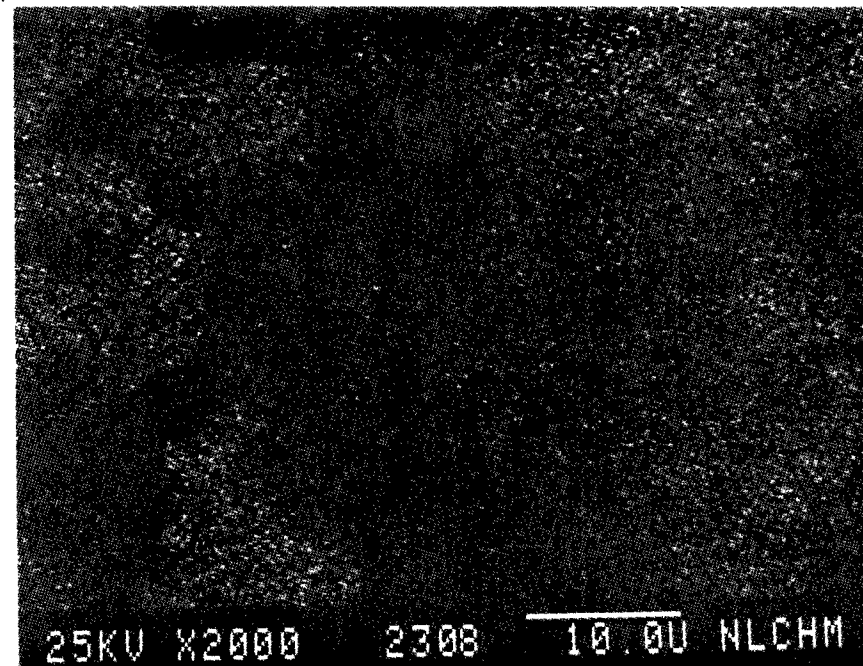


Figure 200

AL X-Ray Image of Figure 199

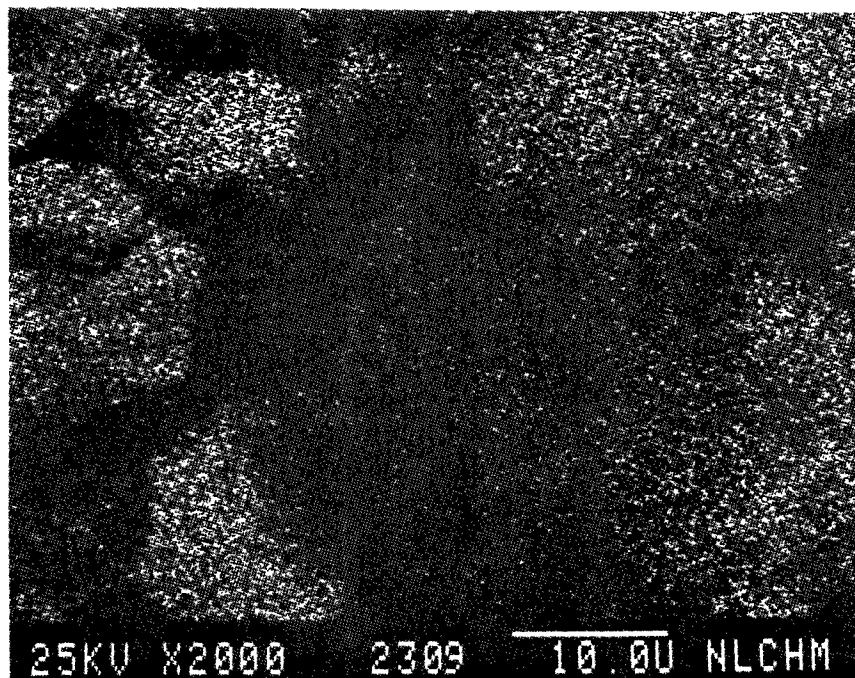


Figure 201

Si X-Ray Image of Figure 199

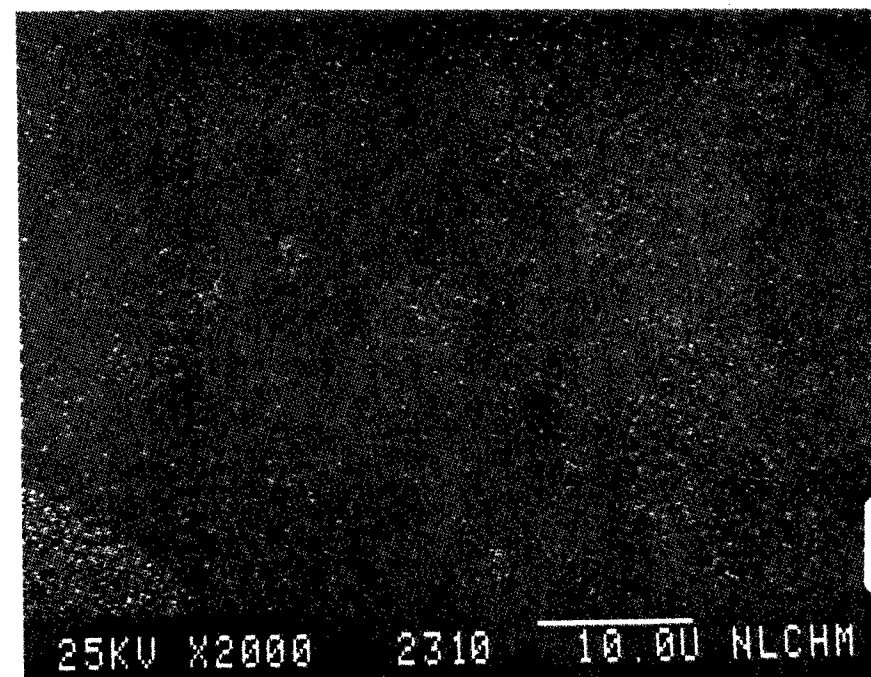


Figure 202

Ca X-Ray Image of Figure 199

SEM IMAGES OF SAMPLE #

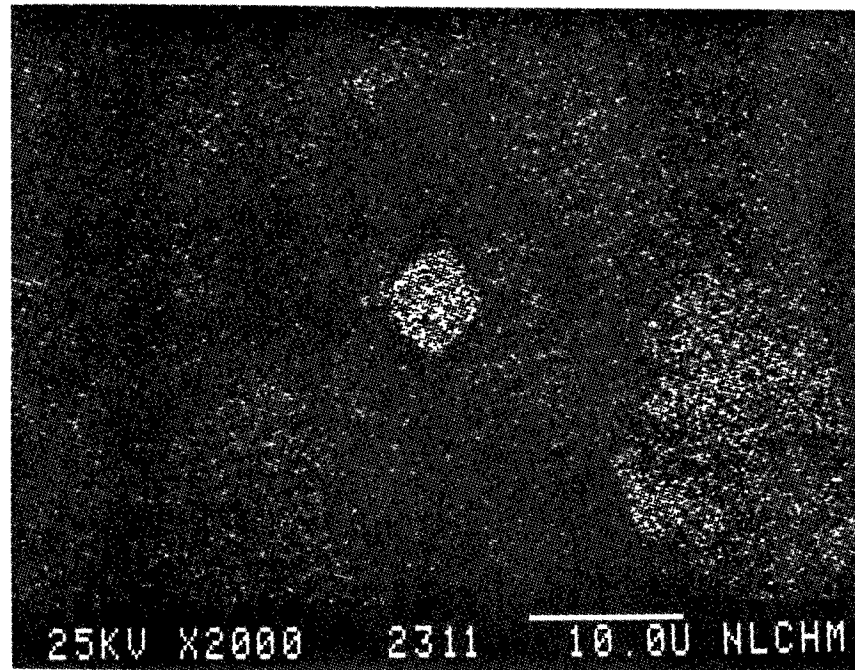


Figure 203

Fe X-Ray Image of Figure 199

SEM IMAGES OF SAMPLE #

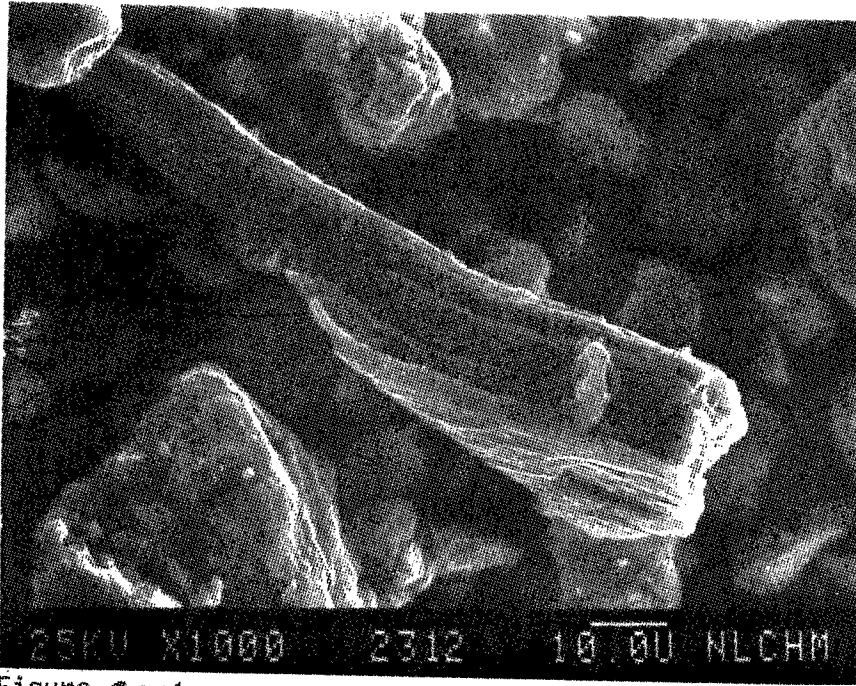


Figure 204

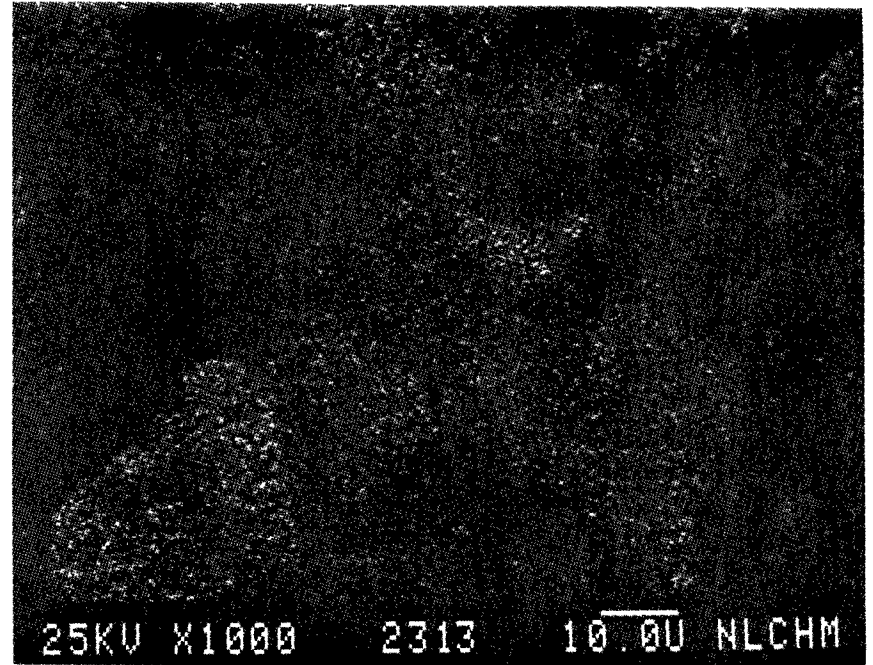


Figure 205

AL X-Ray Image of Figure 204

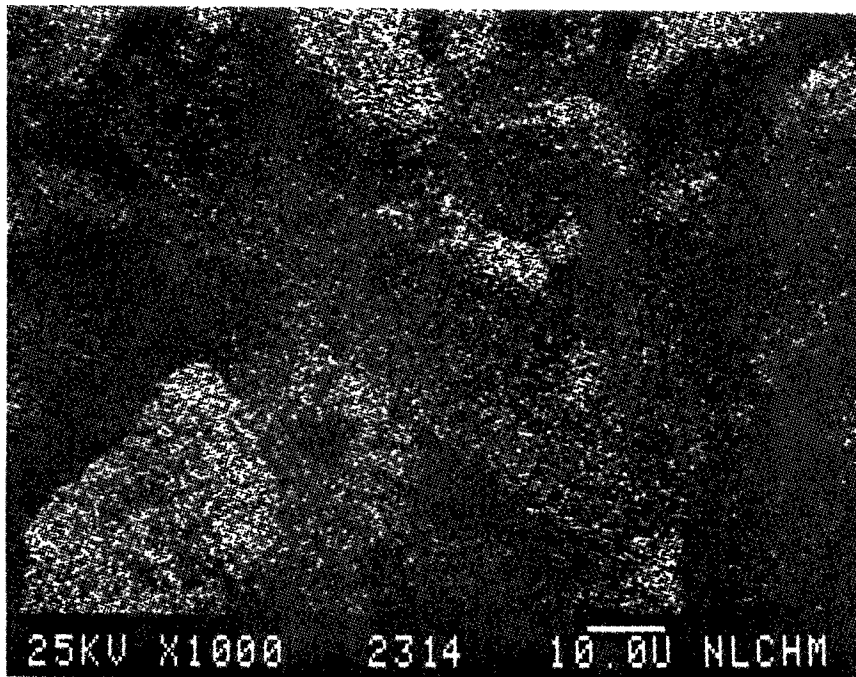


Figure 206

Si X-Ray Image of Figure 204

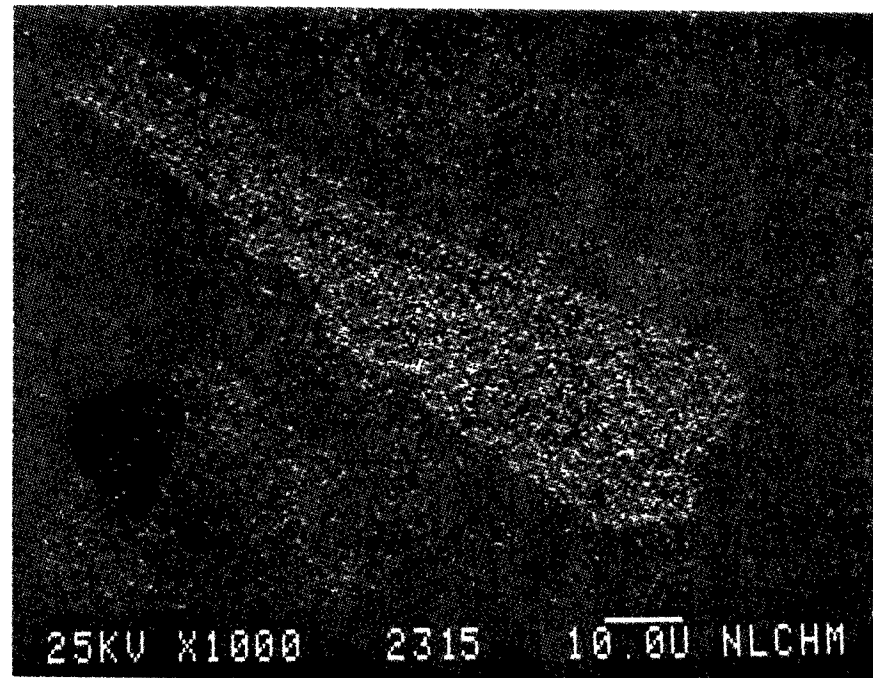


Figure 207

S X-Ray Image of Figure 204



SEM IMAGES OF SAMPLE #

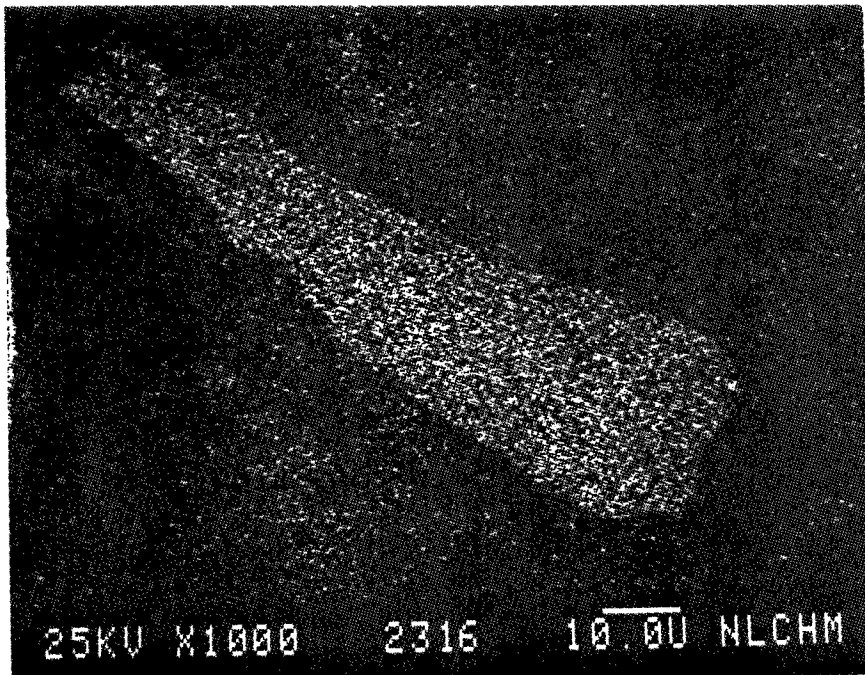


Figure 208

Ca X-Ray Image of Figure 204

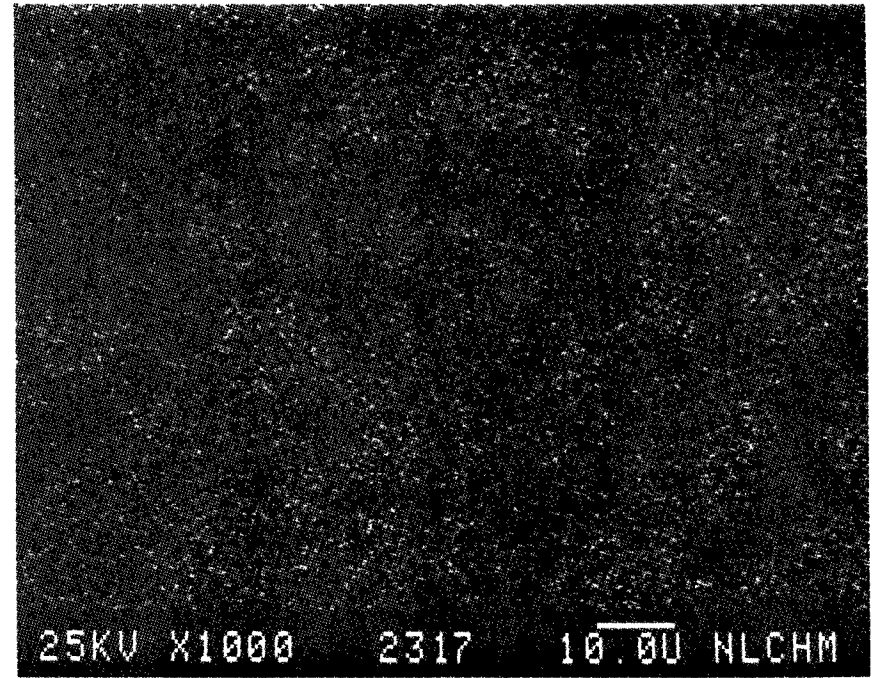


Figure 209

Fe X-Ray Image of Figure 204

ENERGY DISPERSIVE X-RAY ANALYSIS

Analytical Number Bentonite

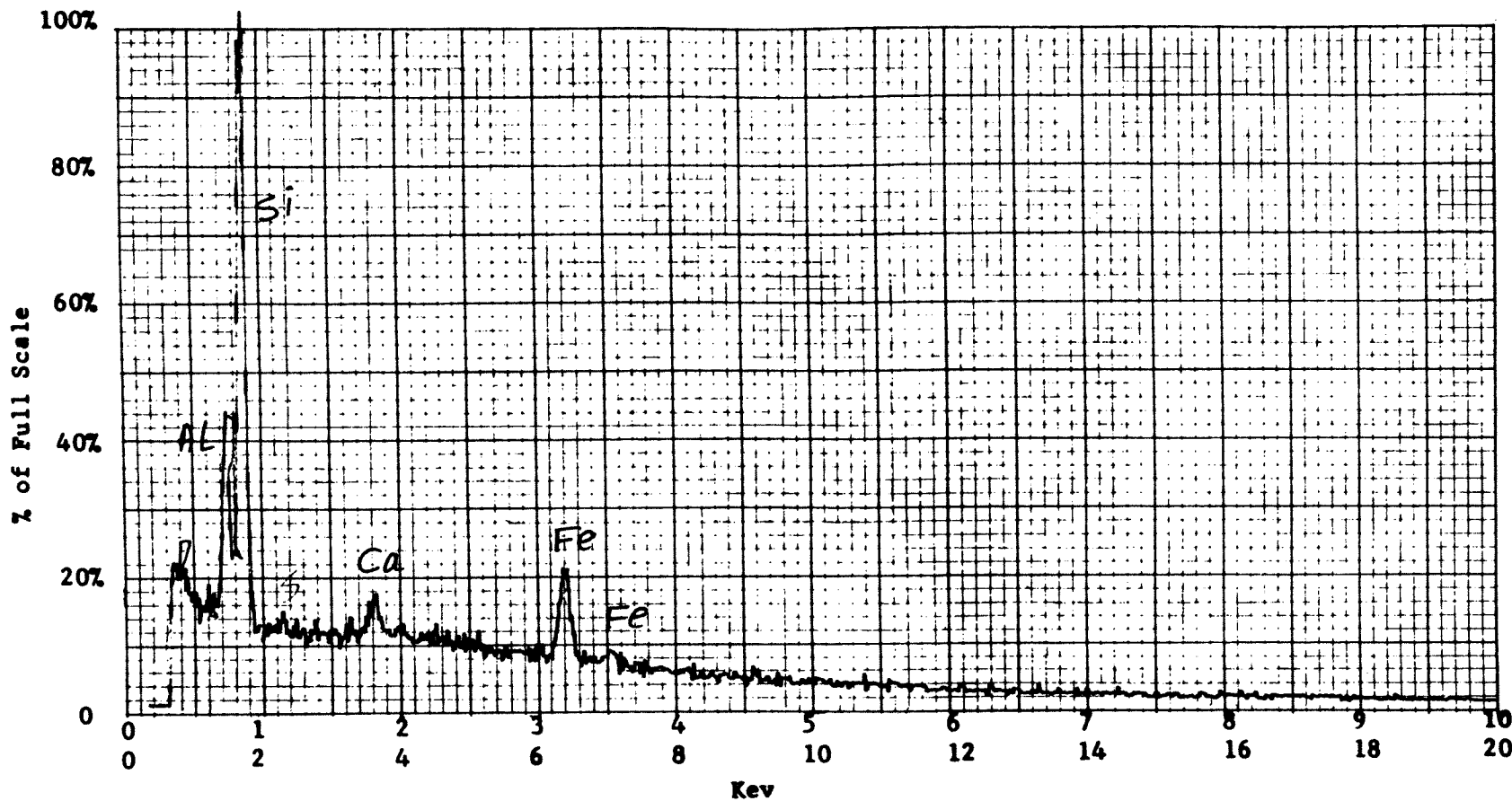
Operator \_\_\_\_\_ Date \_\_\_\_\_

Accelerating Potential 25 KeV

Total Counts Acquired 1.0 min.

Number Counts Full Scale 5K

Number of eV per channel 20



Sample peculiarities and remarks: FIGURE 210: AREA SCAN

ENERGY DISPERSIVE X-RAY ANALYSIS

Analytical Number Bentonite

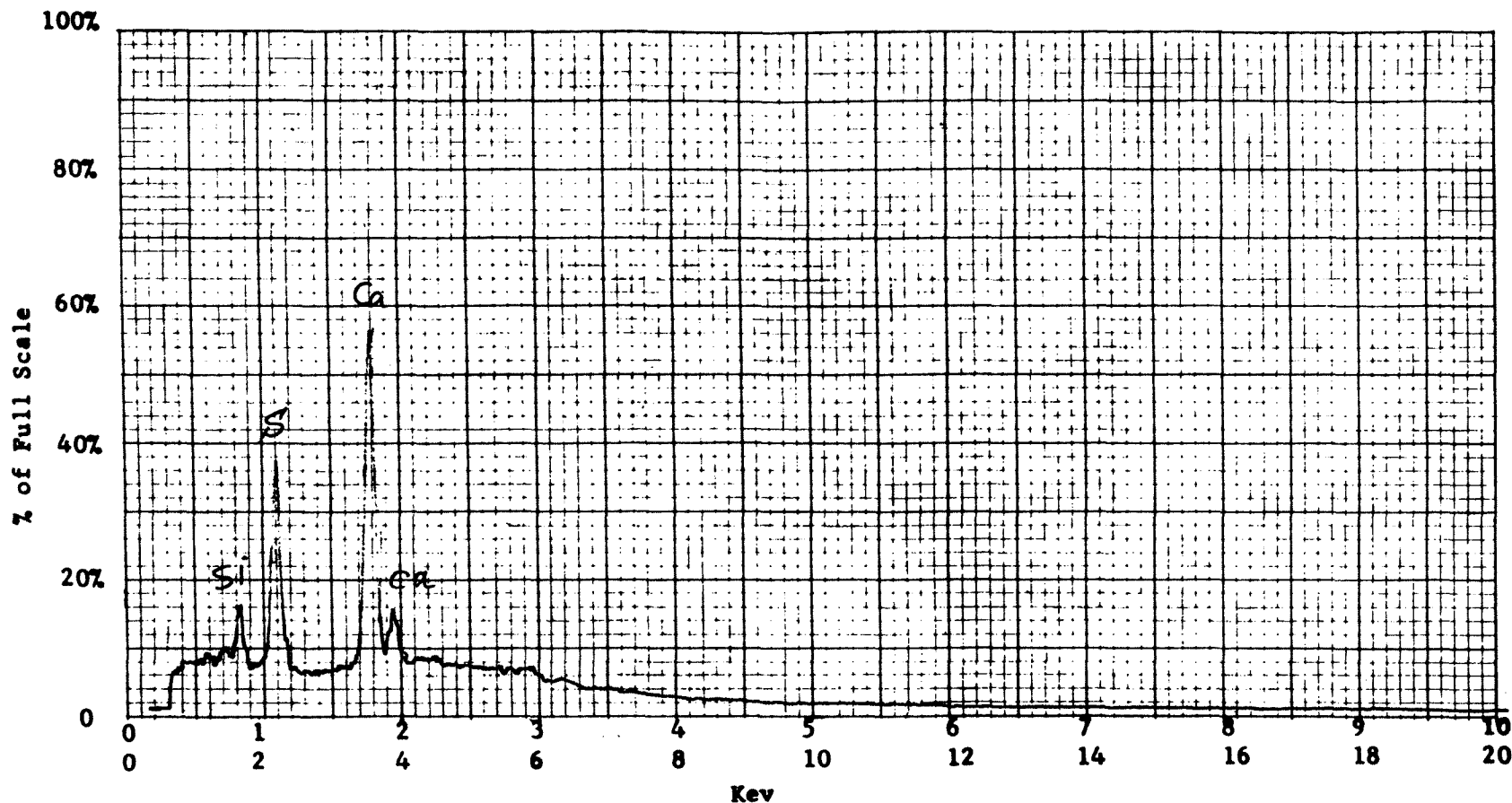
Operator \_\_\_\_\_ Date \_\_\_\_\_

Accelerating Potential 25 KeV

Total Counts Acquired 1.0 min.

Number Counts Full Scale 5K

Number of eV per channel 20



Sample peculiarities and remarks: FIGURE 211: POINT SCAN ON A HIGH Ca-S PARTICLE  
IN FIGURE 187

ENERGY DISPERSIVE X-RAY ANALYSIS

Analytical Number Bentonite

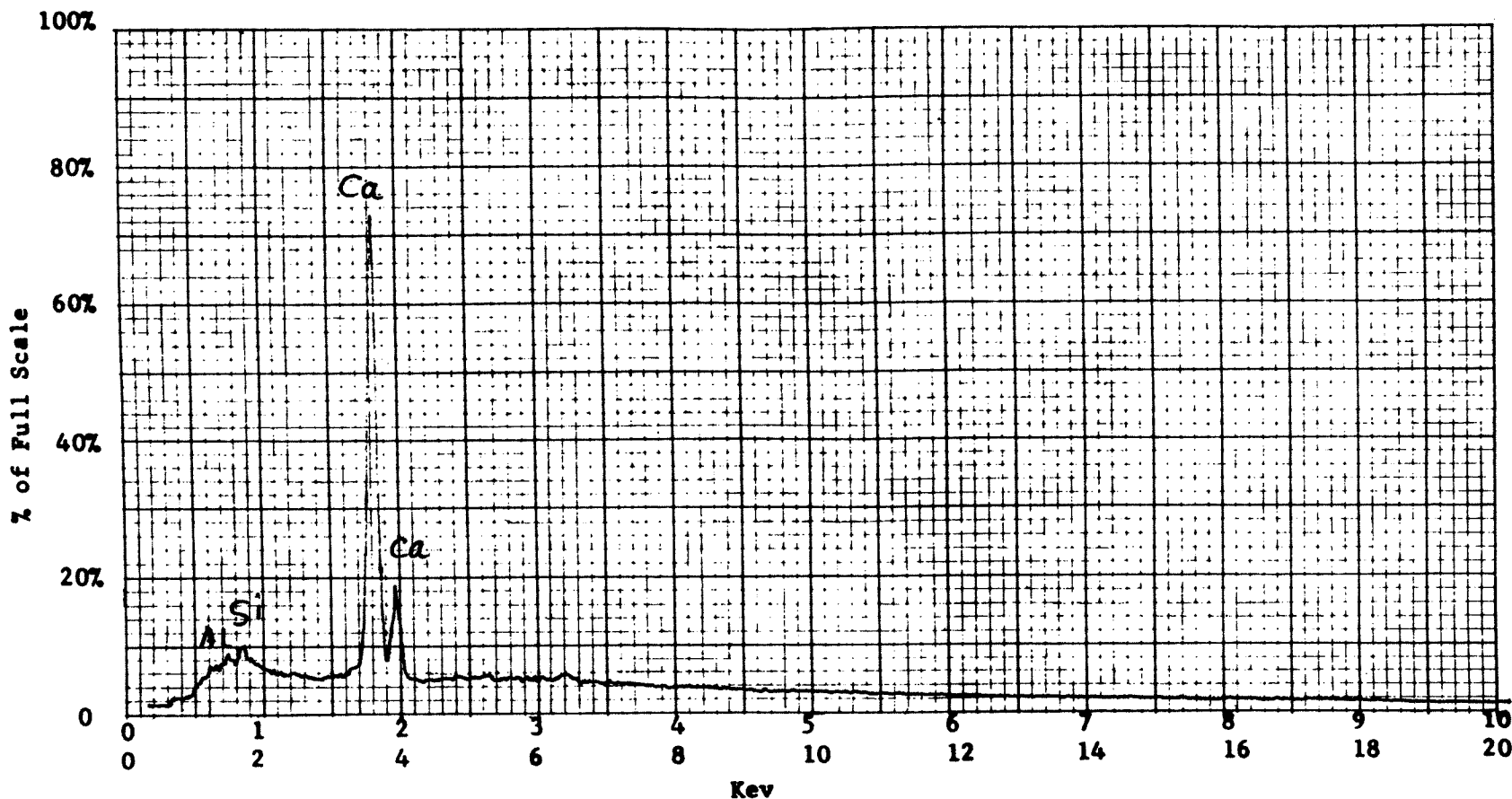
Operator \_\_\_\_\_ Date \_\_\_\_\_

Accelerating Potential 25 KeV

Total Counts Acquired 1.0 min.

Number Counts Full Scale 5K

Number of eV per channel \_\_\_\_\_



Sample peculiarities and remarks: FIGURE 212: POINT SCAN ON A HIGH Ca PARTICLE  
IN FIGURE 193

ENERGY DISPERSIVE X-RAY ANALYSIS

Analytical Number Bentonite

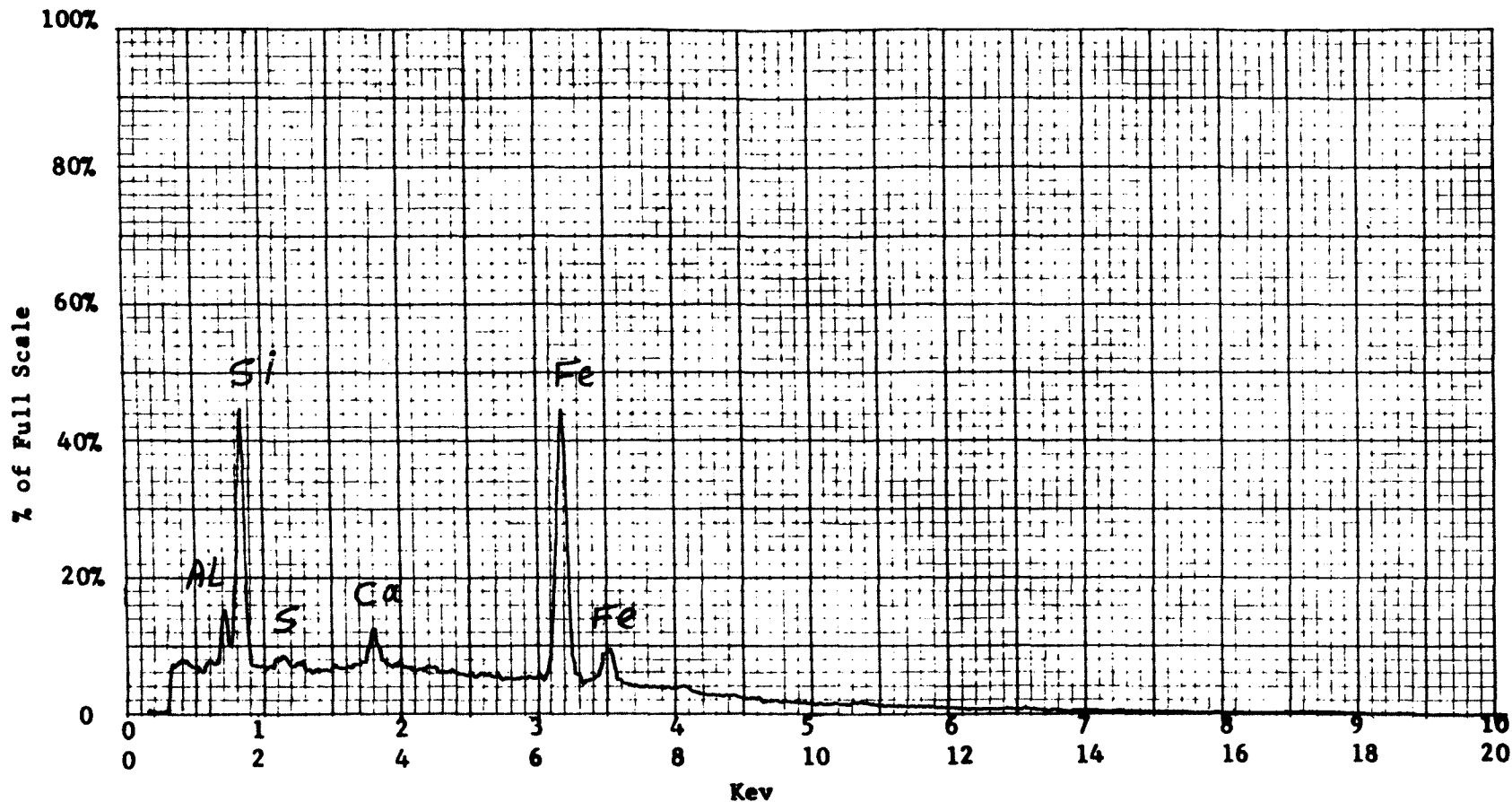
Operator \_\_\_\_\_ Date \_\_\_\_\_

Accelerating Potential 25 KeV

Total Counts Acquired 1.0 min.

Number Counts Full Scale 5K

Number of eV per channel 20



Sample peculiarities and remarks: FIGURE 213: POINT SCAN ON A PARTICLE CONTAINING HIGHER THAN NORMAL Fe IN FIGURE 199

ENERGY DISPERSIVE X-RAY ANALYSIS

Analytical Number Bentonite

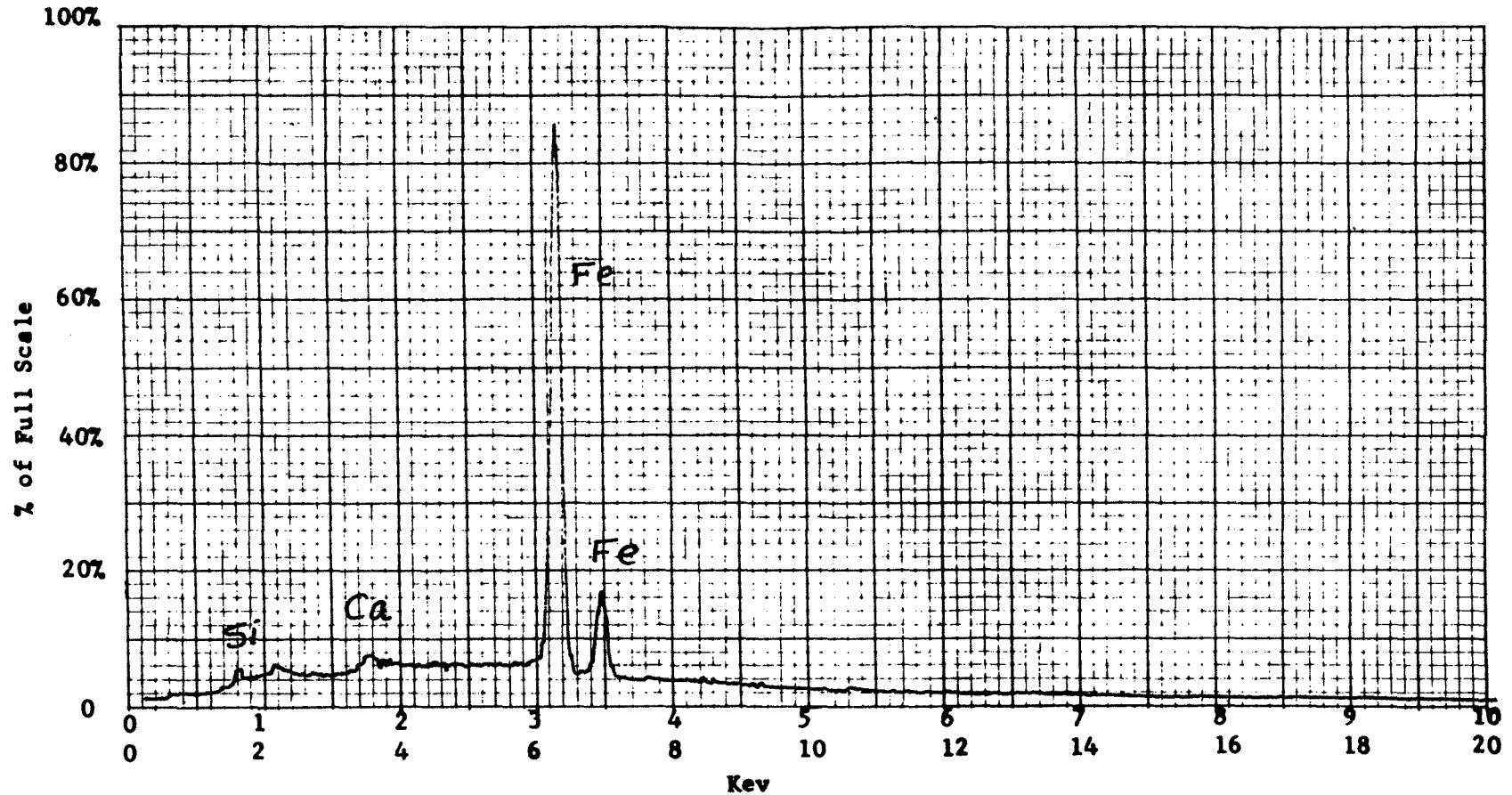
Operator \_\_\_\_\_ Date \_\_\_\_\_

Accelerating Potential 25 KeV

Total Counts Acquired 1.0 min.

Number Counts Full Scale 5K

Number of eV per channel 20



Sample peculiarities and remarks: FIGURE 214: POINT SCAN ON A VERY HIGH Fe PARTICLE  
IN THE MIDDLE OF FIGURE 199

ENERGY DISPERSIVE X-RAY ANALYSIS

Analytical Number Bentonite

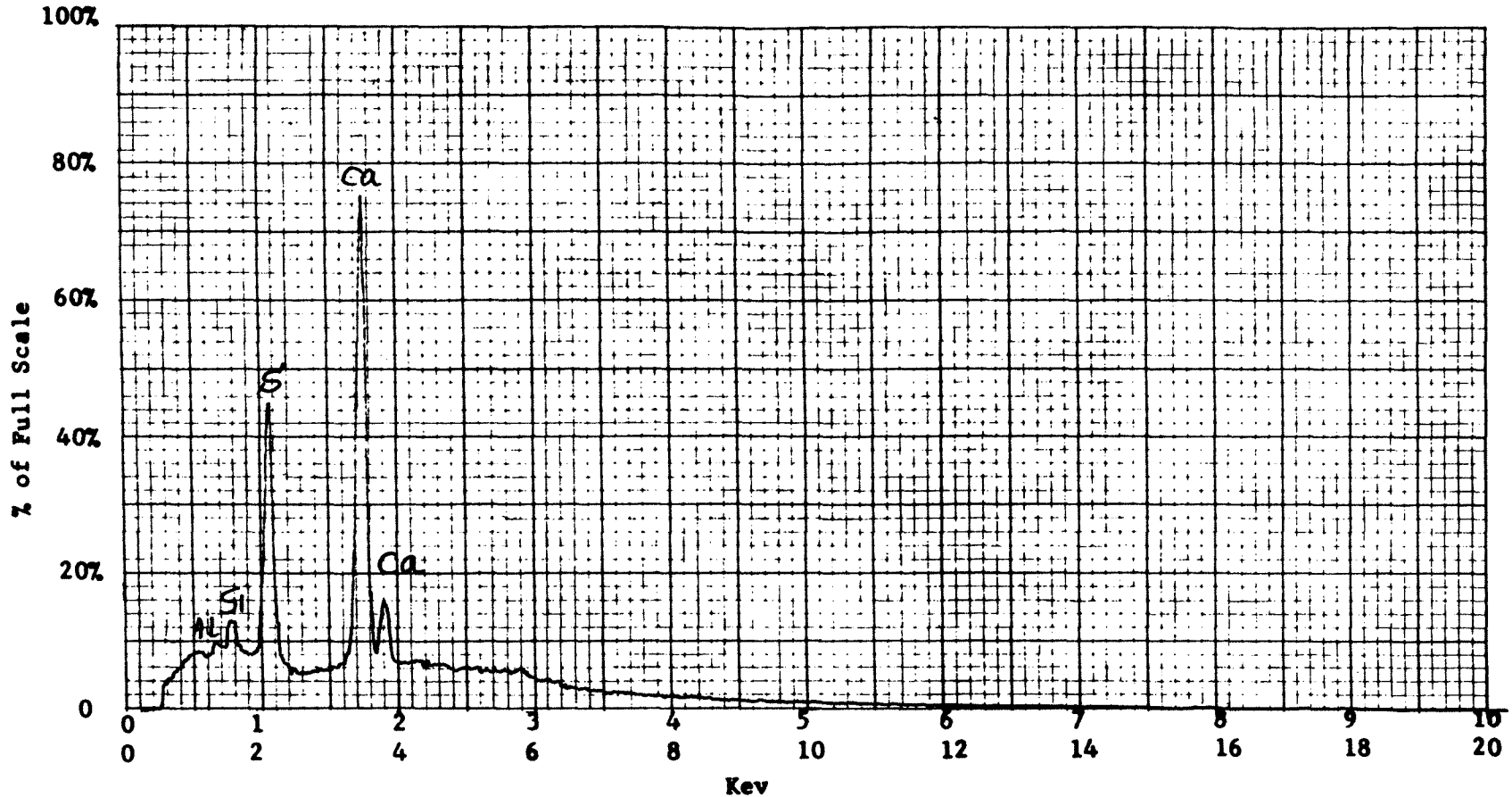
Operator \_\_\_\_\_ Date \_\_\_\_\_

Accelerating Potential 25 KeV

Total Counts Acquired 1.0 min.

Number Counts Full Scale 5K

Number of eV per channel 20



Sample peculiarities and remarks: FIGURE 215: POINT SCAN ON A HIGH Ca-S PARTICLE IN FIGURE 204



Vermiculite:Structural Analysis:

Vermiculite particles were observed to have a laminated and platey structure such as that seen in mica particles. Most of the particles were very large and irregular in shape. A few smaller particles were also observed. Some separation and distortion in the micaceous layers is due to a certain degree of expansion which can be formed by pressure and/or temperature. The degree of expansion of the micaceous layers varies from particle to particle.

SEM micrographs were obtained at very low magnifications because most of the particles were very large. The maximum, average and minimum particle size were measured in microns ( $\mu$ ) as follows:

Maximum	Average	Minimum
2400.0	1000.0	33.0

Elemental Composition and Distribution:

The following elements were detected from the particles: Mg, Al, Si, S, K, Ca, T, Cr and Fe. Fe and Si were the major elements.

Figures 236 and 243 were obtained to illustrate the elemental distribution. The elemental X-ray images of these two figures indicated that all the elements were almost uniformly distributed across the particles.

In a few cases higher than normal concentrations of Si, S, K or Fe were observed from very small areas on the

surfaces of the particles. This abnormal distribution is illustrated in the elemental X-ray images and in the X-ray energy spectrum, Figures 252 and 253.

SEM IMAGES OF SAMPLE #

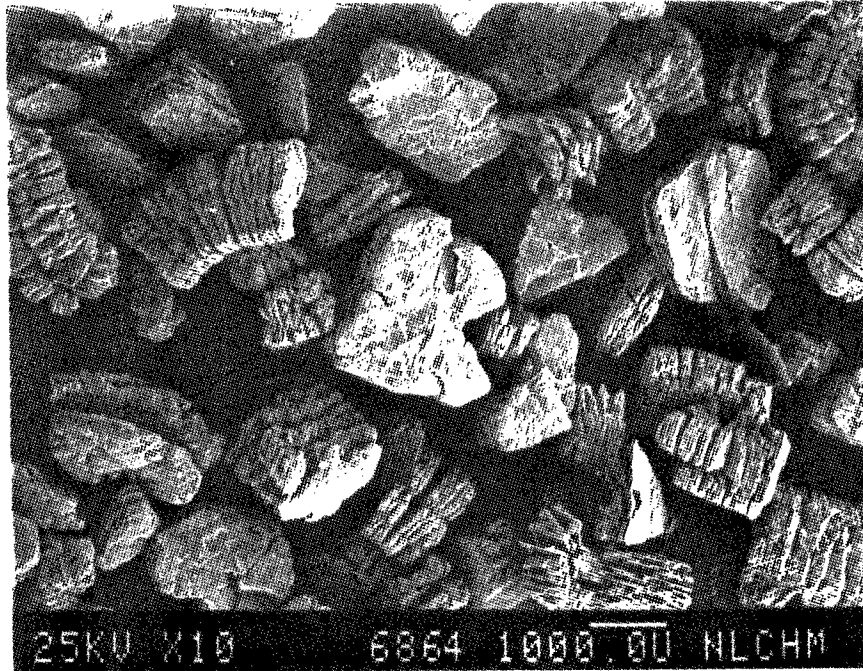


Figure 216



Figure 217

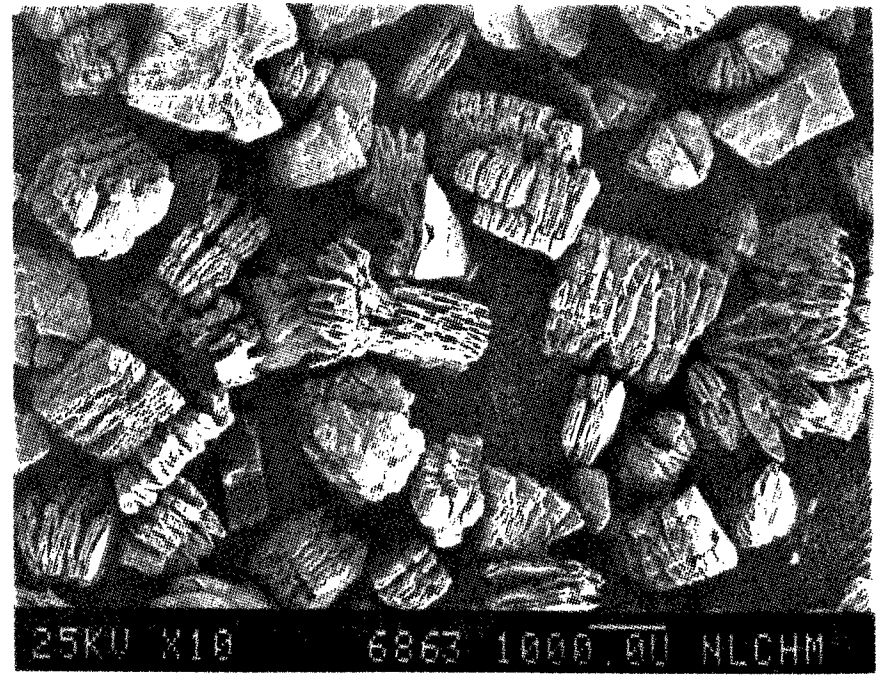


Figure 218

SEM IMAGES OF SAMPLE #

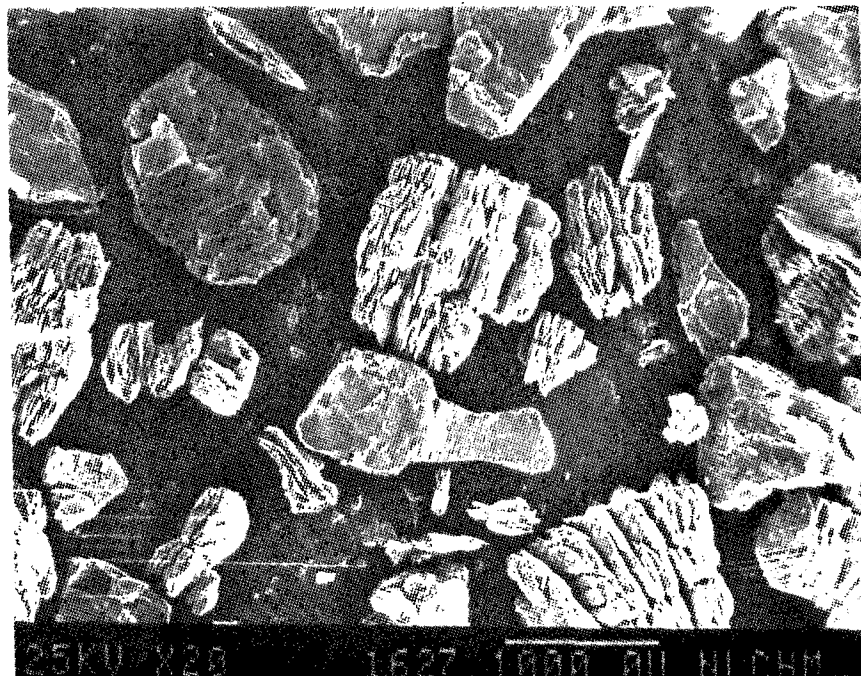


Figure 219

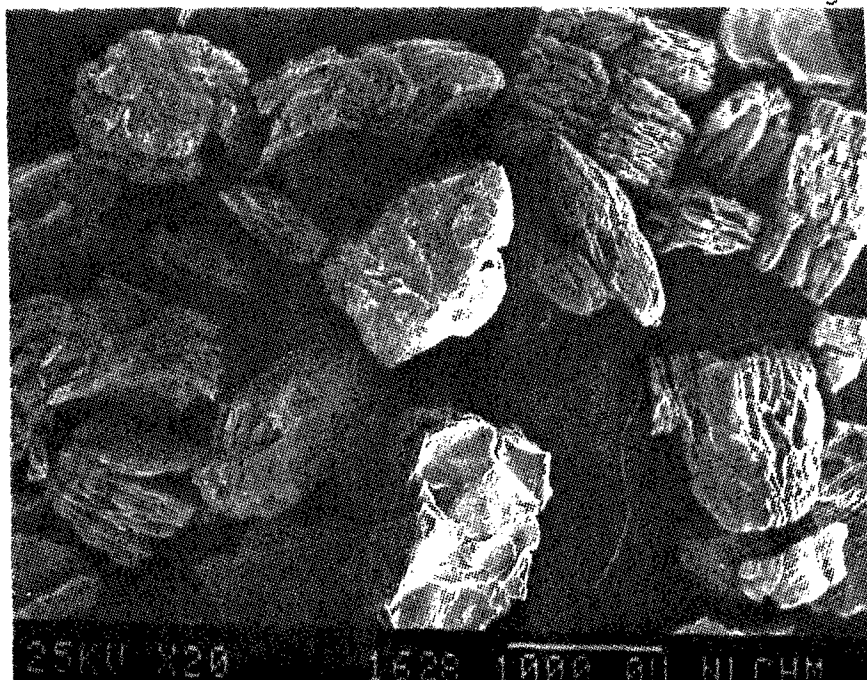


Figure 220

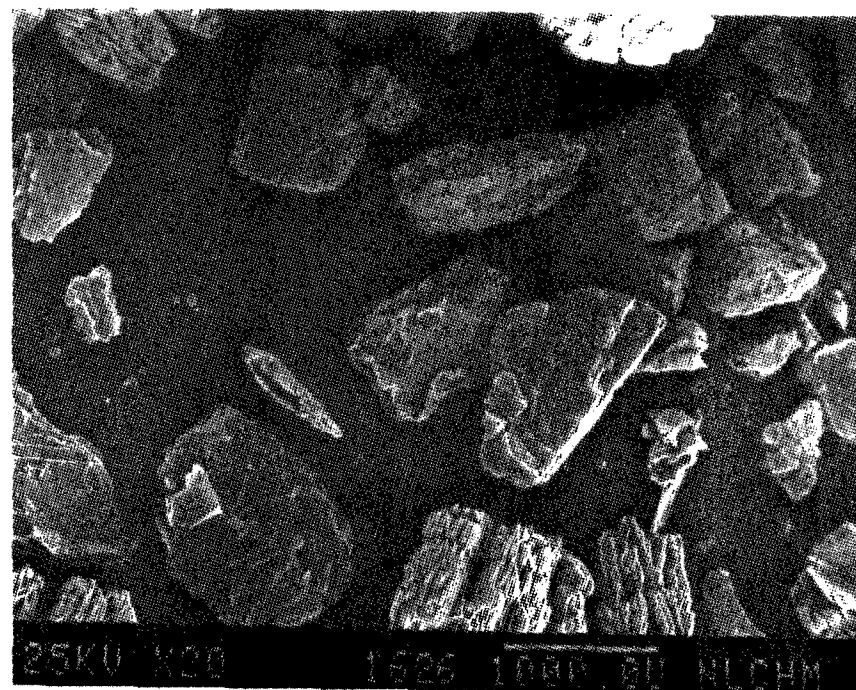


Figure 221

SEM IMAGES OF SAMPLE #

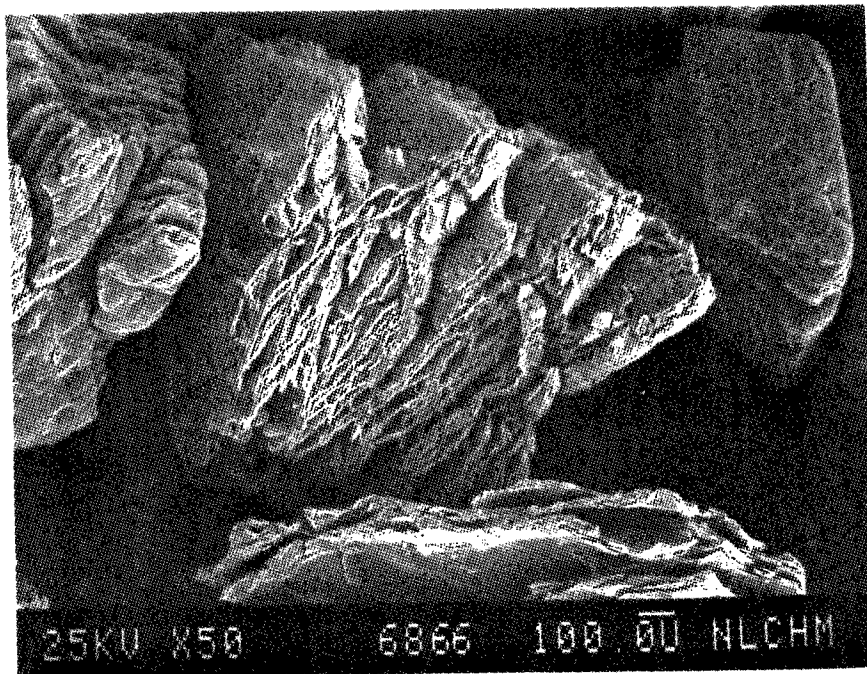


Figure 222

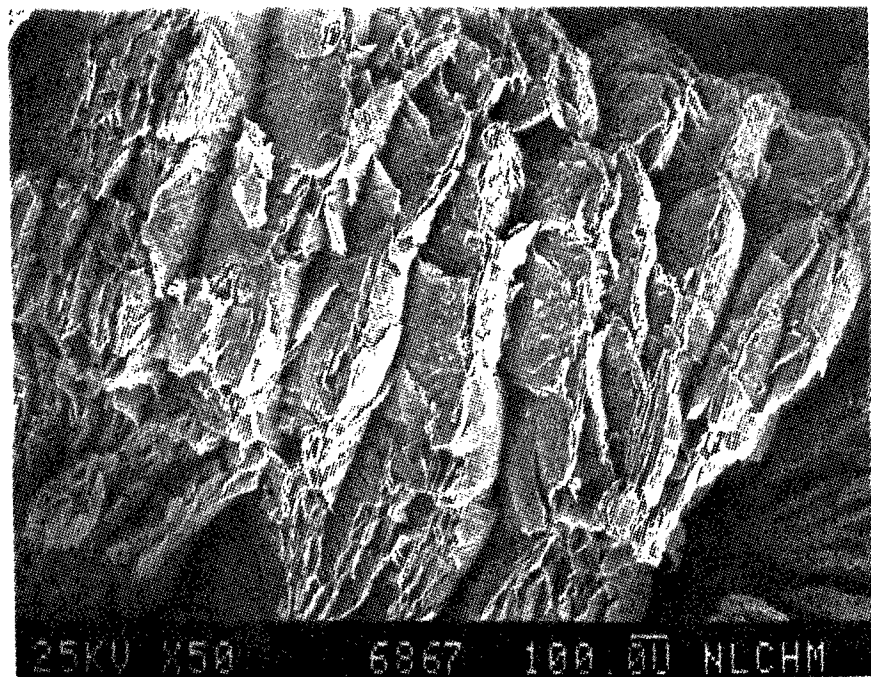


Figure 223

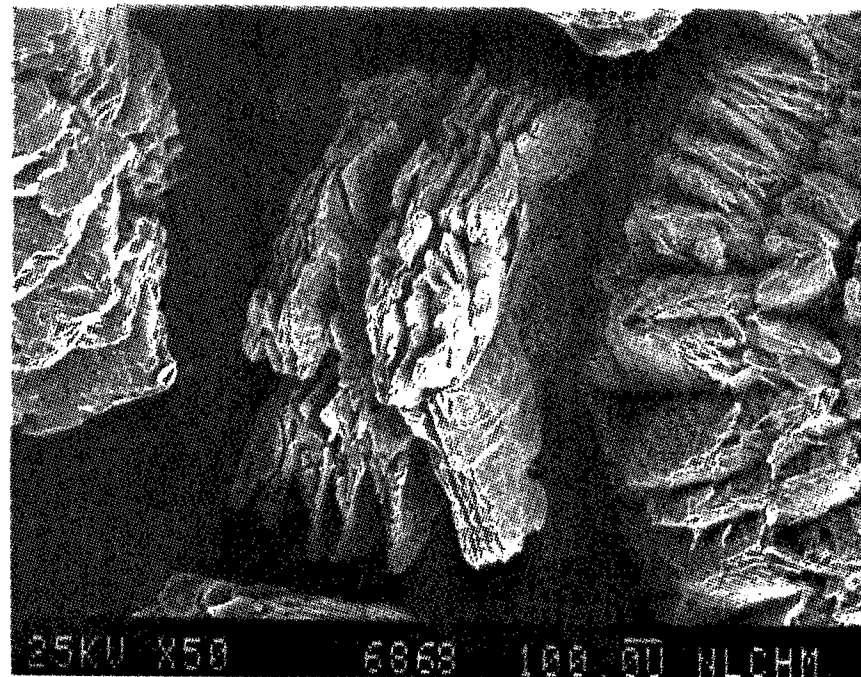


Figure 224



SEM IMAGES OF SAMPLE #

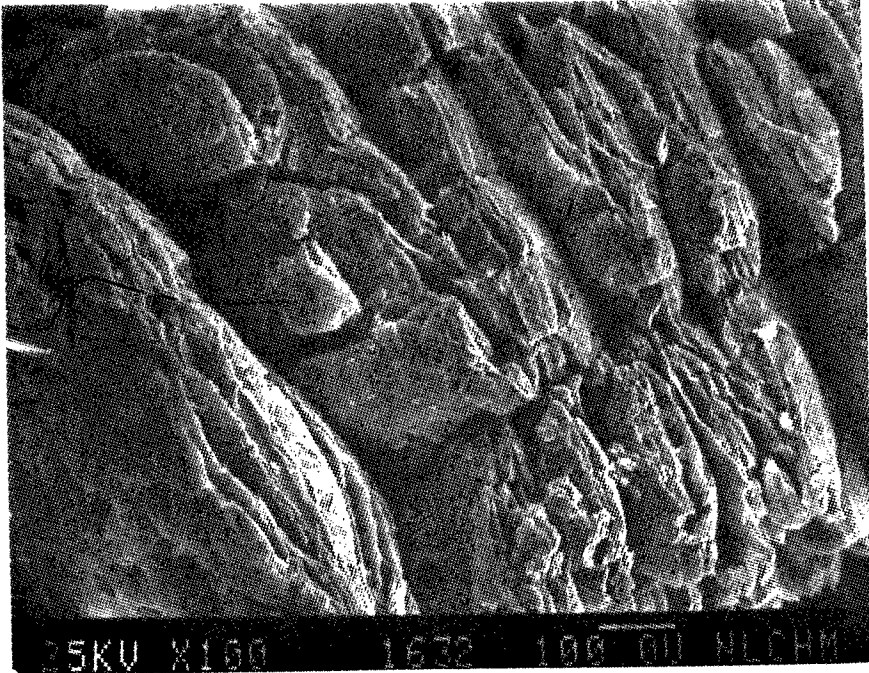


Figure 225

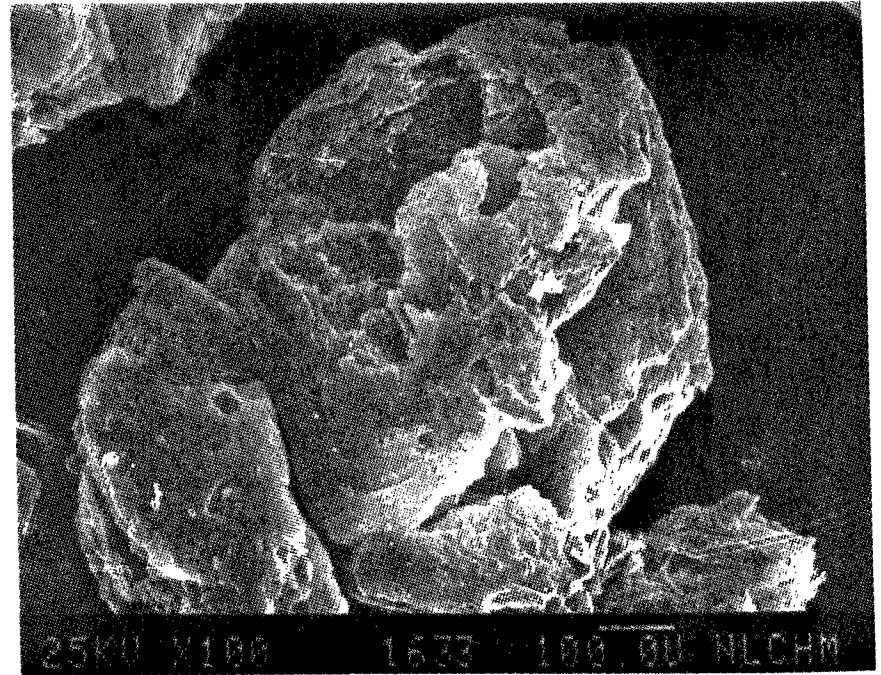


Figure 226

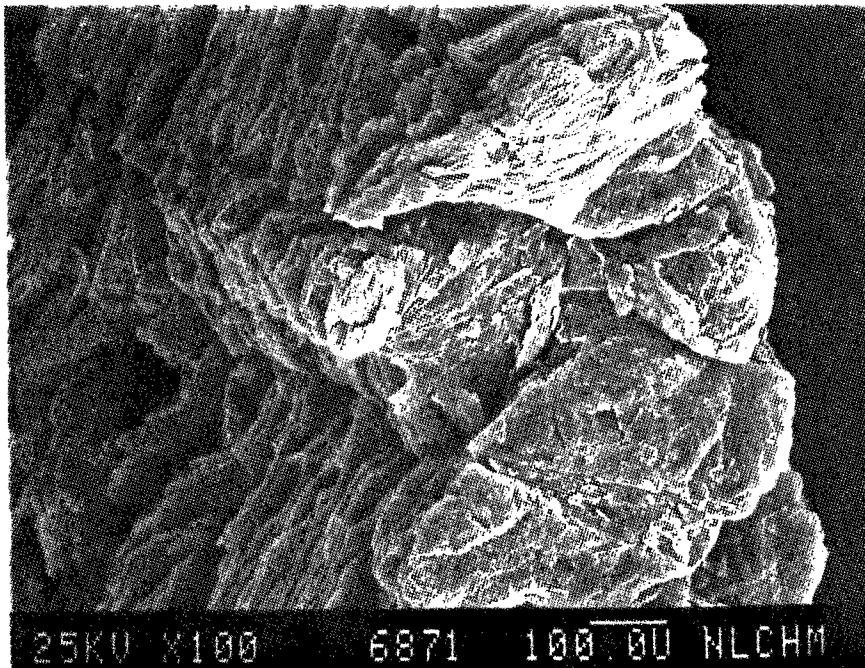


Figure 227

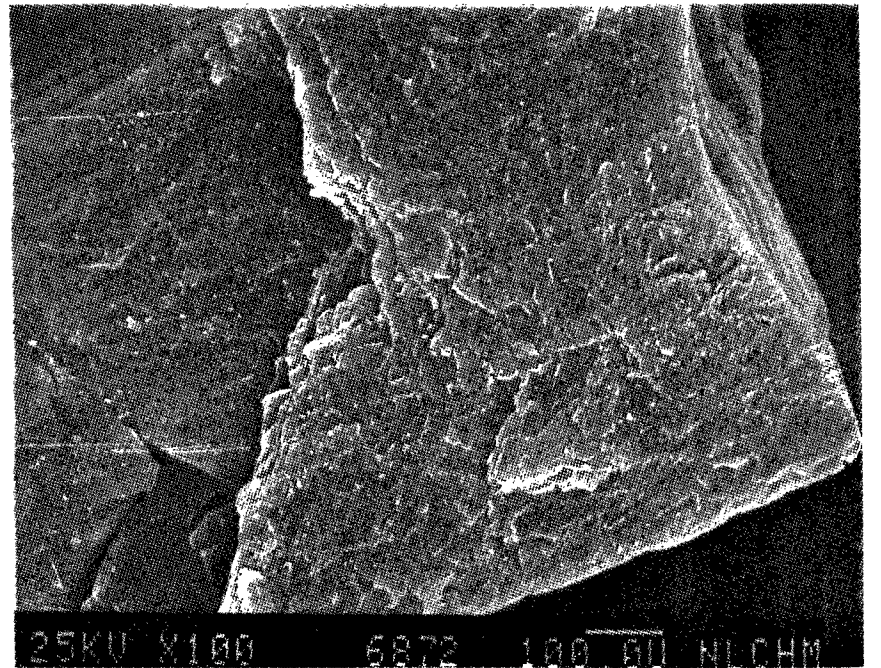


Figure 228

SEM IMAGES OF SAMPLE #

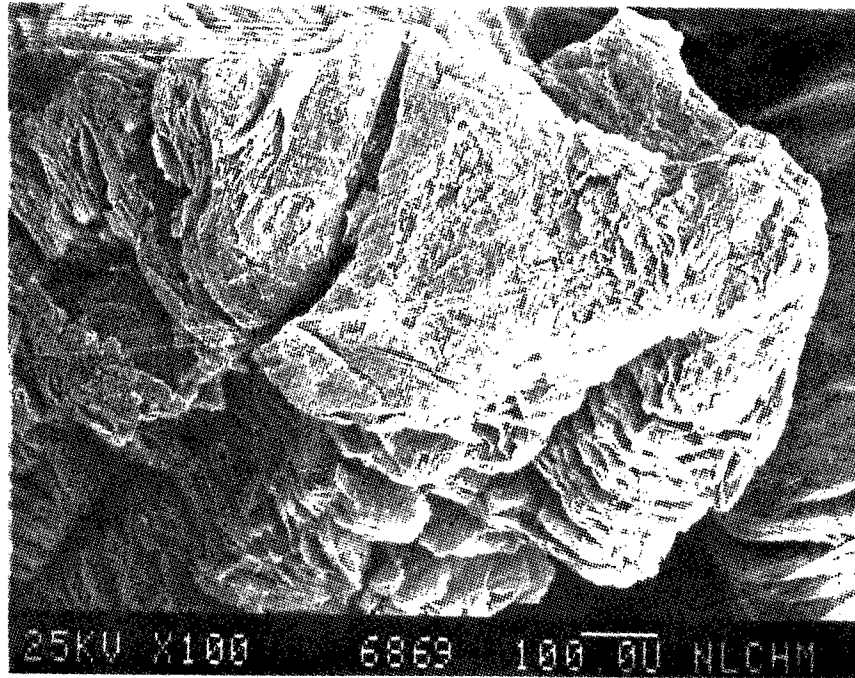


Figure 229



SEM IMAGES OF SAMPLE #

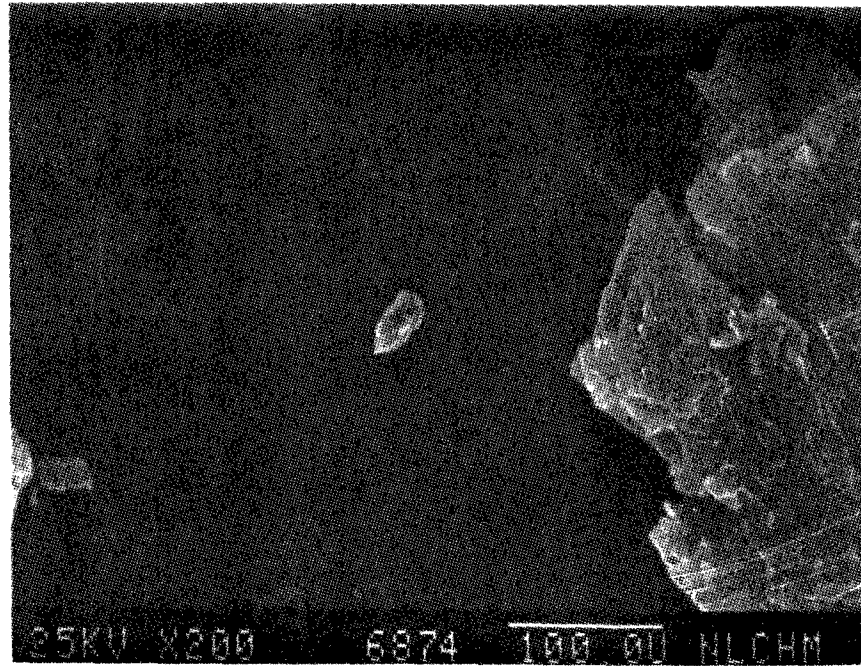


Figure 230

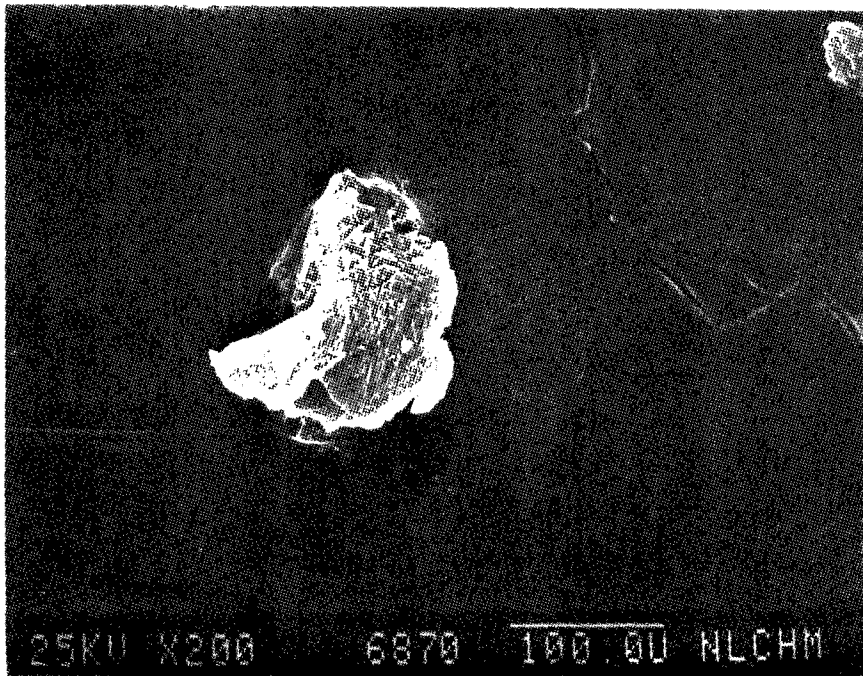


Figure 231

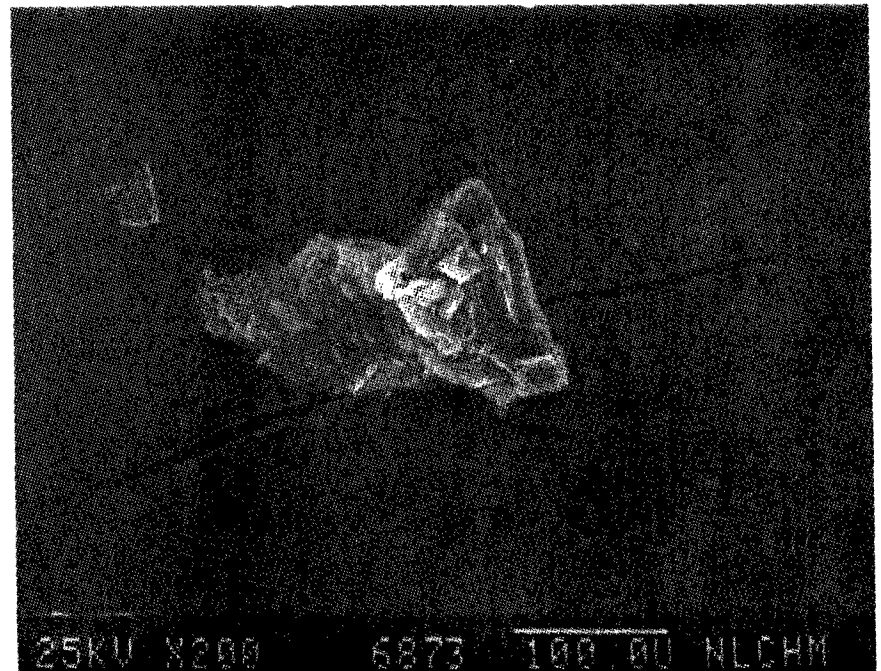


Figure 232

SEM IMAGES OF SAMPLE #

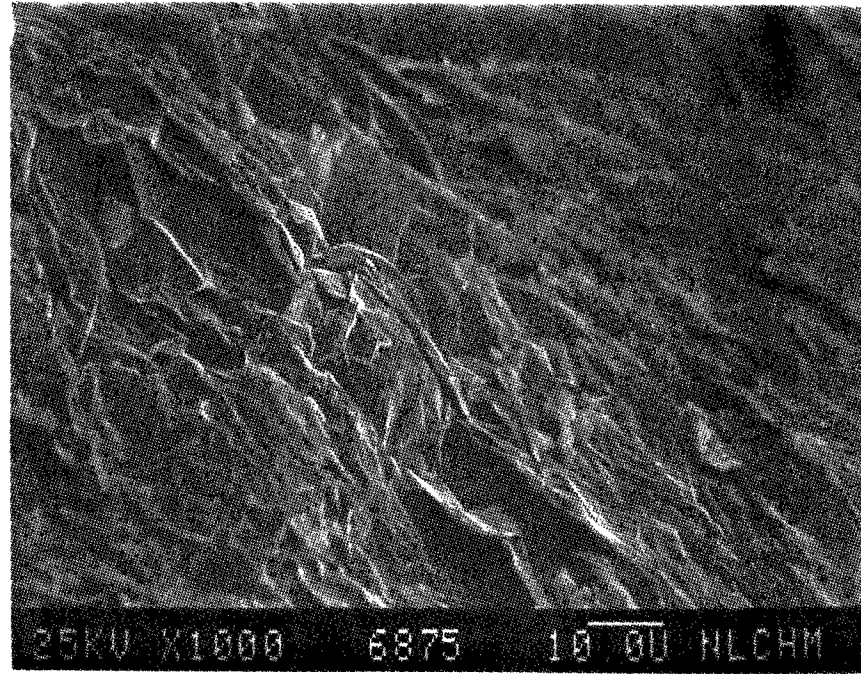


Figure 233

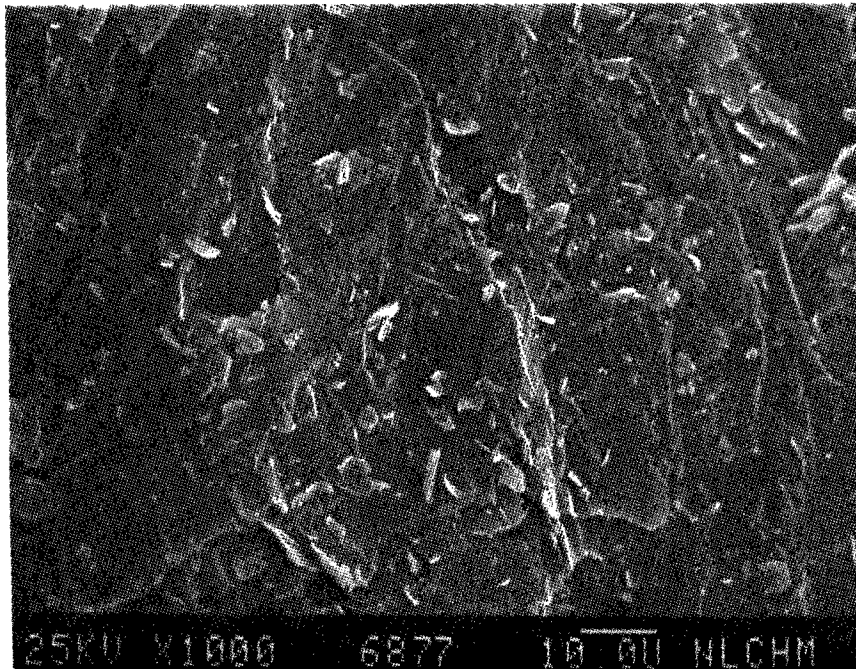


Figure 234

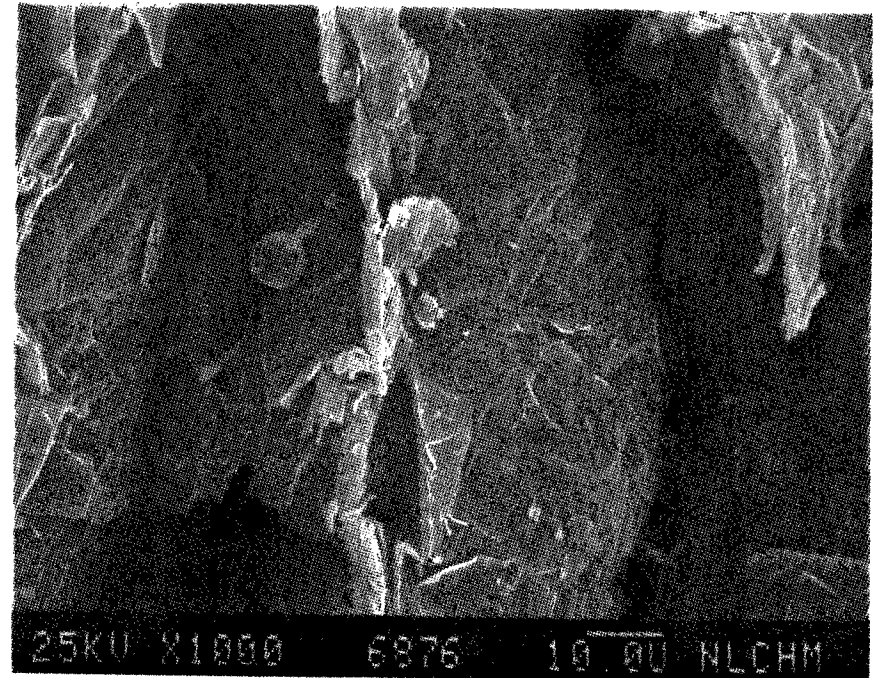


Figure 235

SEM IMAGES OF SAMPLE #

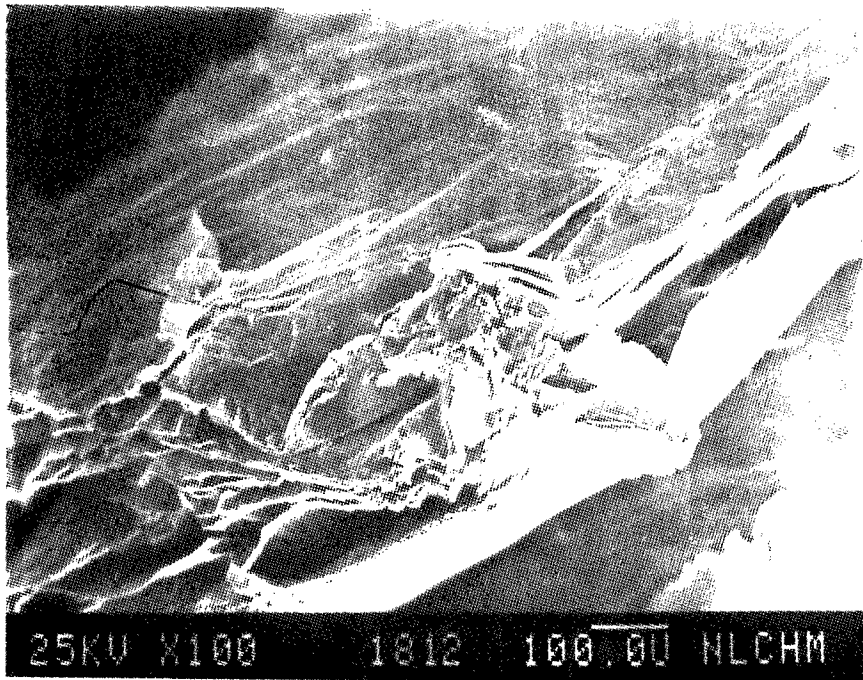


Figure 236

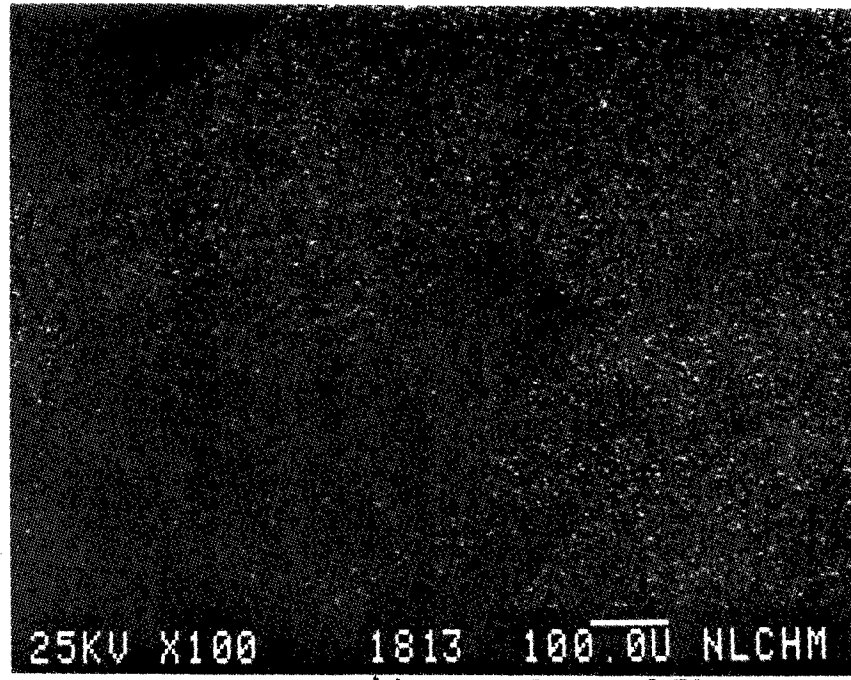


Figure 237

Mg X-Ray Image of Figure 230

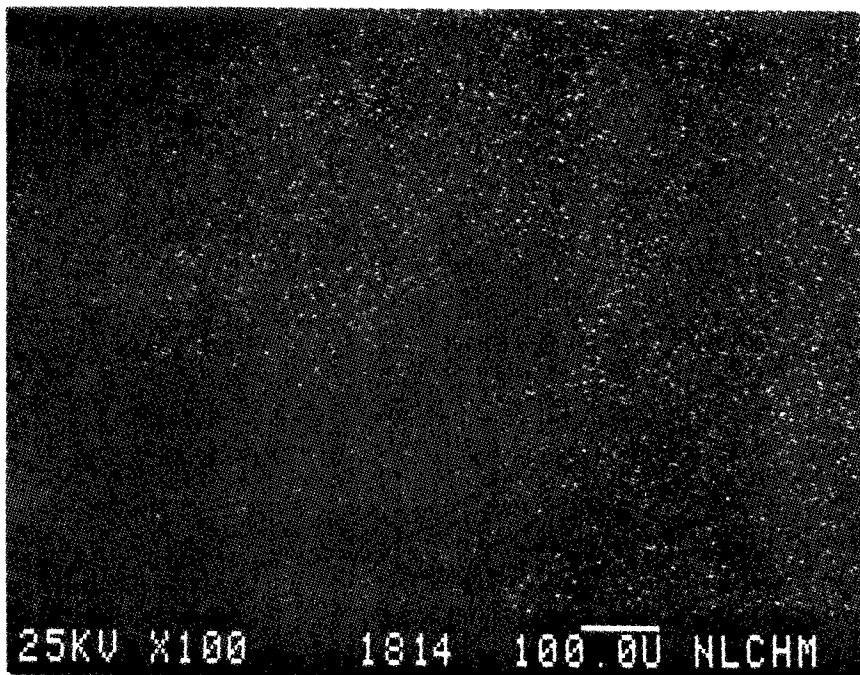


Figure 238

AL X-Ray Image of Figure 230

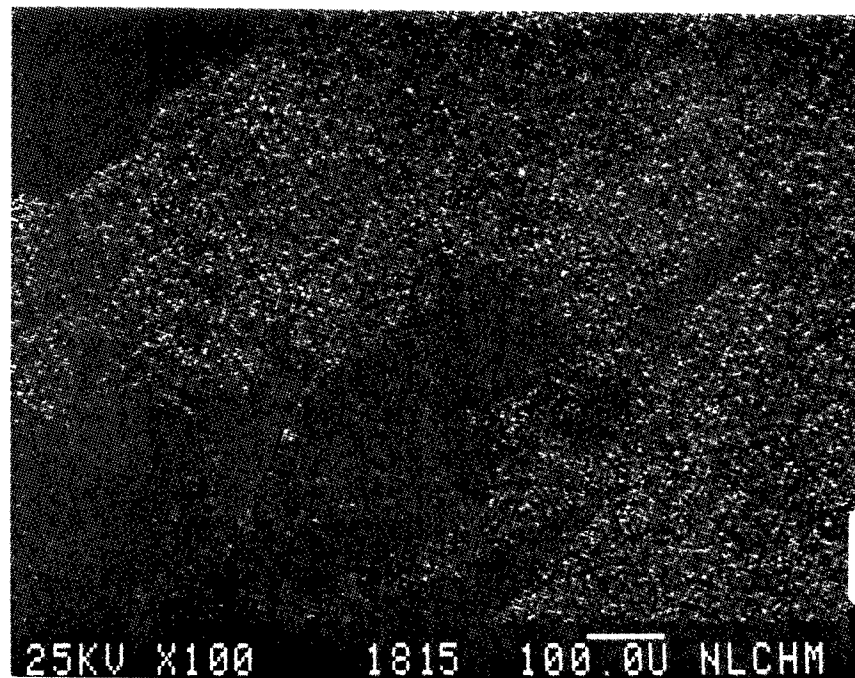


Figure 239

Si X-Ray Image of Figure 230



SEM IMAGES OF SAMPLE #

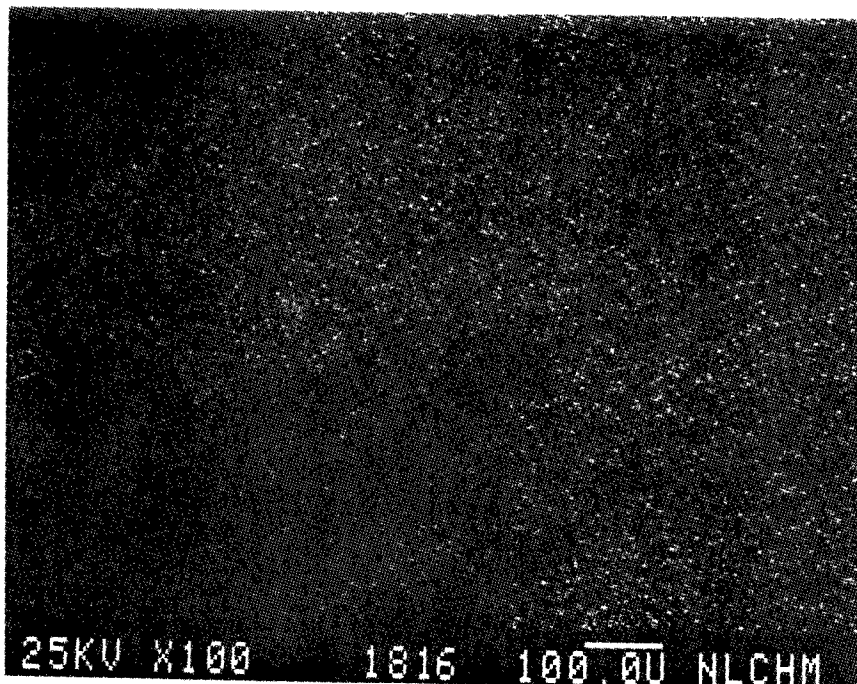


Figure 240

*K* X-Ray Image of Figure 230

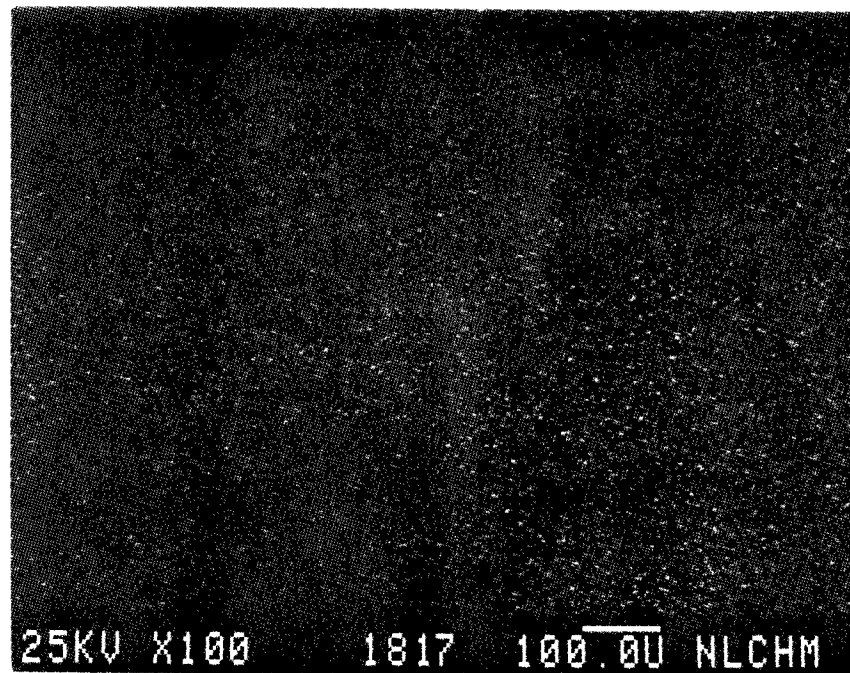


Figure 241

*Ti* X-Ray Image of Figure 230

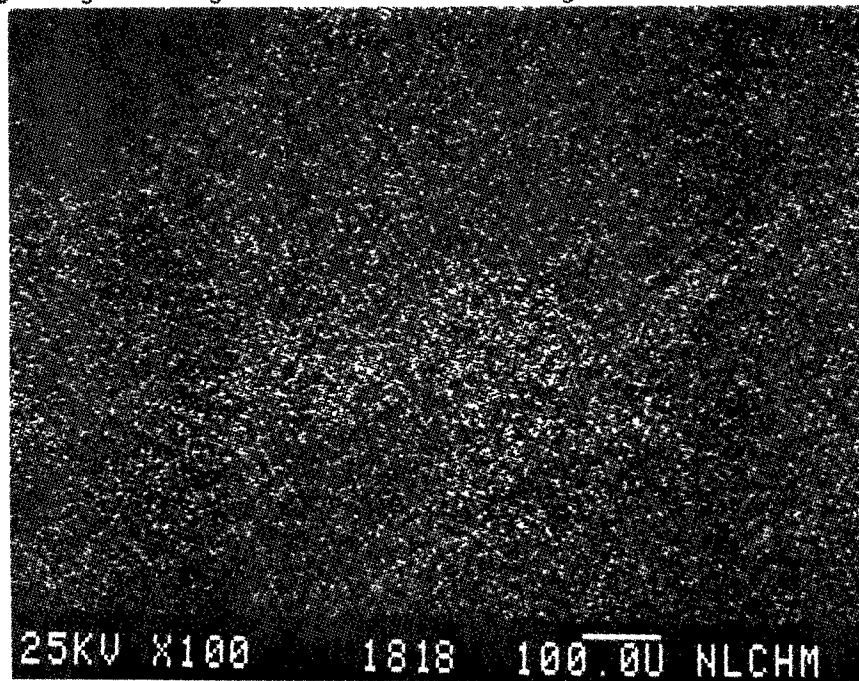


Figure 242

*Fe* X-Ray Image of Figure 230

SEM IMAGES OF SAMPLE #

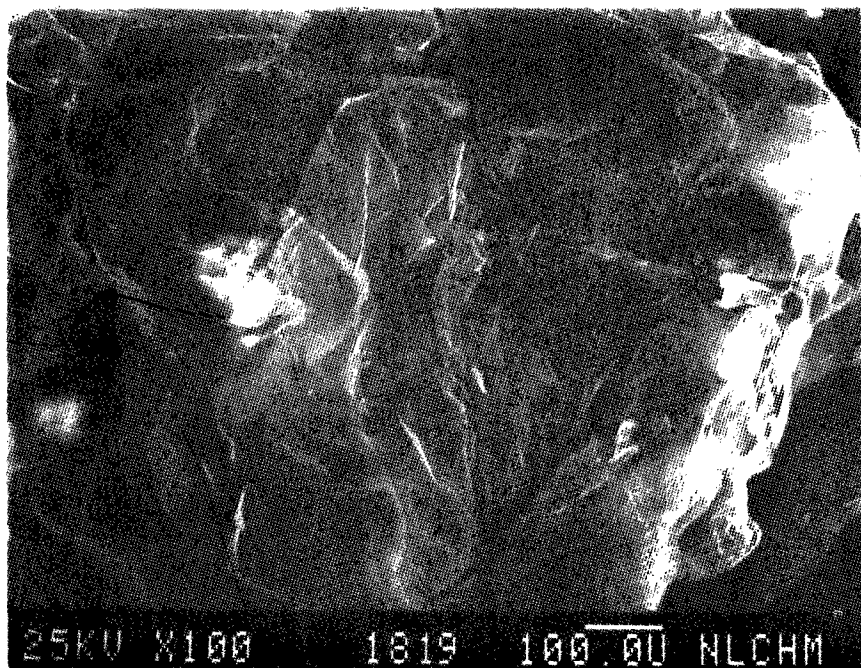


Figure 243

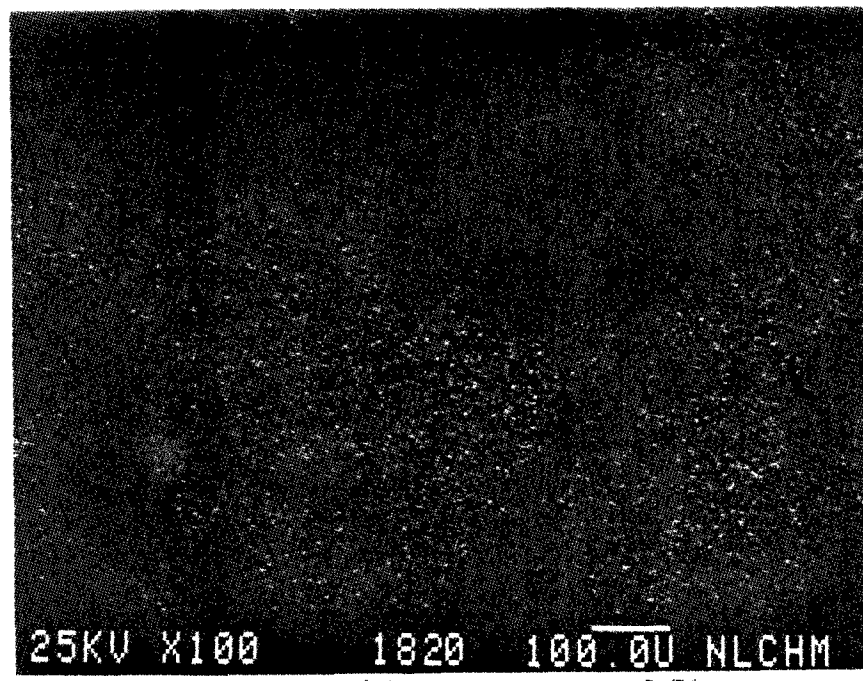


Figure 244

Mg X-Ray Image of Figure 243

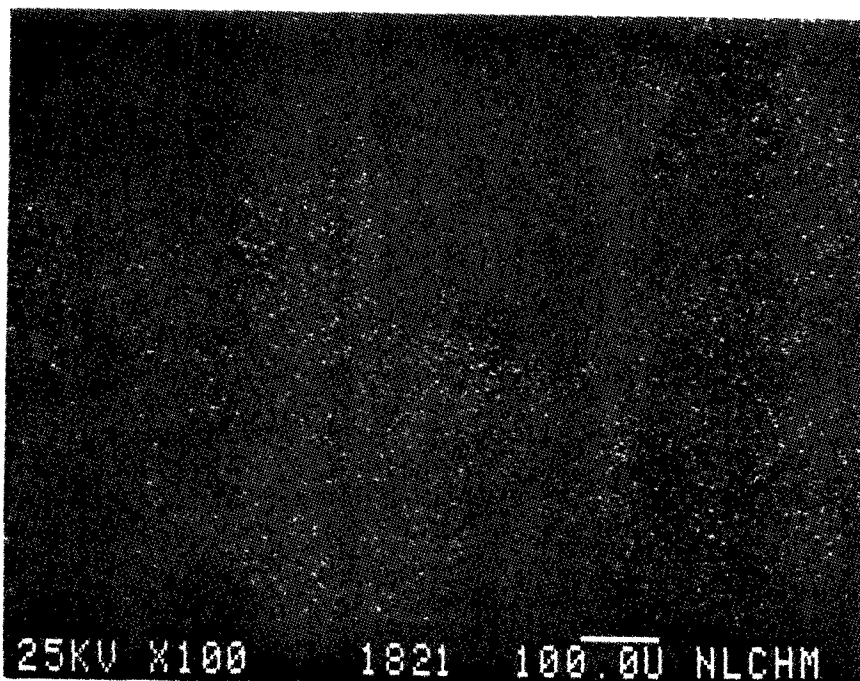


Figure 245

Al X-Ray Image of Figure 243

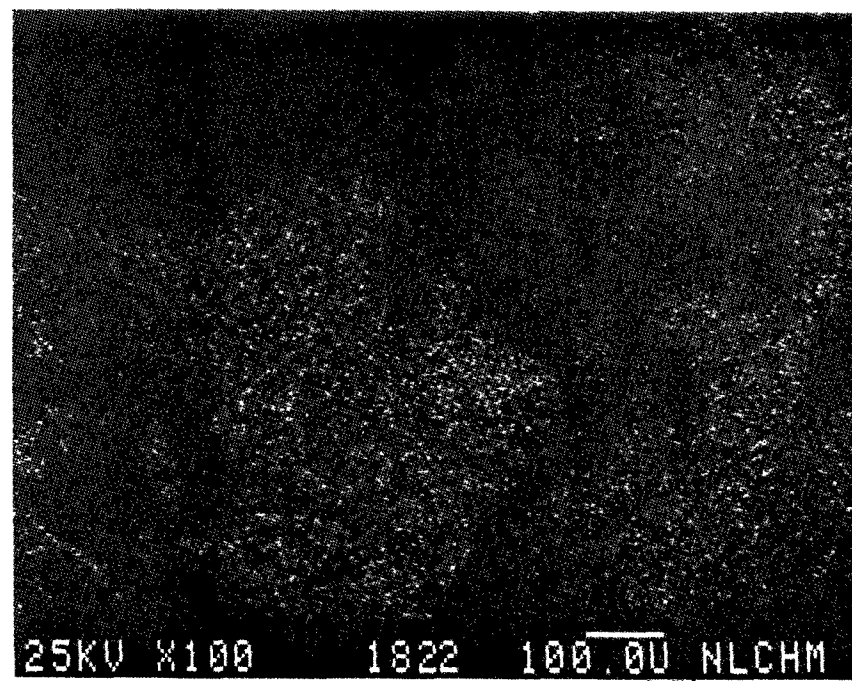


Figure 246

Si X-Ray Image of Figure 243

SEM IMAGES OF SAMPLE #

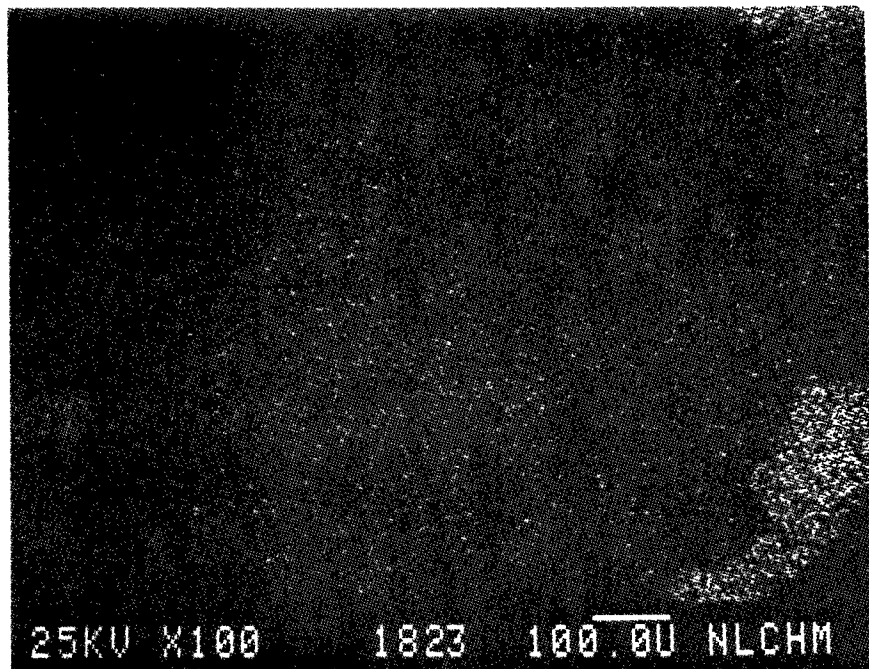


Figure 247 S X-Ray Image of Figure 243

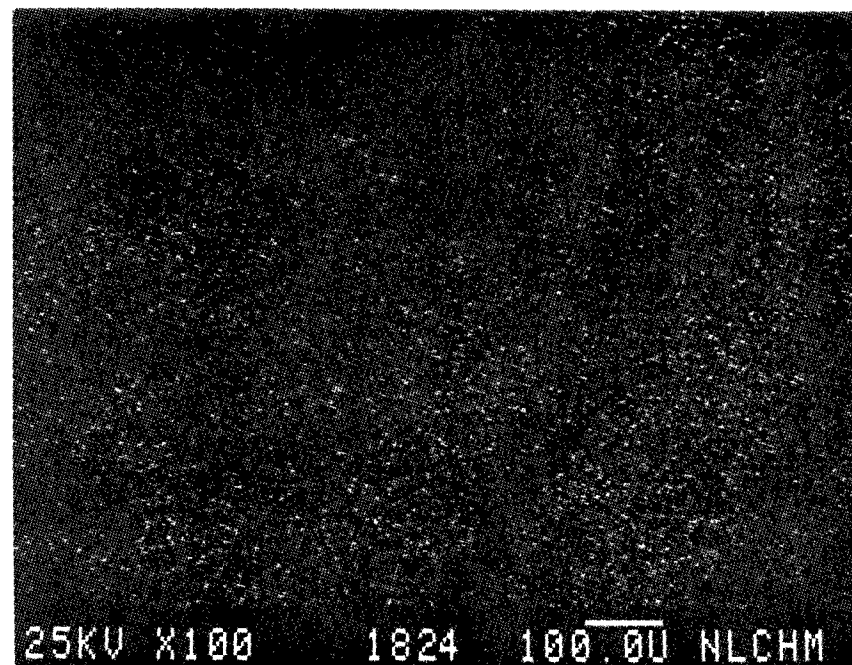


Figure 248 K X-Ray Image of Figure 243

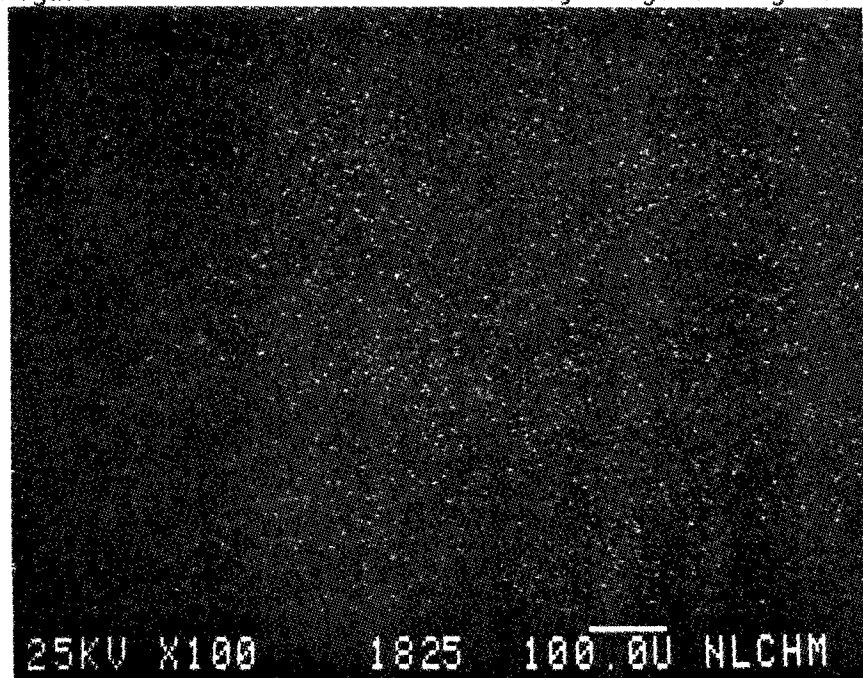


Figure 249 Ti X-Ray Image of Figure 243

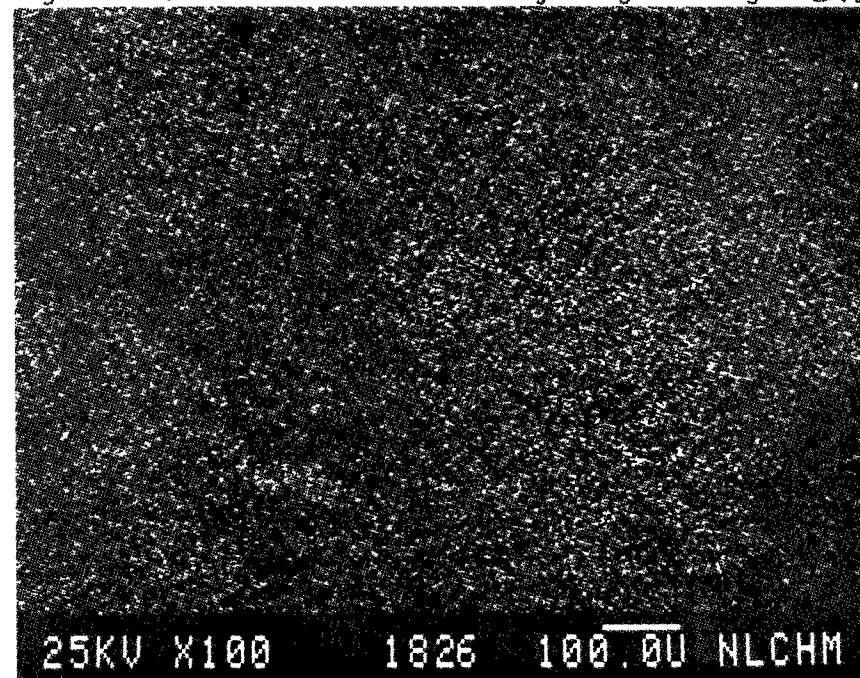


Figure 250 Fe X-Ray Image of Figure 243

ENERGY DISPERSIVE X-RAY ANALYSIS

Analytical Number Vermiculite

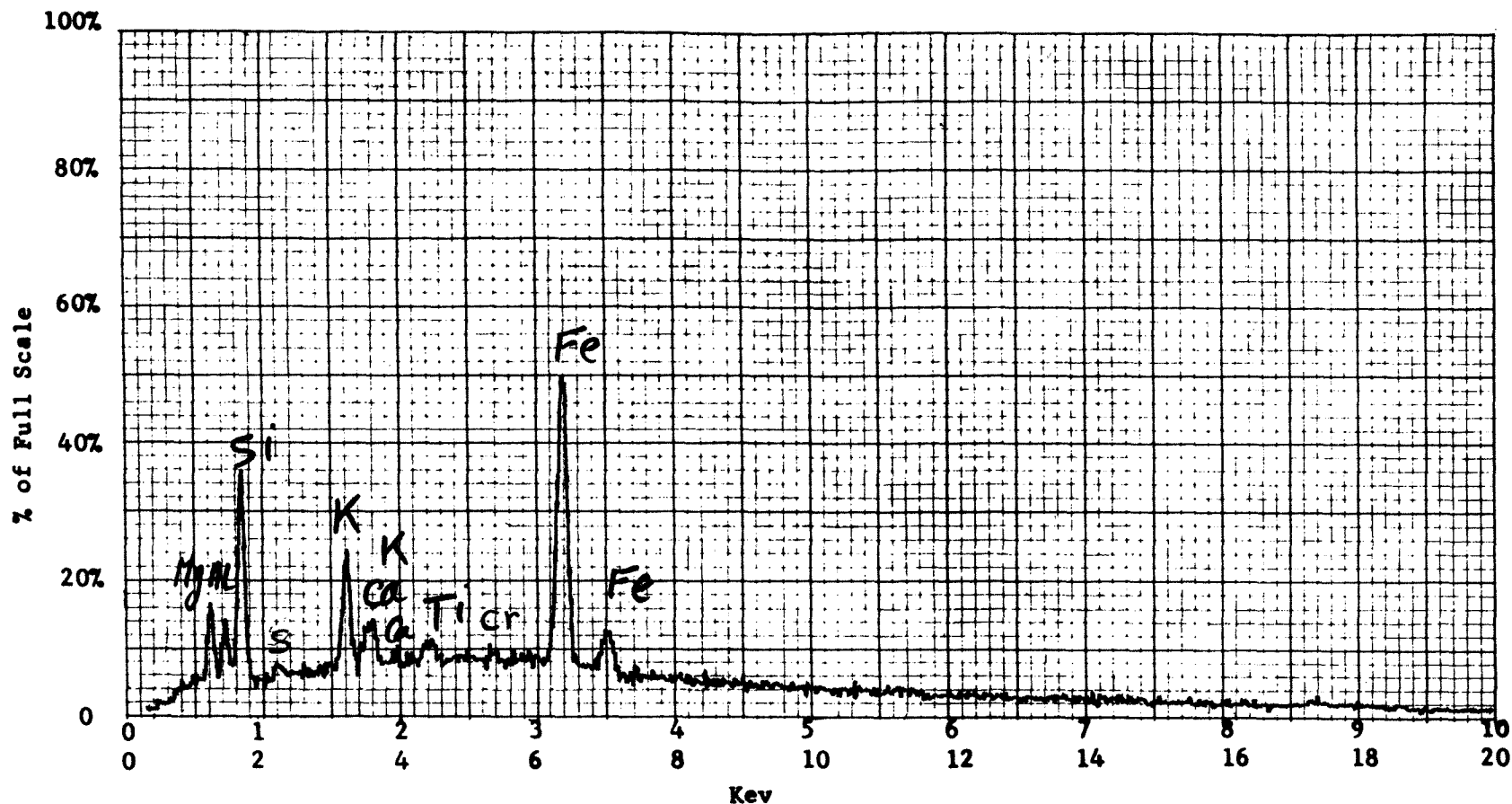
Operator \_\_\_\_\_ Date \_\_\_\_\_

Accelerating Potential 25 KeV

Total Counts Acquired 1.0 min.

Number Counts Full Scale 2K

Number of eV per channel 20



Sample peculiarities and remarks: FIGURE 251: AREA SCAN



ENERGY DISPERSIVE X-RAY ANALYSIS

Analytical Number Vermiculite

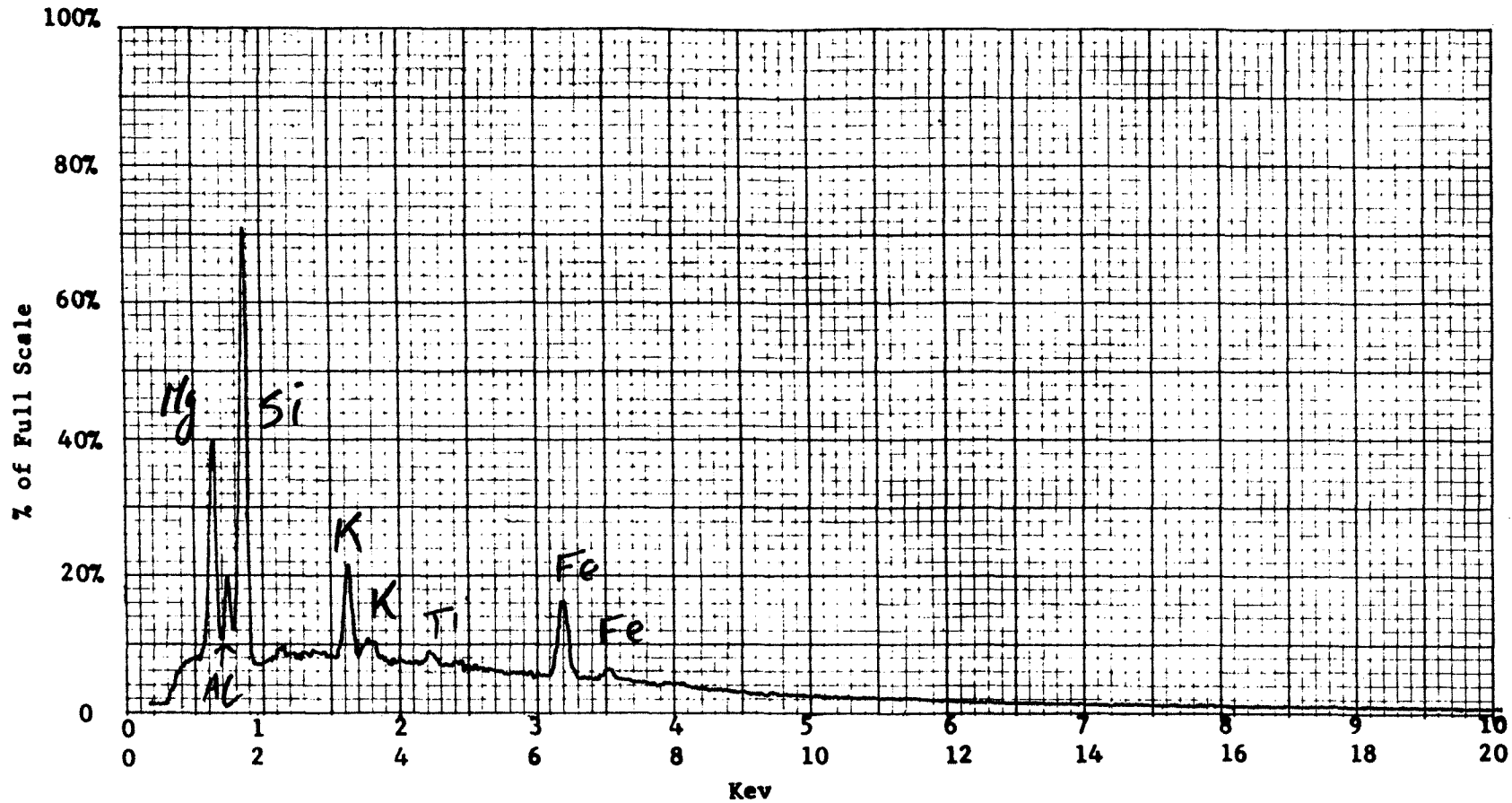
Operator \_\_\_\_\_ Date \_\_\_\_\_

Accelerating Potential 25 KeV

Total Counts Acquired 1.0 min.

Number Counts Full Scale 5K

Number of eV per channel 20



Sample peculiarities and remarks: FIGURE 252: POINT SCAN ON A HIGH Si PARTICLE

ENERGY DISPERSIVE X-RAY ANALYSIS

Analytical Number Vermiculite

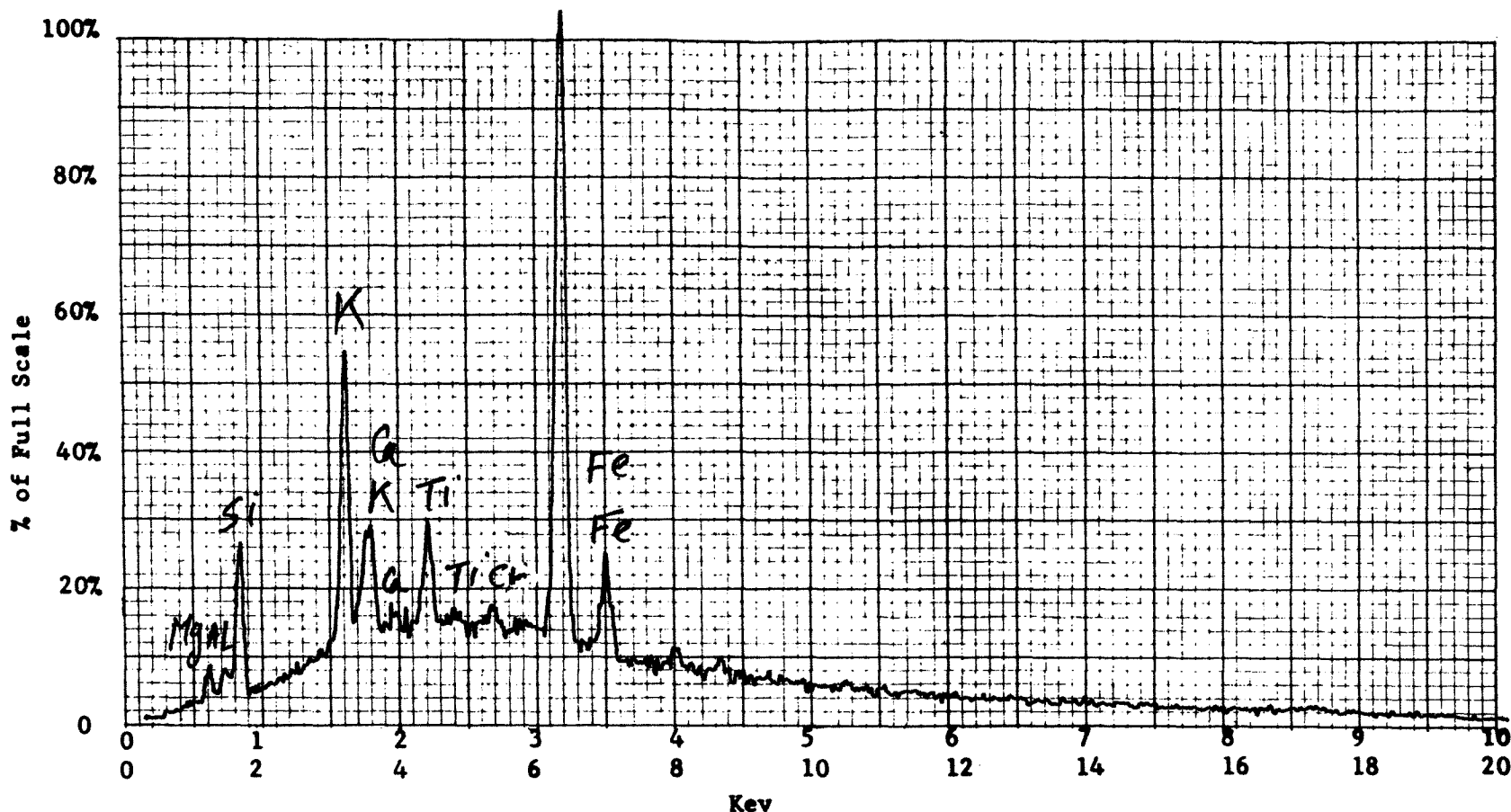
Operator \_\_\_\_\_ Date \_\_\_\_\_

Accelerating Potential 25 KeV

Total Counts Acquired 1.0 min.

Number Counts Full Scale 5K

Number of eV per channel 20



Sample peculiarities and remarks: FIGURE 253: POINT SCAN ON A HIGH Fe PARTICLE

Fly Ash (Basic):Structural Analysis:

Most of the basic fly ash particles were spherical in shape; very small or very large spheres were observed. Some particles that appeared to be irregular in shape at low magnification were found to be formed of many small spheres agglomerated together, and in some cases fused together because of the high temperature they were generated at.

Occasional openings in some small and large spheres disclosed that the hollow center was filled with many more smaller spheres. This is due to efficiently burned fuel at relatively low temperatures. This phenomenon is clearly seen in several particles in Figure 254, by a large spherical particle in Figure 256 and by the large particle in Figure 259.

The surface of the spheres, in most cases, was smooth, in a few cases slightly rough surfaces were observed. Spheres of  $0.1\mu$  to  $0.3\mu$  were seen to be attached to the surface of larger particles in a new micrographs, for example, Figures 260, 262, 265 and 270.

The maximum, average and minimum particle size were measured in microns ( $\mu$ ) as follows:

Maximum	Average	Minimum
140.0	20.0	0.1

Elemental Composition and Distribution:

In most particles, Al, Si, K, Ca, Ti and Fe were detected. Fe concentration in the basic fly ash was higher

than that in the acidic fly ash. Figures 273 and 280 illustrate the general elemental distribution. In both figures, Al and Si were present as major elements. A large number of particles with high Ca or Fe concentrations were also observed.

A large sphere in the top of Figure 287 was found to contain a very high level of Fe, this is presented in the iron X-ray image, Figure 293, and in the X-ray energy spectrum, Figure 240. A few small spheres with high levels of Ca, Ti or Fe were also detected in Figure 294.

A group of fused spheres can be seen in the middle of Figure 301; this figure was obtained to illustrate that some particles contained high concentrations of Ca and S. The elemental distributions are presented in the sulfur X-ray image, Figure 305, the calcium X-ray image, Figure 307, and in the X-ray energy spectrum, Figure 241.

Agglomerated spherical particles are presented in Figures 310 and 324 in which only Ca was high while trace amounts of S were detected. This is illustrated in the calcium X-ray images, Figures 314 and 329, and the X-ray energy spectrum, Figure 242.

Very high concentrations of Fe were detected from a spherical particle in Figure 317 (see also iron X-ray image, Figure 323).

Ti was detected from several very small particles throughout the sample. This is illustrated in the X-ray energy spectrum, Figure 243, and in the titanium X-ray images, (Figures 278, 285, 299 and 315).

Ba was detected at a very high level from a spherical particle seen in Figure 332. The barium X-ray image, Figure 337, and the X-ray energy spectrum, Figure 244, were obtained to illustrate that. The presence of Ti in this particle is possible but cannot be confirmed because the  $L_{\alpha}$  and  $L_{\beta}$  X-ray energy lines of Ba overlap with  $K_{\alpha}$  and  $K_{\beta}$  of Ti.

SEM IMAGES OF SAMPLE #

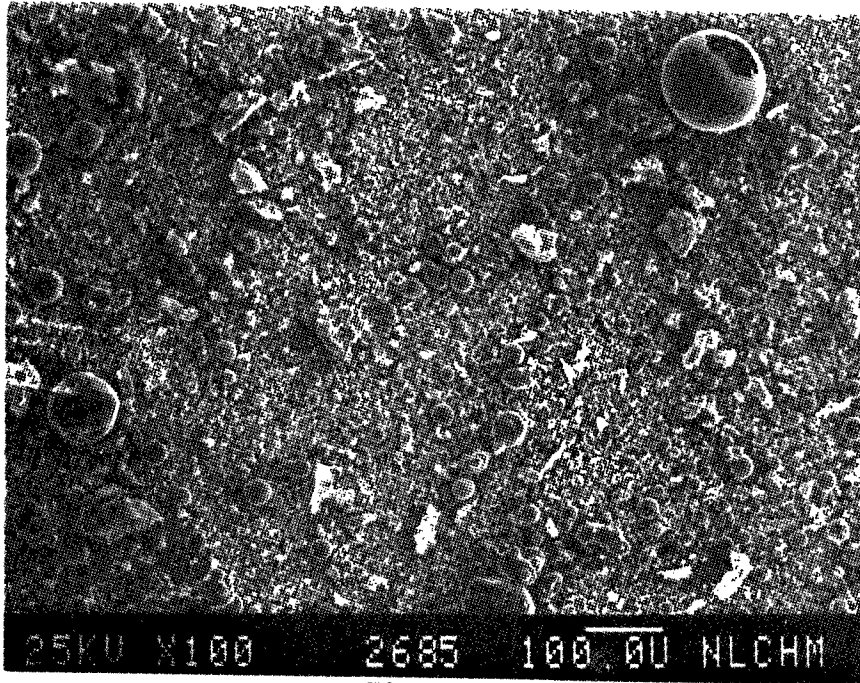


Figure 254

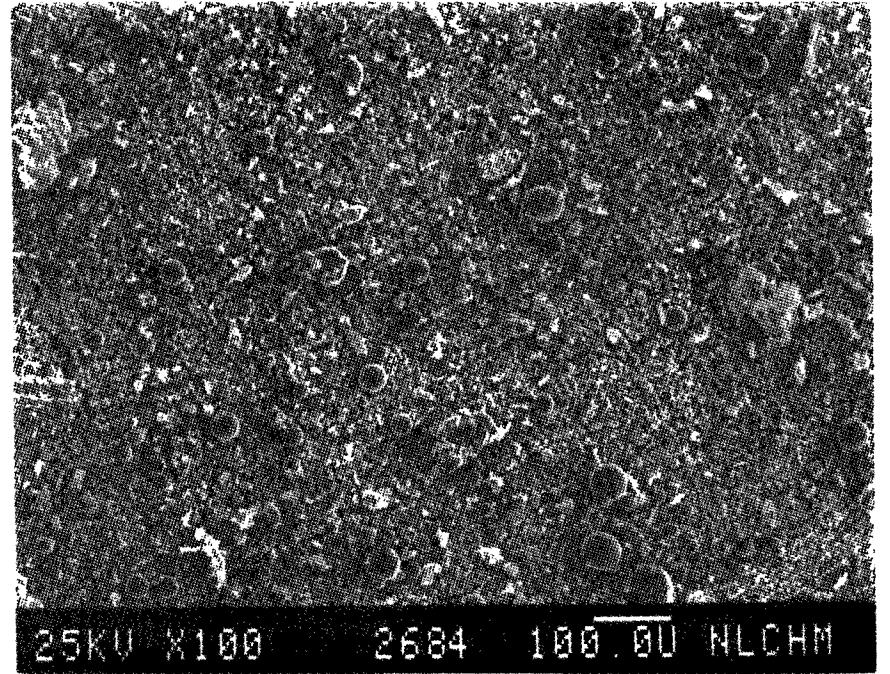


Figure 255

SEM IMAGES OF SAMPLE #

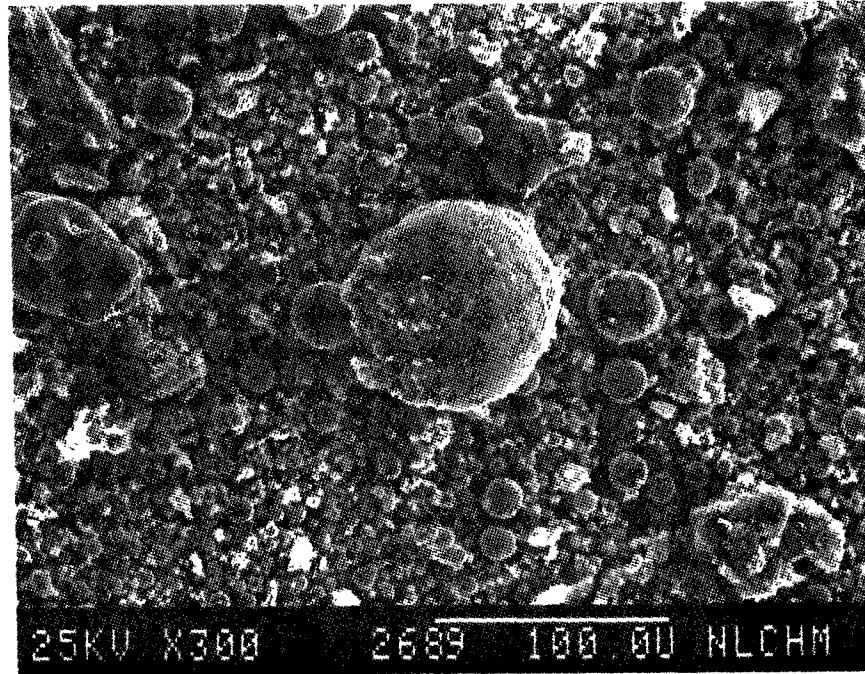


Figure 256

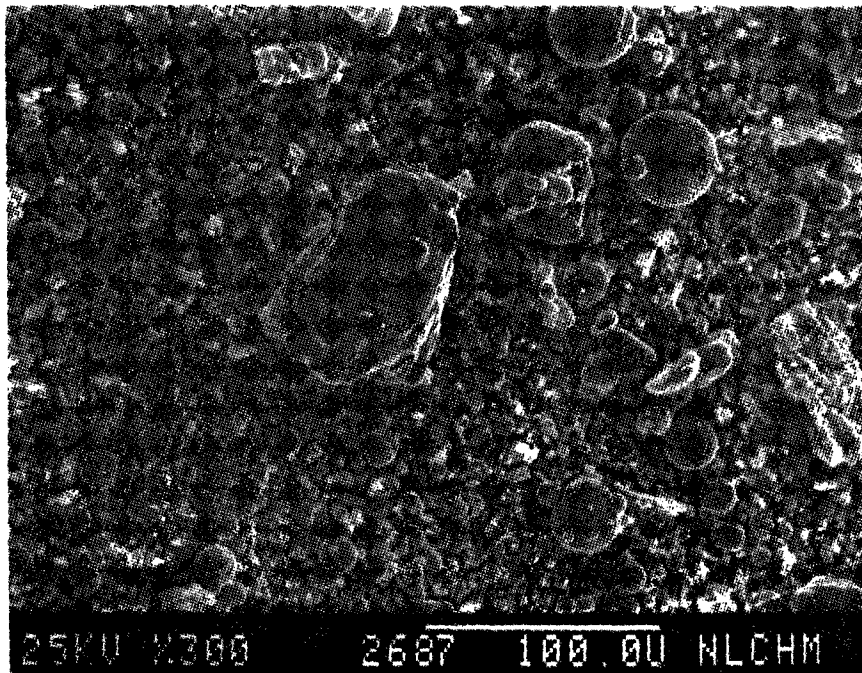


Figure 257

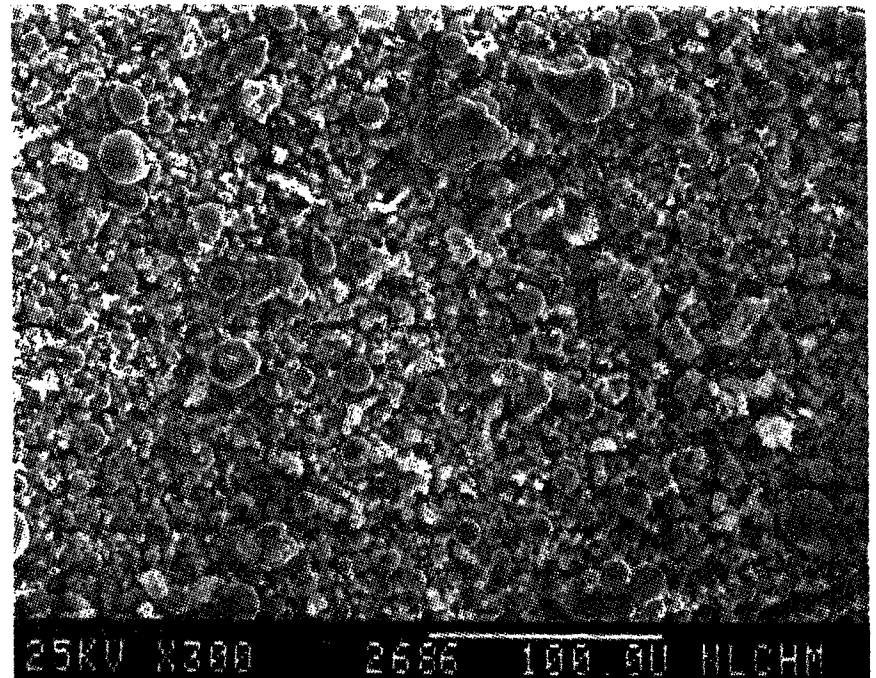


Figure 258



SEM IMAGES OF SAMPLE #

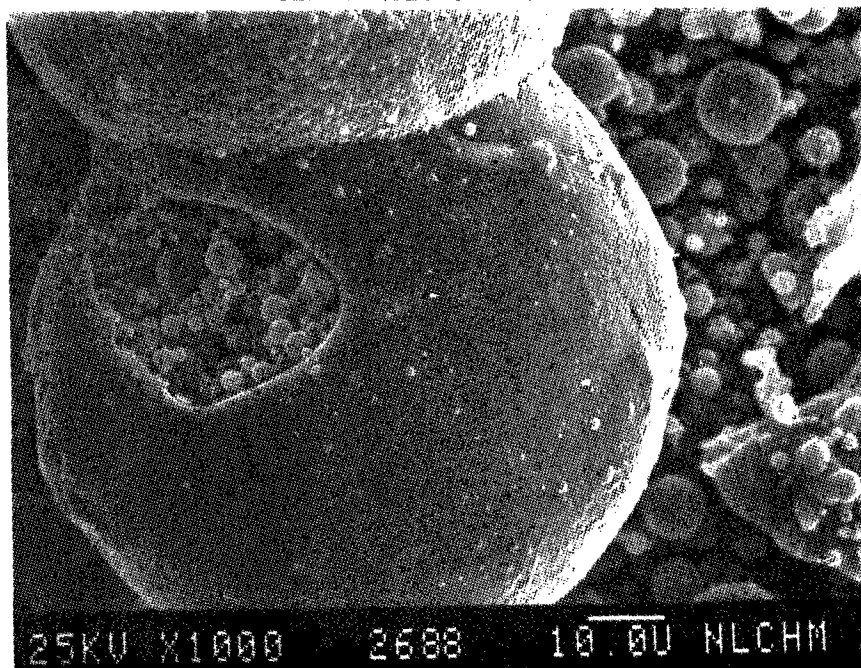


Figure 259

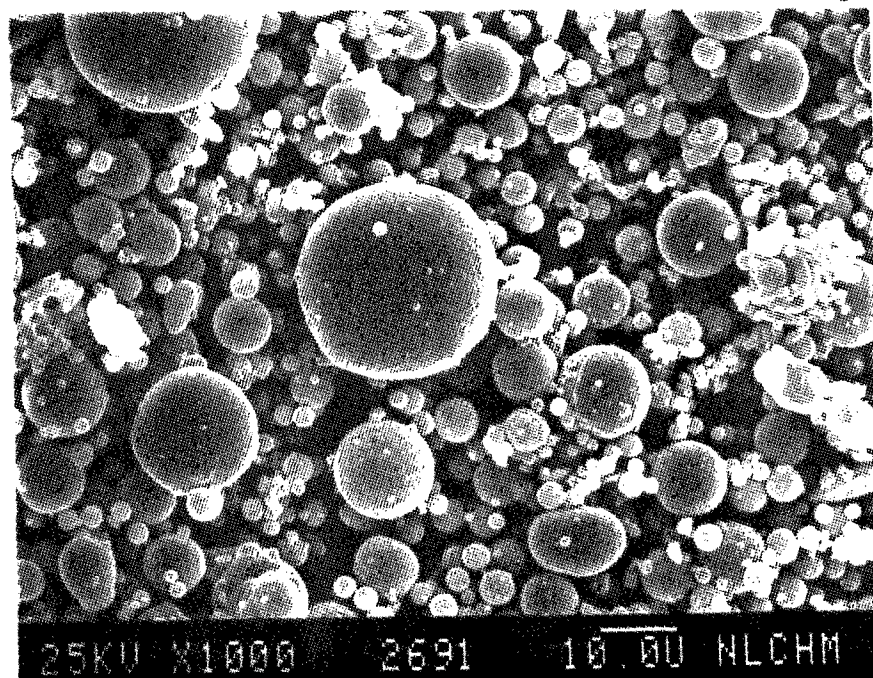


Figure 260

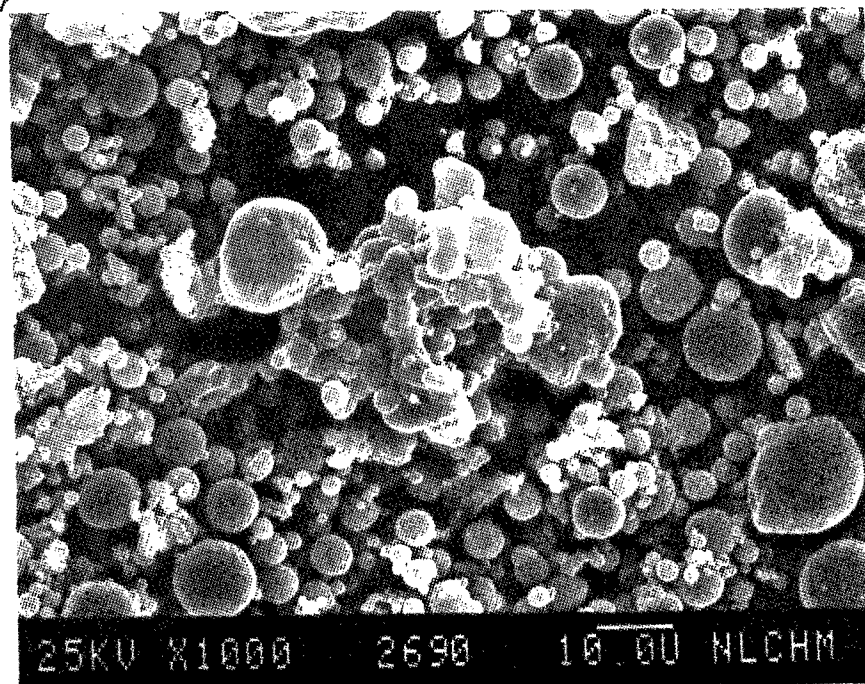
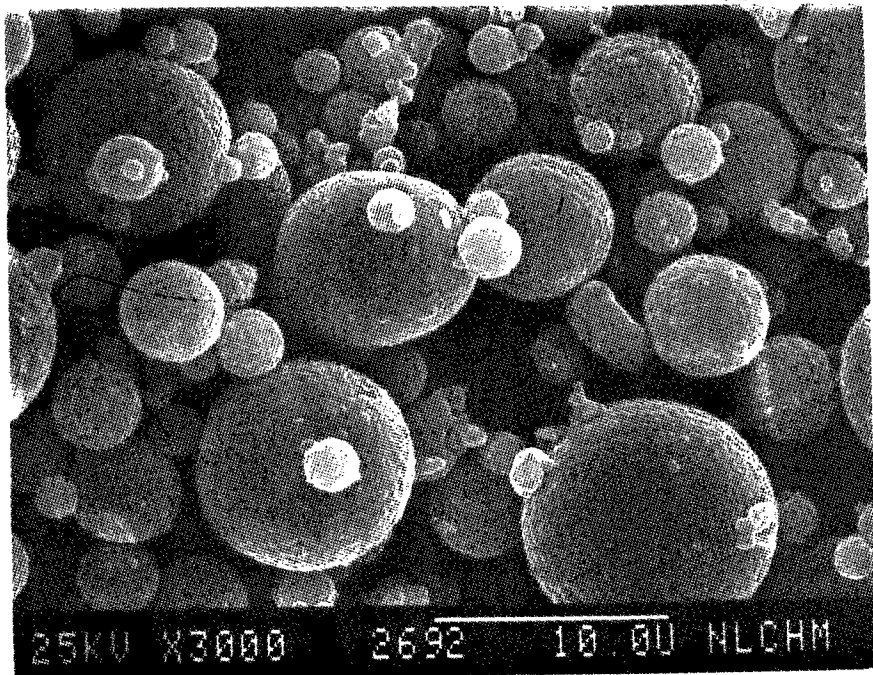


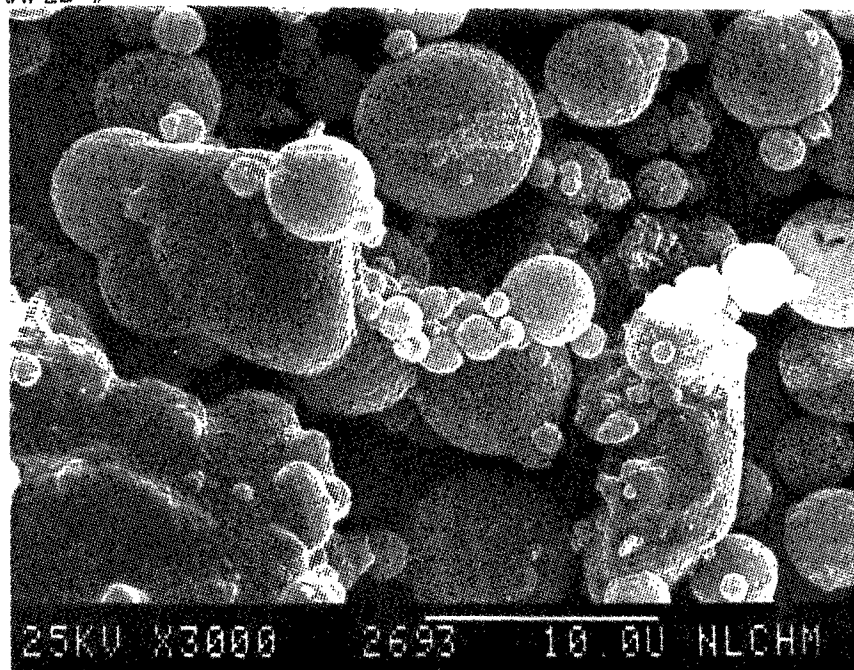
Figure 261

SEM IMAGES OF SAMPLE #



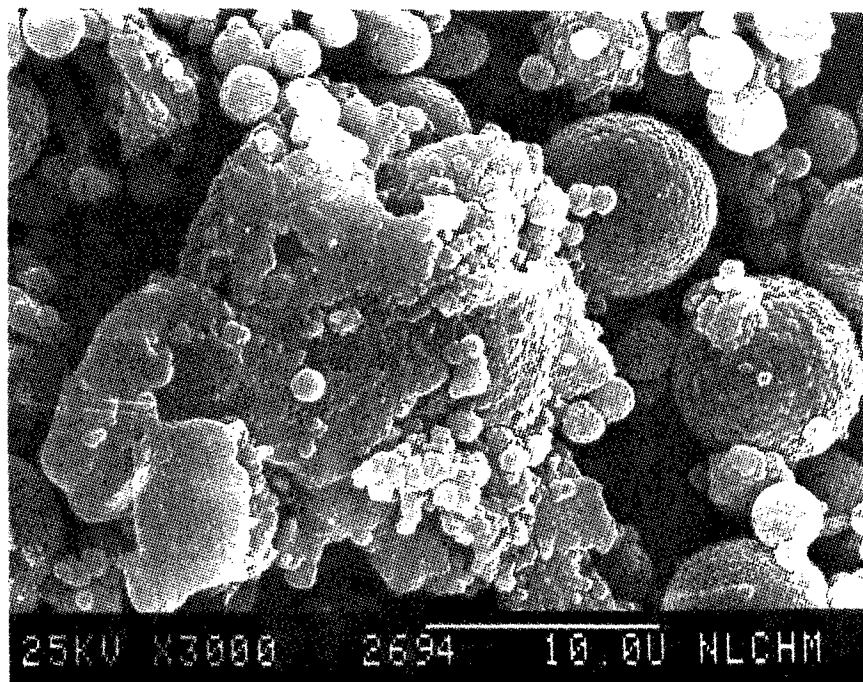
25KV X3000 2692 10.00 NLCHM

Figure 262



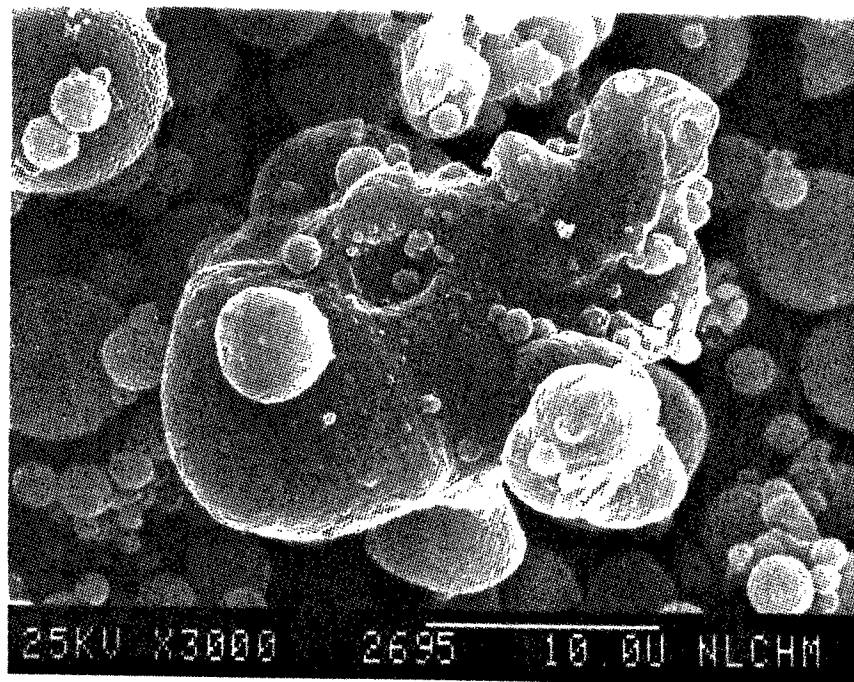
25KV X3000 2693 10.00 NLCHM

Figure 263



25KV X3000 2694 10.00 NLCHM

Figure 264



25KV X3000 2695 10.00 NLCHM

Figure 265



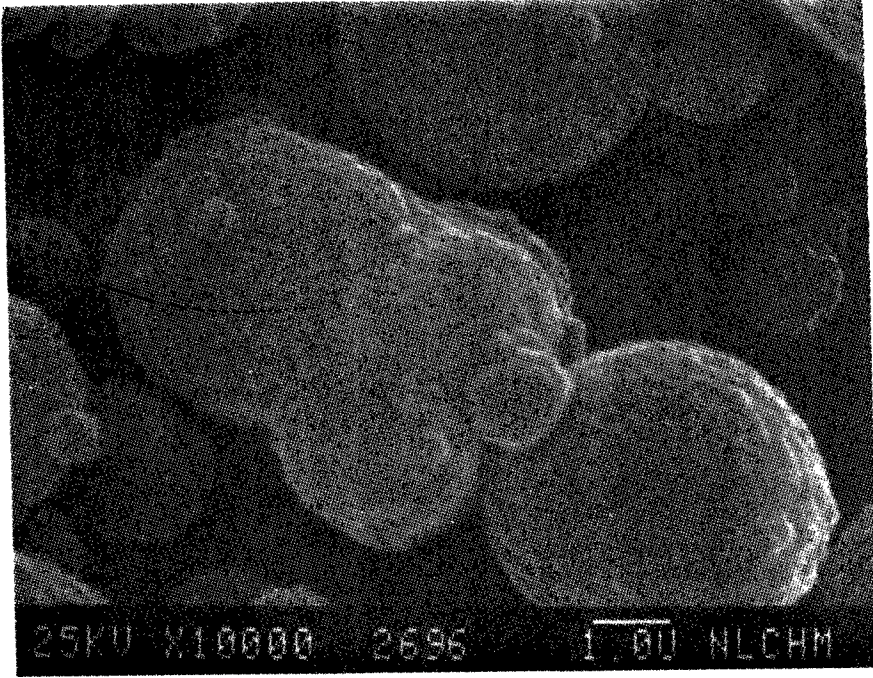


Figure 266

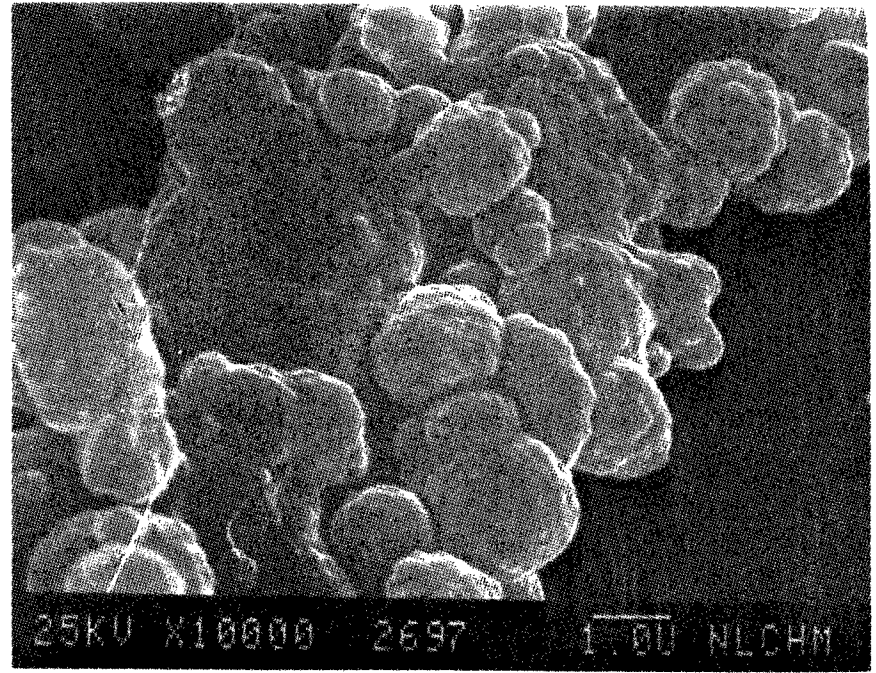


Figure 267

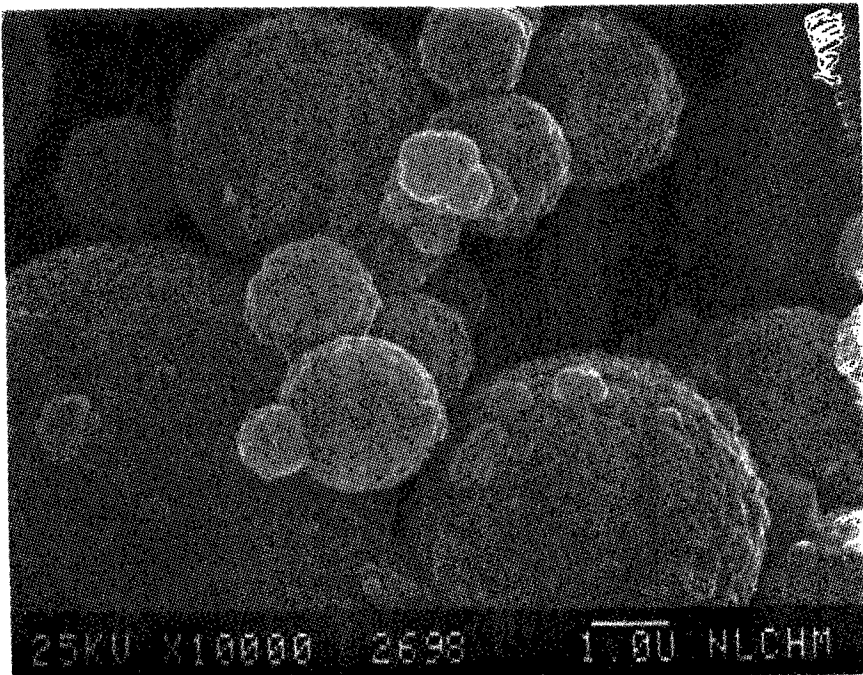


Figure 268

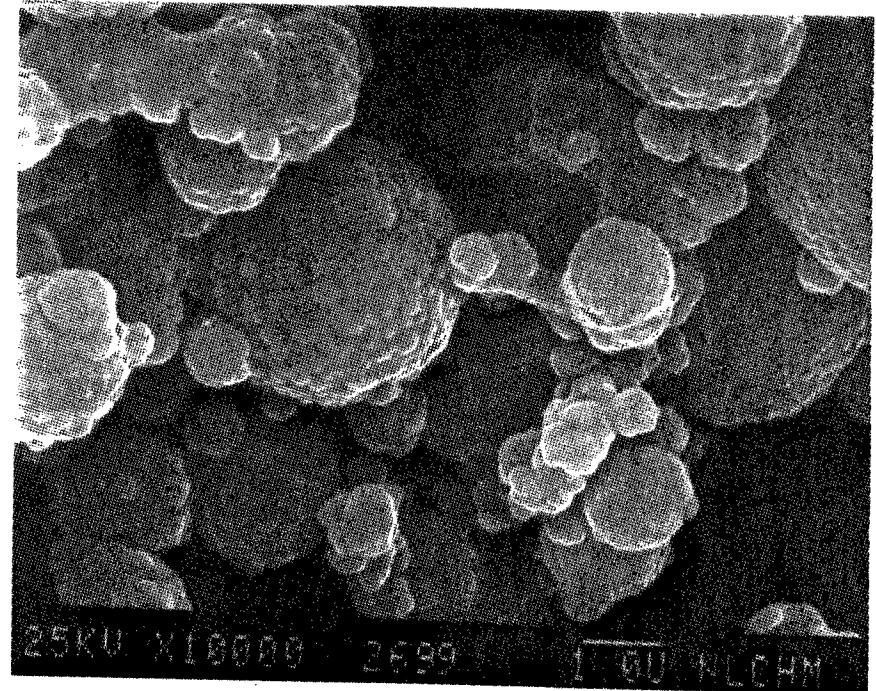


Figure 269

SEM IMAGES OF SAMPLE #

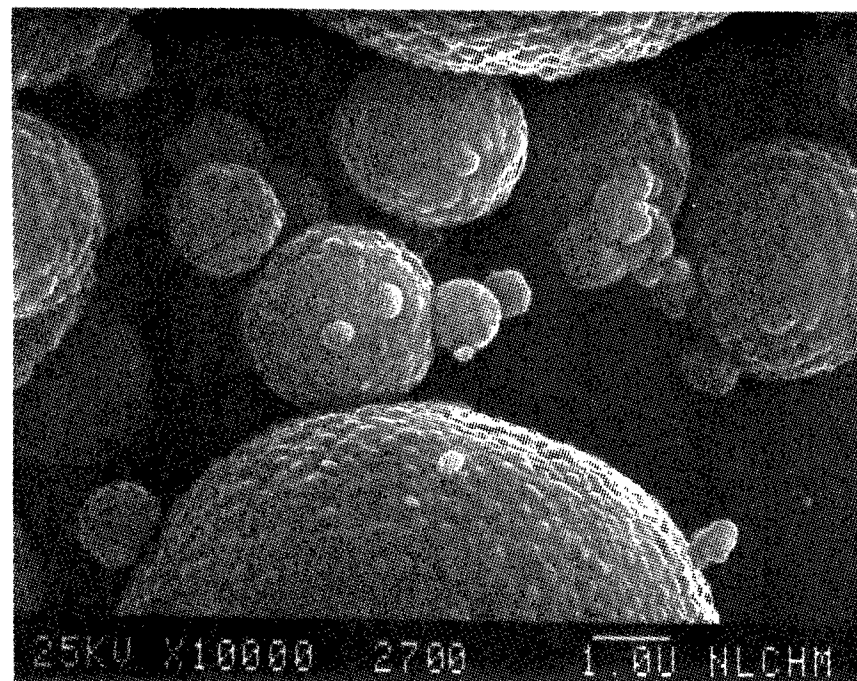


Figure 270

SEM IMAGES OF SAMPLE #

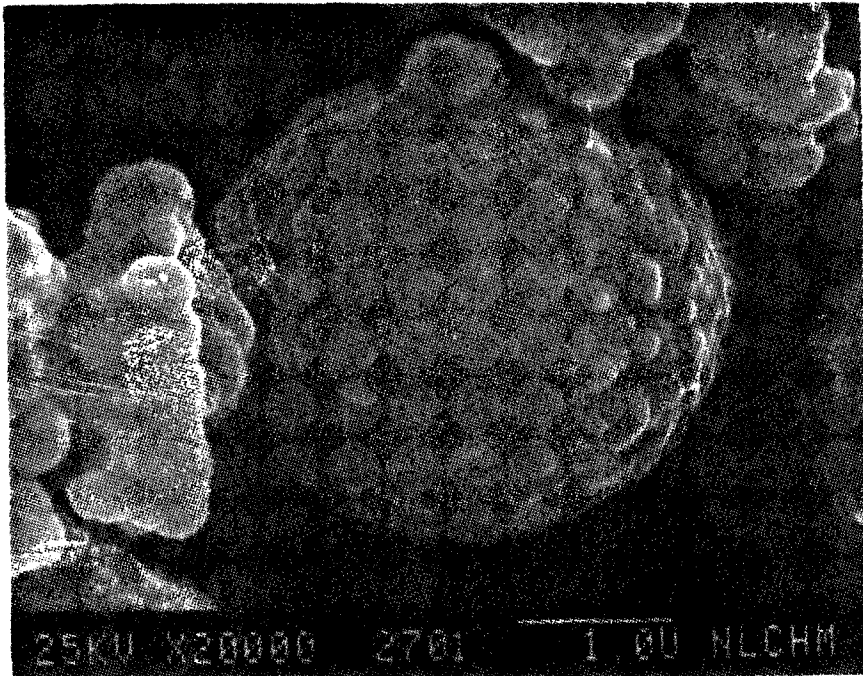


Figure 271

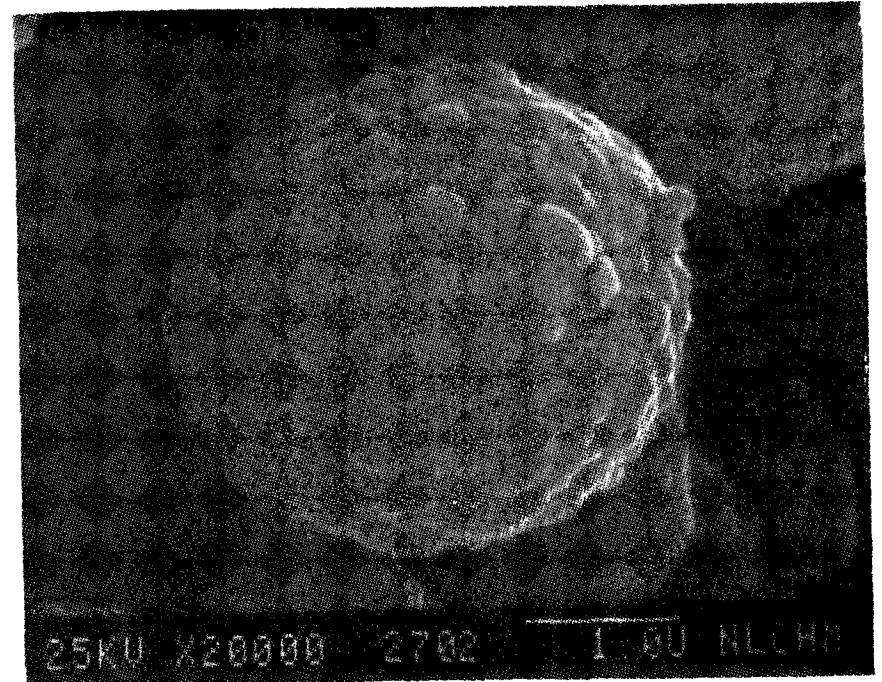


Figure 272



SEM IMAGES OF SAMPLE

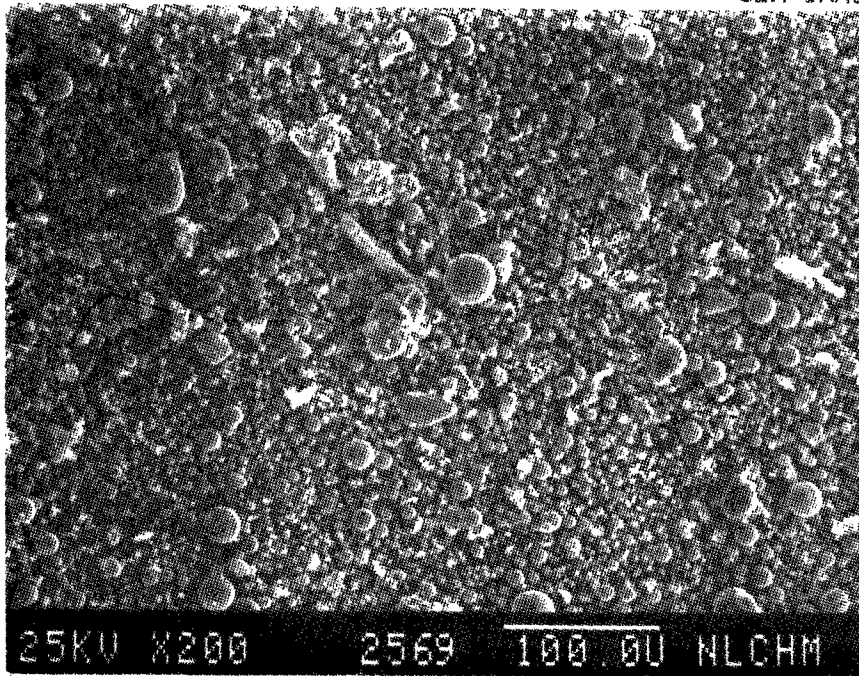


Figure 273

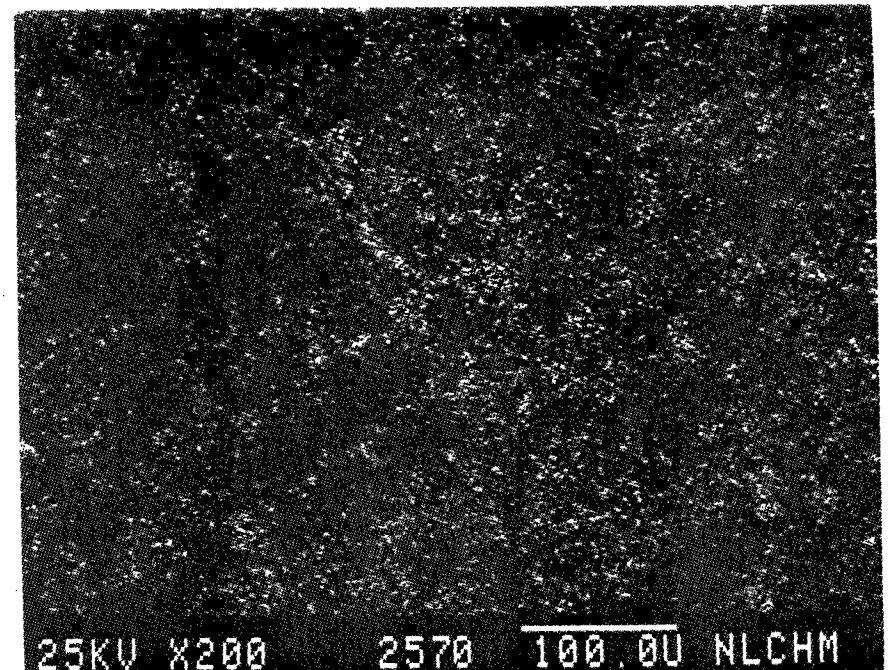


Figure 274

AL X-Ray Image of Figure 273

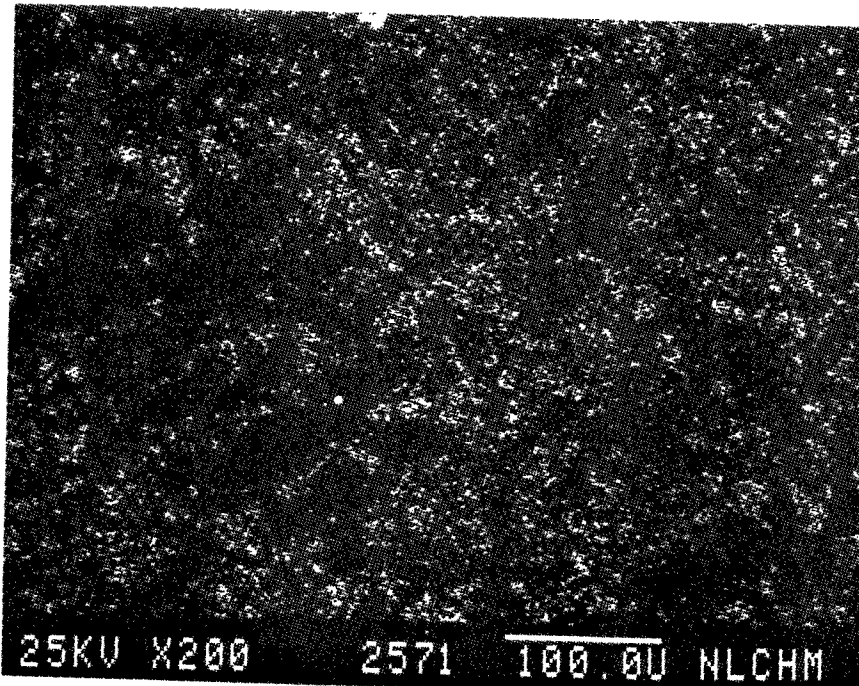


Figure 275

Si X-Ray Image of Figure 273

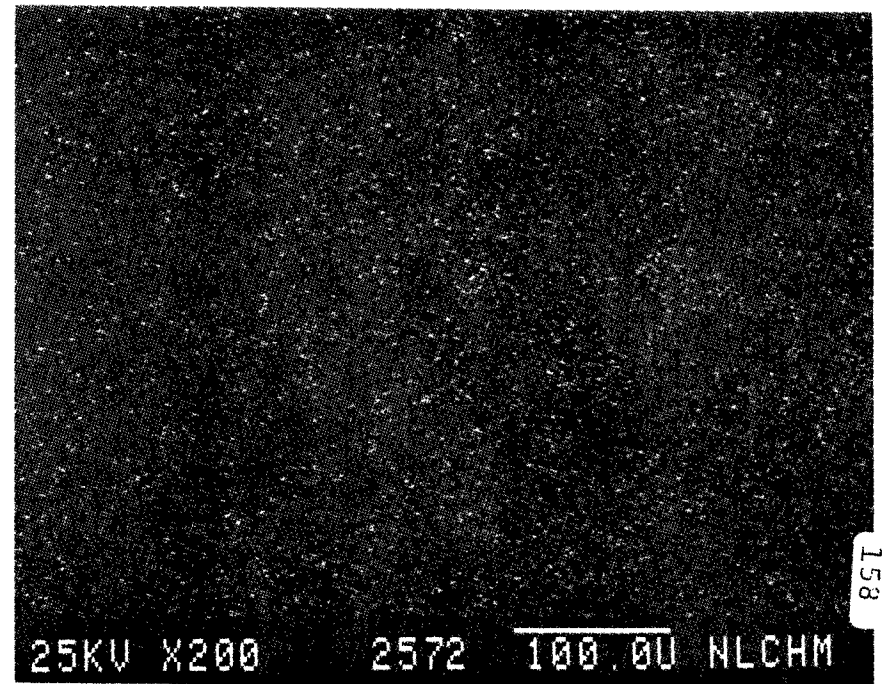


Figure 276

K X-Ray Image of Figure 273

SEM IMAGES OF SAMPLE #

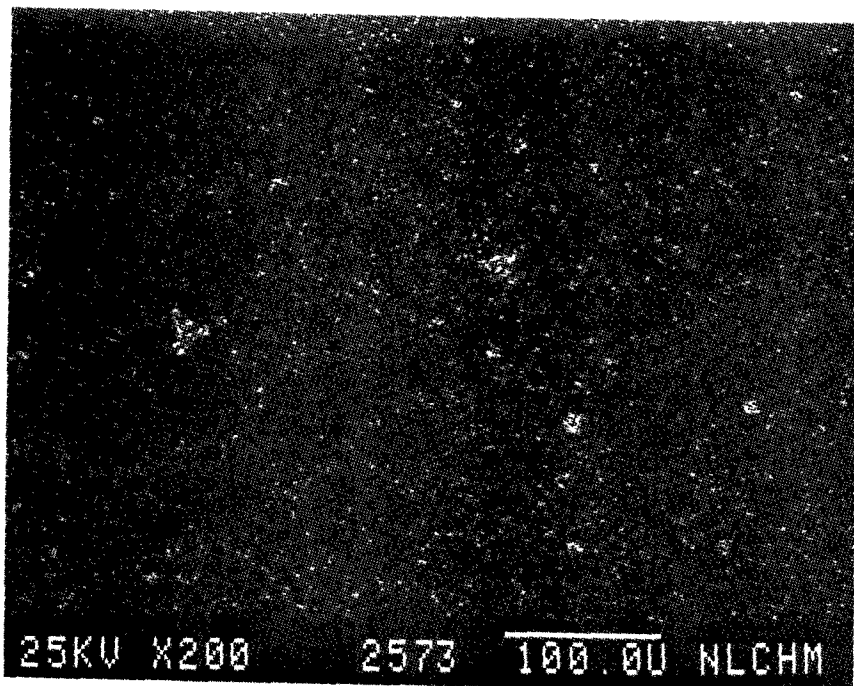


Figure 277

Ca X-Ray Image of Figure 273

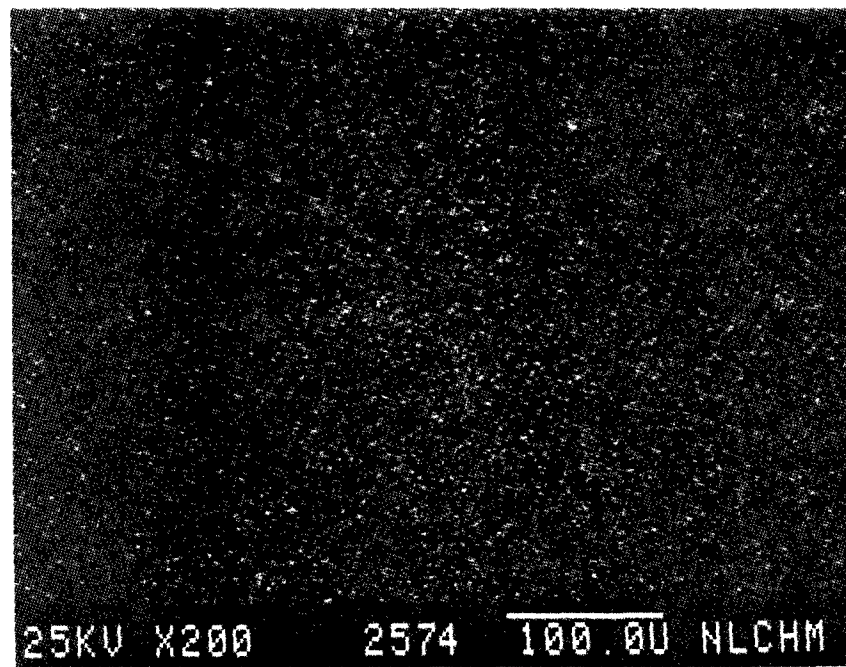


Figure 278

Ti X-Ray Image of Figure 273

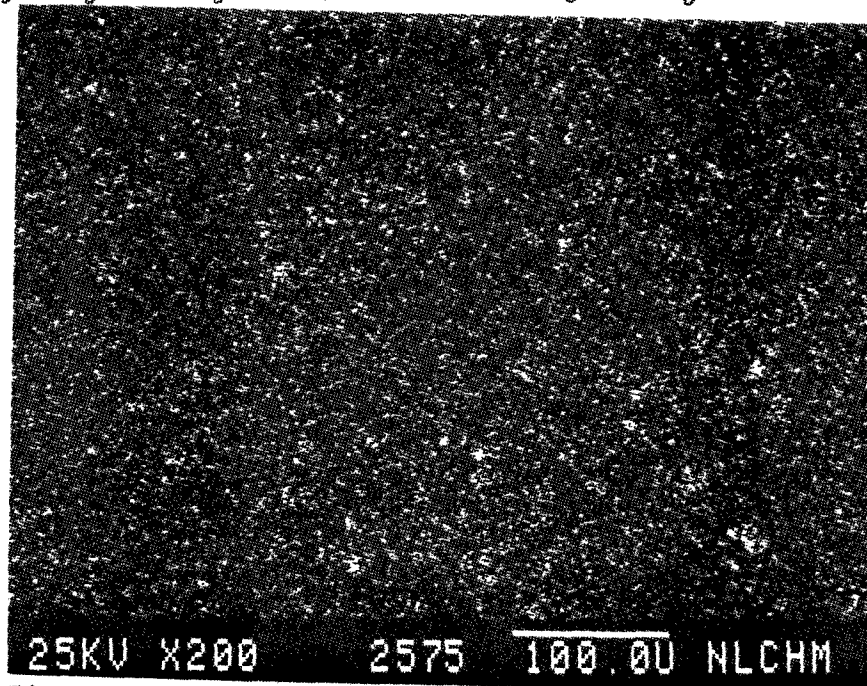


Figure 279

Fe X-Ray Image of Figure 273



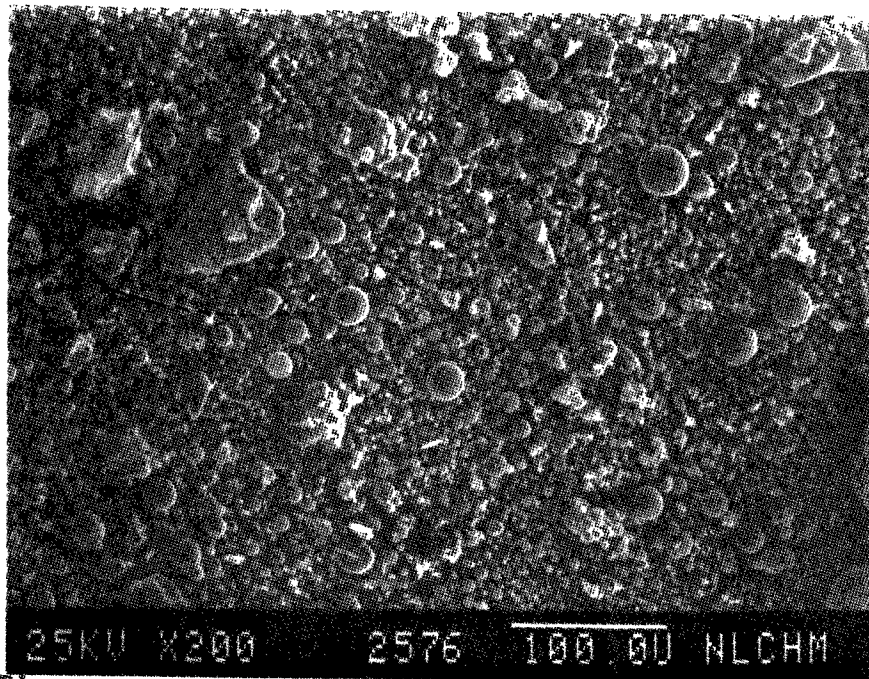


Figure 280

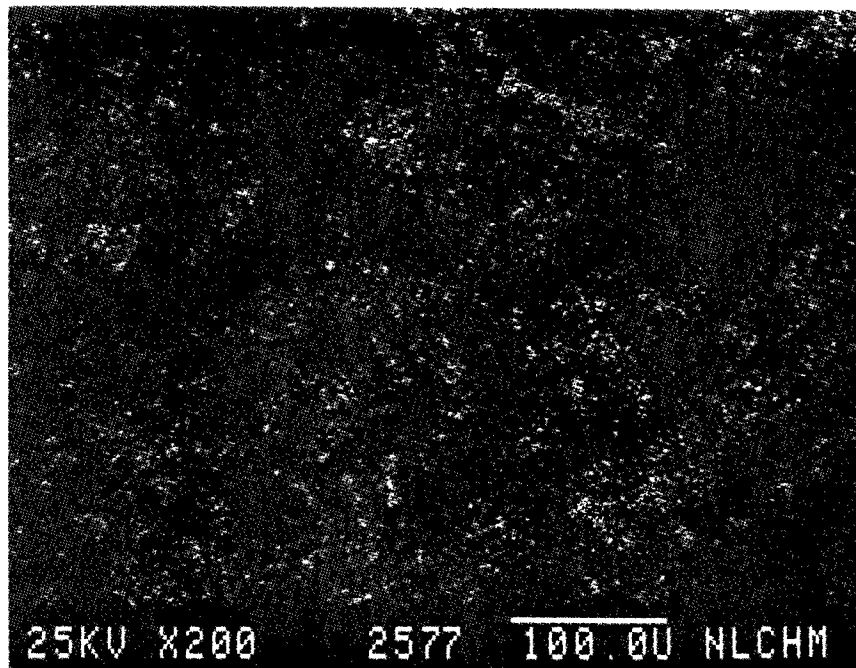


Figure 281

AL X-Ray Image of Figure 280

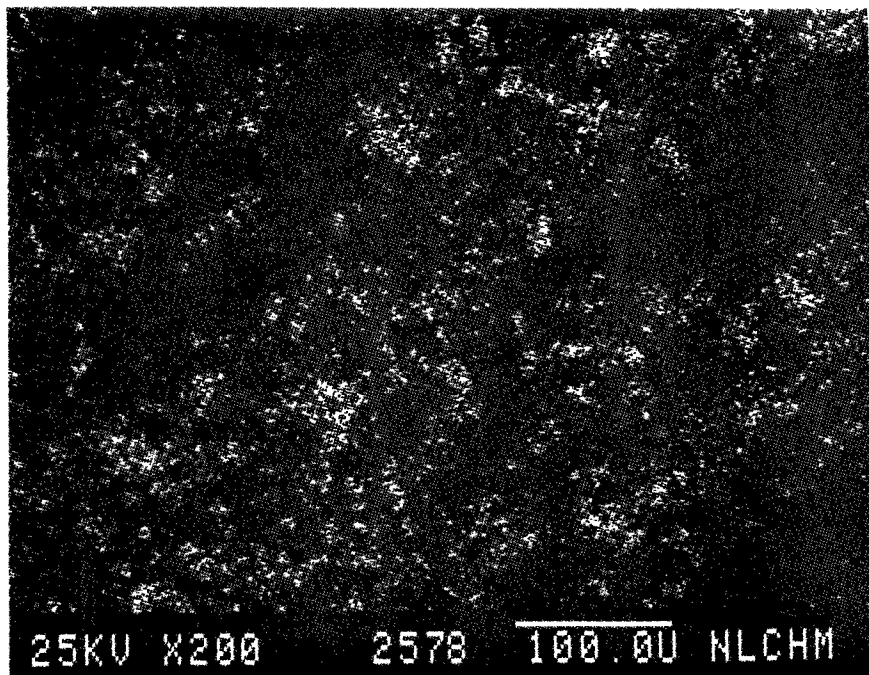


Figure 282

Si X-Ray Image of Figure 280

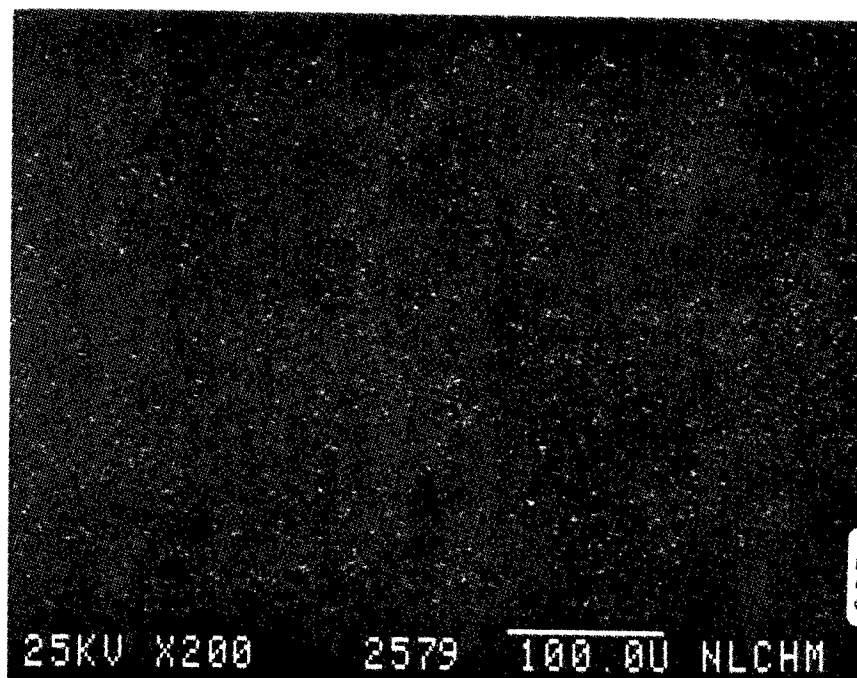


Figure 283

K X-Ray Image of Figure 280

SEM IMAGES OF SAMPLE #

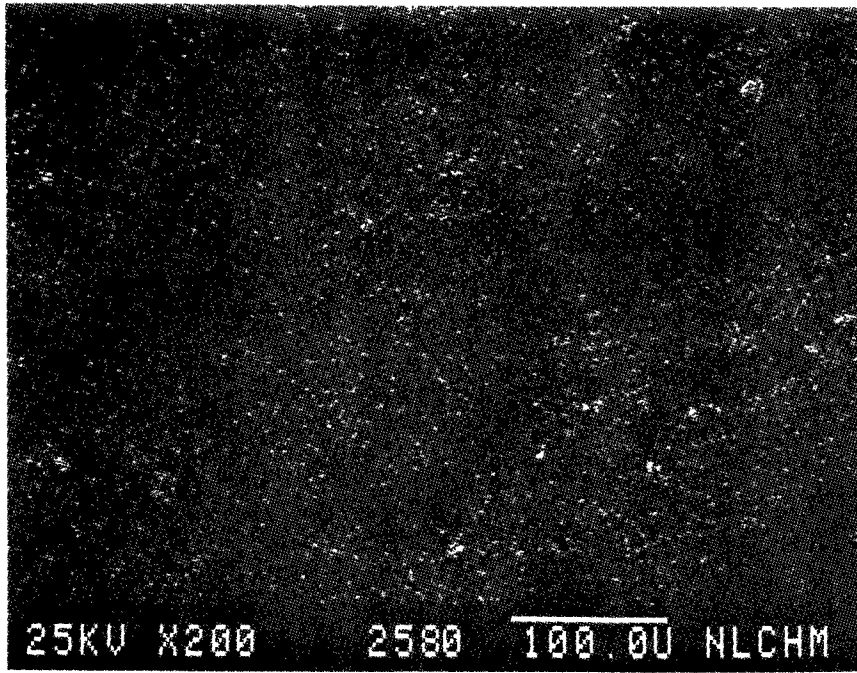


Figure 284

Ca X-Ray Image of Figure 280

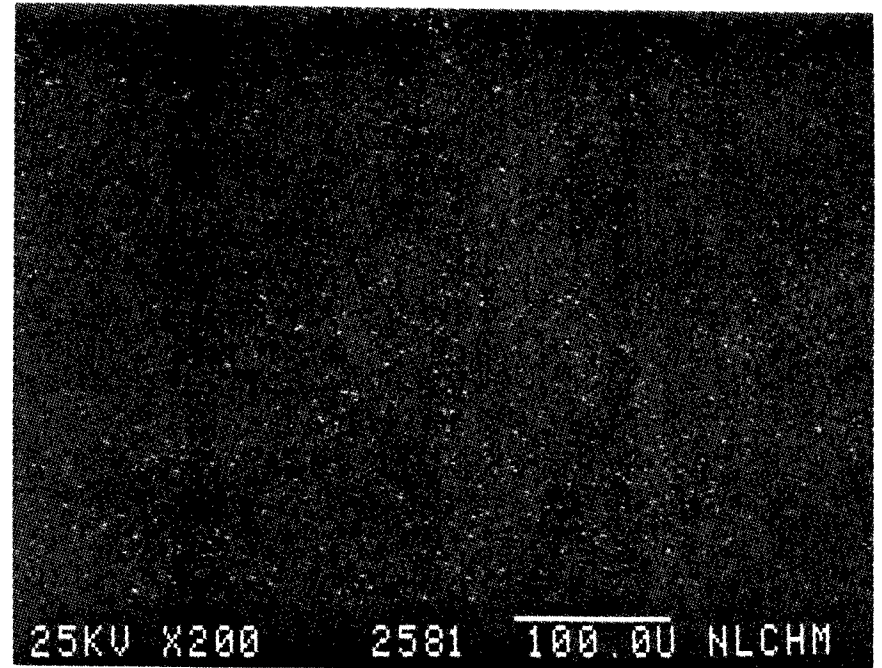


Figure 285

Ti X-Ray Image of Figure 280

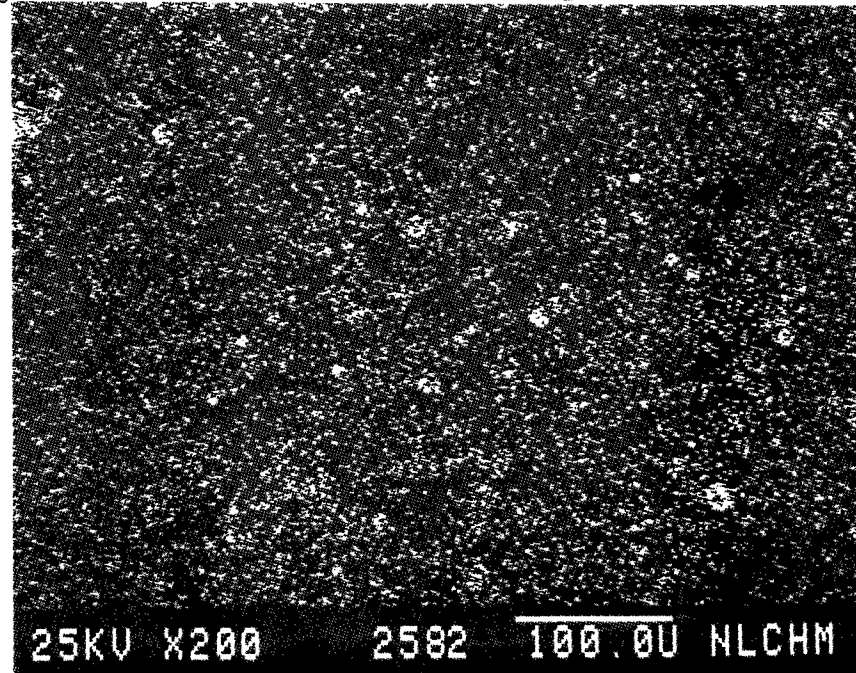


Figure 286

Fe X-Ray Image of Figure 280

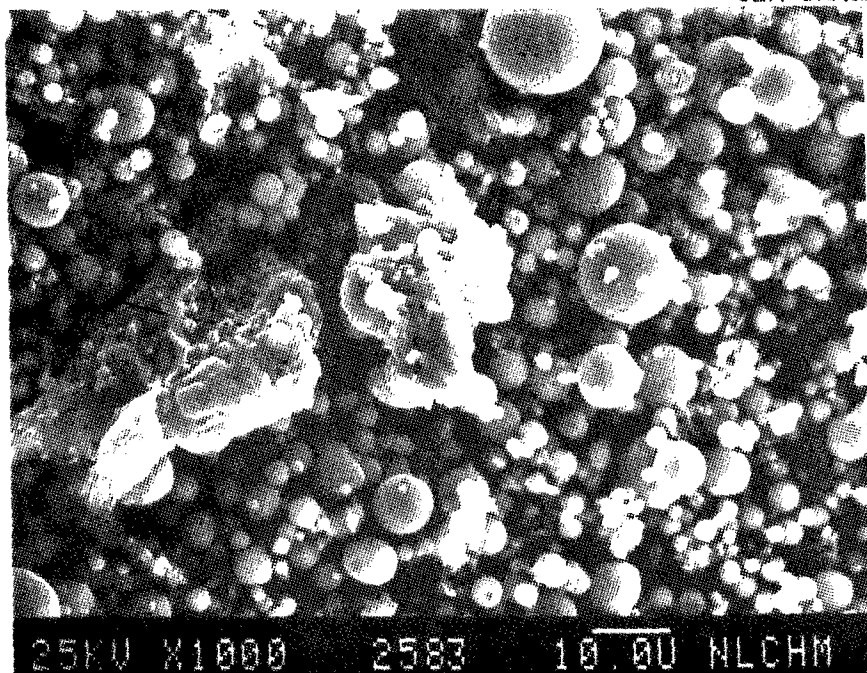


Figure 287

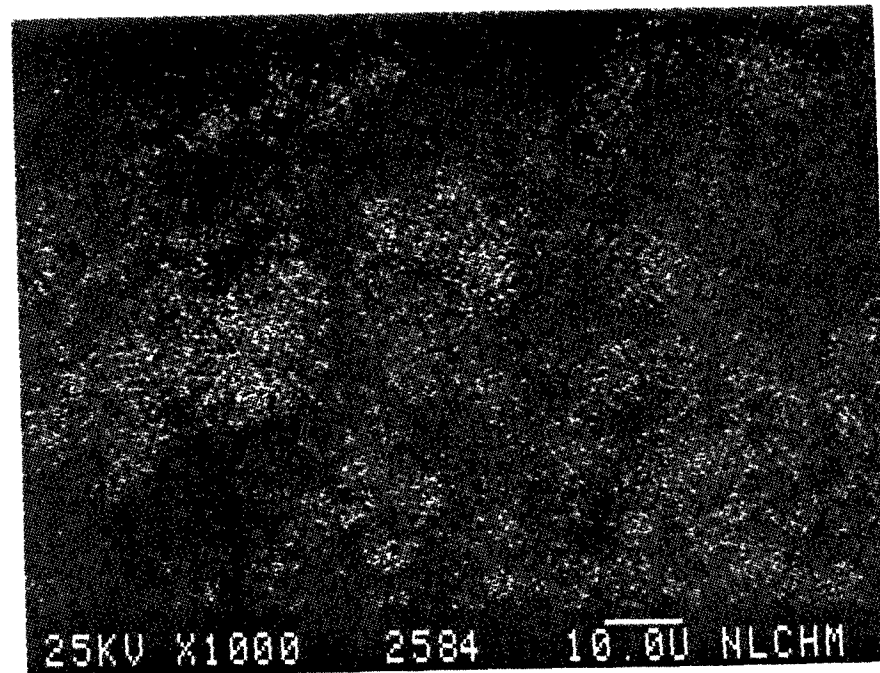


Figure 288

AL X-Ray Image of Figure 287

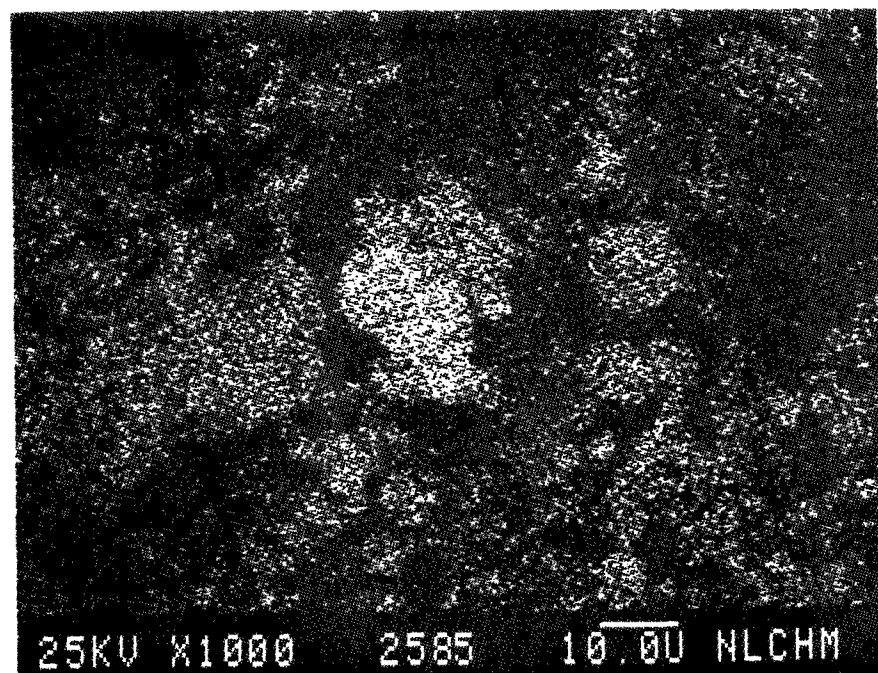


Figure 289

Si X-Ray Image of Figure 287

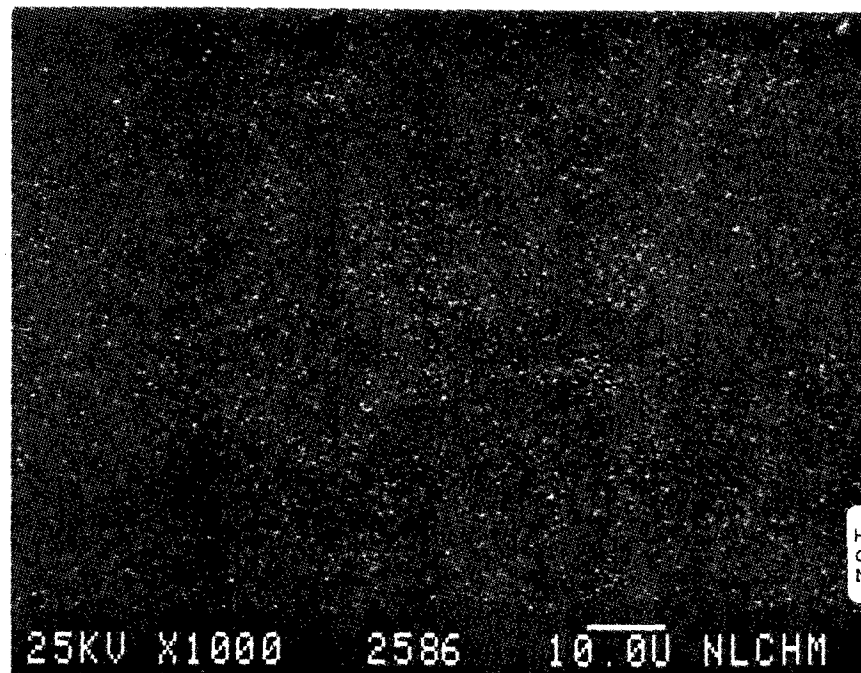


Figure 290

K X-Ray Image of Figure 287

SEM IMAGES OF SAMPLE #

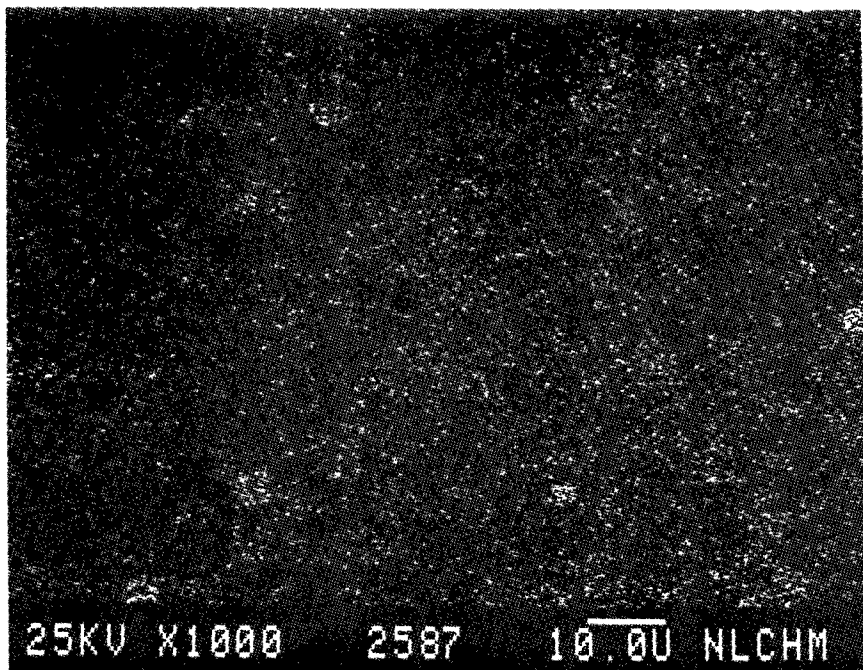


Figure 291

Ca X-Ray Image of Figure 287

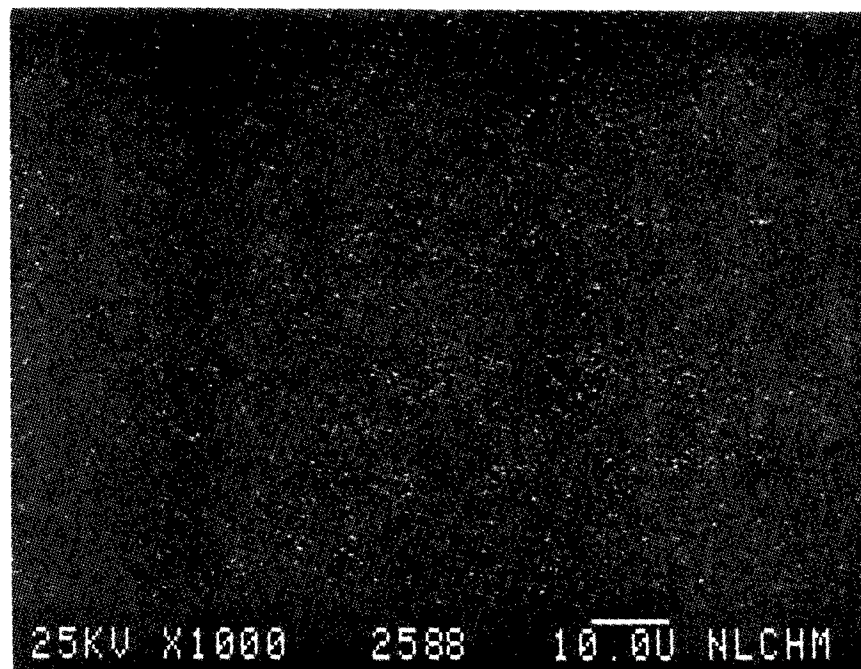


Figure 292

Ti X-Ray Image of Figure 287

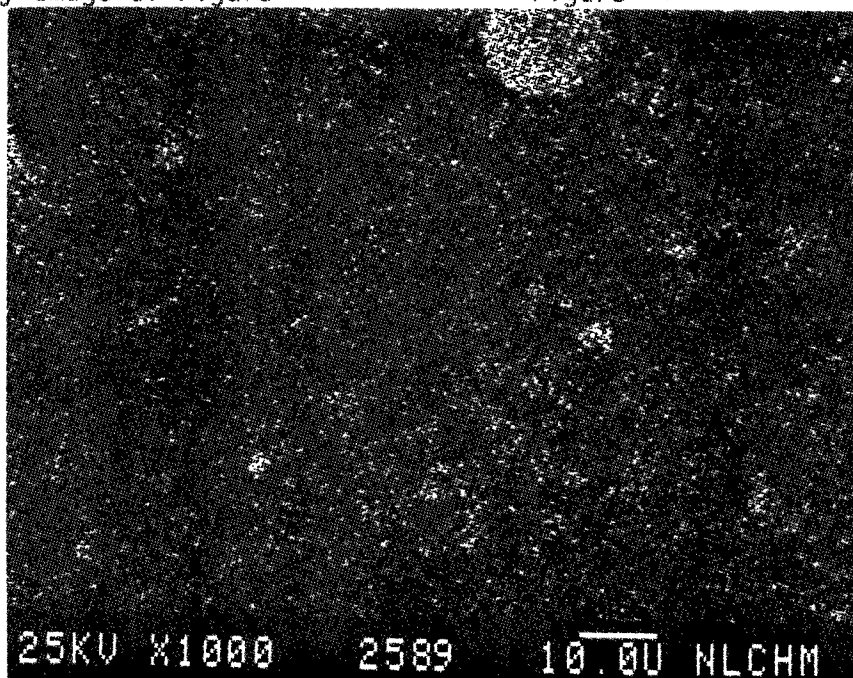


Figure 293

Fe X-Ray Image of Figure 287



SEM IMAGES OF SAMPLE #

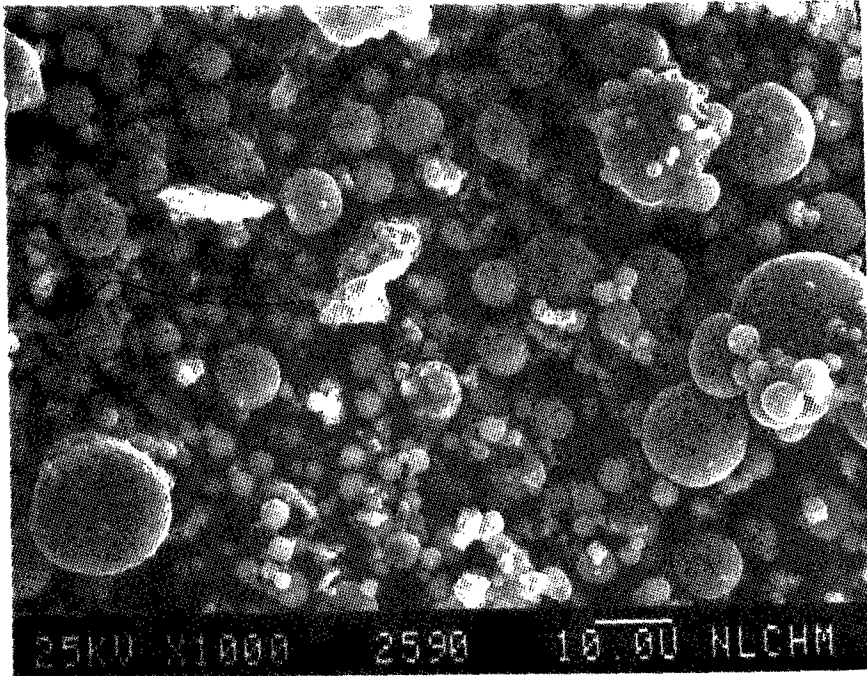


Figure 294

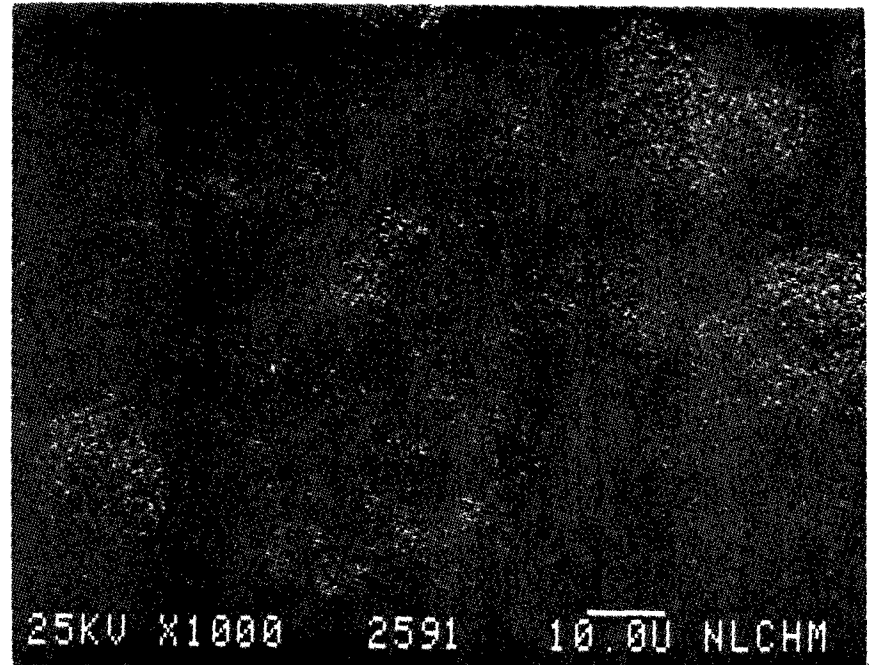


Figure 295

AL X-Ray Image of Figure 294

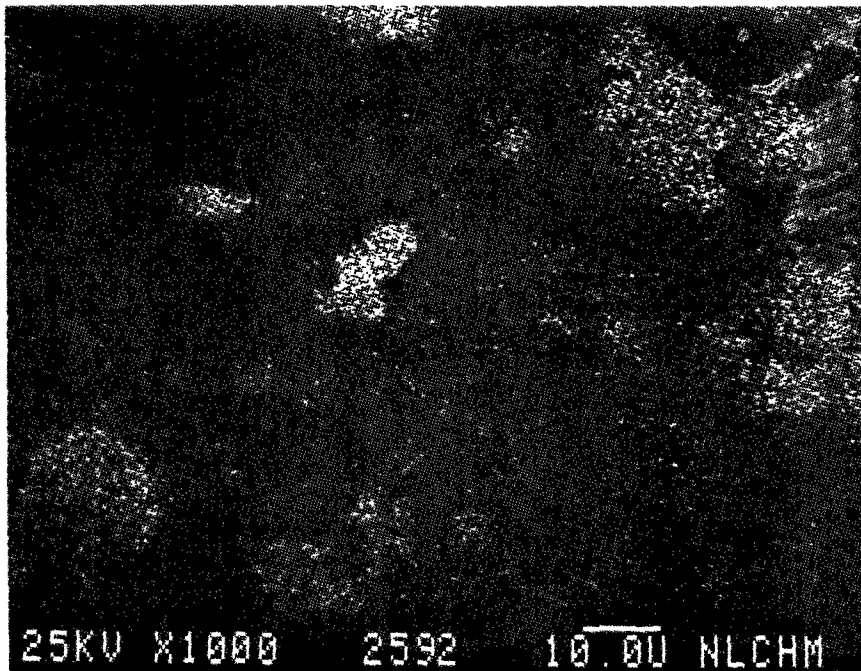


Figure 296

Si X-Ray Image of Figure 294

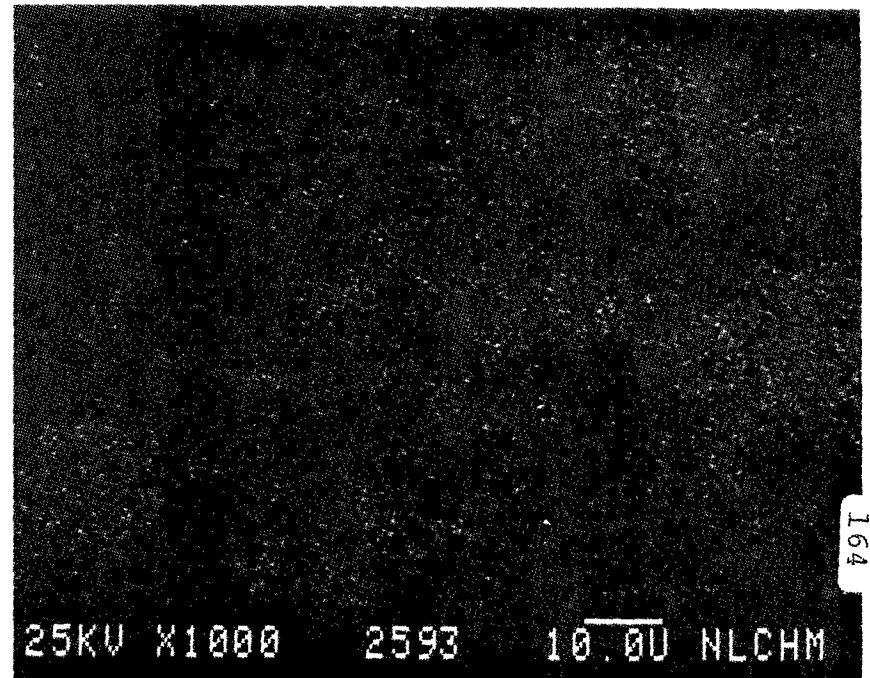


Figure 297

K X-Ray Image of Figure 294

SEM IMAGES OF SAMPLE #

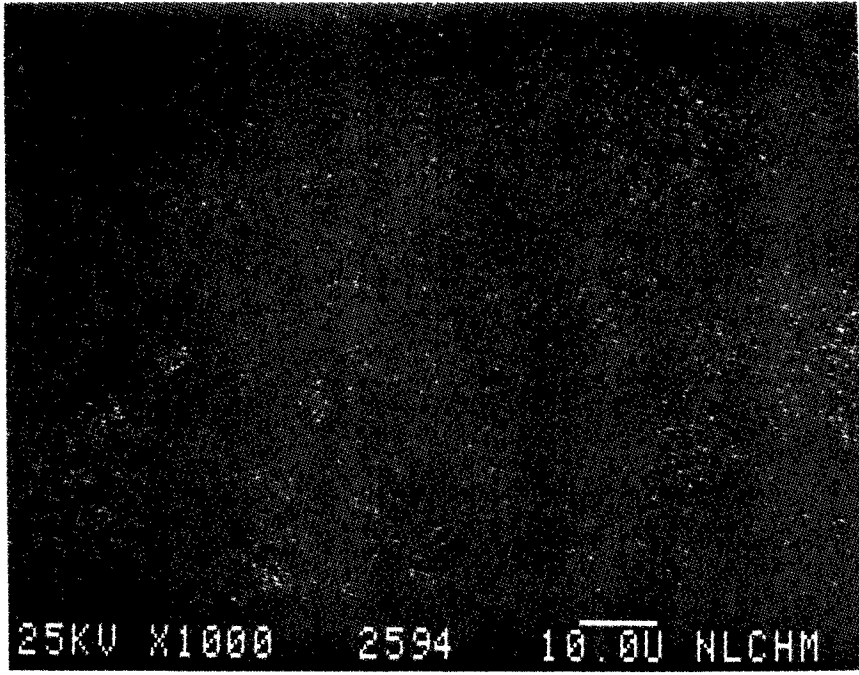


Figure 298

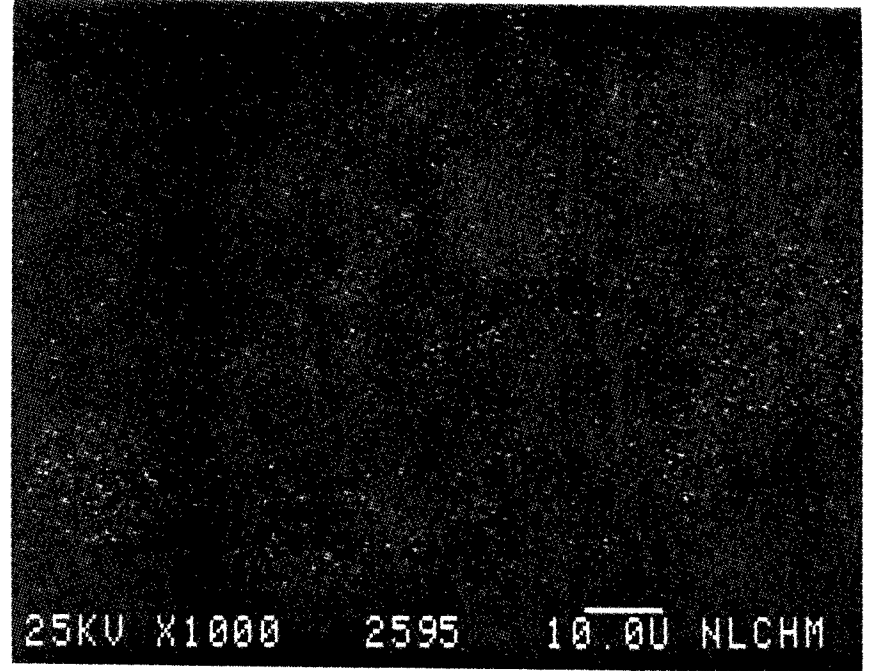


Figure 299

Ca X-Ray Image of Figure 294

Ti X-Ray Image of Figure 294

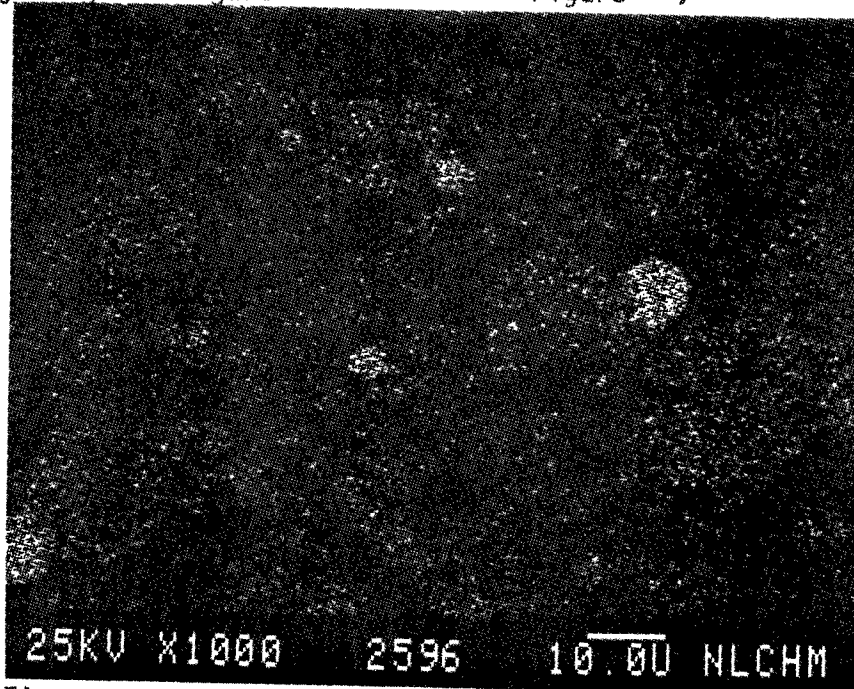


Figure 300

Fe X-Ray Image of Figure 294



SEM IMAGES OF SAMPLE #

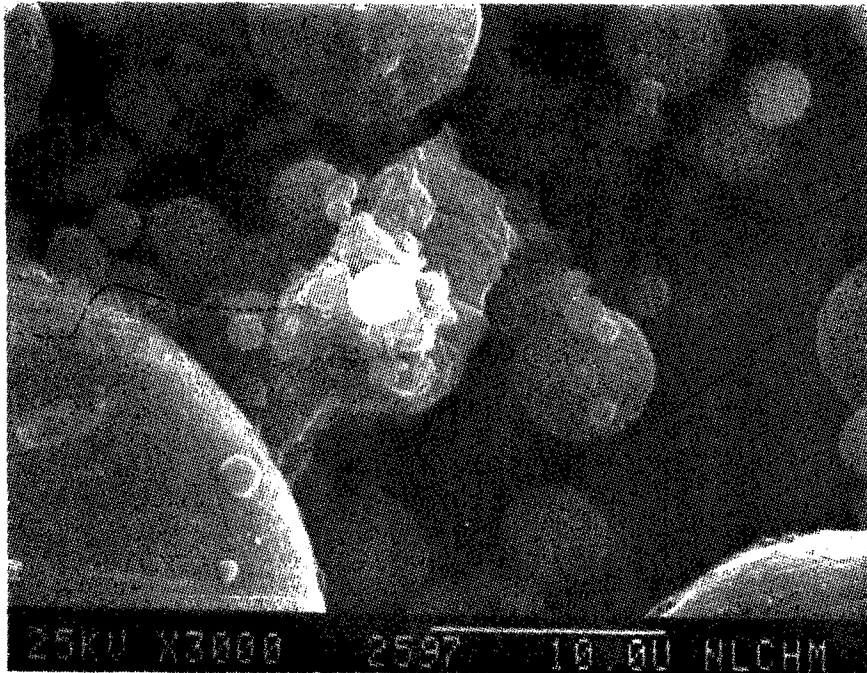


Figure 301

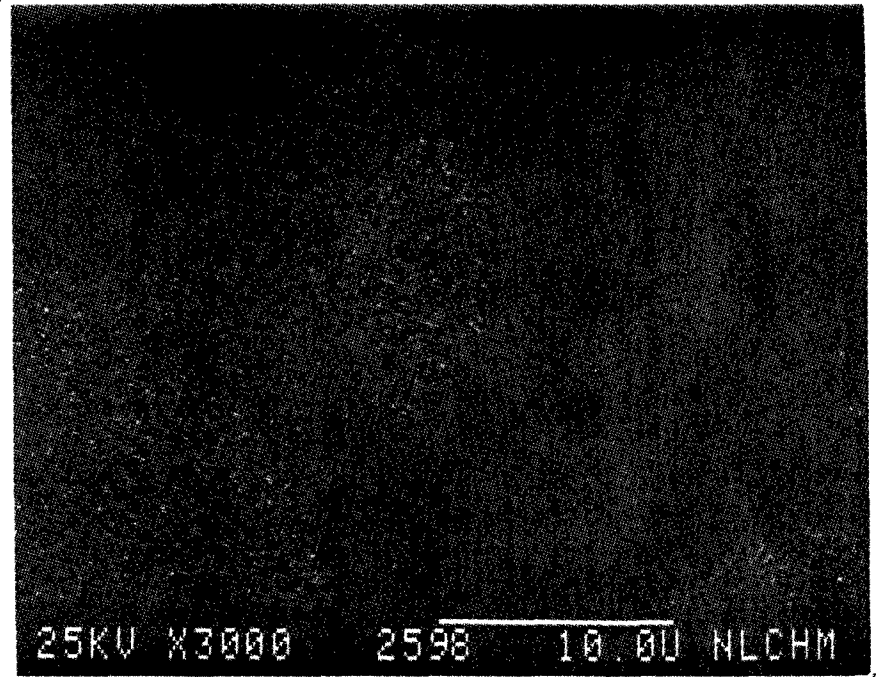


Figure 302

Mg X-Ray Image of Figure 301

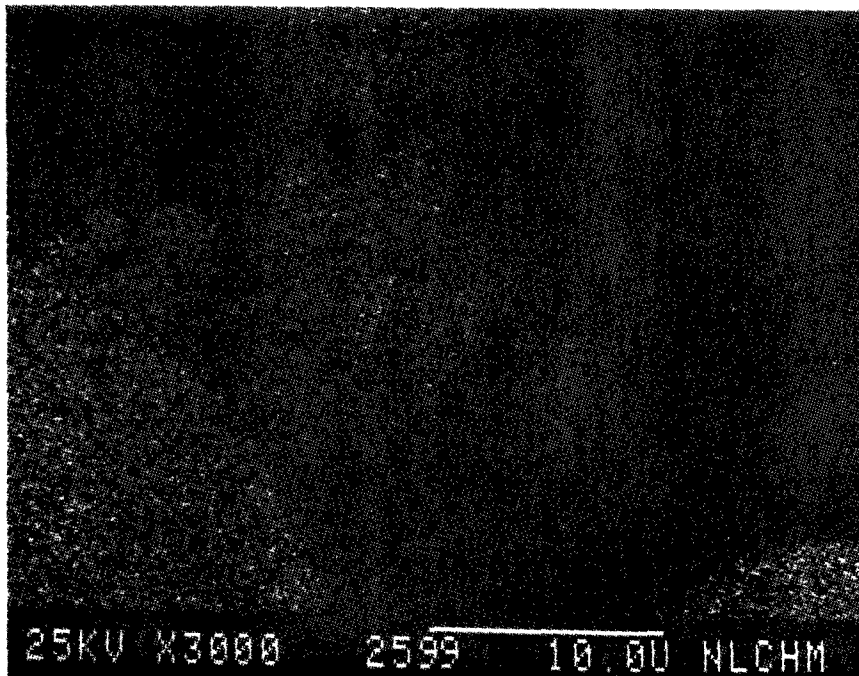


Figure 303

Al X-Ray Image of Figure 301

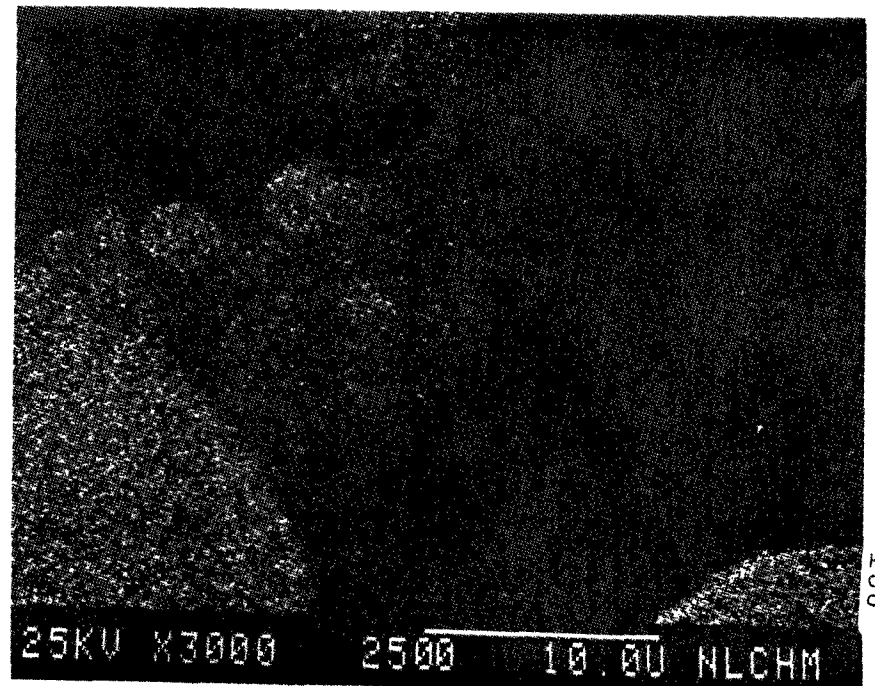


Figure 304

Si X-Ray Image of Figure 301

SEM IMAGES OF SAMPLE #

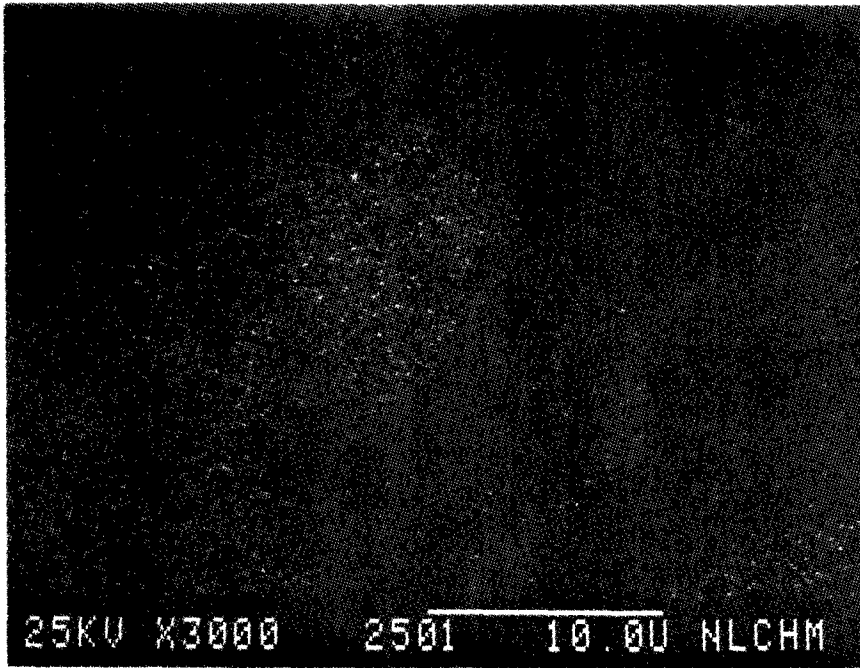


Figure 305 S X-Ray Image of Figure 301

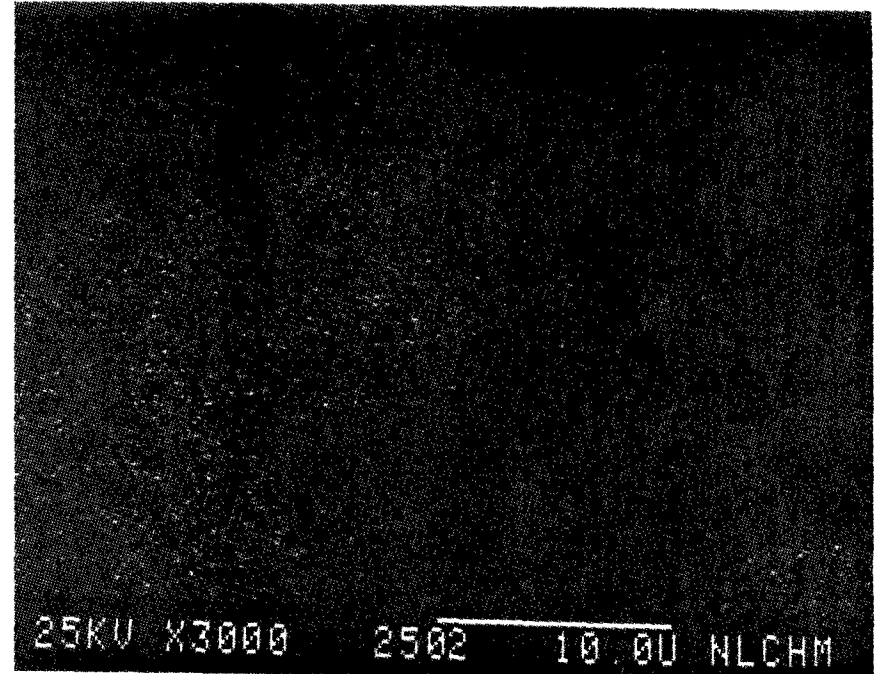


Figure 306 K X-Ray Image of Figure 301

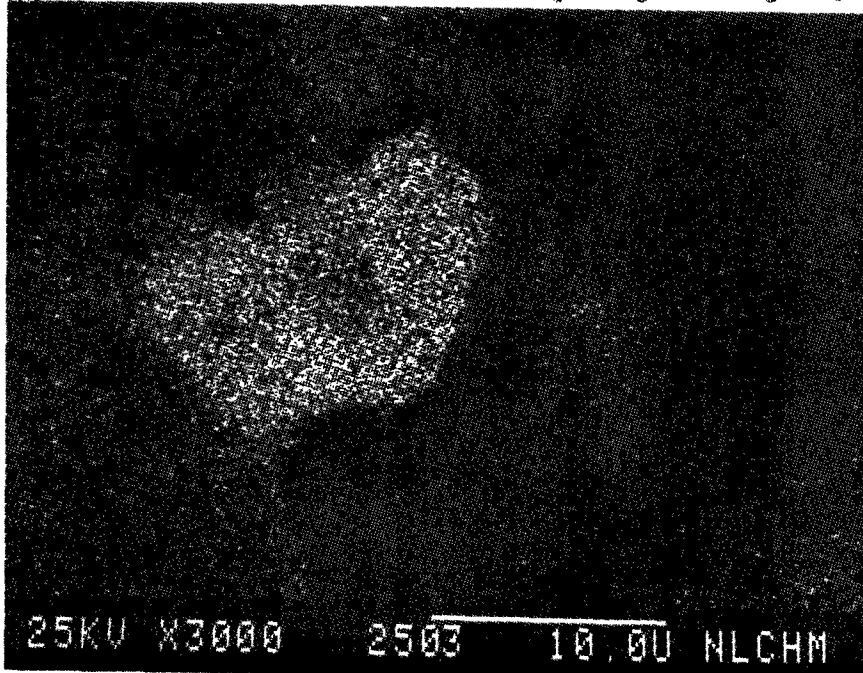


Figure 307 Ca X-Ray Image of Figure 301

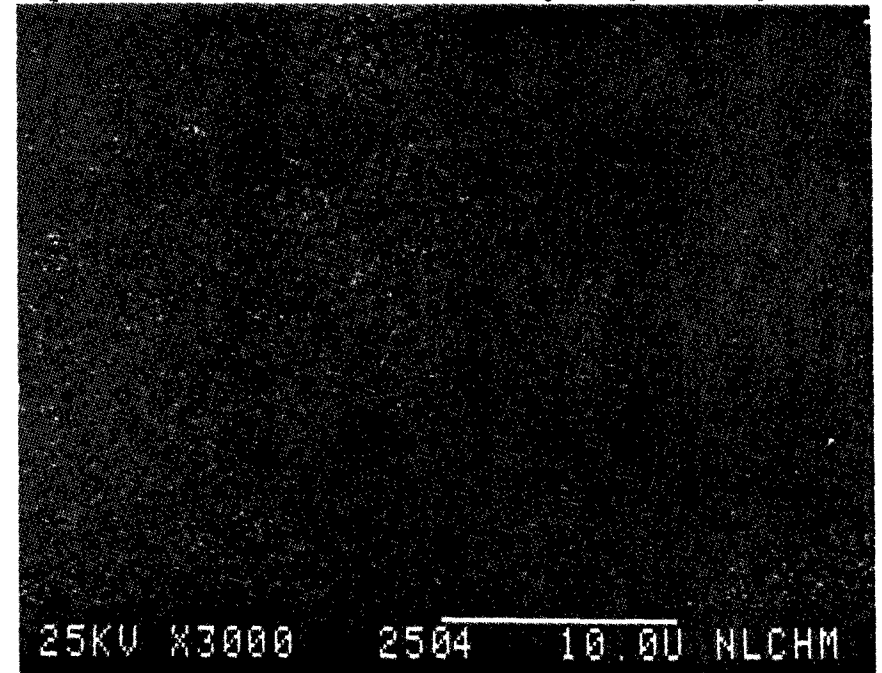


Figure 308 Ti X-Ray Image of Figure 301

SEM IMAGES OF SAMPLE #

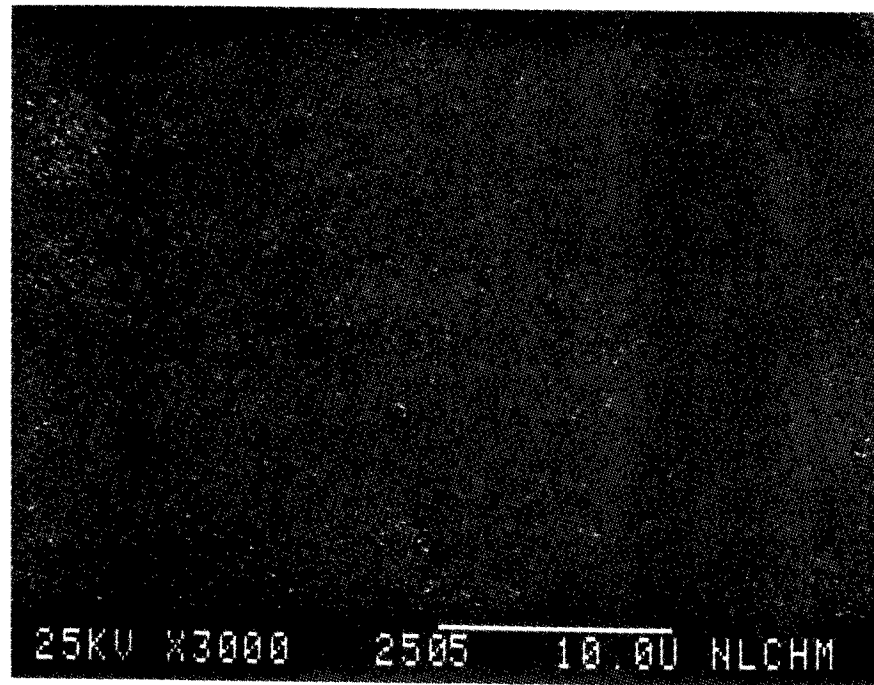


Figure 309

Fe X-Ray Image of Figure 301

SEM IMAGES OF SAMPLE #

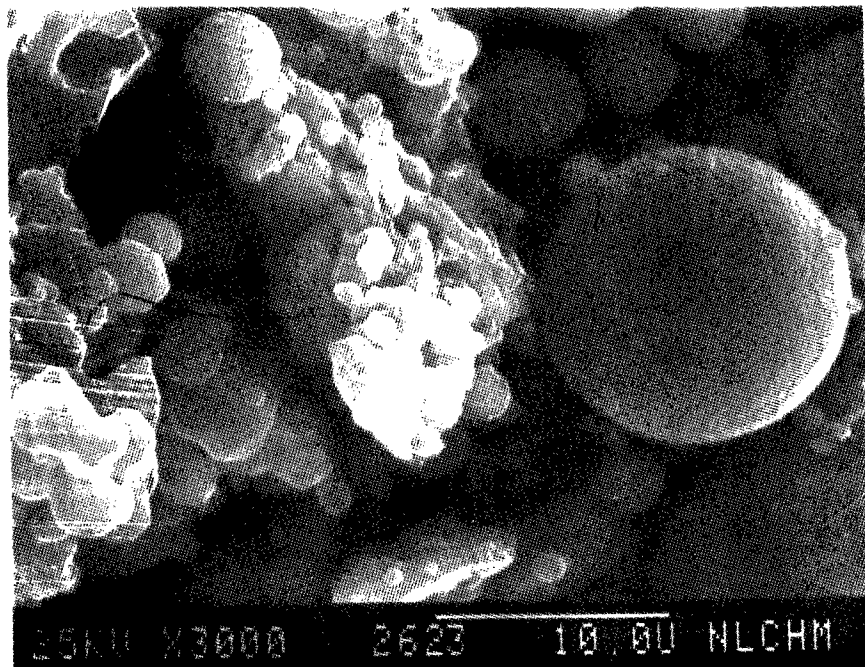


Figure 310

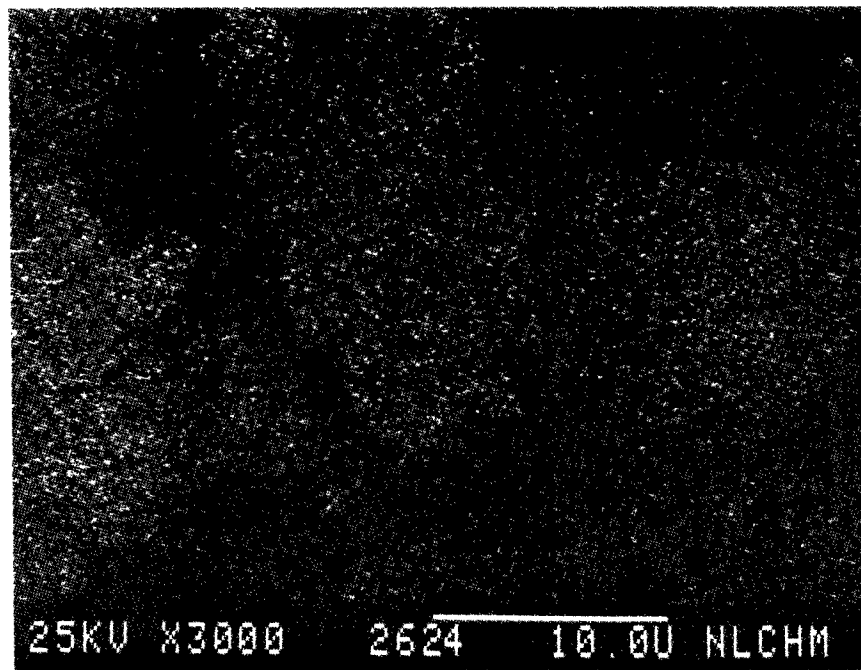


Figure 311

AL X-Ray Image of Figure 310

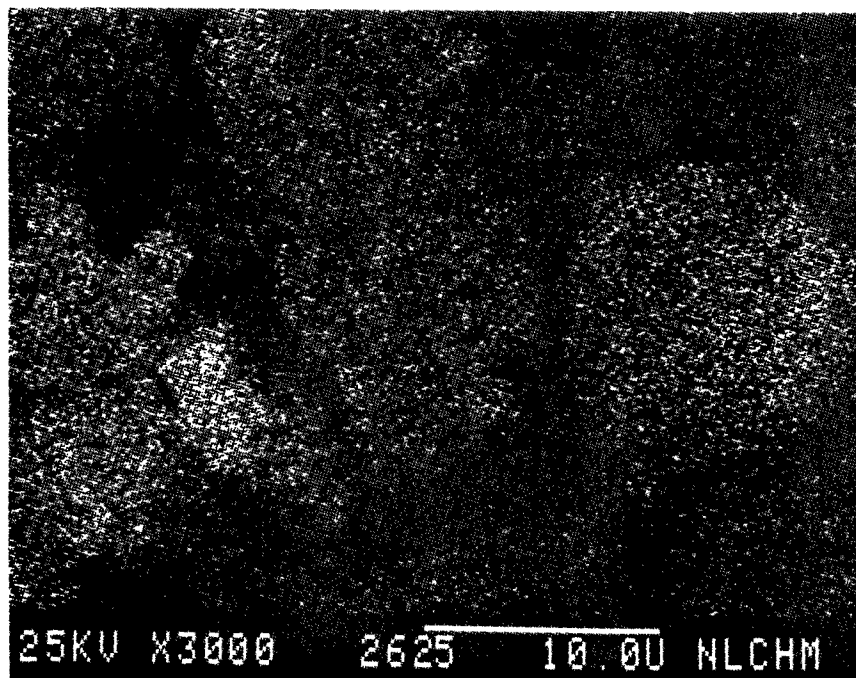


Figure 312

Si X-Ray Image of Figure 310

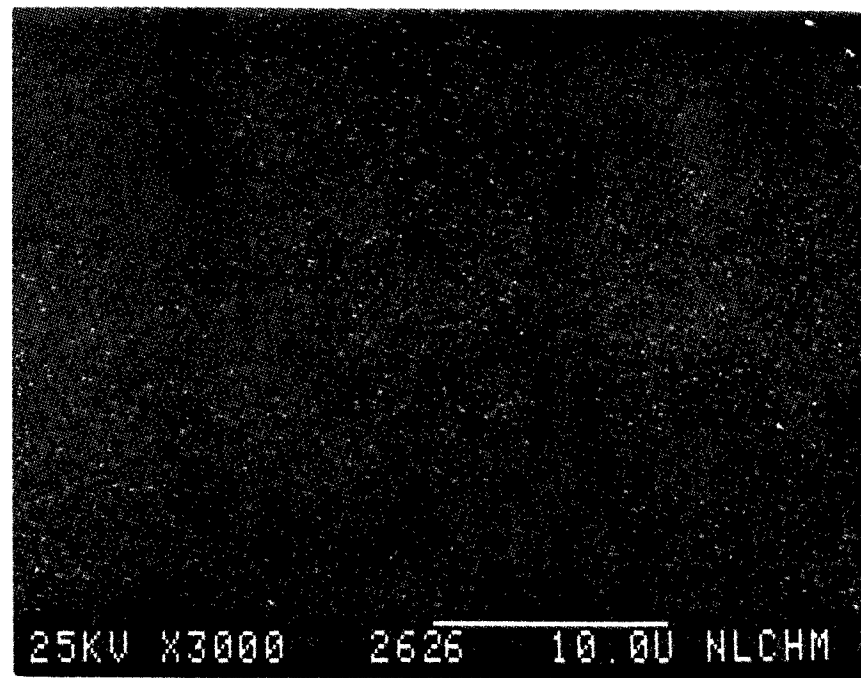


Figure 313

K X-Ray Image of Figure 310

SEM IMAGES OF SAMPLE #

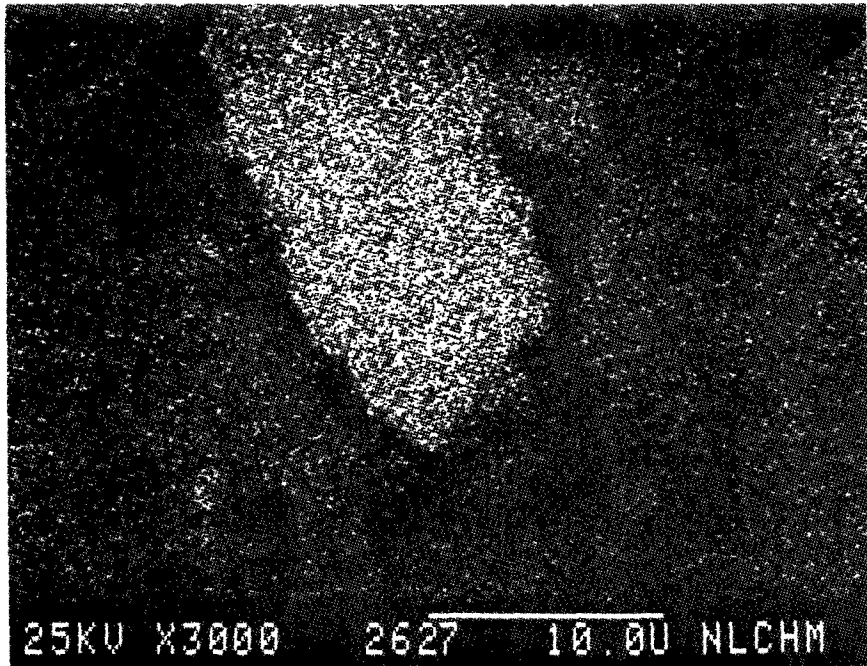


Figure 314

Ca X-Ray Image of Figure 310

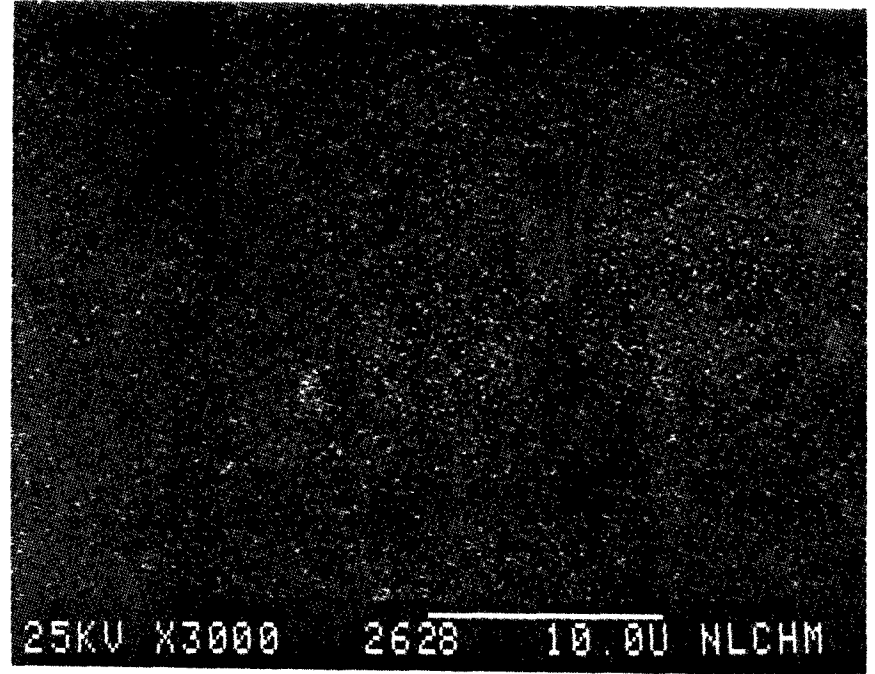


Figure 315

Ti X-Ray Image of Figure 310

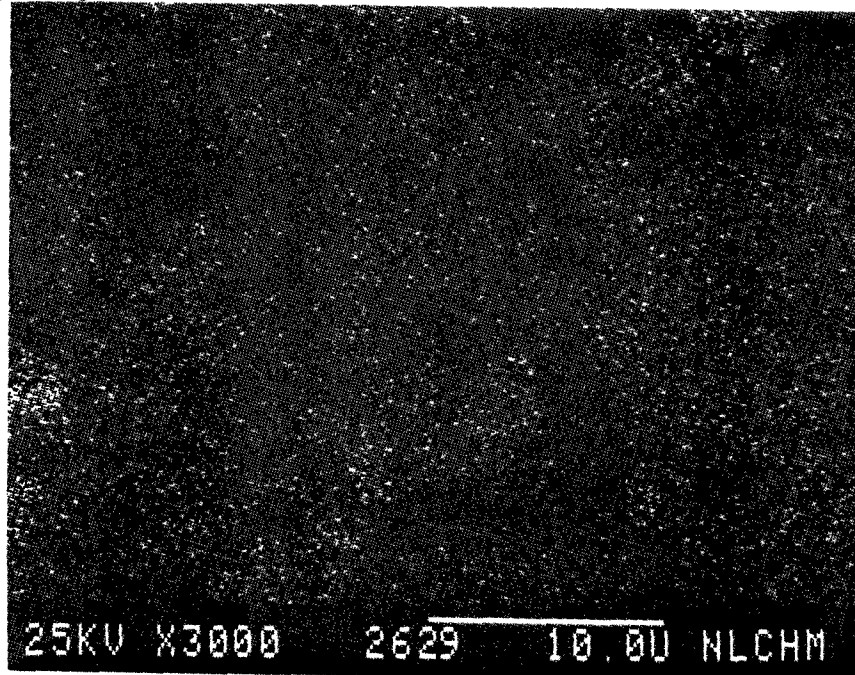


Figure 316

Fe X-Ray Image of Figure 310

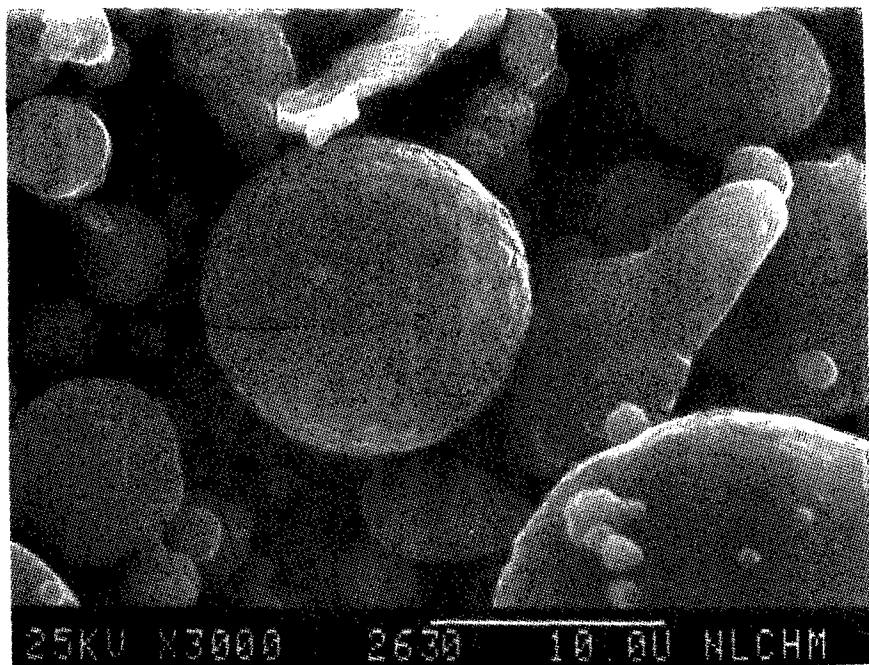


Figure 317

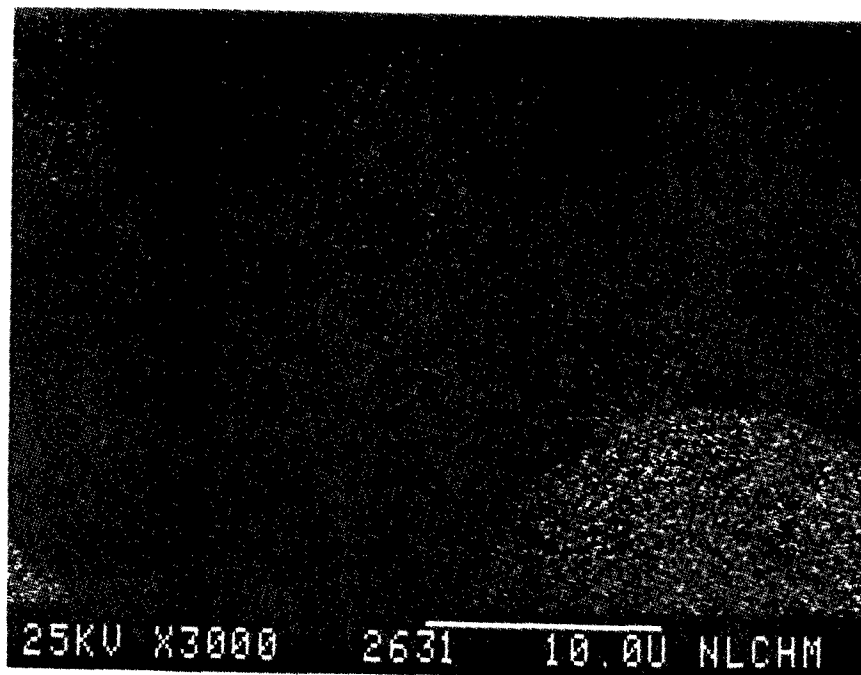


Figure 318

AL X-Ray Image of Figure 317

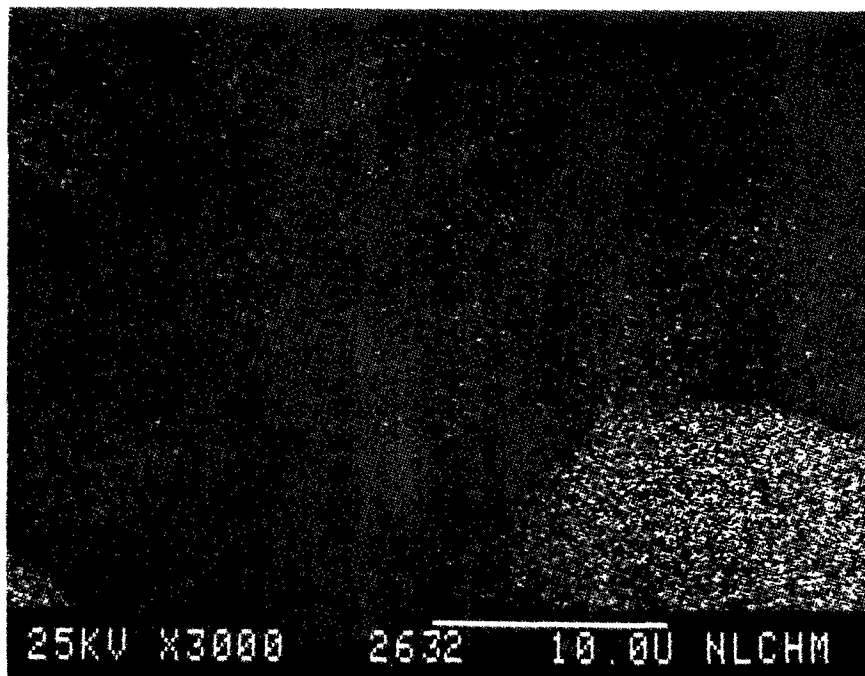


Figure 319

Si X-Ray Image of Figure 317

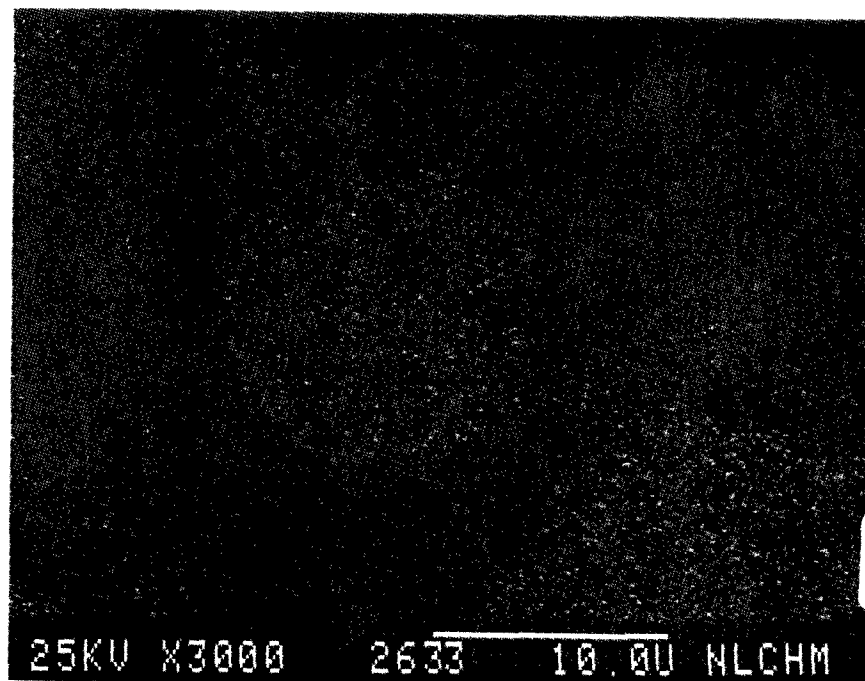


Figure 320

K X-Ray Image of Figure 317



SEM IMAGES OF SAMPLE #

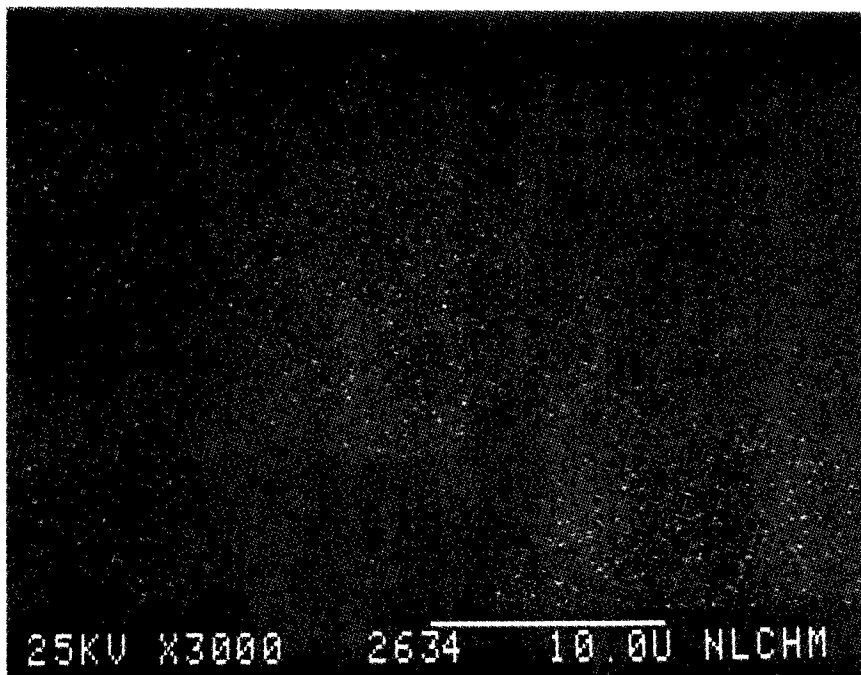


Figure 321

Ca X-Ray Image of Figure 317

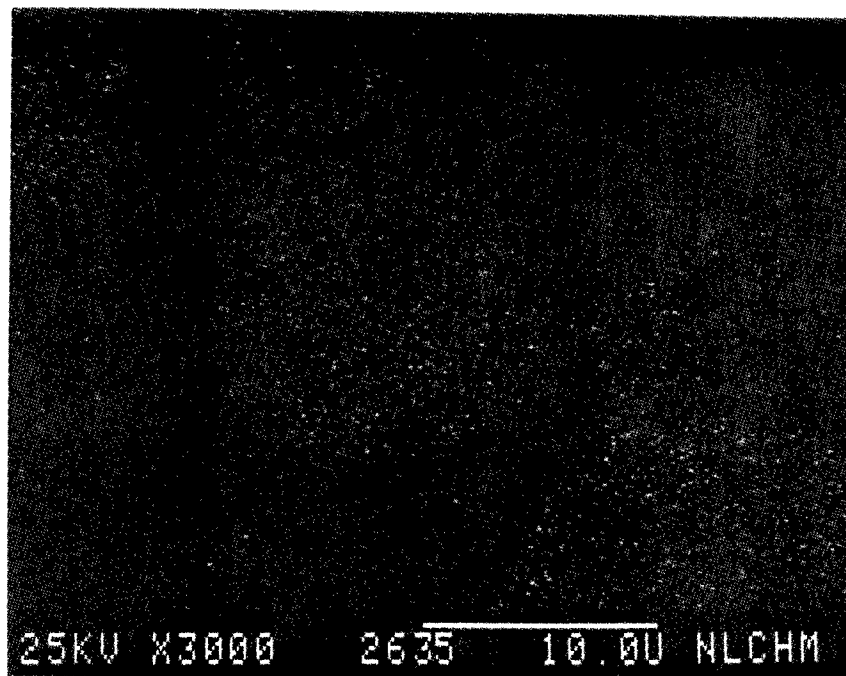


Figure 322

Ti X-Ray Image of Figure 317

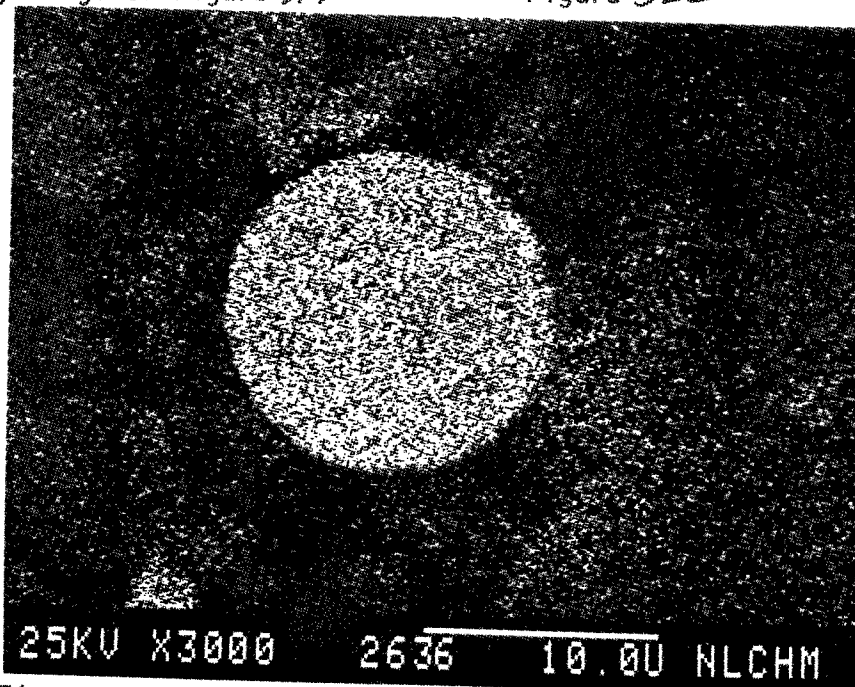


Figure 323

Fe X-Ray Image of Figure 317

SEM IMAGES OF SAMPLE #

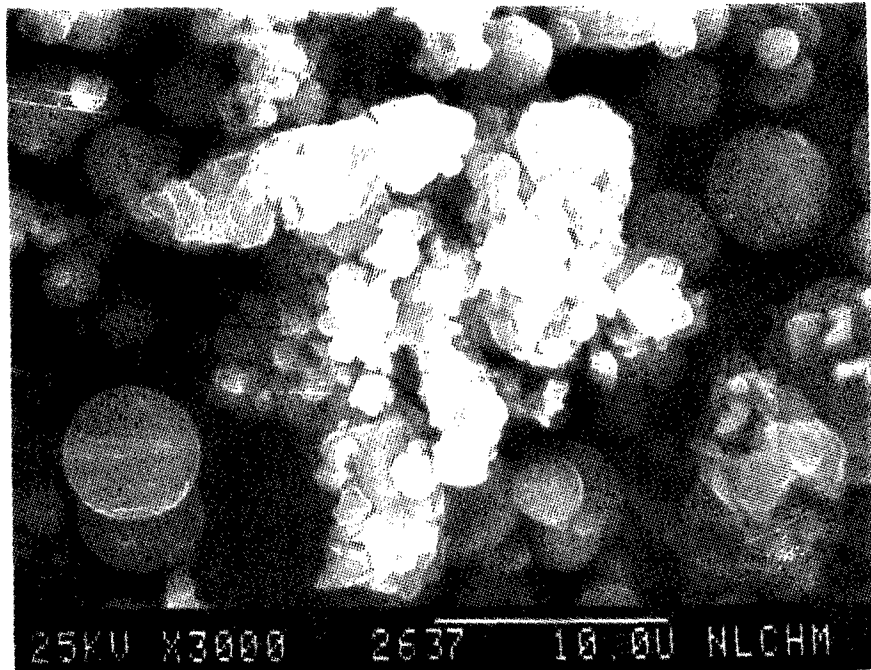


Figure 324

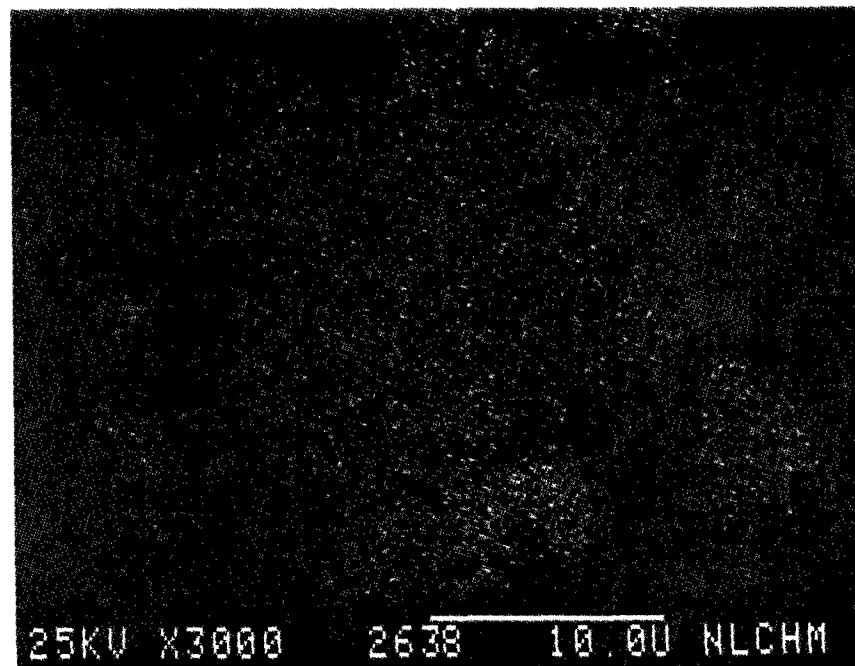


Figure 325

AL X-Ray Image of Figure 324

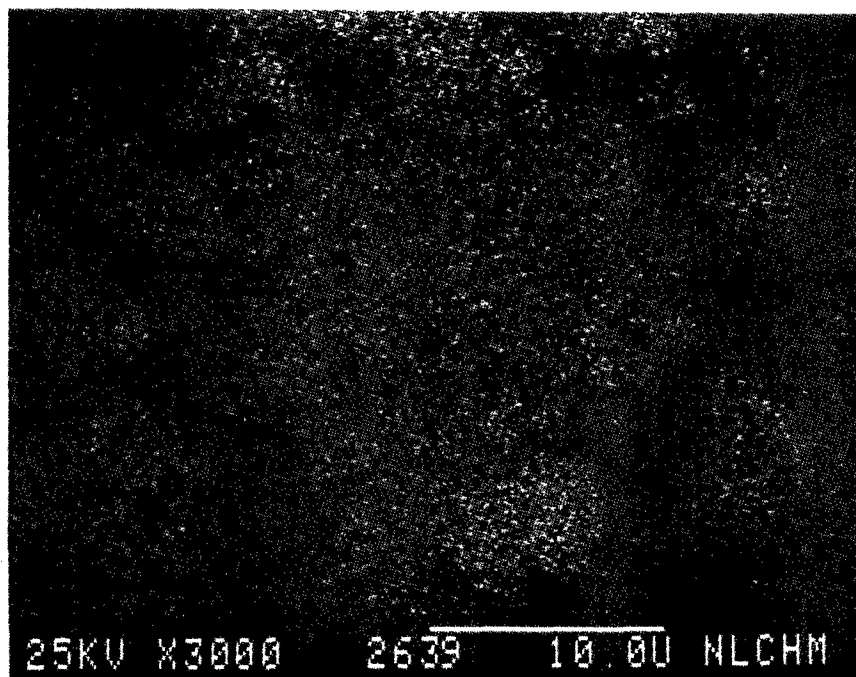


Figure 326

Si X-Ray Image of Figure 324

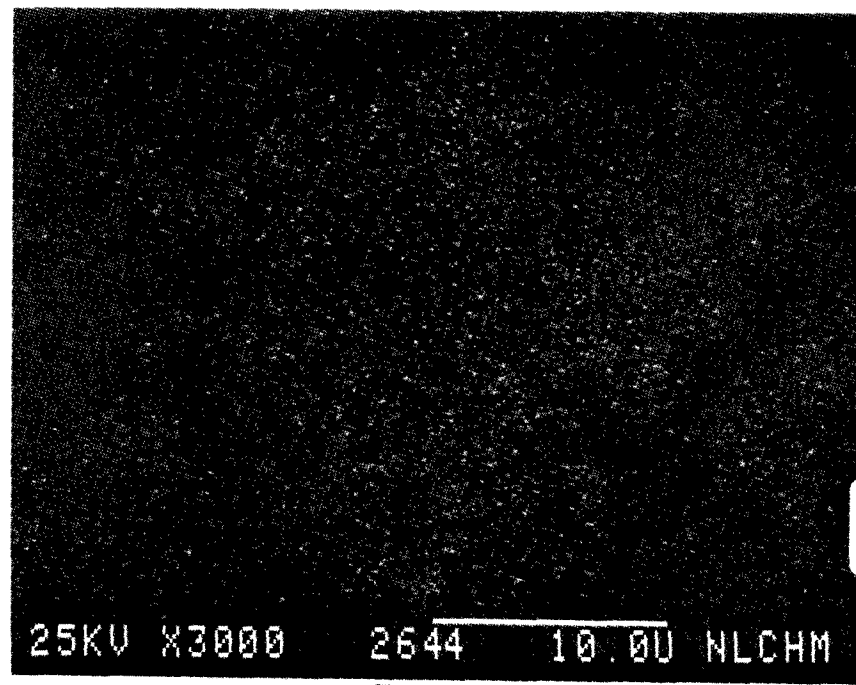


Figure 327

S X-Ray Image of Figure 324

SEM IMAGES OF SAMPLE #

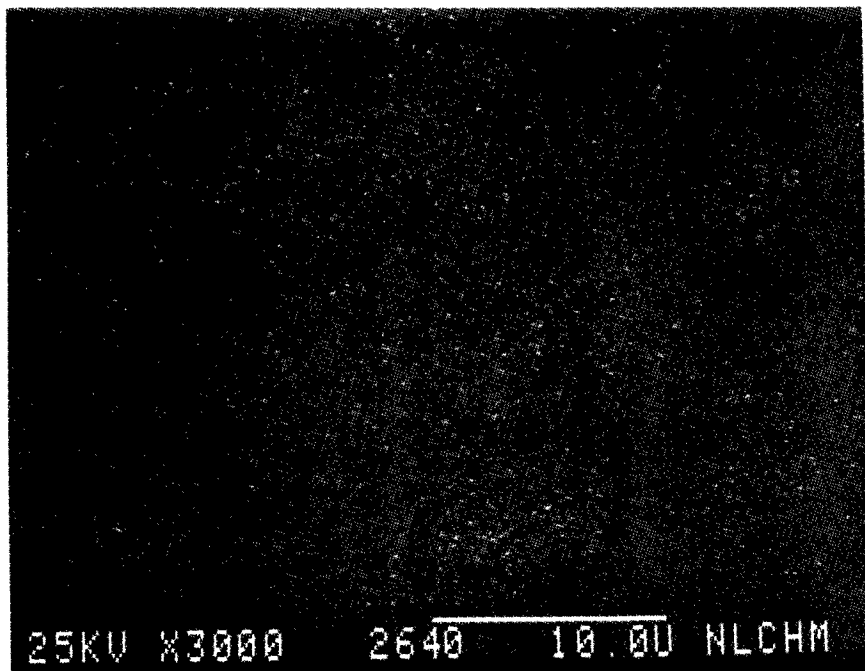


Figure 328

K X-Ray Image of Figure 324

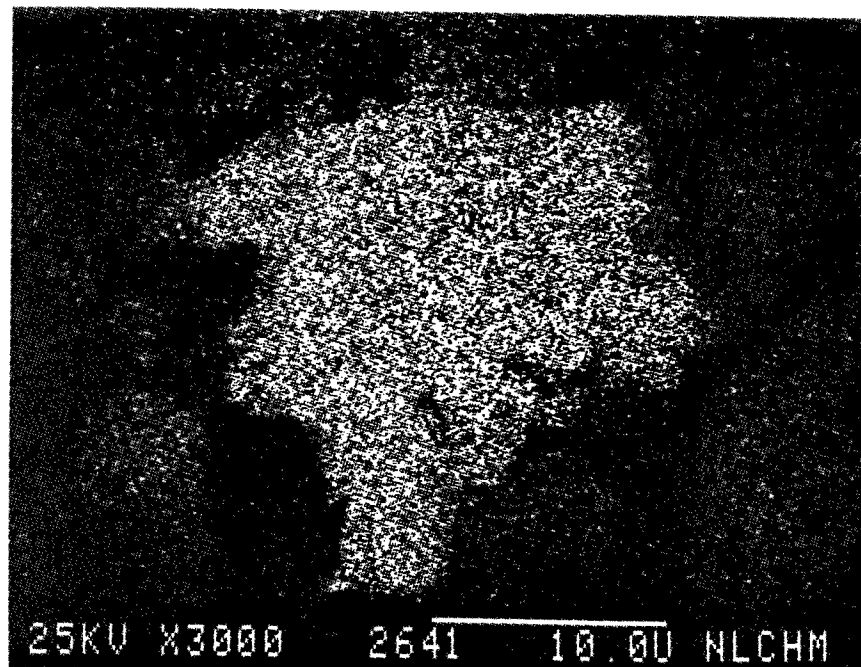


Figure 329

Ca X-Ray Image of Figure 324

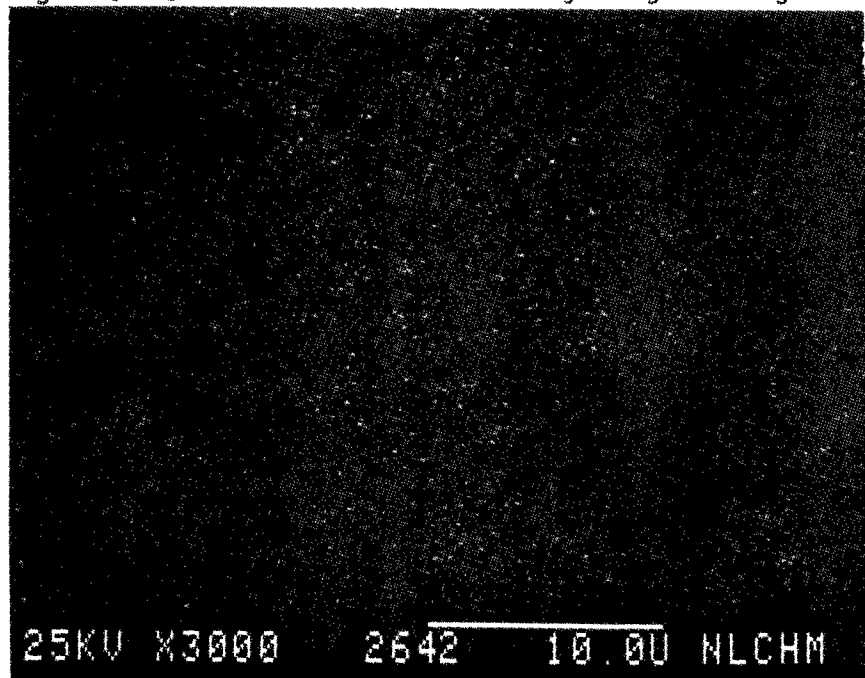


Figure 330

Ti X-Ray Image of Figure 324

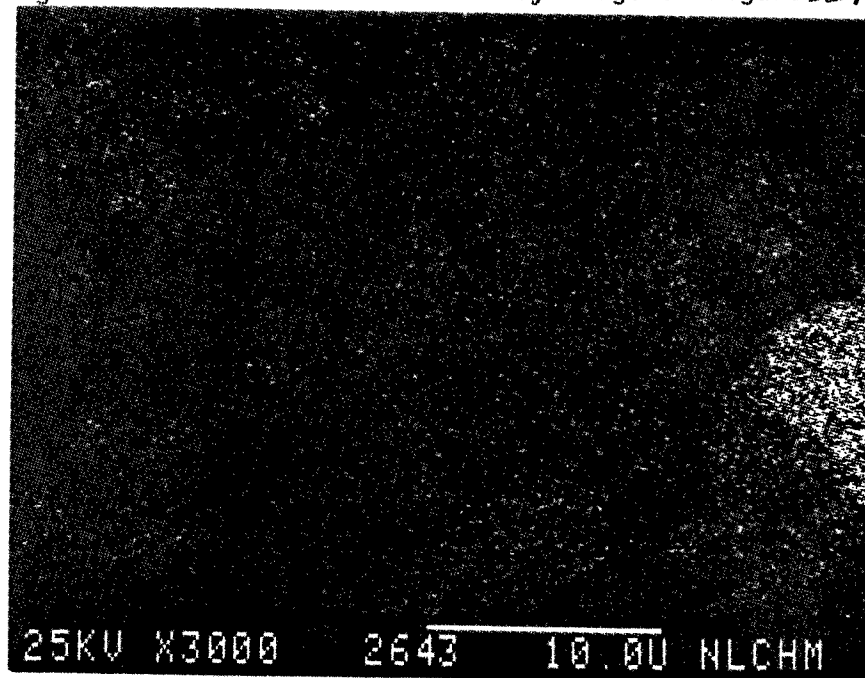


Figure 331

Fe X-Ray Image of Figure 324

SEM IMAGES OF SAMPLE #

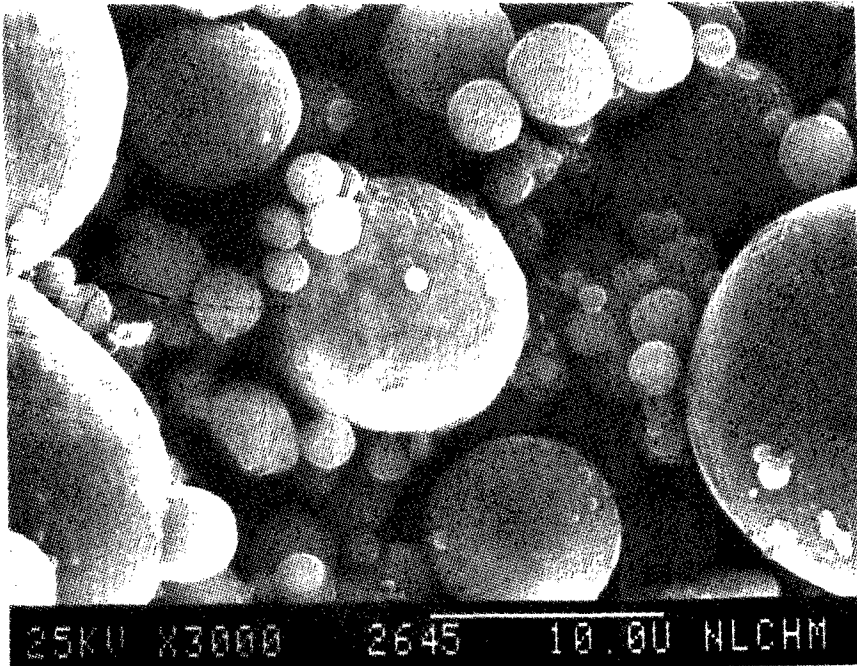


Figure 332

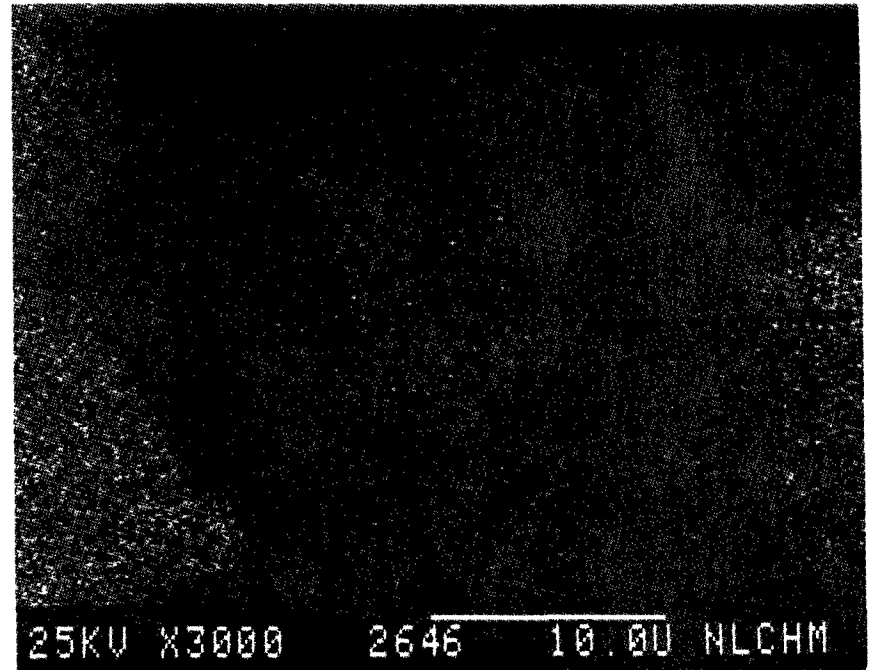


Figure 333

AL X-Ray Image of Figure 332

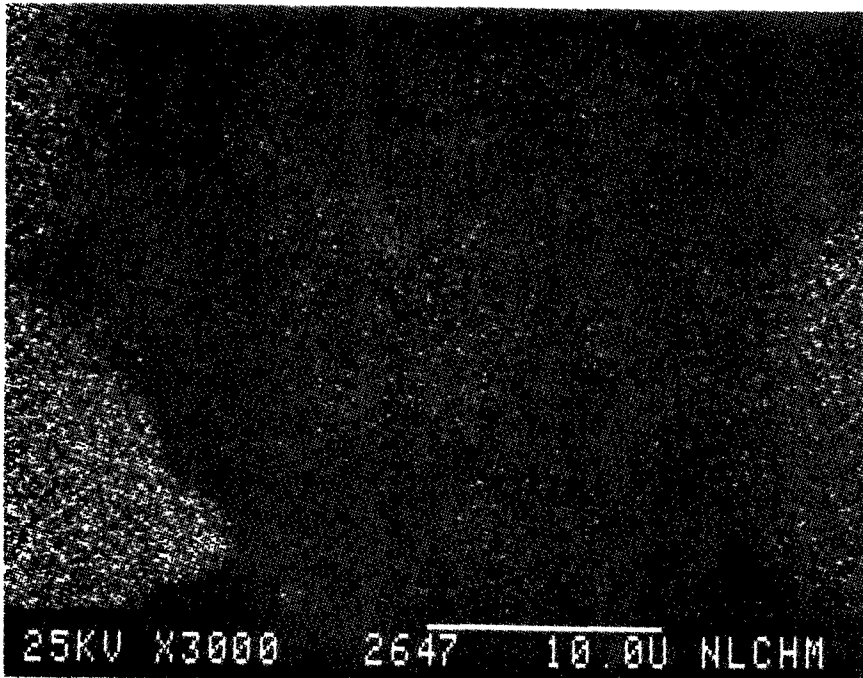


Figure 334

Si X-Ray Image of Figure 332

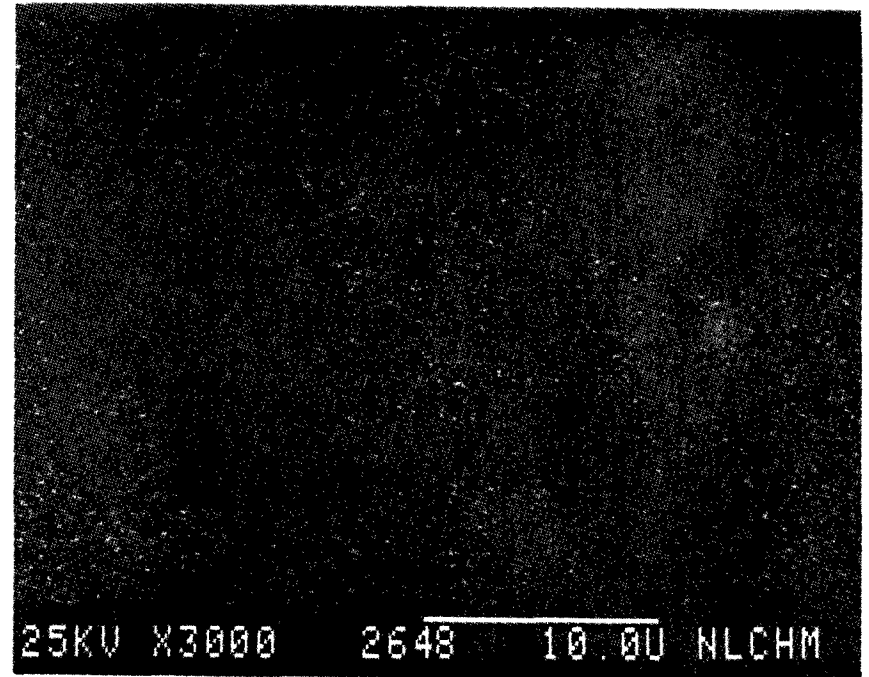


Figure 335

K X-Ray Image of Figure 332

SEM IMAGES OF SAMPLE #

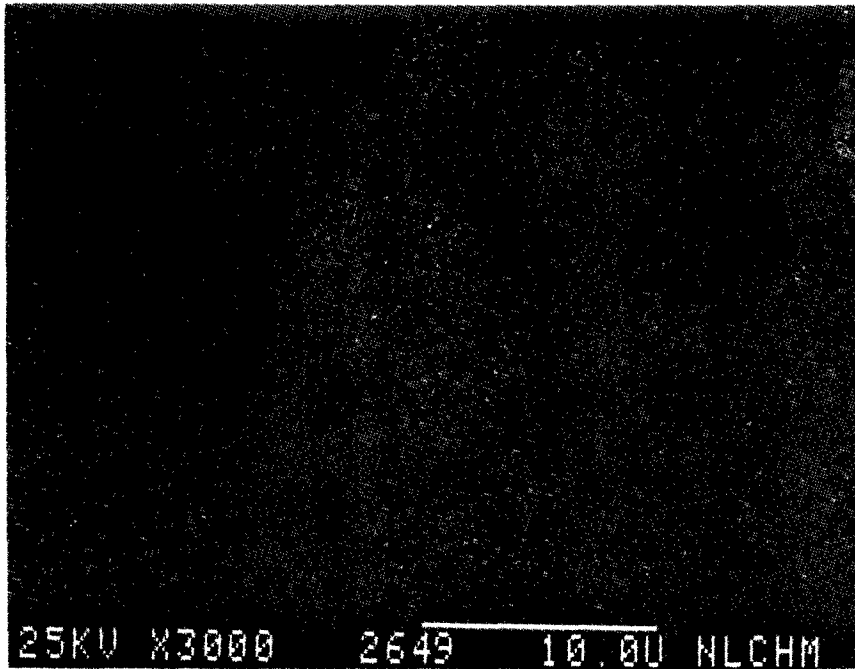


Figure 336

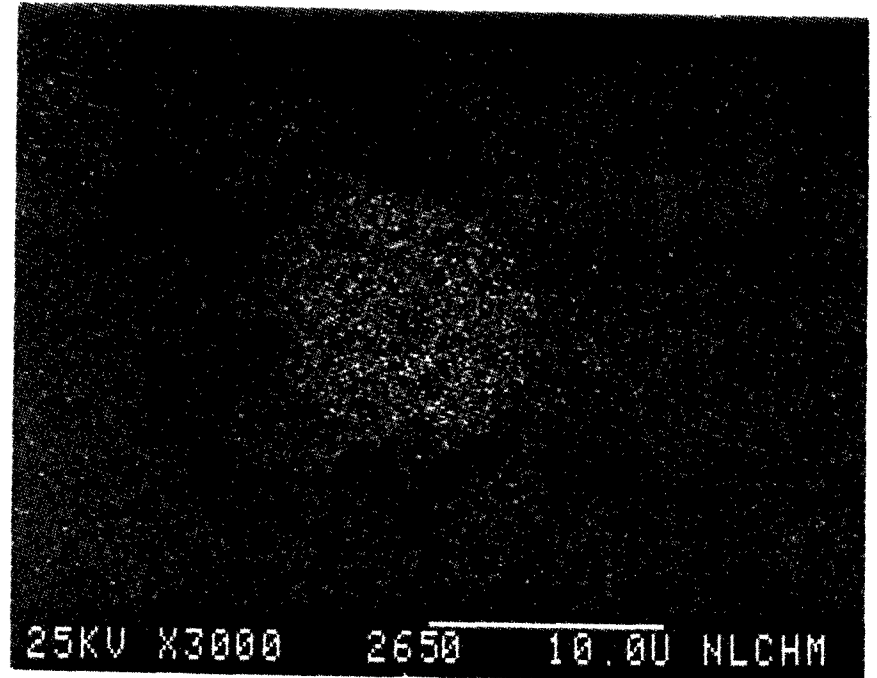


Figure 337

Ca X-Ray Image of Figure 332

Ba X-Ray Image of Figure 332

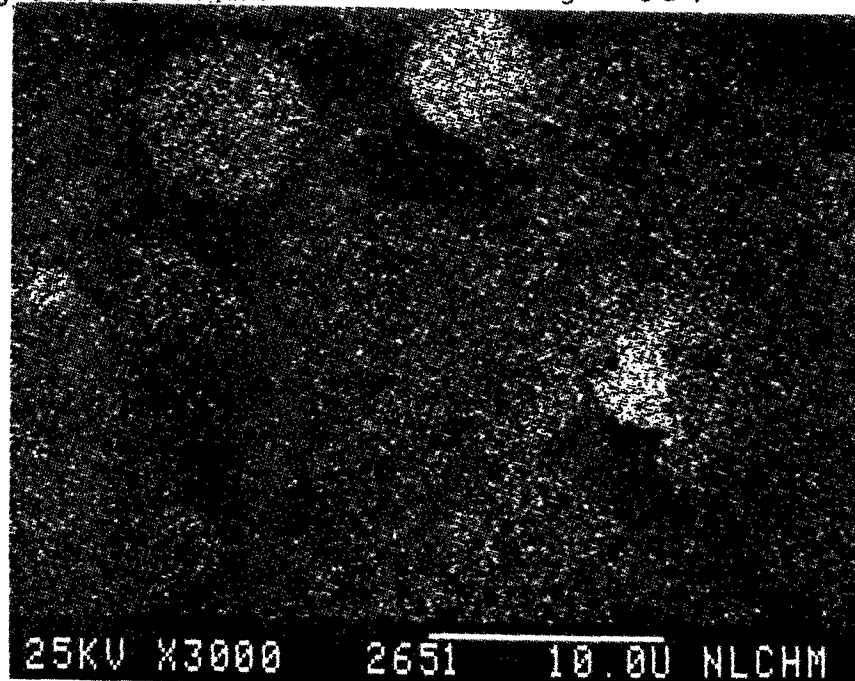


Figure 338

Fe X-Ray Image of Figure 332

ENERGY DISPERSIVE X-RAY ANALYSIS

Analytical Number Fly Ash (Basic)

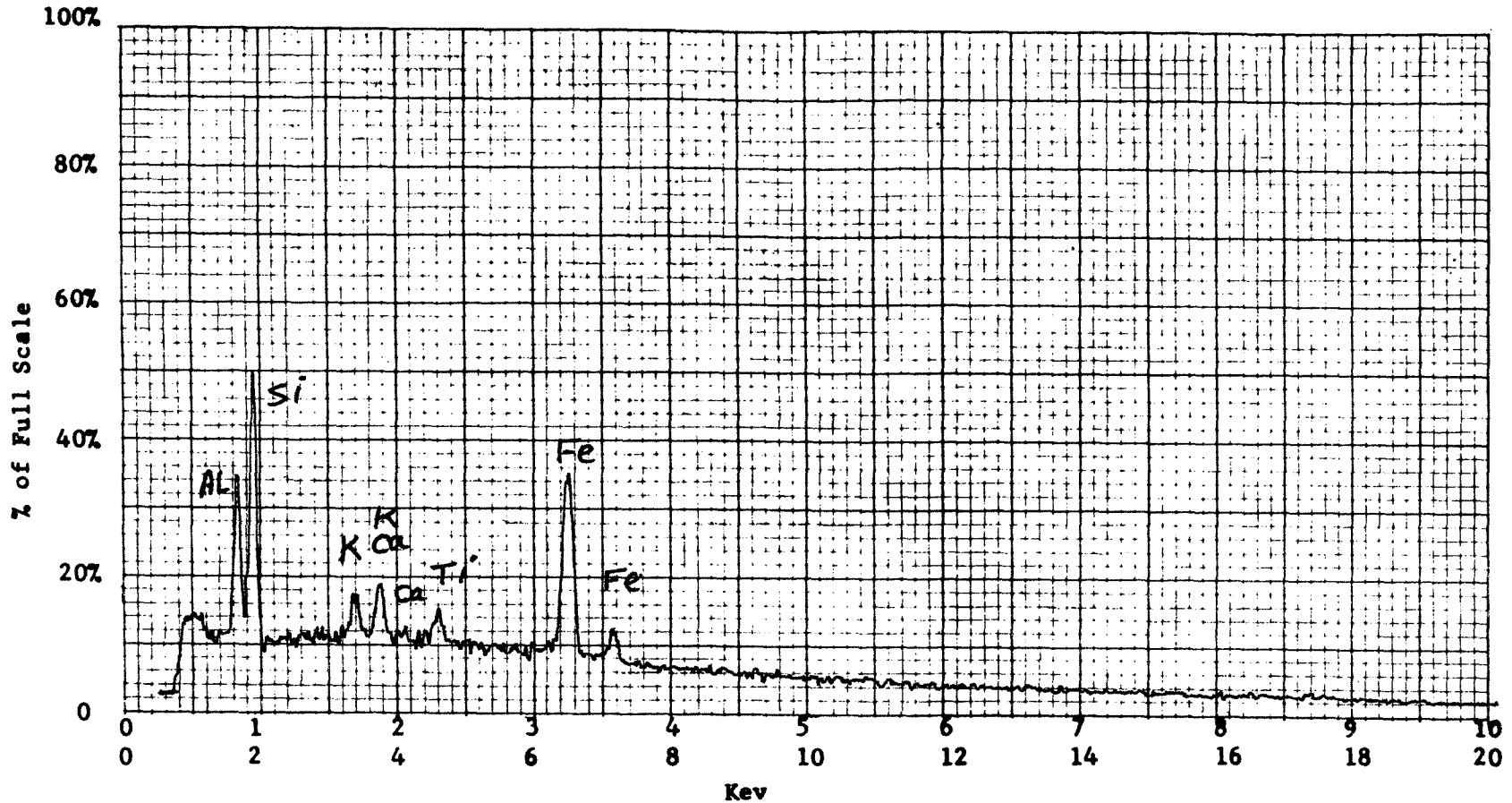
Operator \_\_\_\_\_ Date \_\_\_\_\_

Accelerating Potential 25 KeV

Total Counts Acquired 1.0 min.

Number Counts Full Scale 2K

Number of eV per channel 20



Sample peculiarities and remarks: FIGURE 239: AREA SCAN



**ENERGY DISPERSIVE X-RAY ANALYSIS**

Analytical Number Fly Ash (Basic)

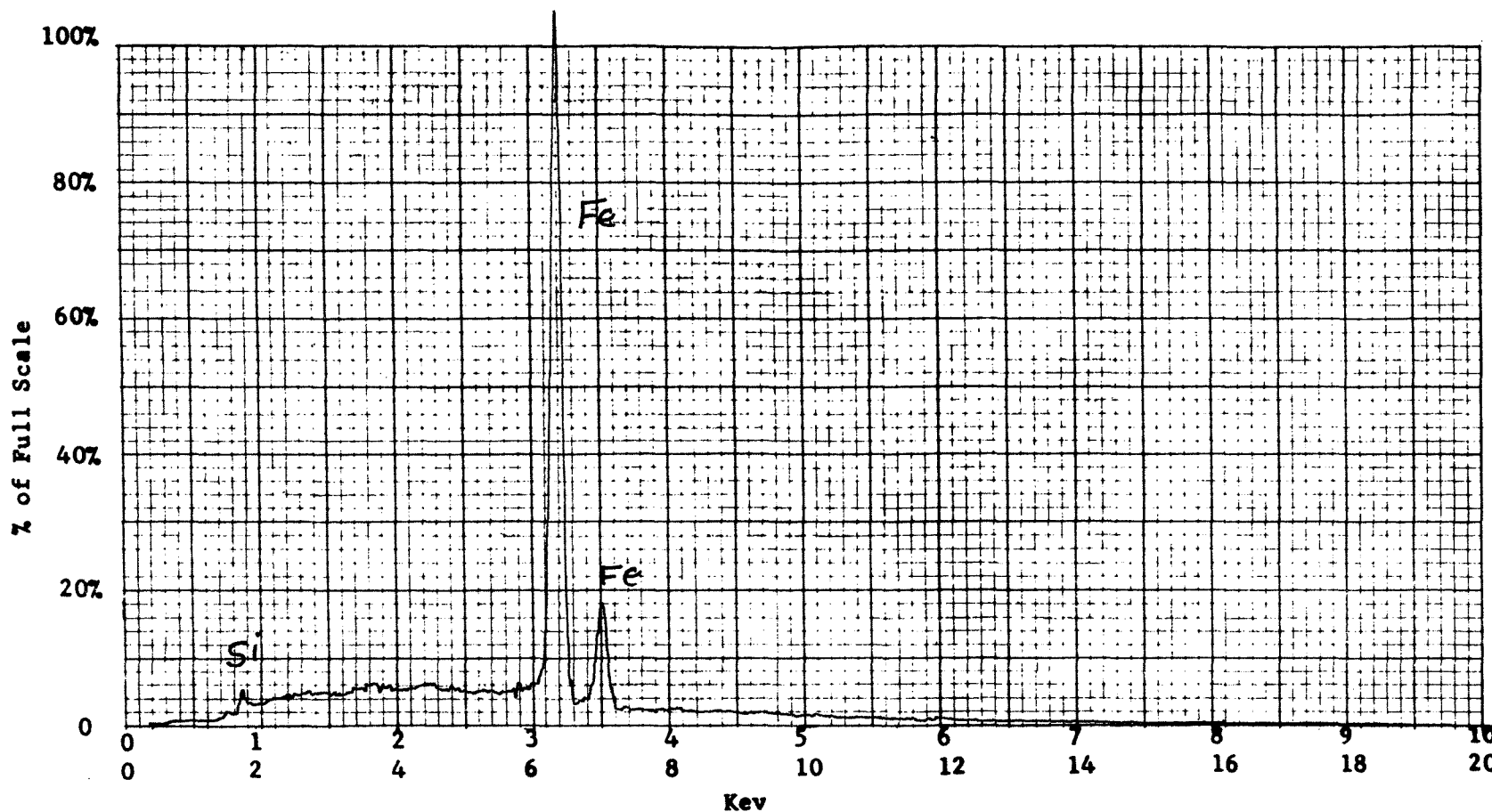
Operator \_\_\_\_\_ Date \_\_\_\_\_

Accelerating Potential 25 KeV

Total Counts Acquired 1.0 min.

Number Counts Full Scale 5K

Number of eV per channel 20



Sample peculiarities and remarks: FIGURE 240: POINT SCAN ON A HIGH Fe LARGE SPHERICAL PARTICLE IN FIGURE 287

ENERGY DISPERSIVE X-RAY ANALYSIS

Analytical Number Fly Ash (Basic)

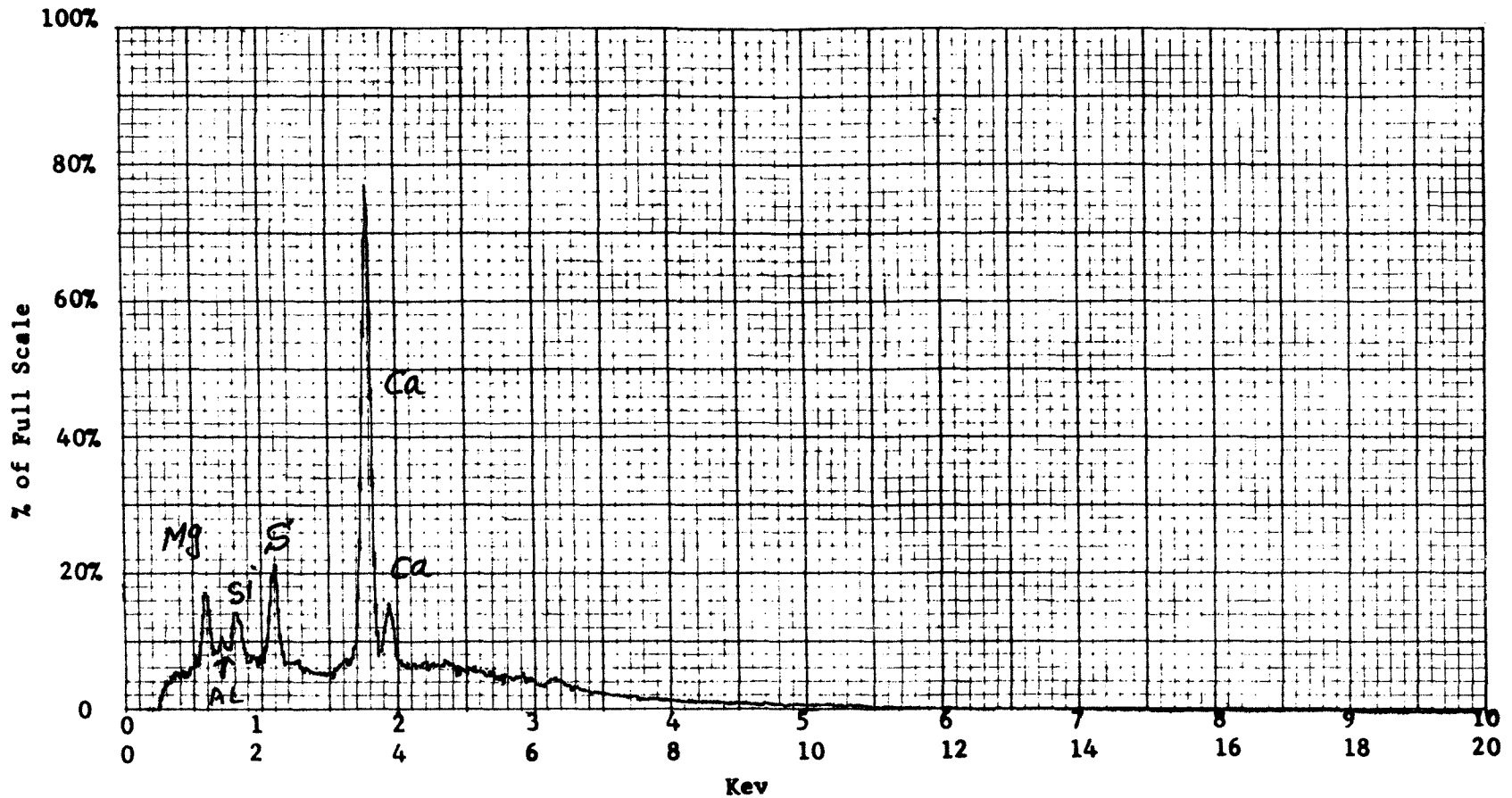
Operator \_\_\_\_\_ Date \_\_\_\_\_

Accelerating Potential 25 KeV

Total Counts Acquired 1.0 min.

Number Counts Full Scale 5K

Number of eV per channel 20



Sample peculiarities and remarks: FIGURE 241: POINT SCAN ON A HIGH Ca-S PARTICLE  
IN FIGURE 301

**ENERGY DISPERSIVE X-RAY ANALYSIS**

Analytical Number Fly Ash (Basic)

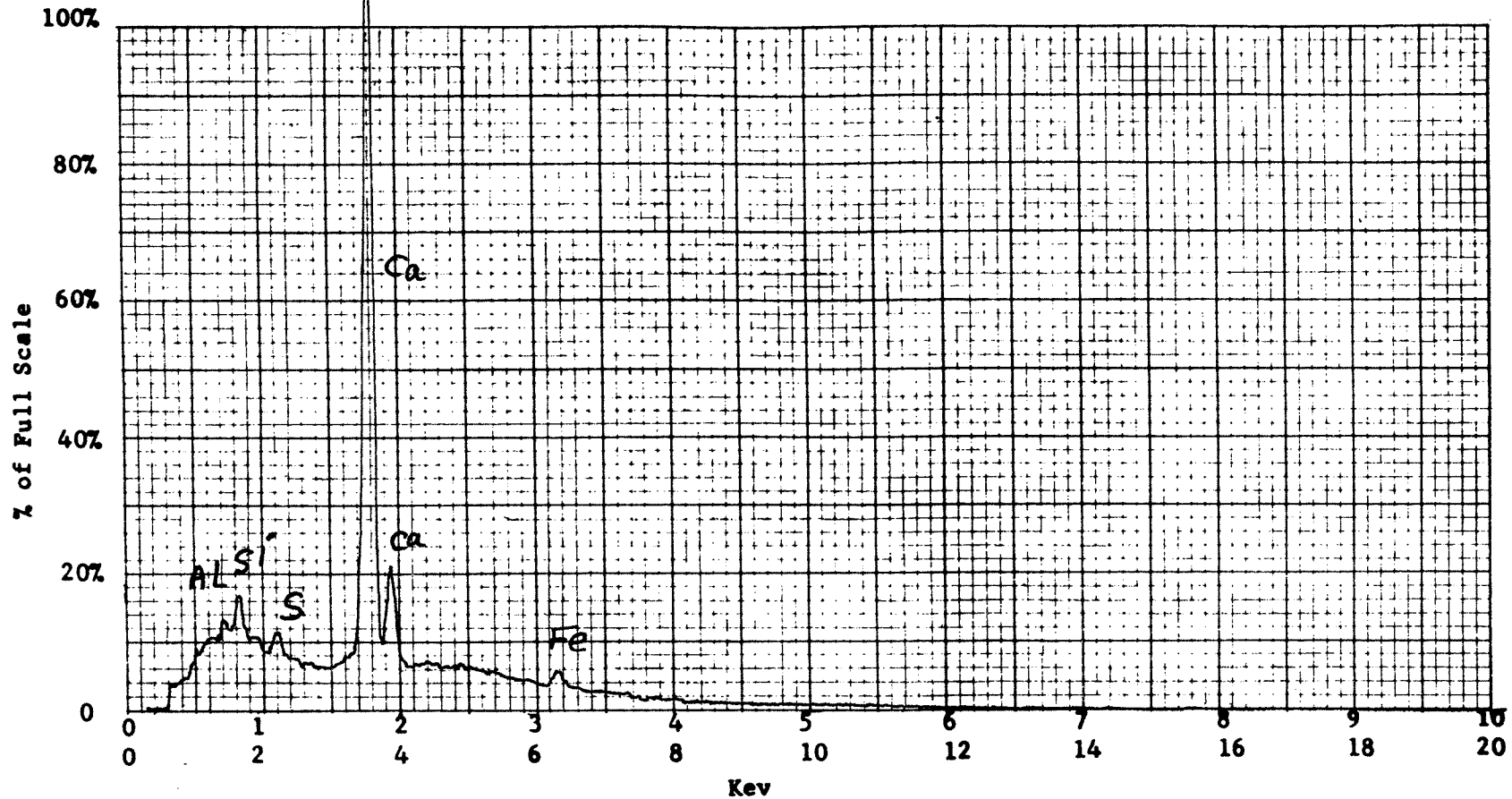
Operator \_\_\_\_\_ Date \_\_\_\_\_

Accelerating Potential 25 KeV

Total Counts Acquired 1.0 min.

Number Counts Full Scale 5K

Number of eV per channel 20



Sample peculiarities and remarks: FIGURE 242: POINT SCAN ON A HIGH Ca PARTICLE  
IN FIGURE 310

ENERGY DISPERSIVE X-RAY ANALYSIS

Analytical Number Fly Ash (Basic)

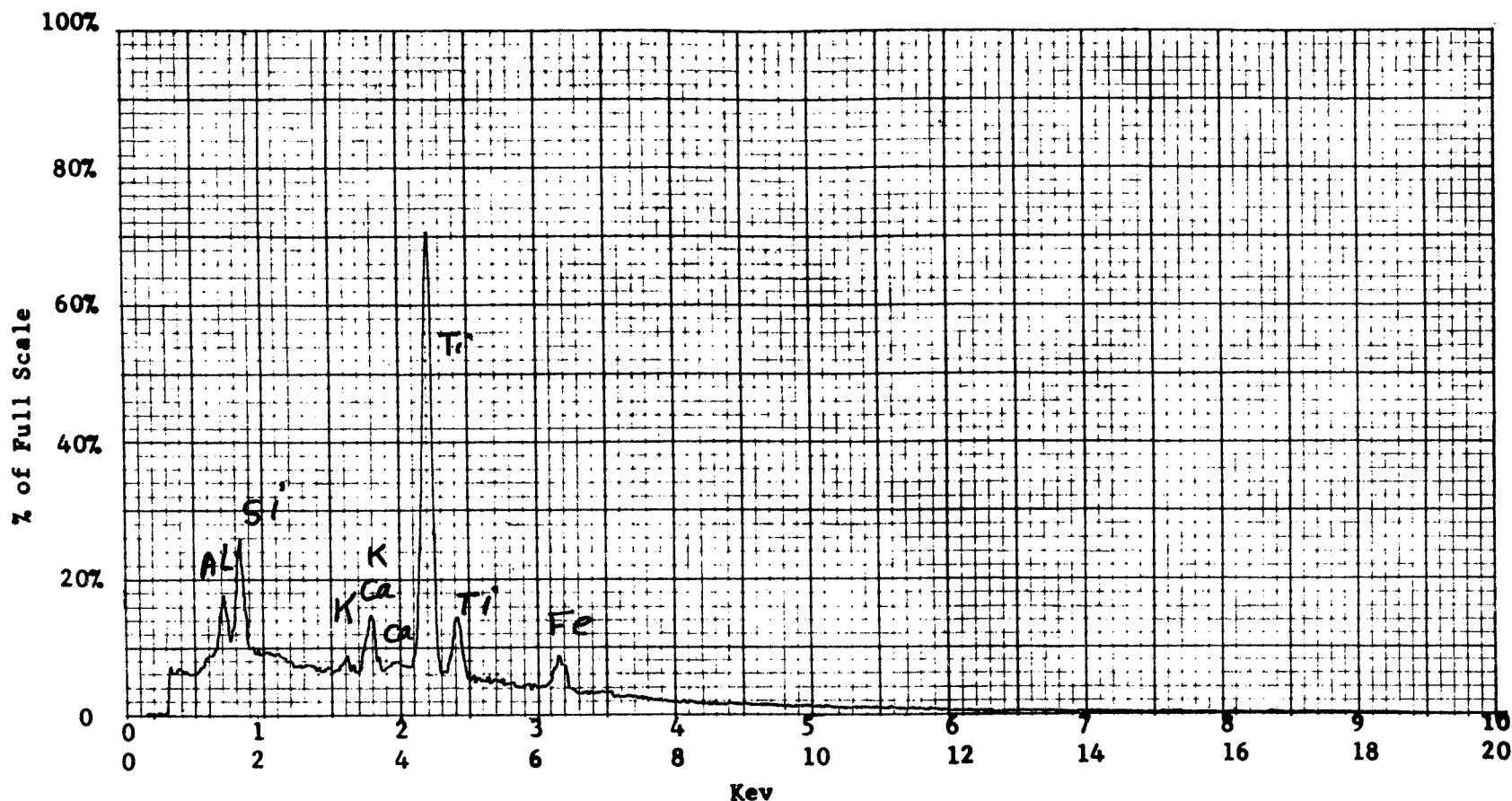
Operator \_\_\_\_\_ Date \_\_\_\_\_

Accelerating Potential 25 KeV

Total Counts Acquired 1.0 min.

Number Counts Full Scale 5K

Number of eV per channel 20



Sample peculiarities and remarks: FIGURE 243: POINT SCAN ON A HIGH Ti PARTICLE  
IN FIGURE 273

ENERGY DISPERSIVE X-RAY ANALYSIS

Analytical Number Fly Ash (Basic)

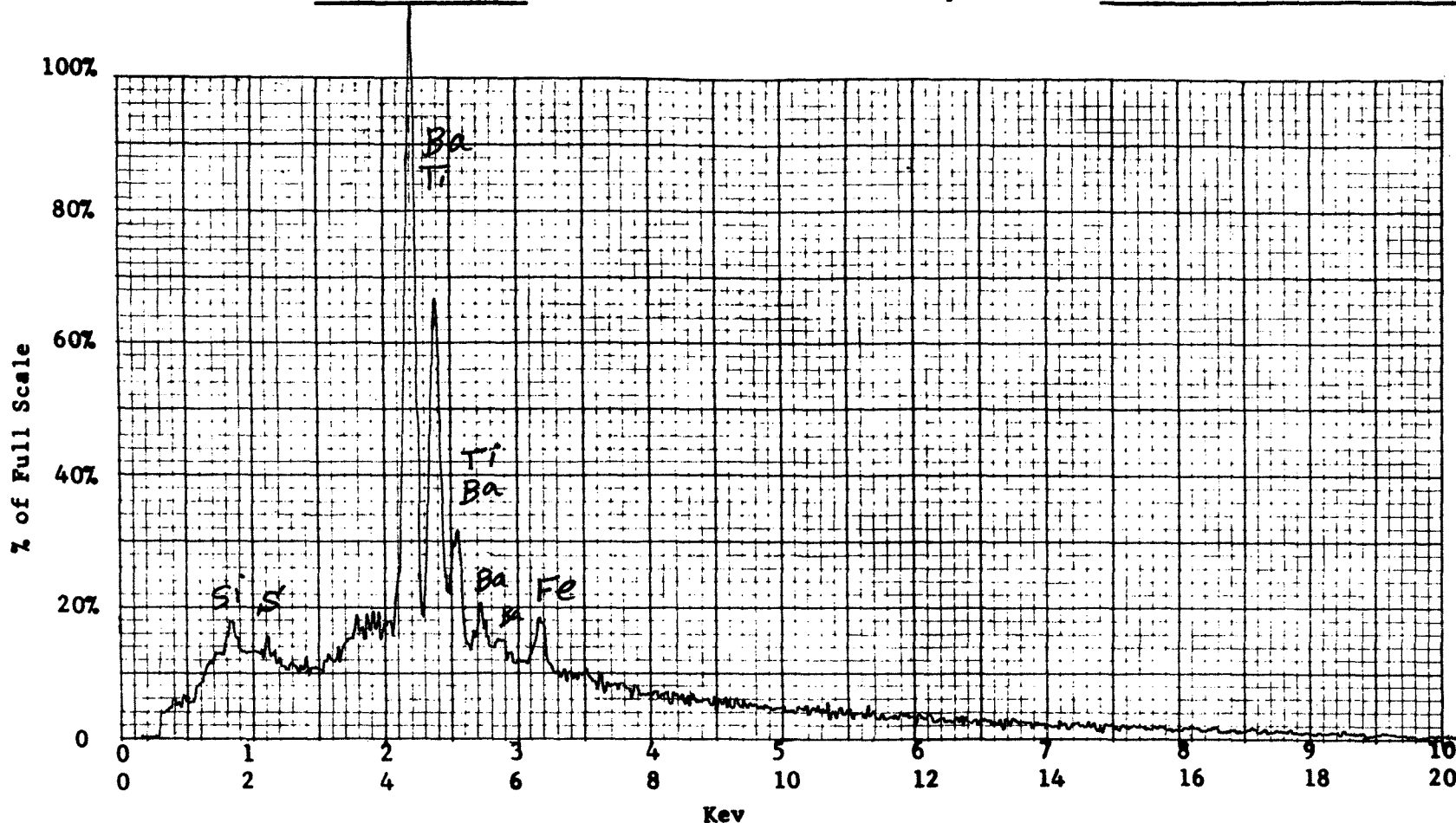
Operator \_\_\_\_\_ Date \_\_\_\_\_

Accelerating Potential 25 KeV

Total Counts Acquired 1.0 min.

Number Counts Full Scale 2K

Number of eV per channel 20



Sample peculiarities and remarks: FIGURE 244: POINT SCAN ON A HIGH Ba PARTICLE IN FIGURE 332.  
Ti (POSSIBLE)

ENERGY DISPERSIVE X-RAY ANALYSIS

Analytical Number Fly Ash (Basic)

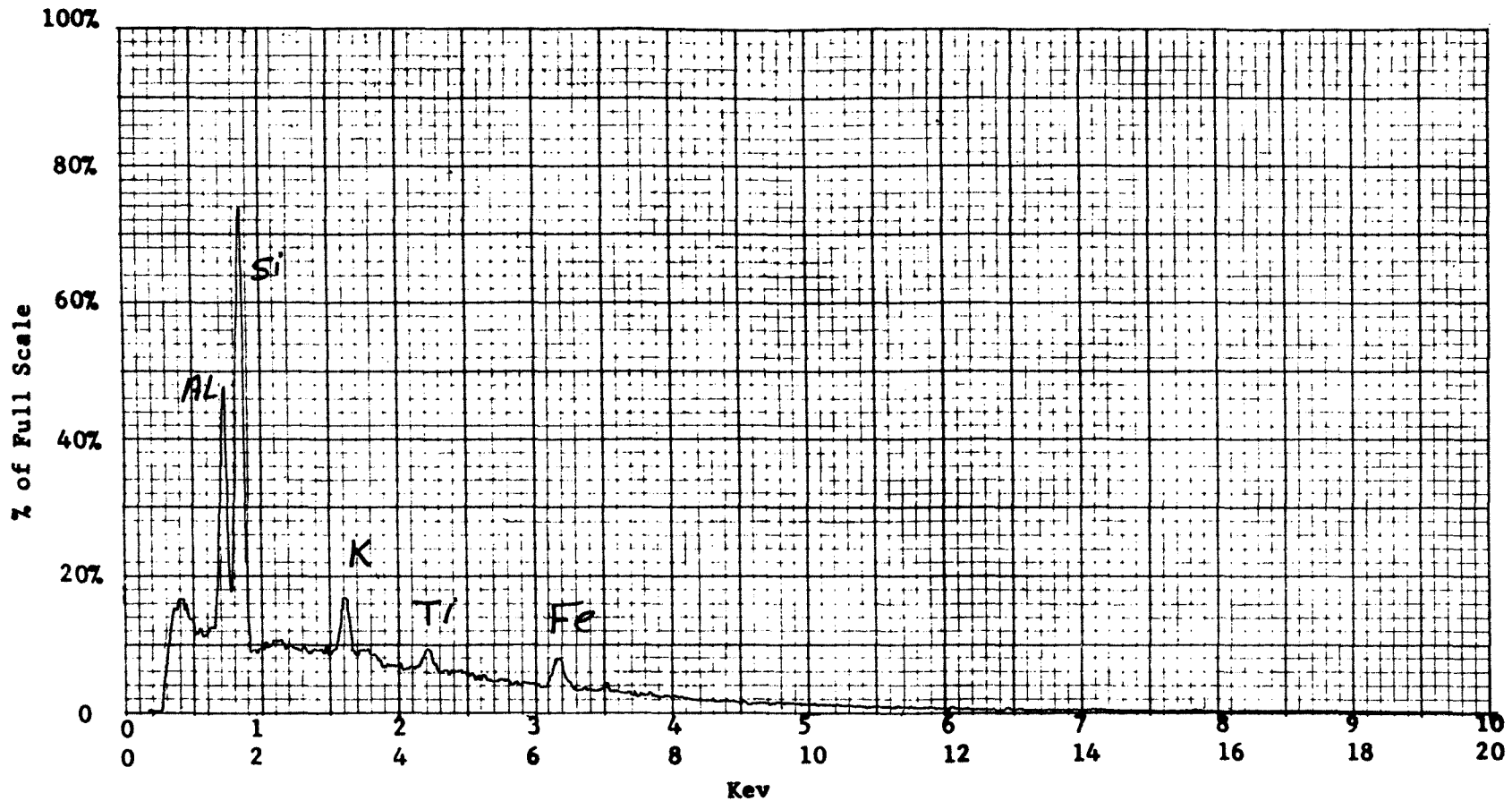
Operator \_\_\_\_\_ Date \_\_\_\_\_

Accelerating Potential 25 KeV

Total Counts Acquired 1.0 min.

Number Counts Full Scale 5K

Number of eV per channel 20



Sample peculiarities and remarks: FIGURE 245: POINT SCAN ON AN ELONGATED PARTICLE IN FIGURE 294



ENERGY DISPERSIVE X-RAY ANALYSIS

Analytical Number Fly Ash (Basic)

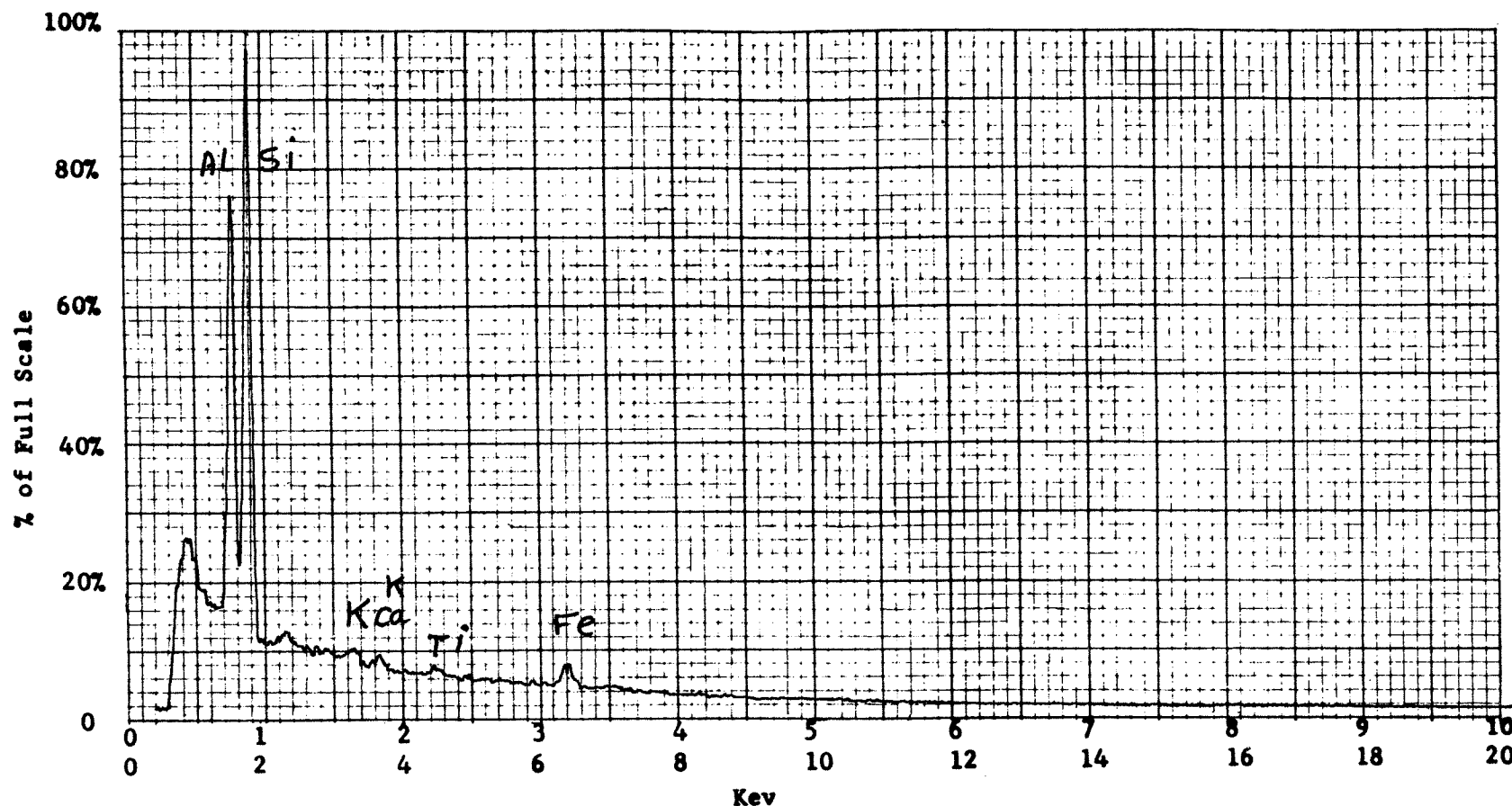
Operator \_\_\_\_\_ Date \_\_\_\_\_

Accelerating Potential 25 KeV

Total Counts Acquired 1.0 min.

Number Counts Full Scale 5K

Number of eV per channel 20



Sample peculiarities and remarks: FIGURE 246: POINT SCAN ON A SPHERICAL PARTICLE OF HIGH Al-Si

## Activated Carbon:

### Structural Analysis:

All the SEM micrographs indicated that the activated carbon particles have very large size, and very rough structures with many pores and deep cracks. The particles have rounded edges and irregular shape. Figures 347 to 354 were obtained at low magnifications of 10X, 20X and 54X to illustrate the particle size distribution, while micrograph Figures 355 to 358 were obtained at relatively higher magnifications such as 100X and 300X. to illustrate the detailed structures present on the particle surfaces.

The maximum, average and minimum particle size were measured in microns ( $\mu$ ) as follows:

Maximum	Average	Minimum
2700.0	1700.0	20.0

### Elemental Composition and Distribution:

As it was previously discussed in the instrumental section, the X-ray energy dispersive spectrometer cannot detect any element below Na in the periodic table. Since the activated carbon contains mainly C and minor impurities, the X-ray energy dispersive spectrometer was only able to detect elements such as S and Fe at very low concentrations. Both elements were distributed uniformly. The uniform distribution can be seen in the SEM micrograph, Figure 359, the sulfur X-ray image, Figure 360, the iron X-ray image, Figure 361, and the X-ray energy spectrum, Figure 362.

SEM IMAGES OF SAMPLE #

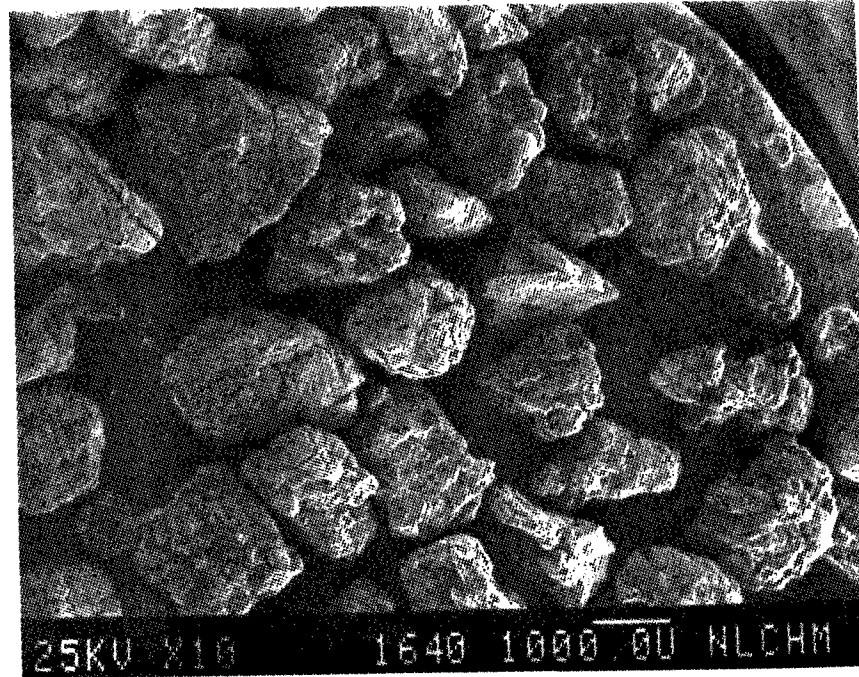


Figure 347

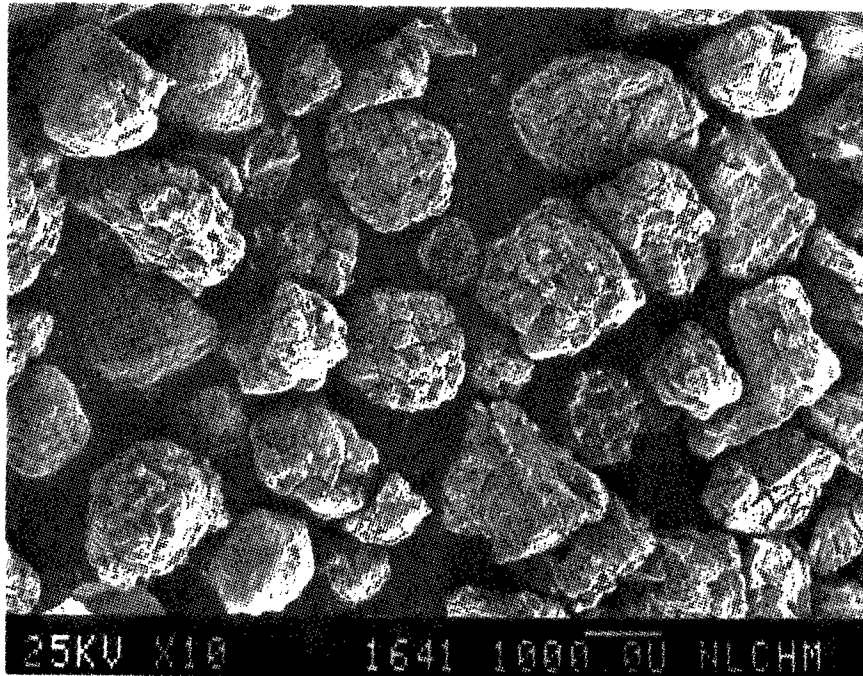


Figure 348

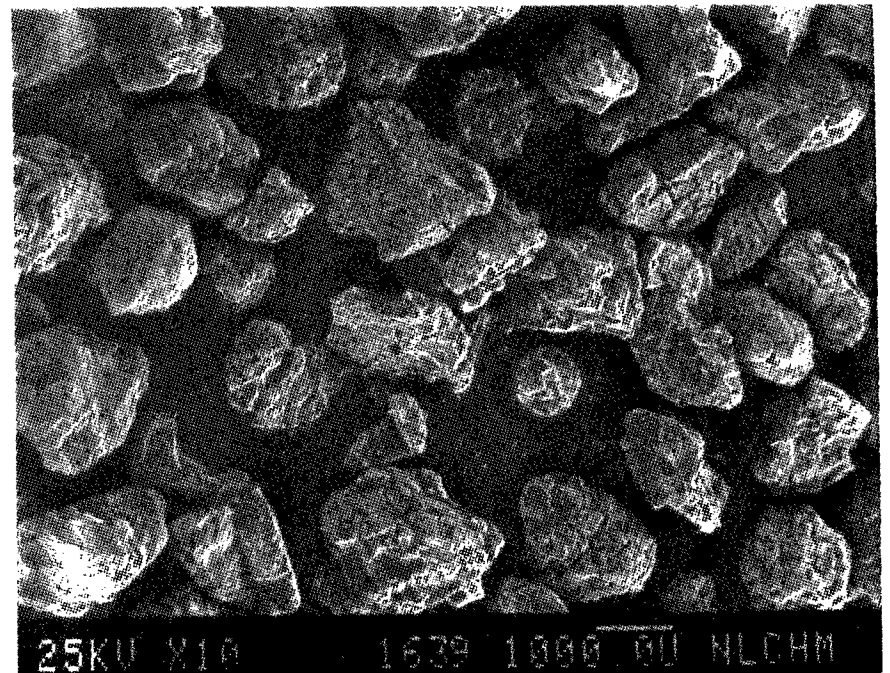


Figure 349

SEM IMAGES OF SAMPLE #

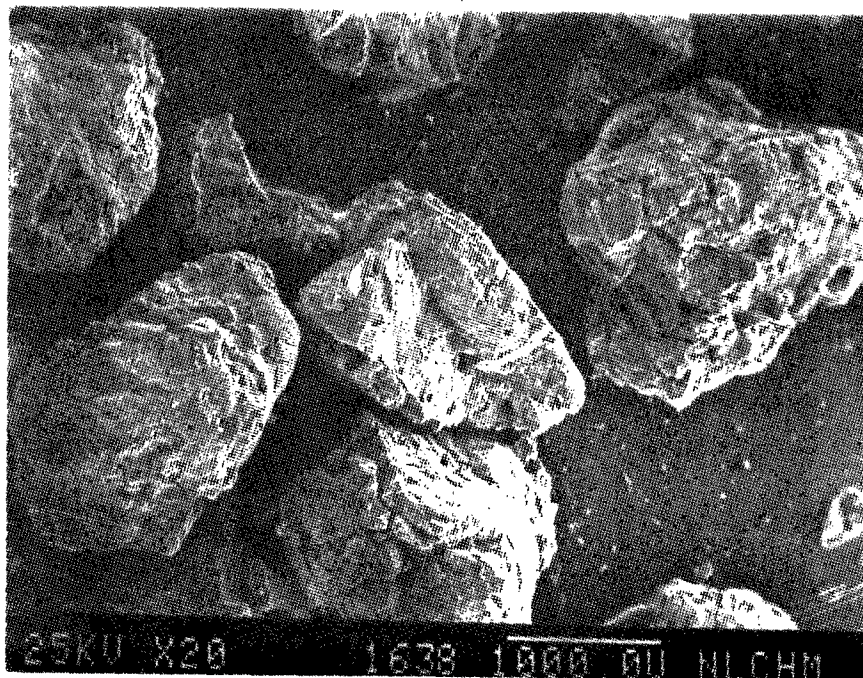


Figure 350

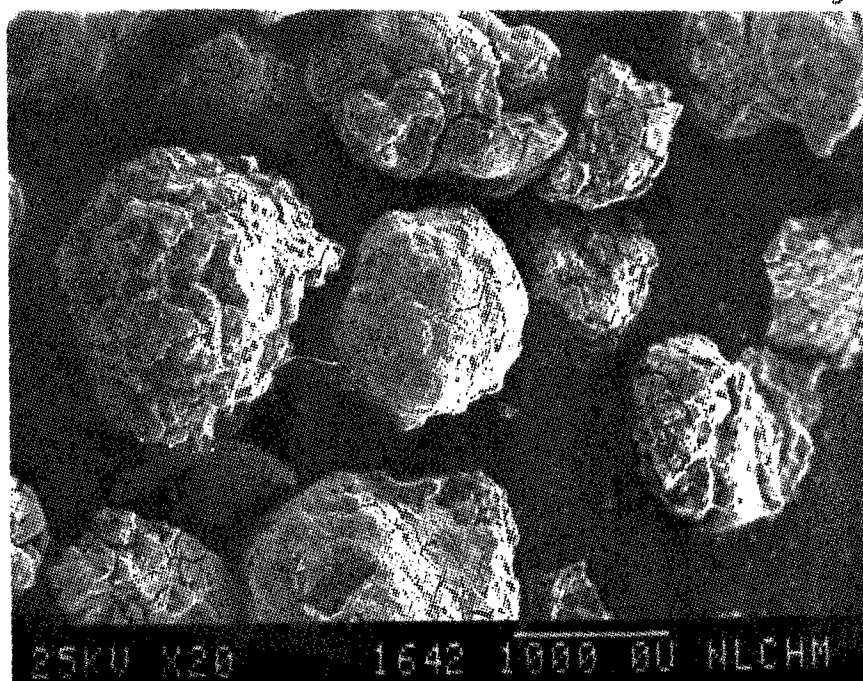


Figure 351

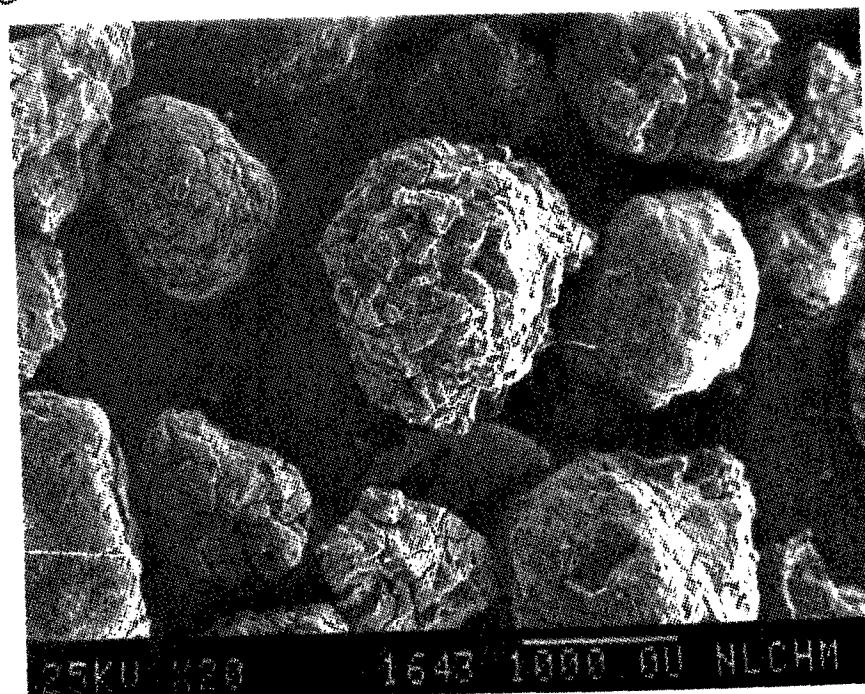


Figure 352

SEM IMAGES OF SAMPLE #

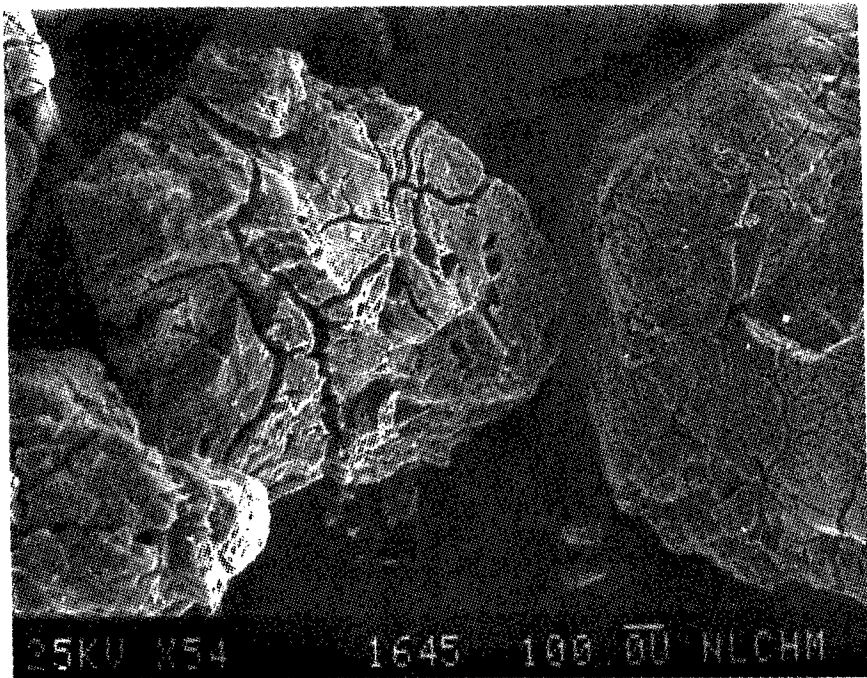


Figure 353

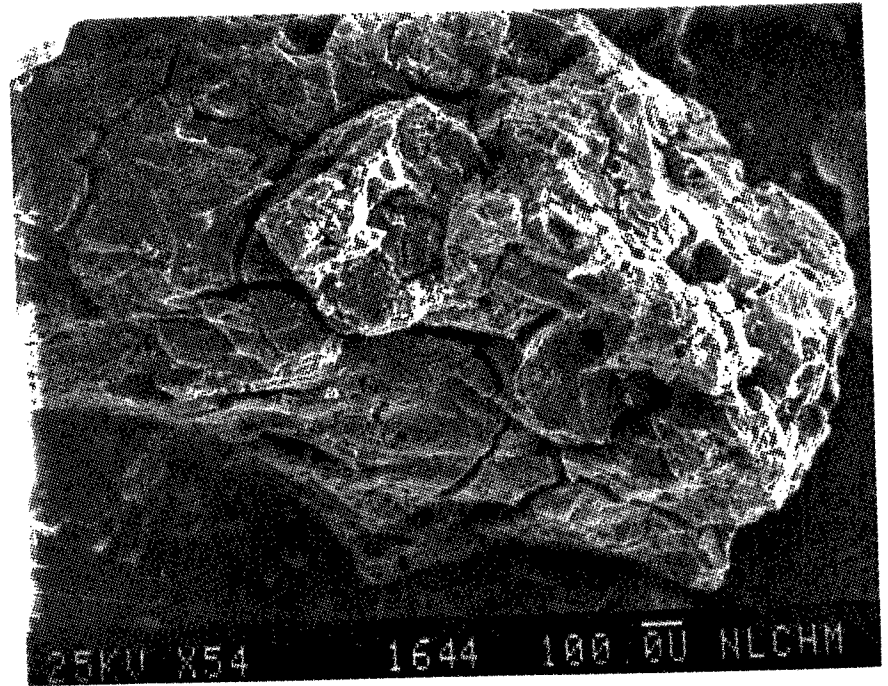


Figure 354



SEM IMAGES OF SAMPLE #

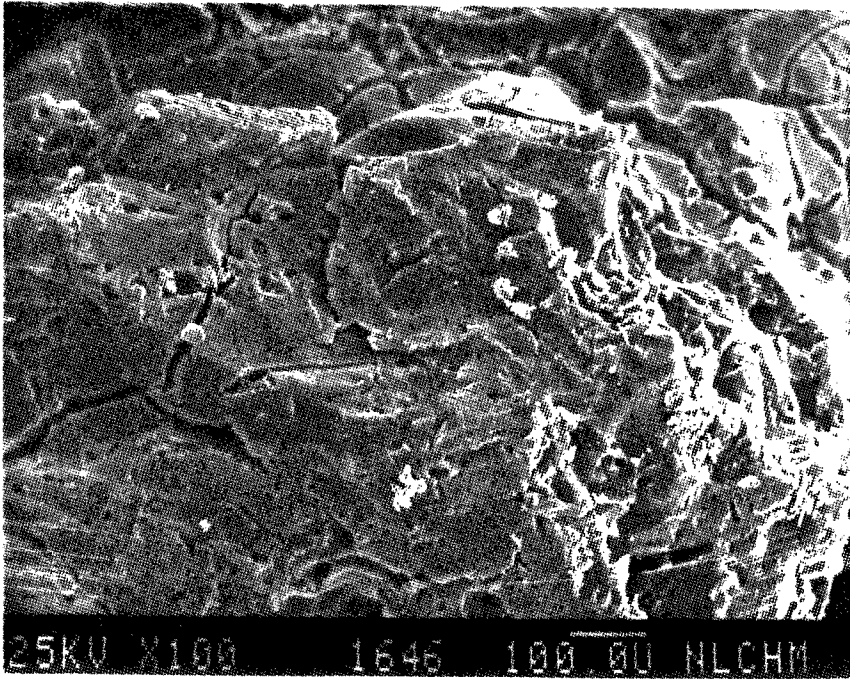


Figure 355

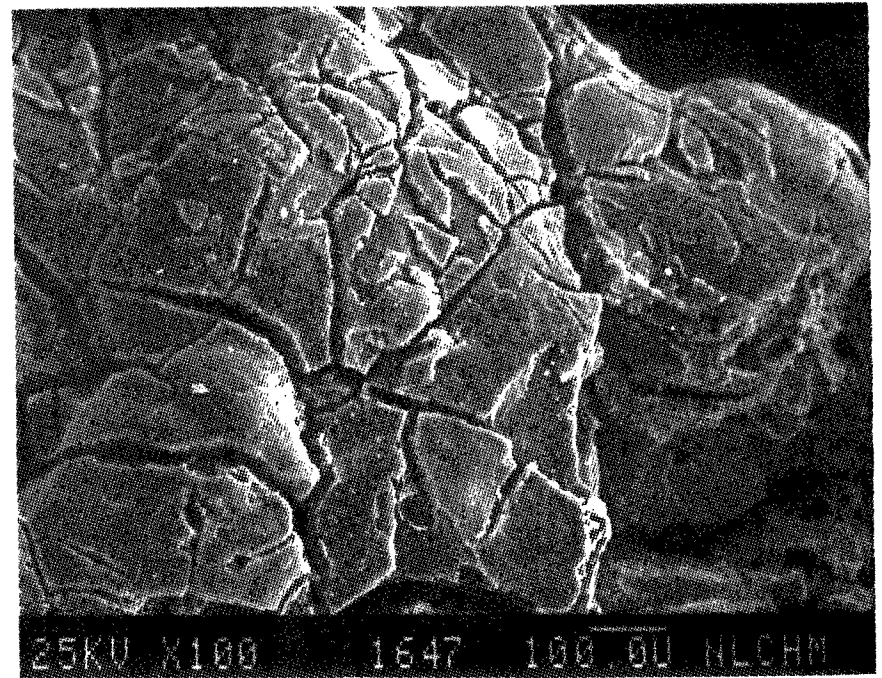


Figure 356



SEM IMAGES OF SAMPLE #

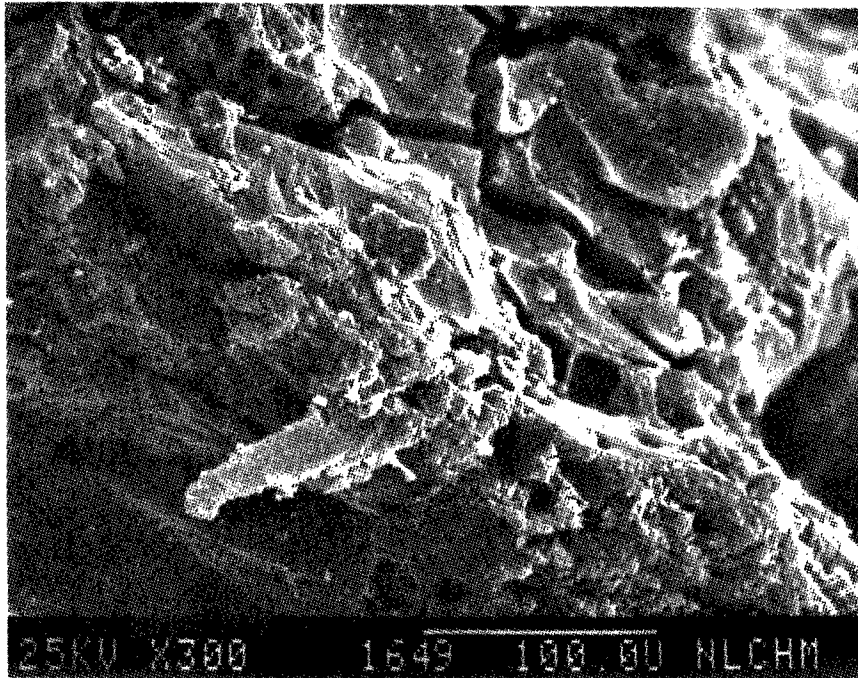


Figure 357

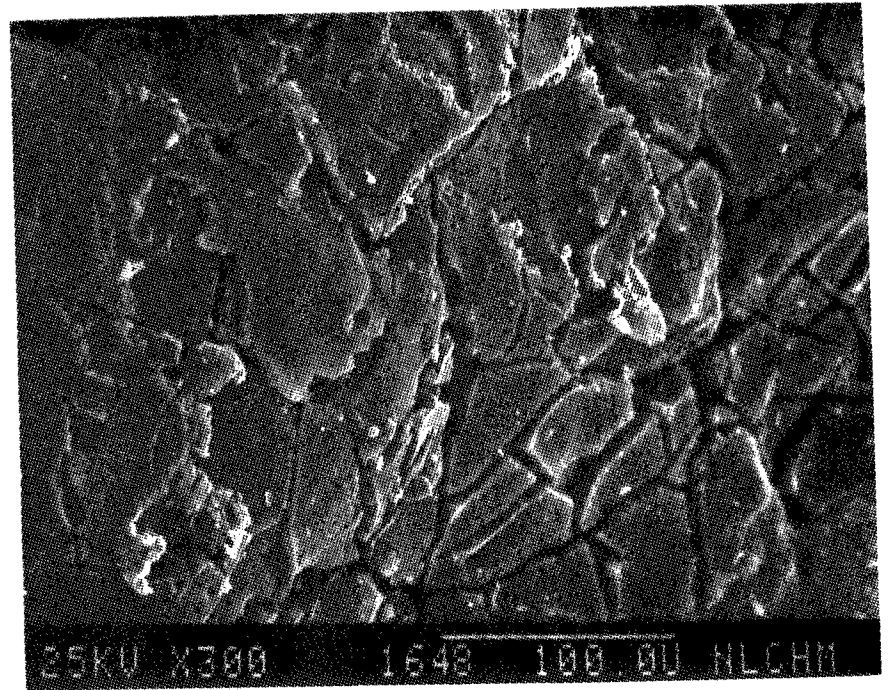


Figure 358

SEM IMAGES OF SAMPLE #

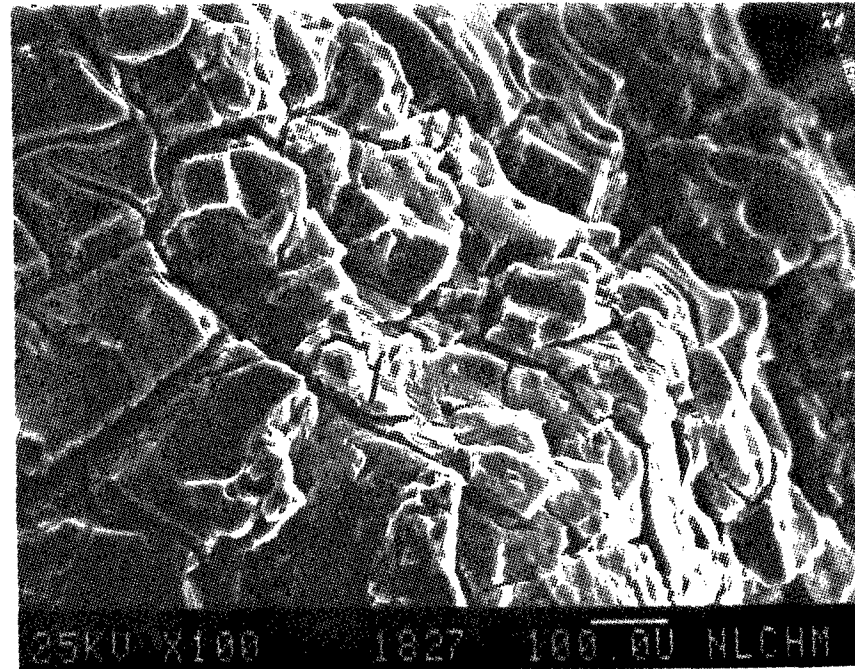


Figure 359

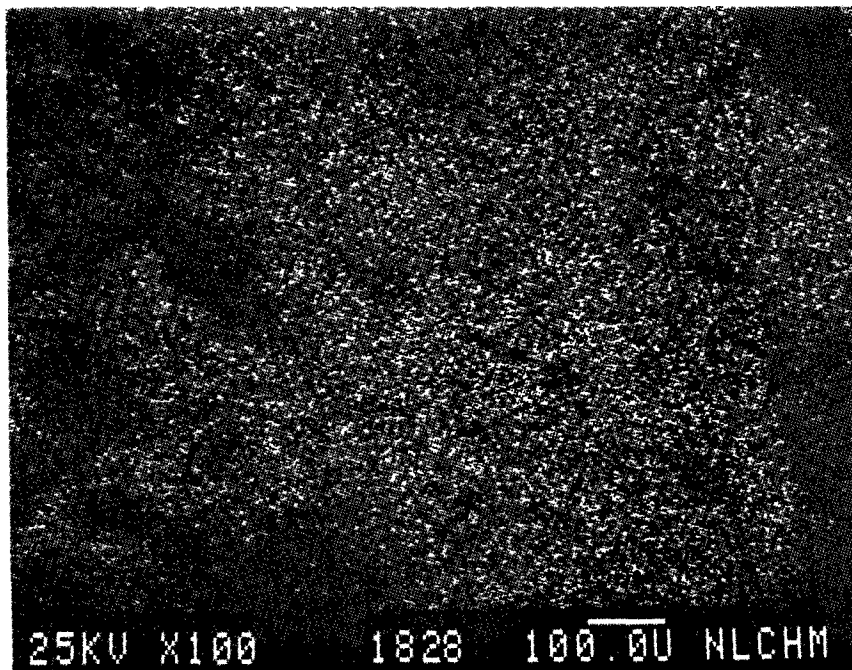


Figure 360

S X-Ray Image of Figure 359

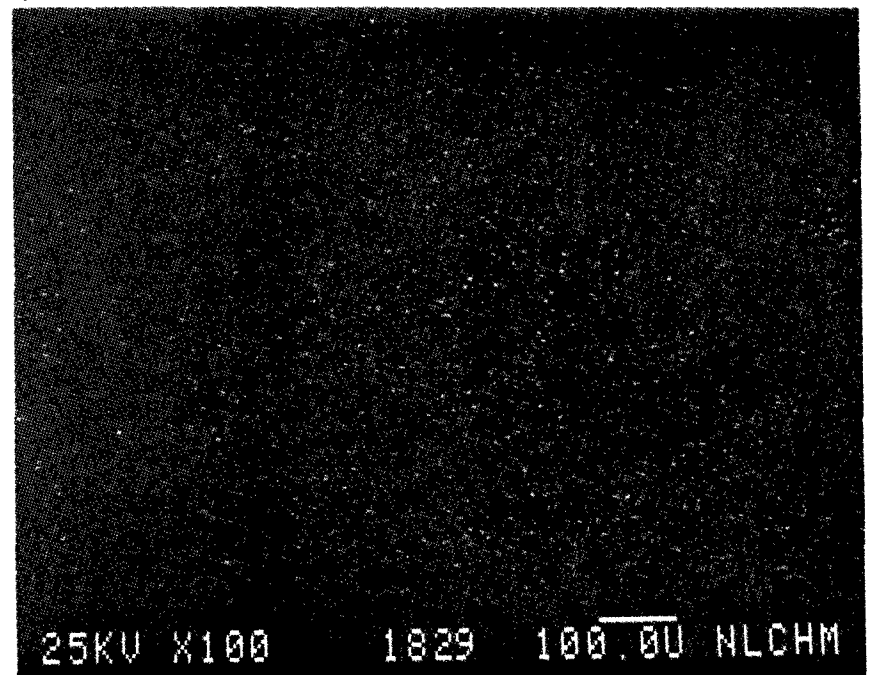


Figure 361

Fe X-Ray Image of Figure 359

ENERGY DISPERSIVE X-RAY ANALYSIS

Analytical Number Activated Carbon

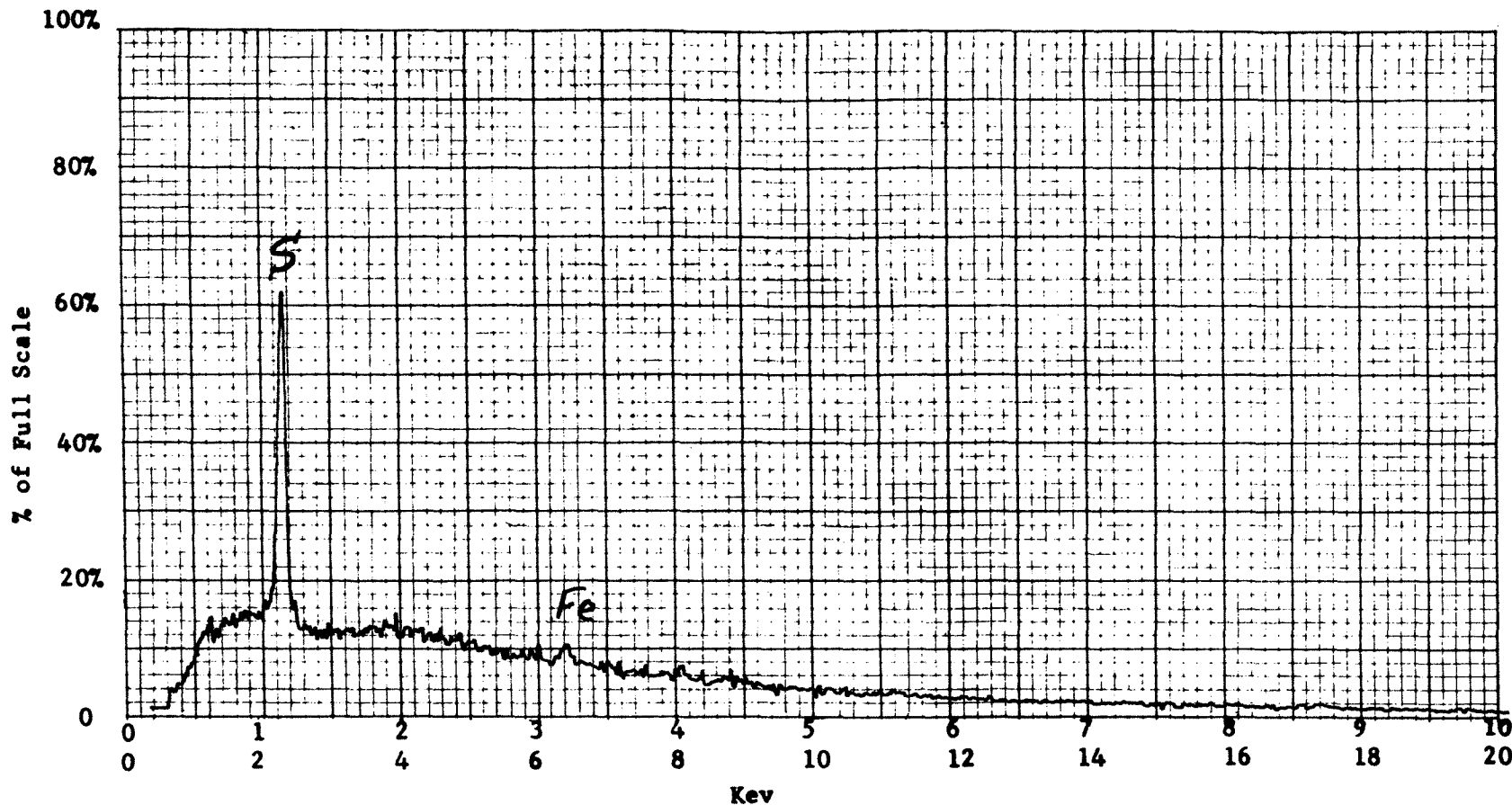
Operator \_\_\_\_\_ Date \_\_\_\_\_

Accelerating Potential 25 KeV

Total Counts Acquired 1.0 min.

Number Counts Full Scale 2K

Number of eV per channel 20



Sample peculiarities and remarks: FIGURE 362: AREA SCAN

Illite:Structural Analysis:

Illite particles were found to be irregular in shape, and only a few particles were elongated. Rough surfaces were observed in all the particles. Most of the particles' edges were rounded, while very few particles had slightly sharpened edges. Particles with pores and small cracks were observed in SEM micrographs obtained at high magnifications, see Figures 381, 384, 385, 386 and 387.

The maximum, average and minimum particle size were measured in microns ( $\mu$ ) as follows:

Maximum	Average	Minimum
85.0	19.0	0.2

Elemental Composition and Distribution:

Al, Si, S, K, Ca, Ti and Fe were detected from two fields present in SEM micrographs, Figures 388 and 396. These figures were obtained at low magnification (200X) to cover larger areas in the sample and in the X-ray energy spectrum, Figure 444. Also, the elemental X-ray images of Figures 388 and 396 indicate that Si is the major element, while elements such as S, Ca and Fe were segregated in a number of particles.

Two particles in Figure 404, the elongated one in the middle of the field and another particle in the lower part of the micrograph contained very high concentrations of Ca and S (possible Ca sulphate). This is illustrated by the sulfur X-ray image, Figure 407, the calcium X-ray

image, Figure 409, and in the X-ray energy spectrum, Figure 445.

The SEM micrograph, Figure 412, was obtained to show a large particle and another smaller one in the middle of the field from which very high levels of Fe and S (possible Fe sulphate) were detected. This is illustrated by the sulfur X-ray image, Figure 415, the iron X-ray image, Figure 419, and in the X-ray energy spectrum, Figure 446.

Very high concentrations of Ti were detected from one particle in the lower part of Figure 420. The titanium X-ray image, Figure 426, and the X-ray spectrum, Figure 447, confirm this result. A very small number of particles in the illite contained Ti in high concentrations. Particles containing high concentrations of Ca and S were also observed in a SEM micrograph, Figure 428.

In Figure 436 a large particle in the right side of the field contained Fe and S at high levels. Also, in the same figure very small spots on the surface of the high Fe-S particle contained much higher concentrations of K than that normally observed. The sulfur X-ray image, Figure 439, the potassium X-ray image, Figure 440, the iron X-ray image, Figure 443, and the X-ray energy spectrum, Figure 448, illustrated that the intensity of K peak was much higher than observed average.

Many particles of very high Si and Al were observed. This is illustrated in X-ray energy spectrum, Figure 449.

SEM IMAGES OF SAMPLE #

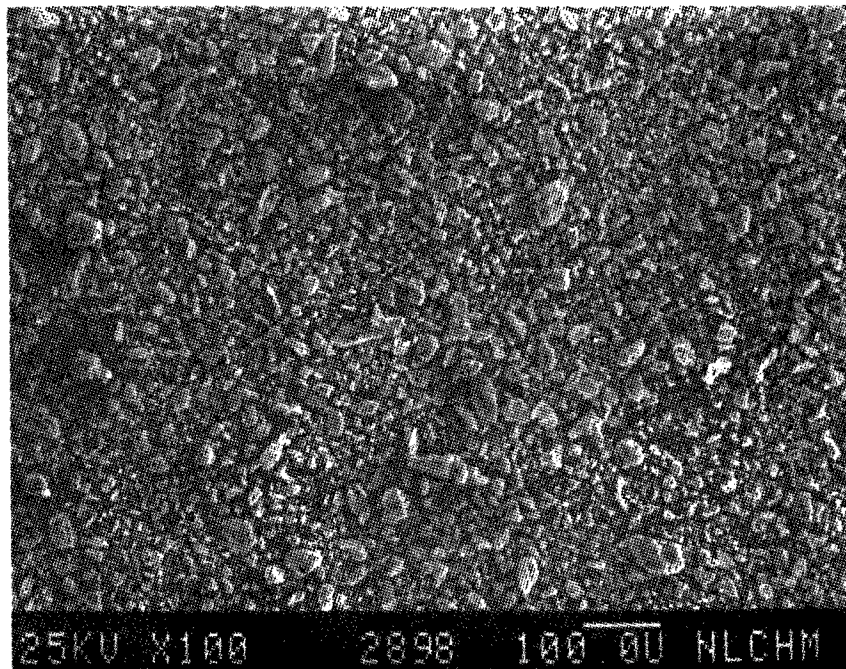


Figure 363

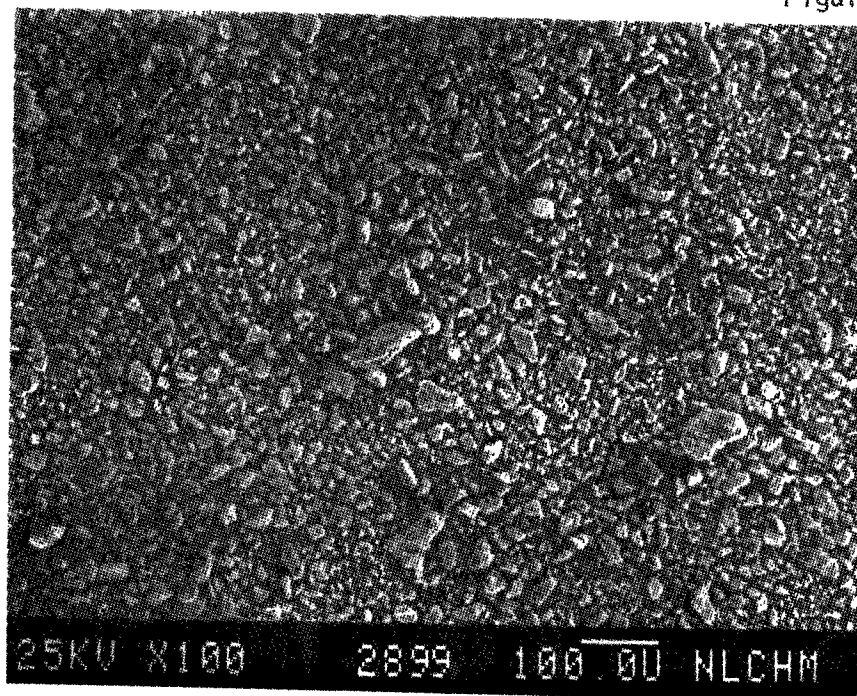


Figure 364

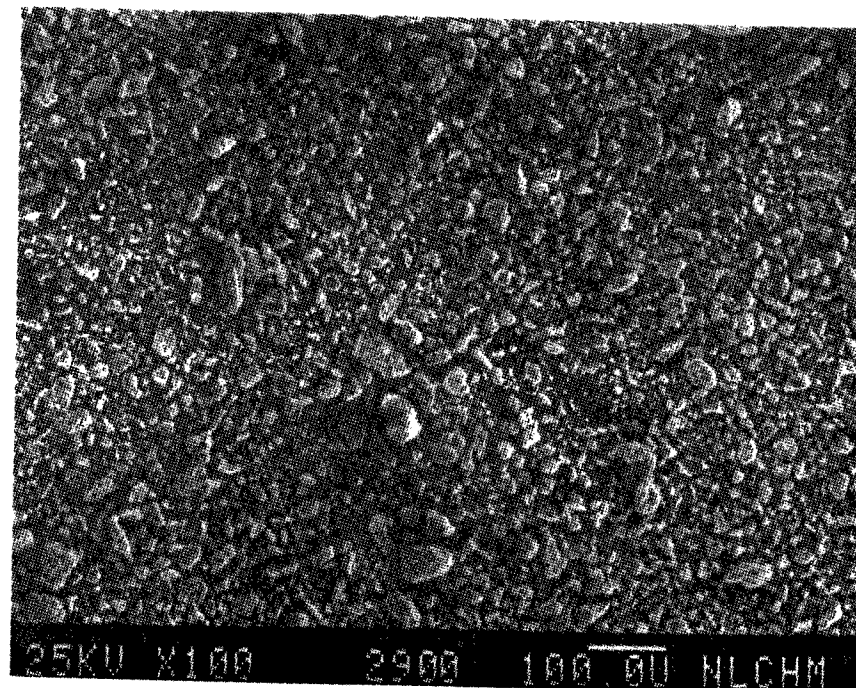


Figure 365



SEM IMAGES OF SAMPLE #

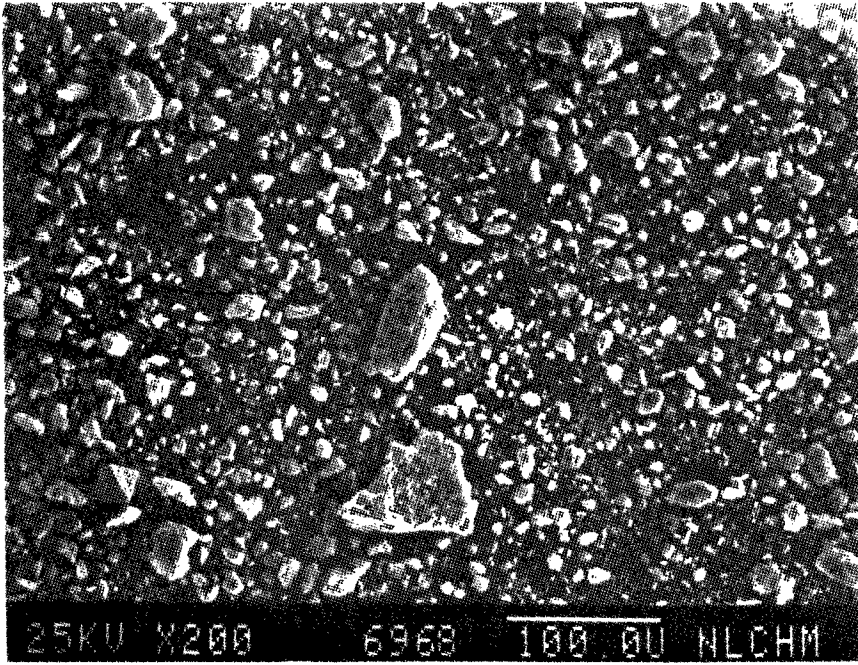


Figure 366

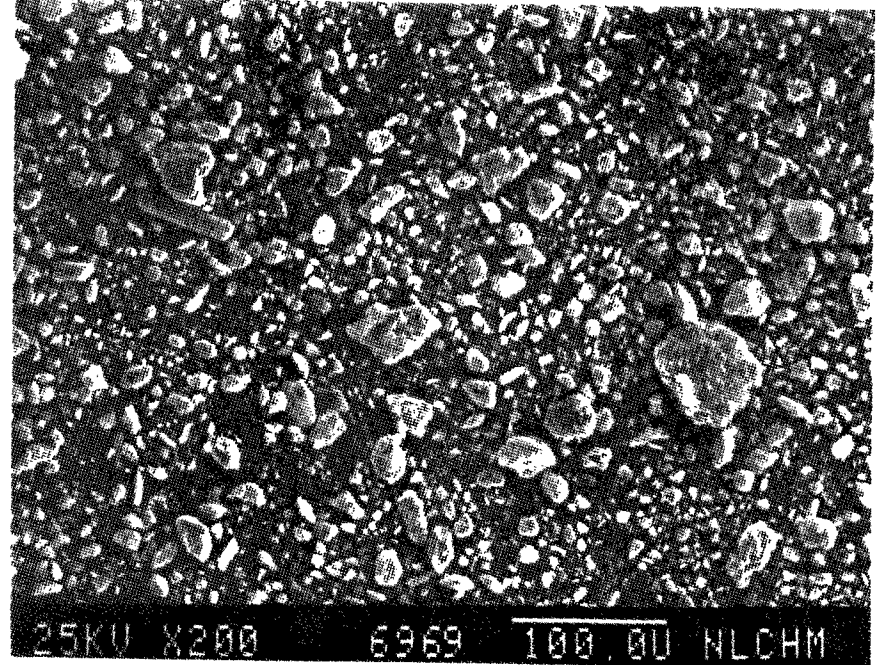


Figure 367

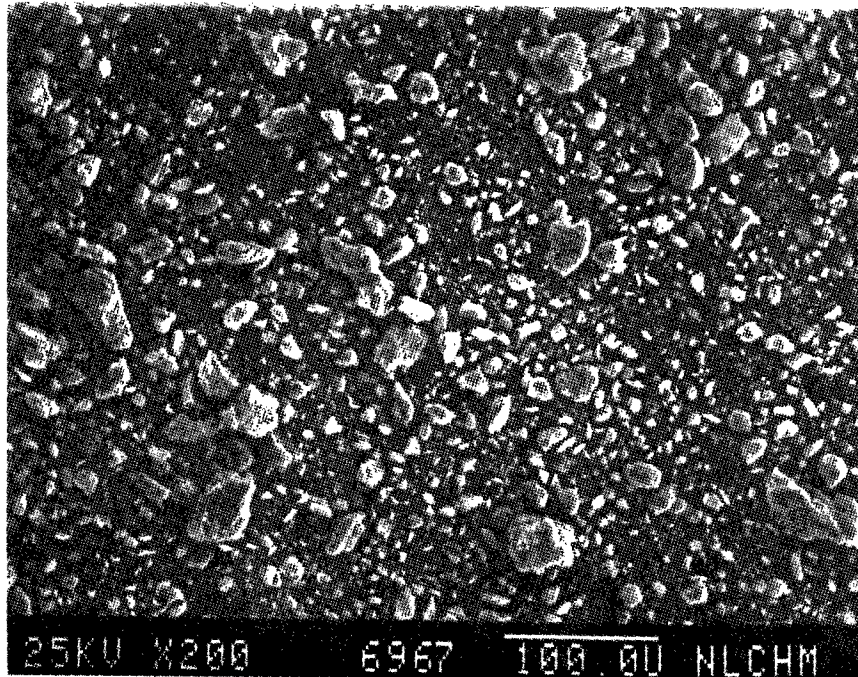


Figure 368

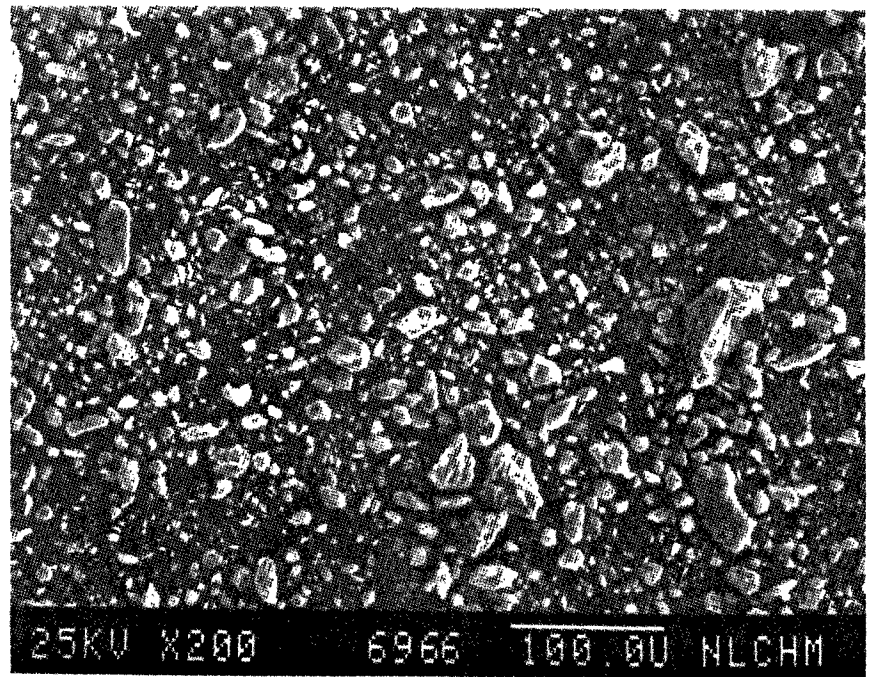


Figure 369

SEM IMAGES OF SAMPLE #

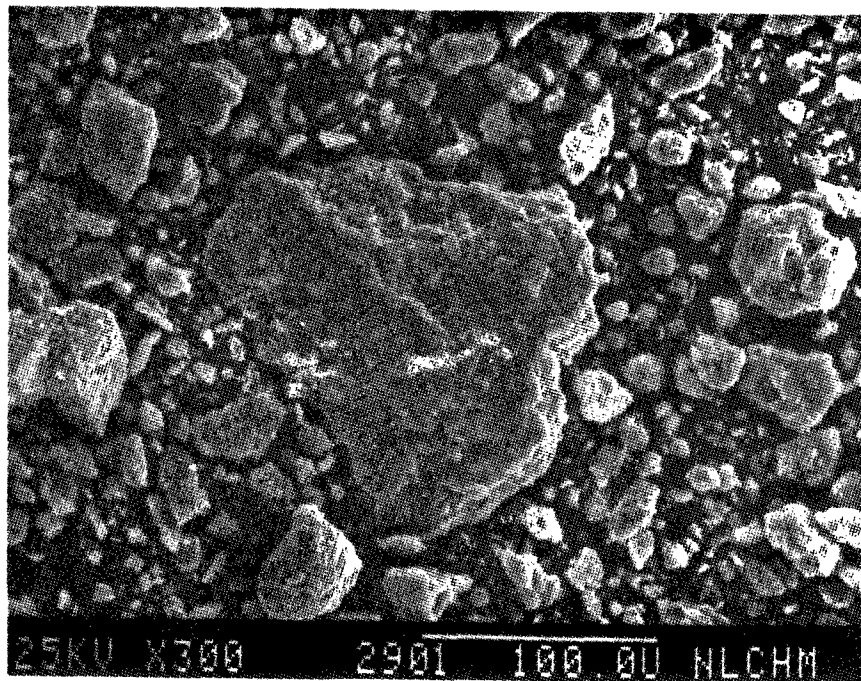


Figure 370

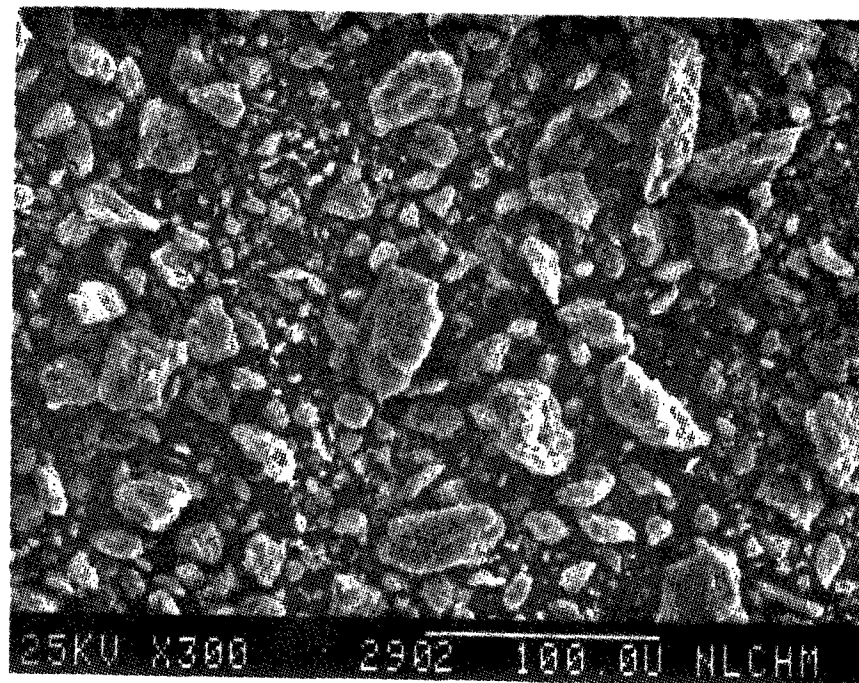


Figure 371

SEM IMAGES OF SAMPLE #

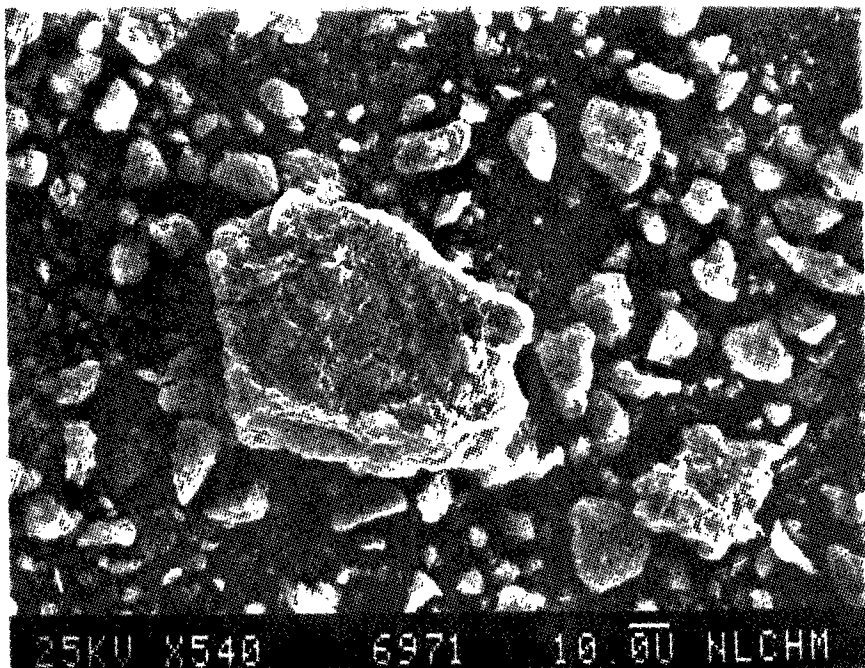


Figure 372

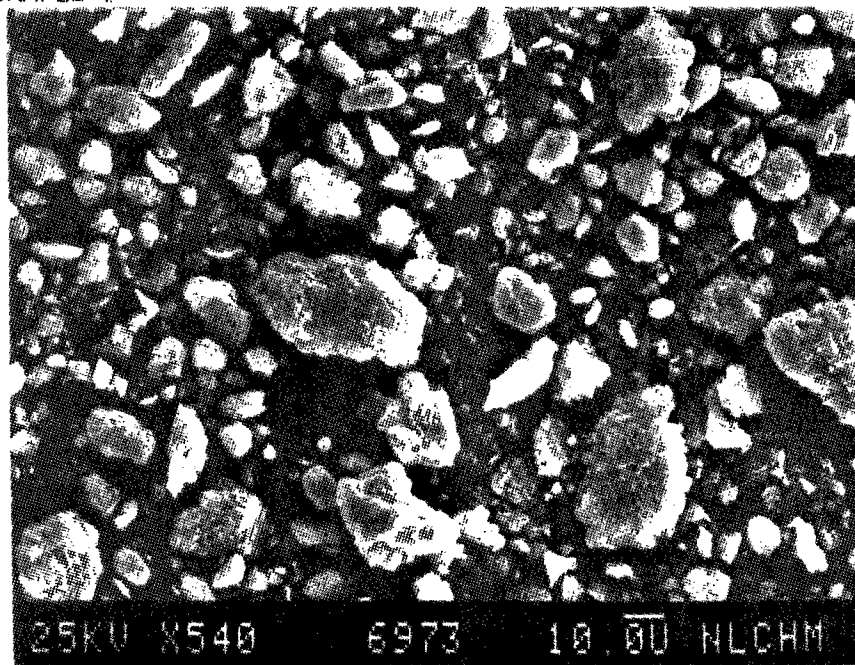


Figure 373

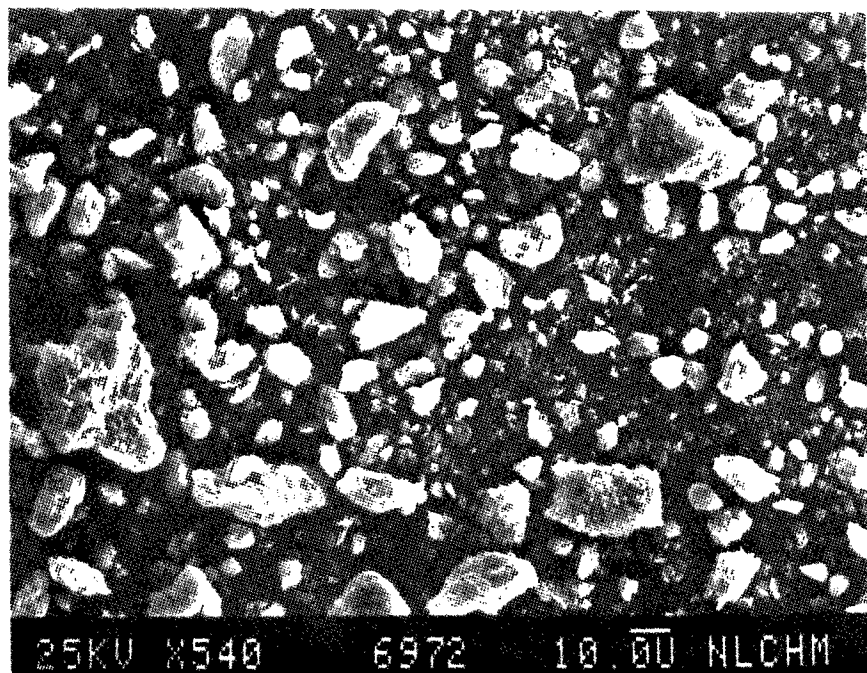


Figure 374

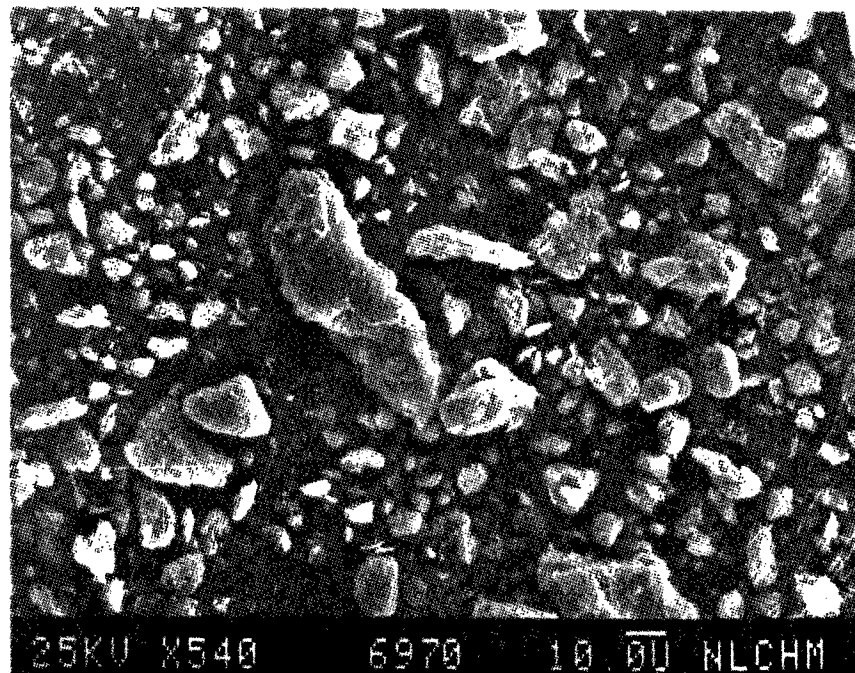


Figure 375



SEM IMAGES OF SAMPLE #

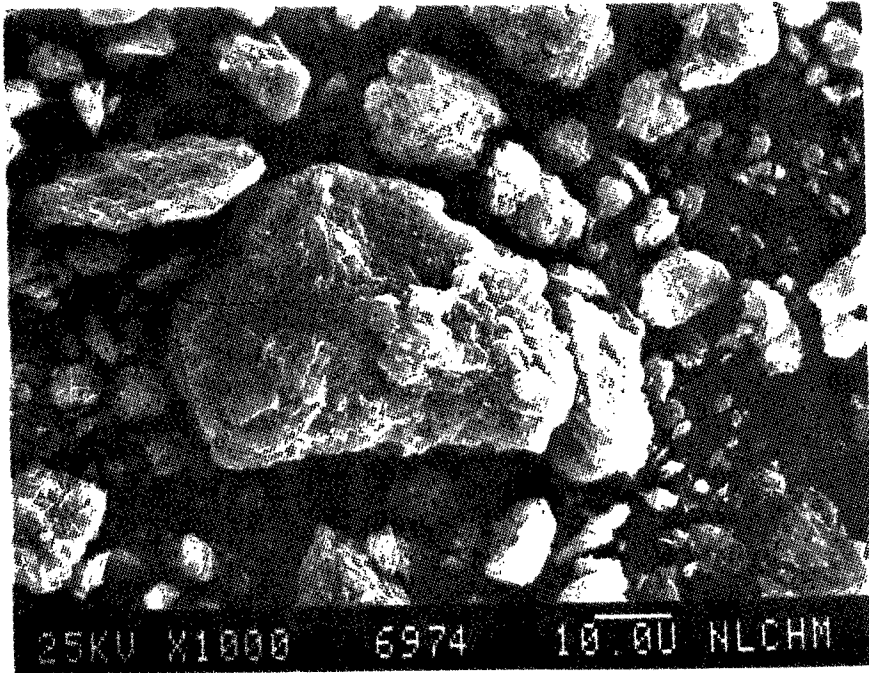


Figure 376

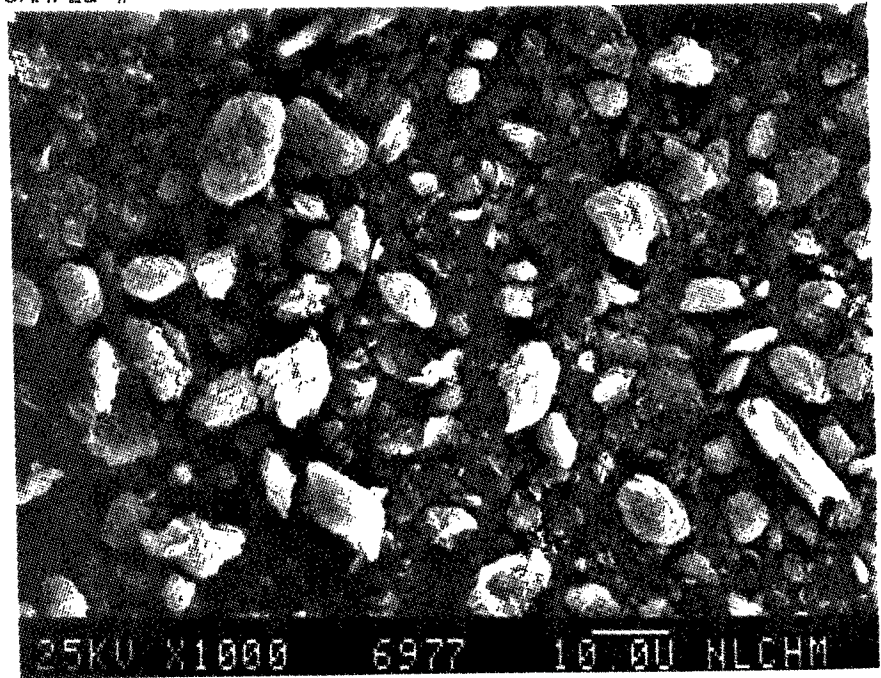


Figure 377

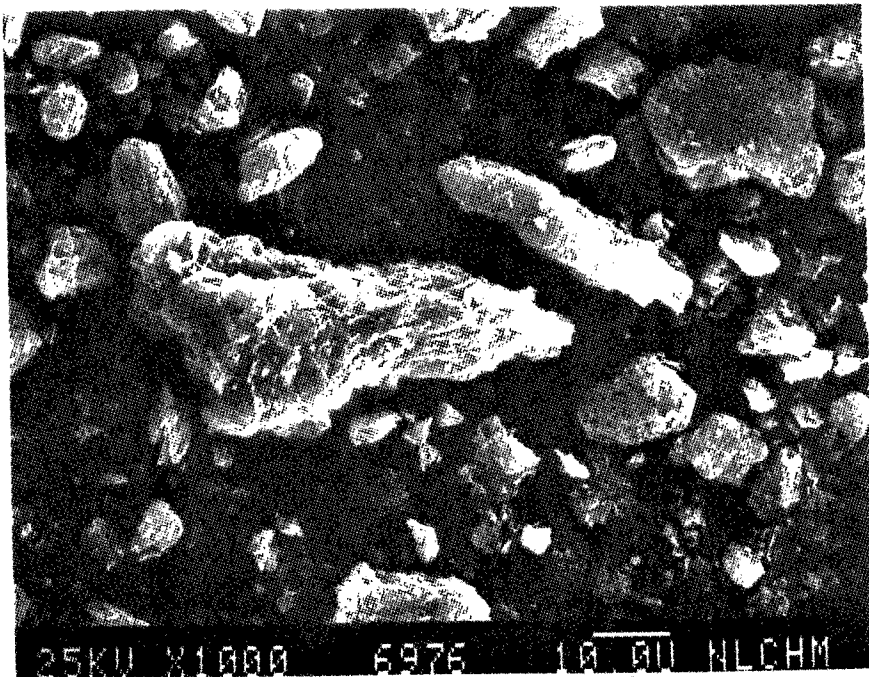


Figure 378

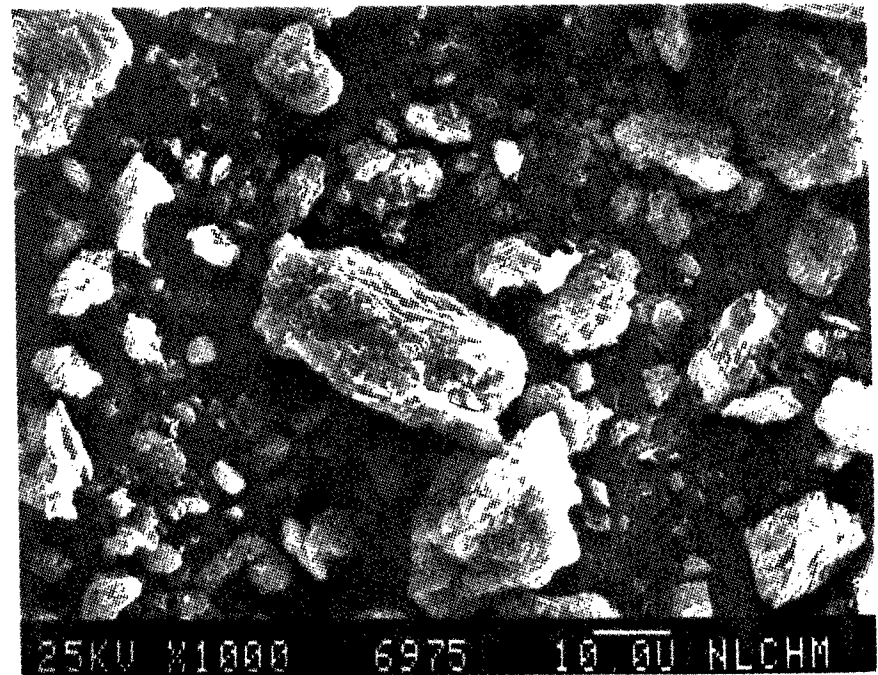


Figure 379

SEM IMAGES OF SAMPLE #

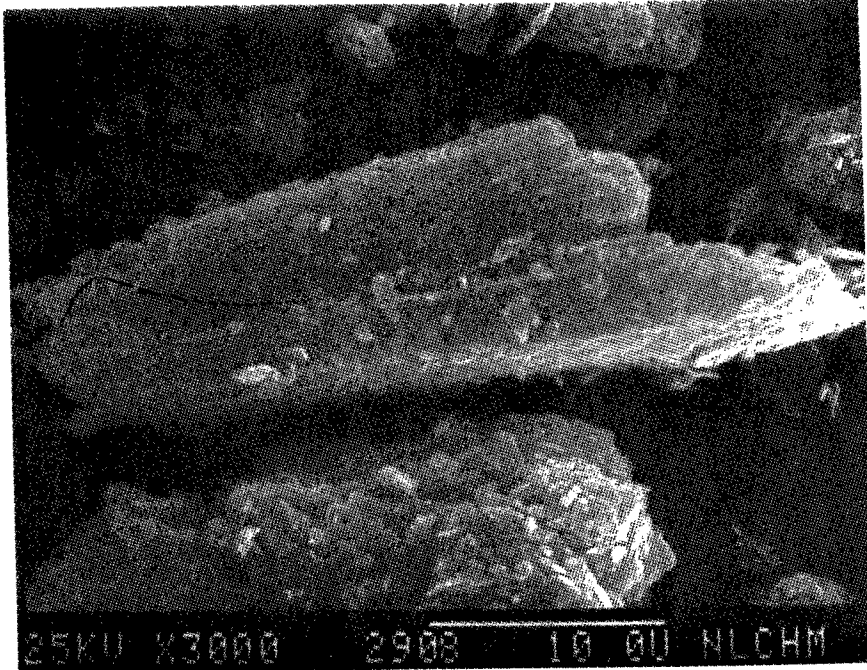


Figure 380

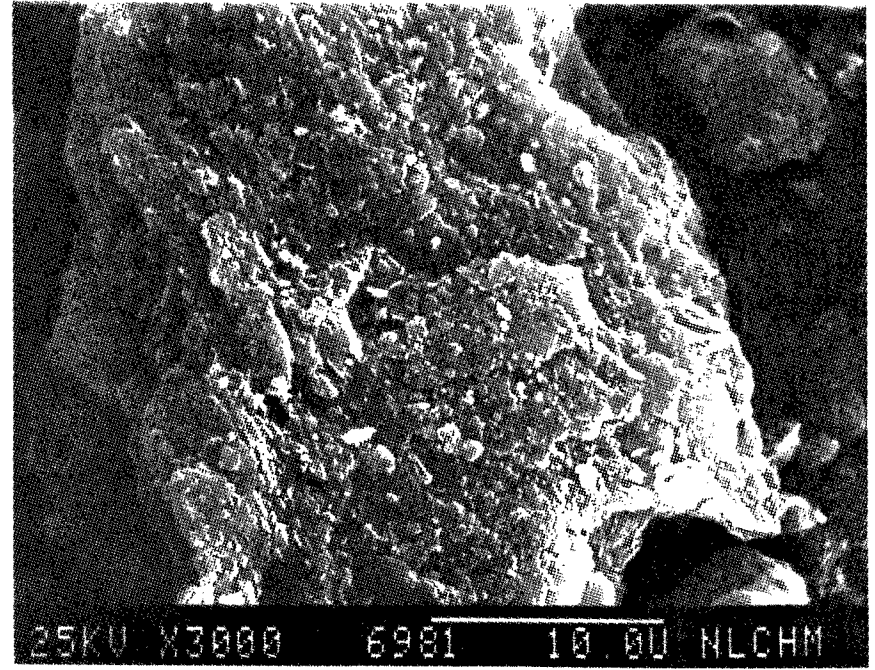


Figure 381

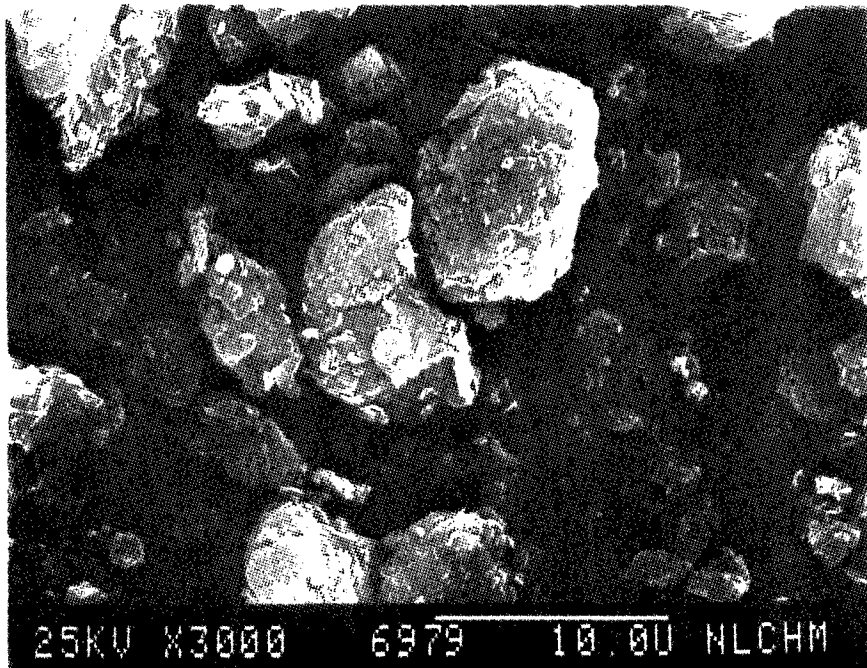


Figure 382

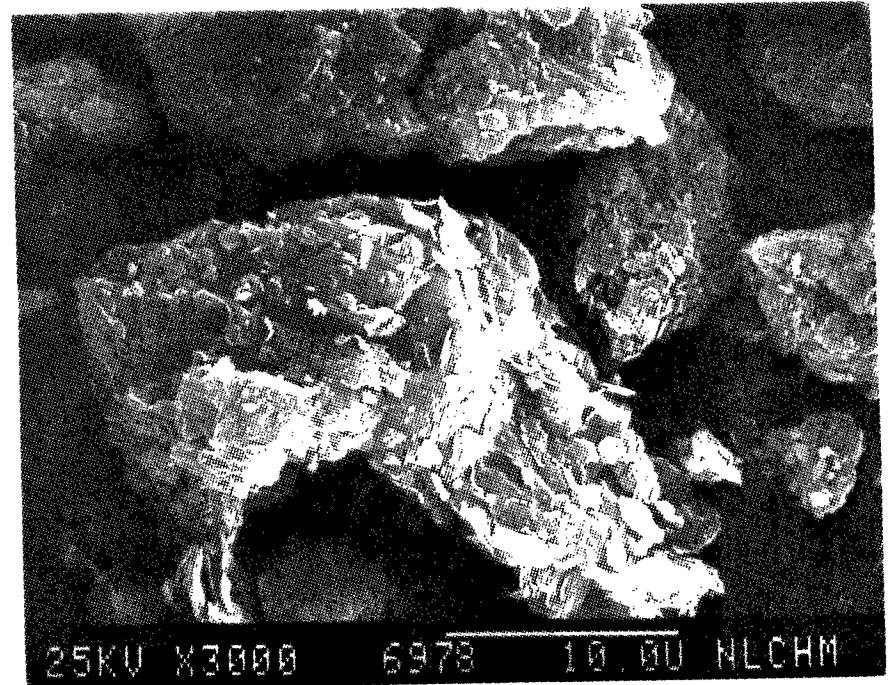


Figure 383



SEM IMAGES OF SAMPLE #

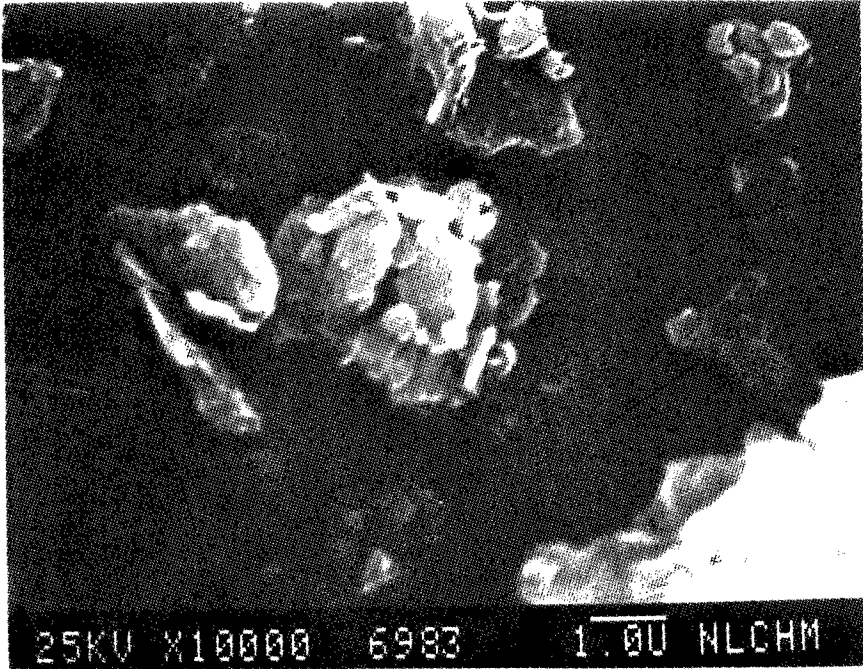


Figure 384

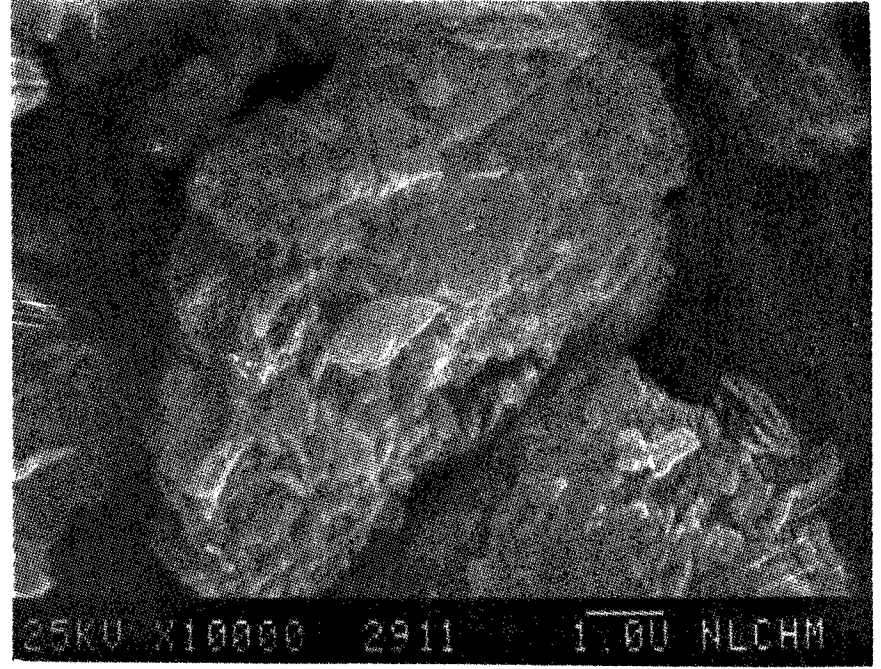


Figure 385

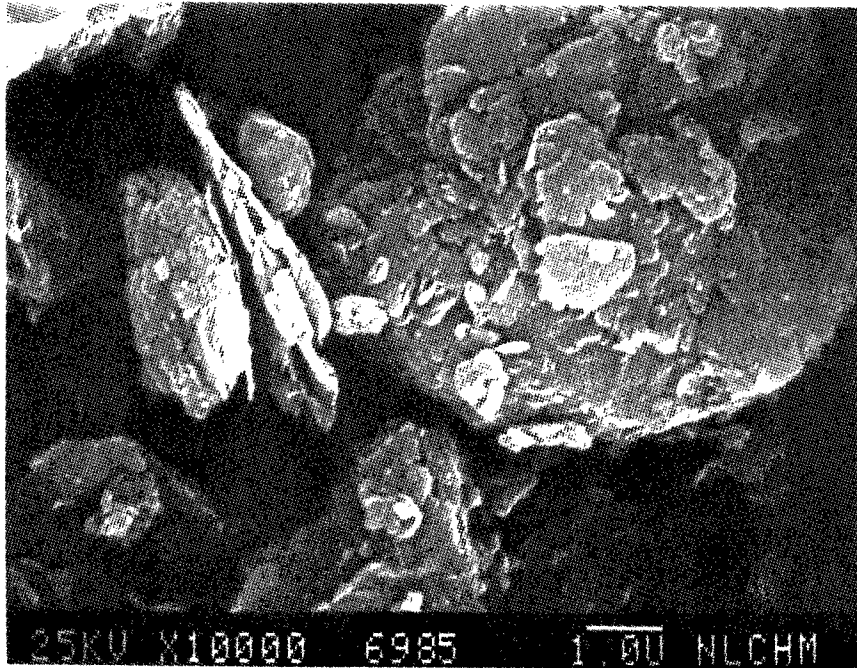


Figure 386

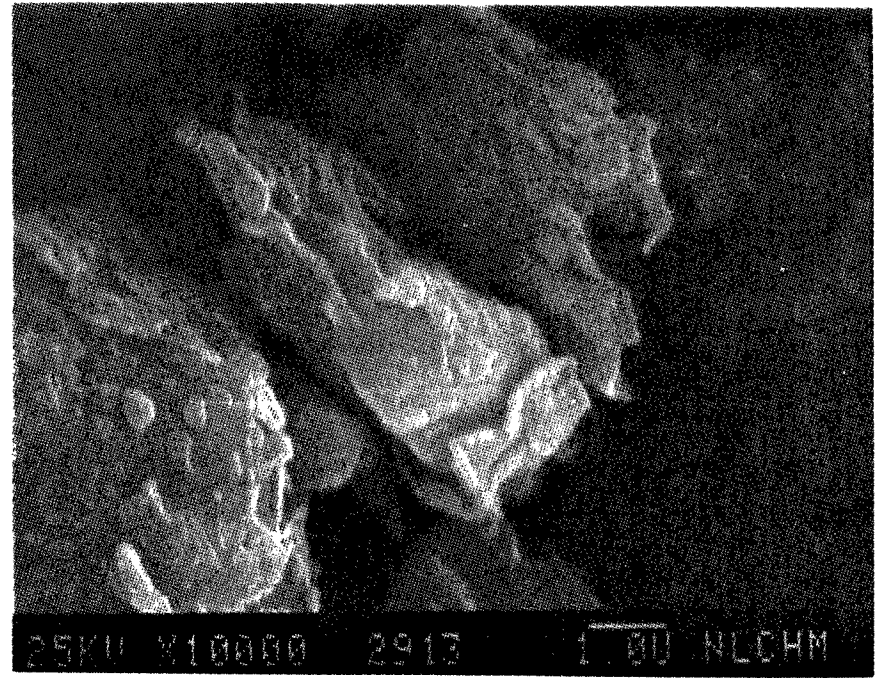


Figure 387



SEM IMAGES OF SAMPLE #

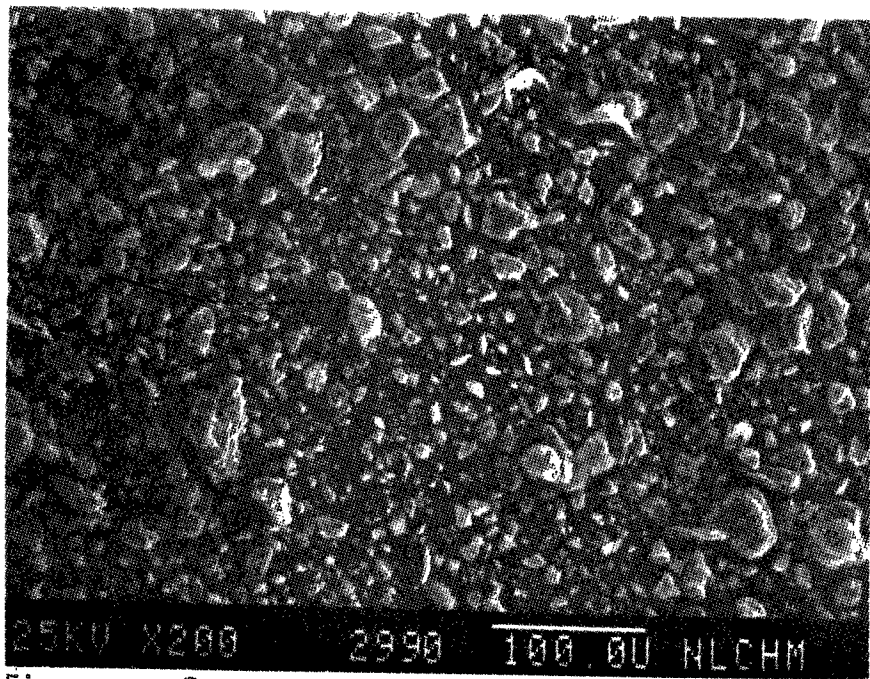


Figure 388

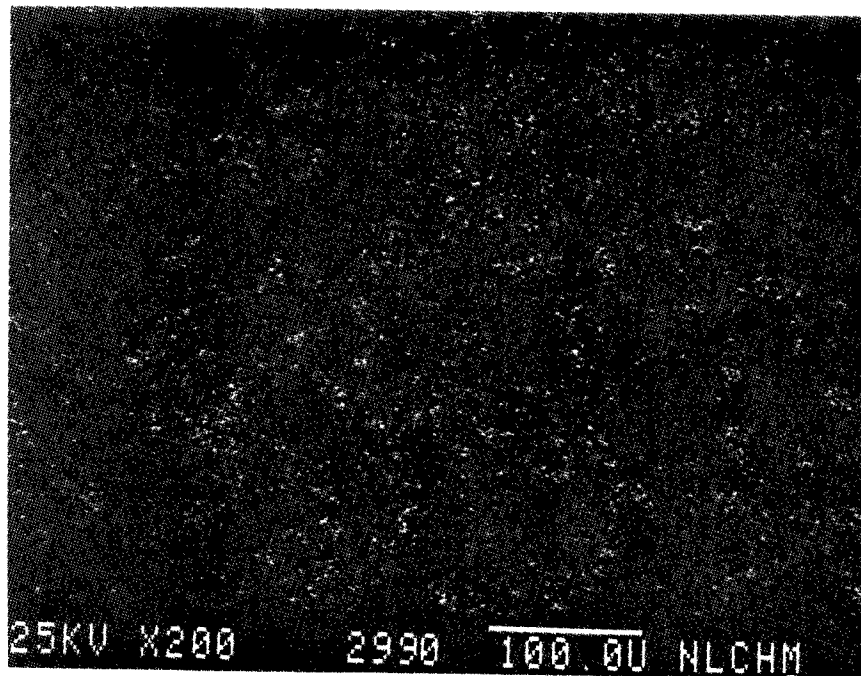


Figure 389

AL X-Ray Image of Figure 388

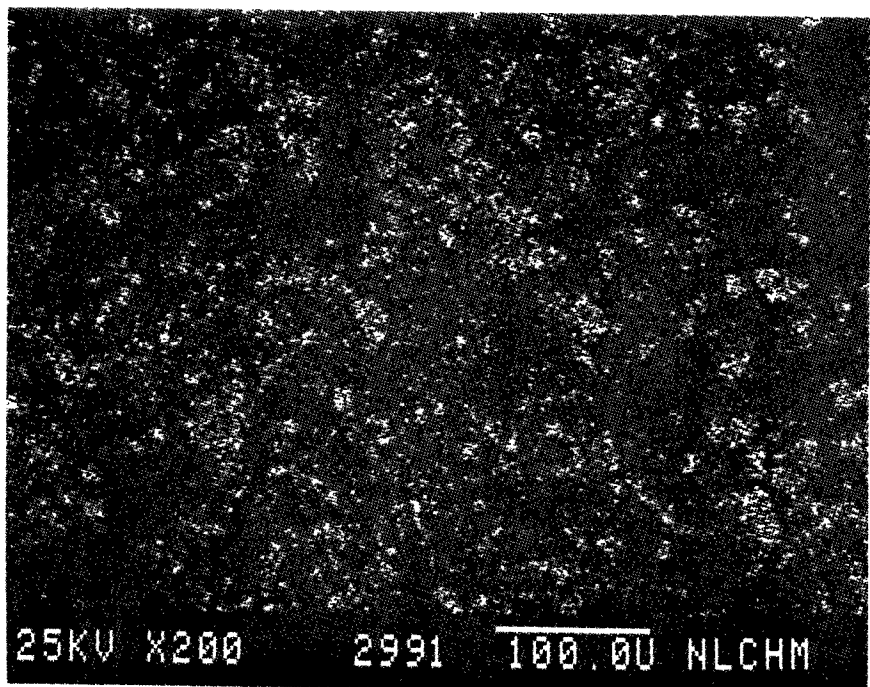


Figure 390

Si X-Ray Image of Figure 388

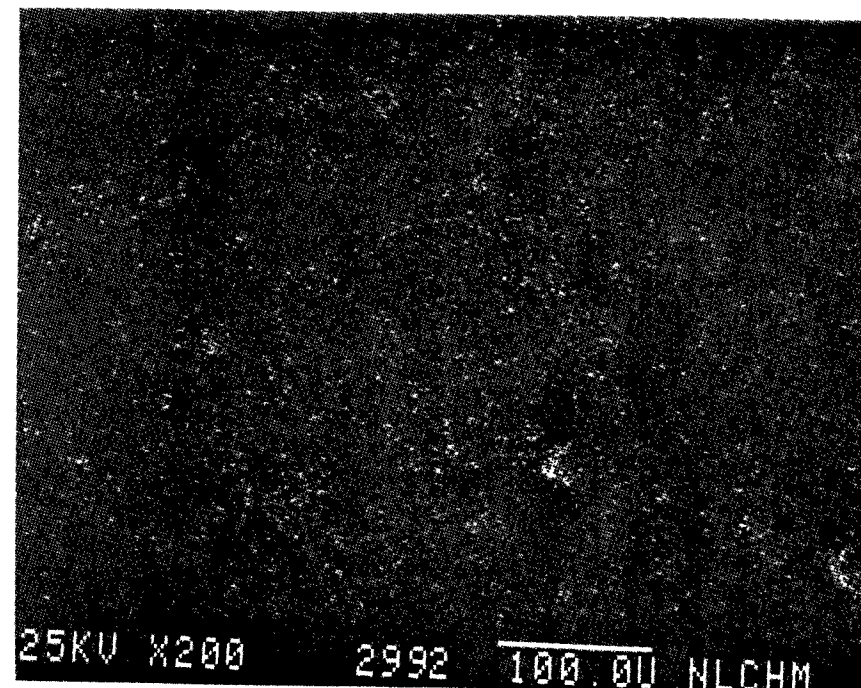


Figure 391

S X-Ray Image of Figure 388

SEM IMAGES OF SAMPLE #

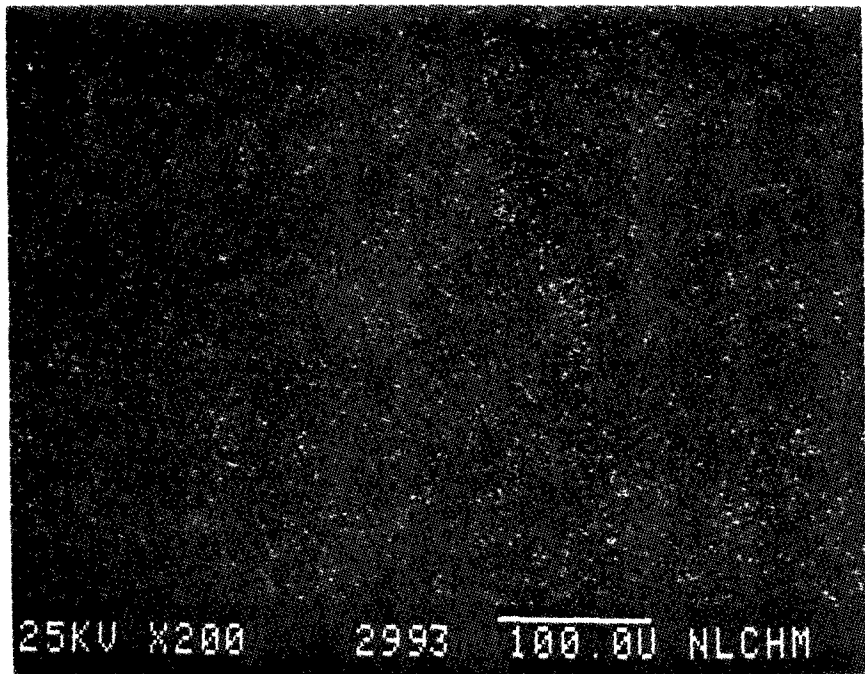


Figure 392

K X-Ray Image of Figure 388

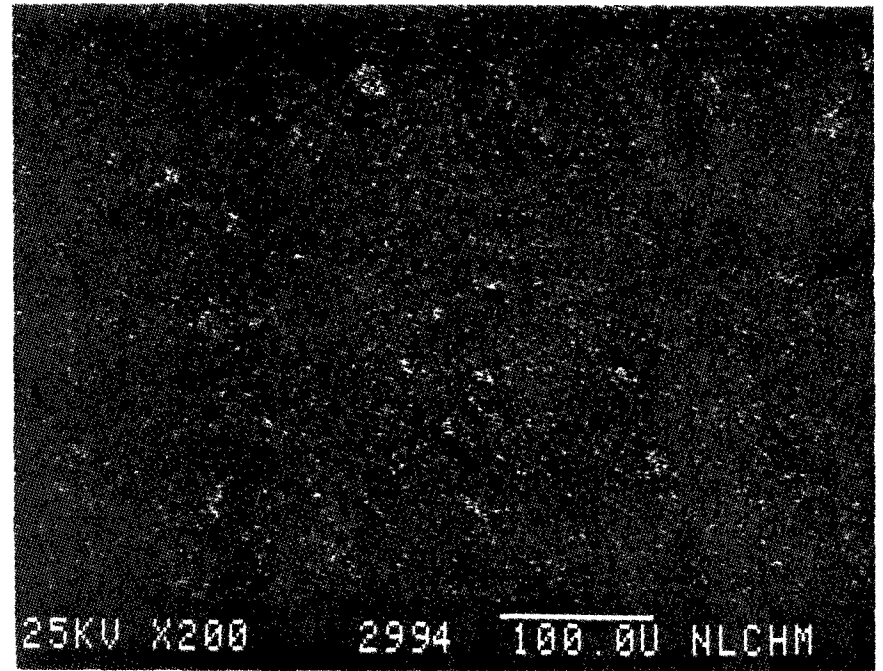


Figure 393

Ca X-Ray Image of Figure 388

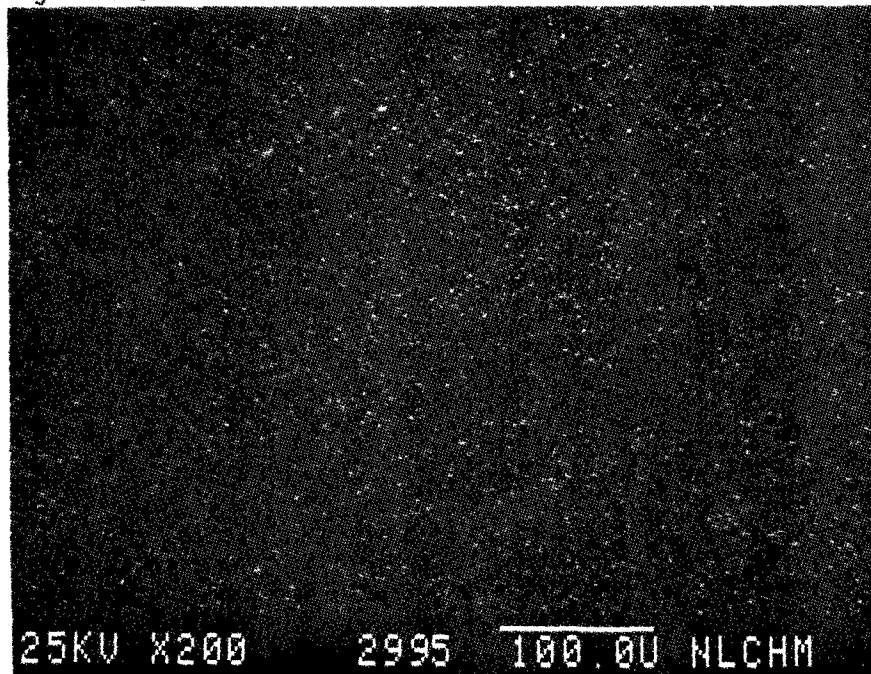


Figure 394

Ti X-Ray Image of Figure 388

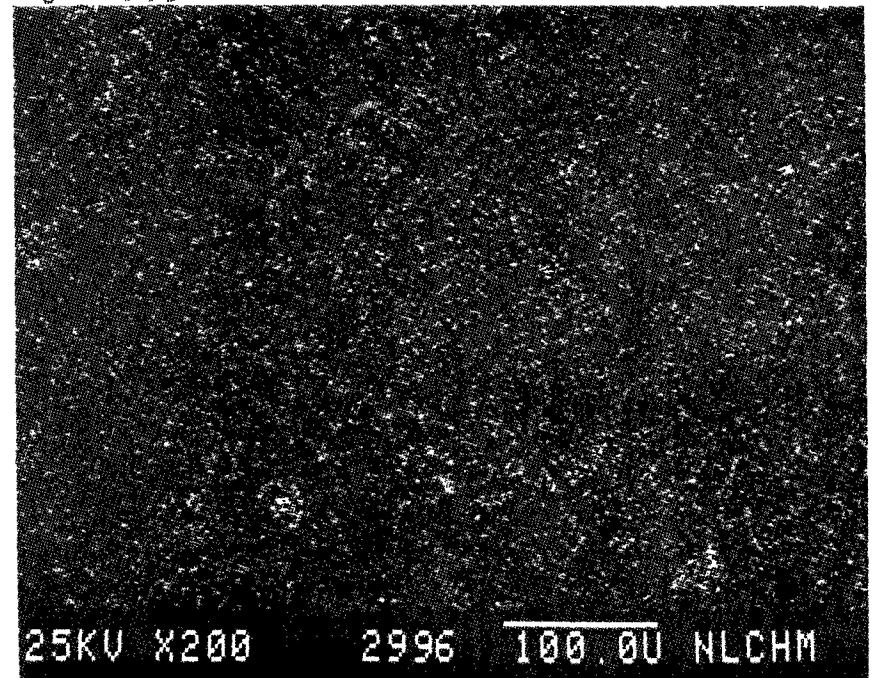


Figure 395

Fe X-Ray Image of Figure 388

SEM IMAGES OF SAMPLE #

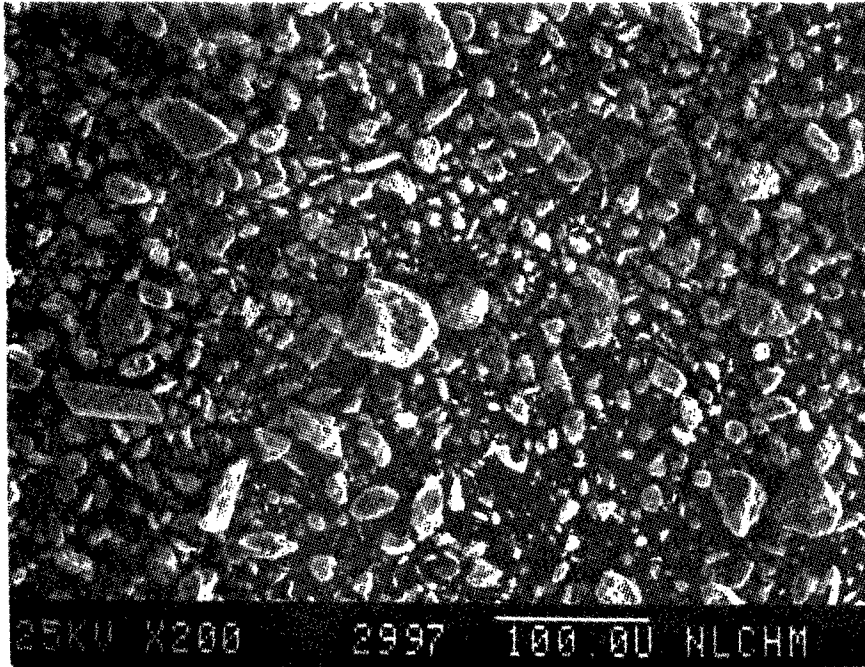


Figure 396

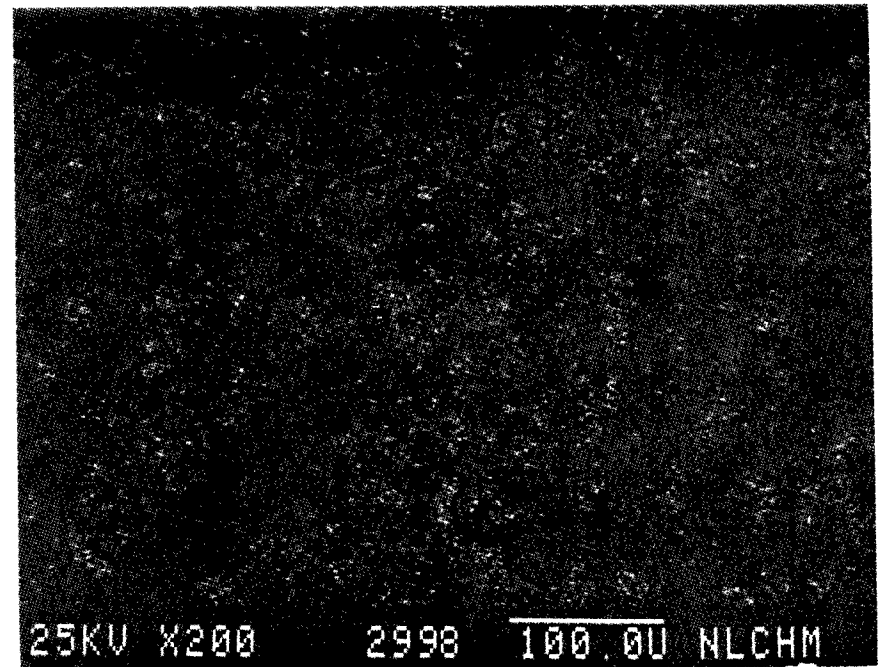


Figure 397

AL X-Ray Image of Figure 396

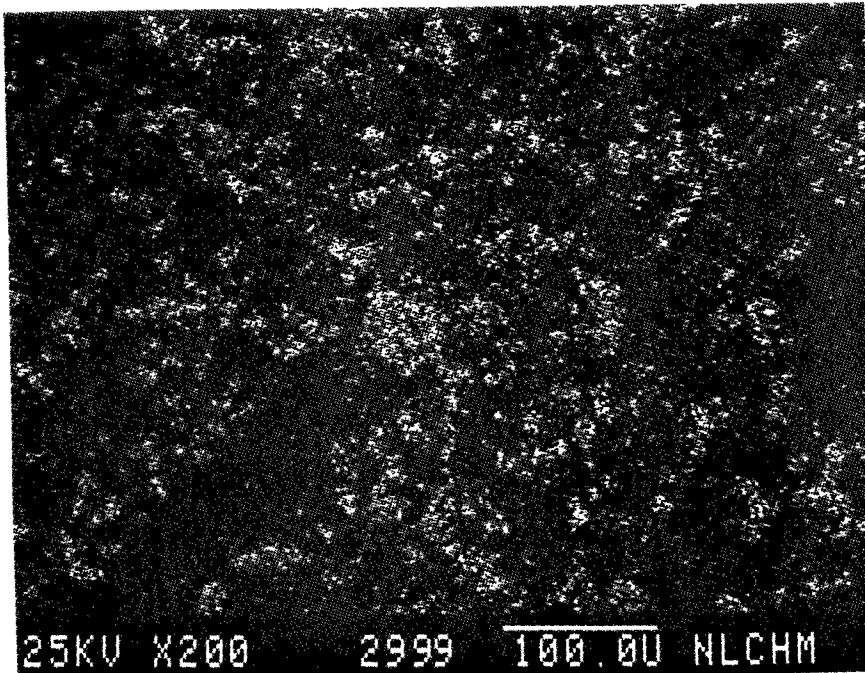


Figure 398

Si X-Ray Image of Figure 396

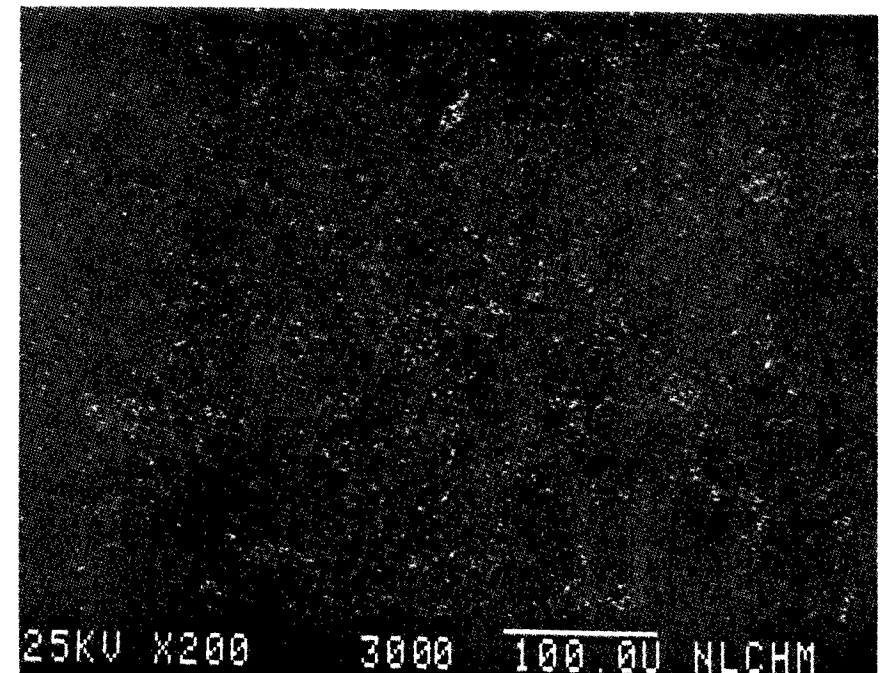


Figure 399

S X-Ray Image of Figure 396

SEM IMAGES OF SAMPLE #

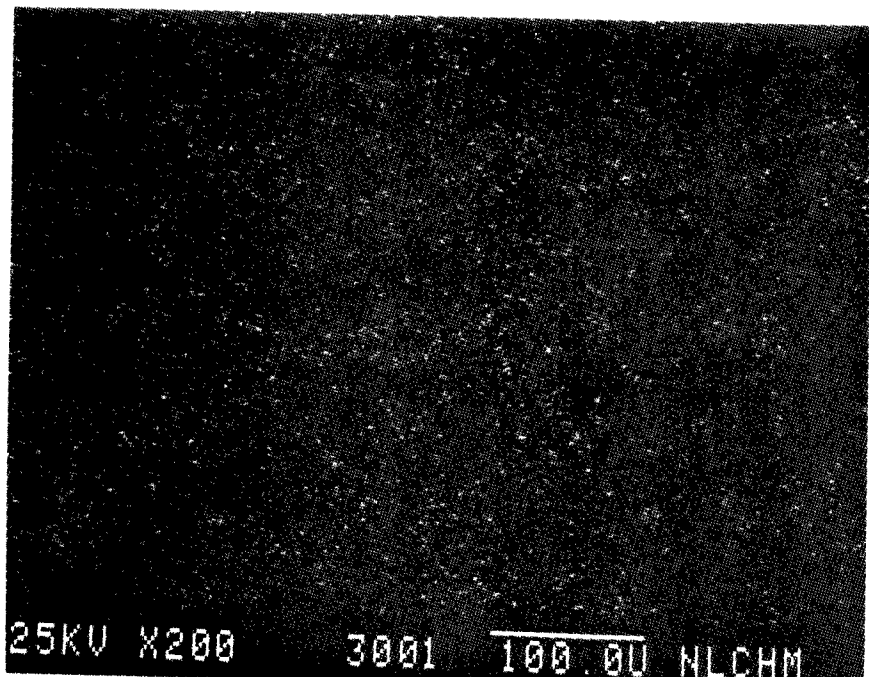


Figure 400 K X-Ray Image of Figure 396

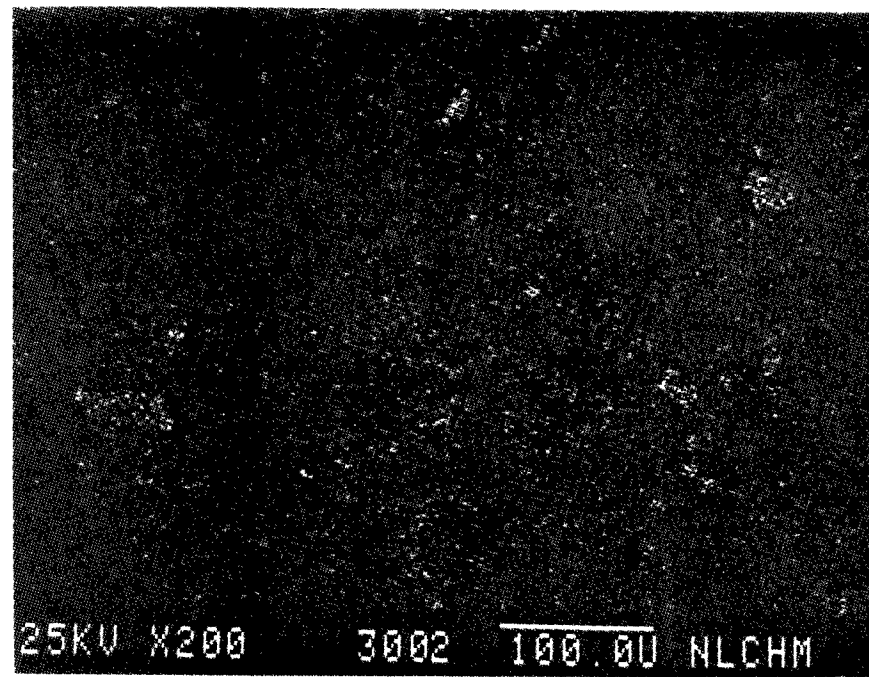


Figure 401 Ca X-Ray Image of Figure 396

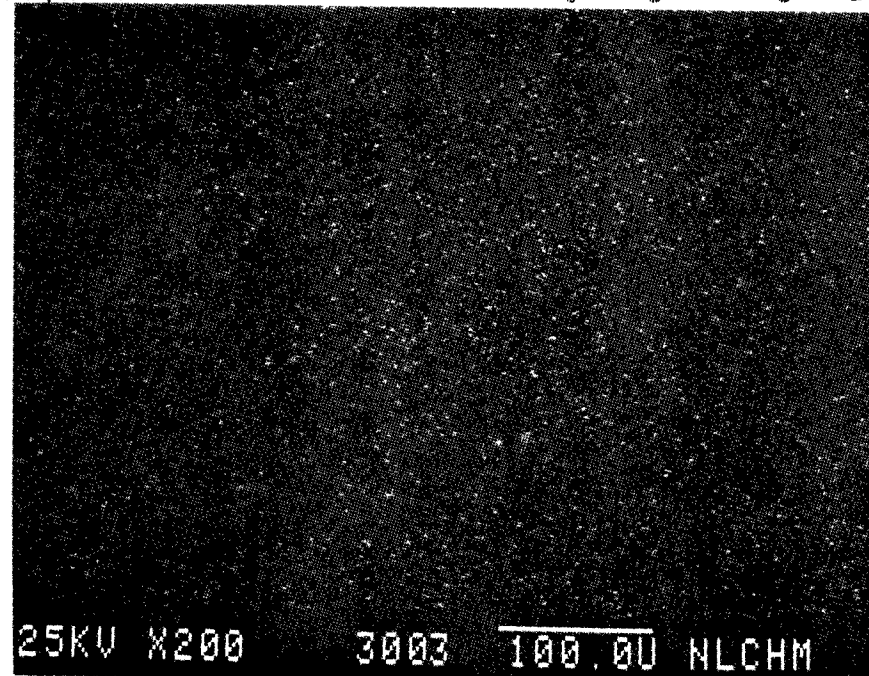


Figure 402 Ti X-Ray Image of Figure 396

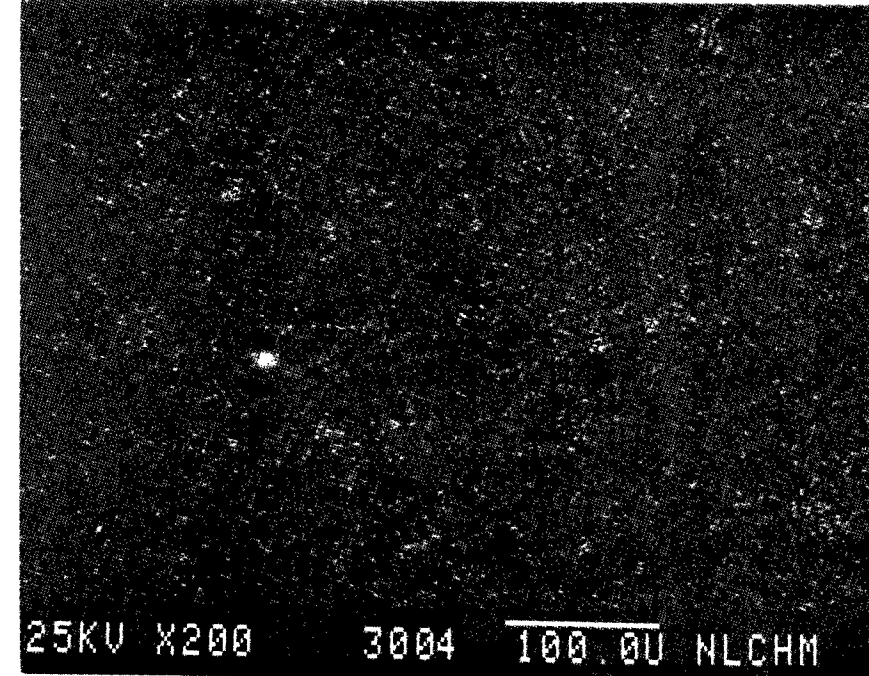


Figure 403 Fe X-Ray Image of Figure 396



SEM IMAGES OF SAMPLE #

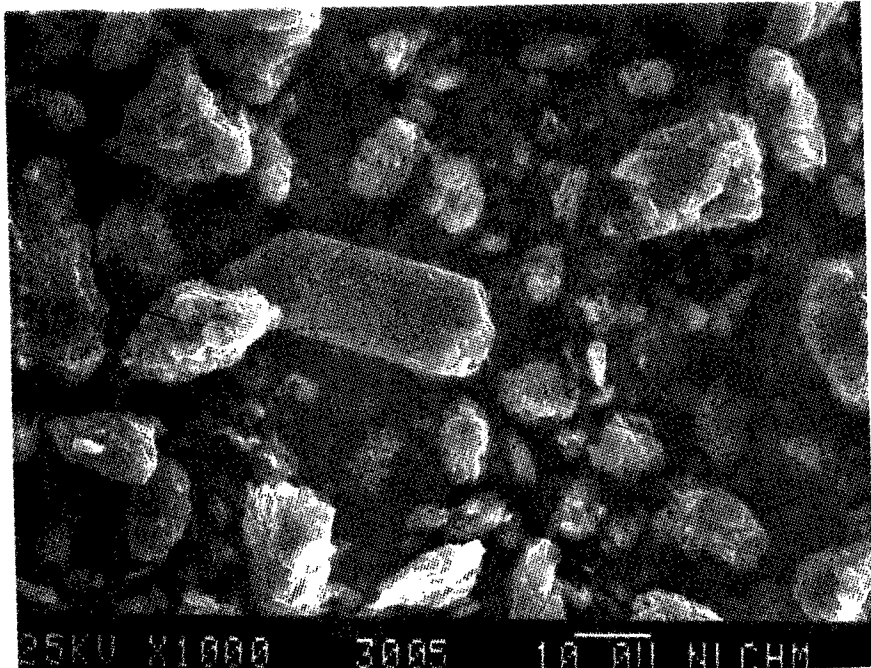


Figure 404

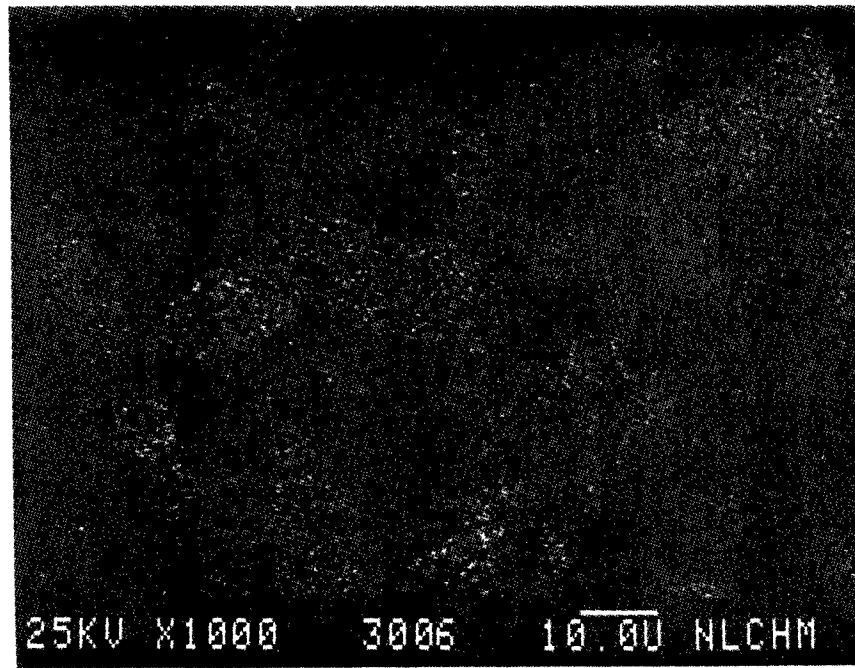


Figure 405

AL X-Ray Image of Figure 404

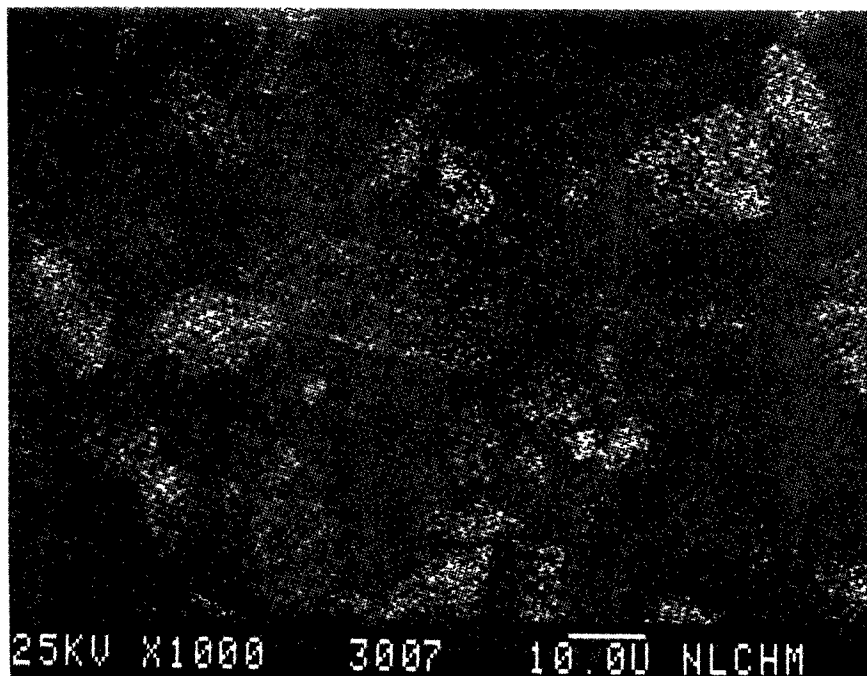


Figure 406

Si X-Ray Image of Figure 404

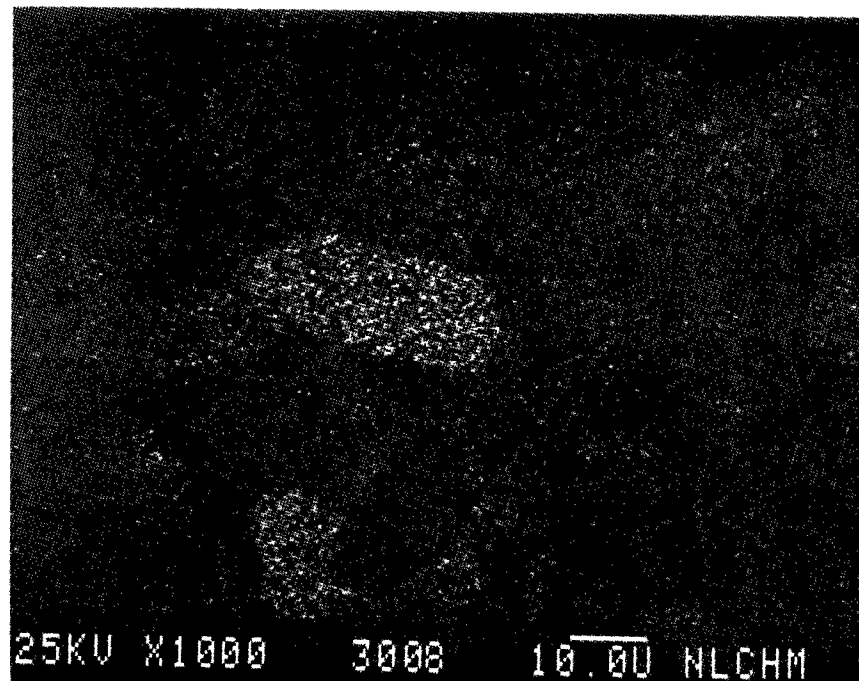


Figure 407

S X-Ray Image of Figure 404

SEM IMAGES OF SAMPLE #

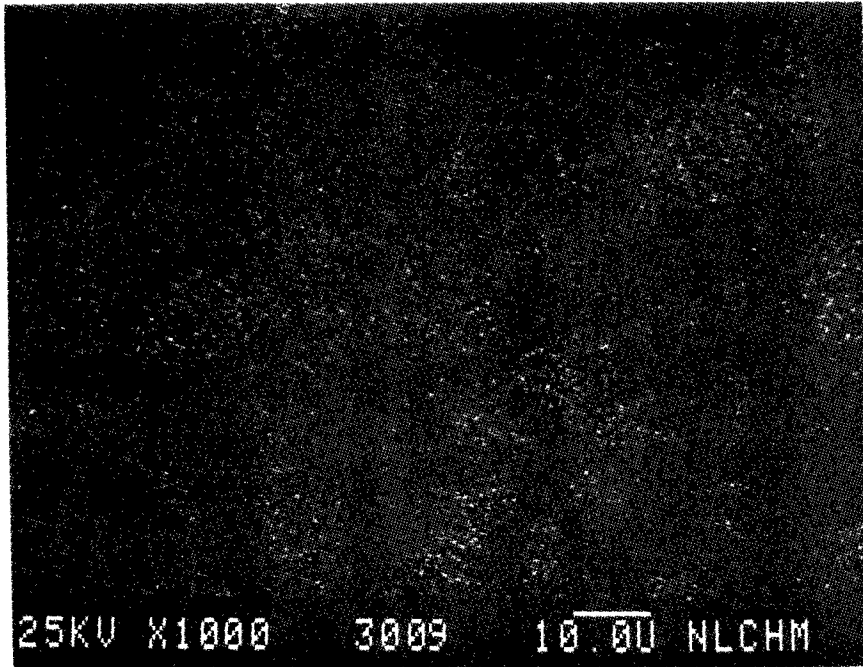


Figure 408

K X-Ray Image of Figure 404

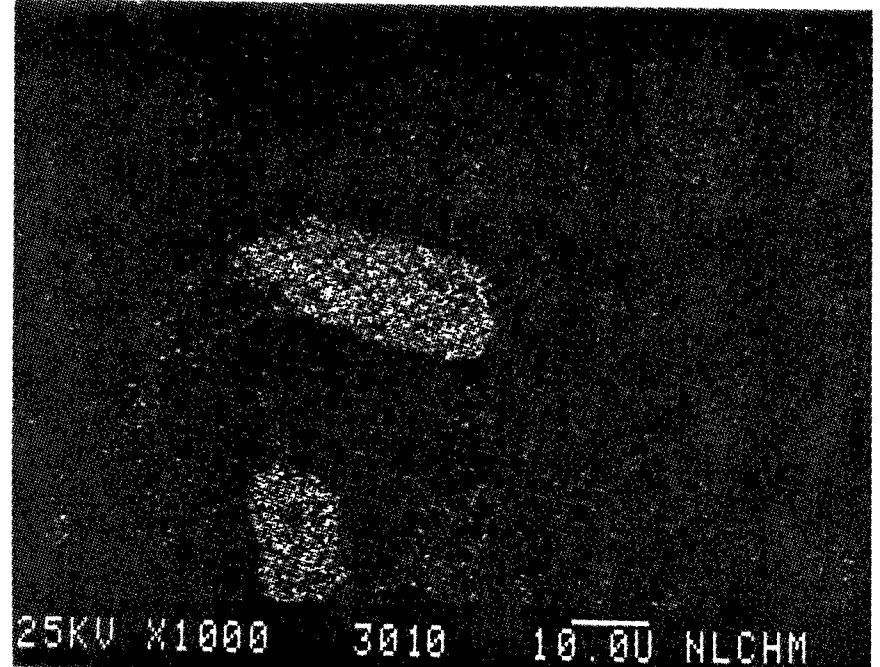


Figure 409

Ca X-Ray Image of Figure 404

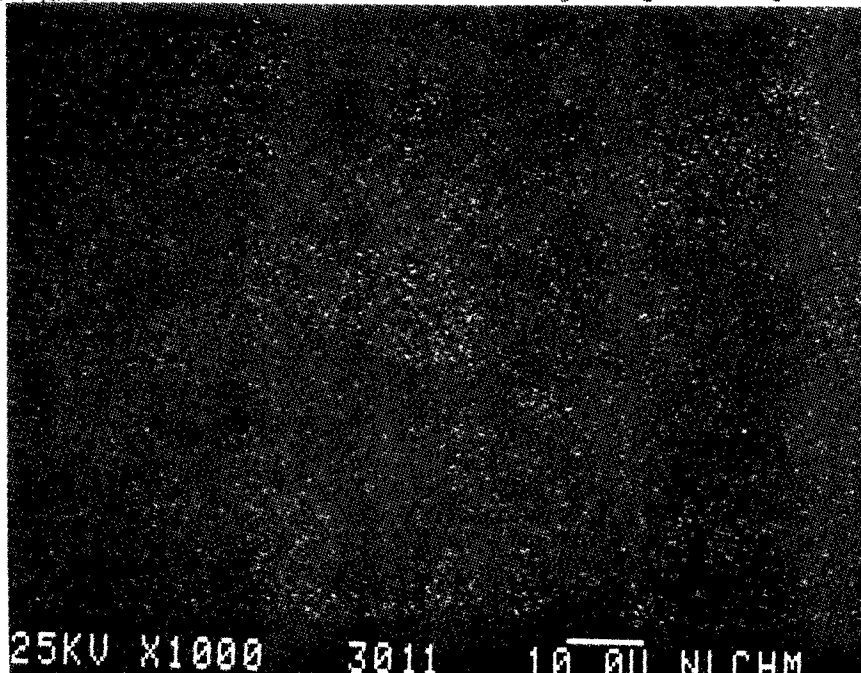


Figure 410

Ti X-Ray Image of Figure 404

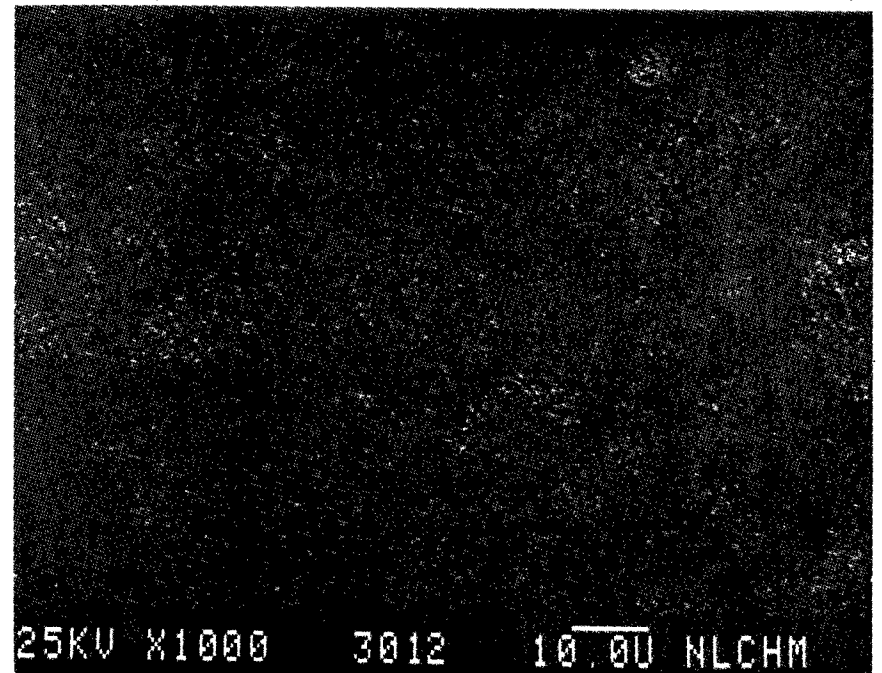


Figure 411

Fe X-Ray Image of Figure 404



SEM IMAGES OF SAMPLE #

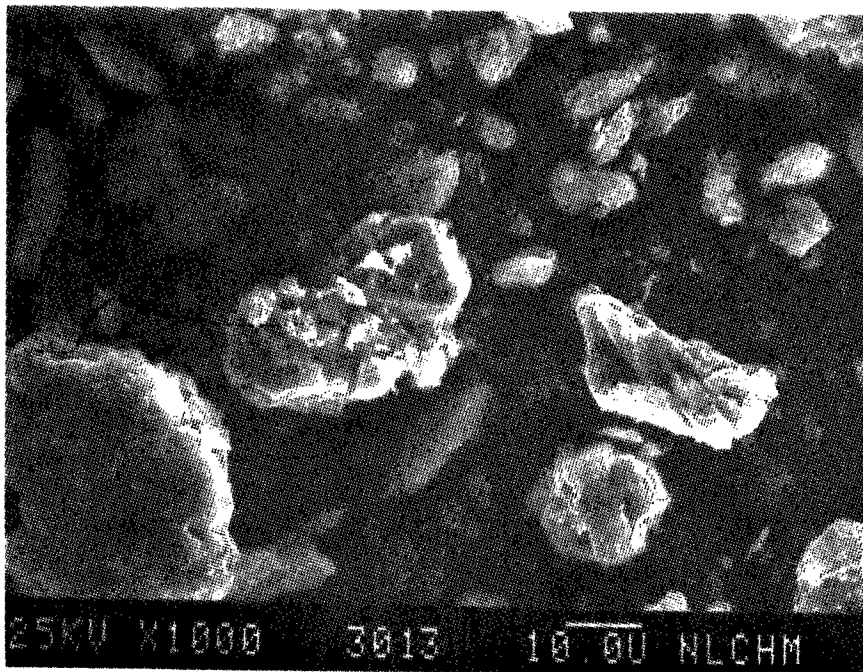


Figure 412

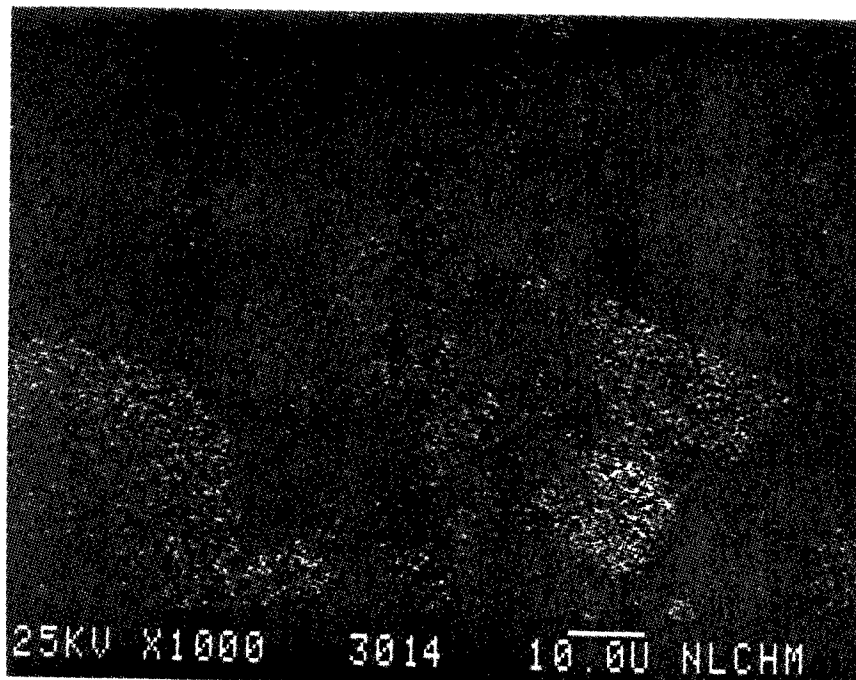


Figure 413

AL X-Ray Image of Figure 412

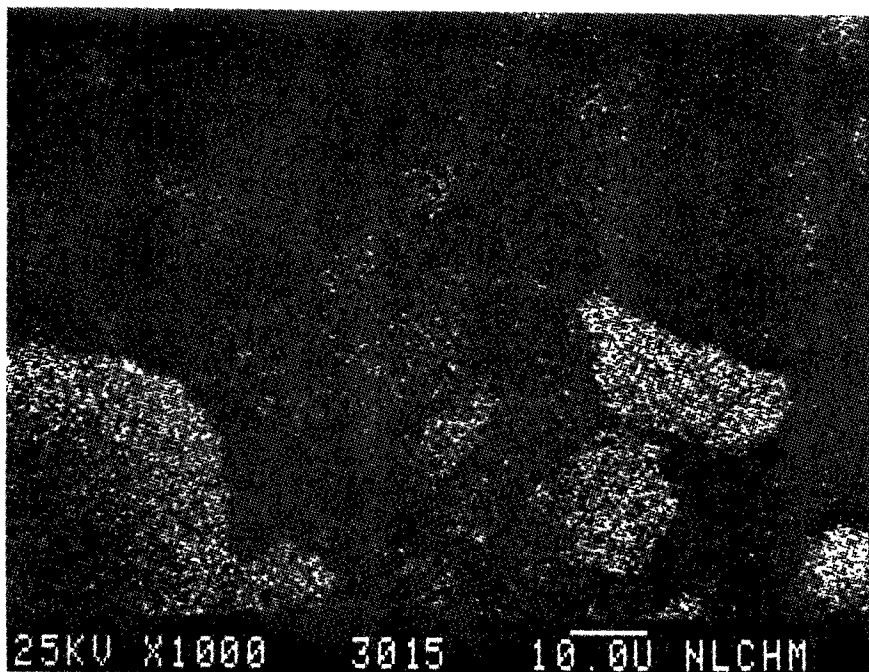


Figure 414

Si X-Ray Image of Figure 412

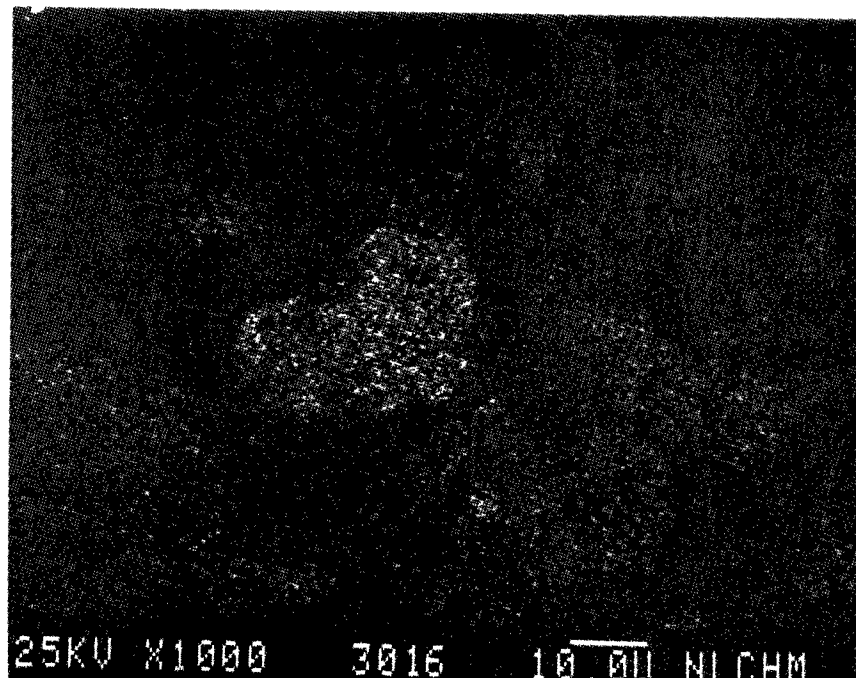


Figure 415

S X-Ray Image of Figure 412

SEM IMAGES OF SAMPLE #

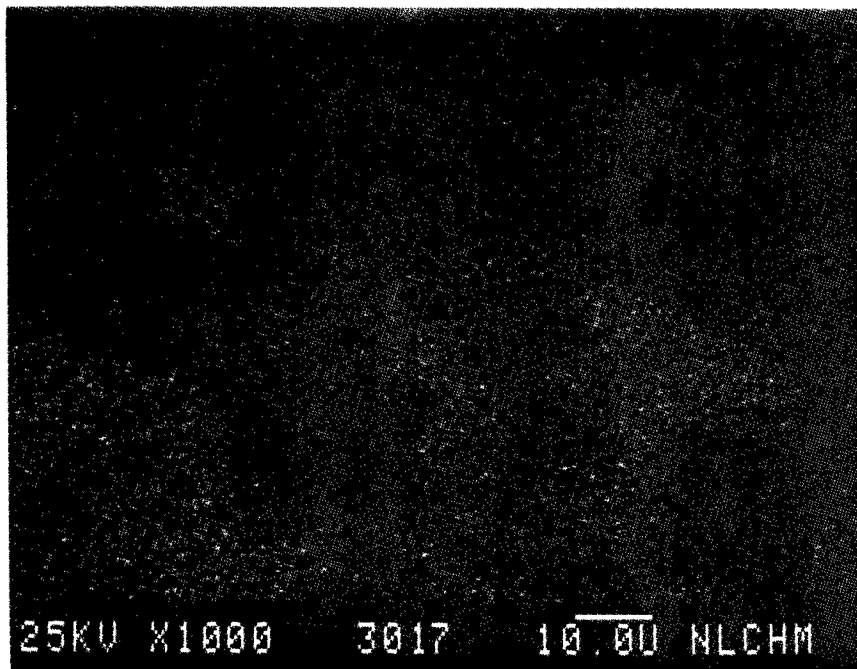


Figure 416

K X-Ray Image of Figure 412

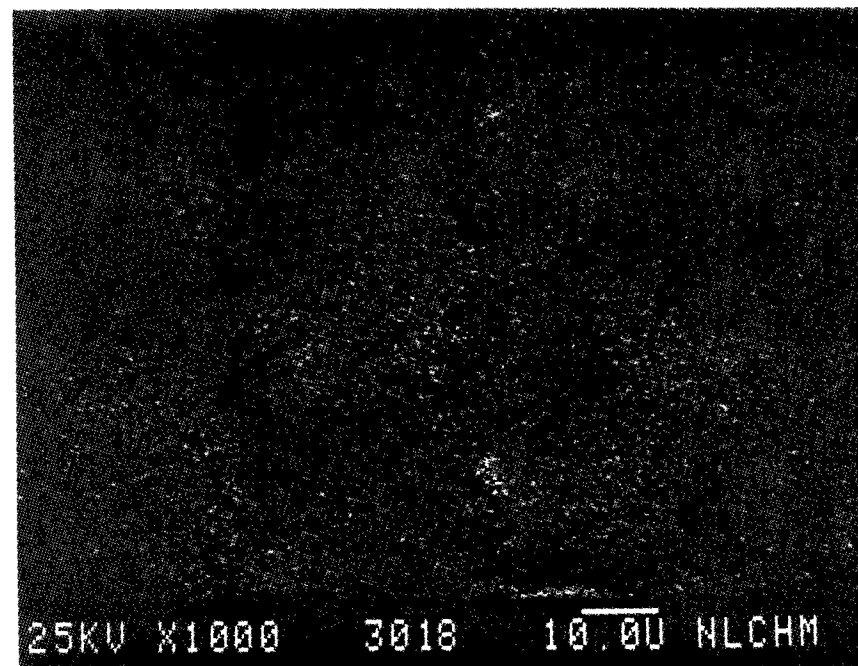


Figure 417

Ca X-Ray Image of Figure 412

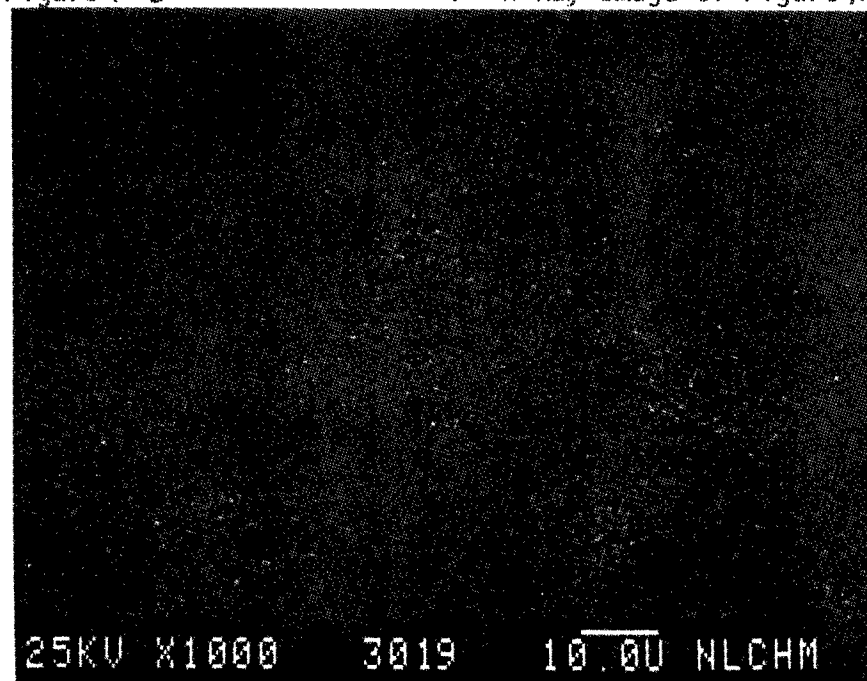


Figure 418

Ti X-Ray Image of Figure 412

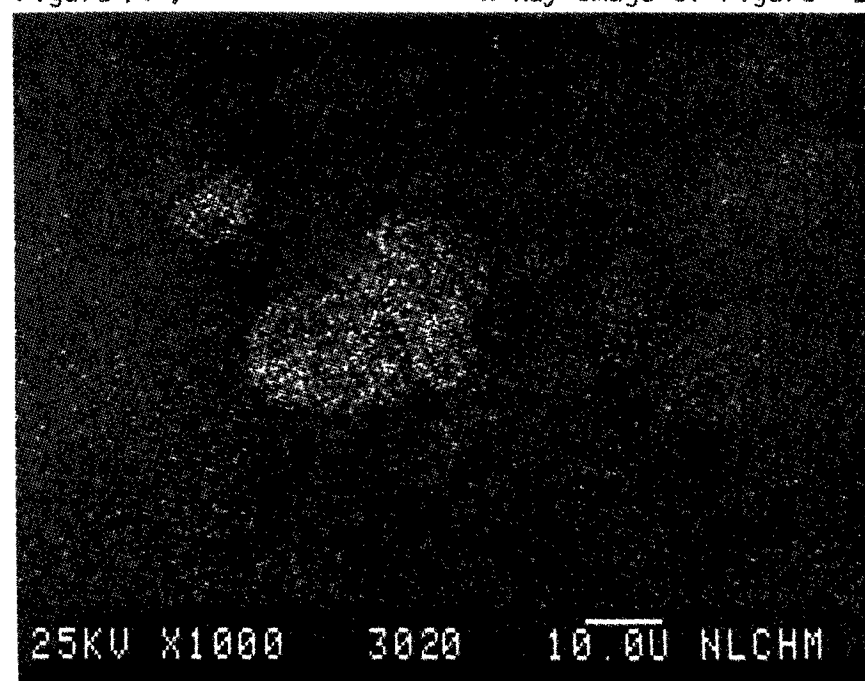


Figure 419

Fe X-Ray Image of Figure 412

SEM IMAGES OF SAMPLE #

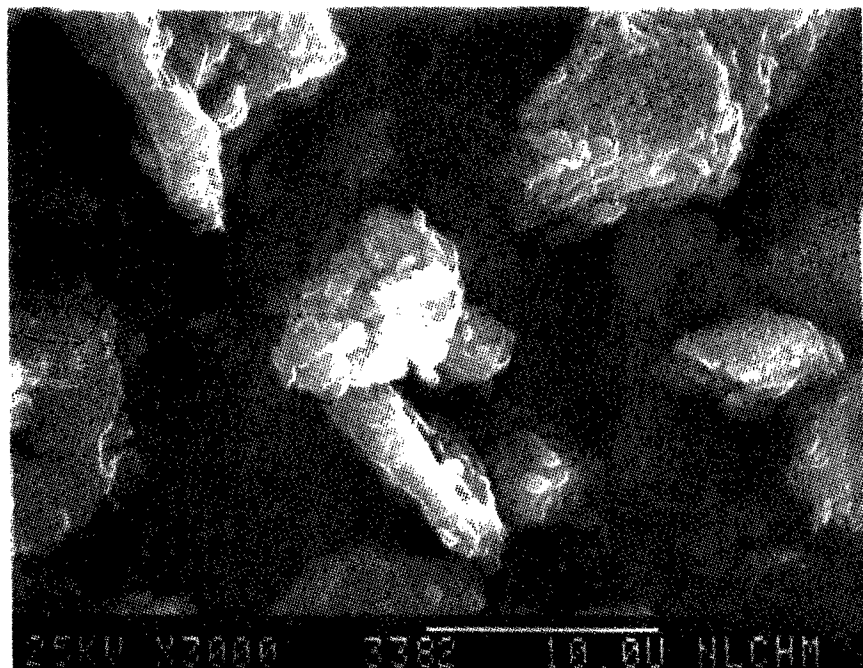


Figure 420

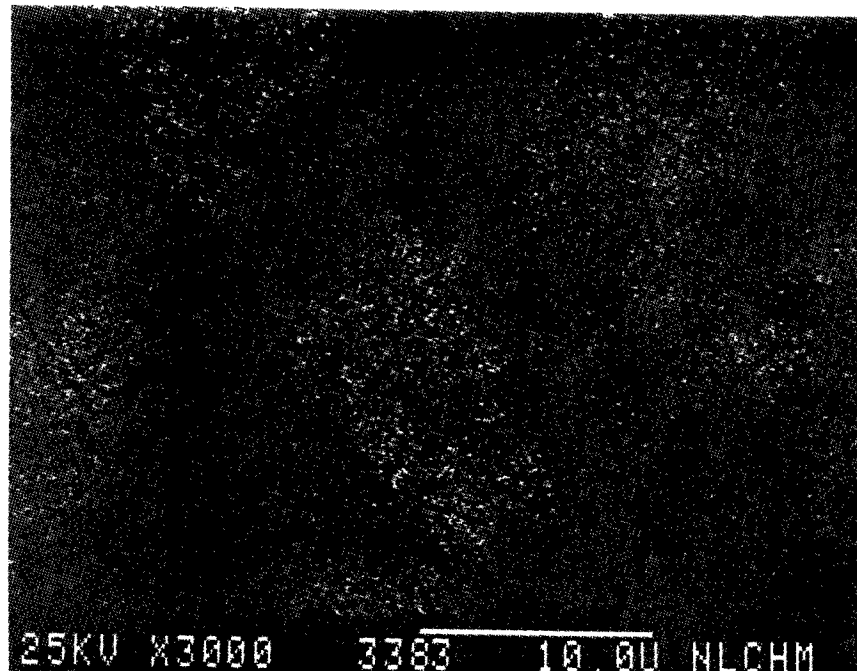


Figure 421

AL X-Ray Image of Figure 420

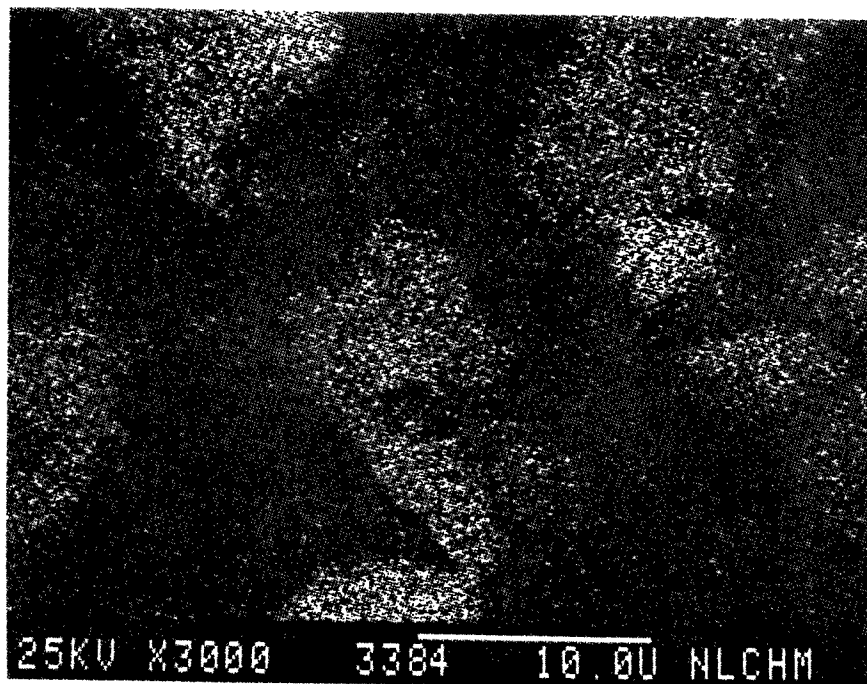


Figure 422

Si X-Ray Image of Figure 420

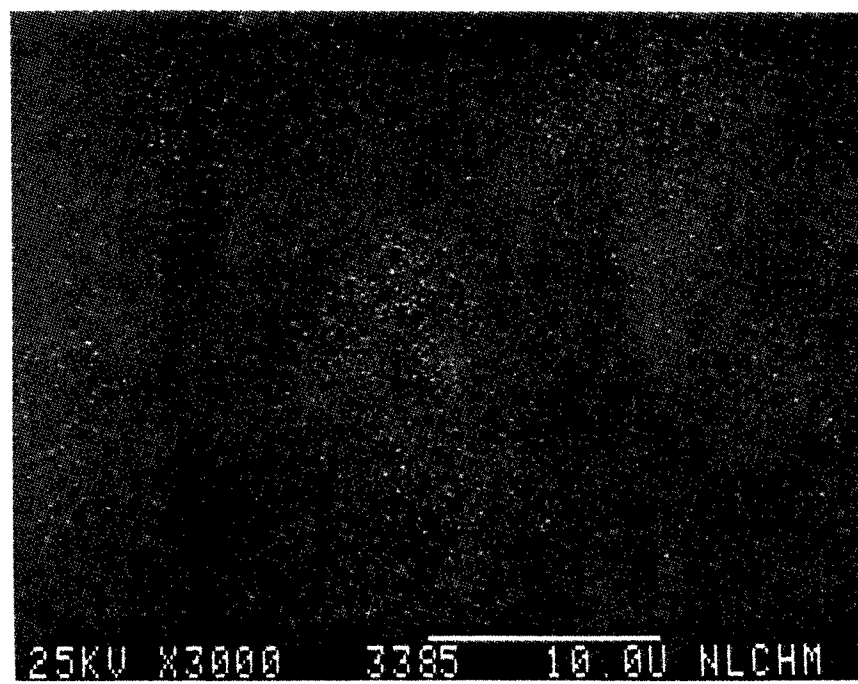


Figure 423

S X-Ray Image of Figure 420

SEM IMAGES OF SAMPLE #

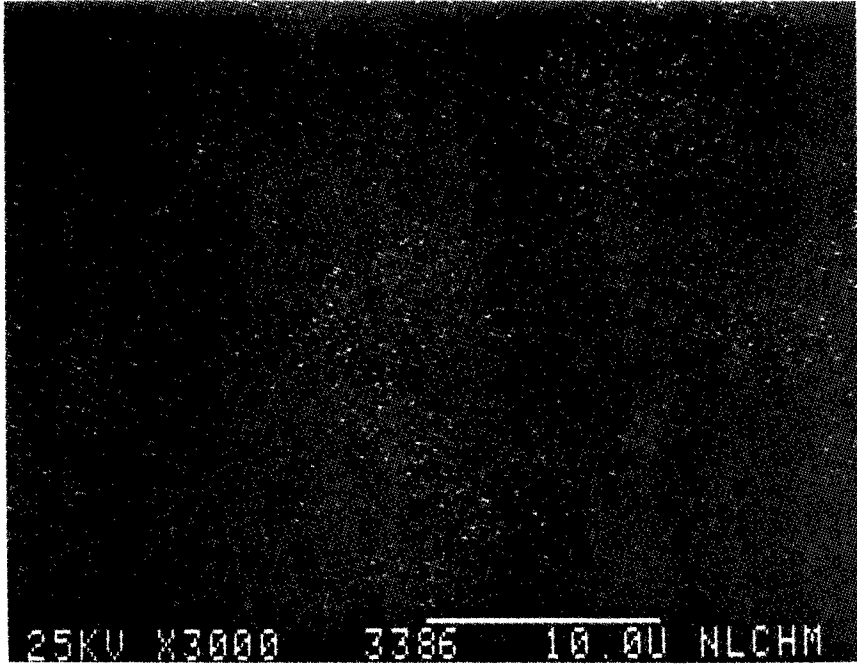


Figure 424

K X-Ray Image of Figure 420

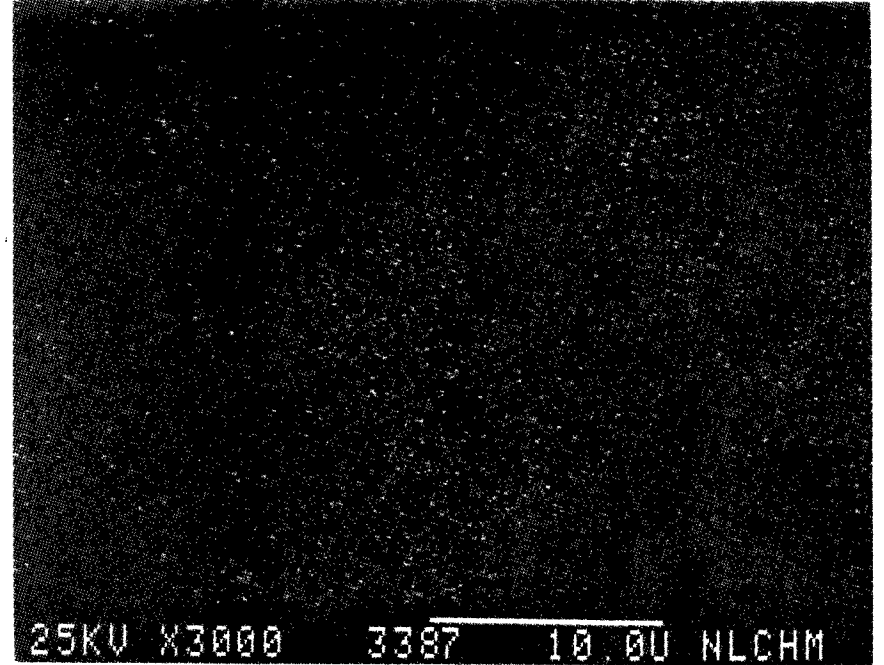


Figure 425

Ca X-Ray Image of Figure 420

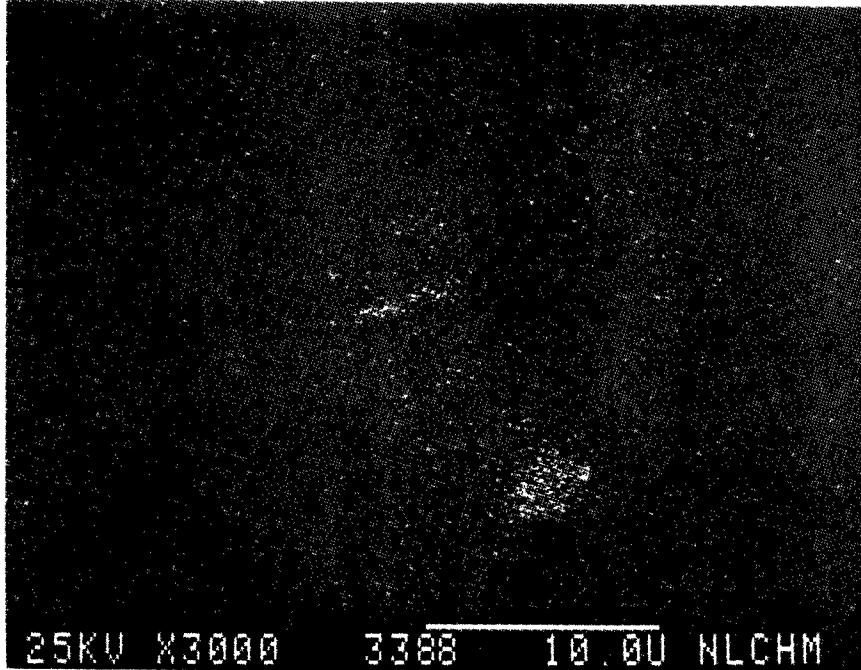


Figure 426

Tr X-Ray Image of Figure 420

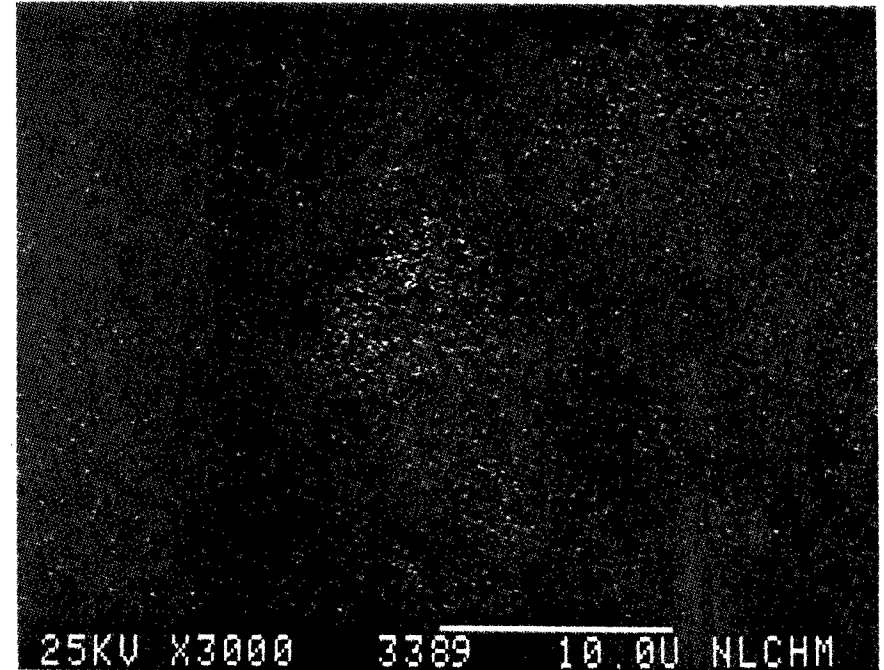


Figure 427

Fe X-Ray Image of Figure 420

SEM IMAGES OF SAMPLE #

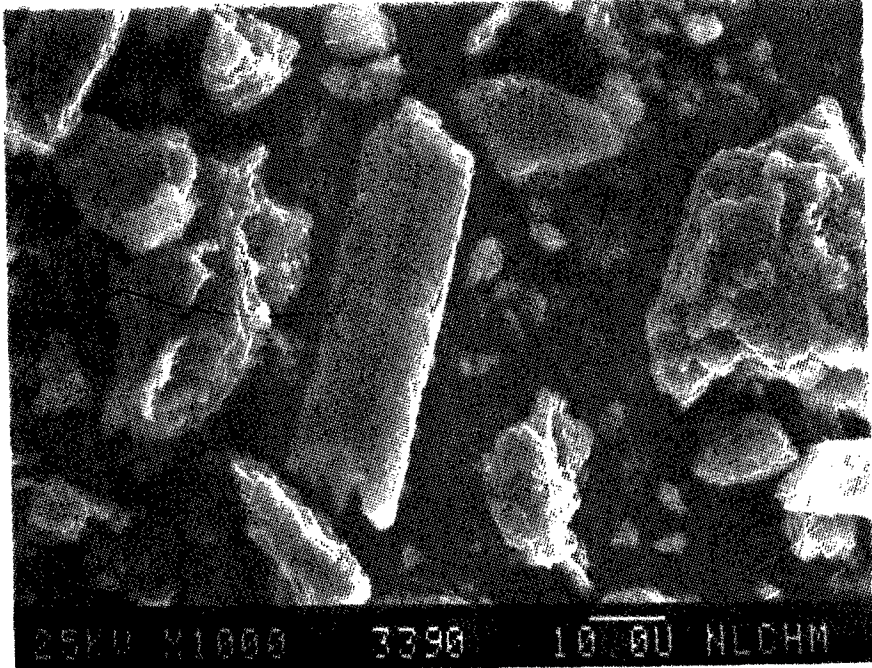


Figure 428

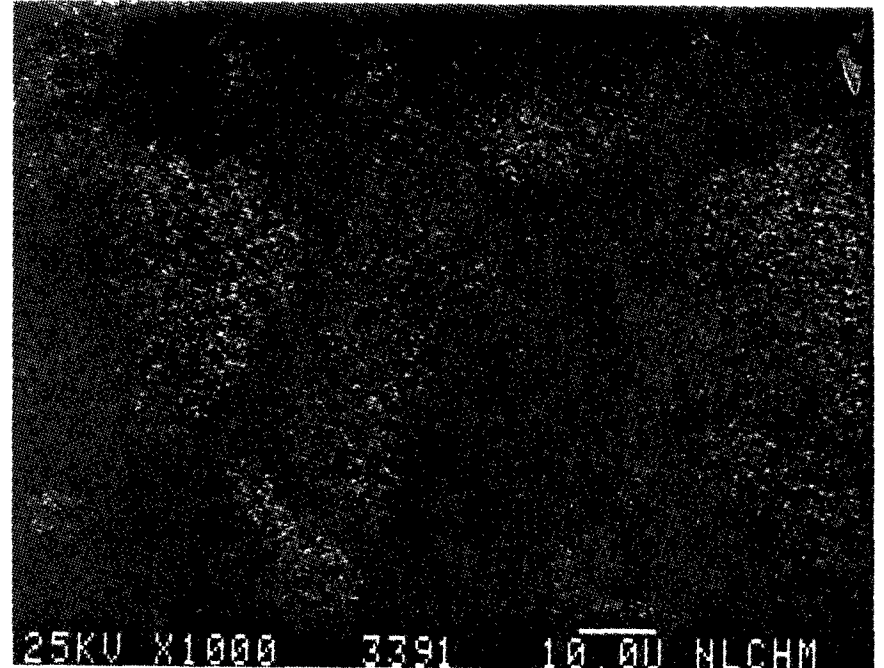


Figure 429

AL X-Ray Image of Figure 428

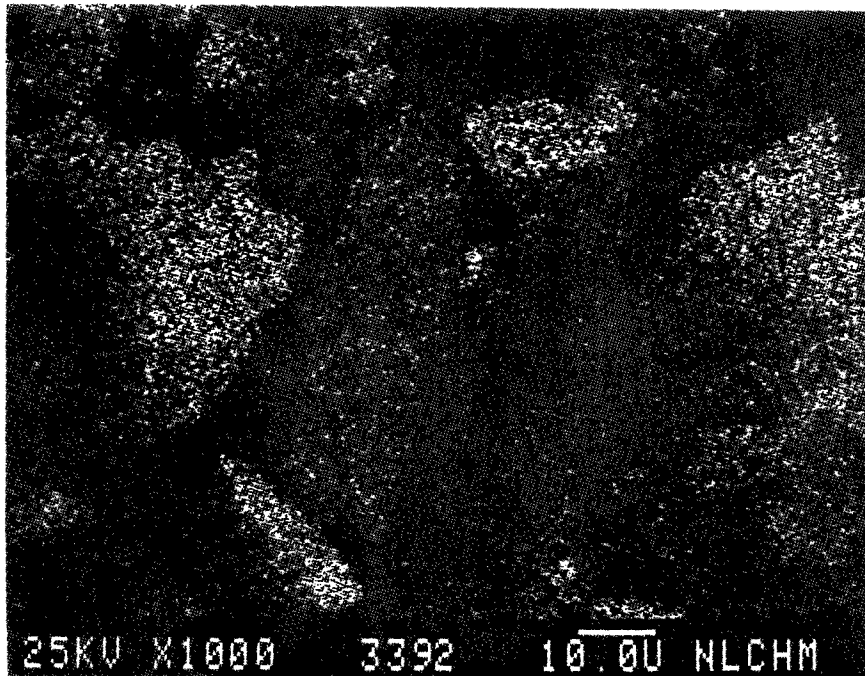


Figure 430

Si X-Ray Image of Figure 428

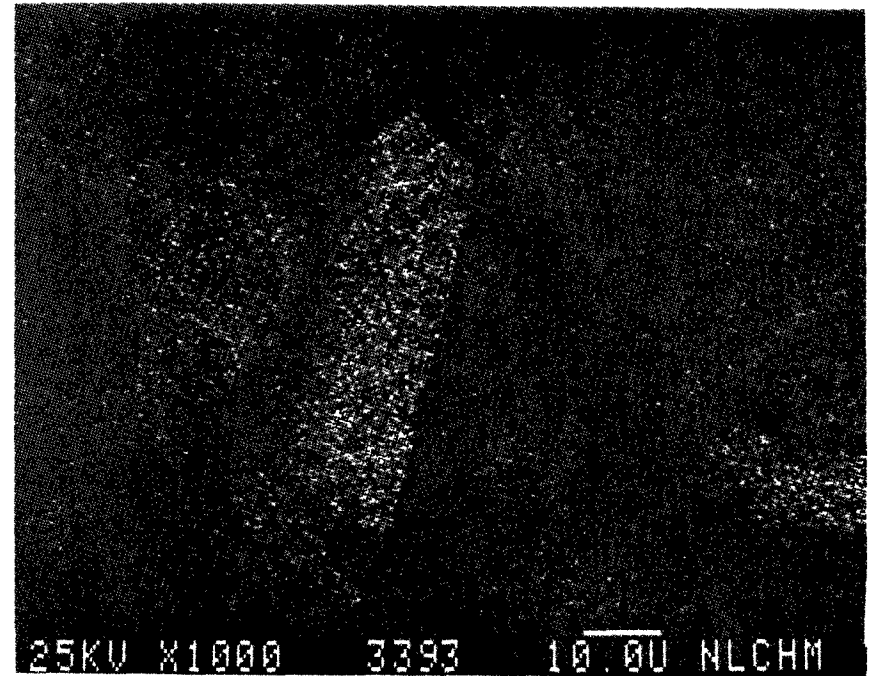


Figure 431

S X-Ray Image of Figure 428



SEM IMAGES OF SAMPLE #

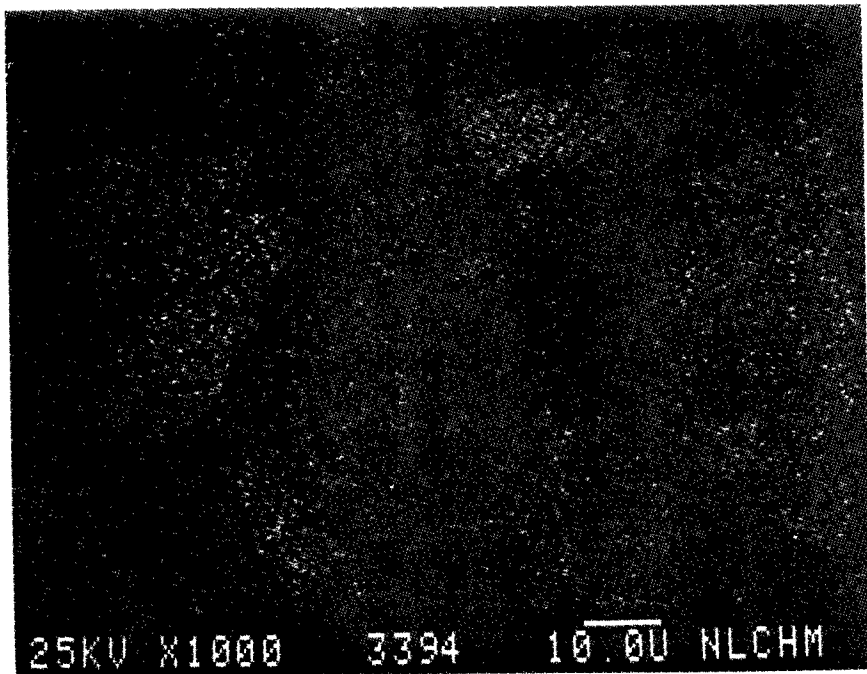


Figure 432

K X-Ray Image of Figure 428

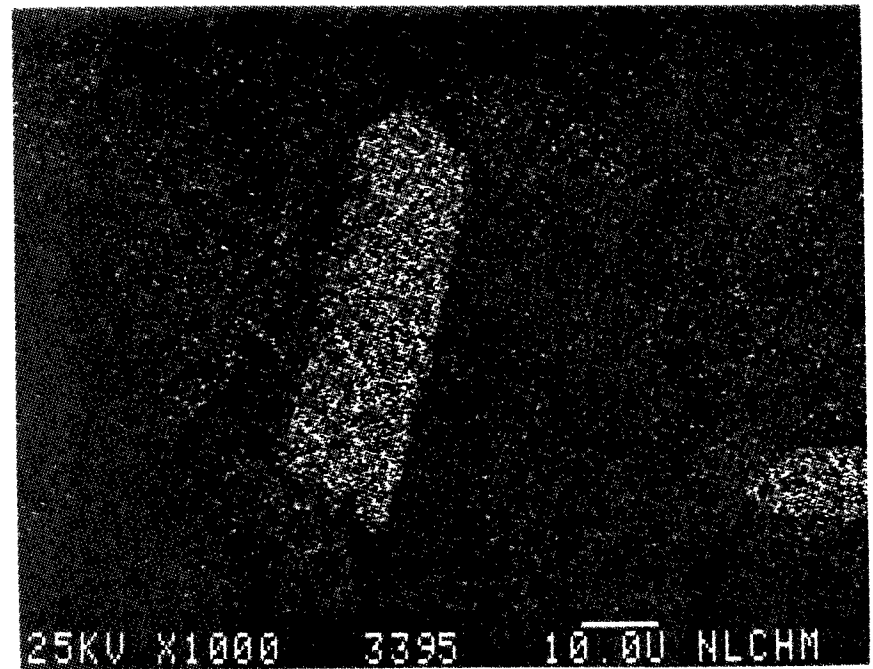


Figure 433

Ca X-Ray Image of Figure 428

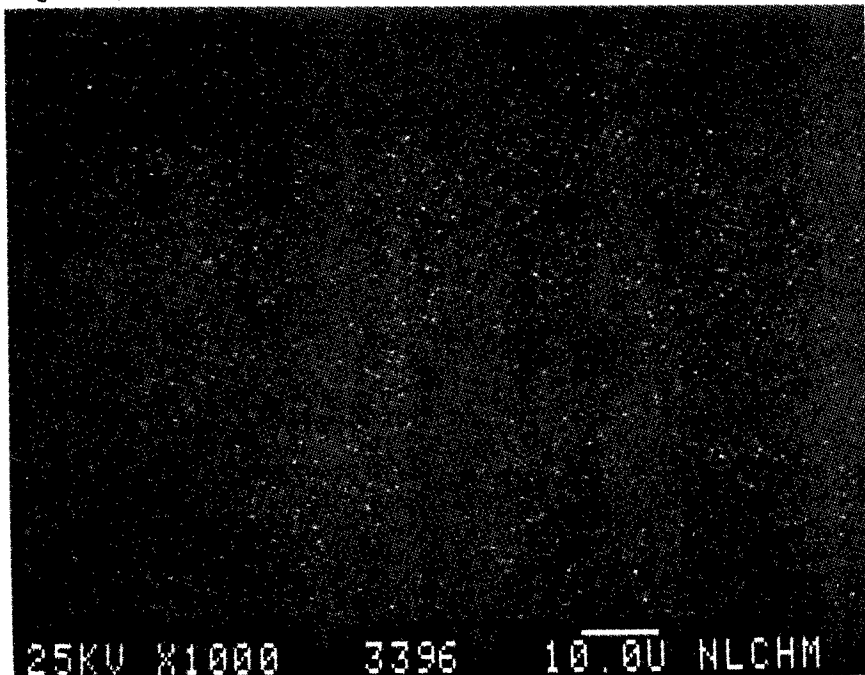


Figure 434

Ti X-Ray Image of Figure 428

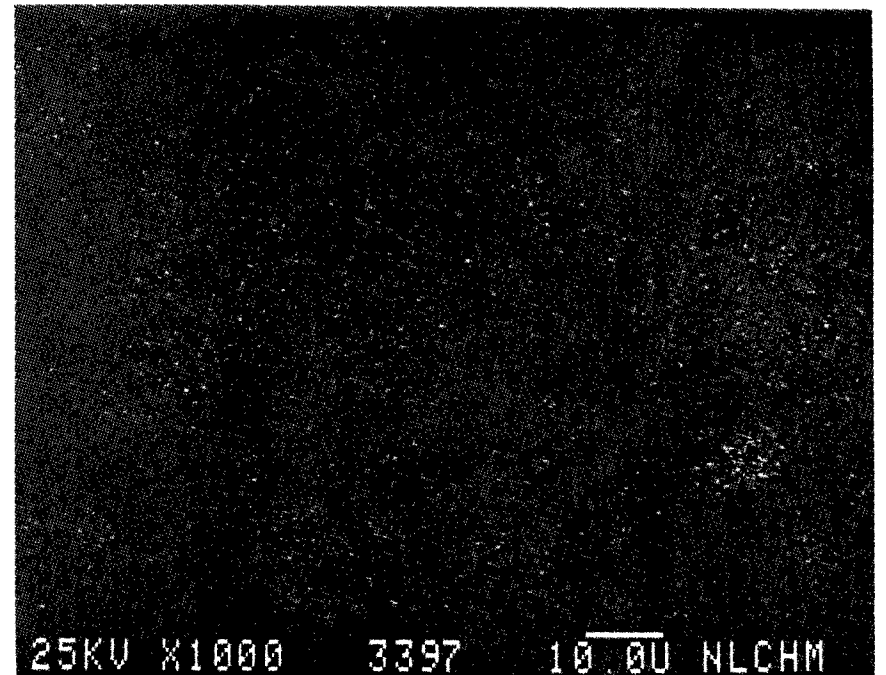


Figure 435

Fe X-Ray Image of Figure 428



SEM IMAGES OF SAMPLE #

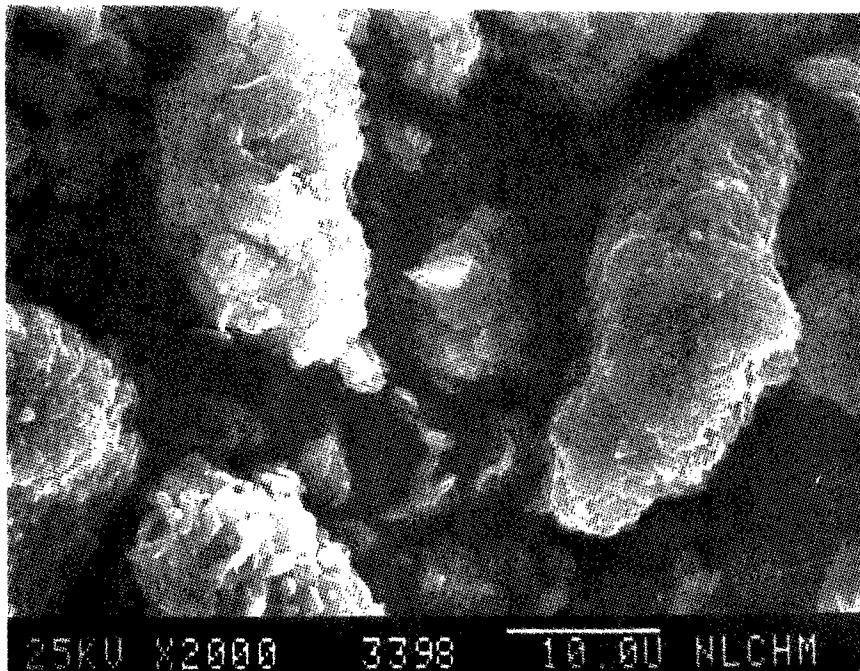


Figure 436

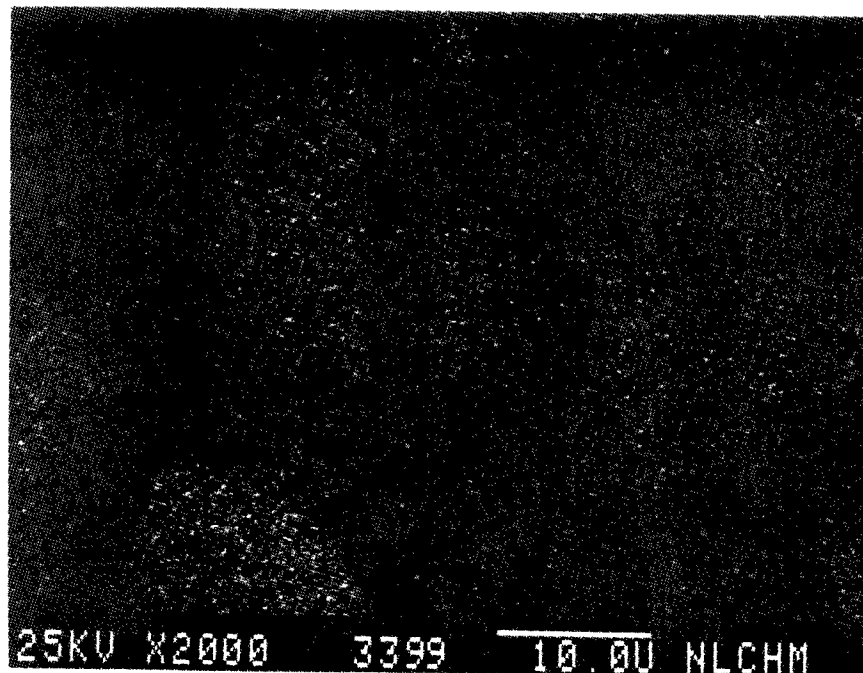


Figure 437

AL X-Ray Image of Figure 436

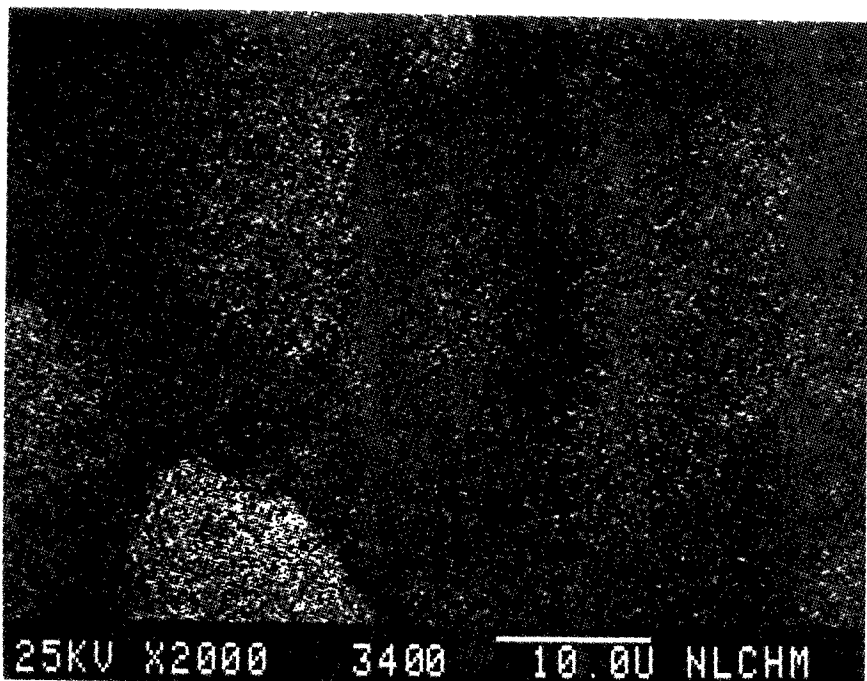


Figure 438

Si X-Ray Image of Figure 436

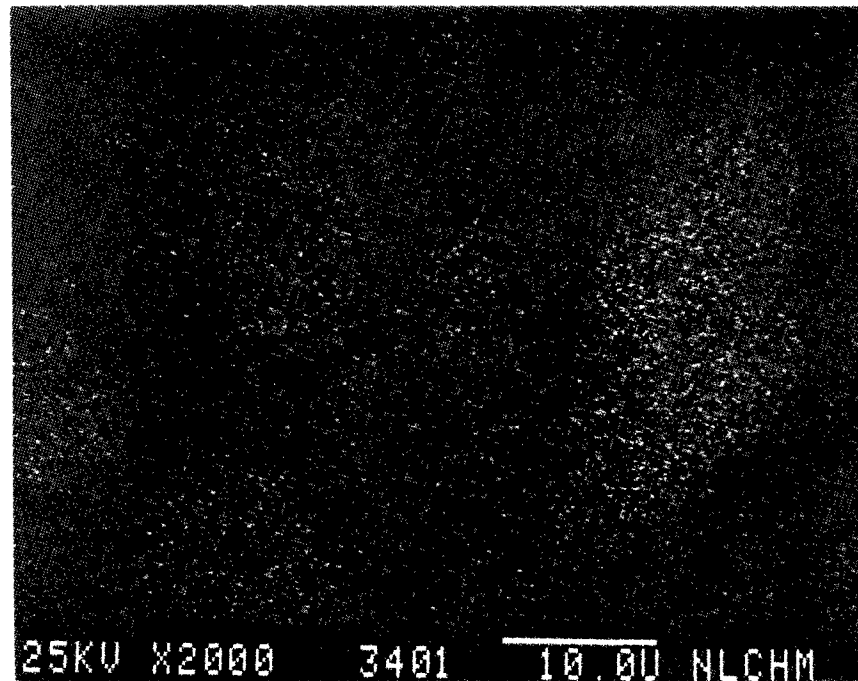


Figure 439

S X-Ray Image of Figure 436

SEM IMAGES OF SAMPLE #

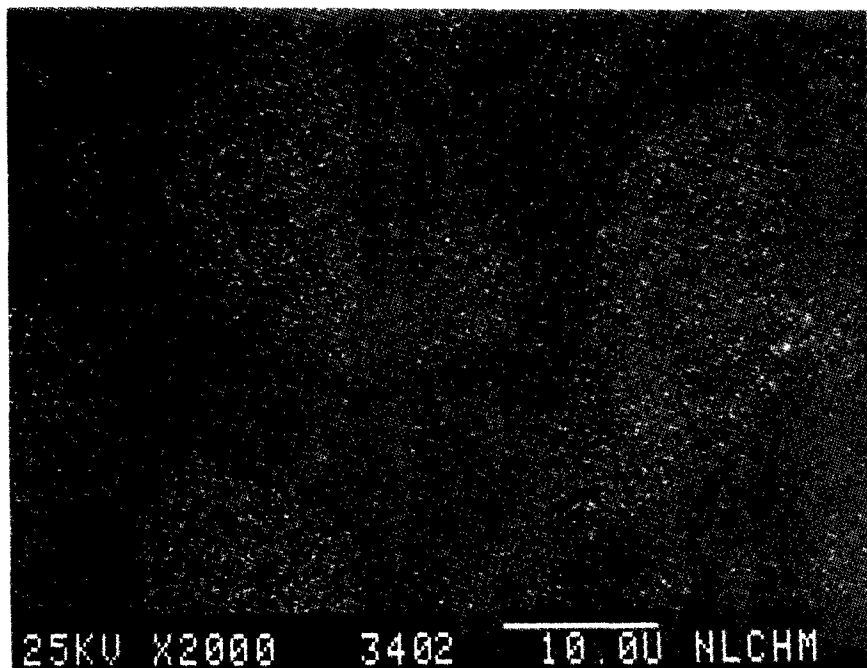


Figure 440

K X-Ray Image of Figure 436

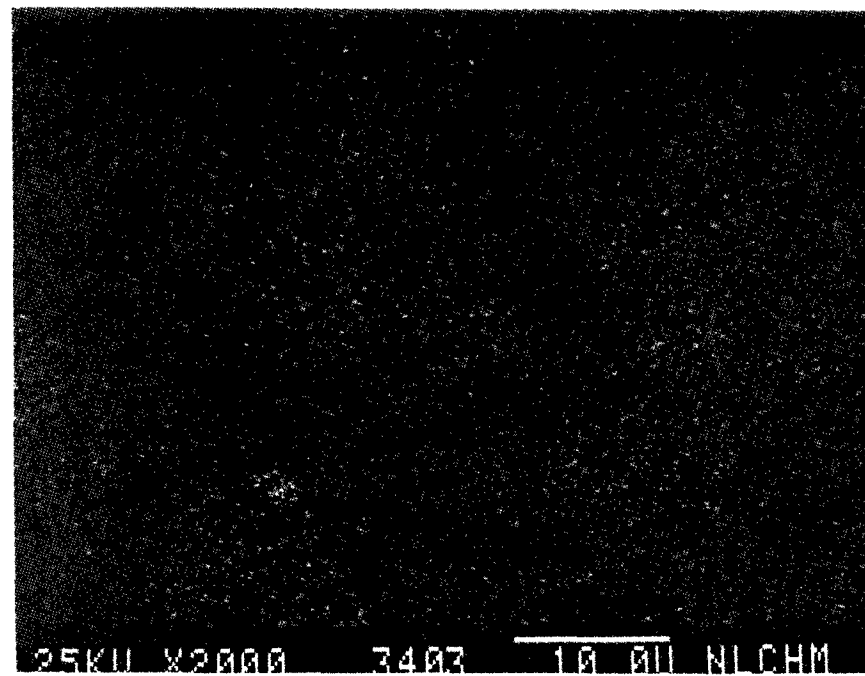


Figure 441

Ca X-Ray Image of Figure 436

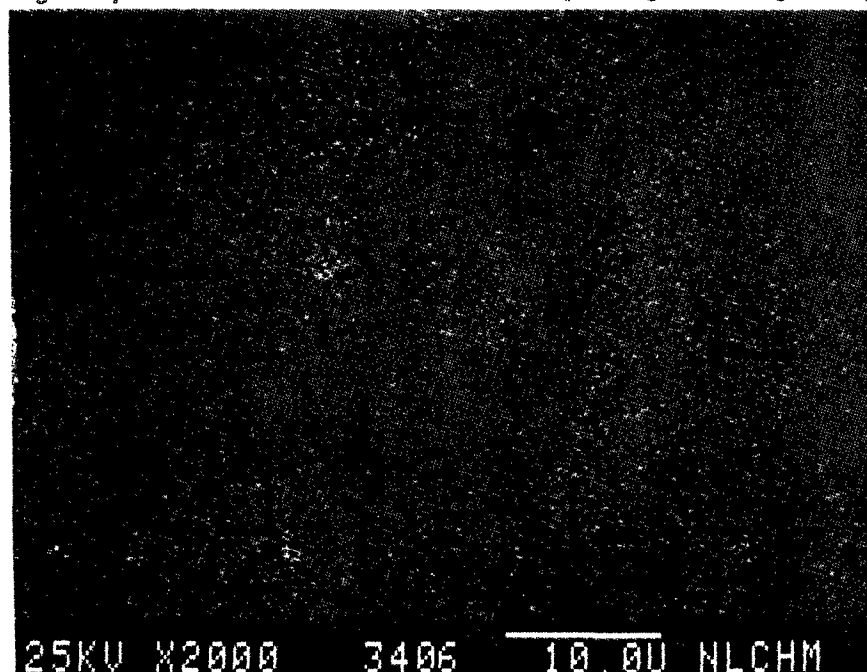


Figure 442

Ti X-Ray Image of Figure 436

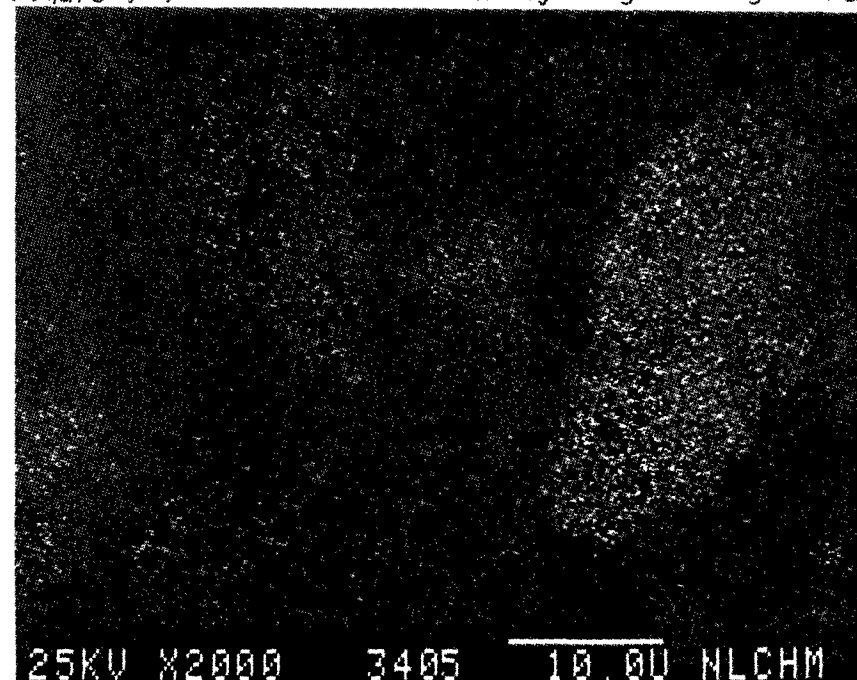


Figure 443

Fe X-Ray Image of Figure 436

ENERGY DISPERSIVE X-RAY ANALYSIS

Analytical Number Illite

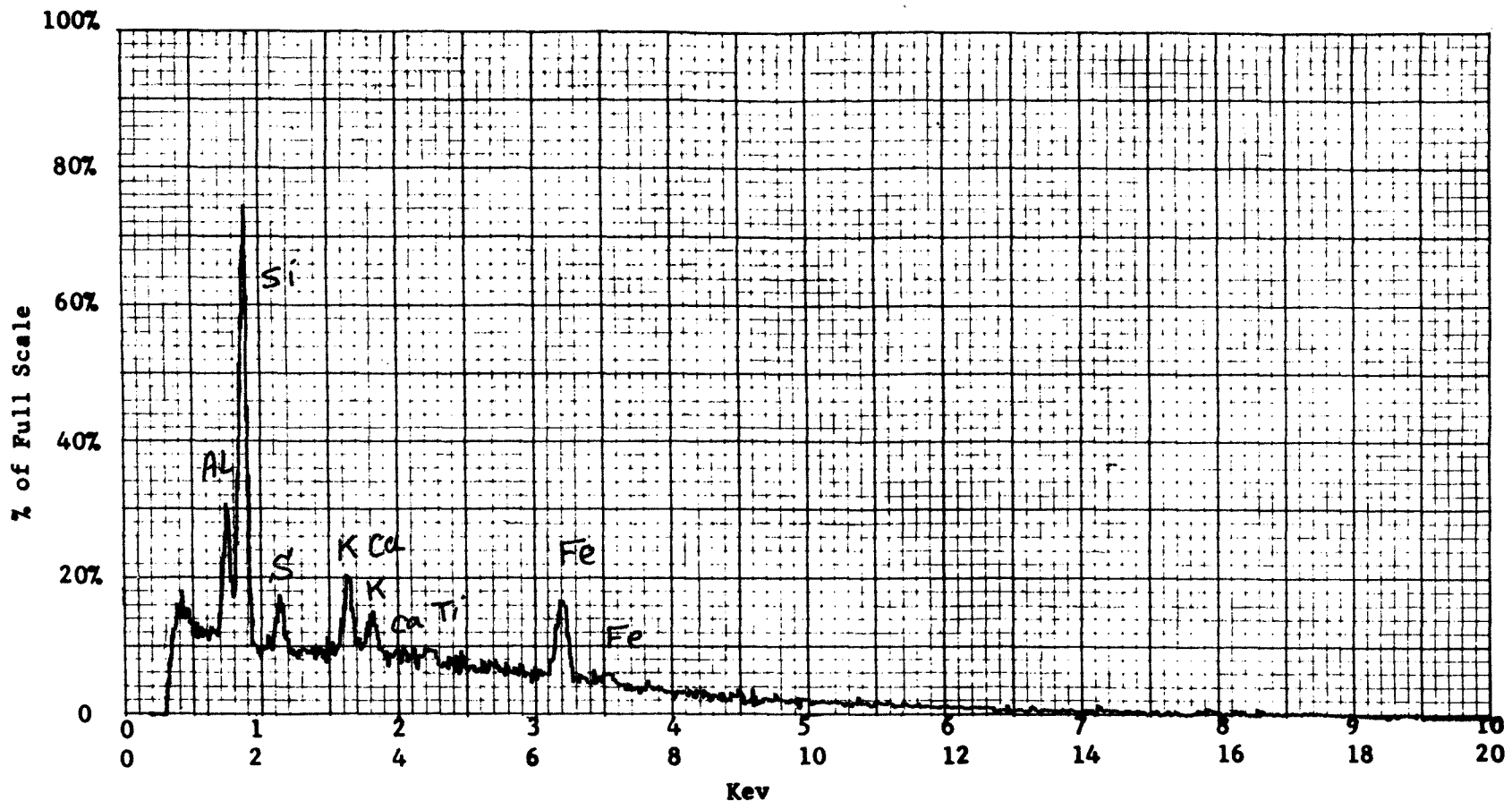
Operator \_\_\_\_\_ Date \_\_\_\_\_

Accelerating Potential 25 KeV

Total Counts Acquired 1.0 min.

Number Counts Full Scale 2K

Number of eV per channel 20



Sample peculiarities and remarks: FIGURE 444: AREA SCAN

ENERGY DISPERSIVE X-RAY ANALYSIS

Analytical Number Illite

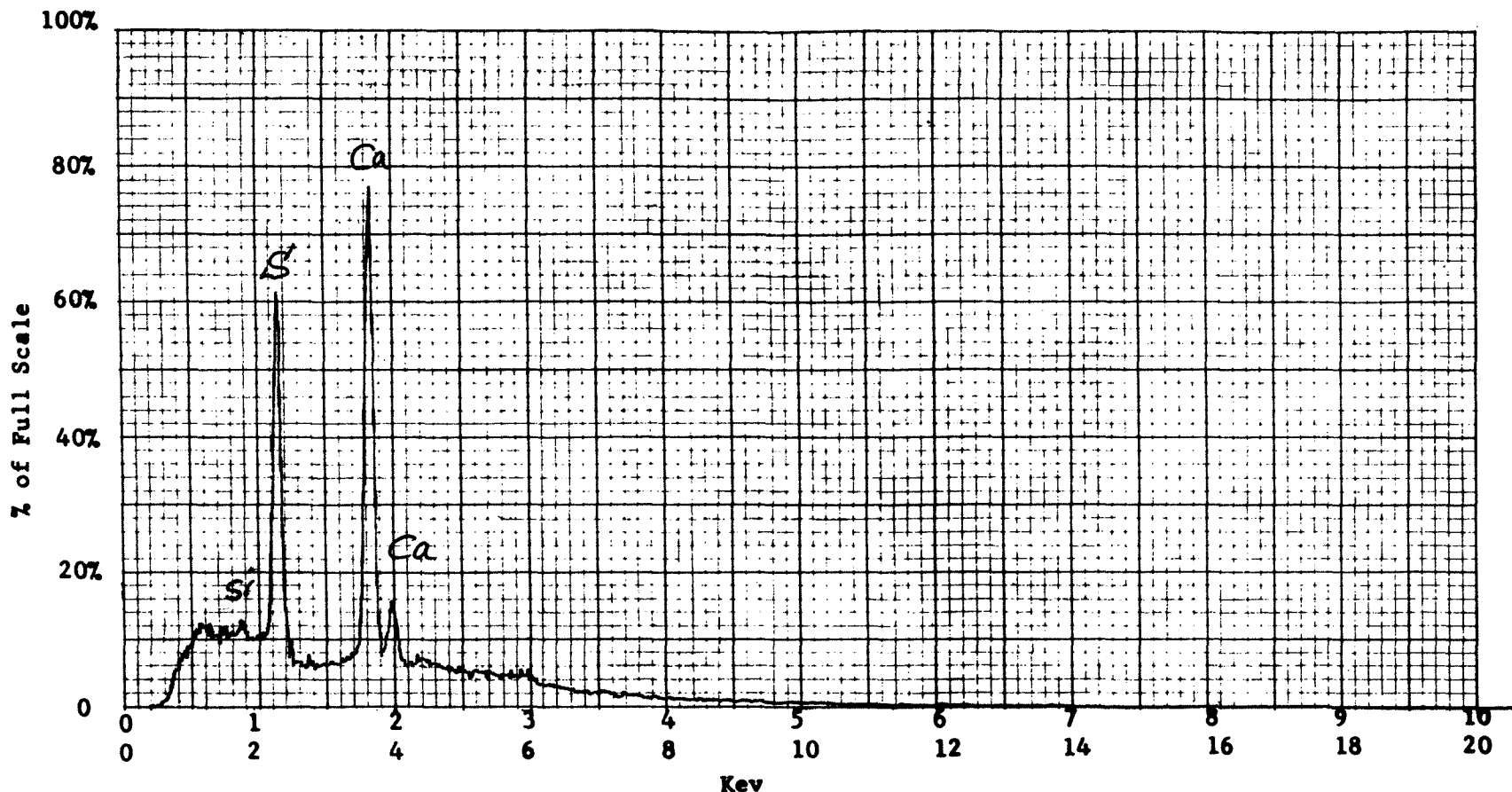
Operator \_\_\_\_\_ Date \_\_\_\_\_

Accelerating Potential 25 KeV

Total Counts Acquired 1.0 min.

Number Counts Full Scale 5K

Number of eV per channel 20



Sample peculiarities and remarks: FIGURE 445: POINT SCAN ON A HIGH Ca-S PARTICLE  
IN FIGURE 404

ENERGY DISPERSIVE X-RAY ANALYSIS

Analytical Number Illite

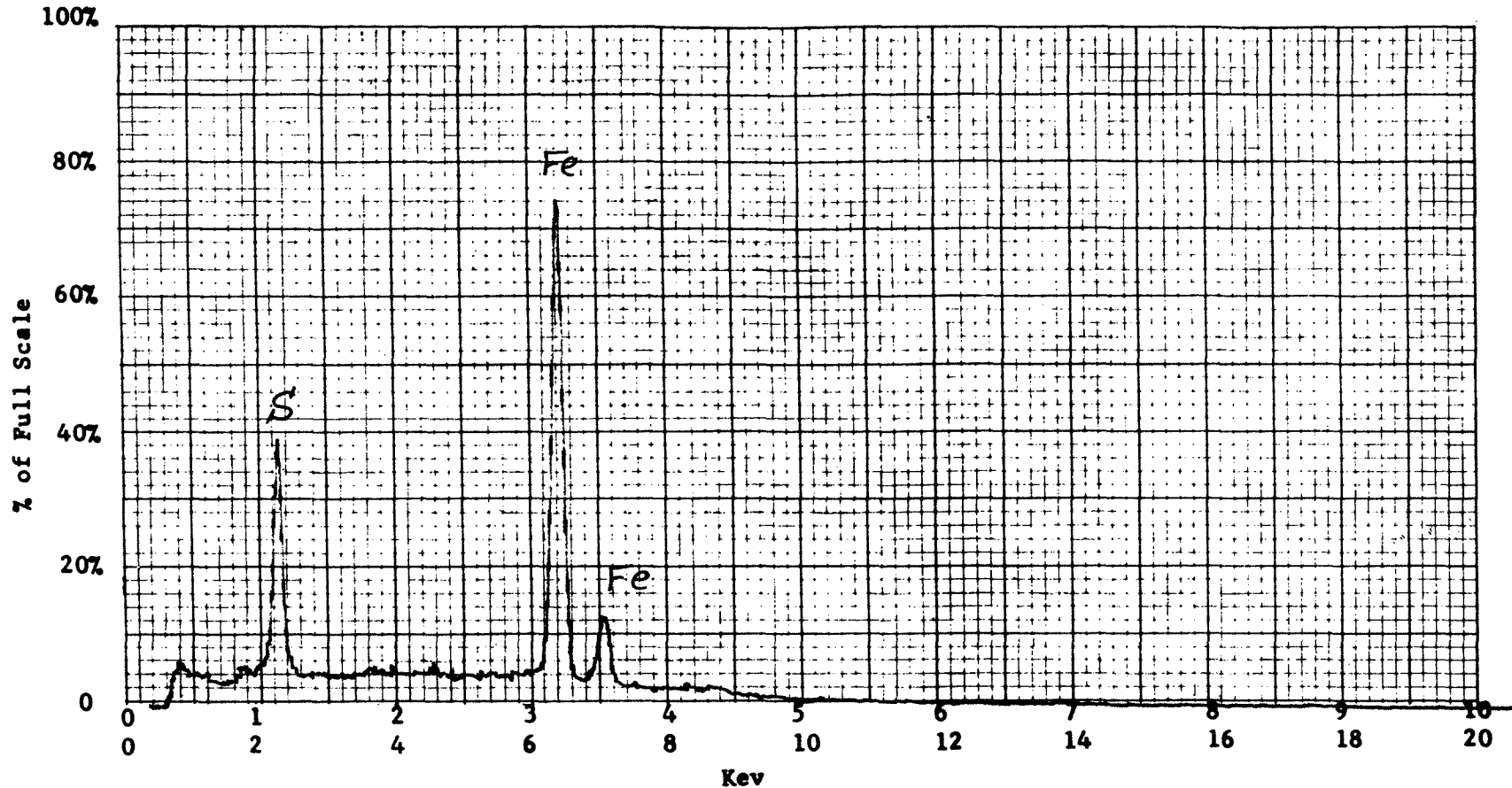
Operator \_\_\_\_\_ Date \_\_\_\_\_

Accelerating Potential 25 KeV

Total Counts Acquired 1.0 min.

Number Counts Full Scale 5K

Number of eV per channel 20



Sample peculiarities and remarks: FIGURE 446: POINT SCAN ON A HIGH Fe-S PARTICLE  
IN FIGURE 412

ENERGY DISPERSIVE X-RAY ANALYSIS

Analytical Number Illite

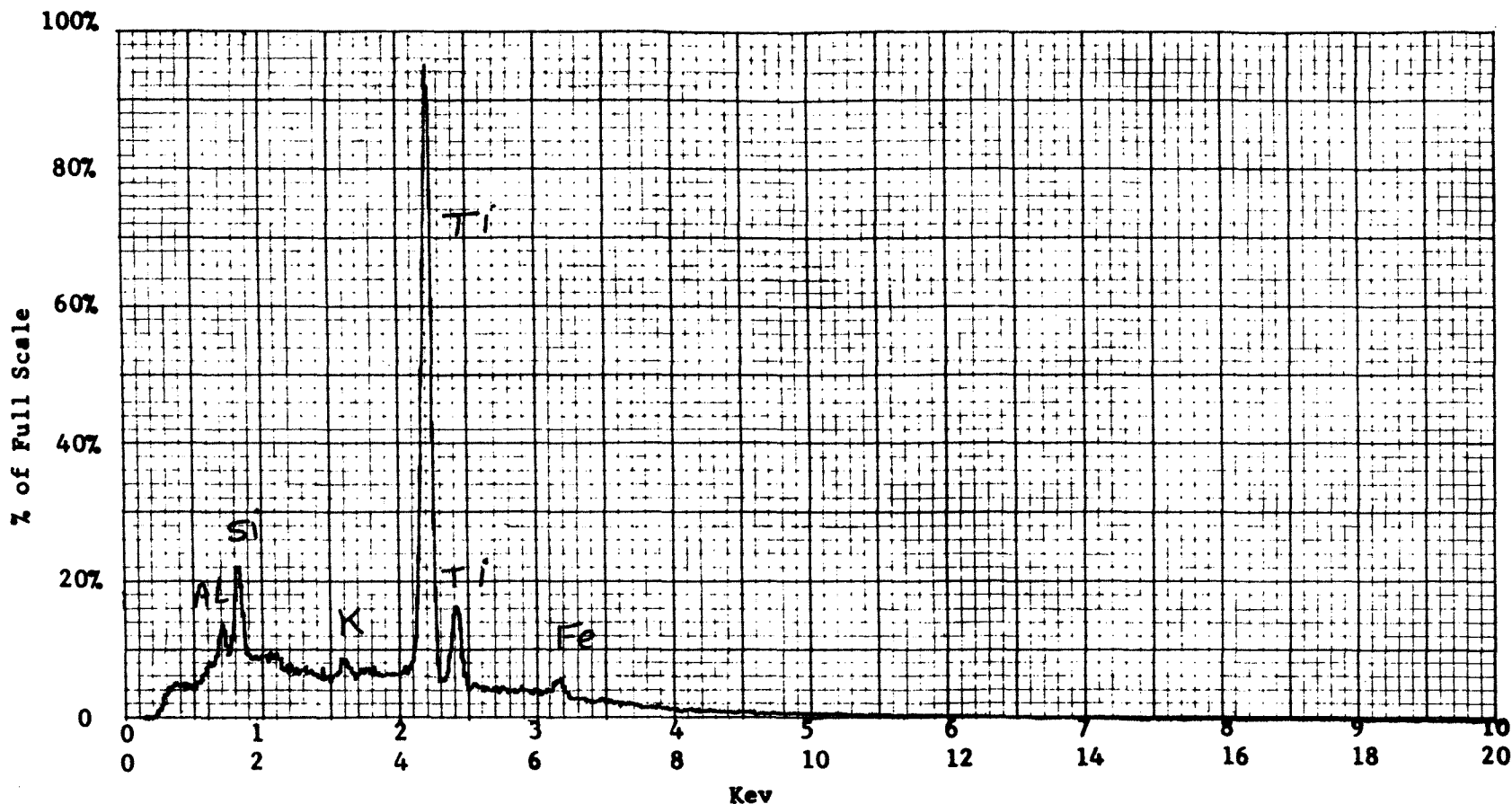
Operator \_\_\_\_\_ Date \_\_\_\_\_

Accelerating Potential 25 KeV

Total Counts Acquired 1.0 min.

Number Counts Full Scale 5K

Number of eV per channel 20



Sample peculiarities and remarks: FIGURE 447: POINT SCAN ON A HIGH Ti PARTICLE  
IN FIGURE 420



ENERGY DISPERSIVE X-RAY ANALYSIS

Analytical Number Illite

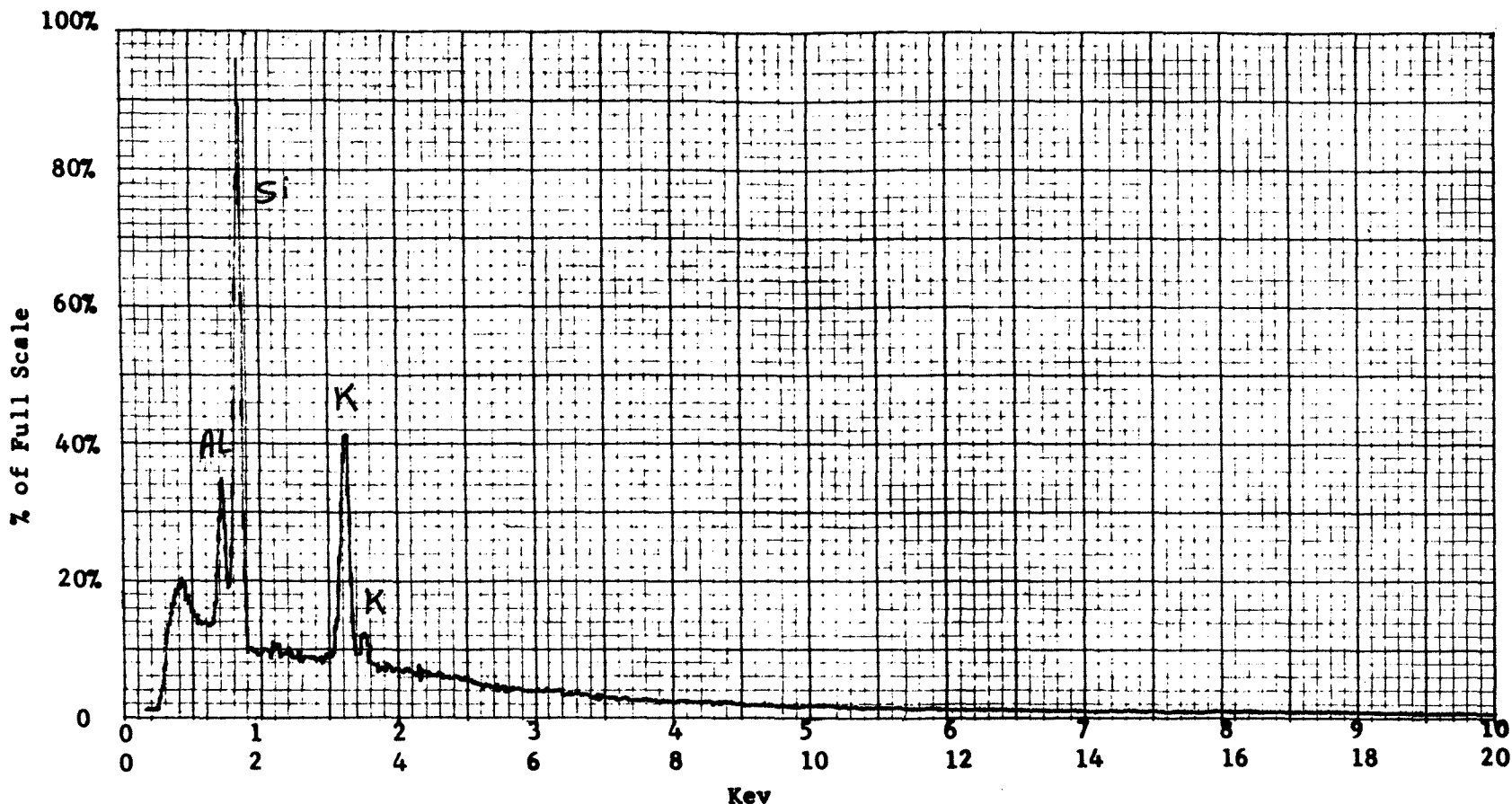
Operator \_\_\_\_\_ Date \_\_\_\_\_

Accelerating Potential 25 KeV

Total Counts Acquired 1.0 min.

Number Counts Full Scale 5K

Number of eV per channel 20



Sample peculiarities and remarks: FIGURE 448: POINT SCAN ON A HIGH K-SPOT IN A PARTICLE  
IN FIGURE 436

ENERGY DISPERSIVE X-RAY ANALYSIS

Analytical Number Illite

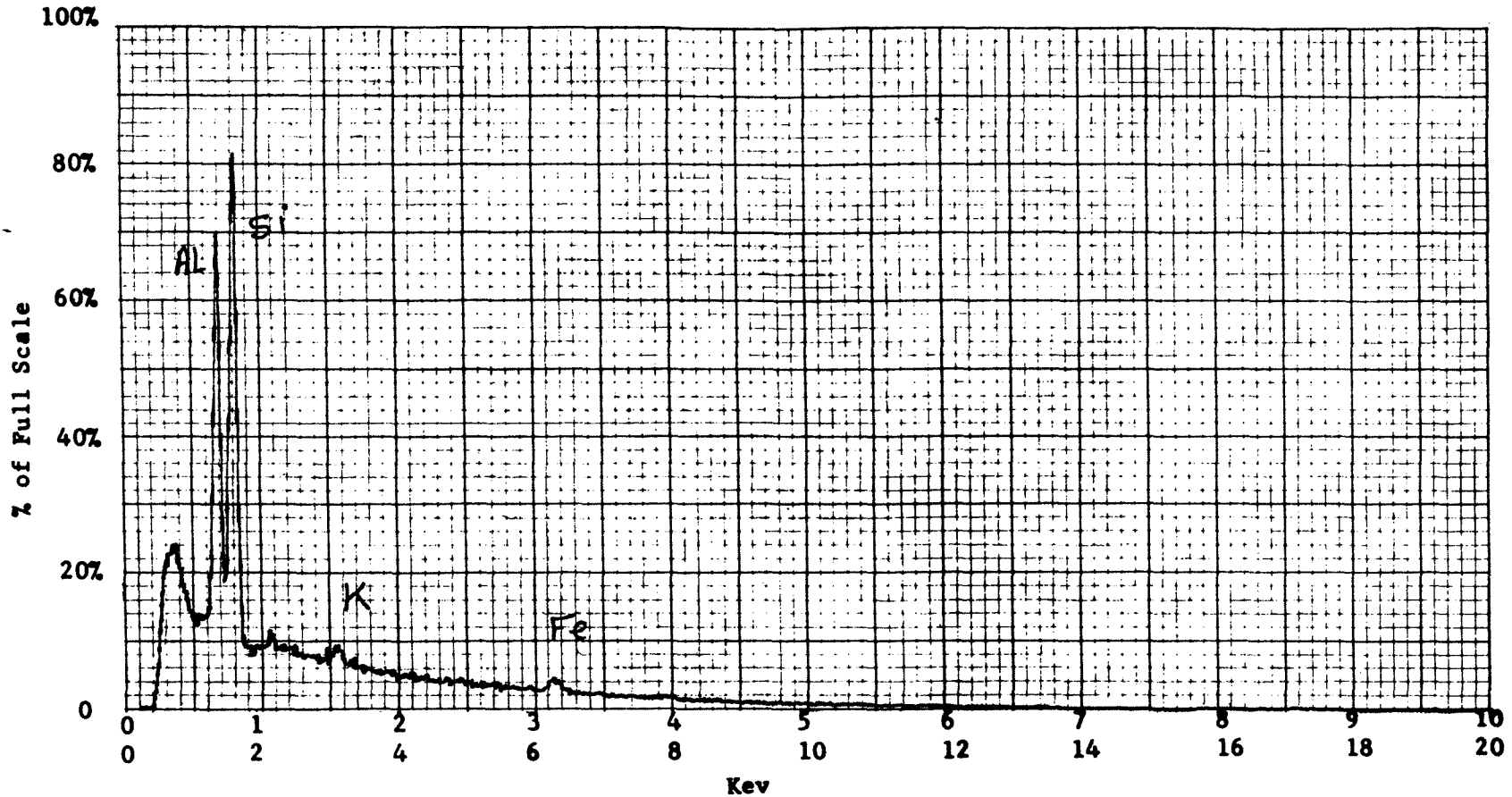
Operator \_\_\_\_\_ Date \_\_\_\_\_

Accelerating Potential 25 KeV

Total Counts Acquired 1.0 min.

Number Counts Full Scale 5K

Number of eV per channel 20



Sample peculiarities and remarks:

FIGURE 449: POINT SCAN ON A HIGH Al-Si PARTICLE

Kaolinite:Structural Analysis:

Kaolinite particles were found to be very small in size; this can be seen clearly in SEM micrographs, Figures 450 and 451, obtained at 300X. The well defined cleavage steps which give the saw-toothed appearance to the fragments (particles) of the mineral are illustrated in SEM micrographs which were obtained at 20,000X, Figures 463 and 464, and also at 40,000X, Figures 465 and 466.

The stacked plates which make up the kaoline particles can be seen in the SEM micrographs which were obtained at 10,000X or higher magnifications.

The maximum, average and minimum particle size were measured in microns ( $\mu$ ) as follows:

Maximum	Average	Minimum
13.0	1.6	0.1

Agglomerations of two or more small particles were observed in almost all the micrographs.

Elemental Composition and Distribution:

All kaolinite particles contained Al and Si and only very few small particles with higher than average concentrations of Ti were detected. This is illustrated in the SEM micrograph, Figure 479, the aluminum X-ray image, Figure 480, the silicon X-ray image, Figure 481, the titanium X-ray image, Figure 482, and X-ray energy spectrum, Figure 485. The other SEM micrographs, elemental X-ray images, and the X-ray energy spectra were obtained to show that Al and Si were the major elements.

SEM IMAGES OF SAMPLE #

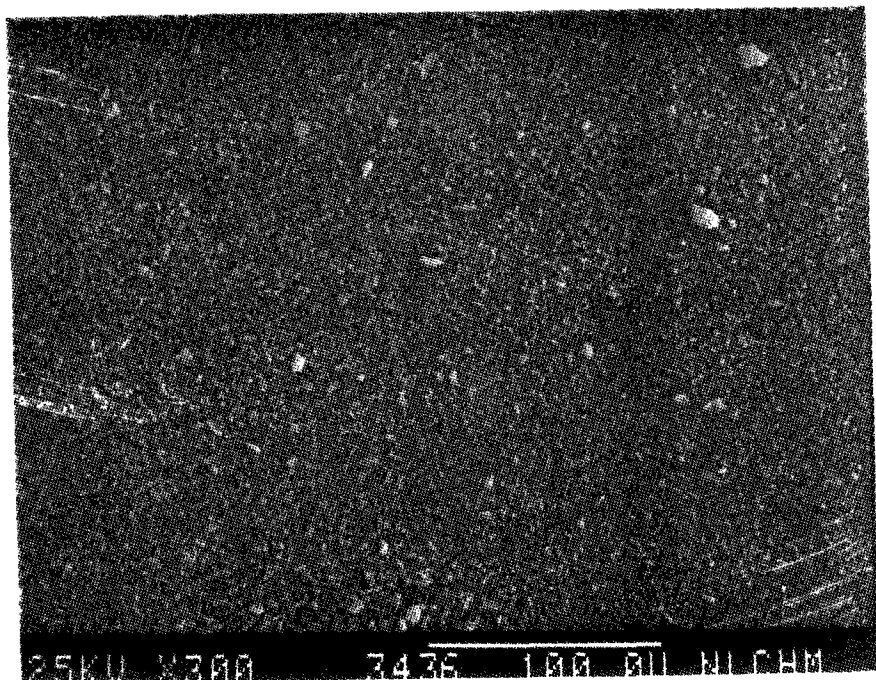


Figure 450

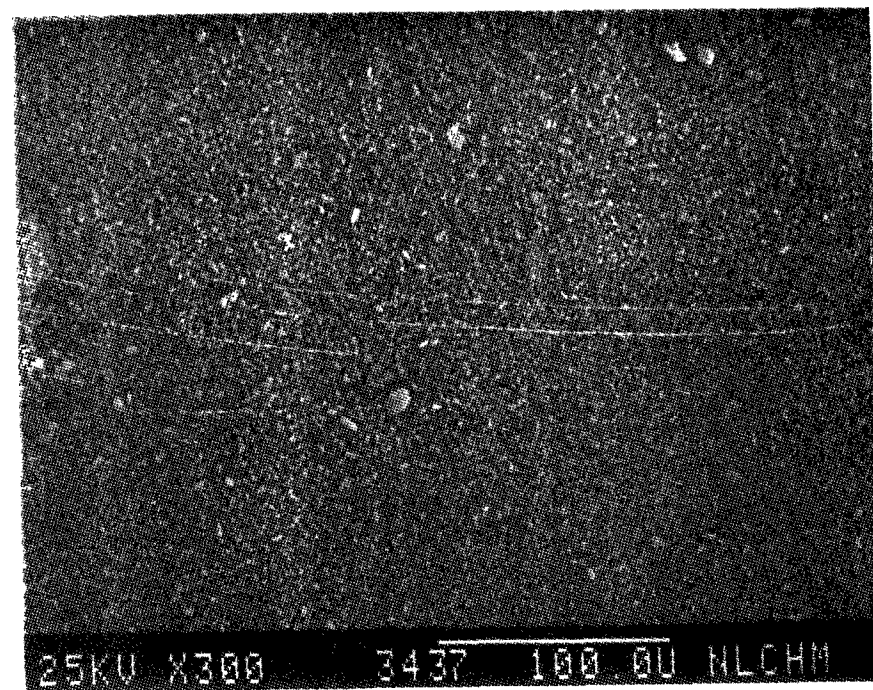


Figure 451

SEM IMAGES OF SAMPLE #

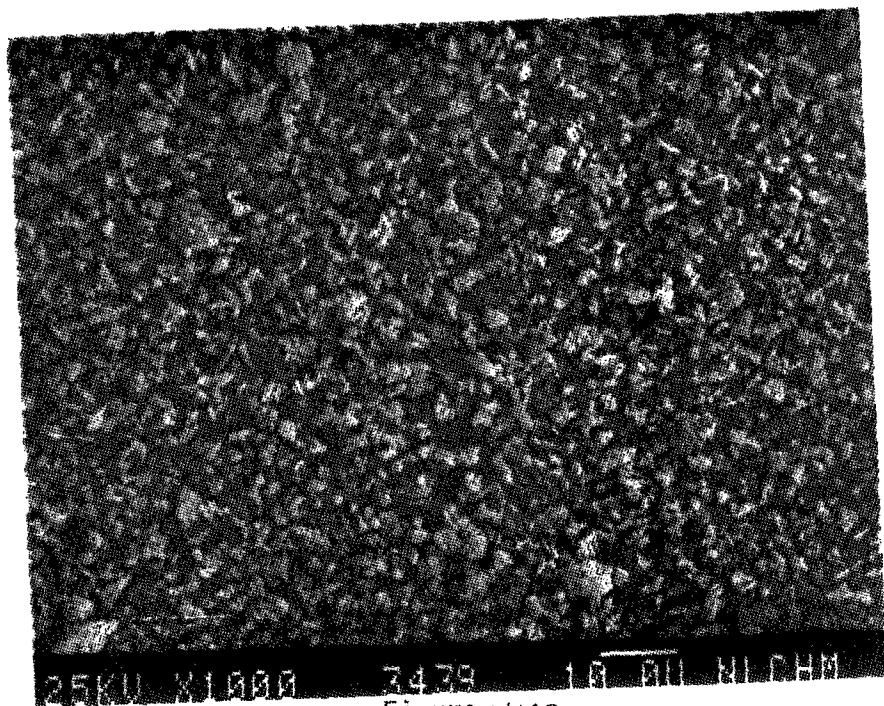


Figure 452

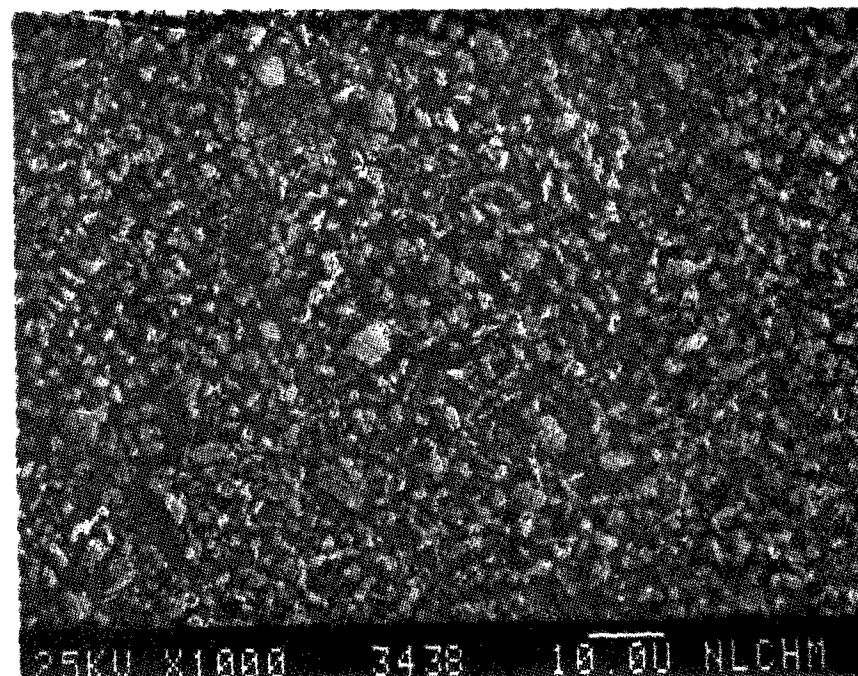


Figure 453

SEM IMAGES OF SAMPLE #

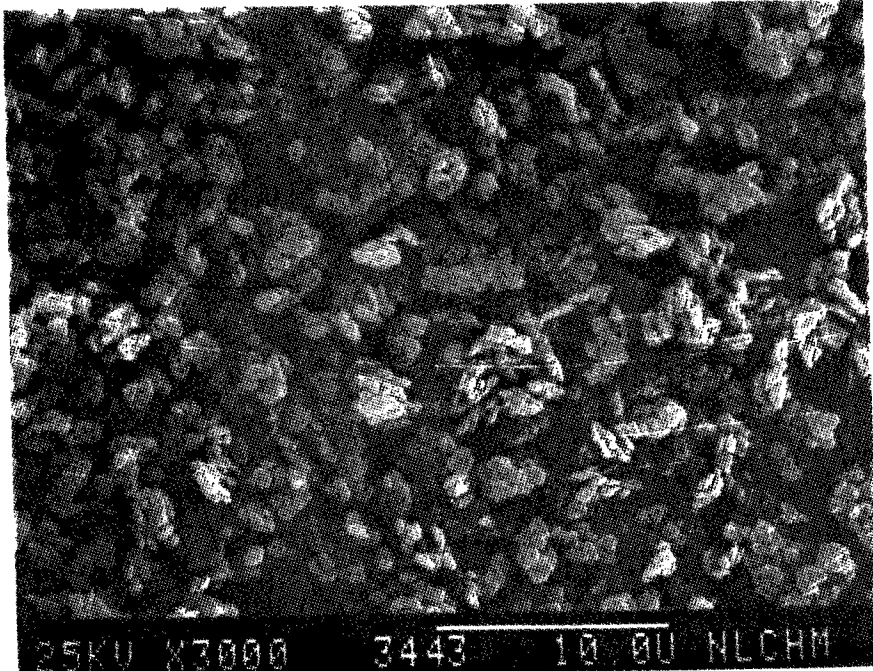


Figure 454

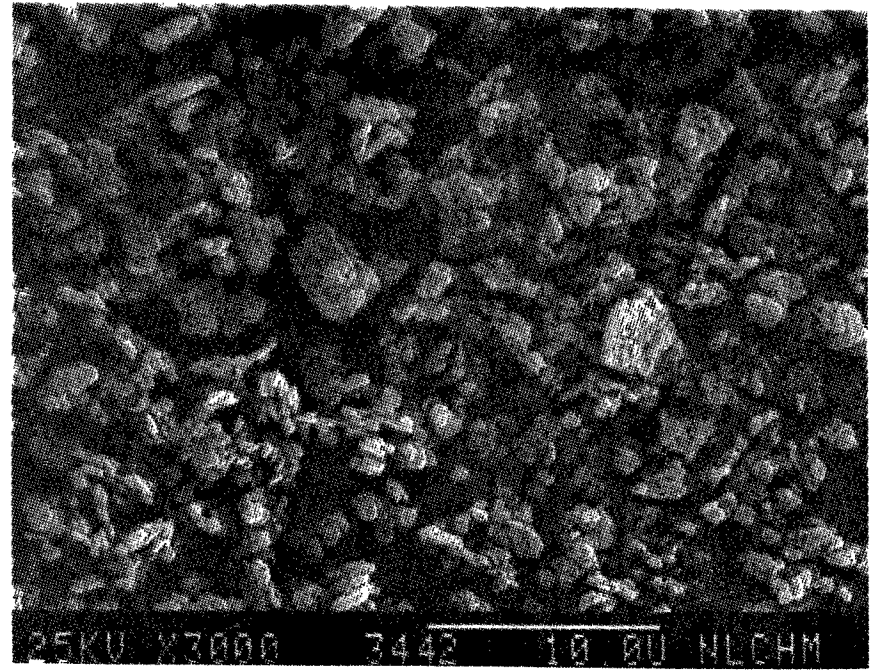


Figure 455

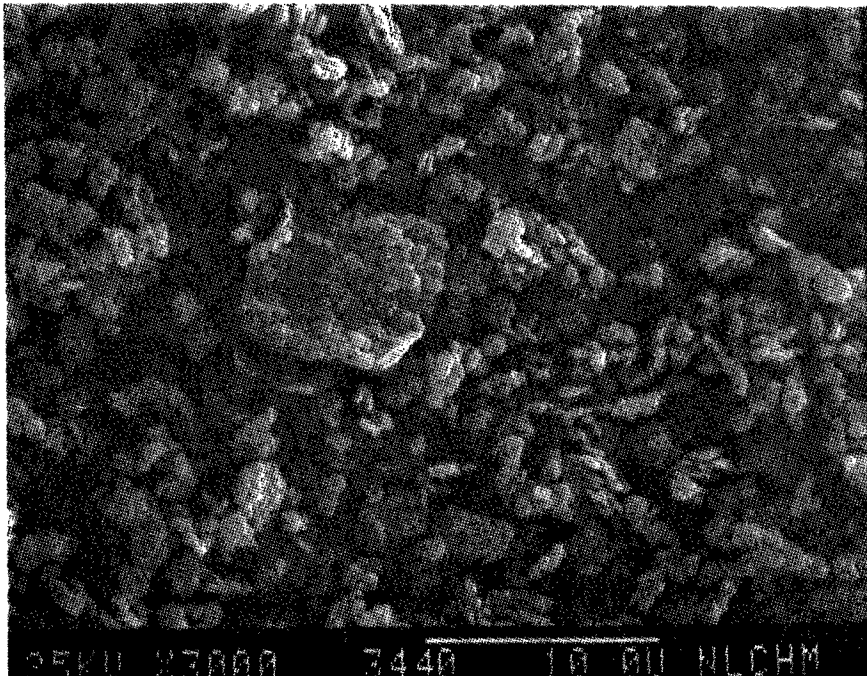


Figure 456

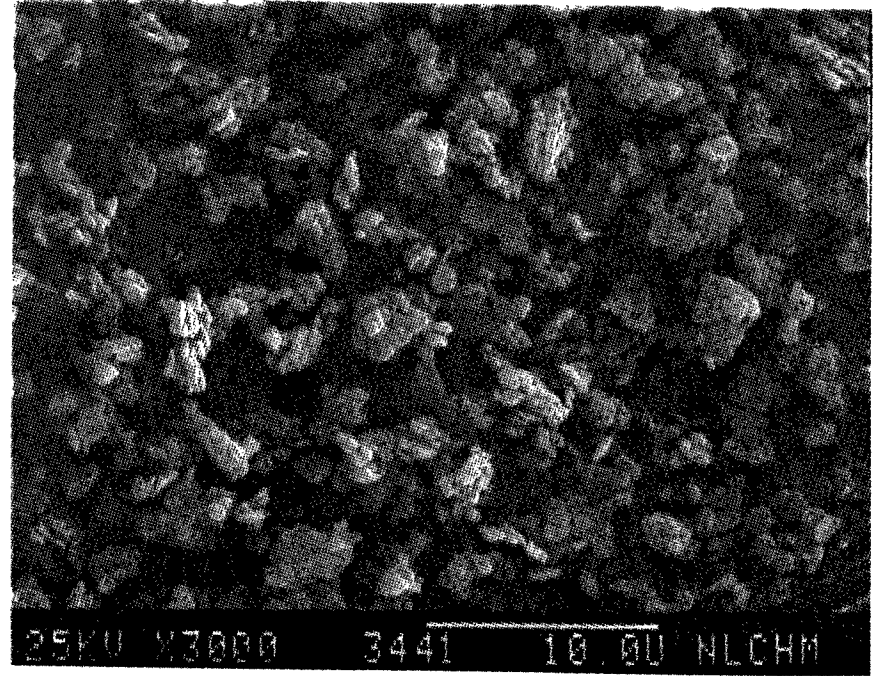


Figure 457



SEM IMAGES OF SAMPLE #

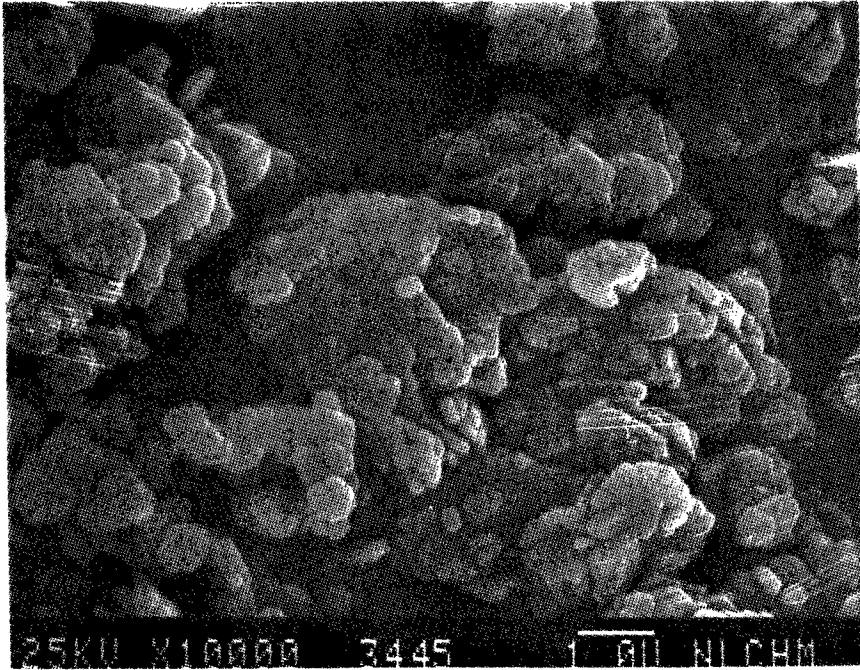


Figure 458

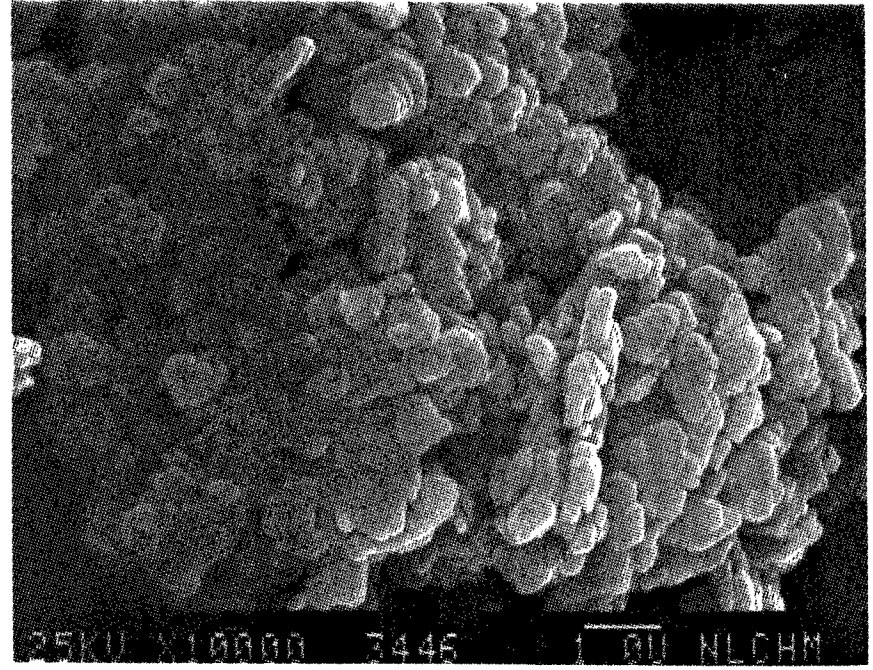


Figure 459

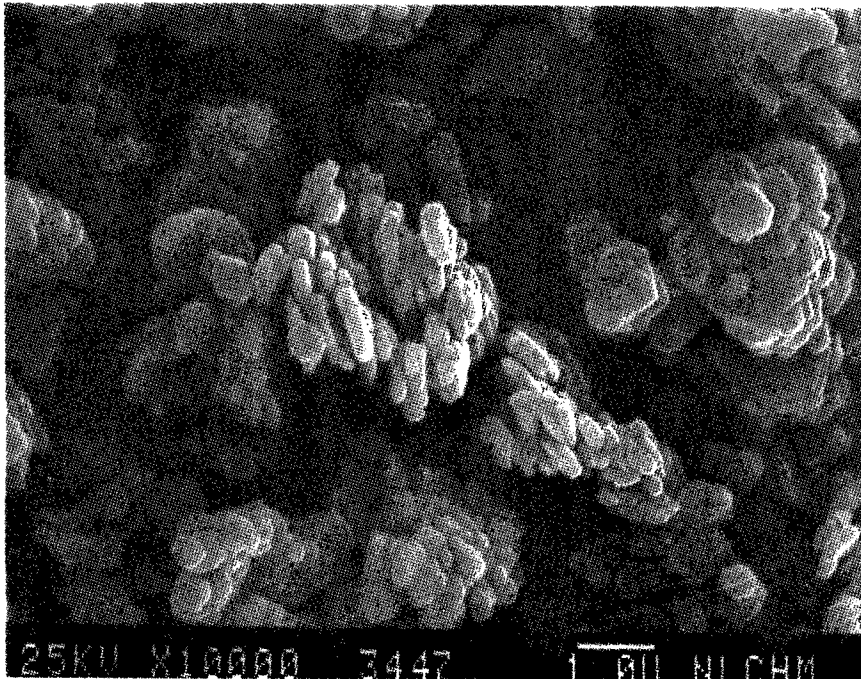


Figure 460

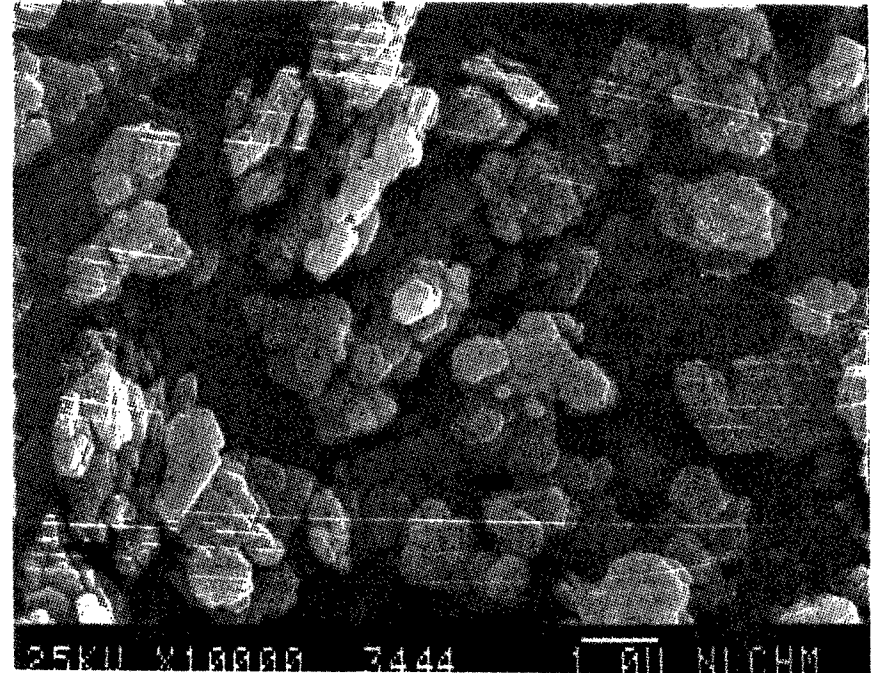


Figure 461

SEM IMAGES OF SAMPLE #

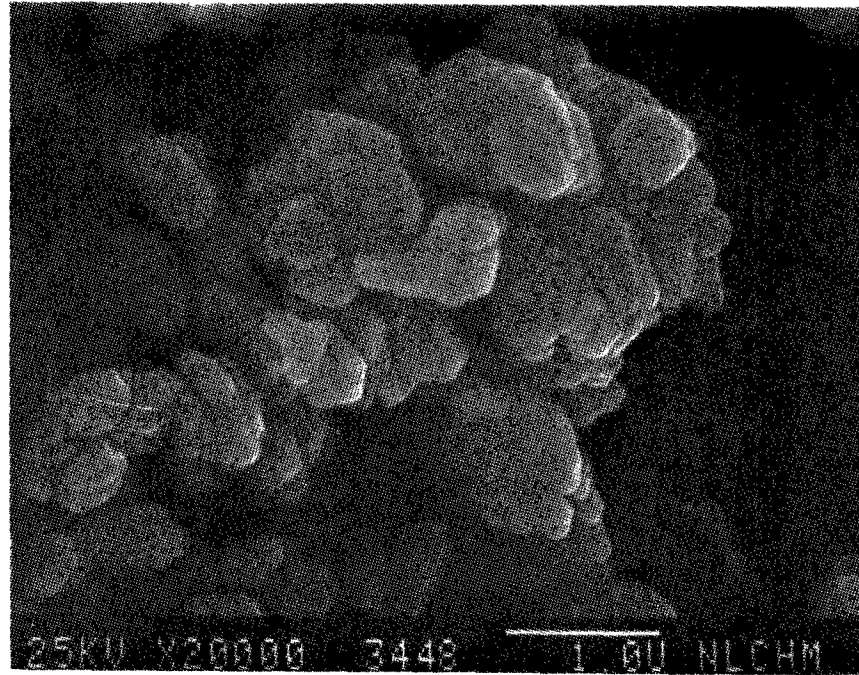


Figure 462

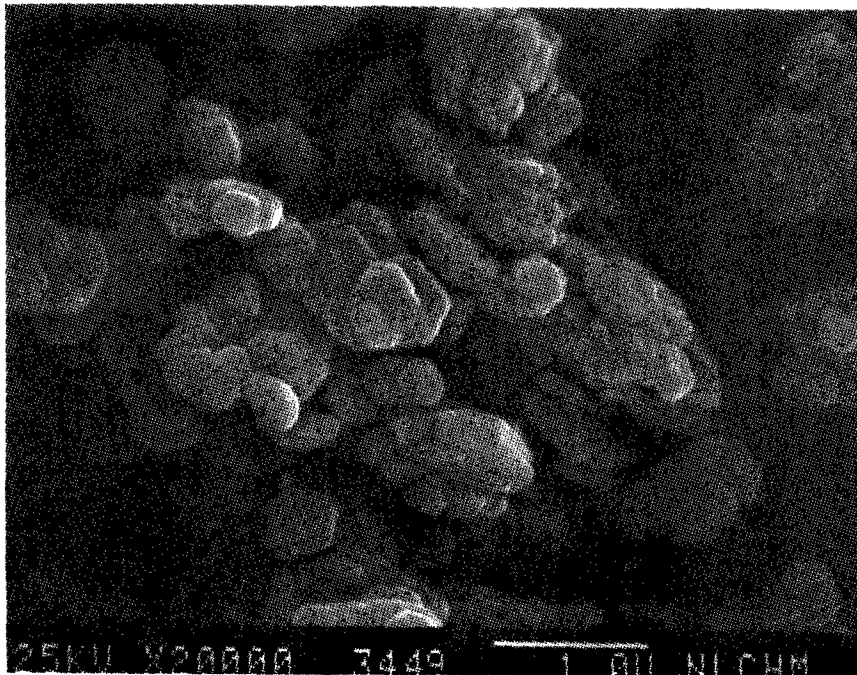


Figure 463

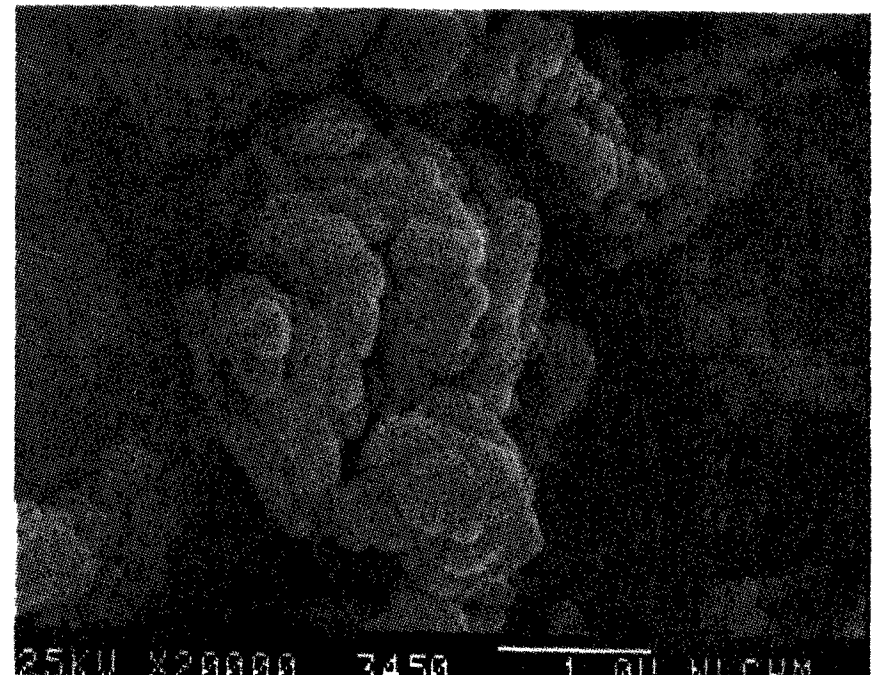


Figure 464

SEM IMAGES OF SAMPLE #

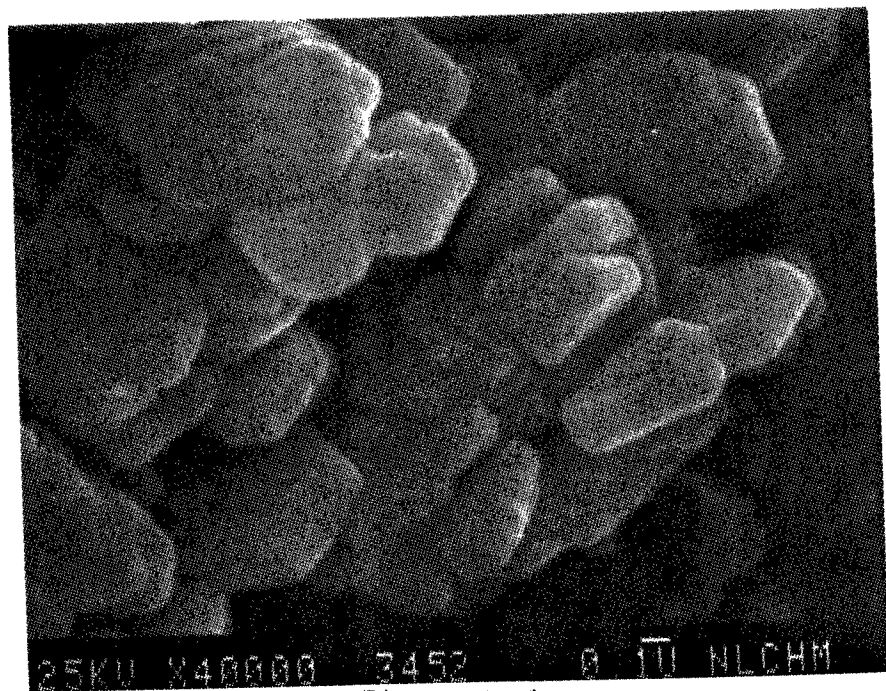


Figure 465

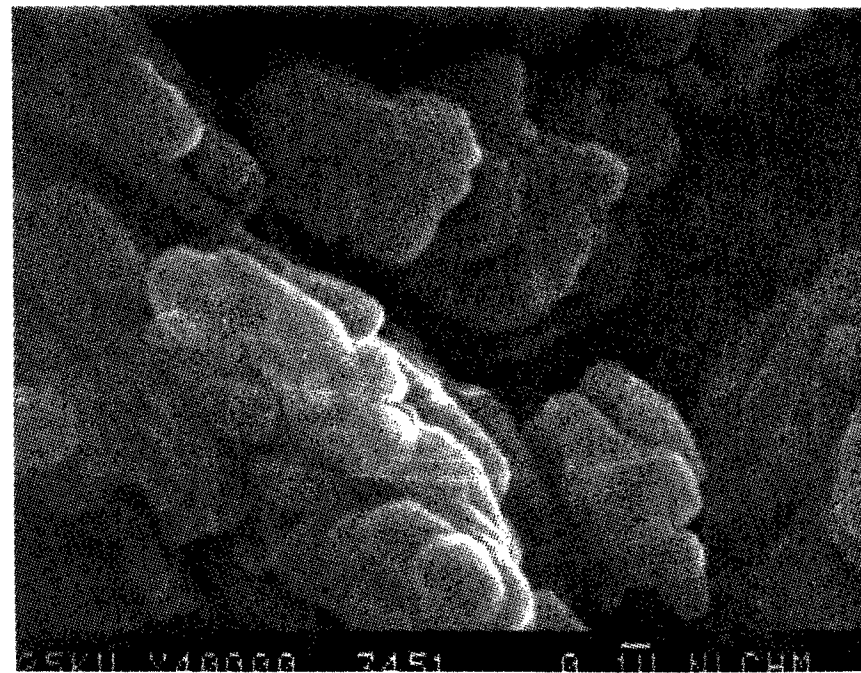


Figure 466



SEM IMAGES OF SAMPLE #

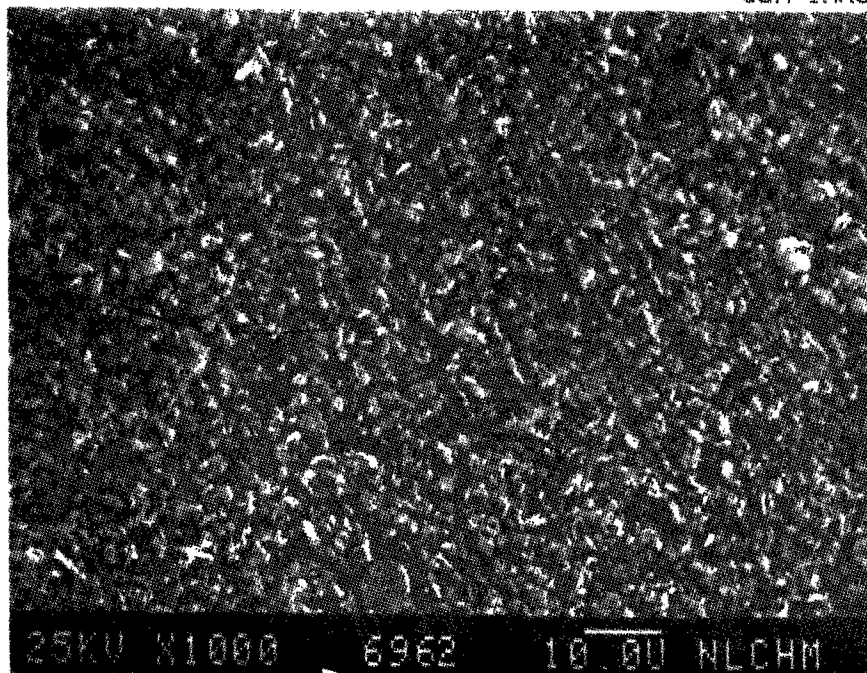


Figure 467

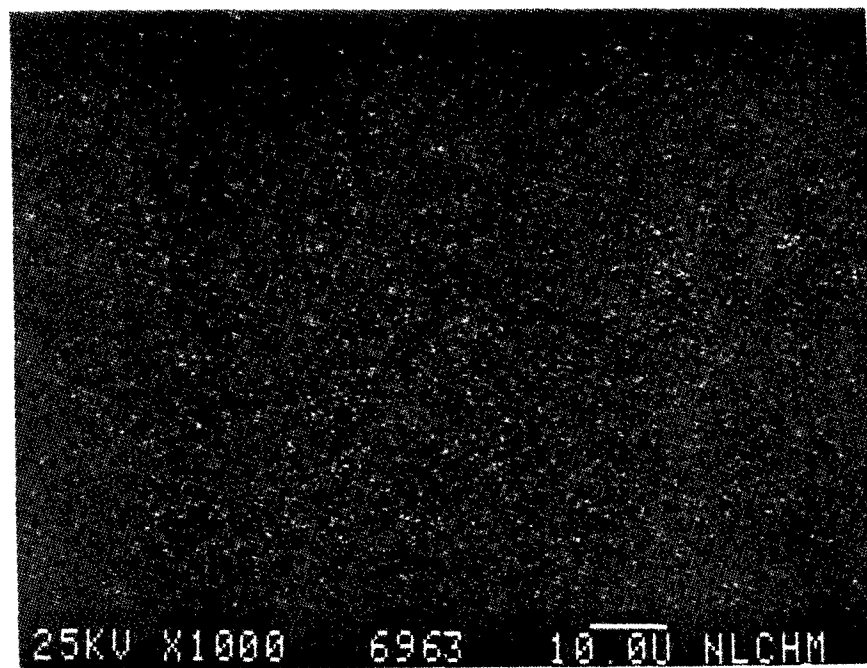


Figure 468

AL X-Ray Image of Figure 467

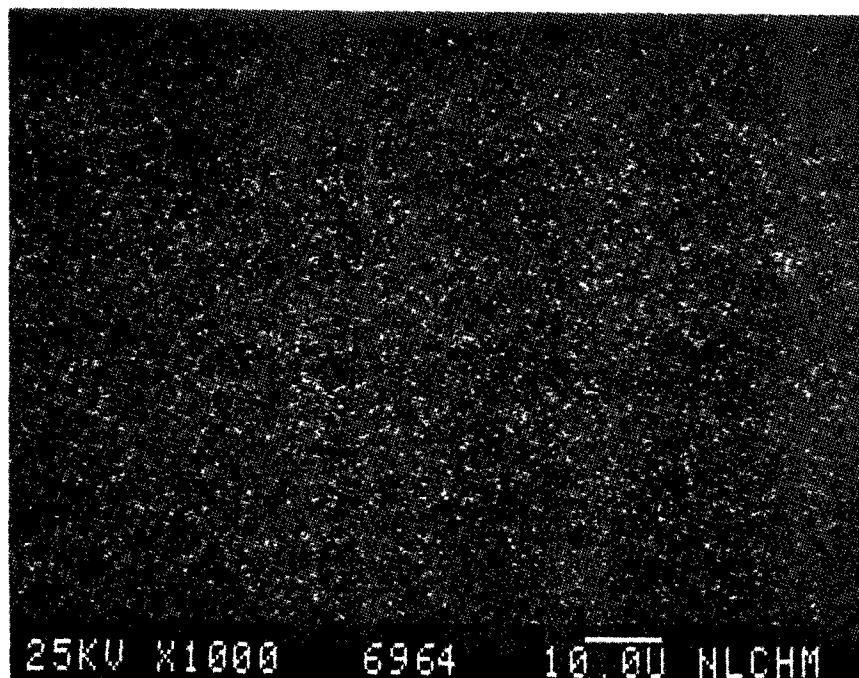


Figure 469

Si X-Ray Image of Figure 467

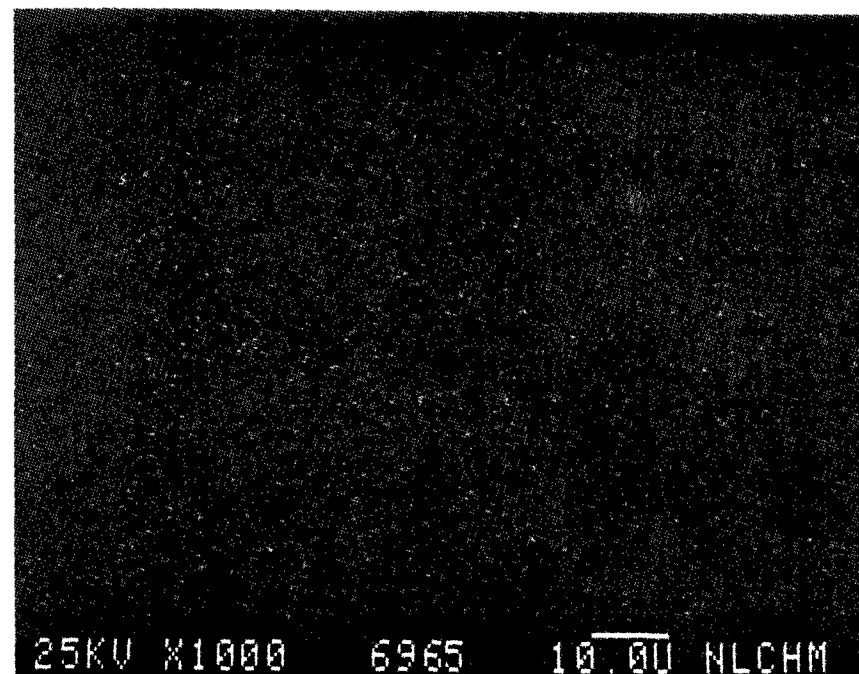


Figure 470

Ti X-Ray Image of Figure 467

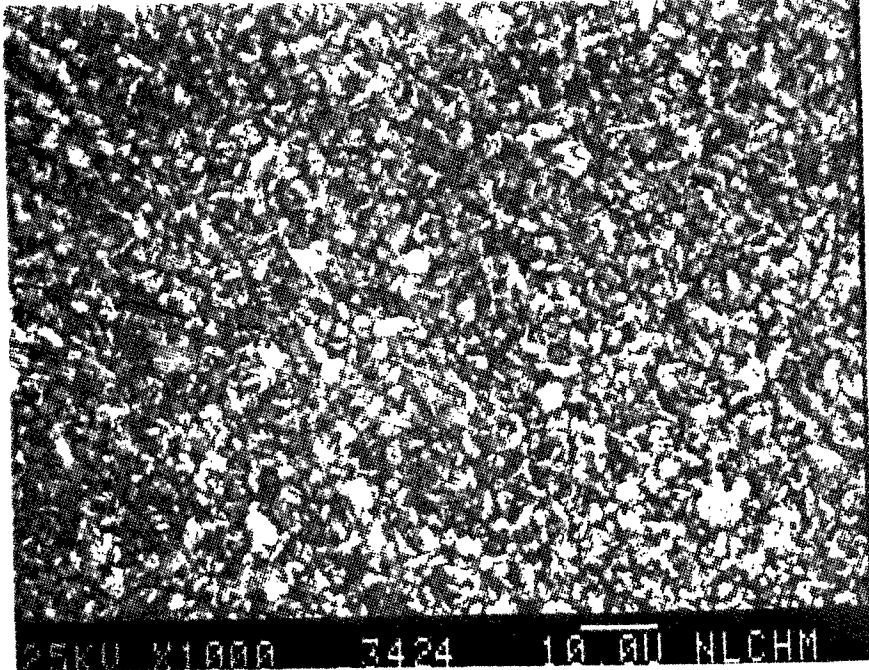


Figure 471

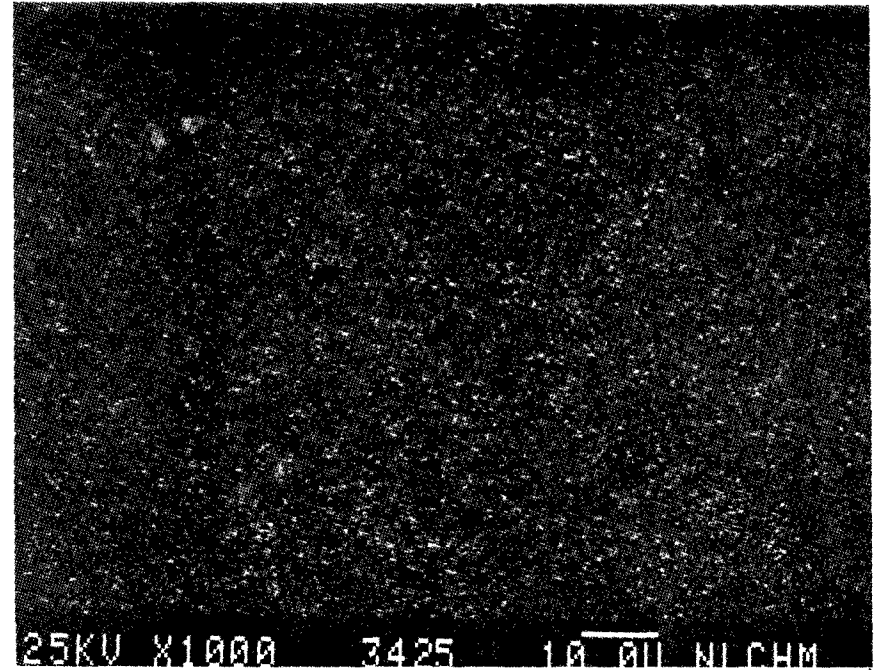


Figure 472

AL X-Ray Image of Figure 471

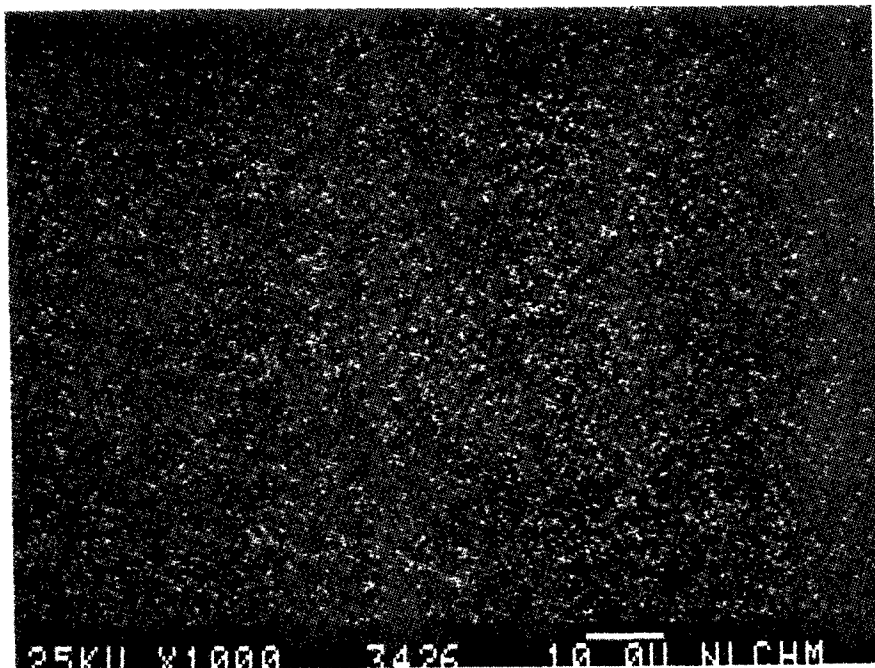


Figure 473

Si X-Ray Image of Figure 471

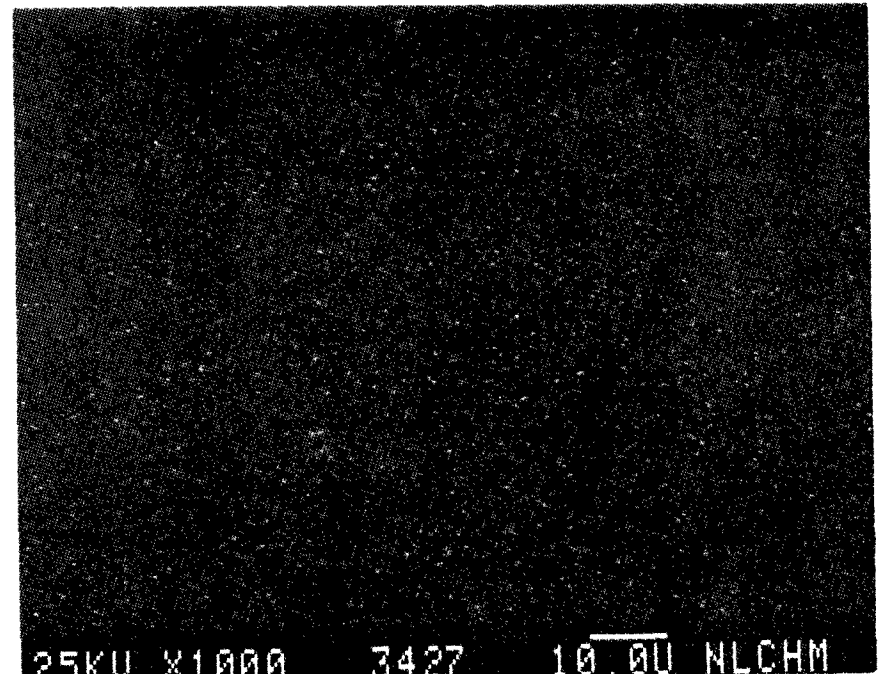


Figure 474

Ti X-Ray Image of Figure 471

SEM IMAGES OF SAMPLE #

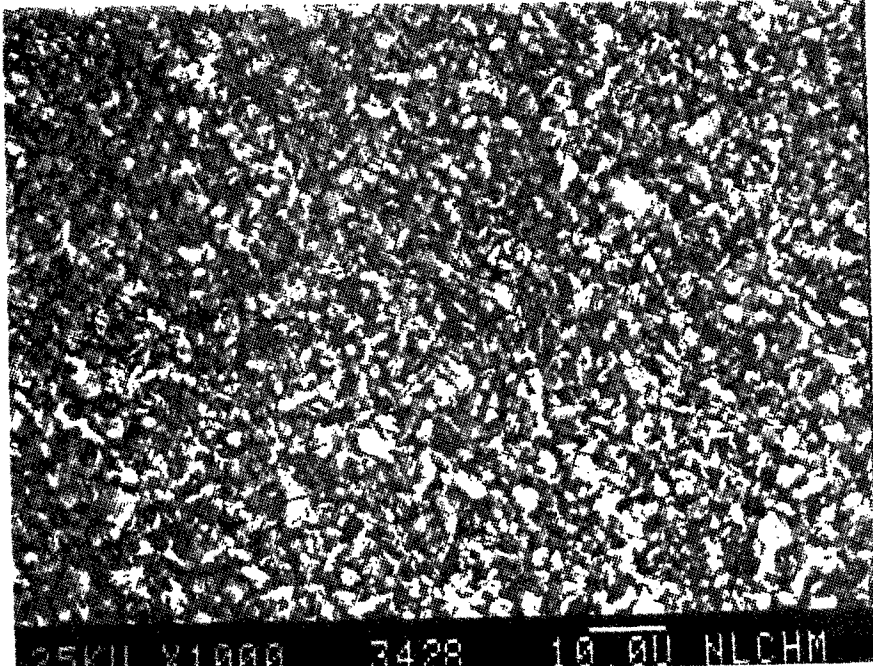


Figure 475

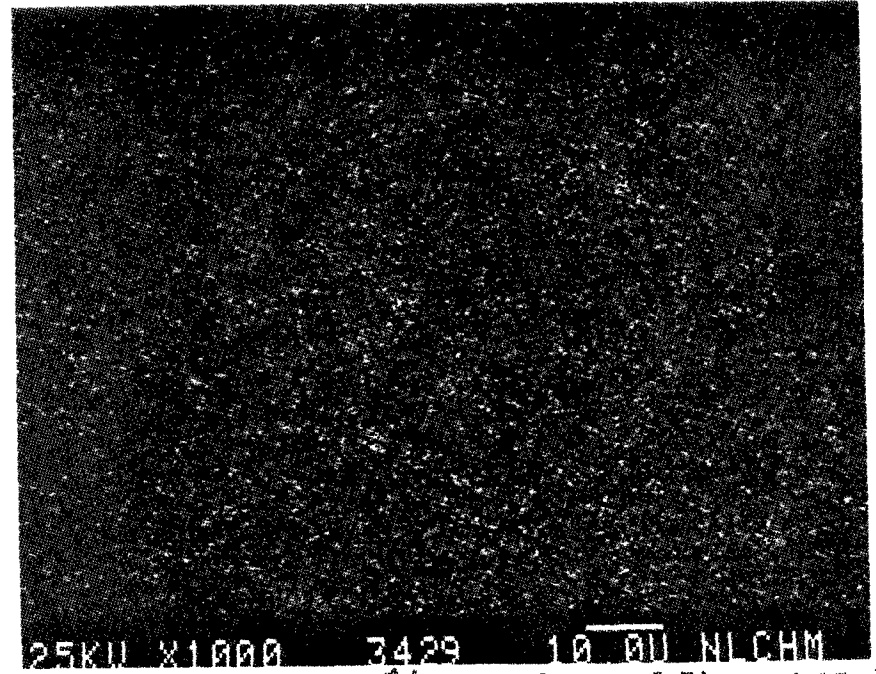


Figure 476

AL X-Ray Image of Figure 475

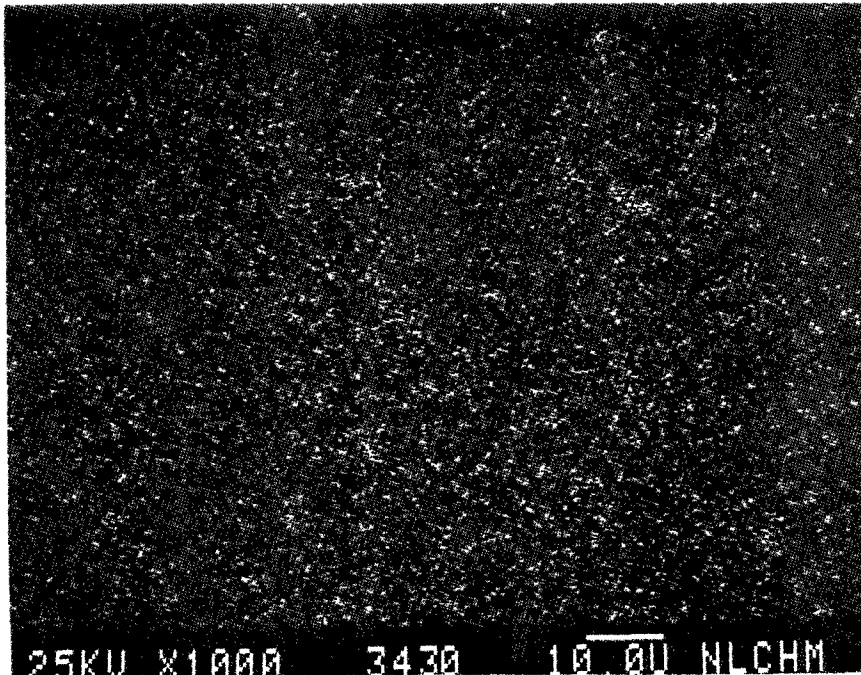


Figure 477

Si X-Ray Image of Figure 475

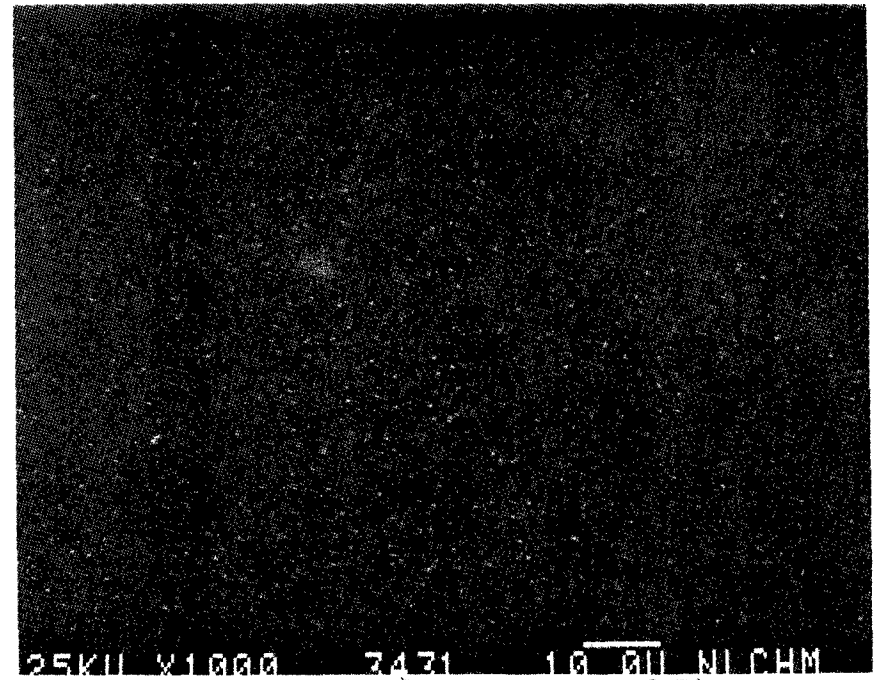


Figure 478

Ti X-Ray Image of Figure 475



SEM IMAGES OF SAMPLE #

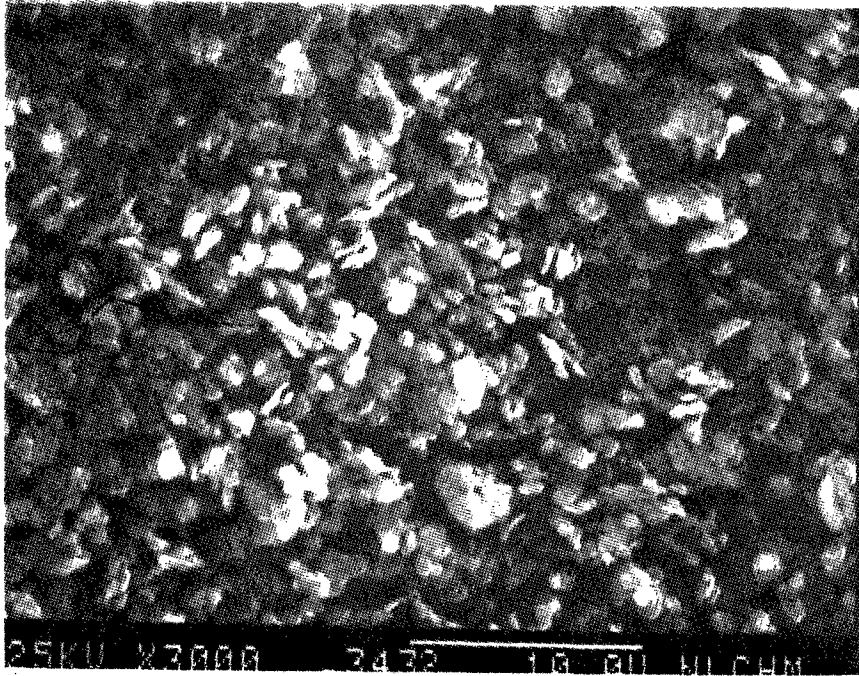


Figure 479

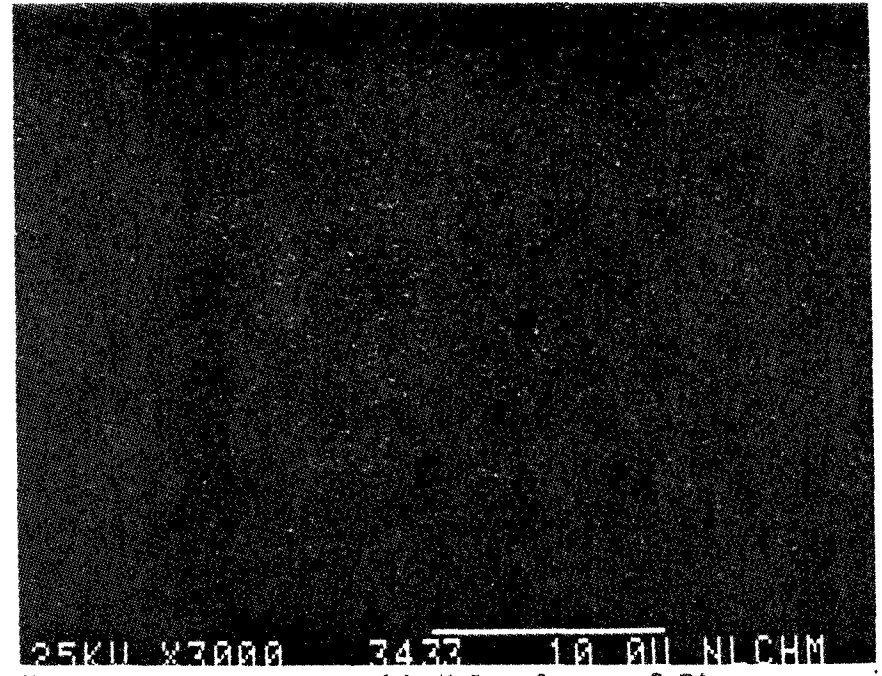


Figure 480

AL X-Ray Image of Figure 479

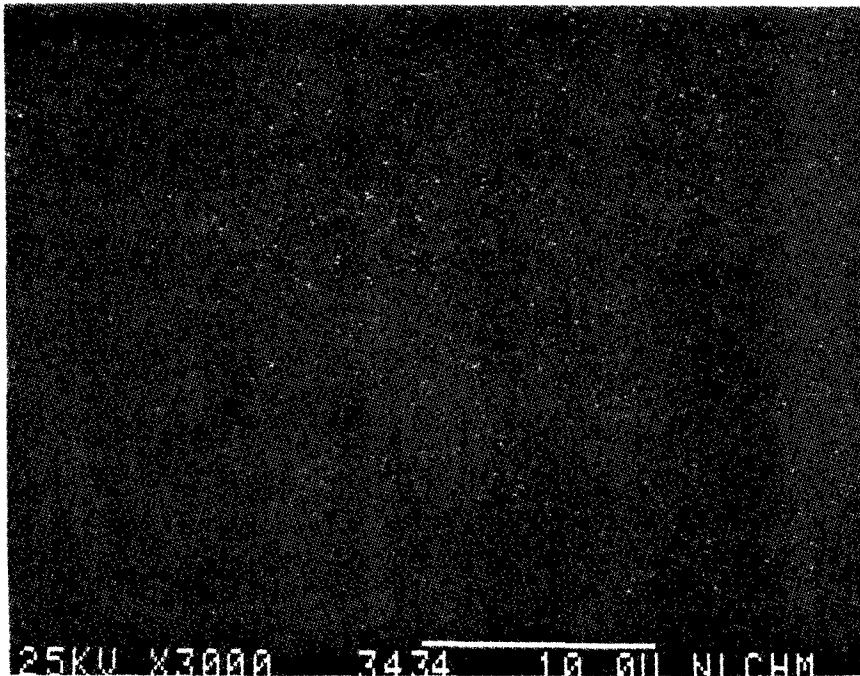


Figure 481

Si X-Ray Image of Figure 479

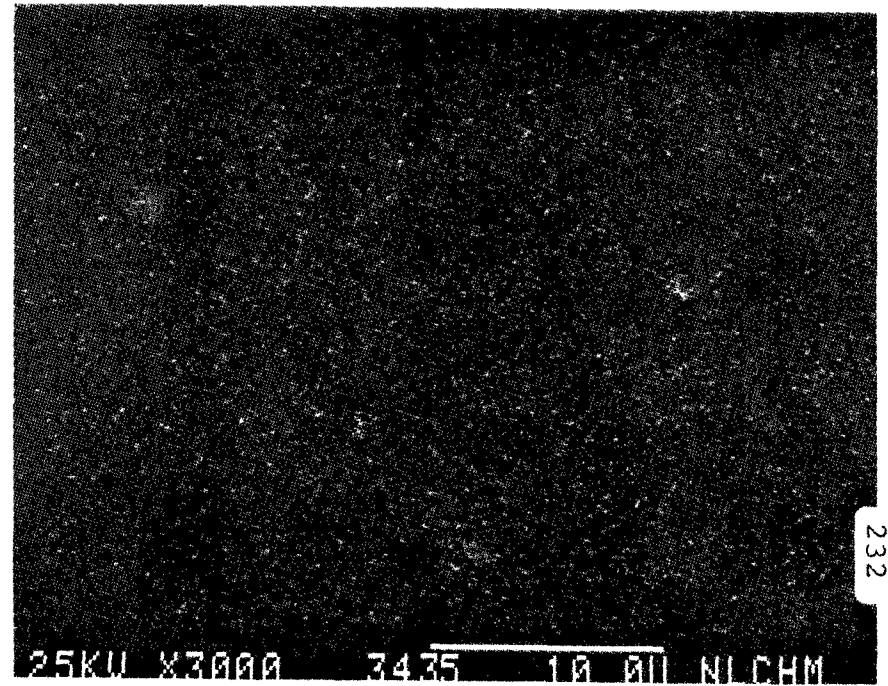


Figure 482

Ti X-Ray Image of Figure 479

ENERGY DISPERSIVE X-RAY ANALYSIS

Analytical Number Kaolinite

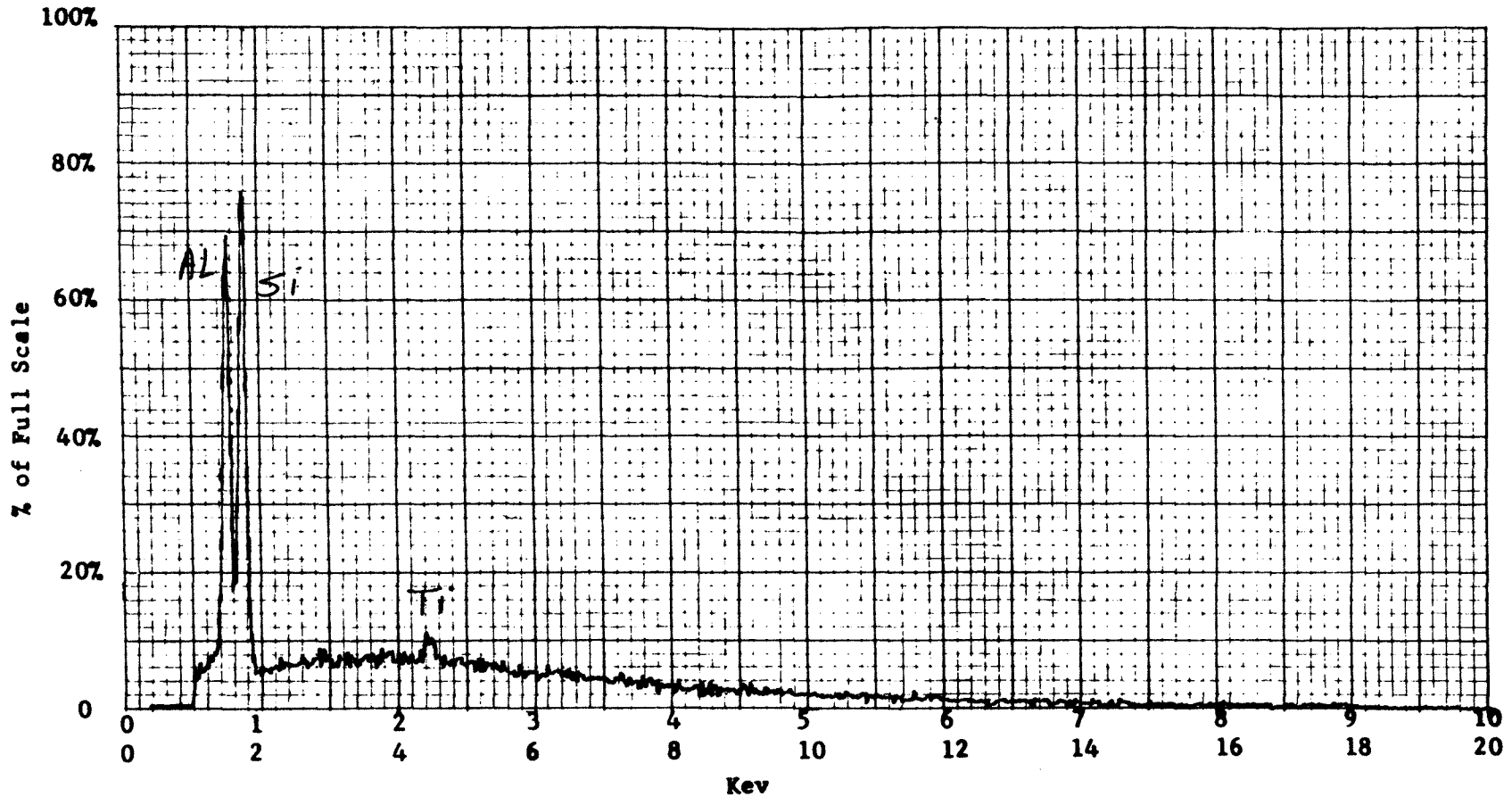
Operator \_\_\_\_\_ Date \_\_\_\_\_

Accelerating Potential 25 KeV

Total Counts Acquired 1.0 min.

Number Counts Full Scale 2K

Number of eV per channel 20



Sample peculiarities and remarks: FIGURE 483: AREA SCAN

ENERGY DISPERSIVE X-RAY ANALYSIS

Analytical Number Kaolinite

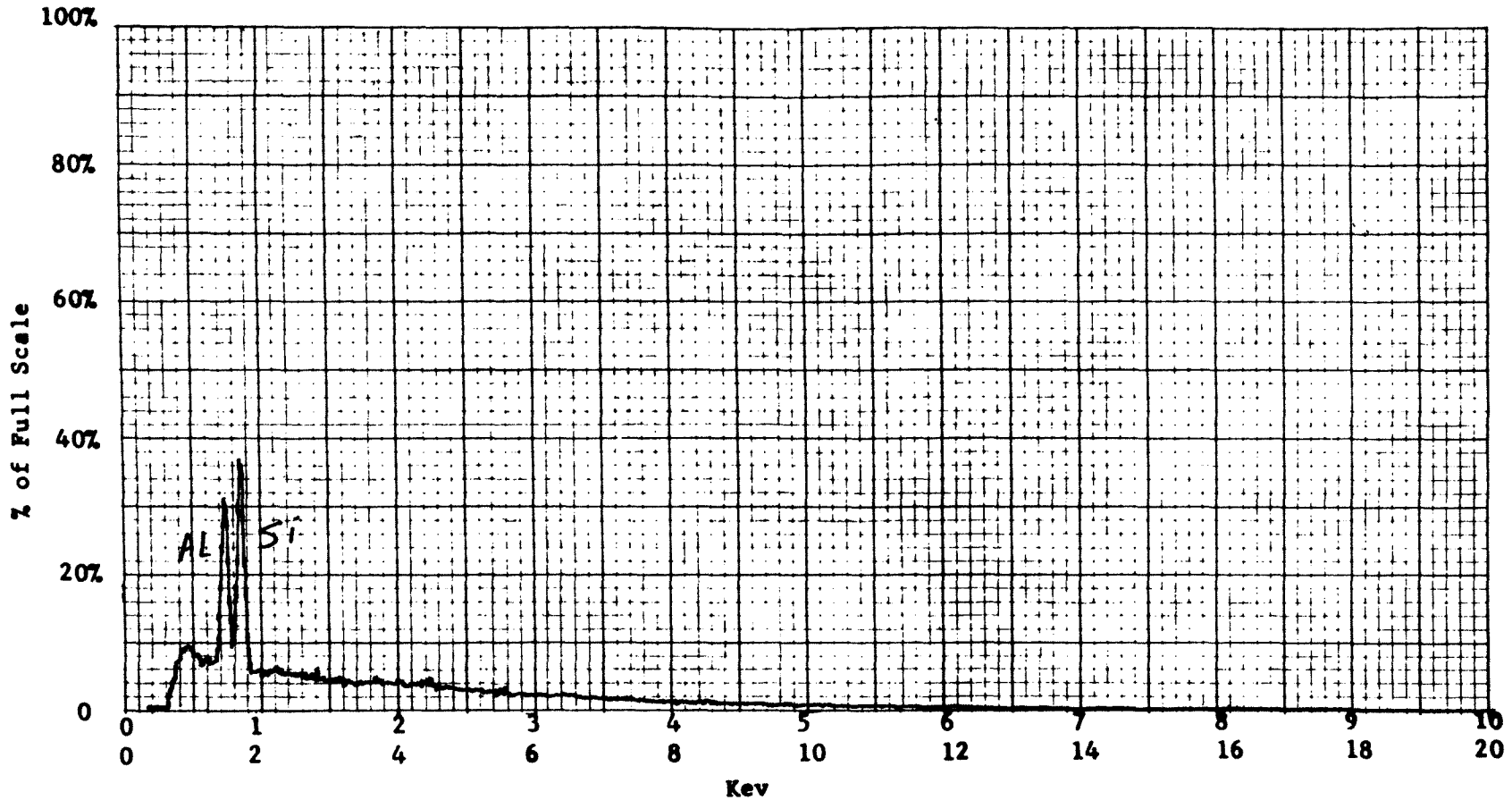
Operator \_\_\_\_\_ Date \_\_\_\_\_

Accelerating Potential 25 KeV

Total Counts Acquired 1.0 min.

Number Counts Full Scale 5K

Number of eV per channel 20



Sample peculiarities and remarks: FIGURE 484: POINT SCAN ON A LARGE PARTICLE

ENERGY DISPERSIVE X-RAY ANALYSIS

Analytical Number Kaolinite

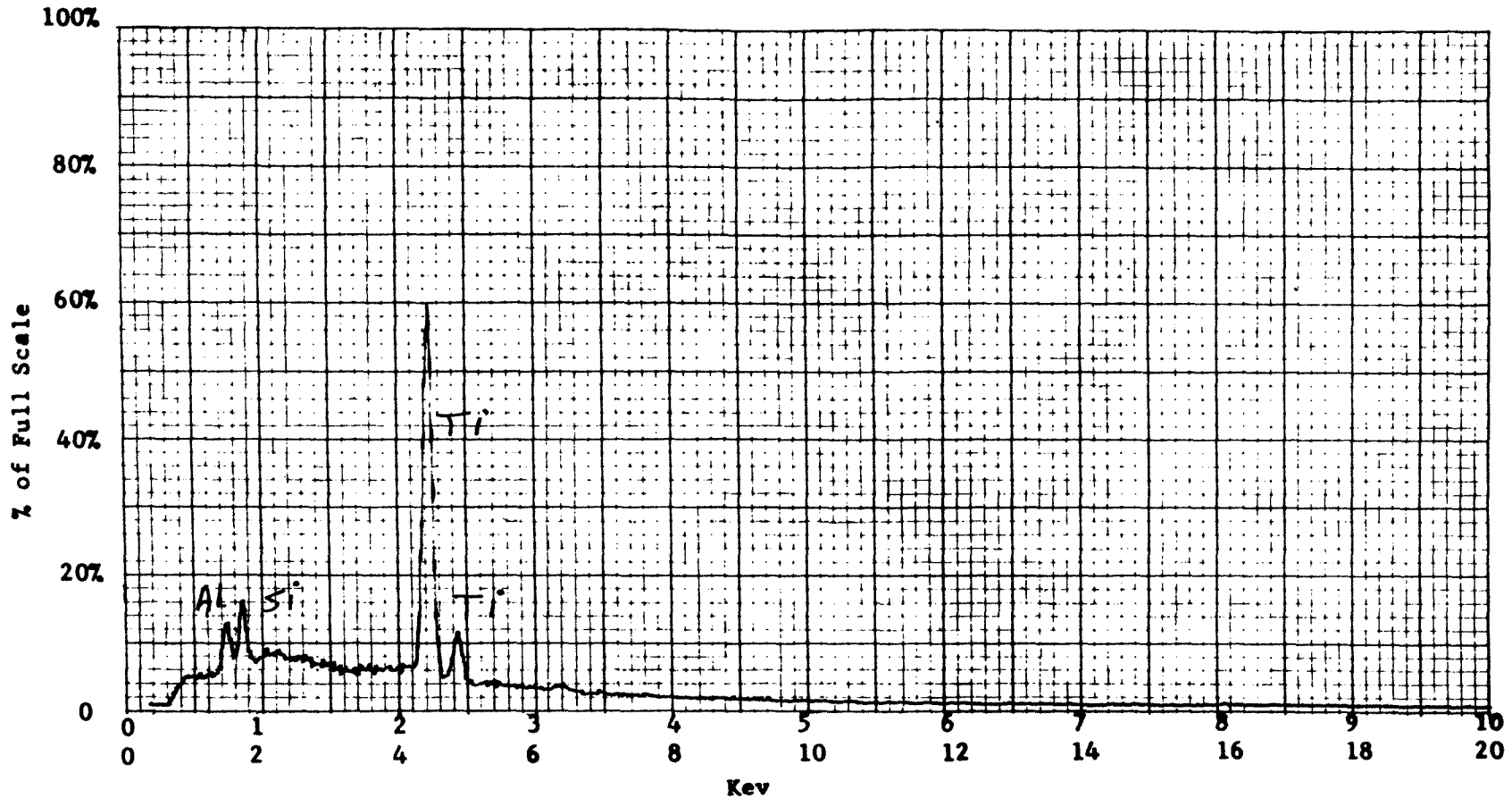
Operator \_\_\_\_\_ Date \_\_\_\_\_

Accelerating Potential 25 KeV

Total Counts Acquired 1.0 min.

Number Counts Full Scale 5K

Number of eV per channel 20



Sample peculiarities and remarks: FIGURE 485: POINT SCAN ON A HIGH Ti PARTICLE  
IN FIGURE 479

Zeolite:Structural Analysis:

Irregular shaped particles were observed in the SEM micrographs which were obtained at low and high magnifications. A few particles observed in Figures 492, 496 and 499 were elongated. SEM micrographs at 3000X or higher magnification indicated that the surface of the particles was rough and in some cases fibrous shaped structures were present on some particle surfaces, for example, Figures 501, 504 and 505.

The elongated plates which were observed in the surface of some particles in SEM micrographs obtained at high magnifications (10,000X) are typical and characteristic structures of zeolite. This is illustrated in Figures 503, 504, 505, 506 and 507.

The maximum, average and minimum particle size were measured in microns ( $\mu$ ) as follows:

Maximum	Average	Minimum
110.0	26.0	0.8

Elemental Composition and Distribution:

Al, Si, K, Ca, Ti and Fe were detected from the sample. For example, Figures 508 and 505 illustrate the general elemental distribution. The elemental X-ray images of these two figures indicates that the major element in most of the zeolite particles is Si, a few particles contain high concentrations of Ca, the other above

mentioned elements were minor. The distribution of elements is illustrated clearly in the X-ray energy spectrum, Figure 555.

Figure 522 is an illustration of a large particle which contains very high level of Ca. By using the point scan technique only Ca with traces of Si could be detected from this particle. This might indicate that this particle is calcium oxide or carbonate. The calcium X-ray image, Figure 526, and X-ray energy spectrum, Figure 556, confirm the high concentration of calcium in this particle.

Three small particles in SEM micrograph, Figure 529, were observed in which high levels of K, Ca or Fe were detected. This is illustrated by the potassium X-ray image, Figure 532, the calcium X-ray image, Figure 533, the iron X-ray image, Figure 535, and X-ray energy spectrum, Figure 557. A small particle in the right side of a large particle in SEM micrograph, Figure 536, was found to contain higher than normal concentrations of Ti and Fe. The titanium X-ray image, Figure 541, and iron X-ray image, Figure 542, also confirm this result.

Two other particles with very high Ca (possible Ca oxide or carbonate) were observed in SEM micrographs, Figures 543 and 549.



SEM IMAGES OF SAMPLE #

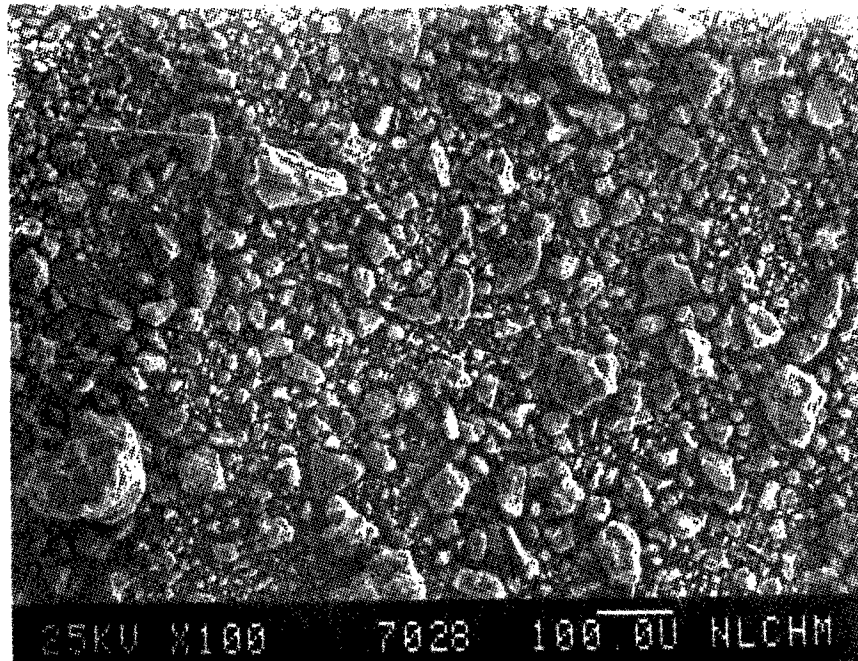


Figure 486

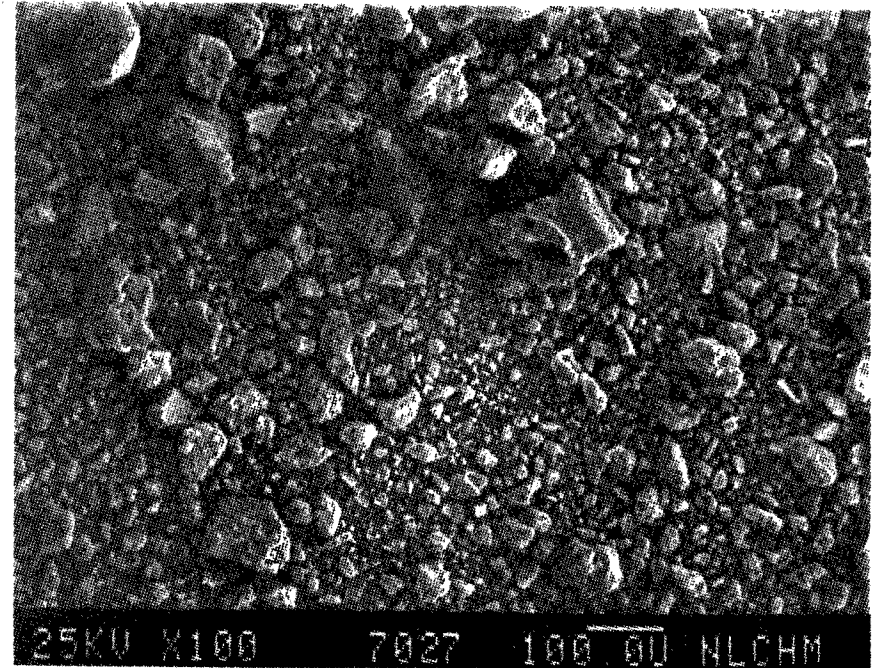


Figure 487

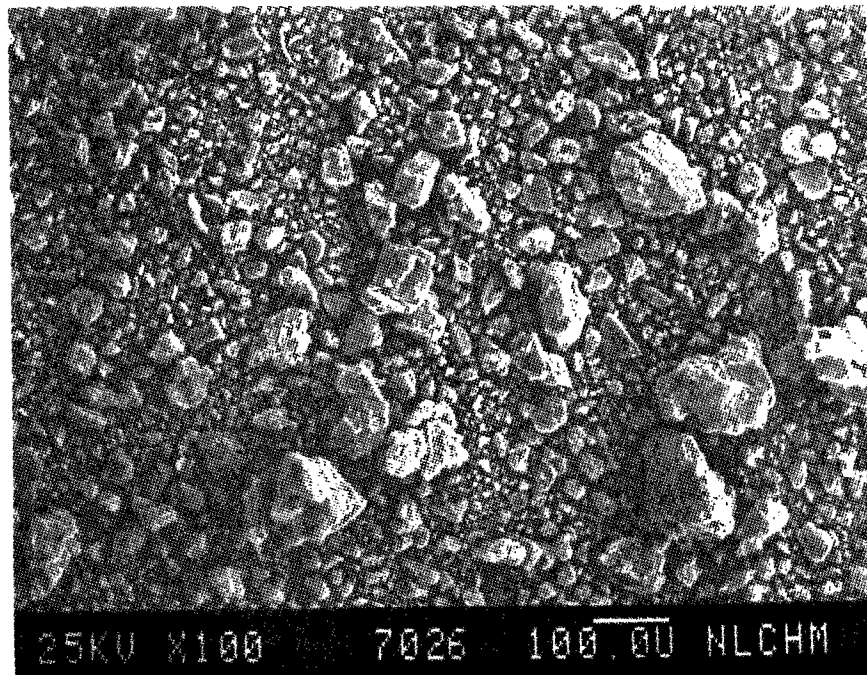


Figure 488

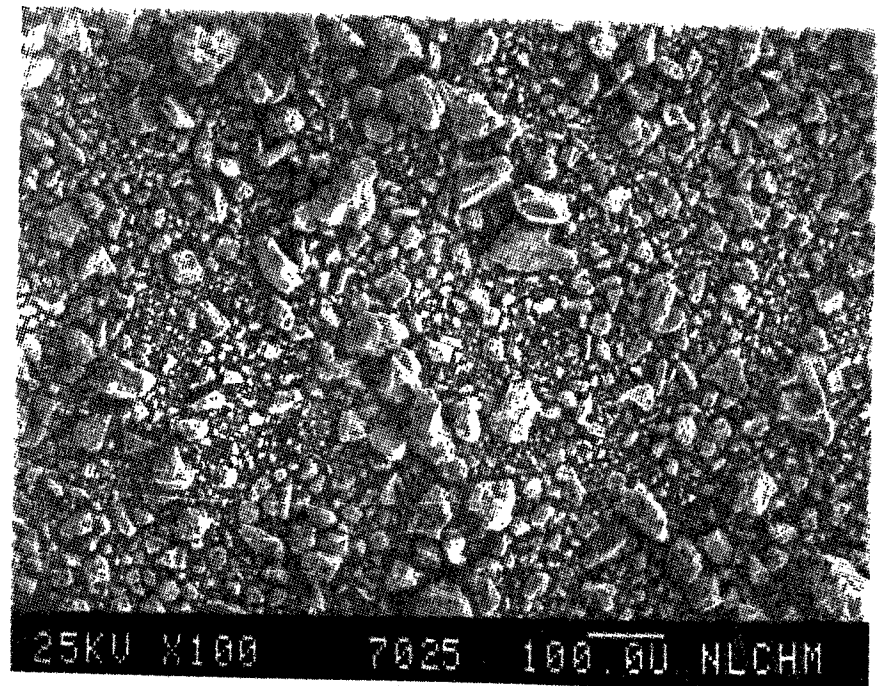


Figure 489

SEM IMAGES OF SAMPLE #

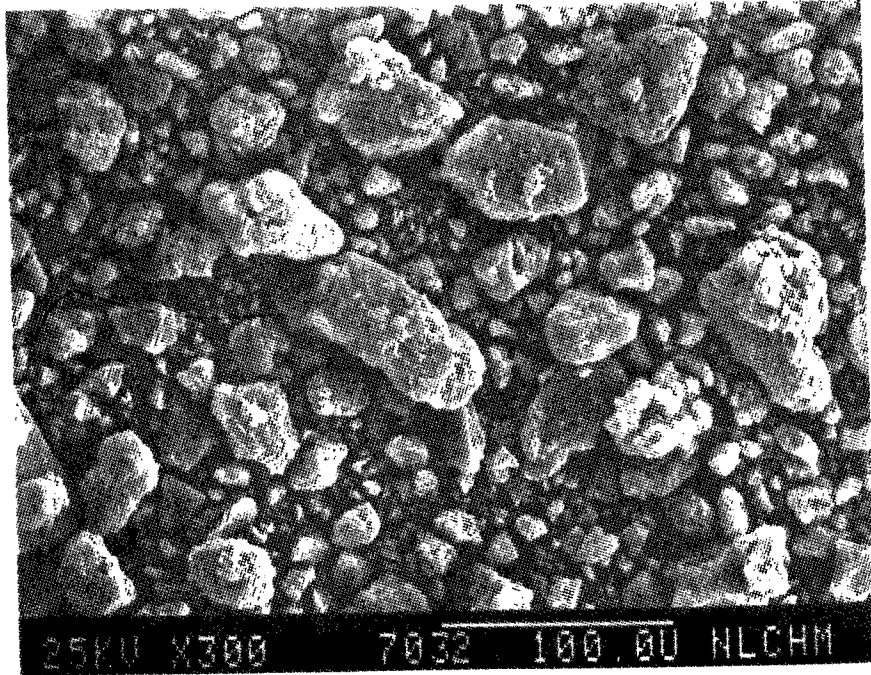


Figure 490

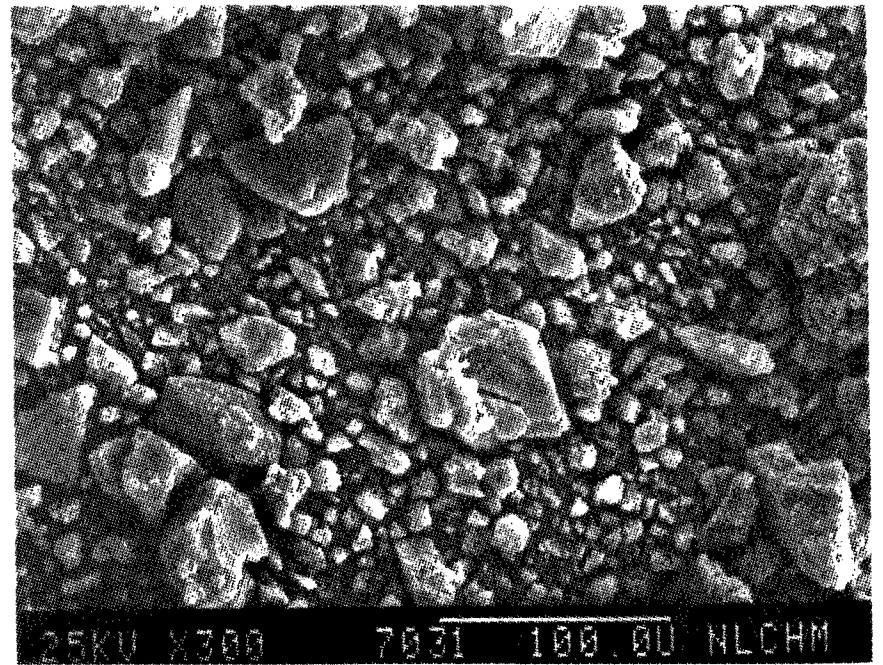


Figure 491

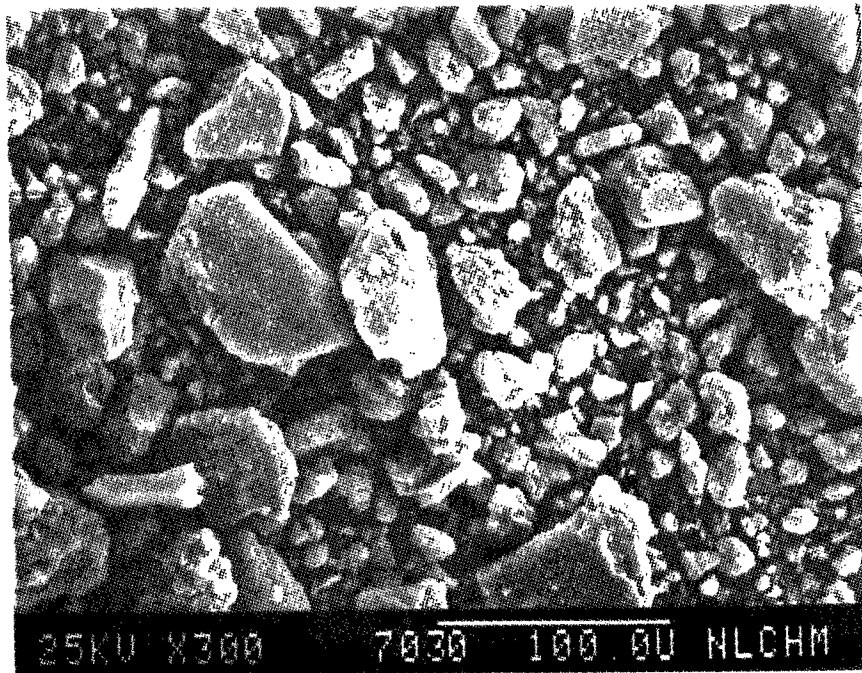


Figure 492

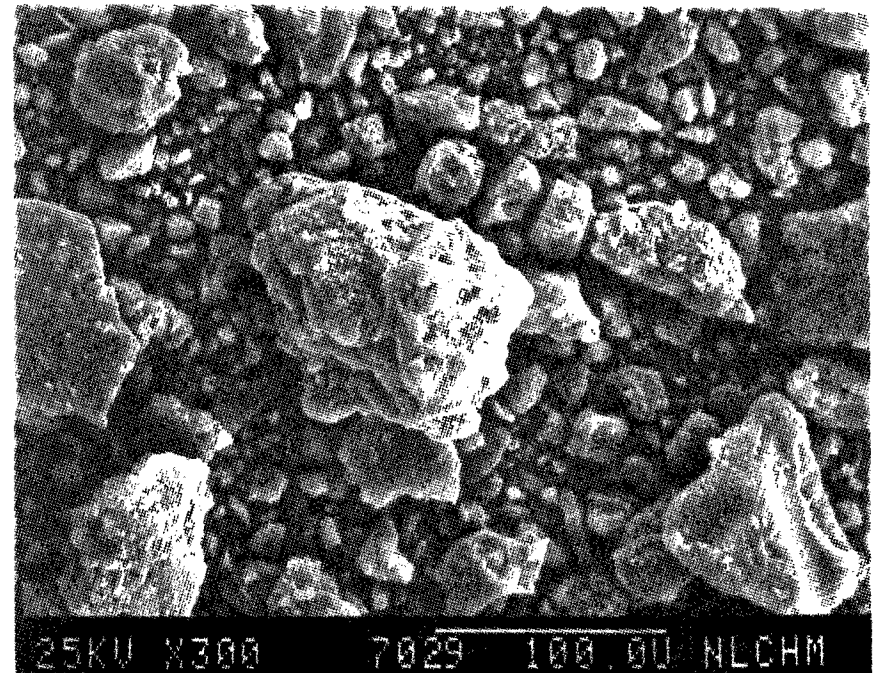


Figure 493



SEM IMAGES OF SAMPLE #

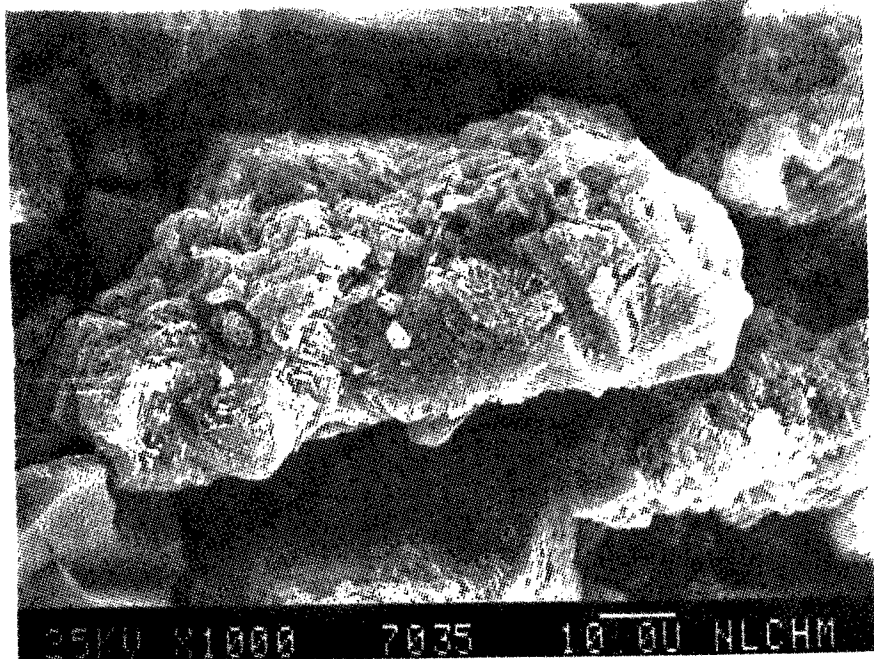


Figure 494

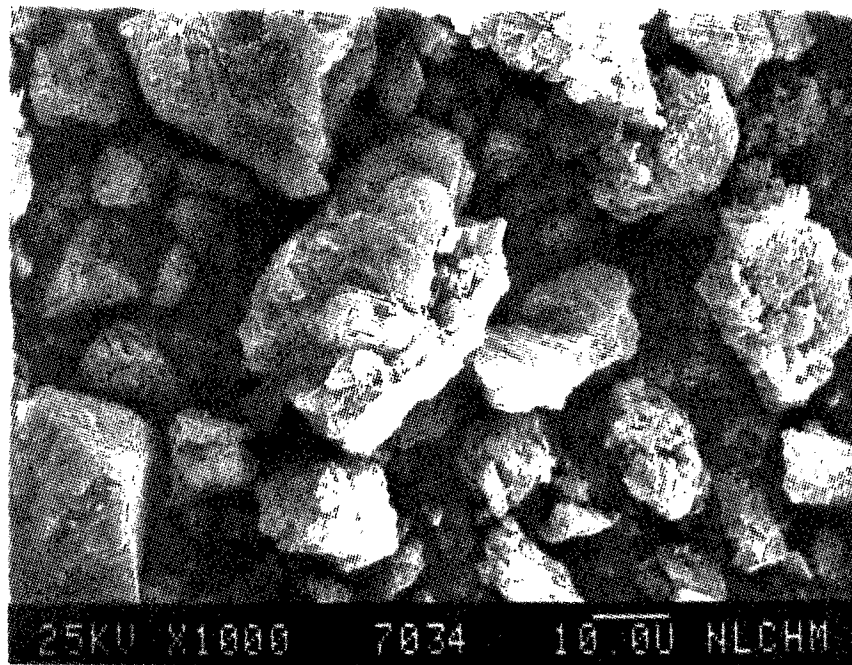


Figure 495

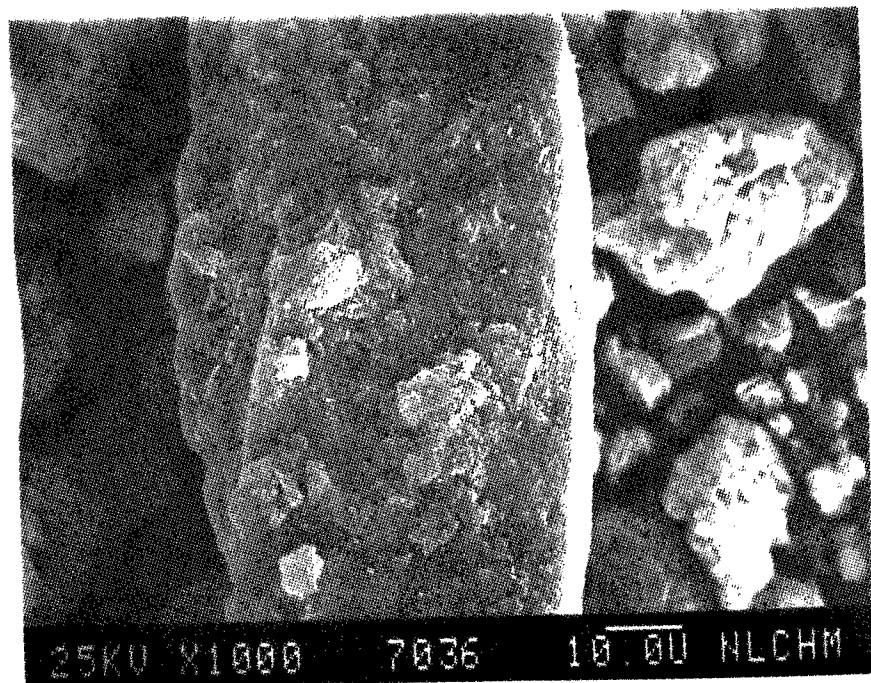


Figure 496

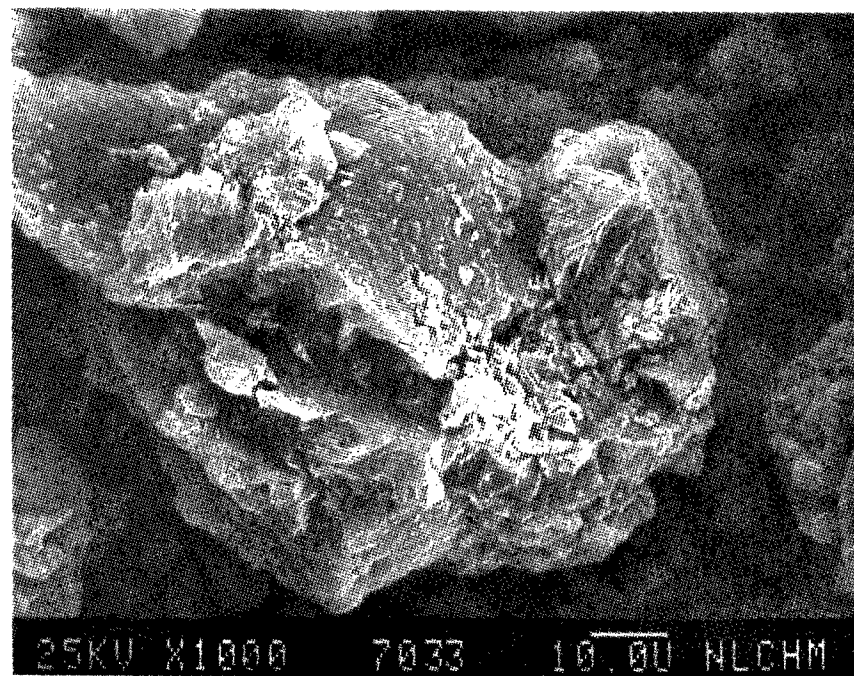
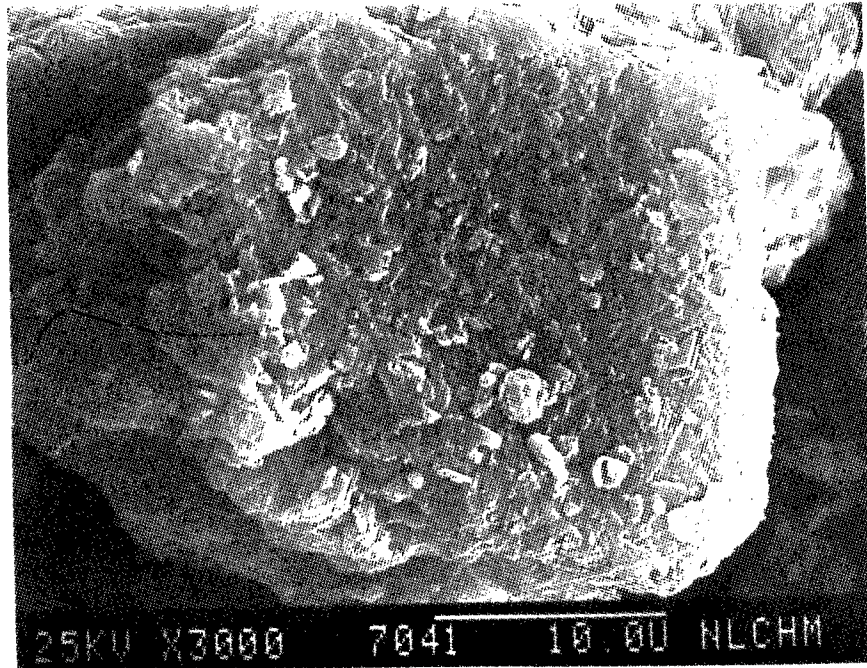


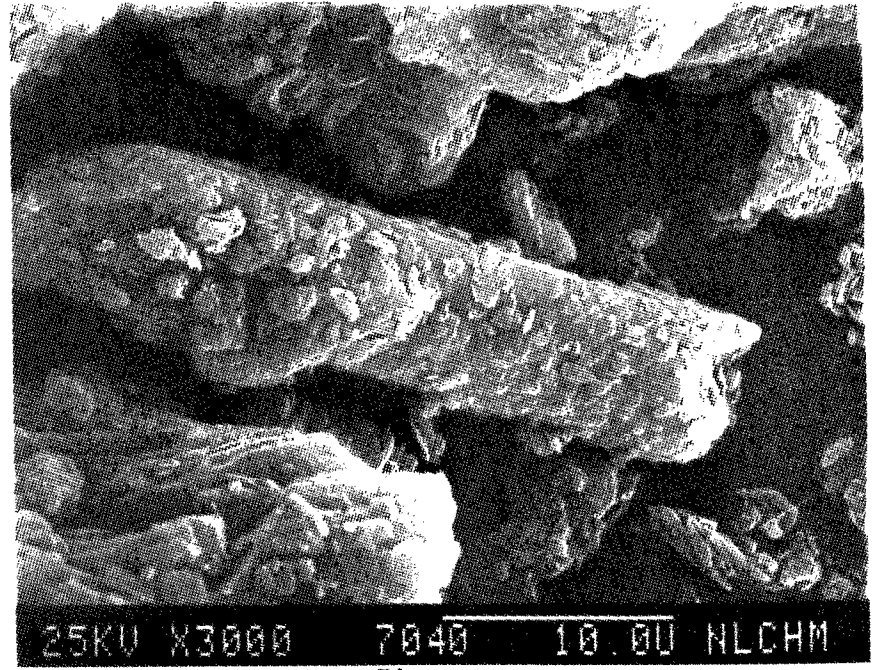
Figure 497

SEM IMAGES OF SAMPLE #



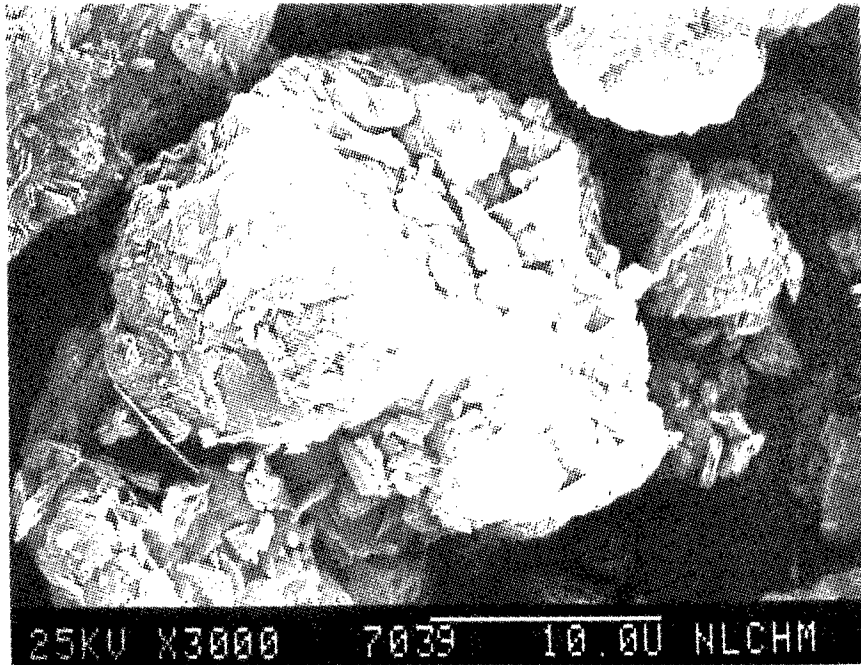
25KV X3000 7041 10.00 NLCHM

Figure 498



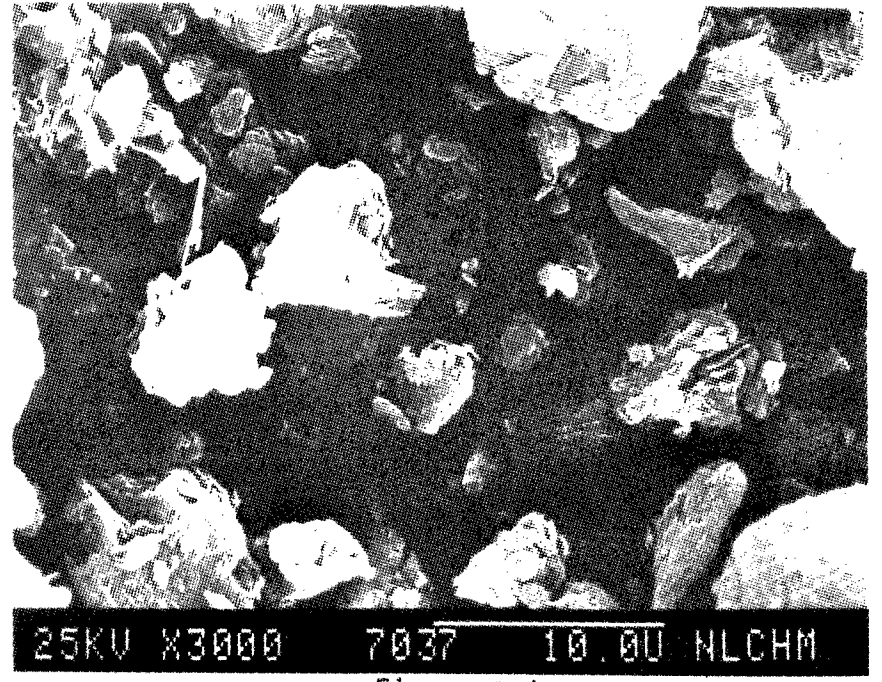
25KV X3000 7040 10.00 NLCHM

Figure 499



25KV X3000 7039 10.00 NLCHM

Figure 500



25KV X3000 7037 10.00 NLCHM

Figure 501



SEM IMAGES OF SAMPLE #

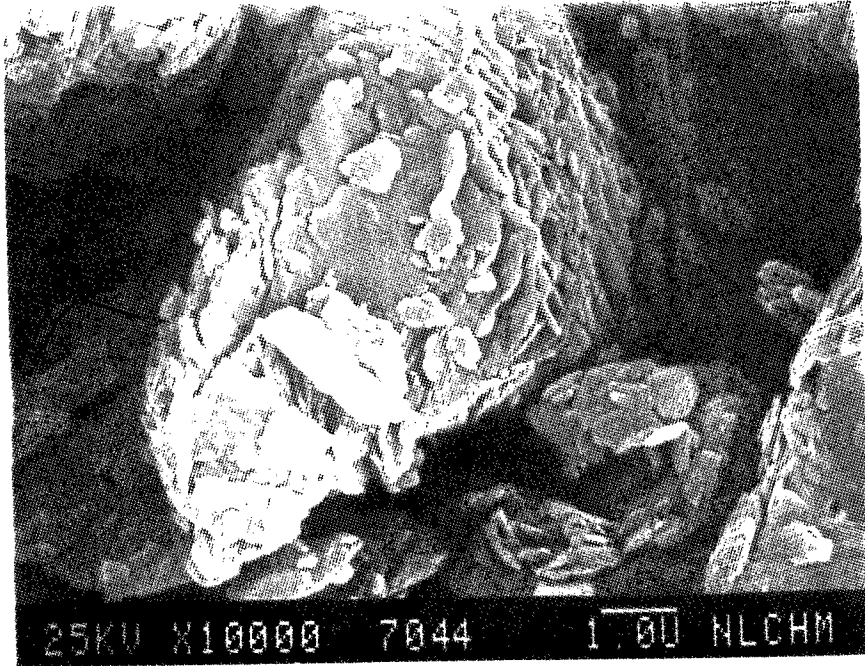


Figure 502

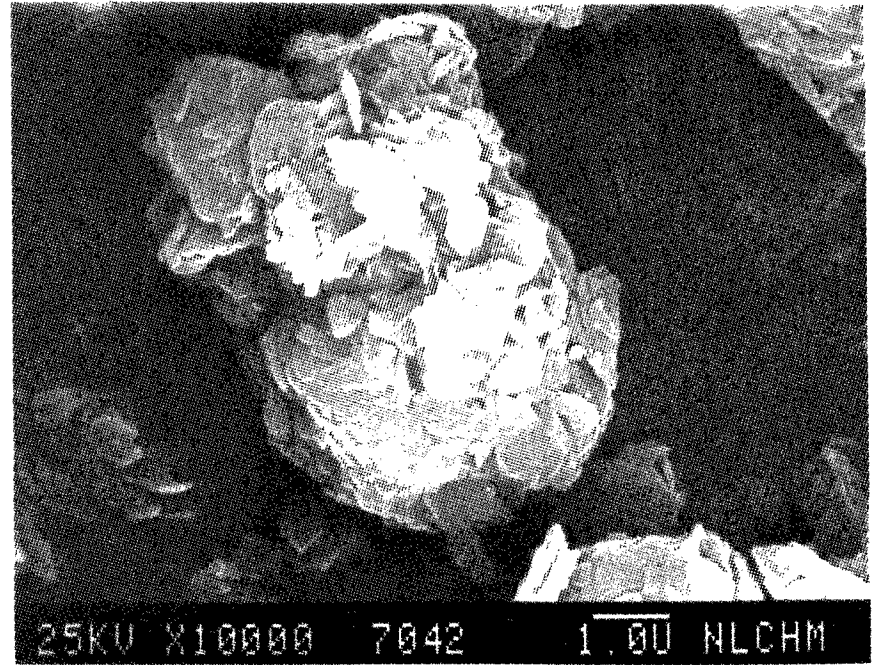


Figure 503

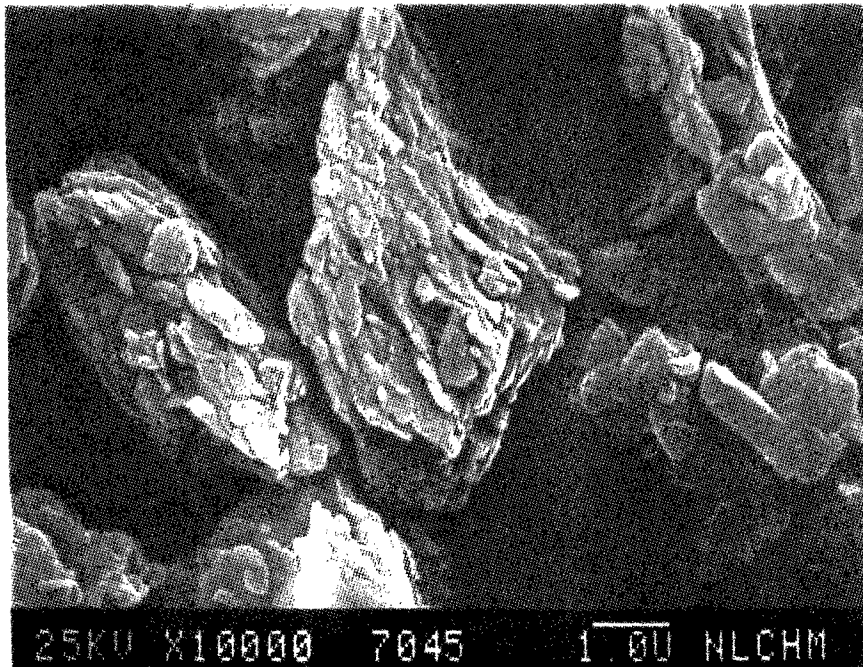


Figure 504

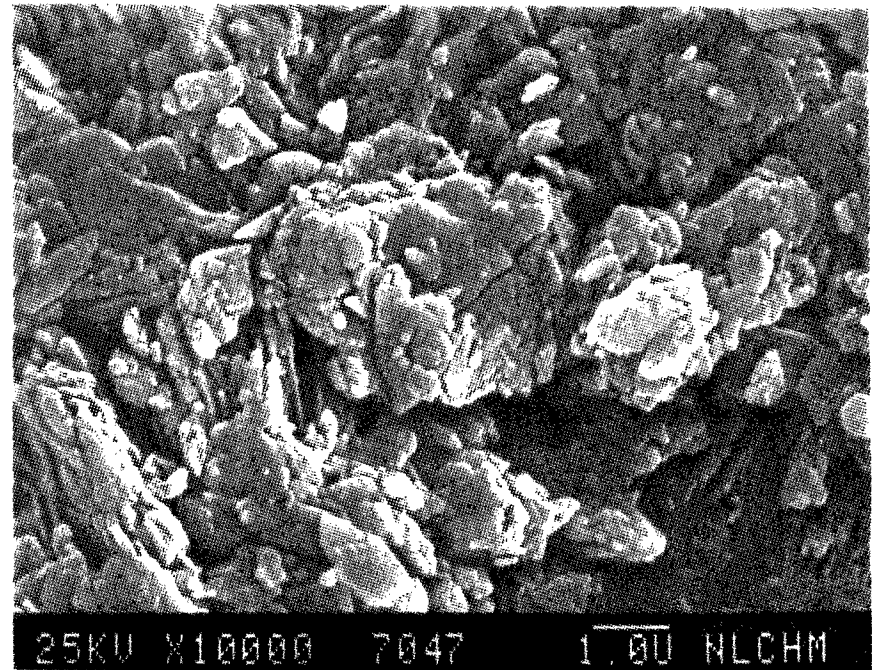


Figure 505

SEM IMAGES OF SAMPLE #

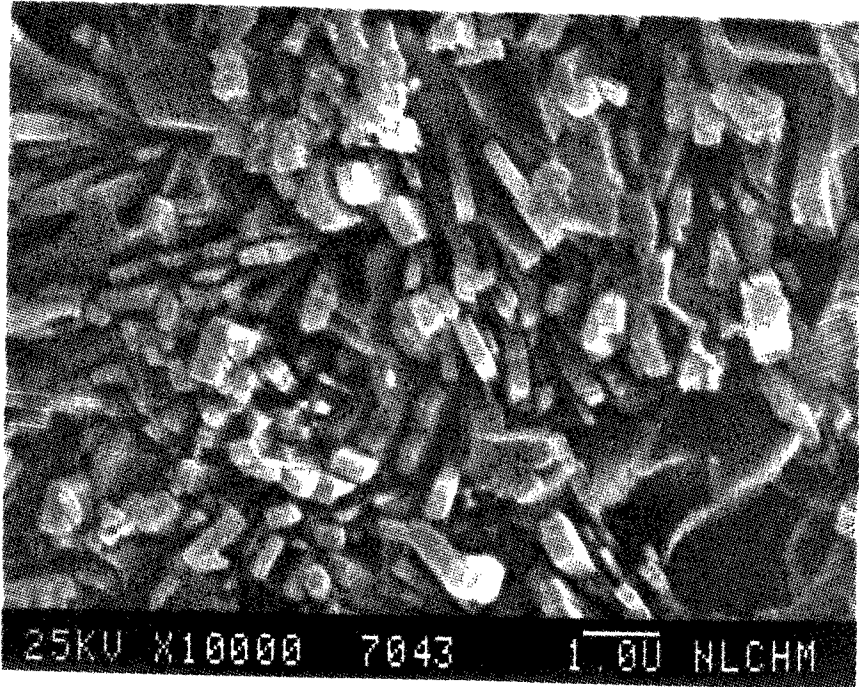


Figure 506

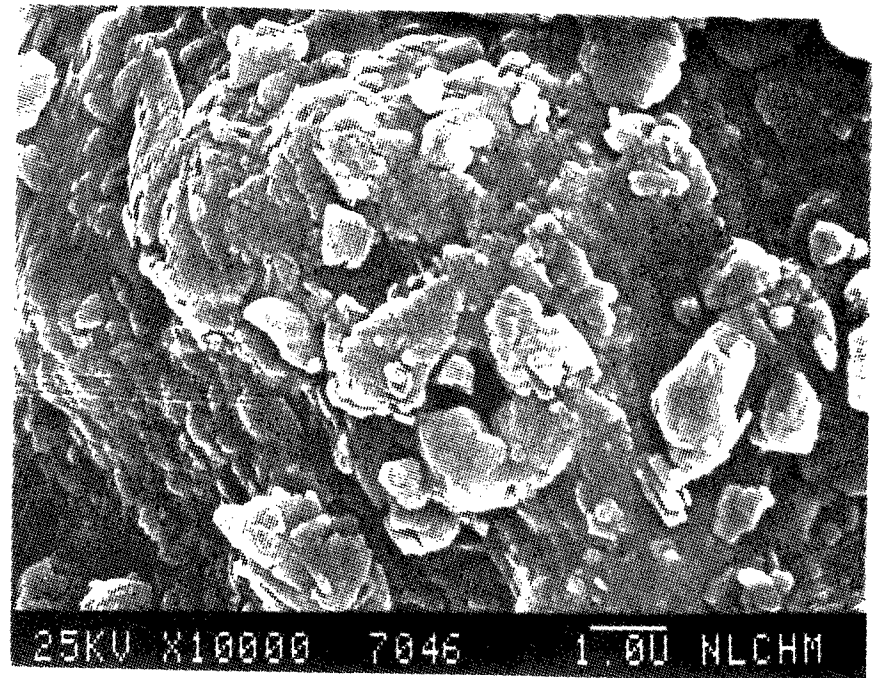


Figure 507



SEM IMAGES OF SAMPLE #

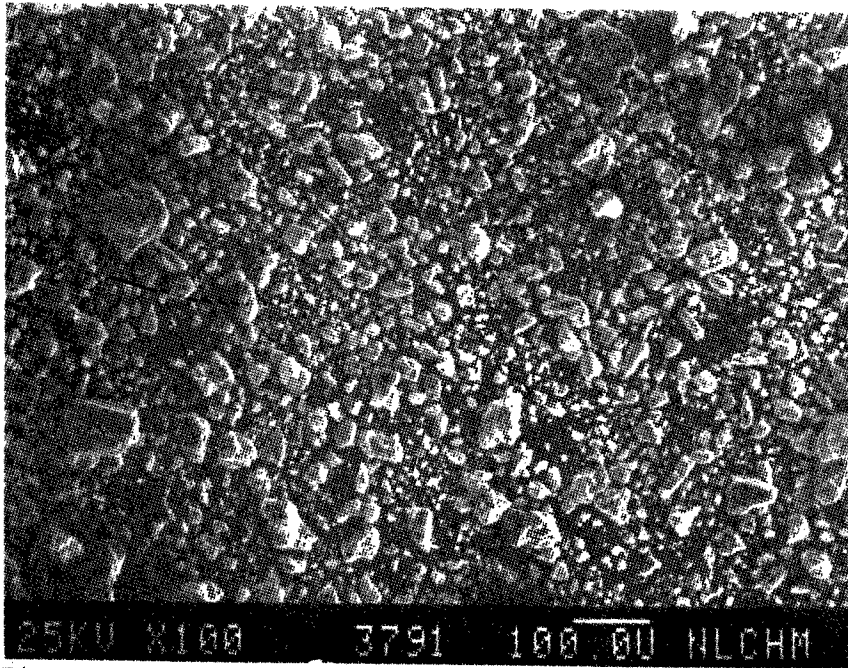


Figure 508

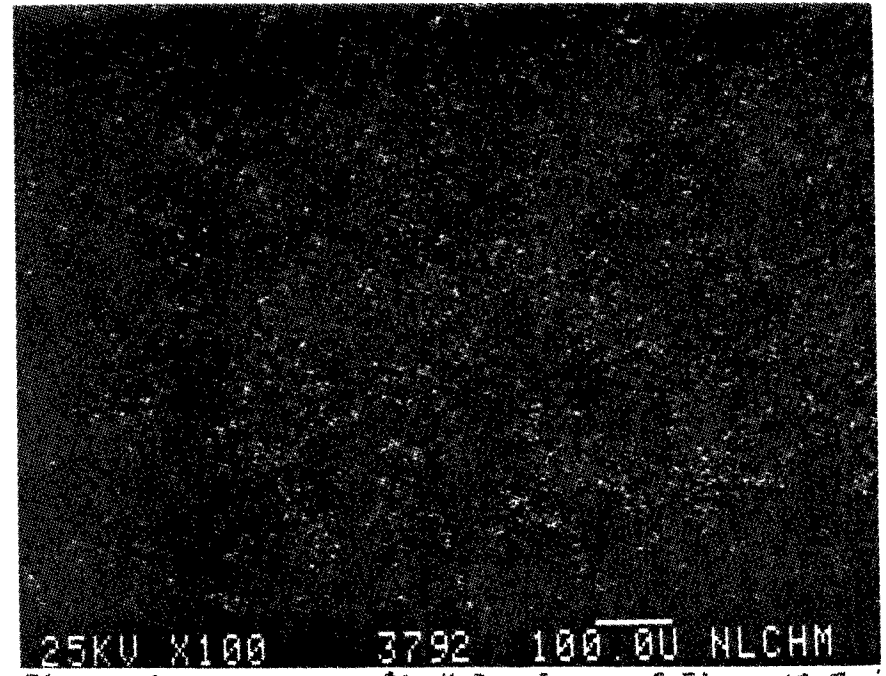


Figure 509

AL X-Ray Image of Figure 508

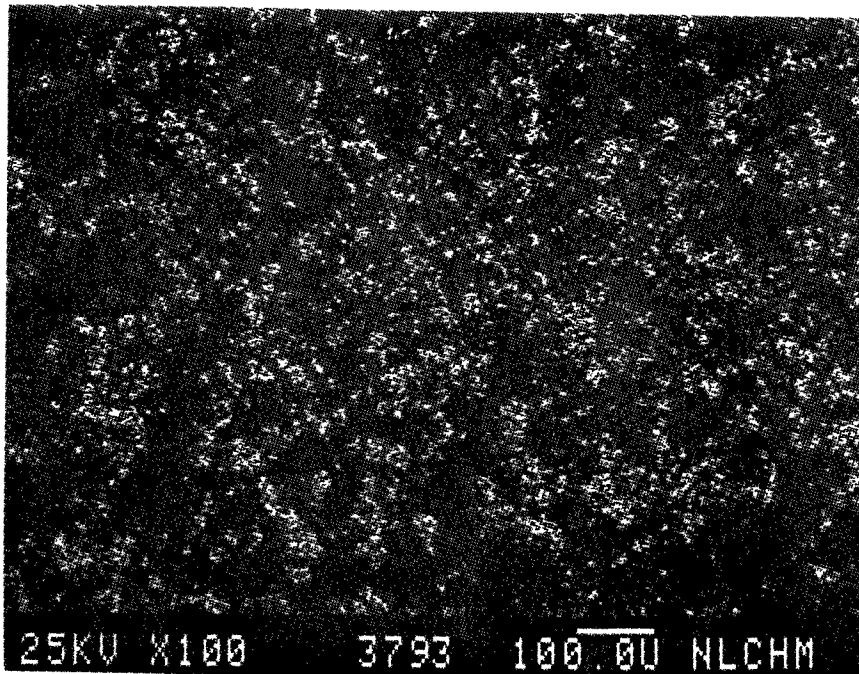


Figure 510

Si X-Ray Image of Figure 508

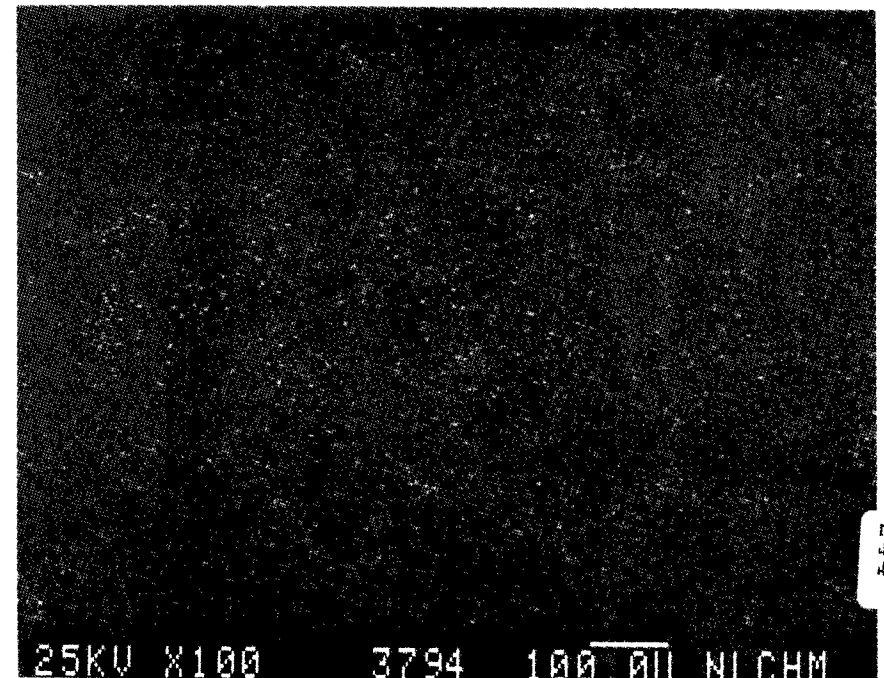


Figure 511

K X-Ray Image of Figure 508

SEM IMAGES OF SAMPLE #

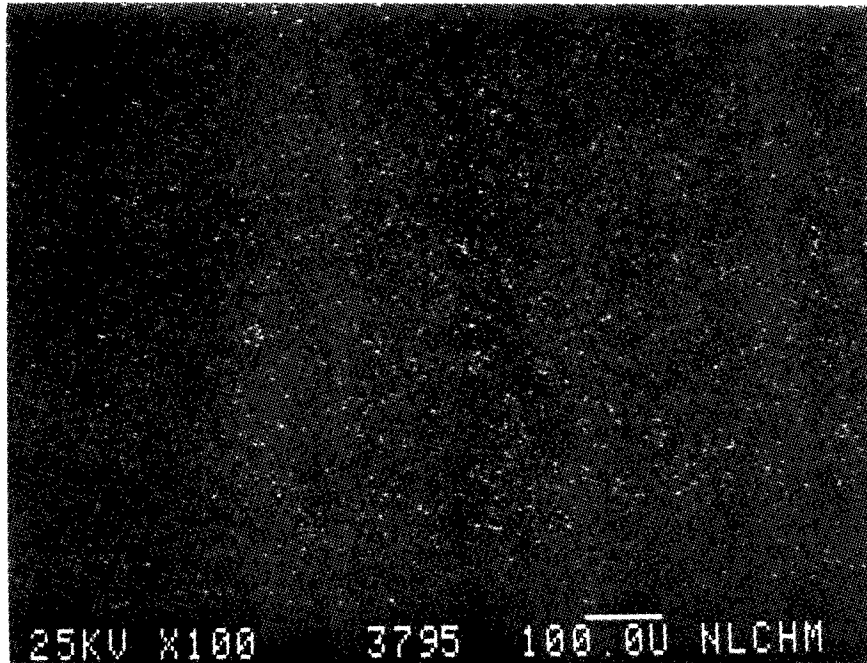


Figure 512

Ca X-Ray Image of Figure 508

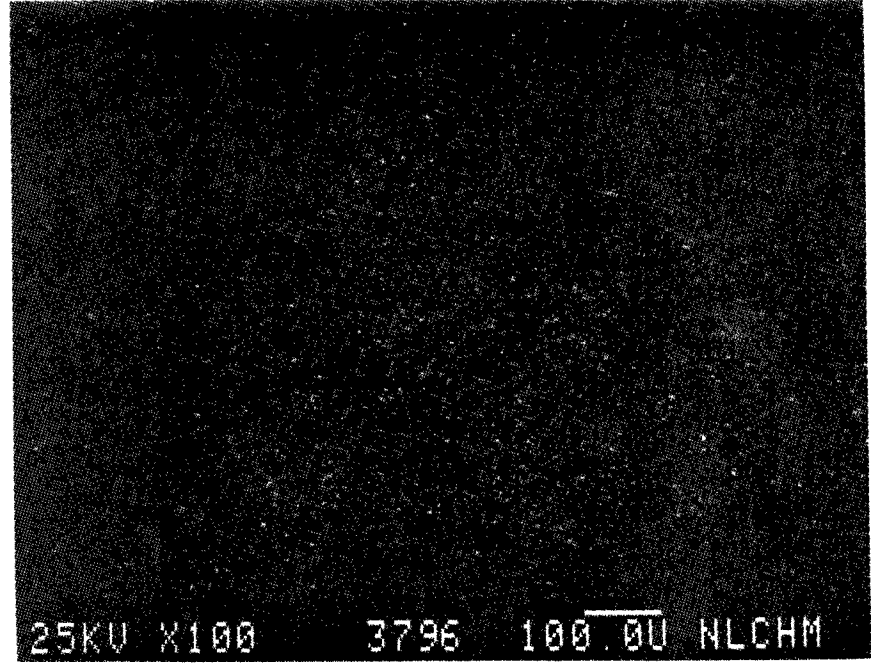


Figure 513

Ti X-Ray Image of Figure 508

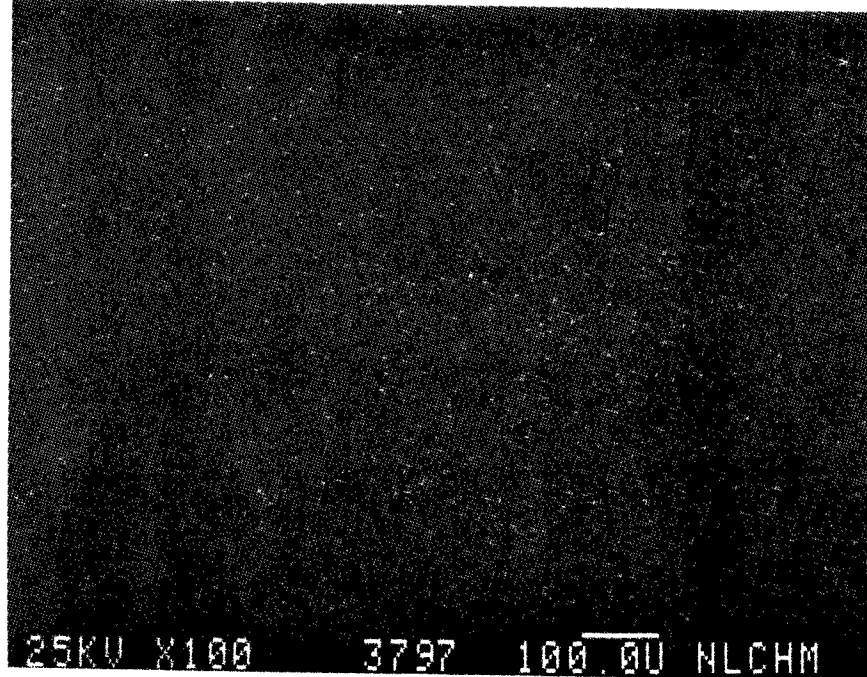


Figure 514

Fe X-Ray Image of Figure 508

SEM IMAGES OF SAMPLE #

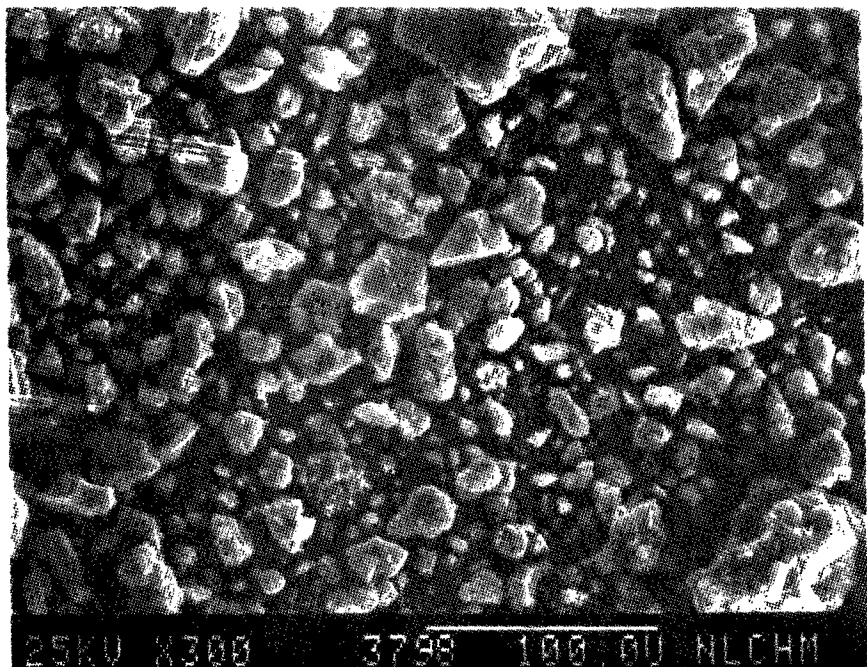


Figure 515

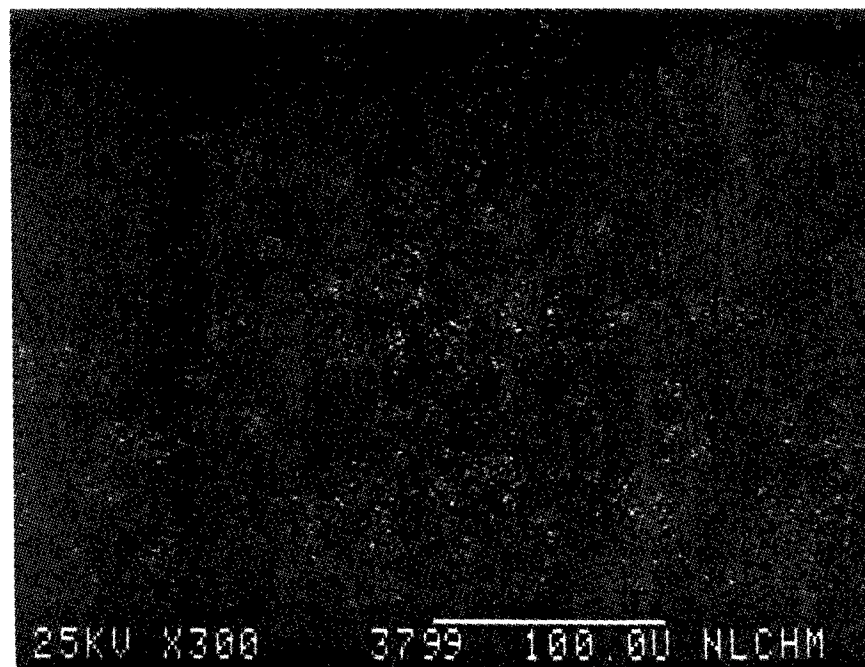


Figure 516

AL X-Ray Image of Figure 515

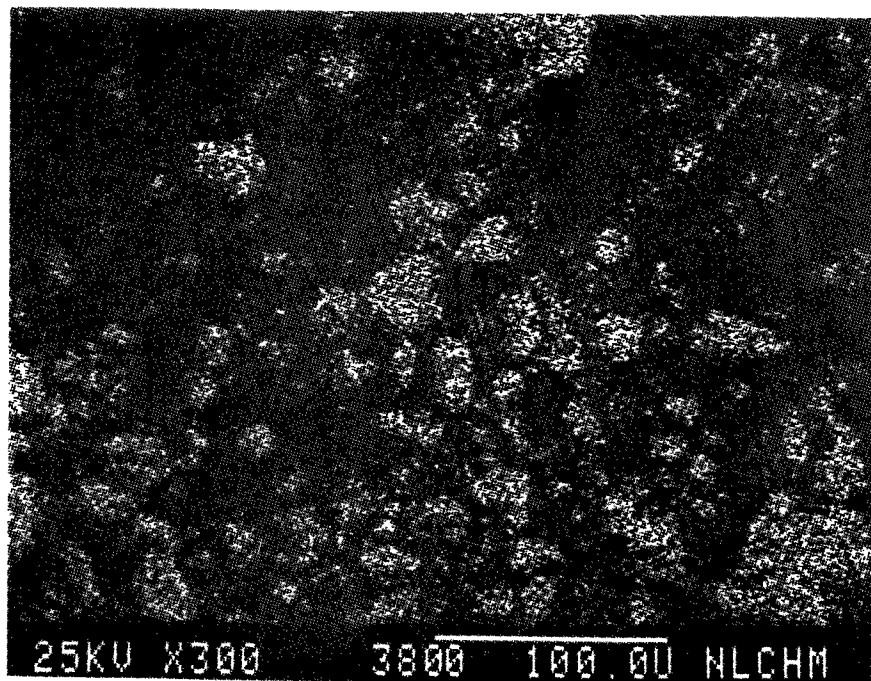


Figure 517

Si X-Ray Image of Figure 515

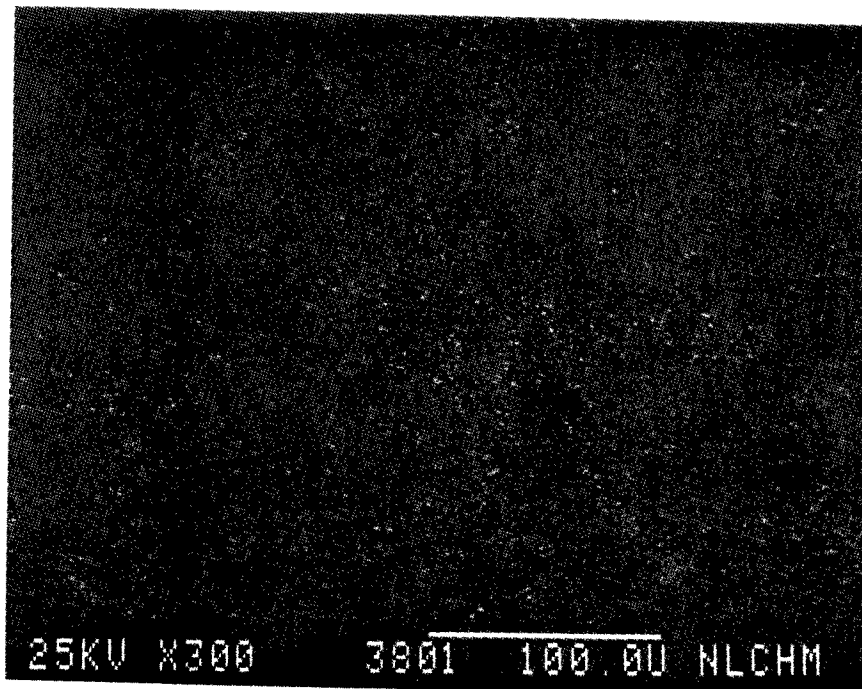


Figure 518

K X-Ray Image of Figure 515

SEM IMAGES OF SAMPLE #

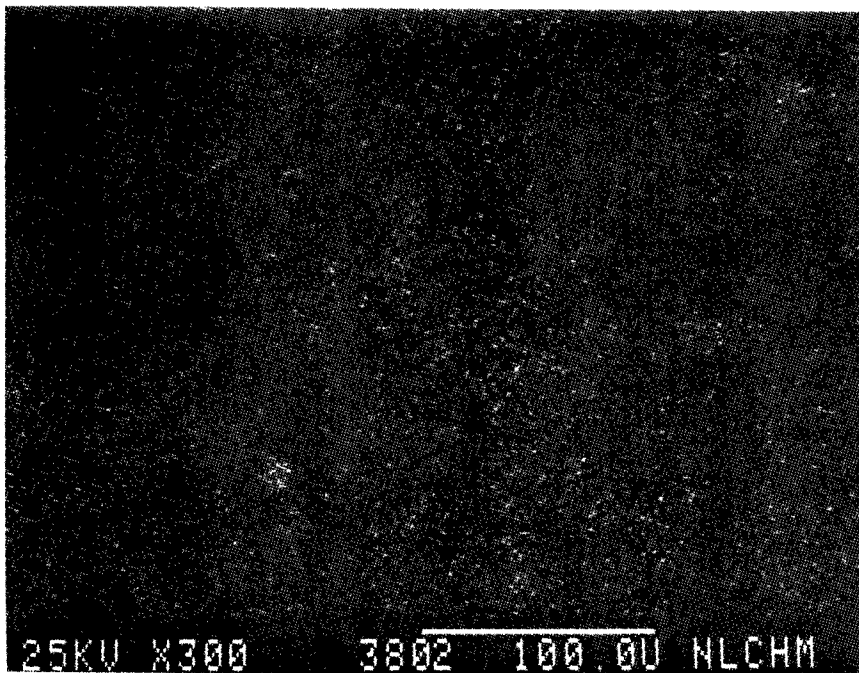


Figure 519

Ca X-Ray Image of Figure 515

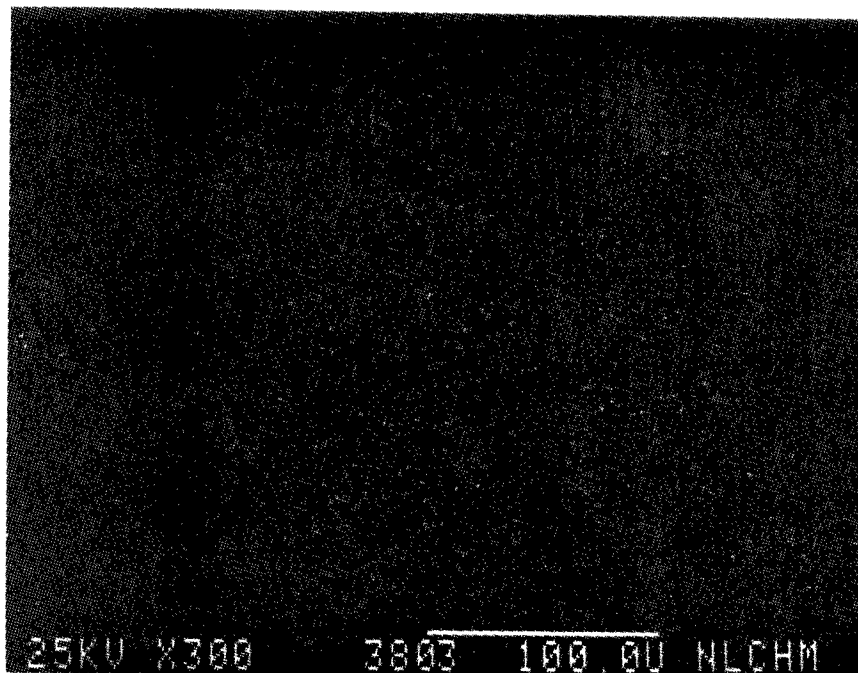


Figure 520

Ti X-Ray Image of Figure 515

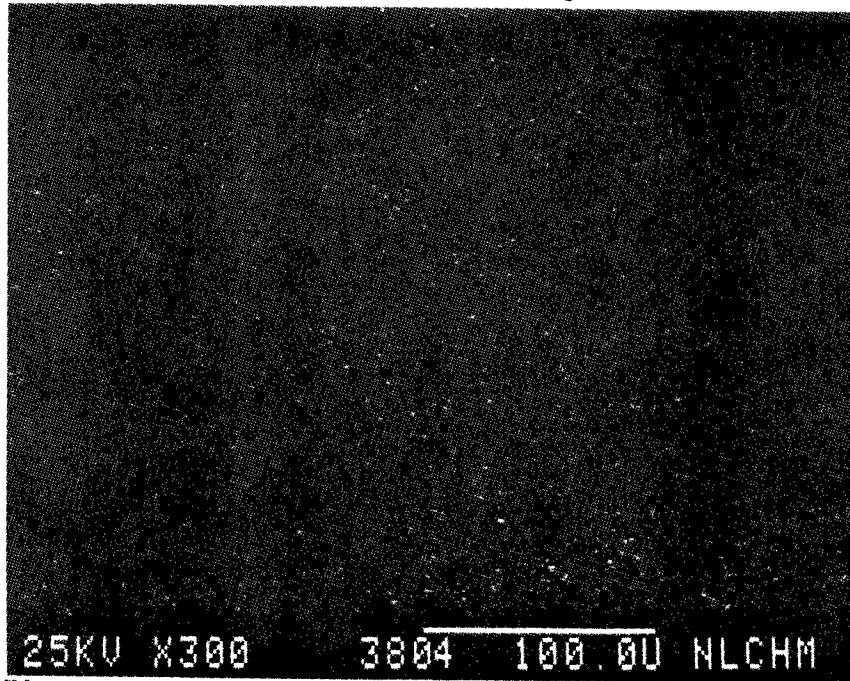


Figure 521

Fe X-Ray Image of Figure 515

SEM IMAGES OF SAMPLE #

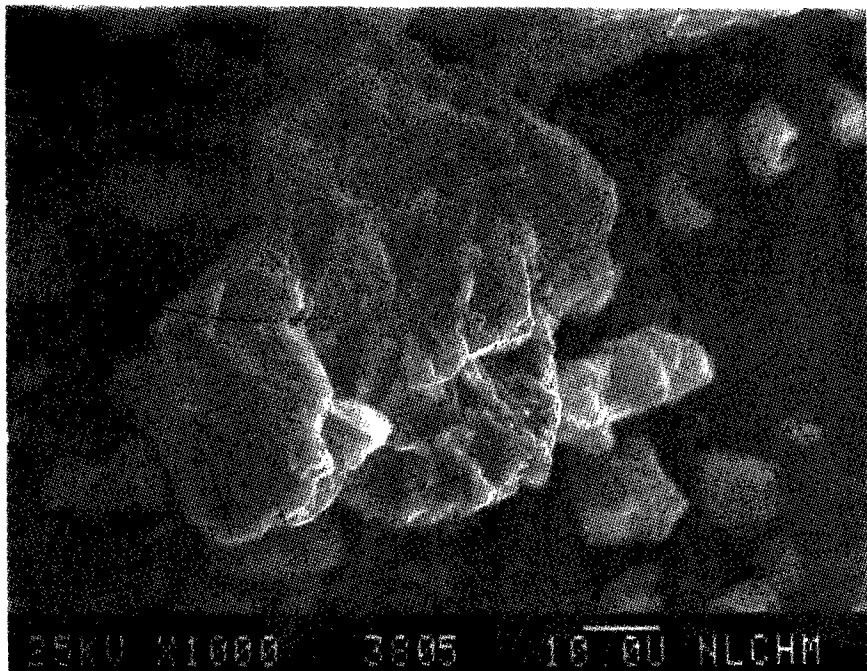


Figure 522

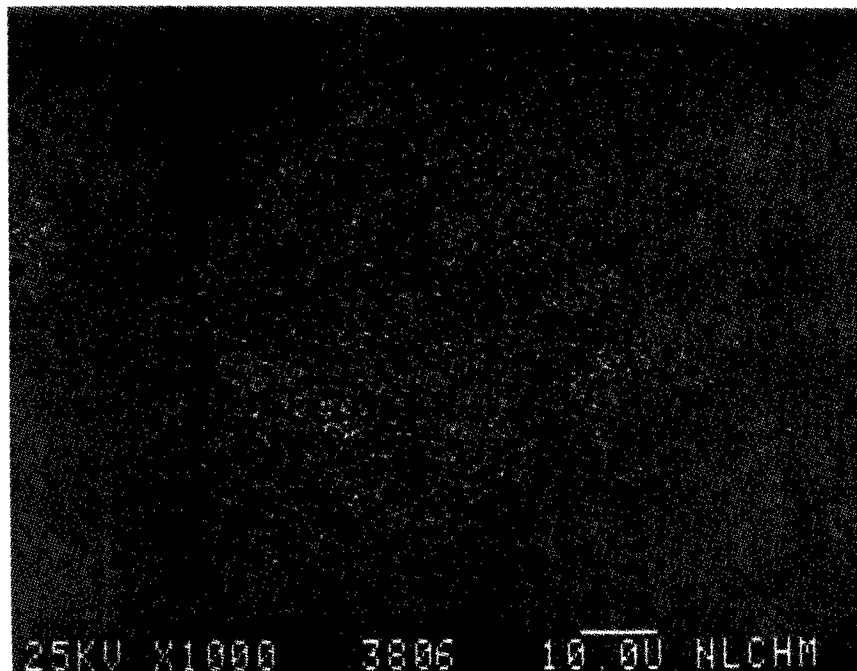


Figure 523

Al X-Ray Image of Figure 522

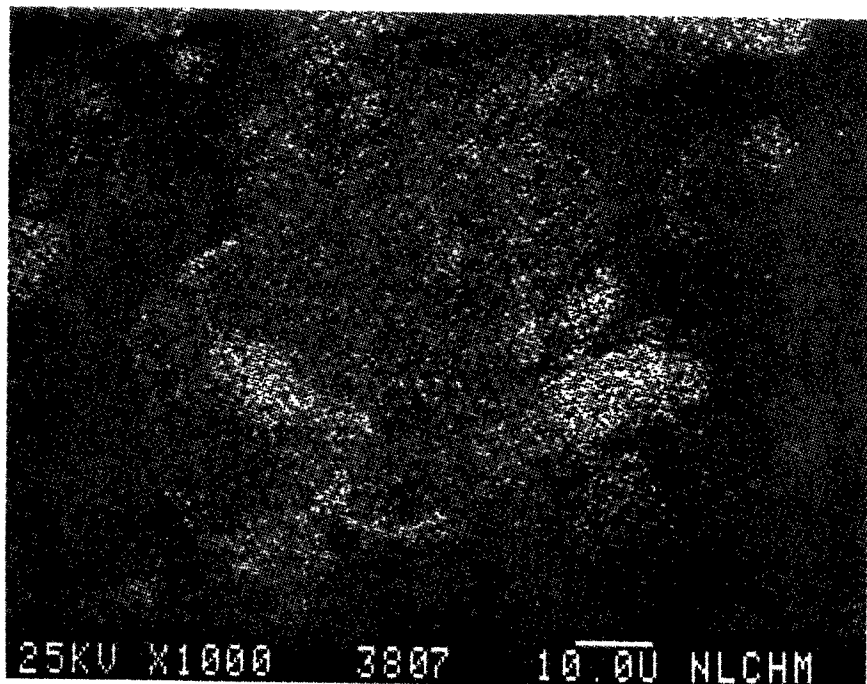


Figure 524

Si X-Ray Image of Figure 522

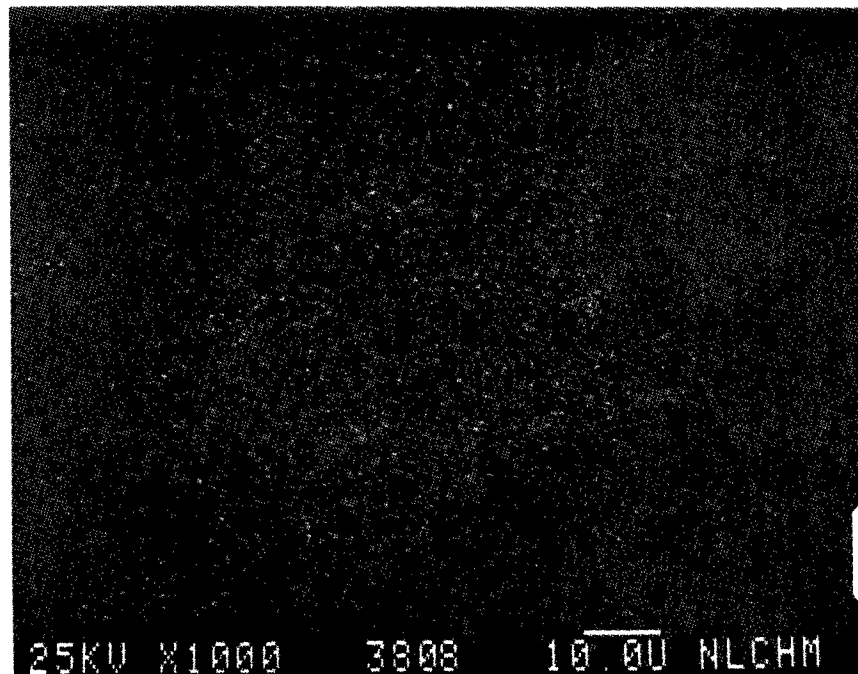


Figure 525

K X-Ray Image of Figure 522



SEM IMAGES OF SAMPLE #

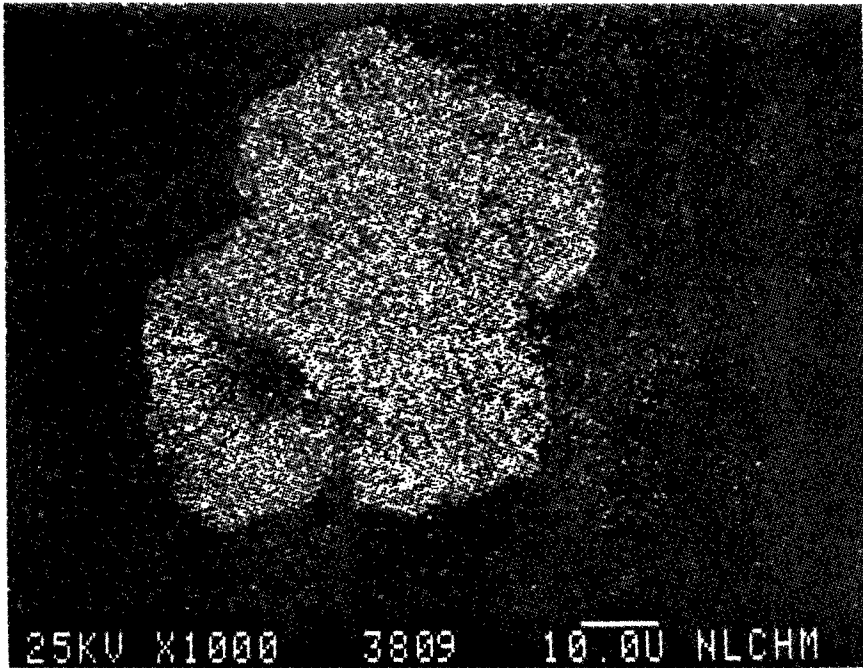


Figure 526

Ca X-Ray Image of Figure 522

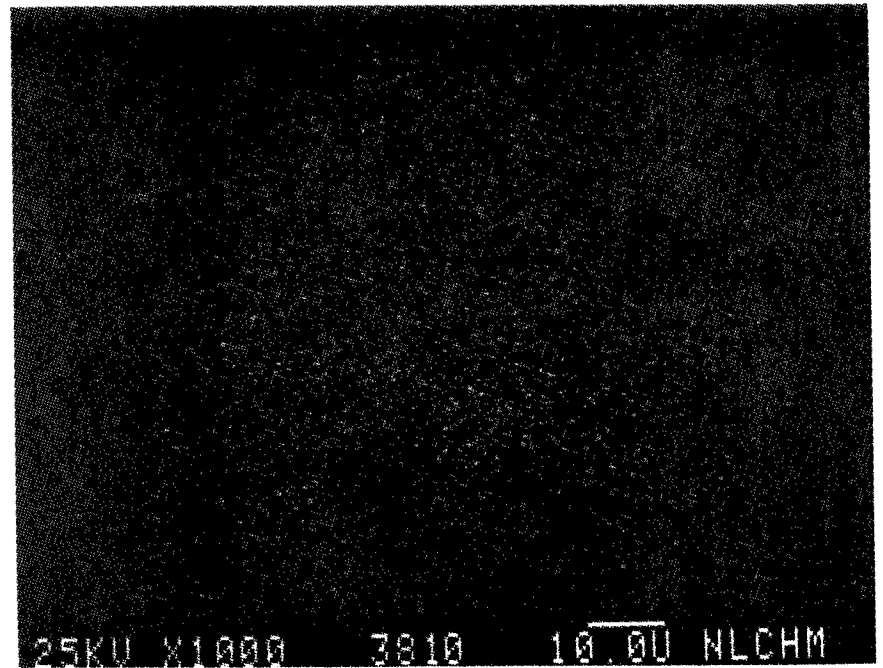


Figure 527

Ti X-Ray Image of Figure 522

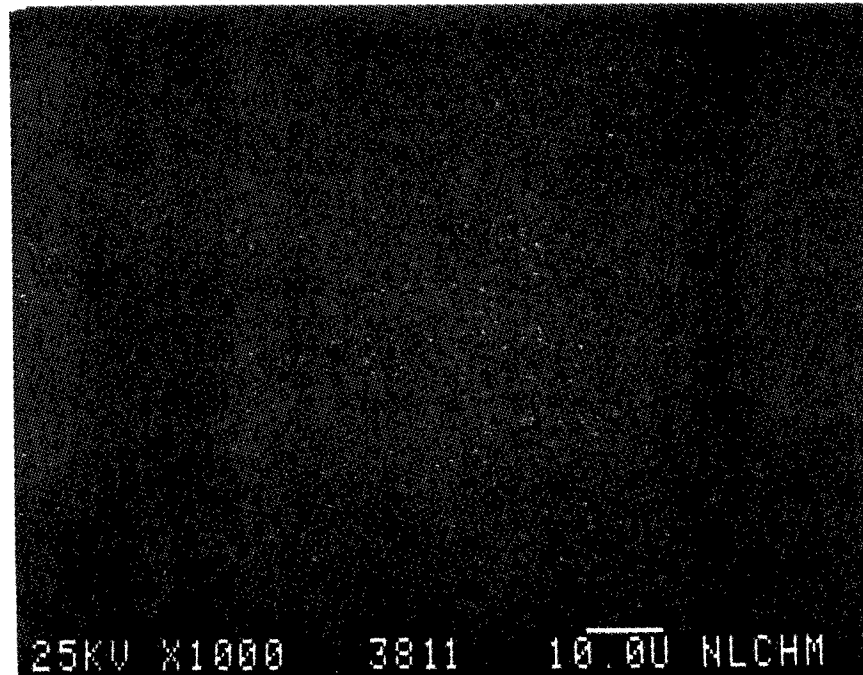


Figure 528

Fe X-Ray Image of Figure 522



SEM IMAGES OF SAMPLE #

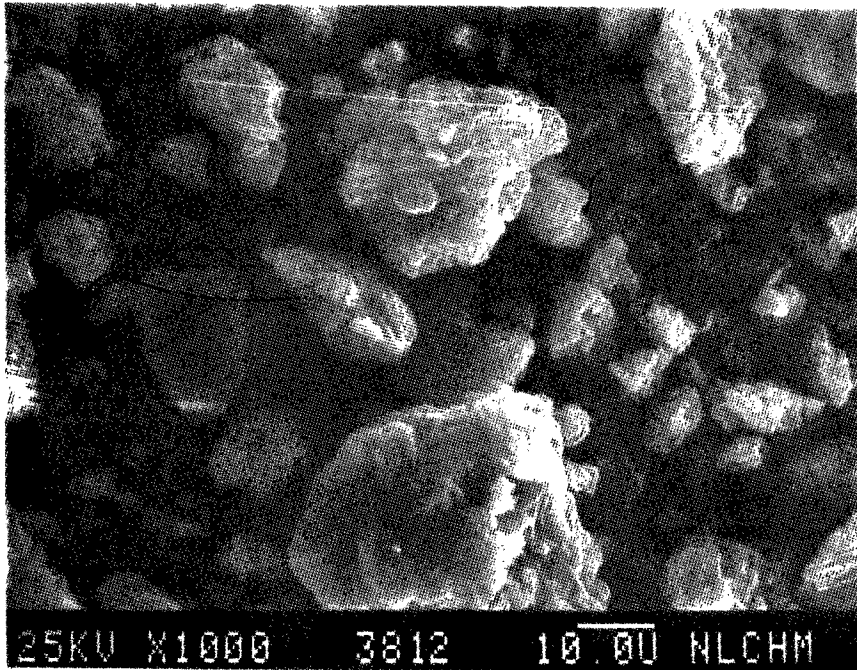


Figure 529

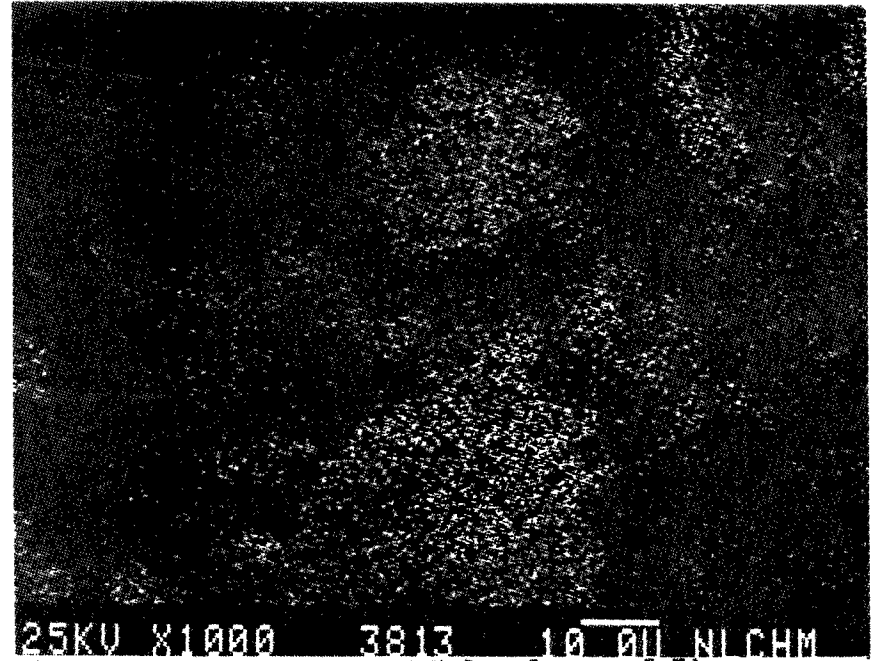


Figure 530

AL X-Ray Image of Figure 529

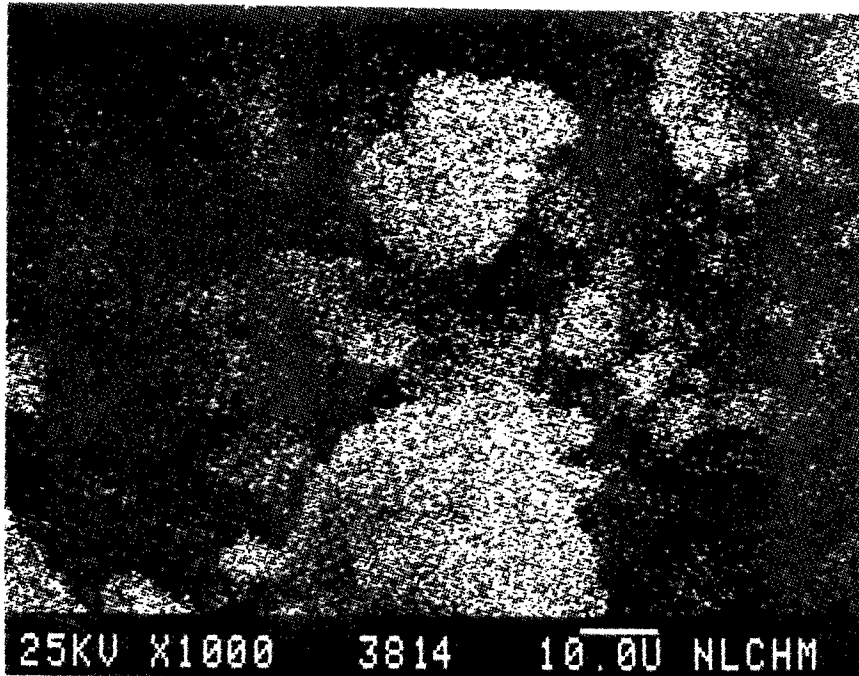


Figure 531

Si X-Ray Image of Figure 529

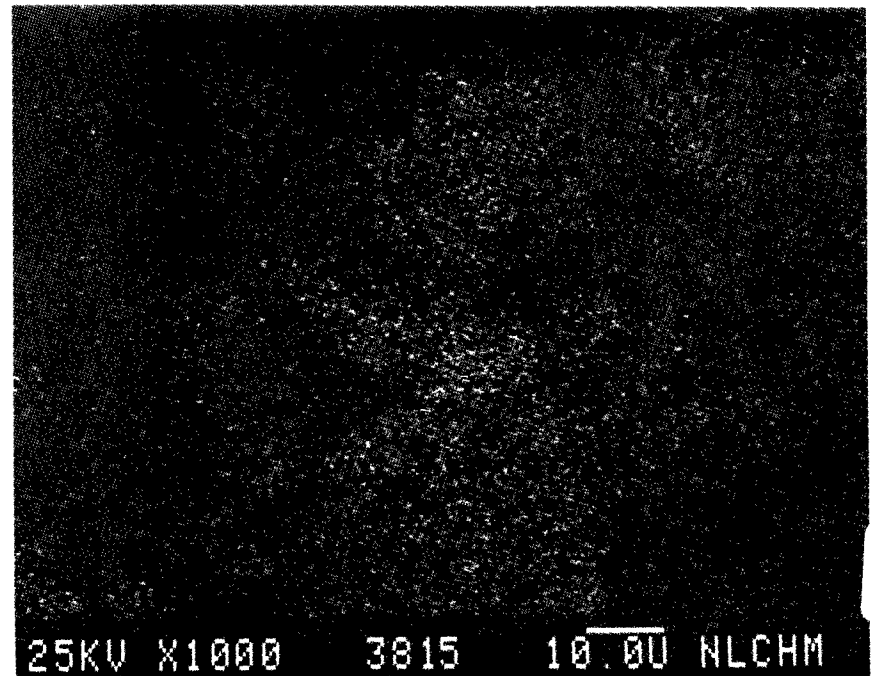


Figure 532

K X-Ray Image of Figure 529

SEM IMAGES OF SAMPLE #

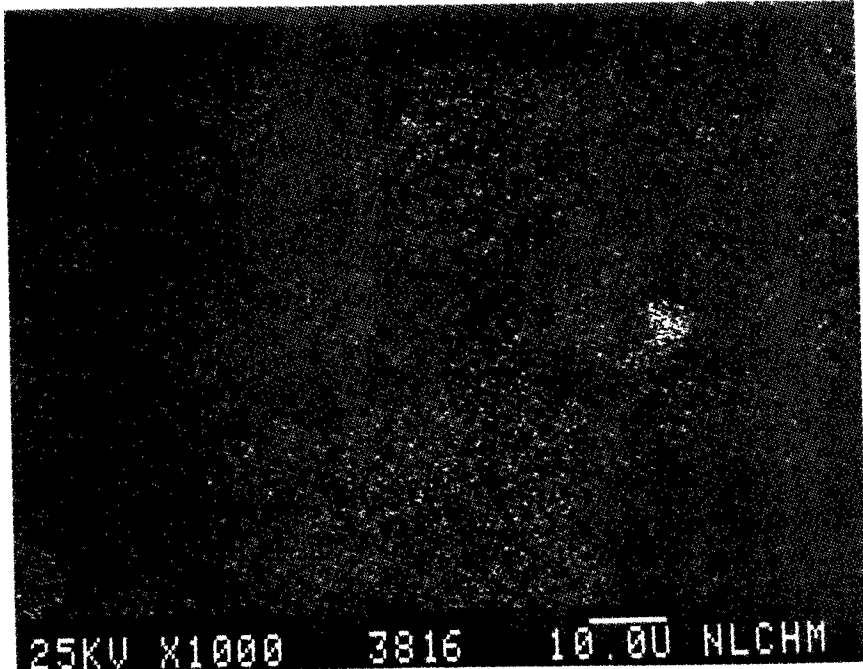


Figure 533

Ca X-Ray Image of Figure 529

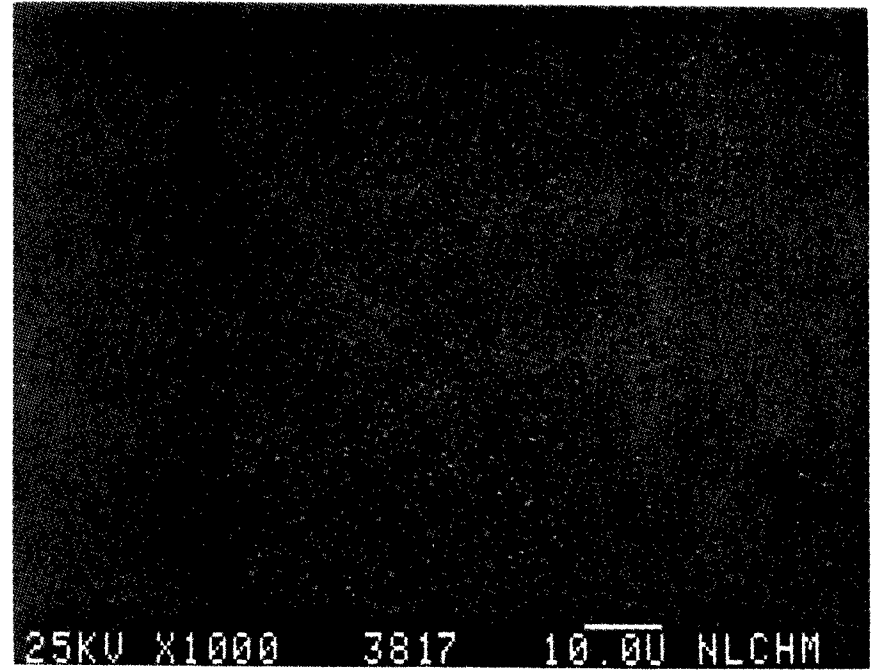


Figure 534

Ti X-Ray Image of Figure 529

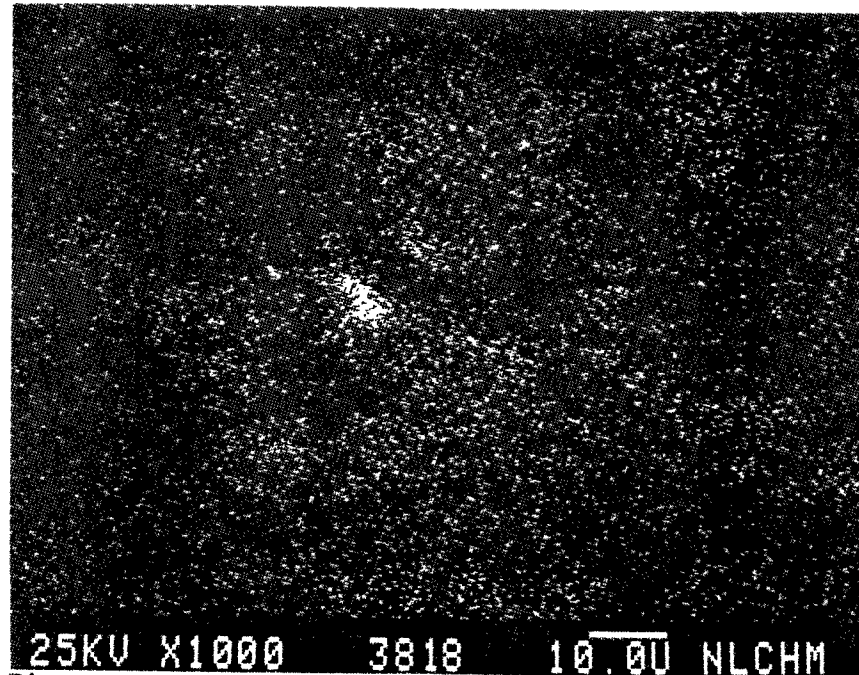


Figure 535

Fe X-Ray Image of Figure 529

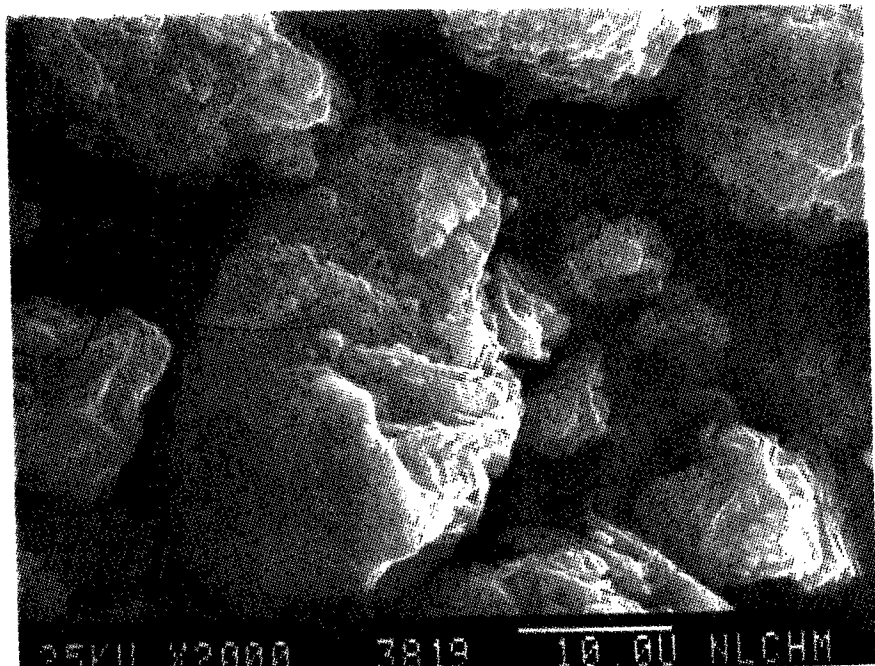


Figure 536

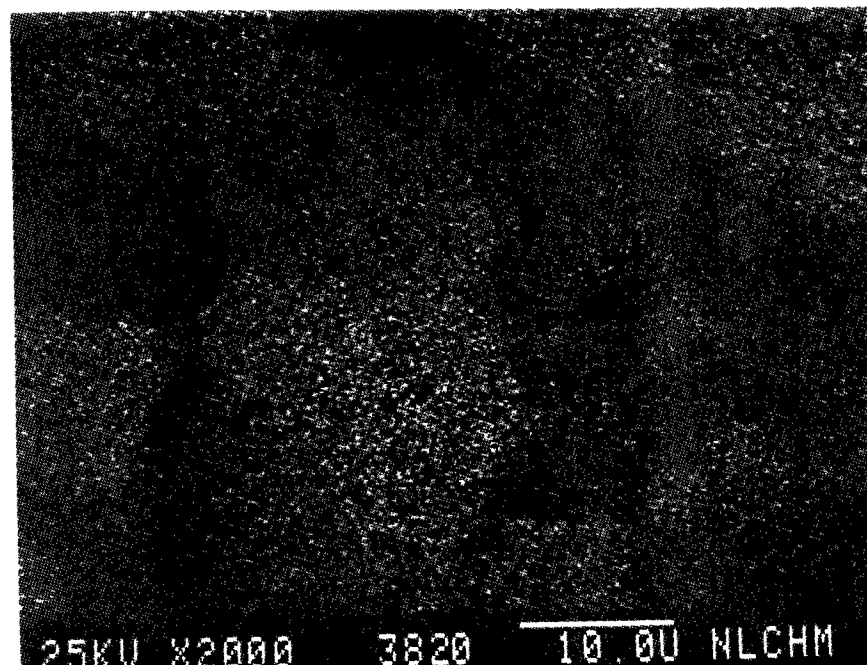


Figure 537

AL X-Ray Image of Figure 536

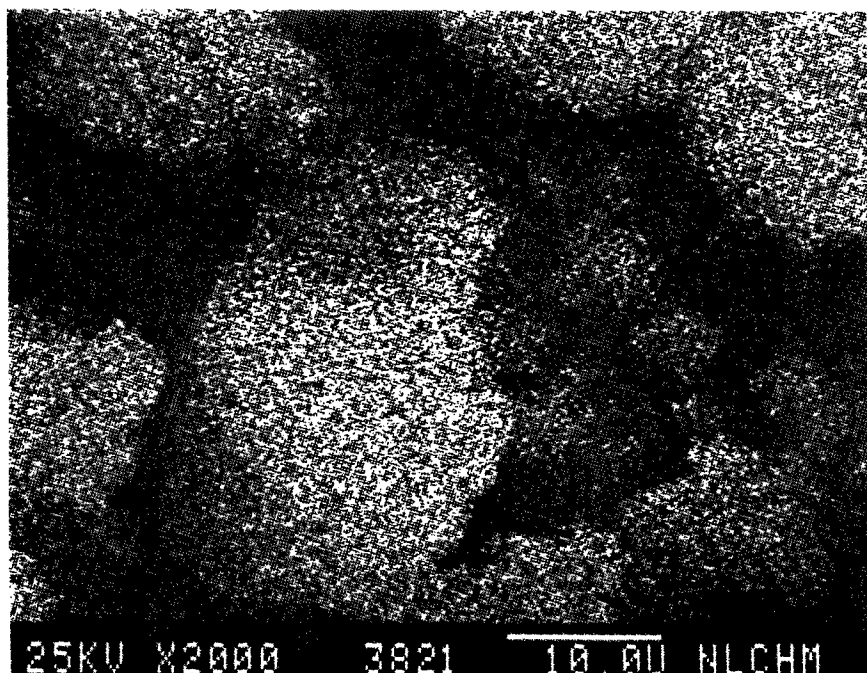


Figure 538

Si X-Ray Image of Figure 536

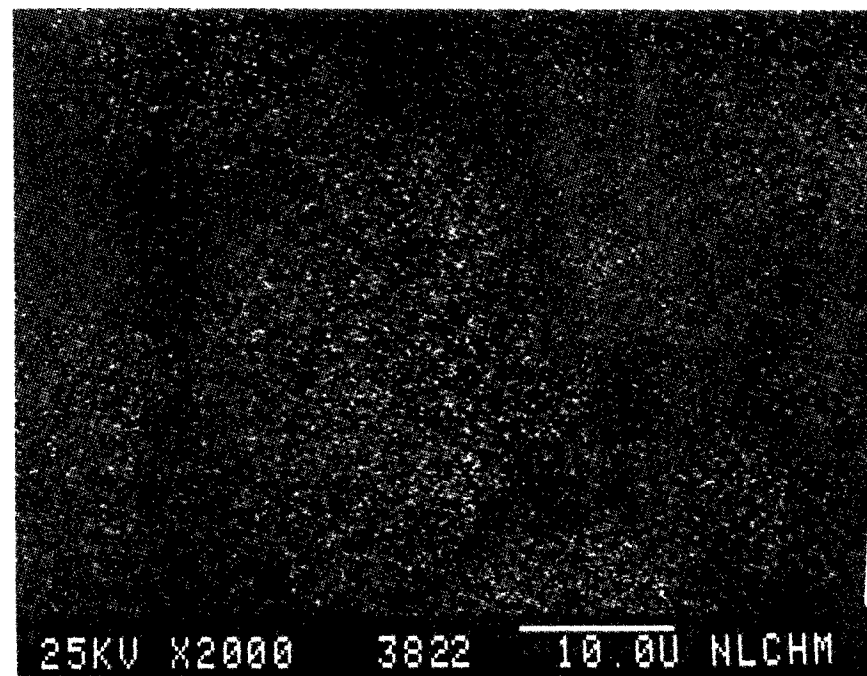


Figure 539

K X-Ray Image of Figure 536

SEM IMAGES OF SAMPLE #

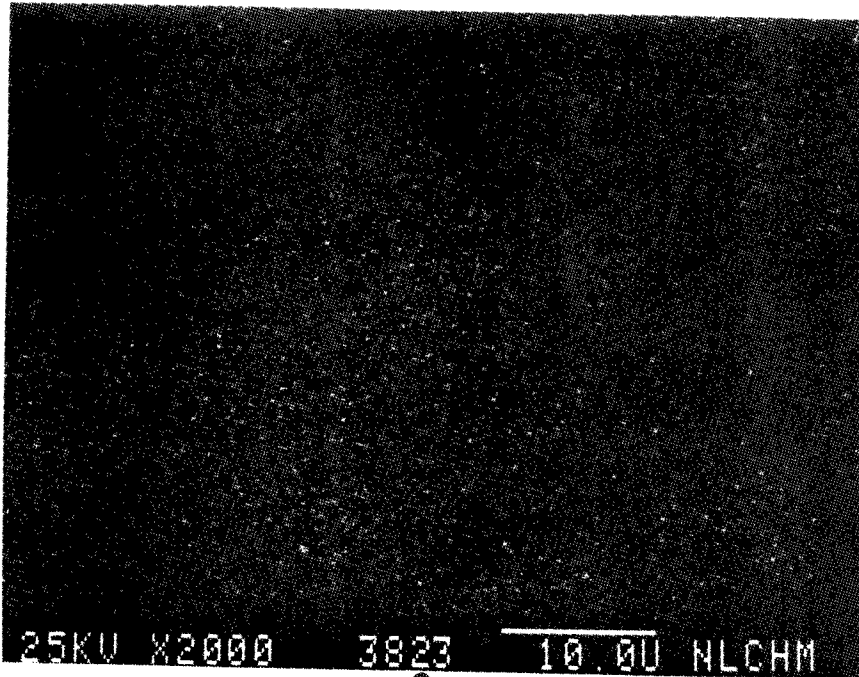


Figure 540

Ca X-Ray Image of Figure 536

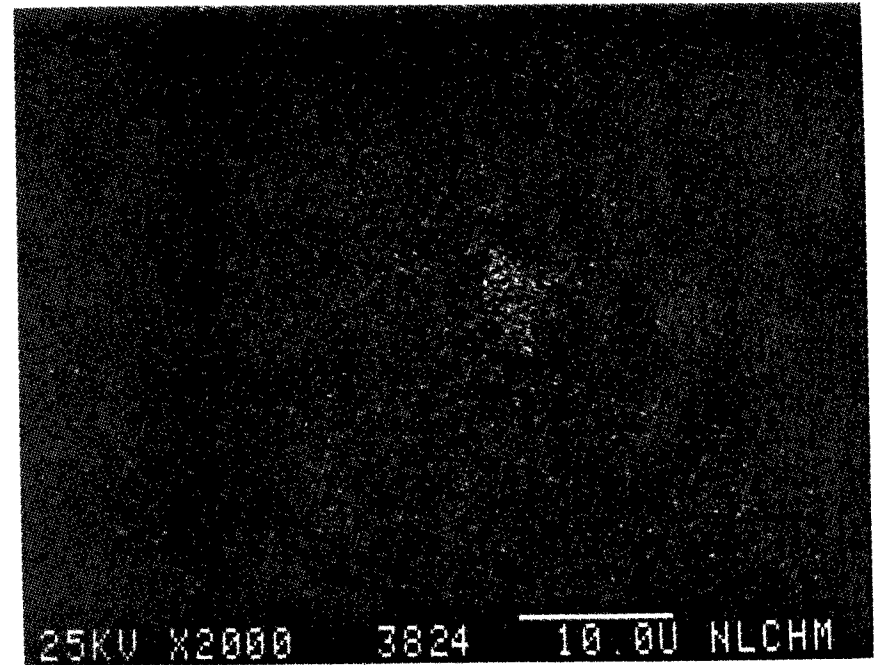


Figure 541

Ti X-Ray Image of Figure 536

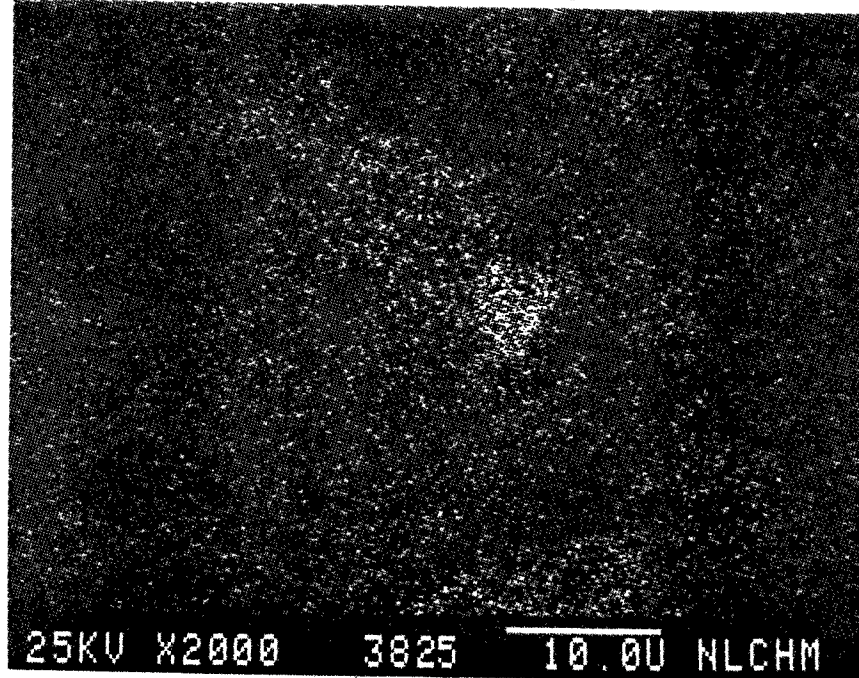


Figure 542

Fe X-Ray Image of Figure 536

SEM IMAGES OF SAMPLE #

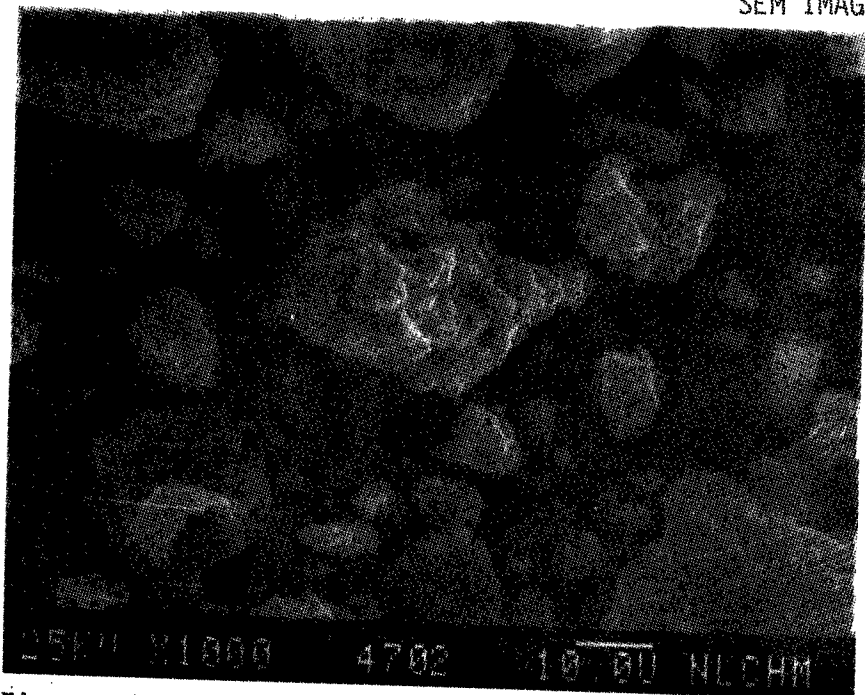


Figure 543

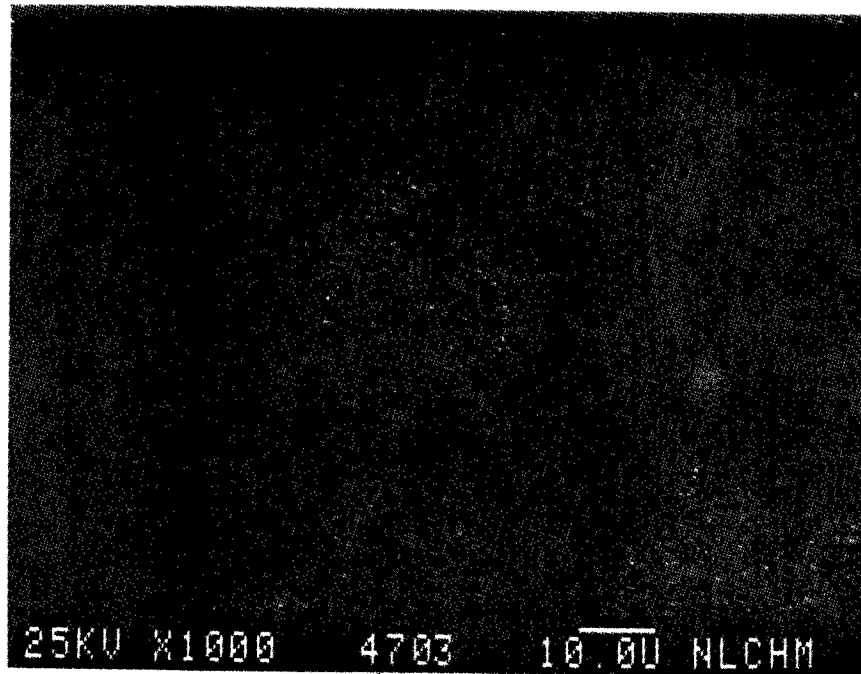


Figure 544

AL X-Ray Image of Figure 543

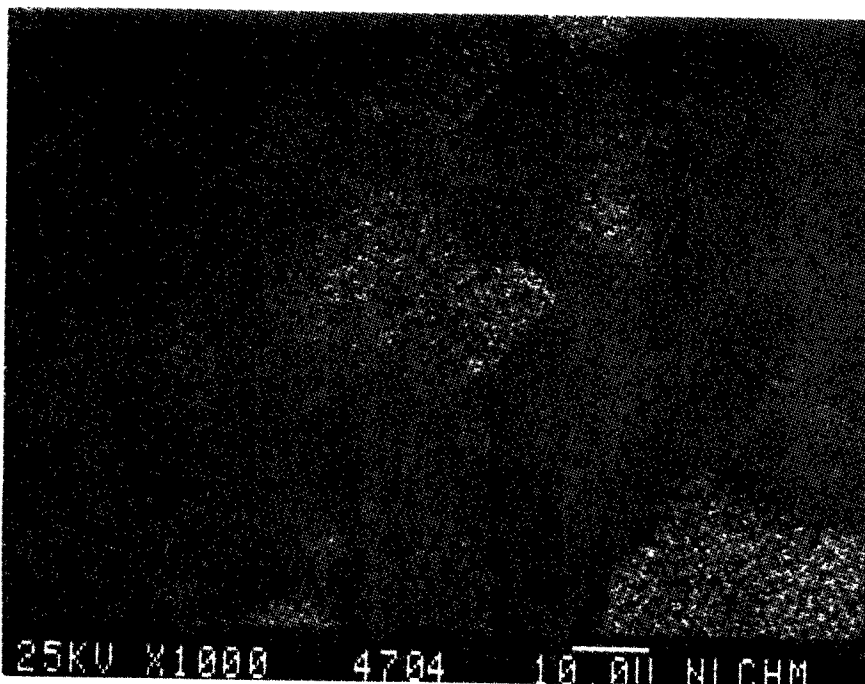


Figure 545

Si X-Ray Image of Figure 543

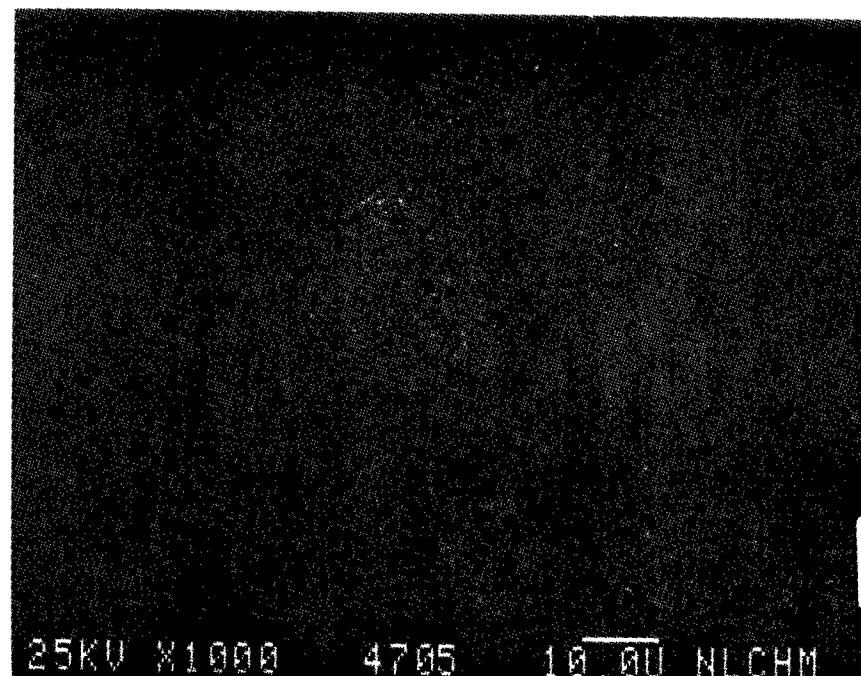


Figure 546

K X-Ray Image of Figure 543

SEM IMAGES OF SAMPLE #

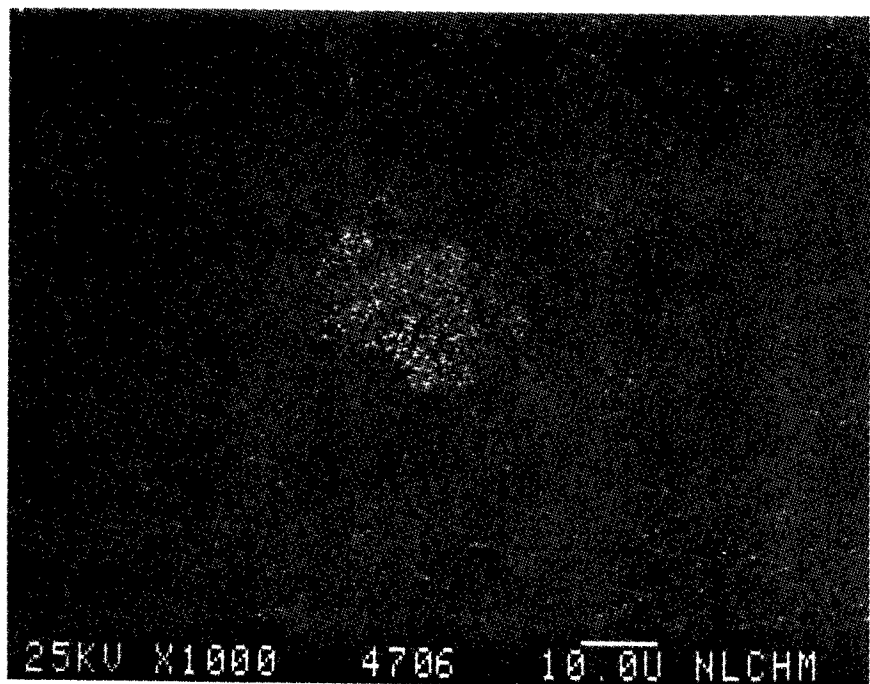


Figure 547

Ca X-Ray Image of Figure 543

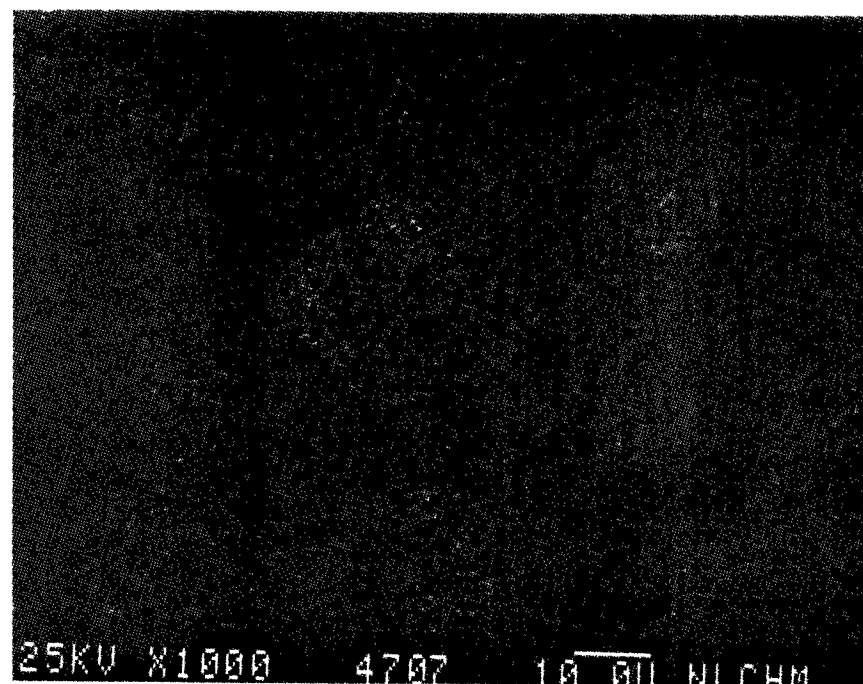


Figure 548

Fe X-Ray Image of Figure 543



SEM IMAGES OF SAMPLE #

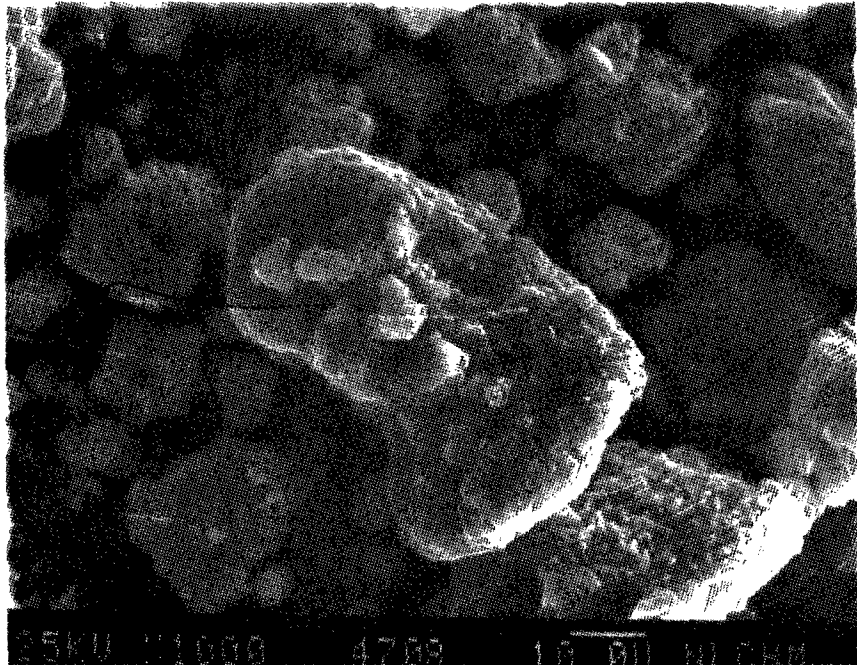


Figure 549

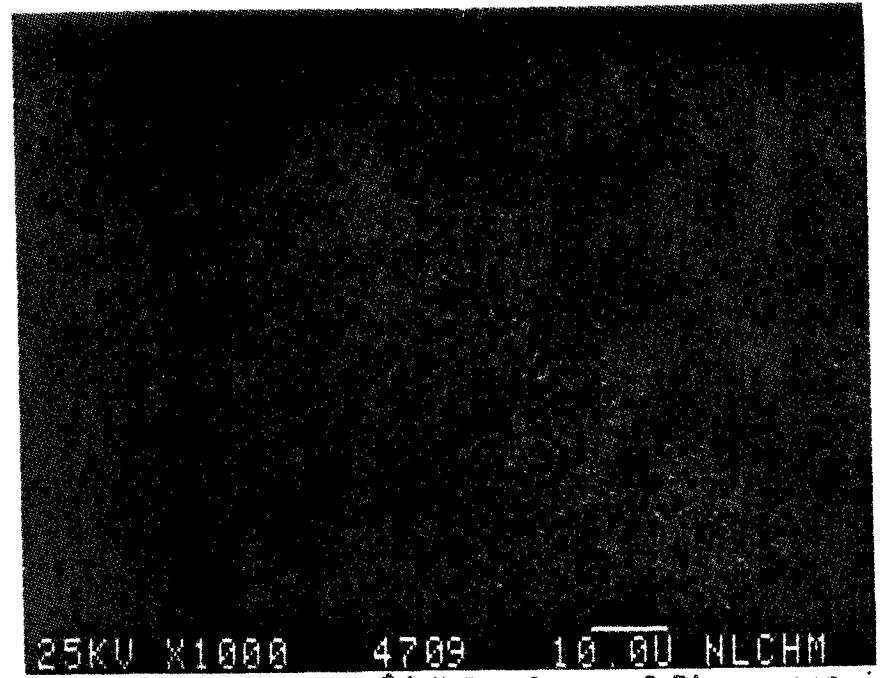


Figure 550

AL X-Ray Image of Figure 549

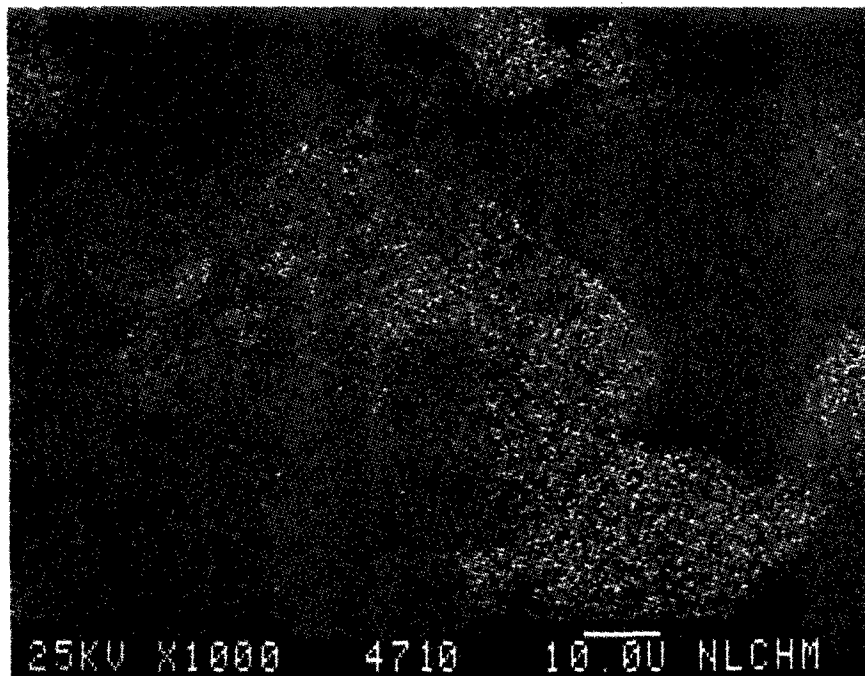


Figure 551

Si X-Ray Image of Figure 549

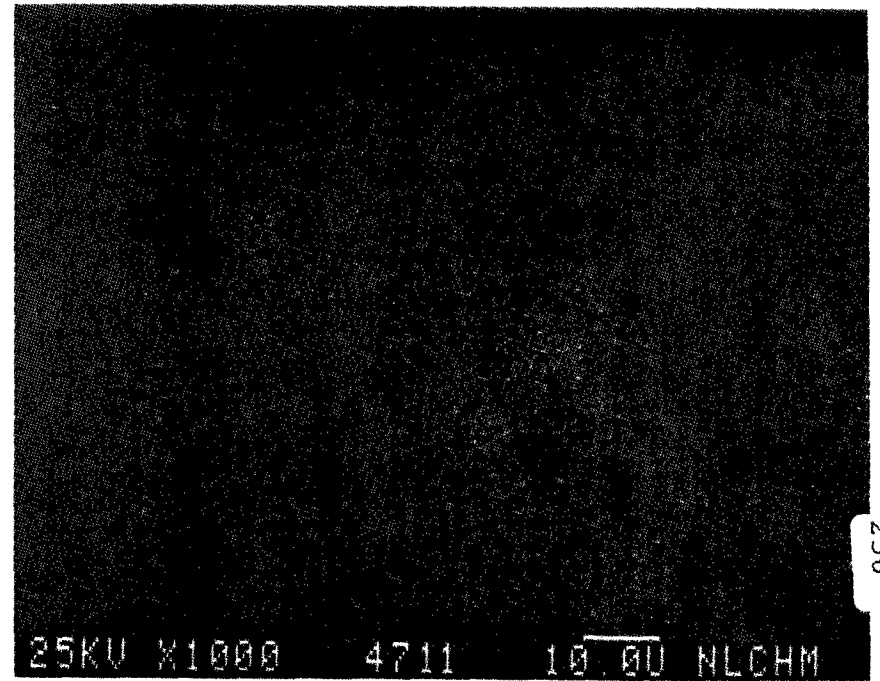


Figure 552

K X-Ray Image of Figure 549

SEM IMAGES OF SAMPLE #

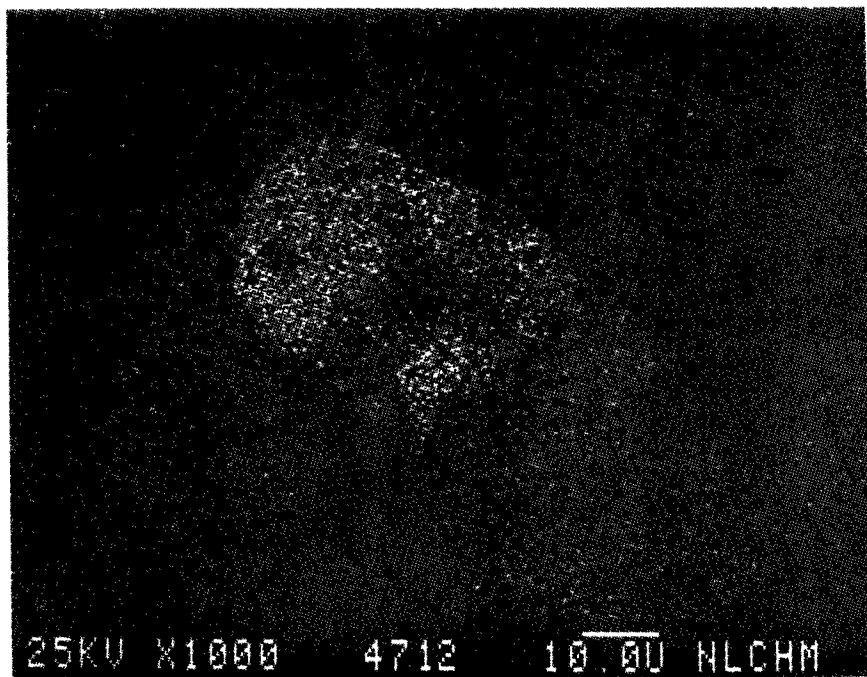


Figure 553

Ca X-Ray Image of Figure 549

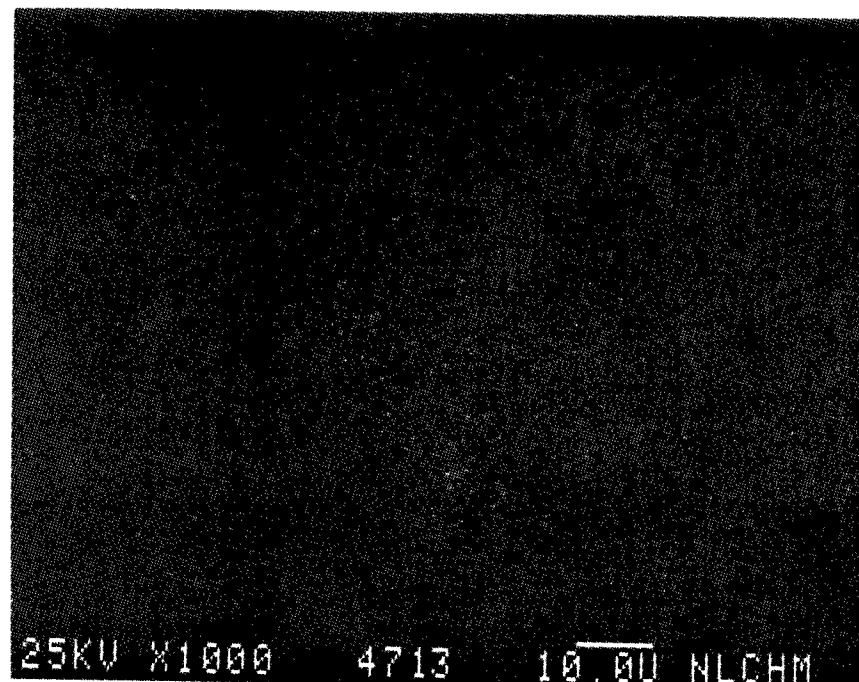


Figure 554

Fe X-Ray Image of Figure 549

**ENERGY DISPERSIVE X-RAY ANALYSIS**

Analytical Number Zeolite

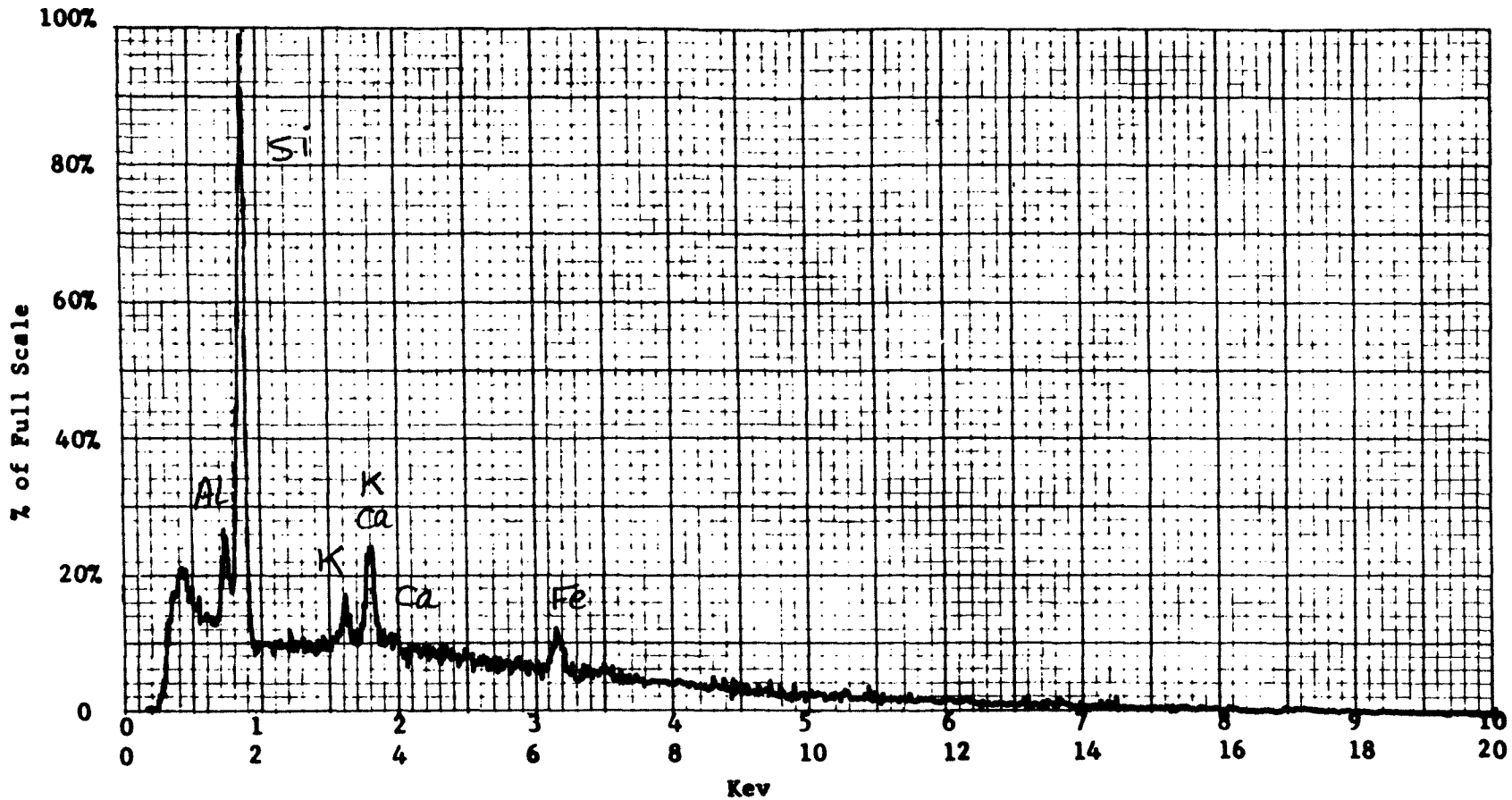
Operator \_\_\_\_\_ Date \_\_\_\_\_

Accelerating Potential 25 KeV

Total Counts Acquired 1.0 min.

Number Counts Full Scale 2K

Number of eV per channel 20



Sample peculiarities and remarks: FIGURE 555: AREA SCAN

ENERGY DISPERSIVE X-RAY ANALYSIS

Analytical Number Zeolite

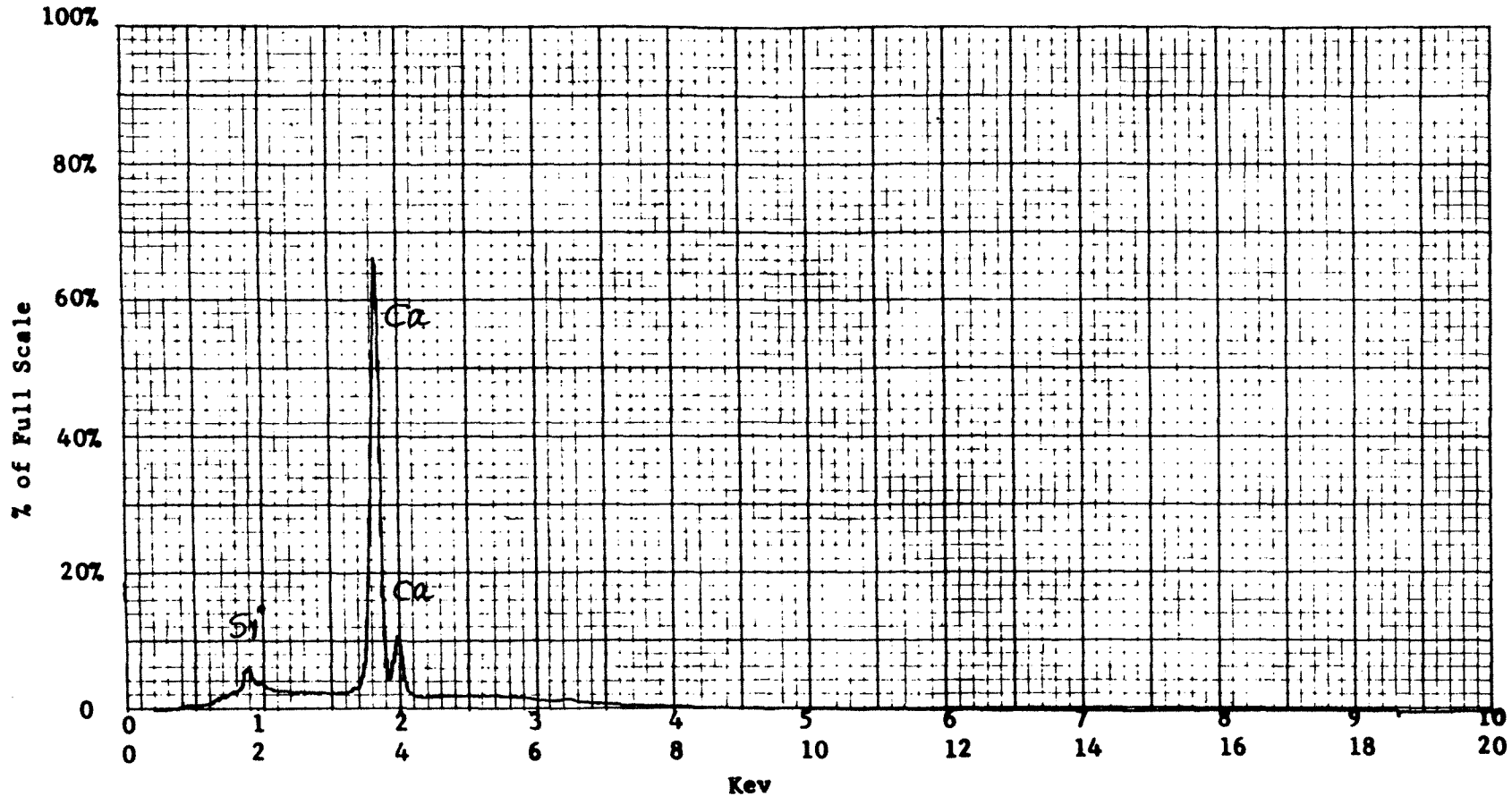
Operator \_\_\_\_\_ Date \_\_\_\_\_

Accelerating Potential 25 KeV

Total Counts Acquired 1.0 min.

Number Counts Full Scale 10K

Number of eV per channel 20



Sample peculiarities and remarks: FIGURE 556: POINT SCAN ON A LARGE PARTICLE  
IN FIGURE 522

ENERGY DISPERSIVE X-RAY ANALYSIS

Analytical Number Zeolite

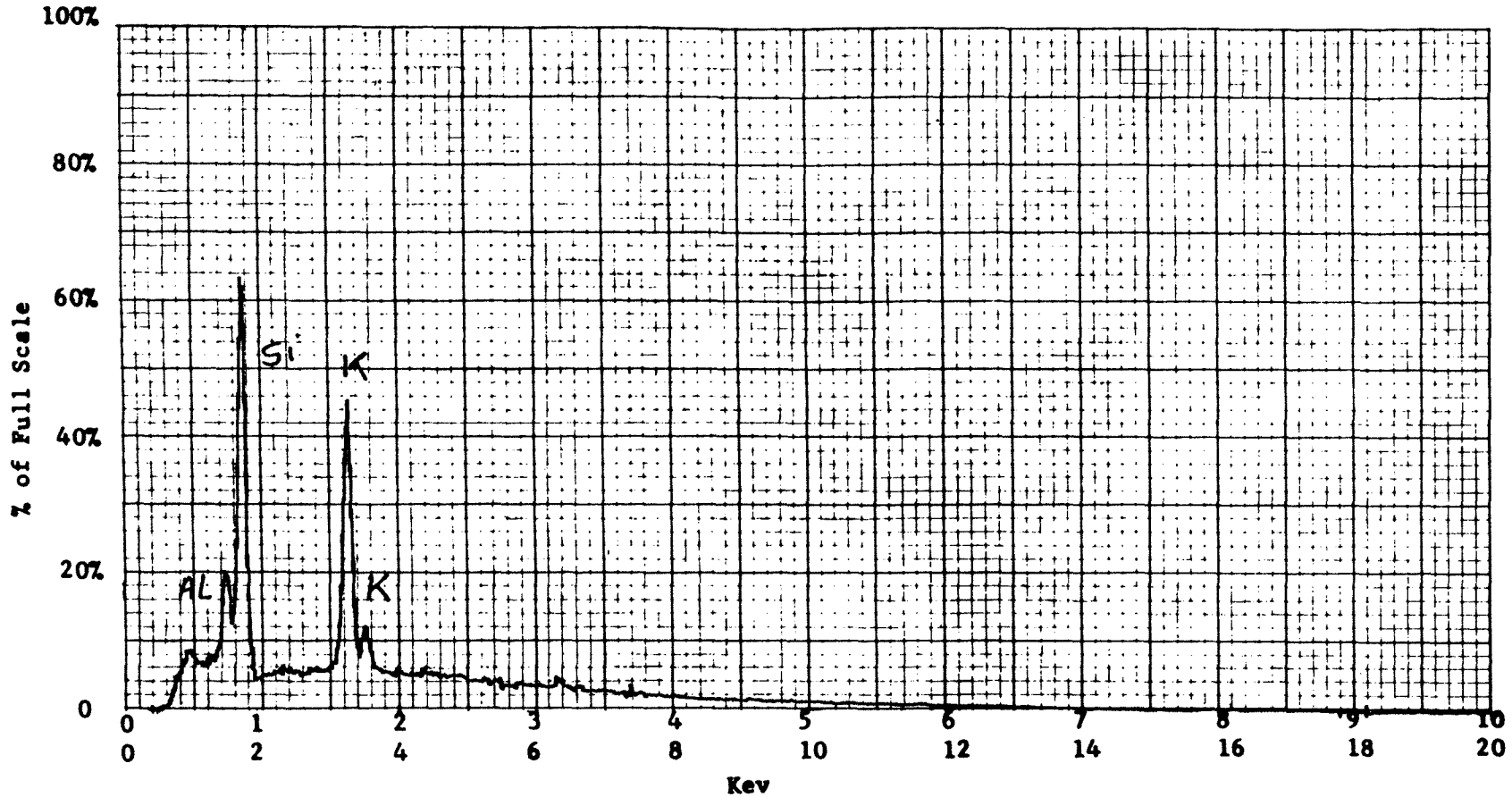
Operator \_\_\_\_\_ Date \_\_\_\_\_

Accelerating Potential 25 KeV

Total Counts Acquired 1.0 min.

Number Counts Full Scale 5K

Number of eV per channel 20



Sample peculiarities and remarks: FIGURE 557: POINT SCAN ON A HIGH K PARTICLE  
IN FIGURE 529

**ENERGY DISPERSIVE X-RAY ANALYSIS**

Analytical Number Zeolite

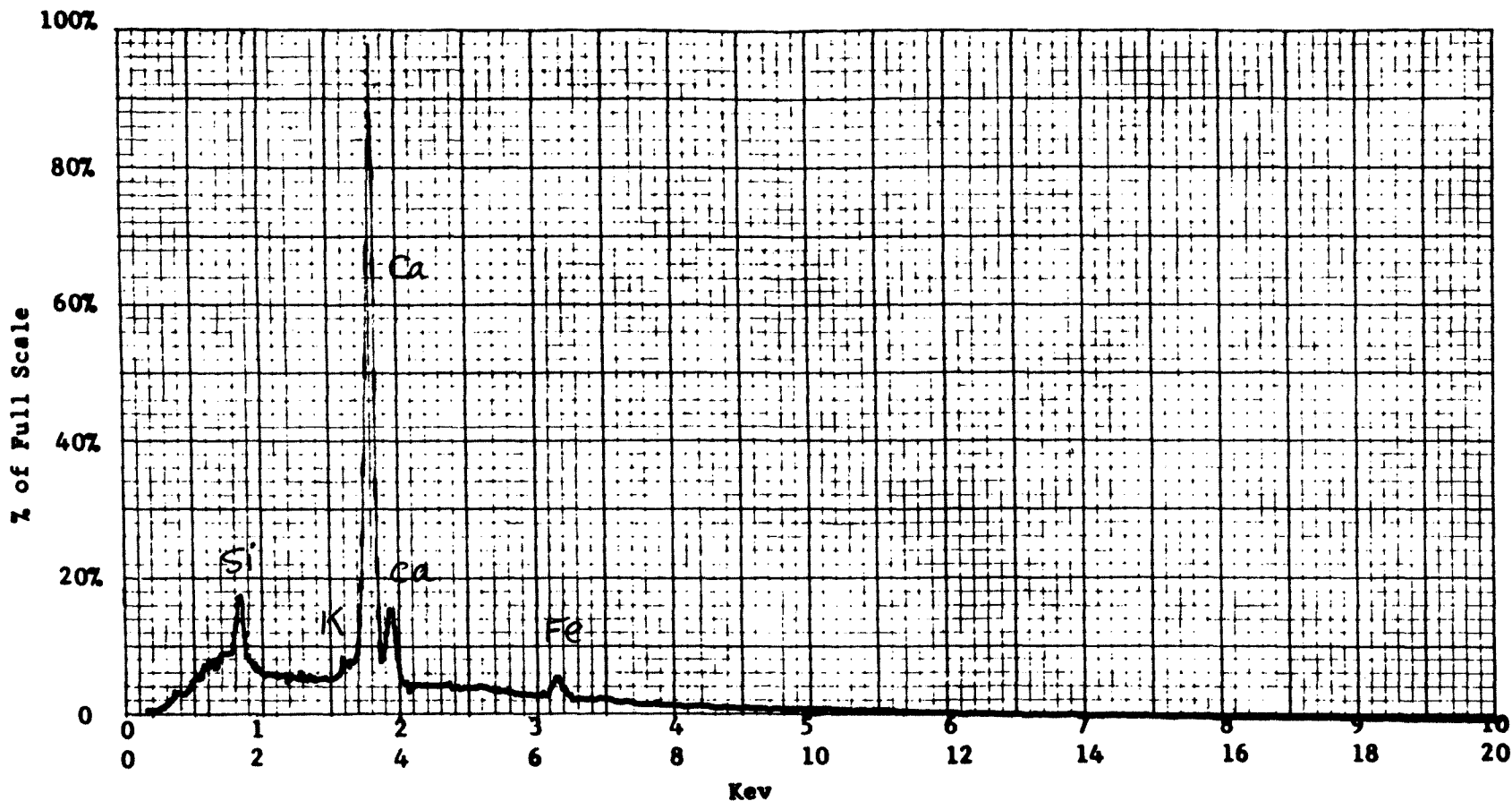
Operator \_\_\_\_\_ Date \_\_\_\_\_

Accelerating Potential 25 KeV

Total Counts Acquired 1.0 min.

Number Counts Full Scale 5K

Number of eV per channel 20



Sample peculiarities and remarks: FIGURE 558: POINT SCAN ON A HIGH Ca PARTICLE  
IN FIGURE 529



ENERGY DISPERSIVE X-RAY ANALYSIS

Analytical Number Zeolite

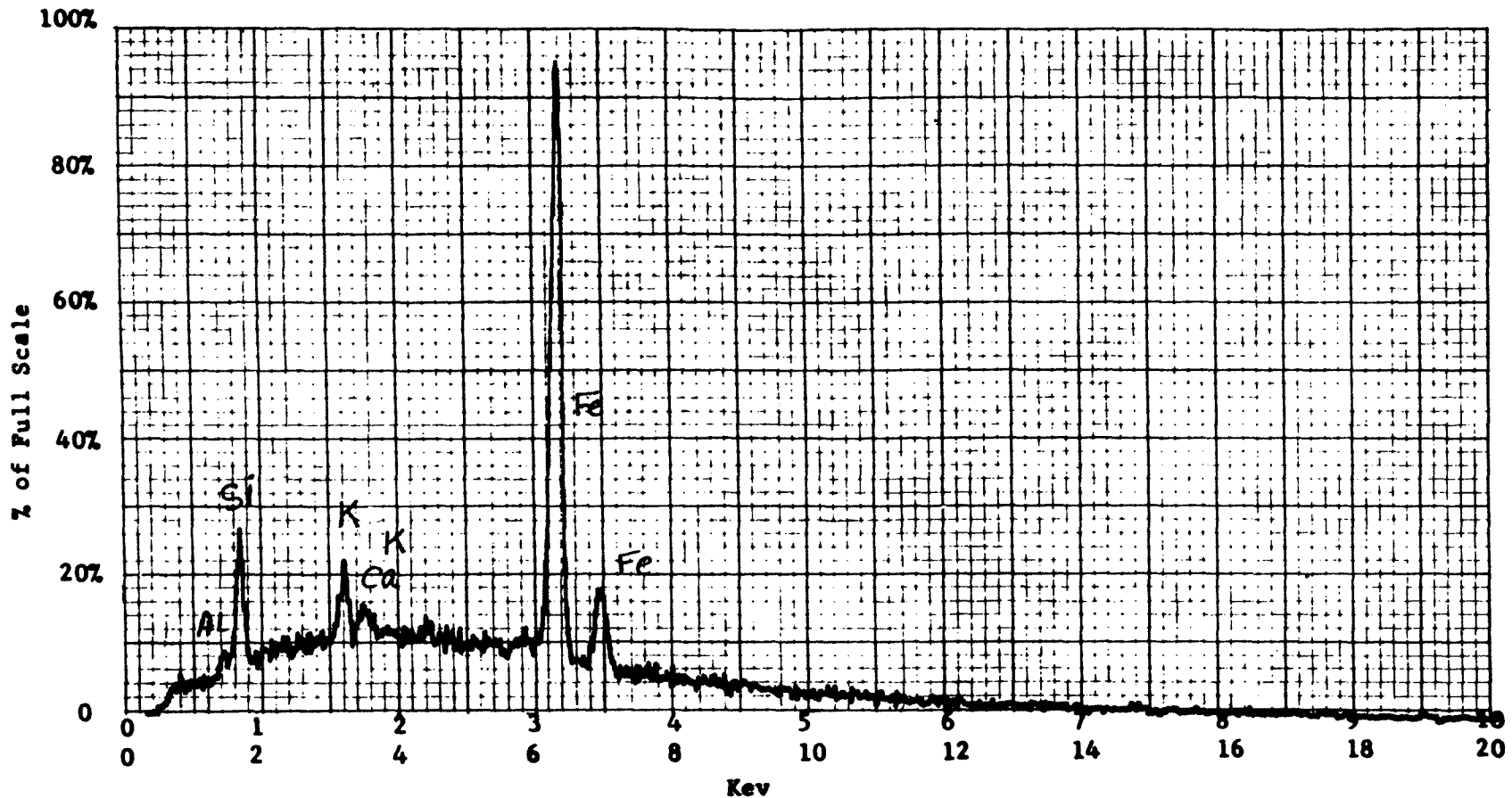
Operator \_\_\_\_\_ Date \_\_\_\_\_

Accelerating Potential 25 KeV

Total Counts Acquired 1.0 min.

Number Counts Full Scale 2K

Number of eV per channel 20



Sample peculiarities and remarks: FIGURE 559: POINT SCAN ON A HIGH Fe PARTICLE  
IN FIGURE 529

ENERGY DISPERSIVE X-RAY ANALYSIS

Analytical Number Zeolite

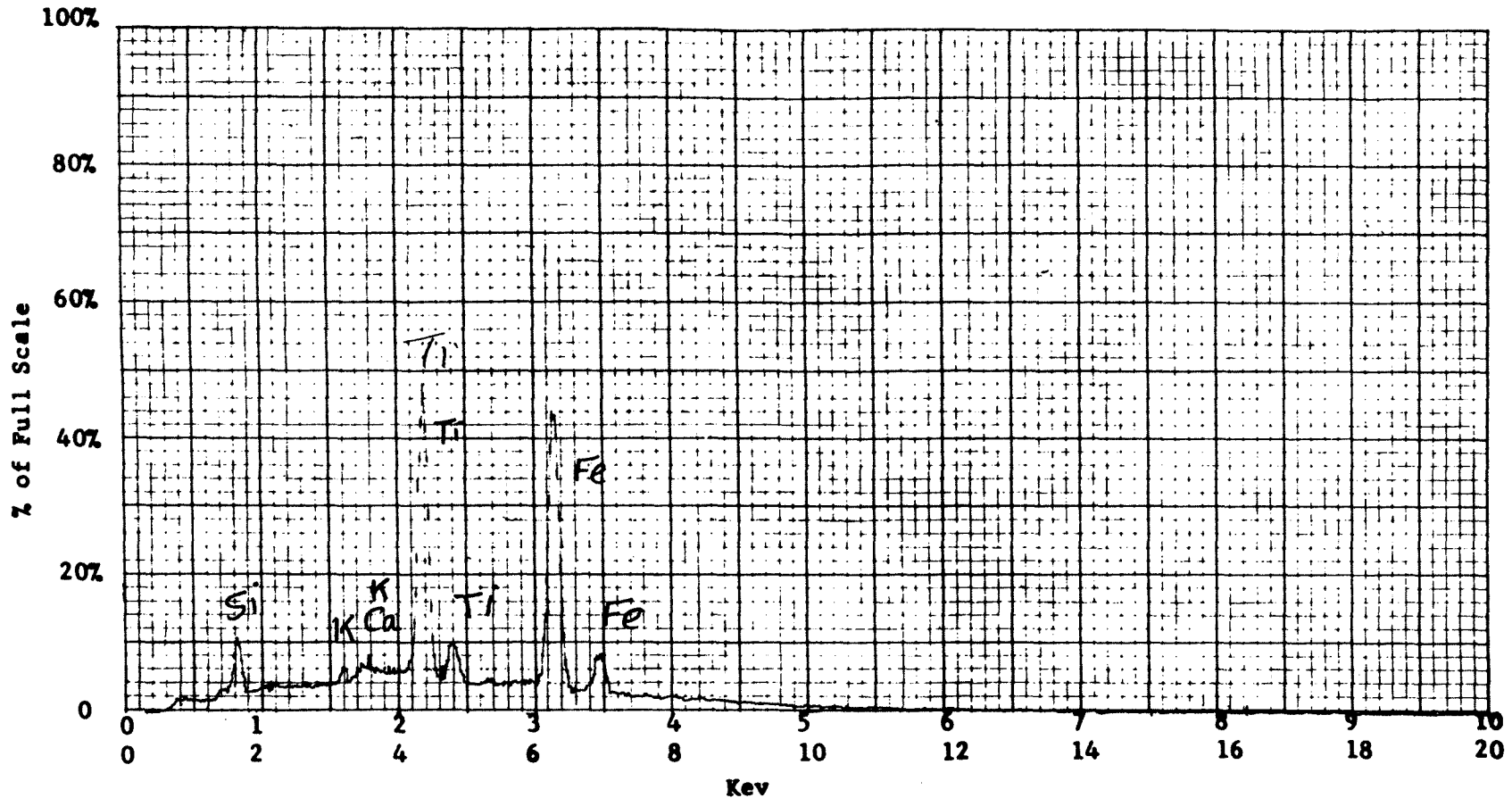
Operator \_\_\_\_\_ Date \_\_\_\_\_

Accelerating Potential 25 KeV

Total Counts Acquired 1.0 min.

Number Counts Full Scale 5K

Number of eV per channel 20



Sample peculiarities and remarks: FIGURE 560: POINT SCAN ON A HIGH Fe-Ti PARTICLE IN FIGURE 536

**ENERGY DISPERSIVE X-RAY ANALYSIS**

Analytical Number Zeolite

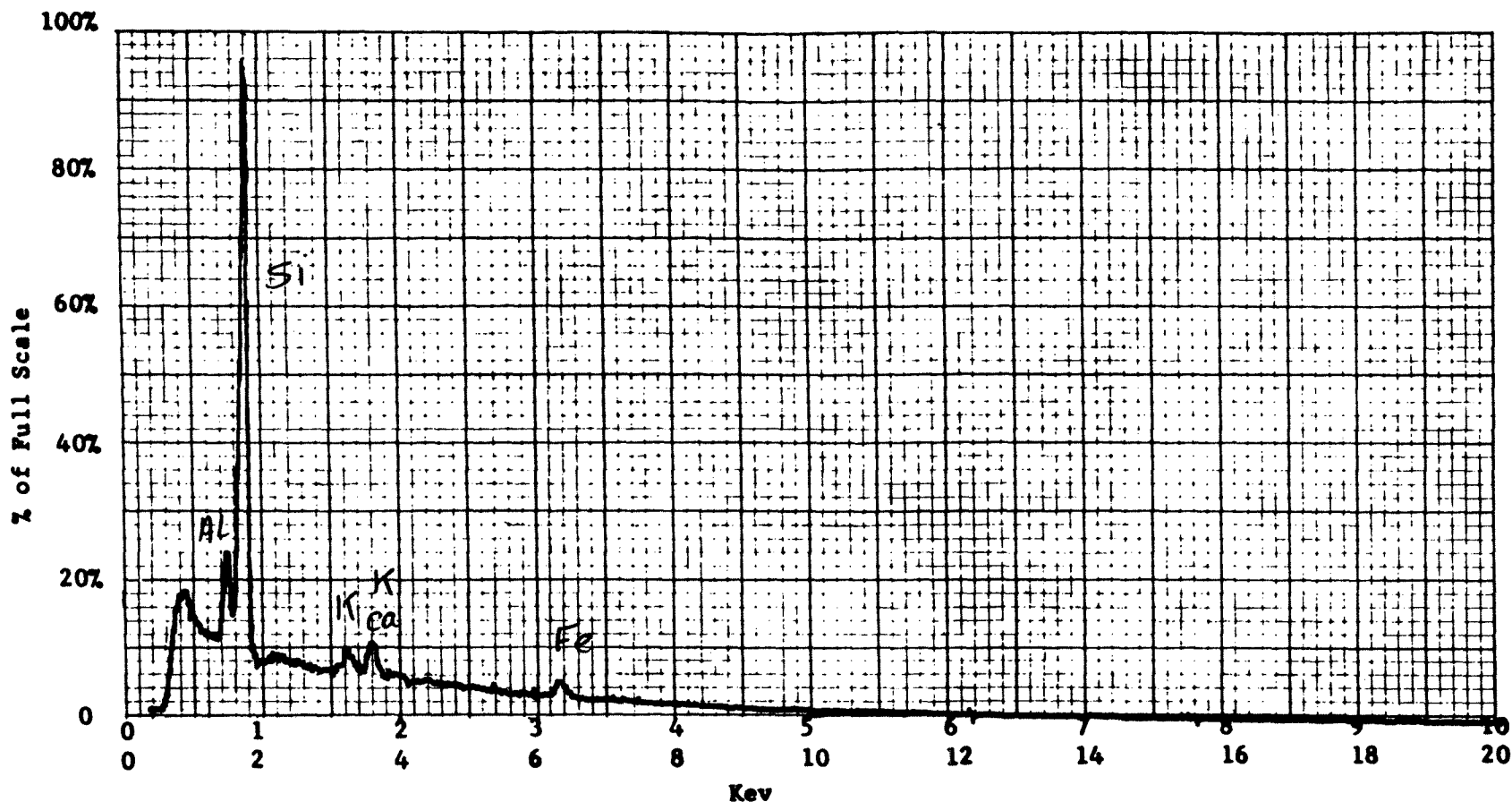
Operator \_\_\_\_\_ Date \_\_\_\_\_

Accelerating Potential 25 KeV

Total Counts Acquired 1.0 min.

Number Counts Full Scale 5K

Number of eV per channel 20



Sample peculiarities and remarks: FIGURE 561: POINT SCAN ON A HIGH Al-Si PARTICLE

Bauxite:Structural Analysis:

Particles of bauxite appeared to be very large and irregular in shape. Most of the particles have rounded edges and a few angular particles were also observed. A few small particles were also detected.

The structures on the surface of the particles were quite smooth. Macro and micro pores were present. The large particles at high magnification appear to be aggregates of smaller ones, or decorated with fine materials.

The maximum, average and minimum particle size were measured in microns ( $\mu$ ) as follows:

Maximum	Average	Minimum
1700.0	700.0	4.0

Elemental Composition and Distribution:

Al is a major element in this sample, other elements such as Si, Ti and Fe were detected in low concentrations in most cases.

Figure 574 illustrates a large particle with uniform distribution of Al (major) and Si, Ti, Fe (minors). This is illustrated by the aluminum X-ray image, Figure 575, the silicon X-ray image, Figure 576, the titanium X-ray image, Figure 577, and the iron X-ray image, Figure 578.

A large particle in the SEM micrograph, Figure 579, was found to contain very high concentrations of Ti. This is illustrated by the titanium X-ray image, Figure 582, and the X-ray energy spectrum, Figure 595.

Small areas of high Ti and larger areas of high Fe were observed in a large particle presented in Figure 584. For example, see the titanium X-ray image, Figure 587, the iron X-ray image, Figure 588, and the X-ray energy spectrum, Figure 595.

Very high Si contents were detected from a small area in a large particle in the SEM micrograph, Figure 579. The silicon X-ray image, Figure 581, and the X-ray energy spectrum, Figure 597, illustrate this.

SEM IMAGES OF SAMPLE #

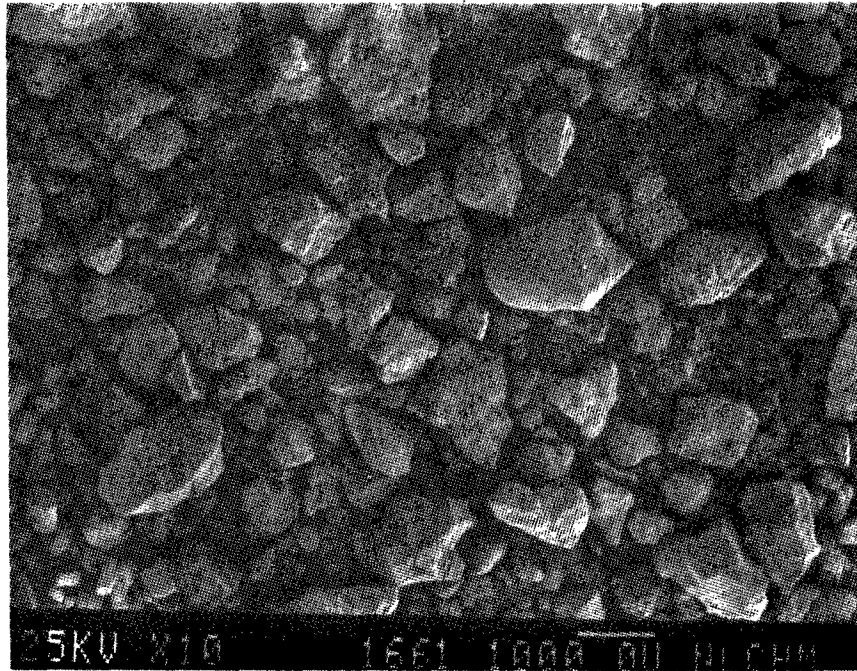


Figure 562

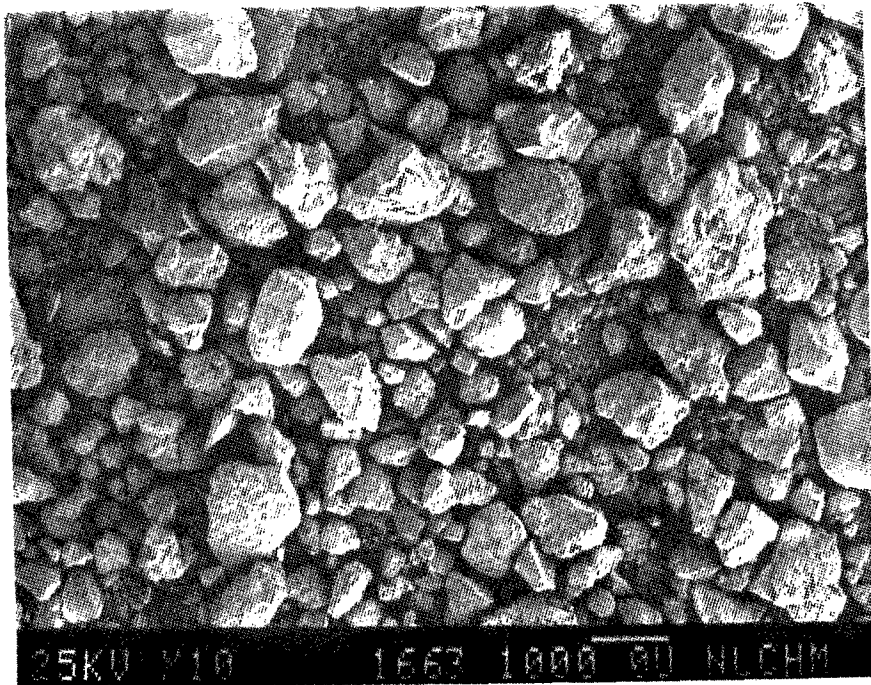


Figure 563

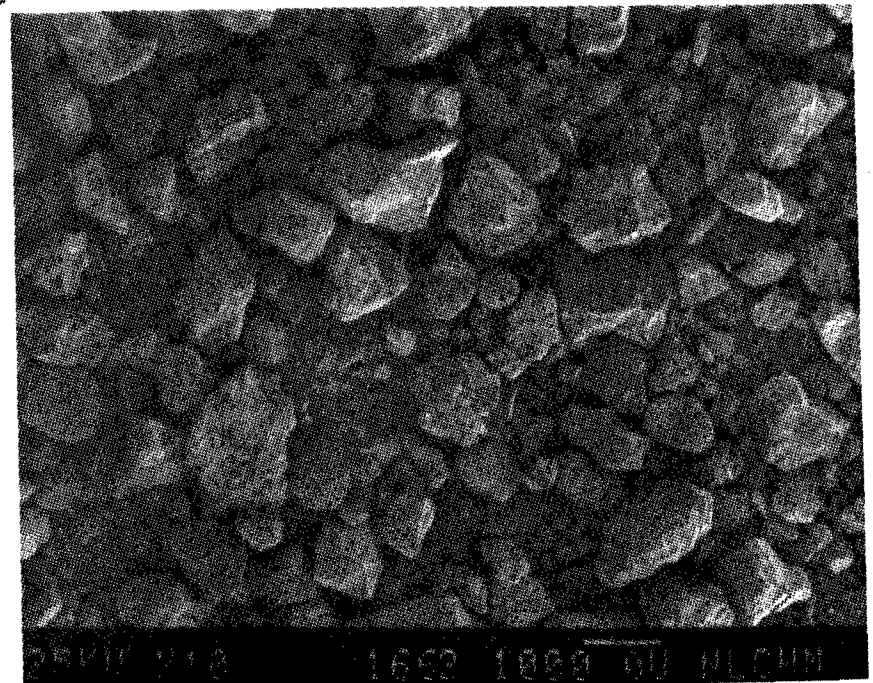


Figure 564



SEM IMAGES OF SAMPLE #

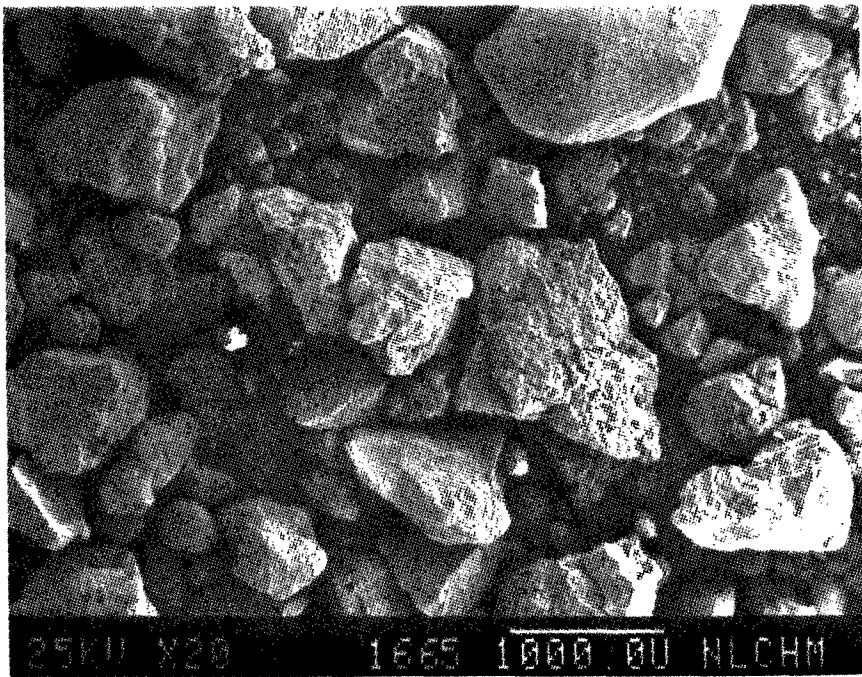


Figure 565

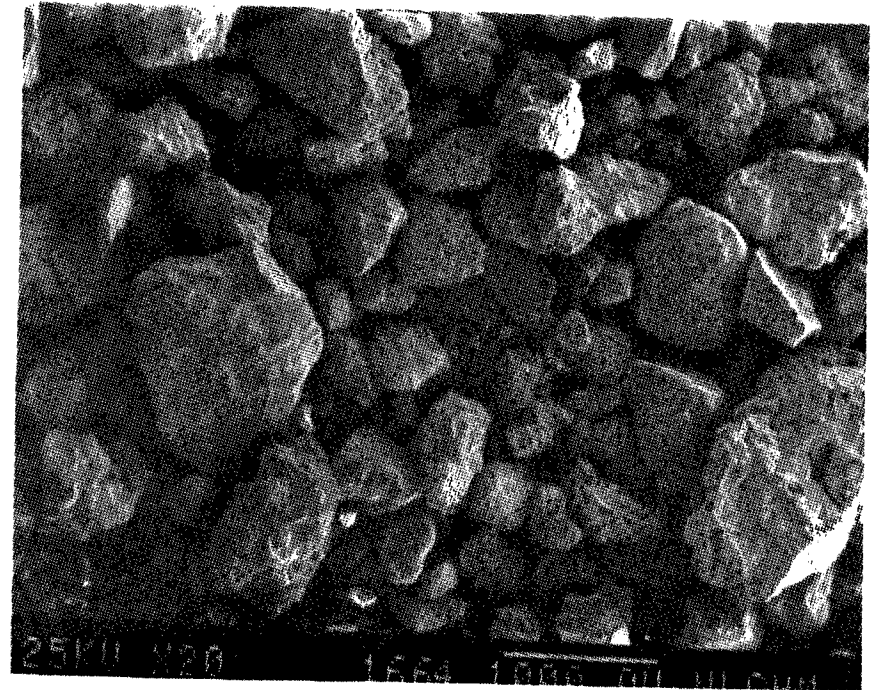


Figure 566

SEM IMAGES OF SAMPLE #

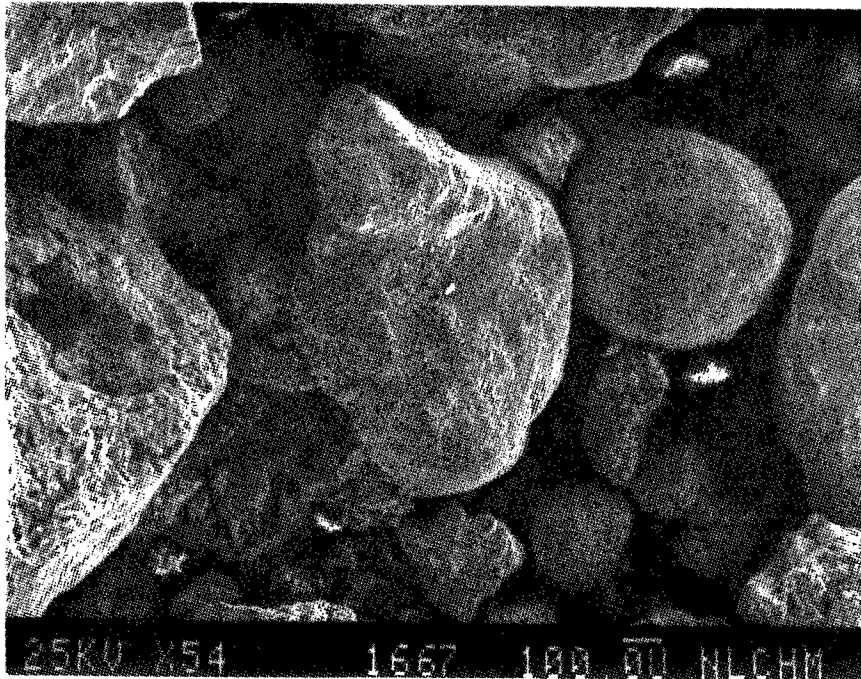


Figure 567

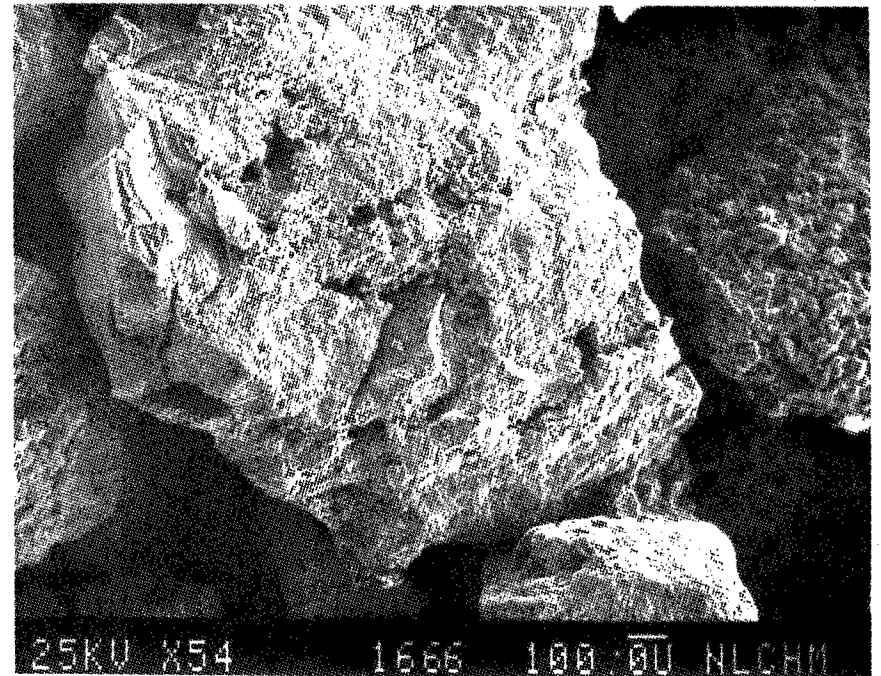


Figure 568

SEM IMAGES OF SAMPLE #

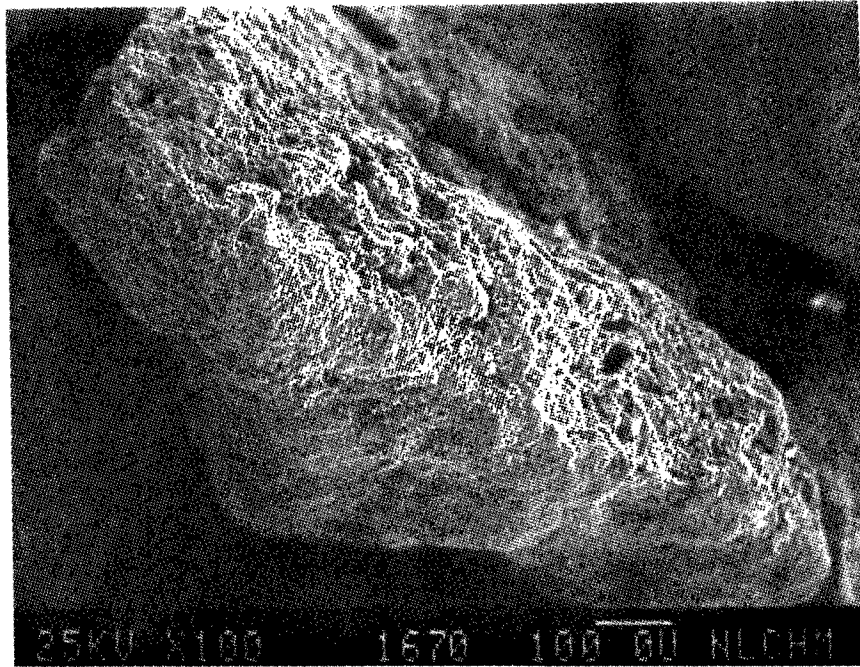


Figure 569

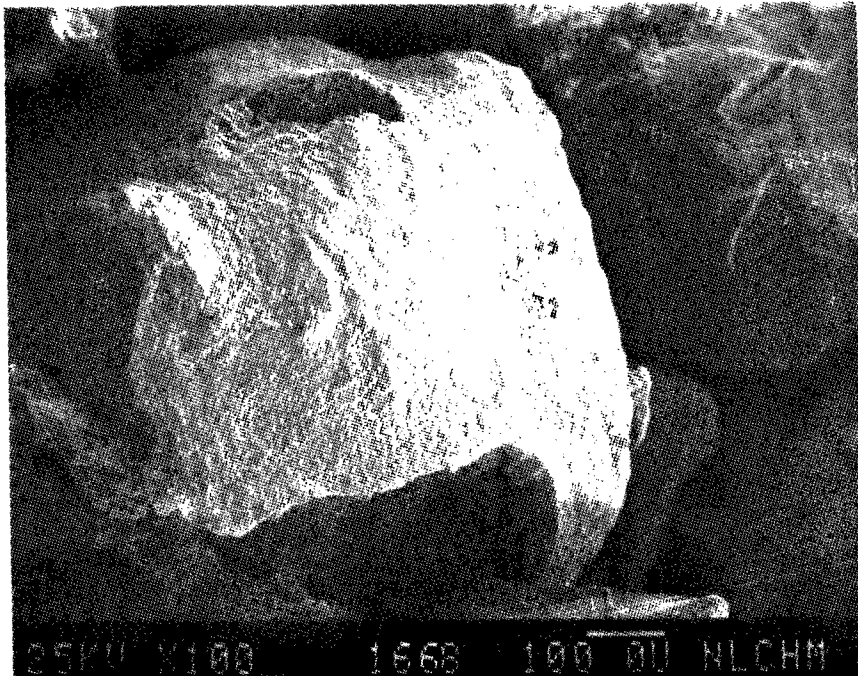


Figure 570



Figure 571

SEM IMAGES OF SAMPLE #

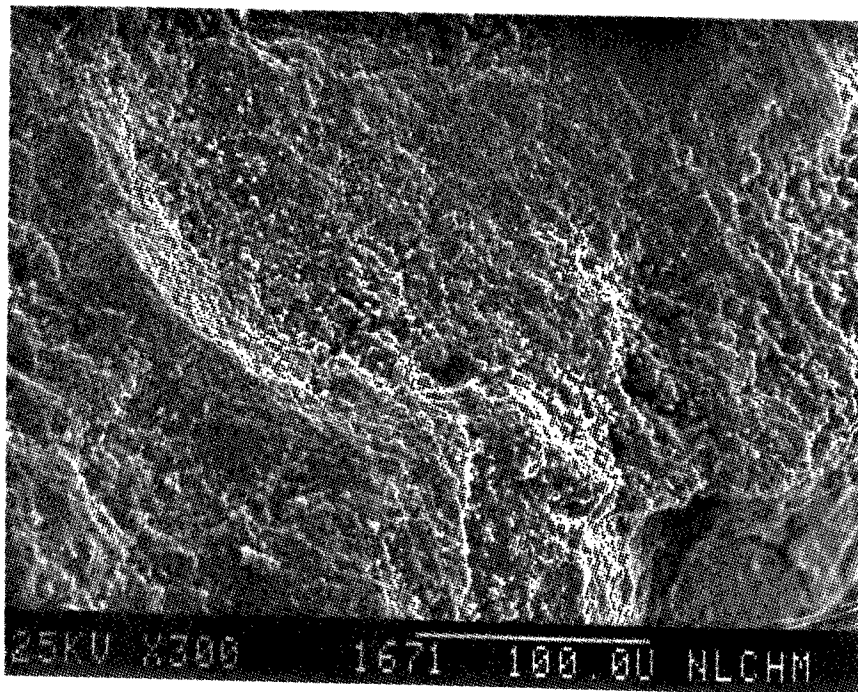


Figure 572

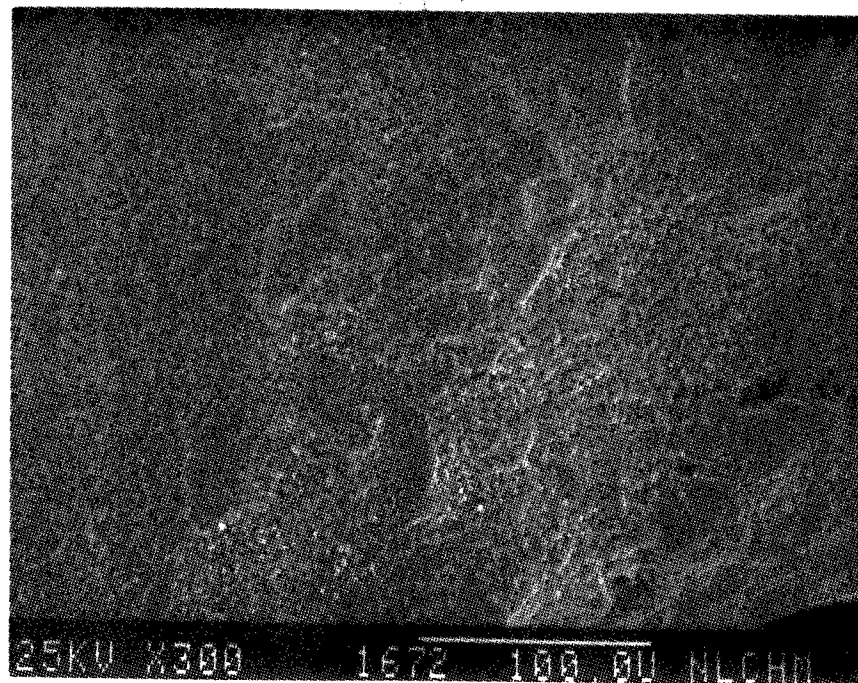


Figure 573



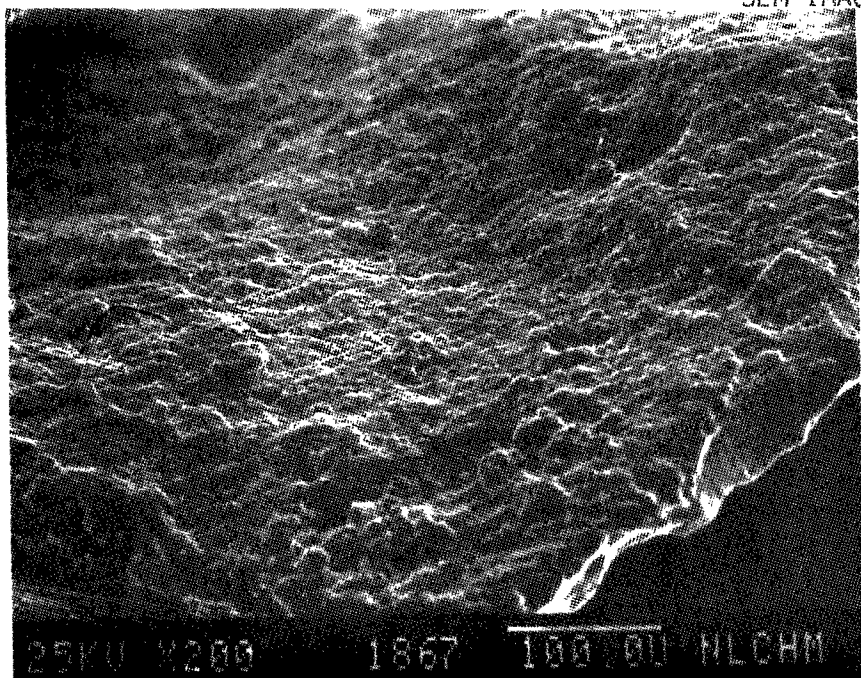


Figure 574

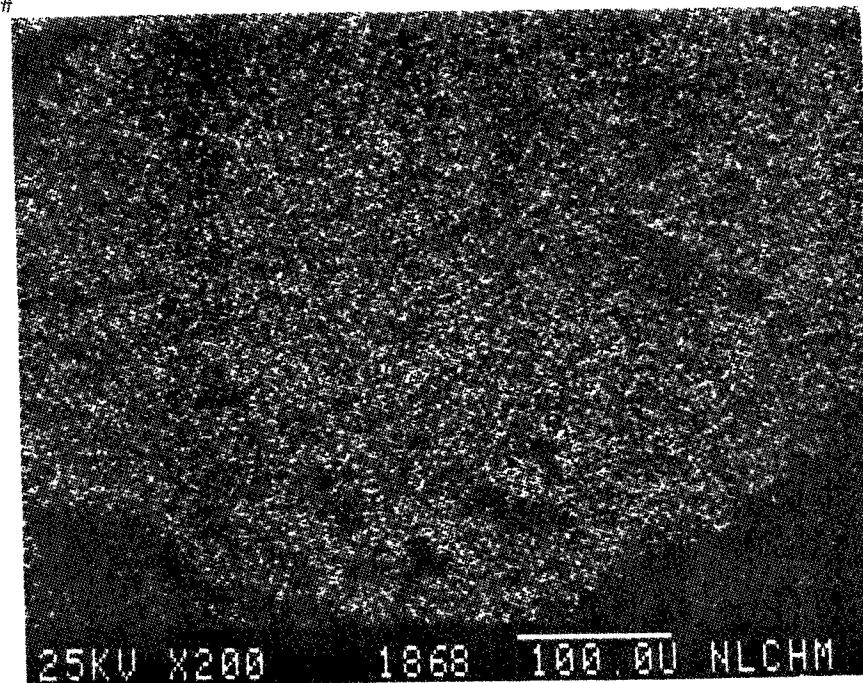


Figure 575

Al X-Ray Image of Figure 574

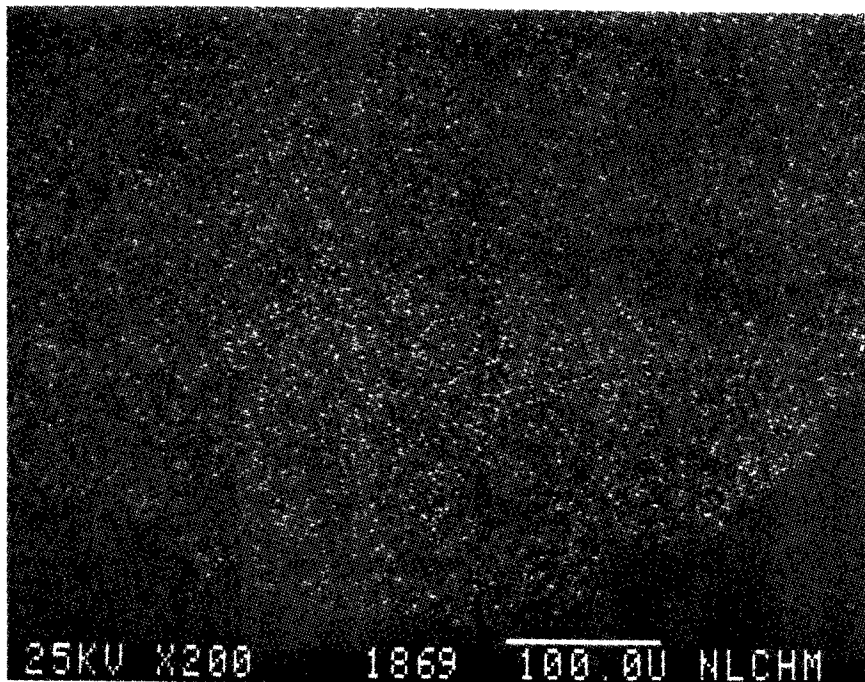


Figure 576

Si X-Ray Image of Figure 574

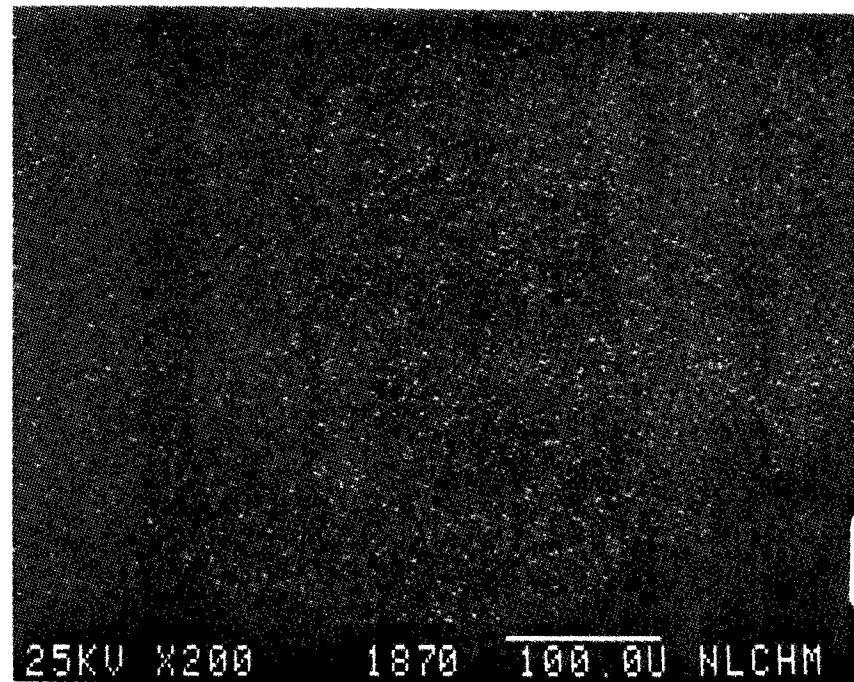


Figure 577

Ti X-Ray Image of Figure 574

SEM IMAGES OF SAMPLE #

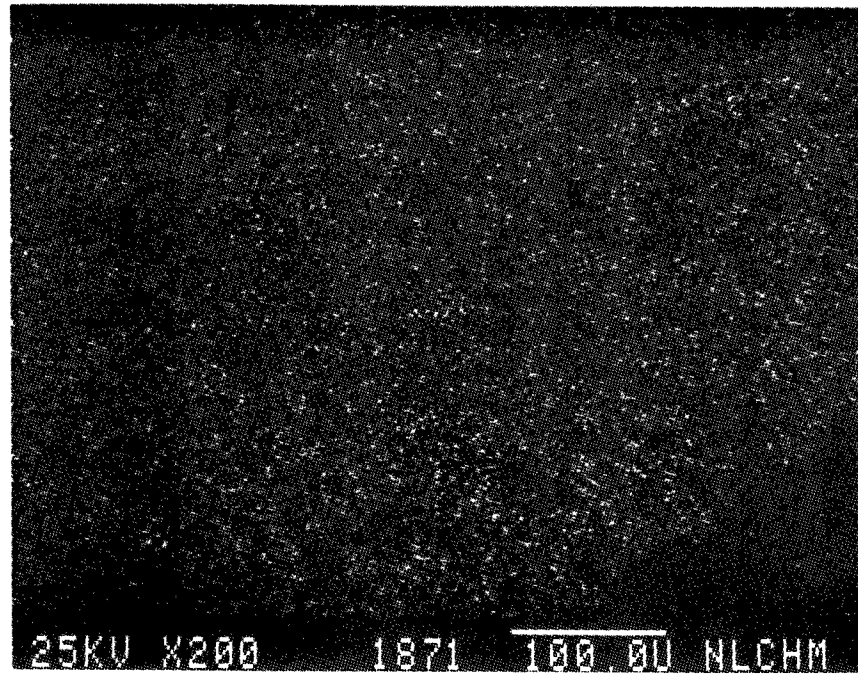


Figure 578

Fe X-Ray Image of Figure 574



SEM IMAGES OF SAMPLE #

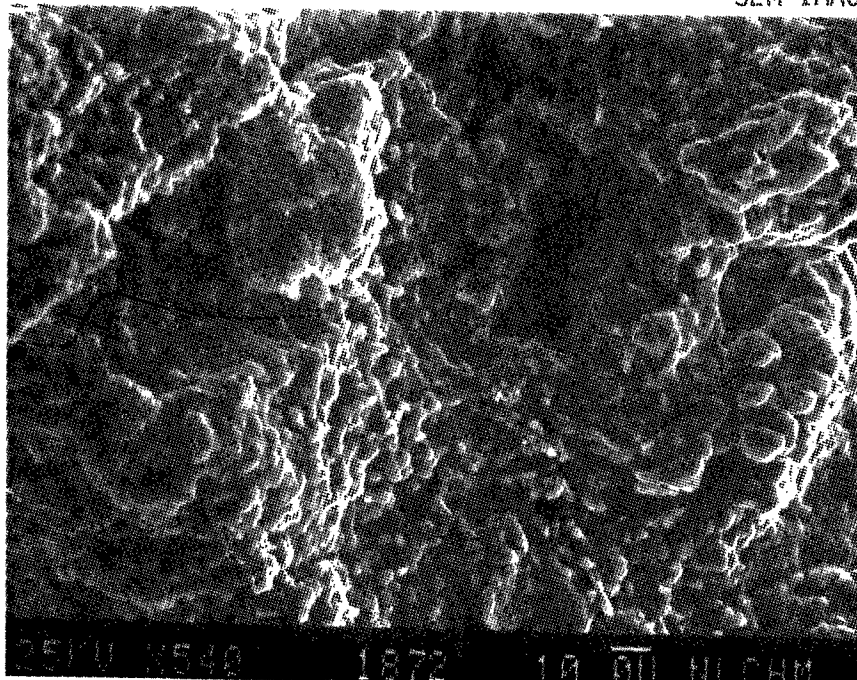


Figure 579

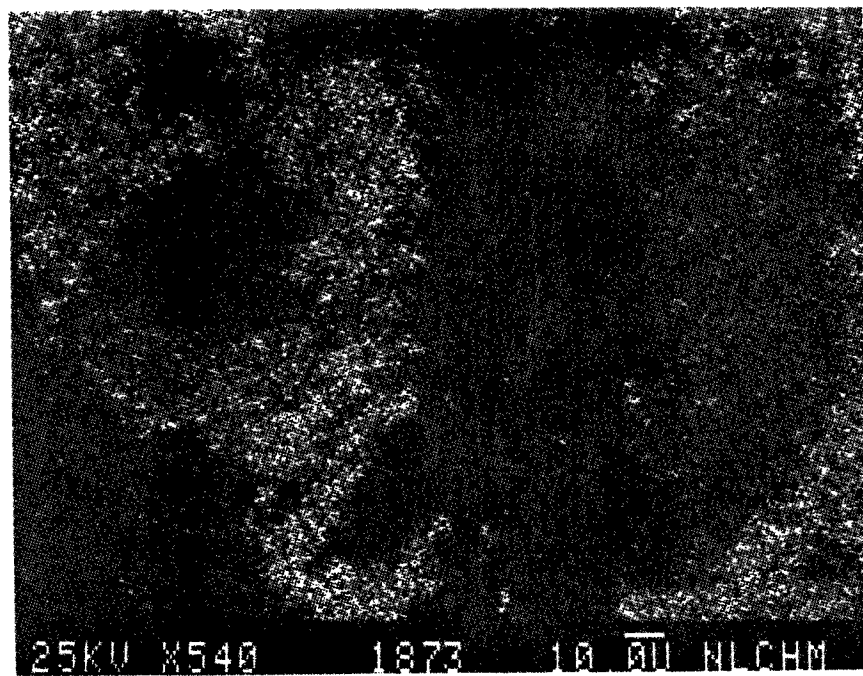


Figure 580

AL X-Ray Image of Figure 579

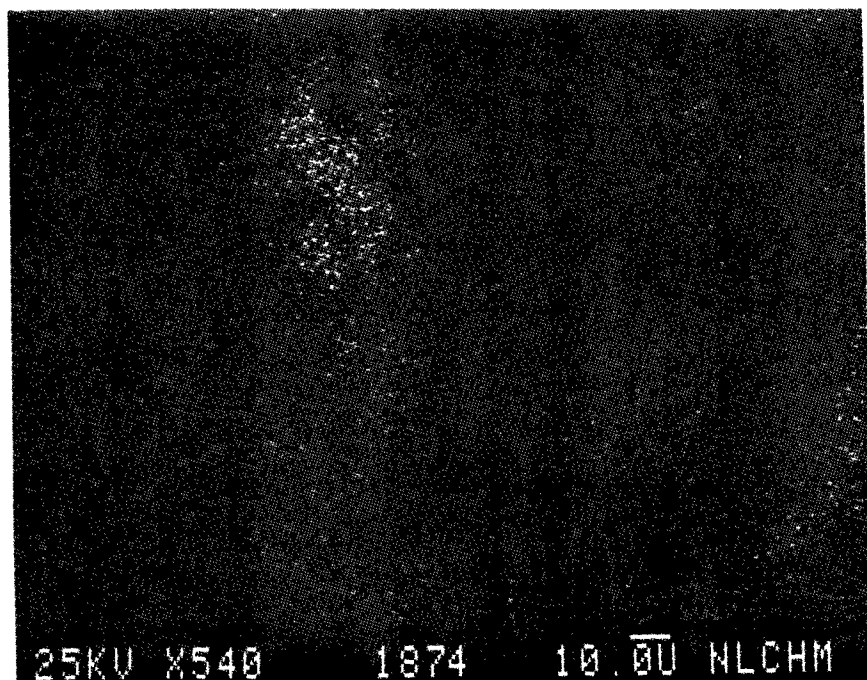


Figure 581

Si X-Ray Image of Figure 579

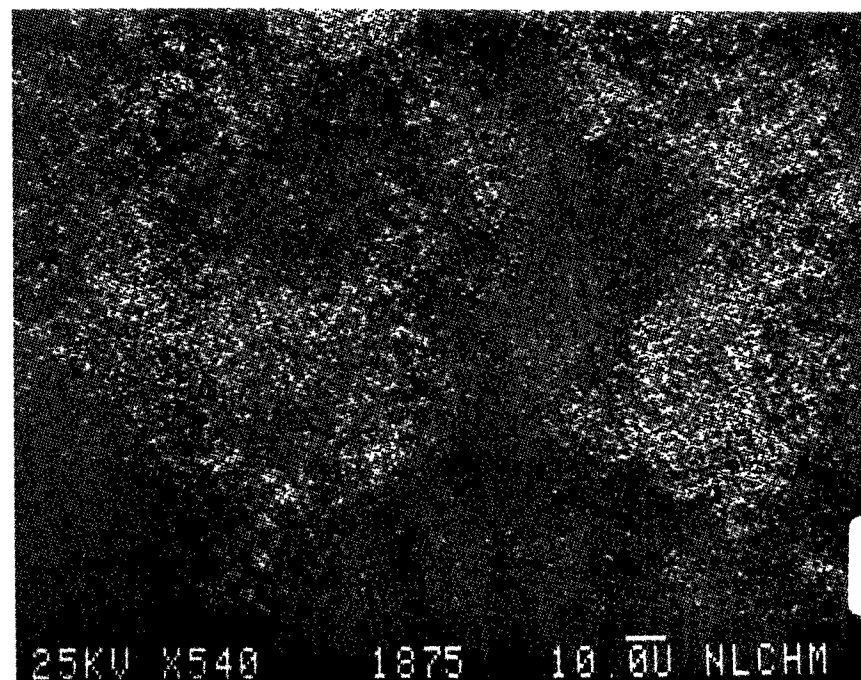


Figure 582

Ti X-Ray Image of Figure 579

SEM IMAGES OF SAMPLE #

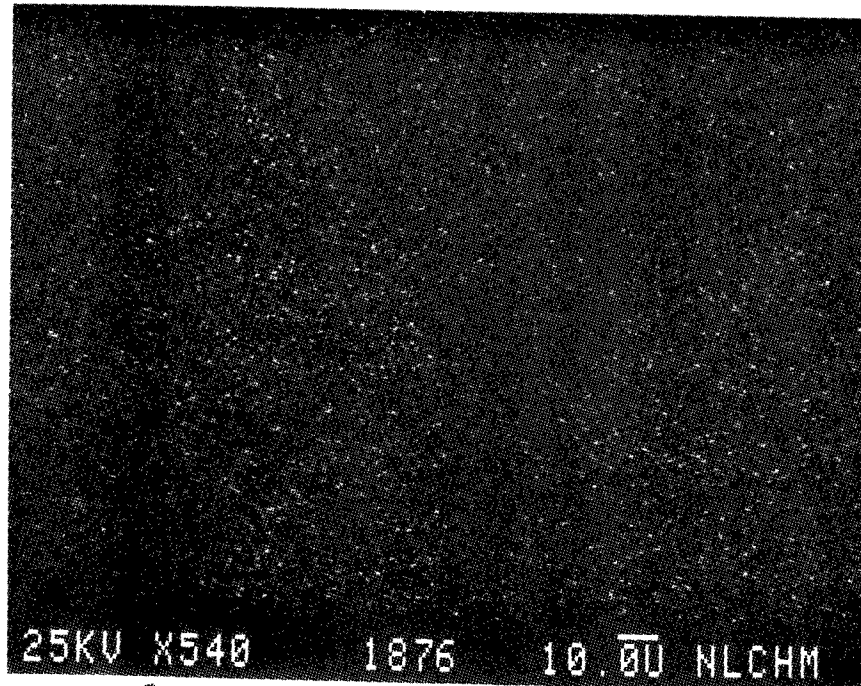


Figure 583

Fe X-Ray Image of Figure 579

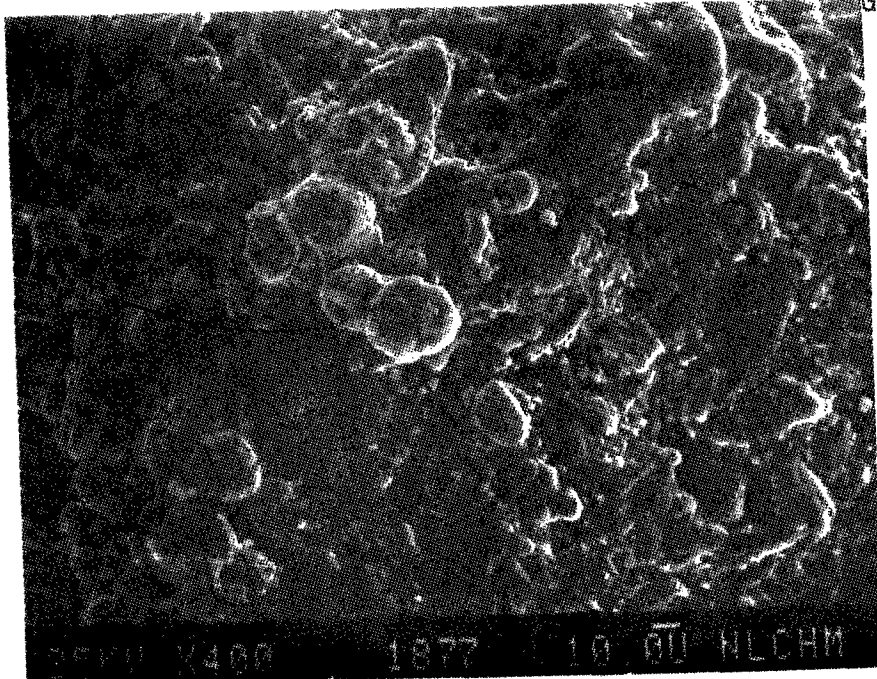


Figure 584

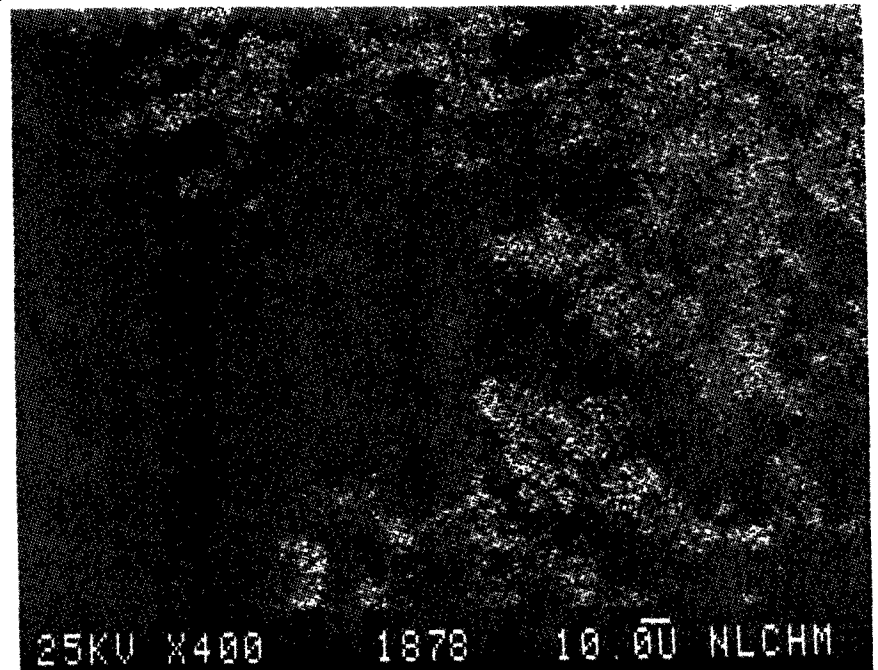


Figure 585

AL X-Ray Image of Figure 584

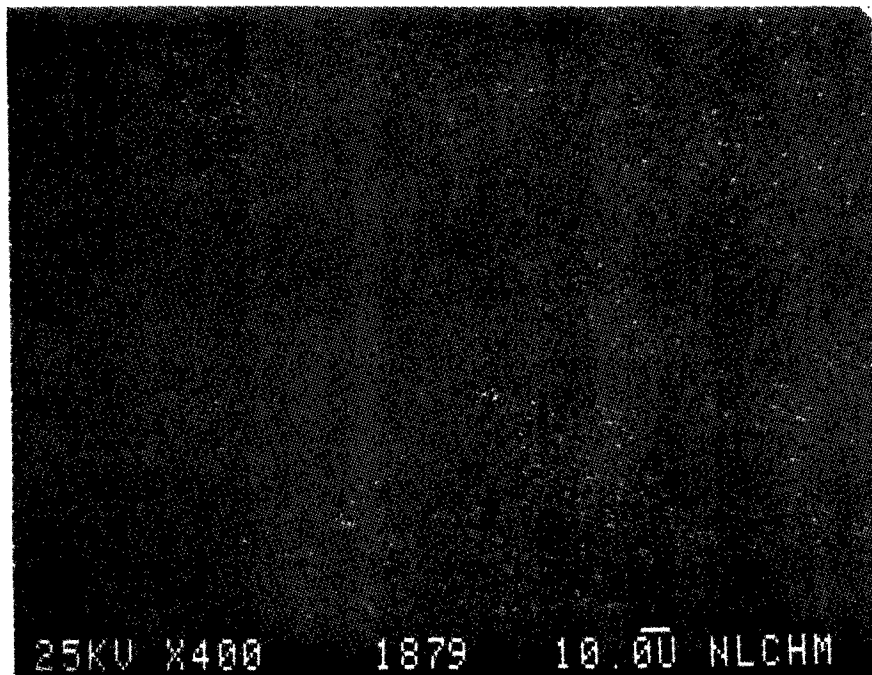


Figure 586

Si X-Ray Image of Figure 584

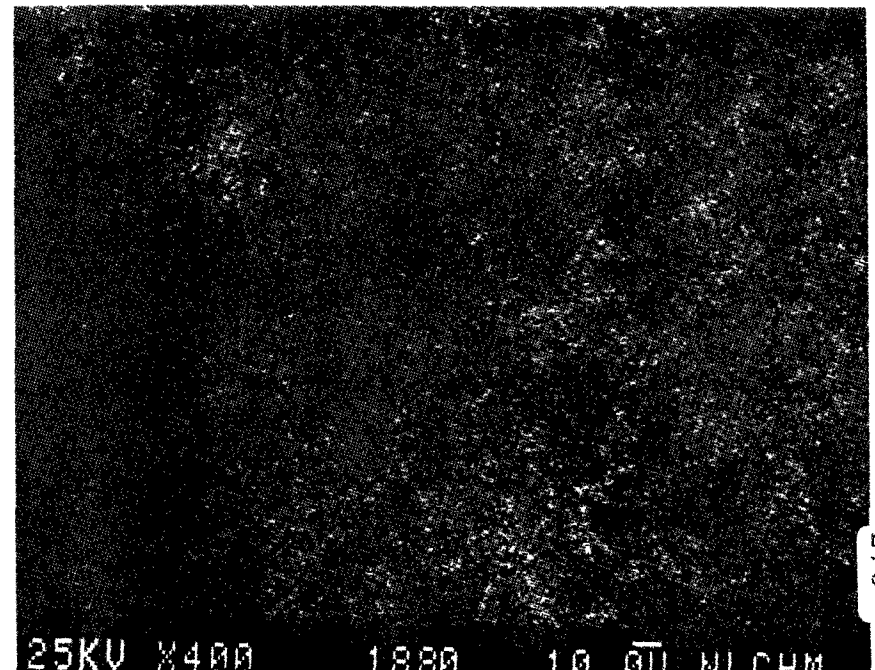


Figure 587

Ti X-Ray Image of Figure 584

SEM IMAGES OF SAMPLE #

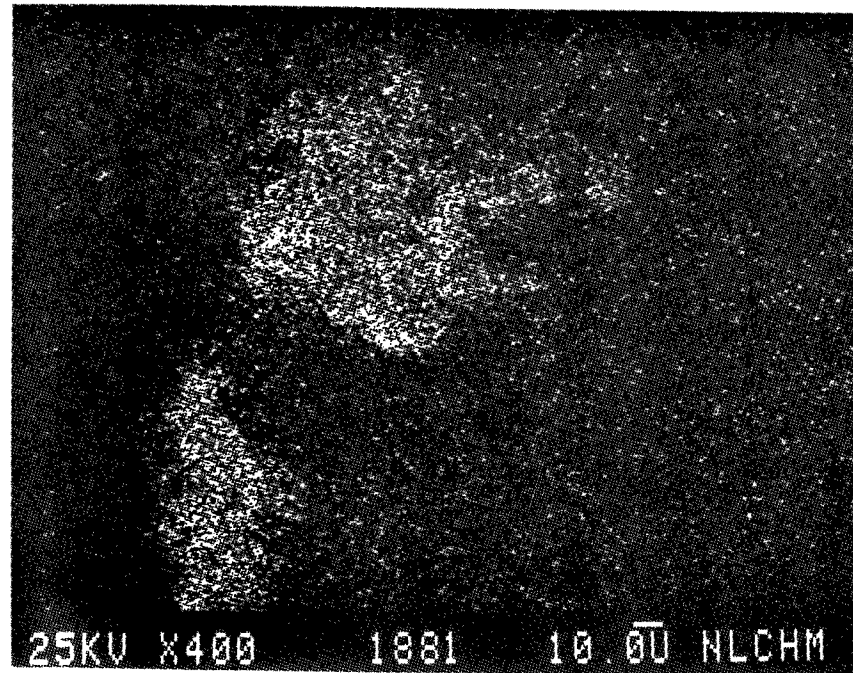


Figure 588

Fe X-Ray Image of Figure 584

SEM IMAGES OF SAMPLE #

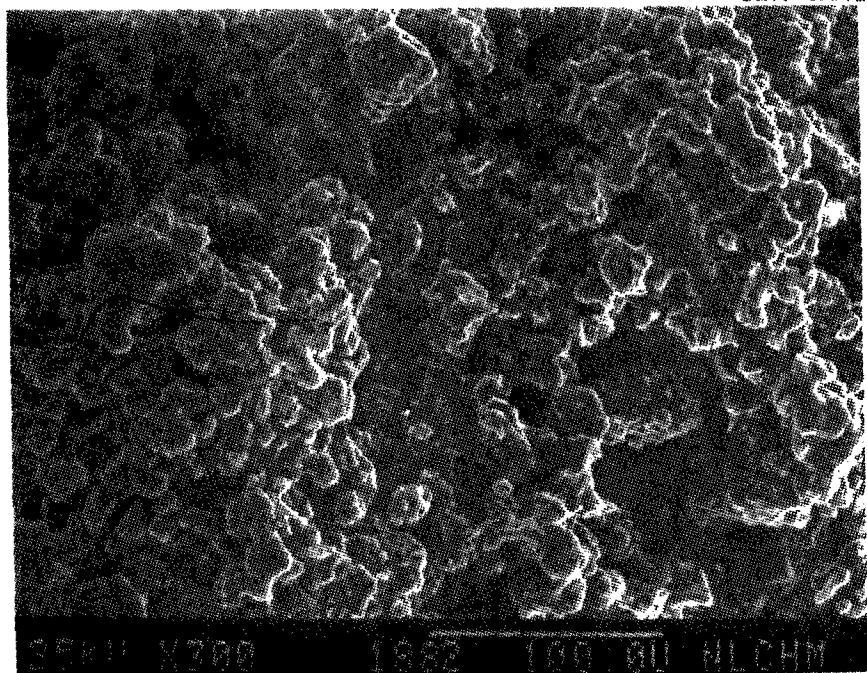


Figure 589

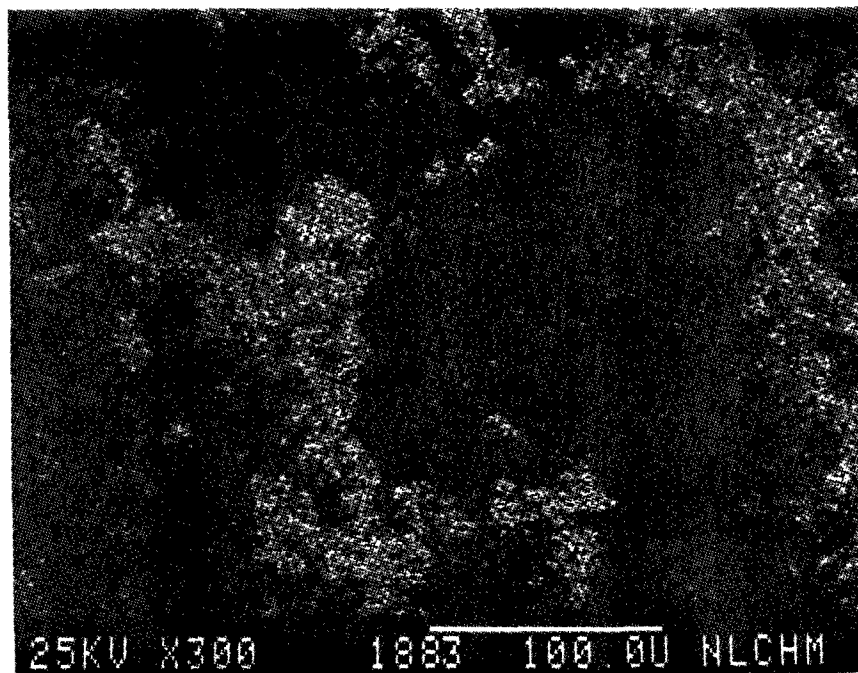


Figure 590

AL X-Ray Image of Figure 589

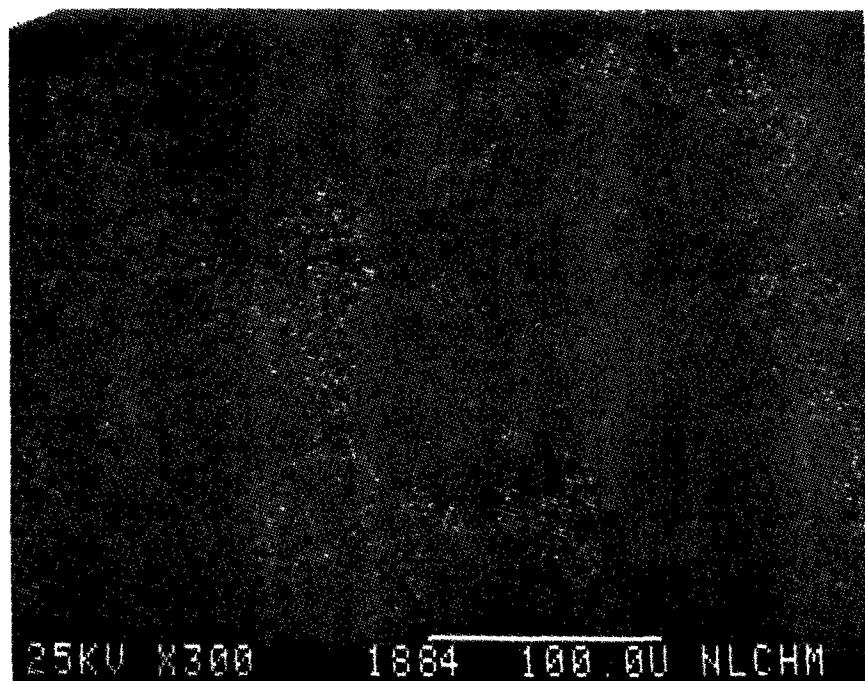


Figure 591

Si X-Ray Image of Figure 589

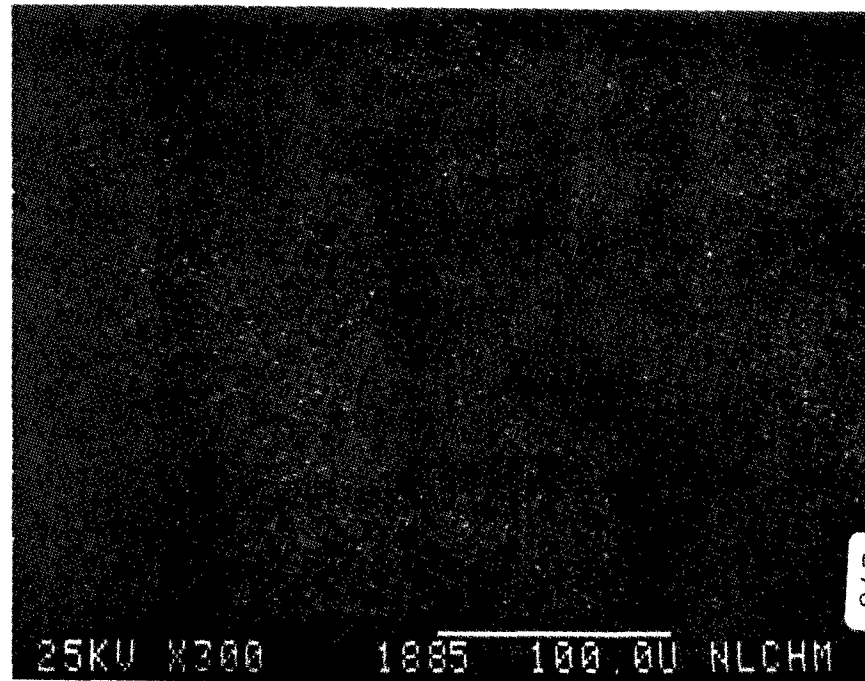


Figure 592

Ti X-Ray Image of Figure 589

SEM IMAGES OF SAMPLE #

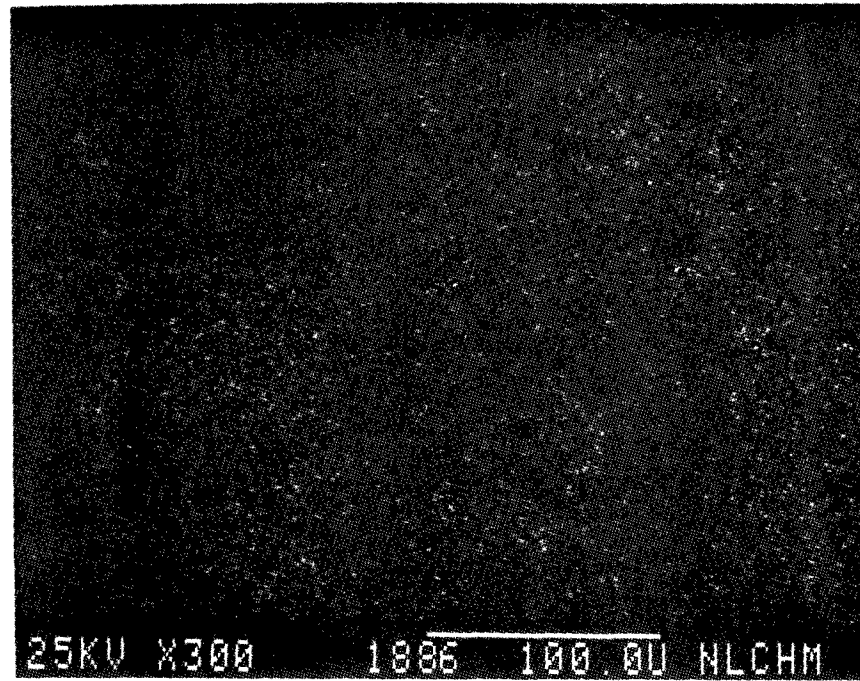


Figure 593

Fe X-Ray Image of Figure 589



ENERGY DISPERSIVE X-RAY ANALYSIS

Analytical Number Bauxite

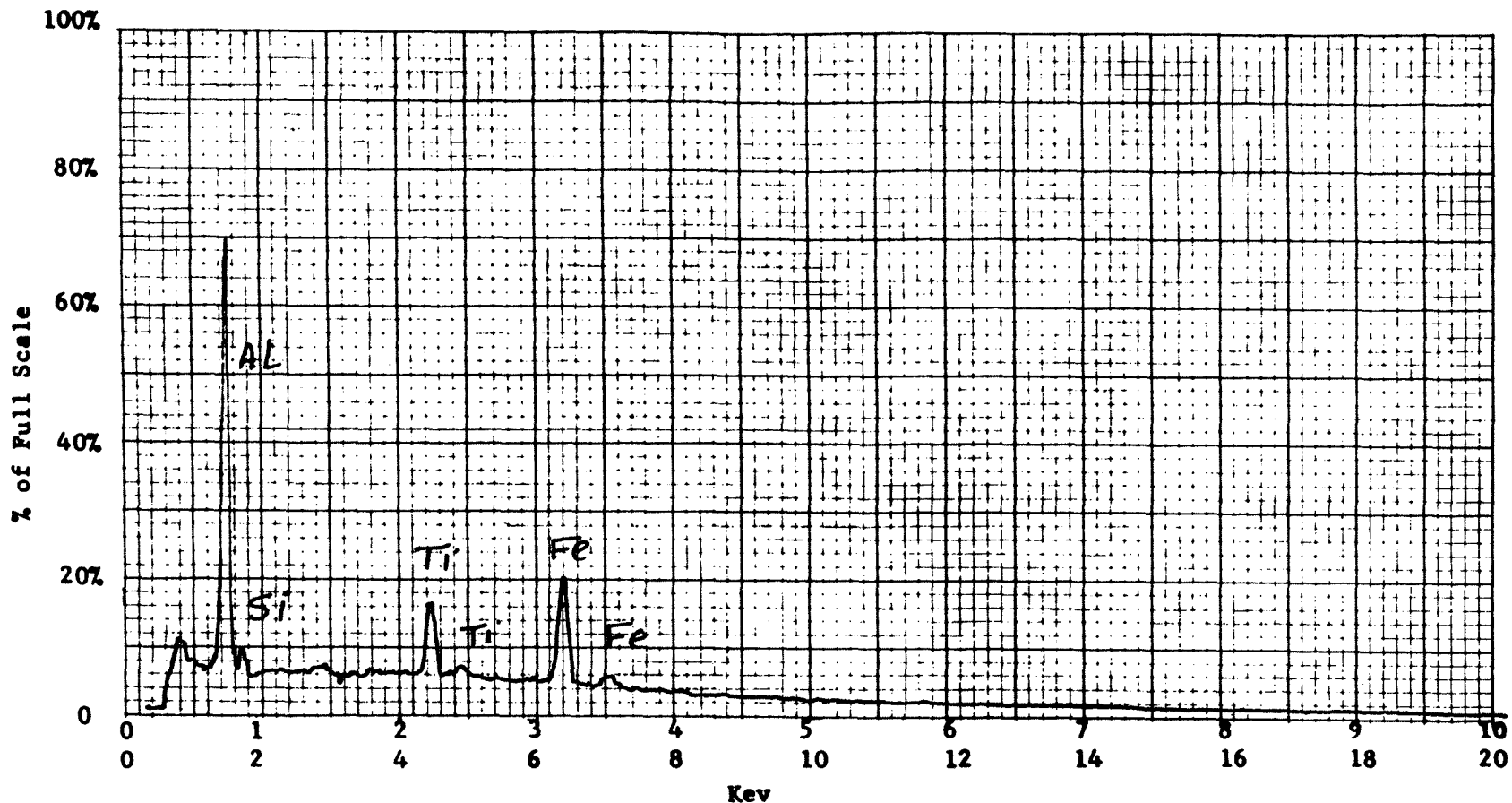
Operator \_\_\_\_\_ Date \_\_\_\_\_

Accelerating Potential 25 KeV

Total Counts Acquired 1.0 min.

Number Counts Full Scale 5K

Number of eV per channel 20



Sample peculiarities and remarks: FIGURE 594: AREA SCAN

**ENERGY DISPERSIVE X-RAY ANALYSIS**

Analytical Number Bauxite

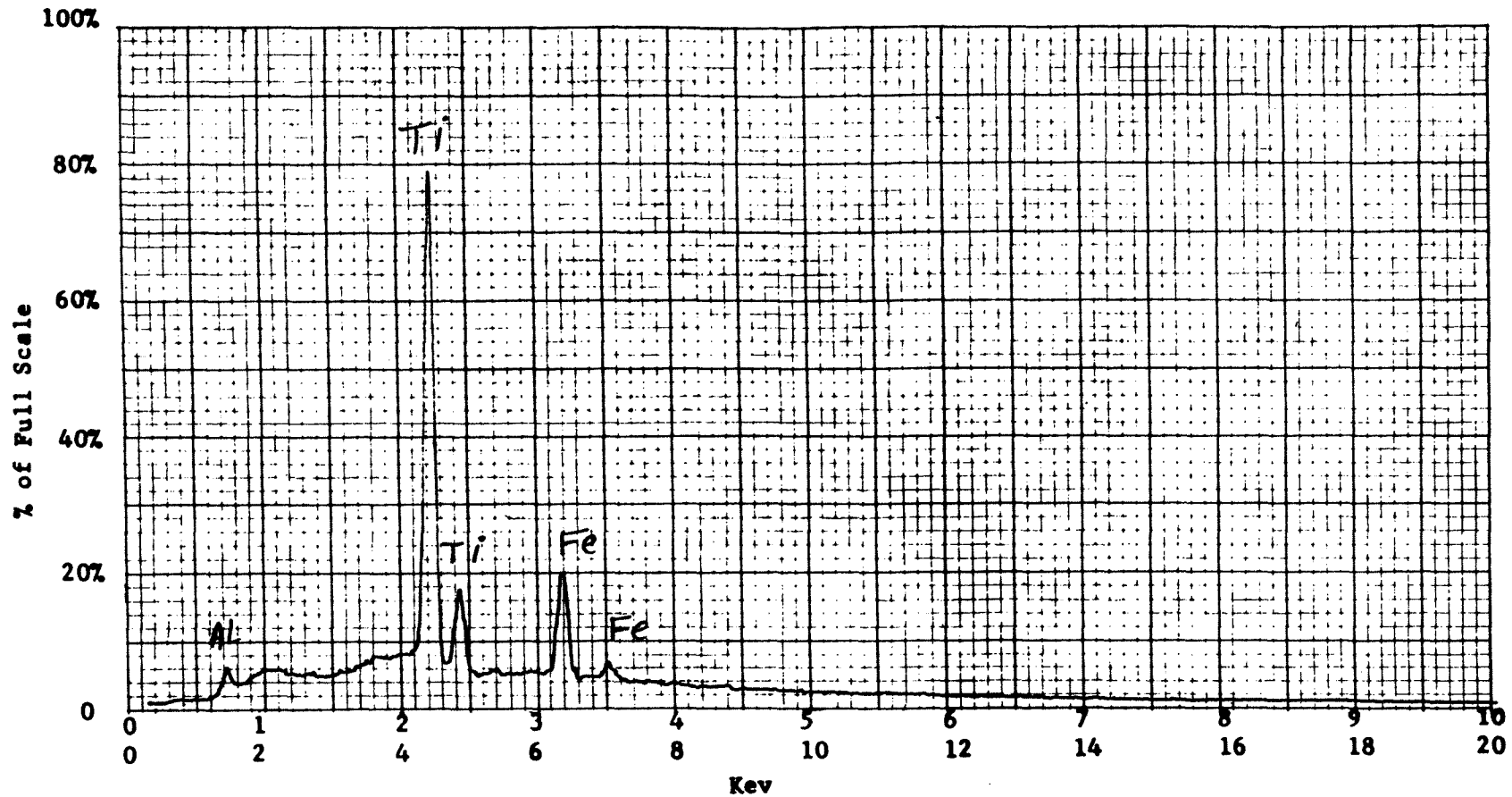
Operator \_\_\_\_\_ Date \_\_\_\_\_

Accelerating Potential 25 KeV

Total Counts Acquired 1.0 min.

Number Counts Full Scale 5K

Number of eV per channel 20



Sample peculiarities and remarks: FIGURE 595: POINT SCAN ON A HIGH Ti PARTICLE  
IN FIGURE 579

ENERGY DISPERSIVE X-RAY ANALYSIS

Analytical Number Bauxite

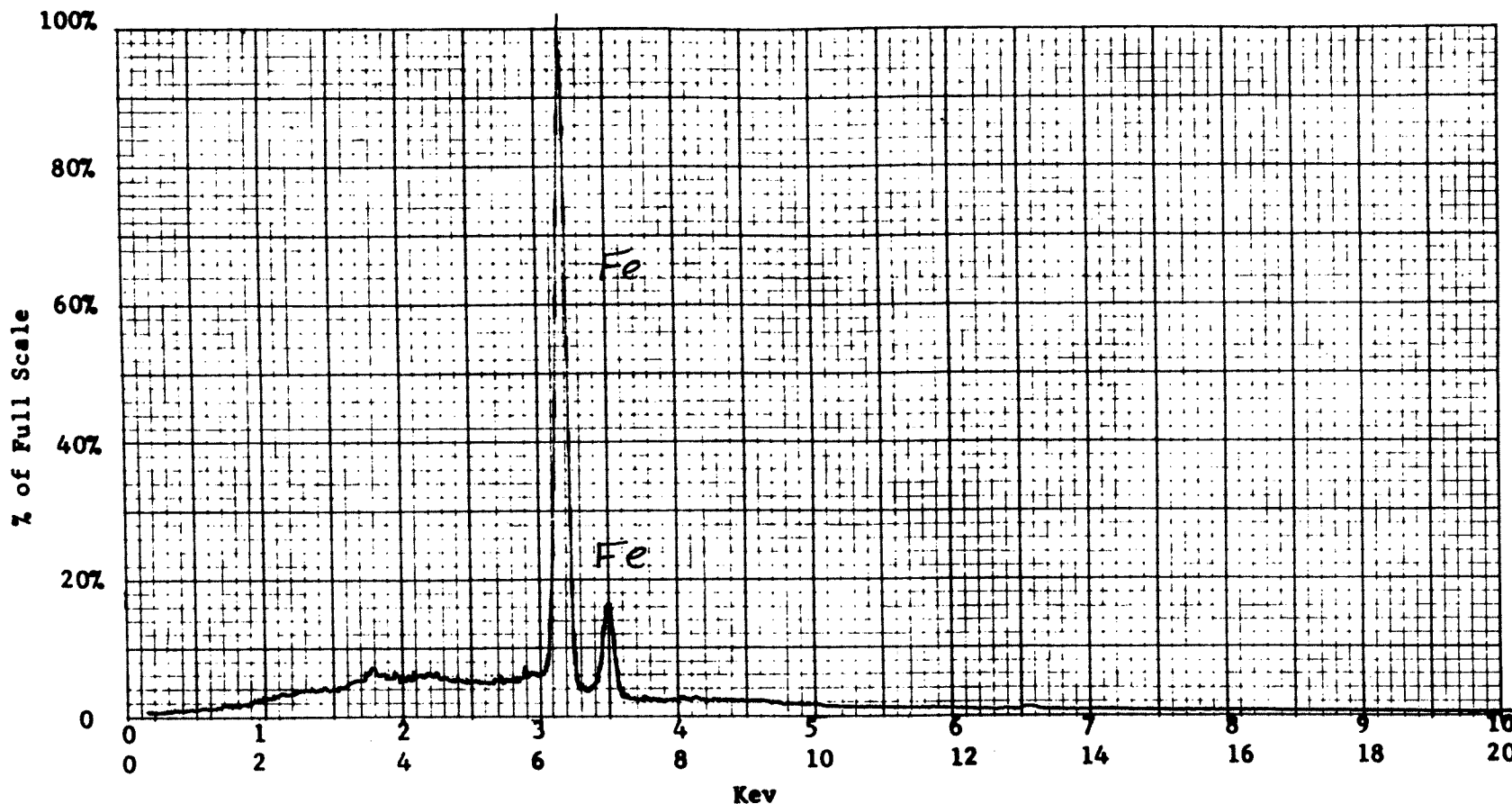
Operator \_\_\_\_\_ Date \_\_\_\_\_

Accelerating Potential 25 KeV

Total Counts Acquired 1.0 min.

Number Counts Full Scale 5K

Number of eV per channel 20



Sample peculiarities and remarks: FIGURE 596: POINT SCAN ON A SMALL SPOT IN A LARGE PARTICLE IN FIGURE 584

ENERGY DISPERSIVE X-RAY ANALYSIS

Analytical Number Bauxite

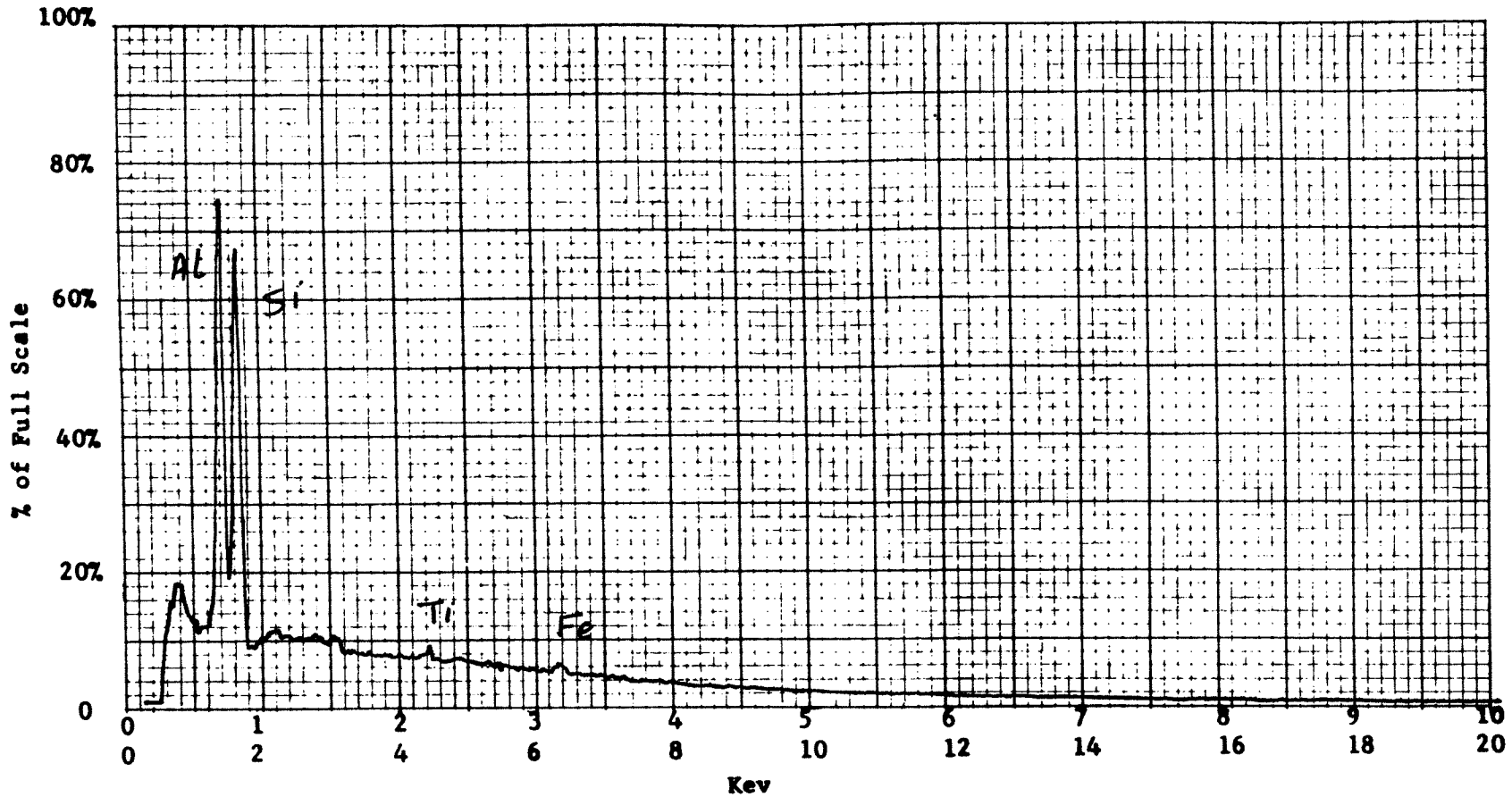
Operator \_\_\_\_\_ Date \_\_\_\_\_

Accelerating Potential 25 KeV

Total Counts Acquired 1.0 min.

Number Counts Full Scale 5K

Number of eV per channel 20



Sample peculiarities and remarks: FIGURE 597: POINT SCAN ON A HIGH Si SPOT ON A LARGE PARTICLE IN FIGURE 579

SECTION 6  
CONCLUSION

A scanning electron microscopy (SEM) and X-ray energy dispersive spectroscopic (EDS) study of selected clay minerals and fly ash samples has been completed. Both methods clearly demonstrate the potential wealth of information that may be gained by such a study. In particular, structural as well as chemical information may be obtained in detail. This type of information may be useful for predicting the efficiency of a sorbent in an actual application for the treatment/control of hazardous leachates.

The detailed results are presented in Section 5, as SEM images, X-ray images and X-ray energy spectra showing the particle size, shape and distribution, also the elemental composition and distribution in each sample. The data are summarized in Tables I and II.

TABLE I  
PARTICLE SIZE IN MICRONS ( $\mu$ )

<u>SAMPLE IDENTIFICATION</u>	<u>MAXIMUM</u>	<u>AVERAGE</u>	<u>MINIMUM</u>
Apautagite (Green Sand)	100.0	11.0	0.1
Fly Ash (Acidic)	105.0	11.0	0.14
Bentonite	135.0	26.0	1.2
Vermiculite	2400.0	1000.0	33.0
Fly Ash (Basic)	140.0	20.0	0.1
Activated Carbon	2700.0	1700.0	20.0
Illite	85.0	19.0	0.2
Kaolinite	13.0	1.6	0.1
Zeolite	110.0	26.0	0.8
Bauxite	1700.0	700.0	4.0



TABLE II  
ELEMENTAL COMPOTISION

<u>SAMPLE IDENTIFICATION</u>	<u>Mg</u>	<u>Al</u>	<u>Si</u>	<u>P</u>	<u>S</u>	<u>K</u>	<u>Ca</u>	<u>Ti</u>	<u>Cr</u>	<u>Mn</u>	<u>Fe</u>	<u>Ba</u>
Apautagite (Green Sand)	X	X	X	X	X	X	X	X		X	X	
Fly Ash (Acidic)		X	X		X	X	X	X			X	
Bentonite		X	X		X		X				X	
Vermiculite	X	X	X			X	X	X	X		X	
Fly Ash (Basic)	X	X	X		X	X	X	X			X	X
Activated Carbon					X							
Illite		X	X		X	X	X	X			X	
Kaolinite		X	X					X				
Zeolite		X	X			X	X	X			X	
Bauxite		X	X					X			X	

REFERENCES

1. Sheih, M. (1979), Doctoral Thesis, New Jersey Institute of Technology.
2. Michaels, A. (1966), Proceeding of the Third National Conference on Air Pollution. U.S. Public Health Service, Publication 1649.
3. Brunner, D.R., Keller, D.J., "Sanitary Landfill Design and Operation", U.S. Environmental Protection Agency, Report SW-65ts, Washington, D.C., 1972.
4. "Sanitary Landfill", ASCE "Manuals of Engineering Practice", No. 39, Sanitary Engineering Division, Am. Soc. Civil Engineers, New York, N.Y. 1959.
5. "Sanitary Landfills in Municipal Refuse Disposal", Chap. 4, p. 91, Institute for Solid Wastes, American Public Works Association, Washington, D.C. 1970.
6. Environmental Protection Agency, "Thermal Processing and Land Disposal of Solid Wastes Guidelines", Federal Register, 39, 158, Part IV, August 14, 1974.
7. Grim, Ralph E. (1953), "Clay Mineralogy".
8. Minerals for the Chemical and Allied Industries by S.J. Johnstone and M.G. Johnstone, 2nd Edition 1961, John Wiley & Son, Inc.
9. The Particle Atlas, Edition II, Vol. IV by Walter C. McCrone & John Delly.
10. Industrial Minerals and Rocks (Nonmetallic Other than Fuels), 3rd Edition, American Institute of Mining, Metallurgical, and Petroleum Engineers.
11. Echlin, P., SEM, 1974 and 1978, "Coating Techniques for SEM".
12. Echlin, P., SEM, 1975, "Sputter Coating Techniques for SEM".
13. Denee, P.N. and Walter, E.R., SEM 1975, "Speciman Coating Techniques for the SEM - A Comparative Study".
14. Coleman, J.R., Practical Scanning Electron Microscopy, Chap. 13, ed. J.I. Goldstein and H. Yakowitz, New York, N.Y. 1975.

15. Holland, L, Vacuum Deposition of Thin Film, Chapman Hall, Ltd, London, England 1970.
16. Maissel, L.I. and Lang, R.G., Handbook of Thin Film Technology, McGraw Hill, New York, N.Y. 1970.
17. Cross, P.M., The Use of the Scanning Electron Microscope, 1972.
18. Introduction to Analytical Electron Microscopy by J. Hren, J. Goldstein and D. Jay, 1979.
19. Practical Scanning Electron Microscopy by J. Goldstein and H. Yakowitz, 1975.
20. Thornton, P.R., Scanning Electron Microscopy, (Chapman Hall, Ltd., London, England, 1968).
21. Wells, O.C., Scanning Electron Microscopy.